NATIONAL CENTER FOR EARTHQUAKE ENGINEERING RESEARCH
Headquartered at the State University of New York at Buffalo

ISSN 1088-3800

Dynamic Response of Unreinforced Masonry Buildings with Flexible Diaphragms

by

A.C. Costley and D.P. Abrams

University of Illinois at Urbana-Champaign
Department of Civil Engineering
1245 Newmark Engineering Laboratory
205 N. Mathews Avenue, MC250
Urbana, Illinois 61801

Technical Report NCEER-96-0001

October 10, 1996

This research was conducted at the University of Illinois at Urbana-Champaign and was supported in whole or in part by the National Science Foundation under Grant No. BCS 90-25010 and other sponsors.

NOTICE

This report was prepared by the University of Illinois at Urbana-Champaign as a result of research sponsored by the National Center for Earthquake Engineering Research (NCEER) through a grant from the National Science Foundation, and other sponsors. Neither NCEER, associates of NCEER, its sponsors, the University of Illinois at Urbana-Champaign, nor any person acting on their behalf:

a. makes any warranty, express or implied, with respect to the use of any information, apparatus, method, or process disclosed in this report or that such use may not infringe upon privately owned rights; or

b. assumes any liabilities of whatsoever kind with respect to the use of, or the damage resulting from the use of, any information, apparatus, method, or process disclosed in this report.

Any opinions, findings, and conclusions or recommendations expressed in this publication are those of the author(s) and do not necessarily reflect the views of NCEER, the National Science Foundation, or other sponsors.

NATIONAL CENTER FOR EARTHQUAKE ENGINEERING RESEARCH
Headquartered at the State University of New York at Buffalo

Dynamic Response of Unreinforced Masonry Buildings with Flexible Diaphragms

by

A.C. Costley[1] and D.P. Abrams[2]

Publication Date: October 10, 1996
Submittal Date: October 7, 1995

Technical Report NCEER-96-0001

NCEER Task Numbers 92-3110, 93-3112 and 94-3110

NSF Master Contract Number BCS 90-25010

1 Structural Engineer, Ficcadenti & Waggoner; former Research Assistant, Department of Civil Engineering, University of Illinois at Urbana-Champaign
2 Professor, Department of Civil Engineering, University of Illinois at Urbana-Champaign

NATIONAL CENTER FOR EARTHQUAKE ENGINEERING RESEARCH
State University of New York at Buffalo
Red Jacket Quadrangle, Buffalo, NY 14261

PREFACE

The National Center for Earthquake Engineering Research (NCEER) was established to expand and disseminate knowledge about earthquakes, improve earthquake-resistant design, and implement seismic hazard mitigation procedures to minimize loss of lives and property. The emphasis is on structures in the eastern and central United States and lifelines throughout the country that are found in zones of low, moderate, and high seismicity.

NCEER's research and implementation plan in years six through ten (1991-1996) comprises four interlocked elements, as shown in the figure below. Element I, Basic Research, is carried out to support projects in the Applied Research area. Element II, Applied Research, is the major focus of work for years six through ten. Element III, Demonstration Projects, have been planned to support Applied Research projects, and will be either case studies or regional studies. Element IV, Implementation, will result from activity in the four Applied Research projects, and from Demonstration Projects.

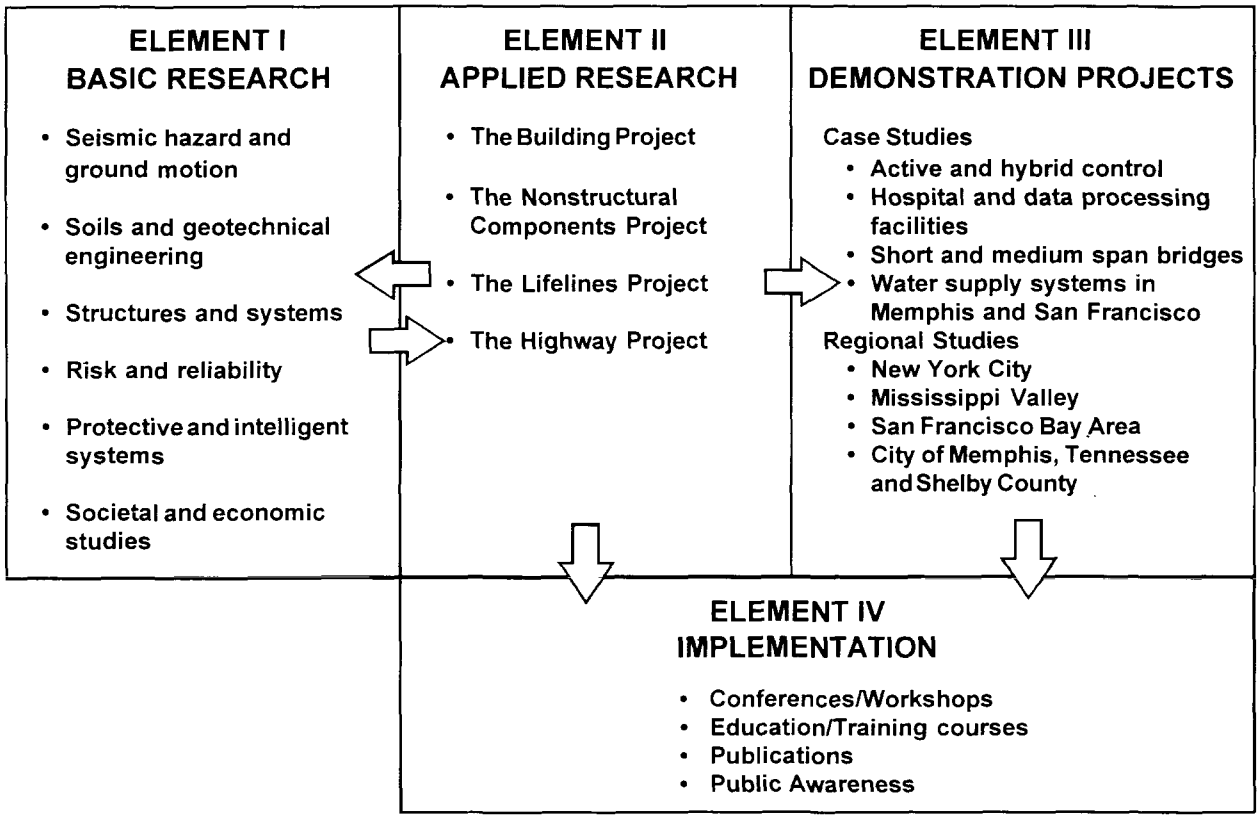

Research in the **Building Project** focuses on the evaluation and retrofit of buildings in regions of moderate seismicity. Emphasis is on lightly reinforced concrete buildings, steel semi-rigid frames, and masonry walls or infills. The research involves small- and medium-scale shake table tests and full-scale component tests at several institutions. In a parallel effort, analytical models and computer programs are being developed to aid in the prediction of the response of these buildings to various types of ground motion.

Two of the short-term products of the **Building Project** will be a monograph on the evaluation of lightly reinforced concrete buildings and a state-of-the-art report on unreinforced masonry

The **structures and systems program** constitutes one of the important areas of research in the **Building Project**. Current tasks include the following:

1. Continued testing of lightly reinforced concrete external joints.
2. Continued development of analytical tools, such as system identification, idealization, and computer programs.
3. Perform parametric studies of building response.
4. Retrofit of lightly reinforced concrete frames, flat plates and unreinforced masonry.
5. Enhancement of the IDARC (inelastic damage analysis of reinforced concrete) computer program.
6. Research infilled frames, including the development of an experimental program, development of analytical models and response simulation.
7. Investigate the torsional response of symmetrical buildings.

This research investigates the dynamic behavior of two reduced-scale URM buildings with flexible diaphragms though laboratory testing. A simple analytical model was created to estimate dynamic response parameters, such as acceleration and displacement. The model showed good agreement with the laboratory results.

Further, conventional methods of analysis for URM structures were investigated to determine their applicability and accuracy. Methods found in present codes for new construction and rehabilitation, finite element models, response spectrum analysis, pushover analysis and nonlinear time-step integration were examined. Recommendations for the analysis and rehabilitation of URM buildings with flexible diaphragms are provided.

ABSTRACT

The overall objective of the research was to provide recommendations for the evaluation and rehabilitation of unreinforced masonry buildings. An experimental study was done to investigate nonlinear dynamic response of two-story building systems with flexible floor diaphragms. Two reduced-scale test structures were subjected to a series of simulated earthquake motions on the University of Illinois shaking table. The experimental parameters were the relative lateral strengths of the two parallel shear walls and the aspect ratios of piers between window and door openings. The accuracy of several computational methods were examined by contrasting estimates with measured response. These methods included procedures that are prescribed in building code requirements for new construction and guidelines for rehabilitation of existing buildings, as well as more complex finite element and dynamic analysis methods. A nonlinear dynamic analysis model was developed to estimate large-amplitude displacements.

This report includes descriptions of the experimental and analytical investigations, and provides a number of recommendations for evaluation and rehabilitation of unreinforced masonry buildings.

ACKNOWLEDGMENTS

The research report herein was funded by the National Center for Earthquake Engineering Research under Project Nos. 92-3110, 93-3112, and 94-3110. This support is sincerely appreciated. The Brick Institute of America donated the bricks used in the construction of the test structures.

Dr. Douglas Foutch, Dr. William Gamble, Dr. German Gurfinkel, and Dr. Sharon Wood are thanked for reviewing the manuscript.

Special acknowledgement is given to Glen Manak for his diligent construction of the two test buildings. The members of the Civil Engineering Machine Shop, Charles Day, Dan Mullis, Bryan Reynolds, Wayne Schillinger, and Roy Walton, under the direction of Carroll Swan, are thanked for their assistance with the laboratory work. Also, special acknowledgement is given to Harold Dalrymple (in memoriam) for his assistance with instrumentation and data collection. The work of his assistant, David Hines, is duly noted. The help of Lee Stoops, Paul Blaszczyk, Tim Lubbe, and Mark Owens with the building construction is appreciated. The thoughtful suggestions of Dr. Arthur Robinson, Dr. G. M. Calvi, Dr. G. Magenes, and Fernando Fonseca during the analysis are also acknowledged.

TABLE OF CONTENTS

TABLE OF CONTENTS (Cont'd)

TABLE OF CONTENTS (Cont'd)

TABLE OF CONTENTS (Cont'd)

LIST OF ILLUSTRATIONS

LIST OF ILLUSTRATIONS (Cont'd)

LIST OF ILLUSTRATIONS (Cont'd)

LIST OF ILLUSTRATIONS (Cont'd)

LIST OF ILLUSTRATIONS (Cont'd)

LIST OF ILLUSTRATIONS (Cont'd)

LIST OF TABLES

SECTION 1. INTRODUCTION

Masonry construction is common in almost all parts of the world. Masonry is the original building material, dating back to ancient Egypt, the Greek and Roman dynasties, and early Latin American and Far Eastern civilizations. Some enduring masonry structures include the Pyramids of Giza, the Roman Colosseum, and the Great Wall of China. For many masonry constructions, only the ravages of time can wear them down.

Recently, masonry has been given a bad reputation due to dramatic media coverage after earthquakes. Piles of bricks on top of sidewalks and parked cars, crumbled walls, toppled chimneys, and cracked masonry facades seem to garner much press following seismic events. However, many of these walls, chimneys, and facades were poorly constructed and were non-engineered, that is they were not designed to resist loads induced by an earthquake. Engineered and/or carefully constructed unreinforced masonry (URM) structures can and do perform well during large seismic events. In a previous study (Tena-Colunga and Abrams, 1992a), an URM firehouse subjected to the 1989 Loma Prieta earthquake was studied. Even though peak ground accelerations in the region of the firehouse were as high as 0.29g, and the flexible timber roof diaphragms amplified ground accelerations as high as 2.5 times, the structure experienced little damage.

Many existing masonry structures are unreinforced because reinforcement was not feasible or was thought to be unnecessary. A growing awareness of the potential insufficiencies of these URM structures has led to the need to know how much resistance these structures have against lateral loads. This awareness has spread beyond the seismically active regions to areas that have been traditionally considered non-seismic. Of particular concern are URM structures with flexible floor and roof diaphragms, usually made of timber. One of the problems with determining the lateral strength of an URM building with flexible floor and/or roof diaphragms is deciding how to analytically model the structure. Typical structural analysis models use lumped masses at the story levels while further simplifications include assuming rigid floor diaphragms in order to collapse the entire story into a single lateral element. An URM building with flexible diaphragms, however, is

not accurately modelled in this way since the flexible diaphragms can amplify wall accelerations and can influence response frequencies.

Seismic evaluation and strengthening of URM structures has started to become accepted engineering practice in the United States over the last ten to fifteen years. Its origins can be tied to a series of reports known as the ABK "Methodology for Mitigation of Seismic Hazards in Existing URM Buildings." Two organizations, one federal and one private, have released code-type provisions and a code which include chapters based on this methodology for the evaluation of URM buildings. In 1992, the Building Seismic Safety Council issued the NEHRP Handbook for the Seismic Evaluation of Existing Buildings (FEMA 178). Here, Appendix C is labeled "Evaluation of Unreinforced Masonry (URM) Bearing Wall Buildings." In 1994, the International Conference of Building Officials (ICBO) released a revised edition of the Uniform Code for Building Conservation (UCBC). Within this code, Appendix Chapter 1 is entitled "Seismic Strengthening Provisions for Unreinforced Masonry Bearing Wall Buildings." Both chapters are similar in nature and scope and are designed to identify potential shortcomings of an existing URM structure's ability to withstand anticipated lateral loads.

The current study was borne from a previous investigation by Tena-Colunga and Abrams (1992a) who examined the dynamic response of an URM firehouse during the Loma Prieta earthquake. This current program is one of the first dynamic laboratory studies of URM buildings aimed at investigating the effects of flexible diaphragms on wall behavior. The study of flexible diaphragms necessitates dynamic testing since static tests do not accurately represent inertial effects, strain rates, and the presence of multiple response frequencies. Inertial and frequency effects are crucial in the study of flexible diaphragms while strain rates play an important role in the dynamic strength of unreinforced masonry.

1.1 Objectives

The objectives of this study can be broken down into three primary areas. The first objective is to investigate the dynamic behavior of two, reduced-scale, URM buildings with flexible

diaphragms. In a laboratory setting, dynamic response of URM bearing wall systems with flexible diaphragms will be observed. A body of response data on URM structures with flexible diaphragms, that can be used by others, will result from the experiments.

A second objective of the research program is to develop a simple analytical model to estimate important dynamic response parameters, such as acceleration and displacement. The model will be reconciled with the data measured during the dynamic tests.

The third objective of the study is to investigate conventional methods of analysis for URM structures to determine their applicability and accuracy. Several methods found in present codes for new construction and rehabilitation, finite element models, and some simple dynamic analyses will be reviewed. Calculated response will be compared with the measured response. Other methods, such as response spectrum analysis, pushover analysis, and nonlinear time-step integration will be examined more carefully to see how well these methods model the behavior of the test structures. The end result of the study will be recommendations for the evaluation and rehabilitation of URM buildings with flexible diaphragms.

1.2 Previous Masonry Research

Masonry research has been conducted in many nations around the world. Static and dynamic tests of masonry structures and components have been completed. Studies have also been undertaken to model and analyze the response of masonry structures to lateral loadings. In addition, researchers have reported on the actual response of masonry buildings during earthquakes through post-earthquake reconnaissance reports. This section will briefly summarize previous research relating to the dynamic and static testing of masonry structures and components, the modeling and analysis of masonry structures, and the response of masonry structures during earthquakes.

1.2.1 Dynamic Tests

A large number of shaking-table tests of masonry structures has been completed in what is now Slovenia (formerly Yugoslavia). In 1987, Tomazevic reported on dynamic tests of a one-seventh scale, four-story, unreinforced brick, building. Since all the damage occurred in the first story during these tests, Tomazevic proposed a story mechanism as a simple model when overturning forces can be neglected. In 1990, Tomazevic, et al, described the effects of reinforcement and structural layout on masonry structures as a result of dynamic tests on four, one-fifth scale, block buildings. Two of the buildings had a central reinforced concrete column while the other two had a central cross-shaped masonry wall. The unreinforced buildings were determined to be less "ductile" than those with reinforcement while among the unreinforced models, the one with the cross-shaped wall performed better than the one with the reinforced concrete column. Tomazevic and Weiss revisited the tests of the latter two buildings (with the cross-shaped walls) in 1994. Dynamic tests on four, one-fourth scale, two-story, stone masonry buildings were discussed in 1992 by Tomazevic, et al. The primary variable in this series of tests was the effect of different types of floor systems on the seismic performance of the buildings. Results indicated that the type of floor system (wood, reinforced concrete or brick) was less important than how well the floor system was connected to the walls and how well the walls were tied together. A series of tests on four, one-fourth scale, two-story, unreinforced brick buildings were reported on in 1993 and 1994 by Tomazevic, et al. The main issue being studied in this test series was the connectivity of the walls. Preliminary results showed that adding ties to buildings with wooden floor systems can prevent serious damage to the out-of-plane walls.

Other European shaking-table tests of masonry structures have been conducted by researchers in Italy, Macedonia, and England. In 1992, Modena, La Mendola, and Terrusi reported on a one-fifth scale, three-story, test building composed of reinforced block perimeter walls and a central reinforced concrete column. Magenes and Calvi described dynamic tests of eight unreinforced brick walls in 1994. Variables in this test series included two mortar strengths, two aspect ratios, and two levels of axial load. Wall rocking was reported for the four walls with the stronger mortar and one of the four walls with the weaker mortar (more slender, lighter axial

load). A joint Macedonian/Italian shaking-table testing program of mixed brick masonry and reinforced concrete systems was discussed by Jurukovski, et al, in 1992. Three, one-third scale, four-story, models with reinforced concrete elements in the first story and brick walls in all stories were tested, the latter two models being strengthened versions of the first. Also in 1992, Pomonis, et al, reported on shaking-table tests of a total of six unreinforced concrete block and concrete brick walls. The purpose of the tests was to study the effects of frequency content of the ground motion on wall damage.

A considerable amount of dynamic testing of masonry structures has also taken place in the Peoples Republic of China (PRC). In 1986, Zhu summarized the Chinese shaking-table testing programs. Three, reduced-scale, one-story, unreinforced brick buildings were tested at the Institute of Engineering Mechanics (Harbin) while three, one-fourth scale, five-story, unreinforced block buildings were tested at Tongji University (Shanghai). Dynamic tests of masonry walls, with and without openings, were also conducted at Tongji University. A more detailed report by Zhu, Wu, and Zhou in 1986 (Tongji) described a shaking-table test of a one-fourth scale, five-story, block building, this one strengthened by reinforced concrete corner columns and tie beams. In 1990, Xia, et al, (IEM) described dynamic tests of a one-sixth scale, seven-story, block building with reinforced concrete tie columns and beams. The main interest of these tests was the lightweight blocks that were used.

Some dynamic testing of masonry structures has been conducted in Peru. Bariola, Ginocchio, and Quiun described shaking-table tests of seven unreinforced brick walls in 1990. The walls had varying slenderness and were tested in the out-of-plane direction. After flexural cracking at the base, rigid-body rocking (out-of-plane) was prevalent. In 1992, San Bartolomé, Quiun, and Torrealva reported on dynamic tests of a reduced-scale (1:2.5), three-story, confined brick masonry structure. One facet of the tests was the type of failure, either shear or flexural, and the effect of this failure on the current design practice. Even though a flexural failure was expected, a shear failure was recorded.

In the United States, shaking-table tests have been conducted on brick, block, and abode structures. In 1979, Clough, Mayes, and Gülkan summarized a series of dynamic tests of four,

full-size, one-story, partially-reinforced houses. One of the buildings was brick while the others were block. One of the block buildings was first tested unreinforced. In addition, walls, both reinforced and unreinforced, were tested simultaneously with some of the houses. During the testing of the first house, rocking of the walls was found to strongly influence the response and was minimized in subsequent tests. In 1983, Manos, Clough, and Mayes reported on tests of a fifth house, this time under triaxial excitation. This block house was also first tested unreinforced before being partially reinforced. Sucuoglu, Mengi, and McNiven used shaking-table tests of a pair of unreinforced brick walls to develop a linear, mathematical model for the dynamic response of masonry walls in 1982. In 1986, Mengi and McNiven used the results from the previous tests to extend the model to include nonlinear behavior. Also in 1986, Scawthorn and Becker used shaking-table tests of a three-fourth scale adobe house to test various strengthening measures. Tolles, et al, reported on dynamic tests of strengthened adobe houses (one-fifth scale) in 1994. Lastly, in 1990, Paulson and Abrams used shaking-table tests of two, one-fourth scale, reinforced concrete block buildings to examine dynamic response characteristics of reinforced masonry buildings.

1.2.2 Static Tests

Statics tests on unreinforced masonry have been conducted in Italy. Anthoine, Magenes, and Magonette reported on cyclic, in-plane tests of unreinforced masonry piers with different aspect ratios in 1994. The static tests showed that the more slender wall rocked while the stockier wall failed by diagonal cracking. When retested with a larger axial load, the more slender wall also exhibited diagonal cracking. Also in 1994, Calvi, et al, reported on preliminary studies relating to the static testing of a full-scale, unreinforced brick building at the University of Pavia.

In the United States, in 1989, Epperson and Abrams reported on in-plane static tests of full-scale walls extracted from an existing building. Although the primary mode of failure for the five walls was shear, the walls all continued to resist increasing lateral loads after initial flexural cracking. Abrams and Shah reported on cyclic, in-plane, static tests of unreinforced masonry walls in 1992. The primary test variables in this study were aspect ratio and vertical compressive stress.

Results indicated that aspect ratio influenced the mode of failure, with the more slender walls exhibiting a greater degree of flexural cracking. Also noted was that deformation capacity was quite large when flexural cracking was present. In 1995, in-plane static tests of three, one-third scale, unreinforced masonry shear walls were reported by Mahmoud, Hamid, and El Magd. The authors concluded that the more slender walls were controlled primarily by rigid-body rocking. In addition, lowering the unit strength did not have a significant effect on the strength of the more slender walls.

Static tests on confined masonry components have been conducted in Mexico. Alcocer and Meli reported on tests of five confined masonry walls in 1993. Test variables included the degree of (in-plane) coupling between the walls, the absence or presence of joint reinforcement, and the aspect ratios of the walls. Results indicated that for these types of systems, diagonal cracking was predominant independent of wall aspect ratio.

In 1986, Feng summarized the results of in-plane static tests conducted in Xian, China. Eighty-six unreinforced masonry walls were tested in this study. The tests showed that under low loads the walls rocked while remaining intact. Under larger loads, shear sliding occurred. Feng concluded that lateral resistance decreased with both an increase in aspect ratio (more slender) and an increase in vertical compressive stress.

1.2.3 Modeling of Masonry Buildings

In 1978, Adham and Ewing reported on the modeling of unreinforced masonry buildings with wooden roof diaphragms. Their model consisted of rigid end (in-plane) walls, a flexible roof diaphragm, and the weight of the out-of-plane walls which were assumed to be cracked. The results from computer simulations using earthquake input motions indicated that stiffer diaphragms transmitted more shear force to the in-plane walls than the more flexible diaphragms, yet the more flexible diaphragms had greater deflections.

Like the Adham and Ewing paper, the ABK "Methodology" report, published in 1984, also recommended the assumption of modeling in-plane shear walls as rigid to determine dynamic

excitations of the diaphragms. In another section, this report discussed restoring shear capacity, i.e., rocking capacity, for piers with flexural cracks at the base and top.

In a 1987 paper, Ewing, et al, described a "lumped parameter model (LPM)" for reinforced masonry buildings with flexible roof diaphragms. This model consisted of *flexible* end (in-plane) walls, a flexible roof diaphragm, and additional masses to account for the out-of-plane walls. A paper by El-Mustapha and Kariotis in 1990 extended this LPM to allow uplift of the masonry walls from their bases. Results from computer simulations using the uplift model indicated that shear in the masonry walls was greatly reduced and in some cases collapse was prevented.

Xu and Abrams, in a 1992 report, discussed different failure modes for unreinforced masonry walls. Among the failure modes was flexural cracking, where overturning would occur with little damage to the wall. The load-deflection curve for this behavior showed that once a flexural crack reached the toe, deflection would increase with no increase in load.

In a 1994 paper about the assessing the performance of masonry buildings in Canada during earthquakes, Bruneau mentioned rigid-body rocking as a contributor to an "effective `ductility'" for unreinforced masonry structures. Bruneau went on to state that ductility in masonry structures has not yet been reliably quantified, nor has it been accurately modeled analytically.

1.2.4 Response of Masonry Buildings During Earthquakes

A 1993 paper by Hamid, Magd, and Salama reported on damage to loadbearing masonry buildings during the 1992 Cairo earthquake. The authors noted that out-of-plane walls well restrained at both ends maintained their integrity after cracking horizontally. Some behavioral differences between concrete and wooden floors in masonry buildings also were discussed.

In a 1994 paper, Schultz reviewed the response of masonry buildings during recent earthquakes through much of the North and South American continents. While reinforced and confined masonry generally have performed well during seismic events, the performance of unreinforced masonry ranges from excellent to disastrous. Unreinforced masonry structures performed well during the Mexico City earthquake (1985) primarily due a mismatch between

ground and structural frequencies. Thousands of brick residential units were severely damaged during the 1976 Guatemalan earthquakes while a large number survived with minimal damage. Out-of-plane failures due to poor connections within the masonry and poor anchorages between diaphragms and walls have been reported by a number of authors (ie - Bermudez 1994, Bruneau 1994a, Gallegos 1994, Garcia & Yamin 1994, and Schultz 1994) in the American hemisphere.

A 1994 paper by Bruneau (1994b) reviewed the seismic performance of North American unreinforced masonry buildings. Two common types of failures listed, based largely in part on damage observed during the 1989 Loma Prieta earthquake, were lack of anchorage (between walls and floor and roof systems) and out-of-plane failures (also related to floor and roof systems). The author went on to discuss codes being used in Canada and the United States to design and evaluate unreinforced masonry buildings.

In 1995, Bruneau gave a preliminary report of failures of masonry buildings during the 1995 Hansin-Awaji (Kobe, Japan) earthquake. Most of the unreinforced masonry buildings located by the author were found to have suffered severe damage, much of which was attributable to out-of-plane failures of the walls. In-plane behavior, meanwhile, was quite good in some of these buildings.

1.3 Organization of Report

The report is divided into eight sections. Specimen design, material tests, construction techniques, instrumentation, ground motion, and testing procedures are detailed in Section 2. Section 3 covers static and dynamic response calculated with conventional methods. Estimates of response as given by building codes, rehabilitation codes, finite element models and several simple dynamic models are given to compare with the measured response.

Measured dynamic response is described in Section 4, with the measured data appearing in Appendices C and E. A comparison of the measured response with the response calculated using codes and simple dynamic models, and important experimental conclusions are given at the end of Section 4.

Section 5 examines response spectrum analysis, pushover analysis, and a nonlinear time-step integration for their applicability to analyzing URM structures with flexible diaphragms. The third model examined, the nonlinear, three-degree-of-freedom model, was developed during the course of the study. Section 6 compares the response of S1 with S2 and presents some recommendations for the evaluation and rehabilitation of URM structures based on the correlation between the measured response in Section 4 and the analysis methods discussed in Sections 3 and 5.

A summary of the report is provided in Section 7. Comparisons between the various analytical methods and the measured response are reviewed and conclusions and recommendations of the entire study are presented. Some suggestions for future research on the subject of URM buildings are given. References are provided in Section 8.

SECTION 2. EXPERIMENTAL PROGRAM

2.1 Overview

Two reduced-scale buildings were constructed in the Newmark Civil Engineering Laboratory for the experimental phase. Although the buildings were reduced scale, no prototype building was intended or should be inferred. The two test buildings were each composed of four, two-story, unreinforced brick masonry walls and incorporated steel floor systems which were designed to simulate the flexible timber diaphragms common in older, unreinforced masonry structures. The layout of the openings, windows and doors, was varied in order to produce piers with several different aspect ratios. Configuration and construction of the test buildings were similar to that of an actual instrumented building which was investigated in a previous study (Tena-Colunga and Abrams, 1992a). Material strengths and construction procedures are documented. Both buildings were instrumented with almost 40 channels of accelerometers, displacement transducers, and strain gauges. Using the Newmark Lab's earthquake simulator, the two test structures were tested dynamically by subjecting them to simulated earthquake ground motions.

2.2 Description of Test Structures

The design of the test structures was directed by creating test buildings representative of older, unreinforced brick buildings, but not too complex to prevent an understanding of the dynamic behavior exhibited. A further constraint was the size and weight limits of the earthquake simulator (Section 2.4). As such, four-walled, box-type structures were devised each with two perforated shear/bearing walls and two solid transverse walls (Figures 2.1 and 2.2). The four-wall box measured 89.1" long, 65.8" wide, and 95.4" high. The designation of shear and transverse walls refers to the direction of shaking and perpendicular to the direction of shaking, respectively. Bearing walls are those resisting floor loadings. The number of stories was limited by construction practicalities as well as by the weight of the structures.

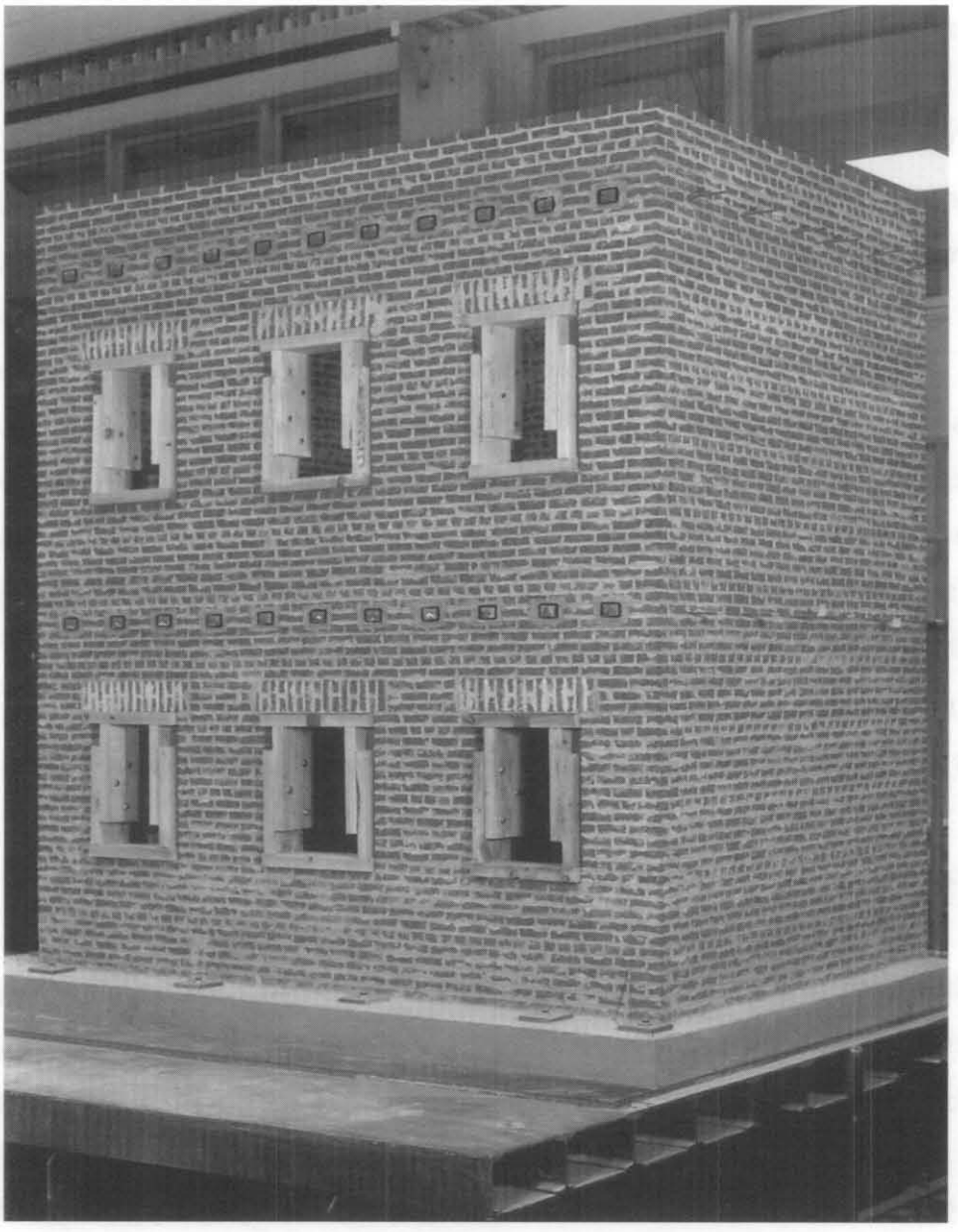

Figure 2.1 First Test Structure (S1) on the Earthquake Simulator (View of "Window-wall")

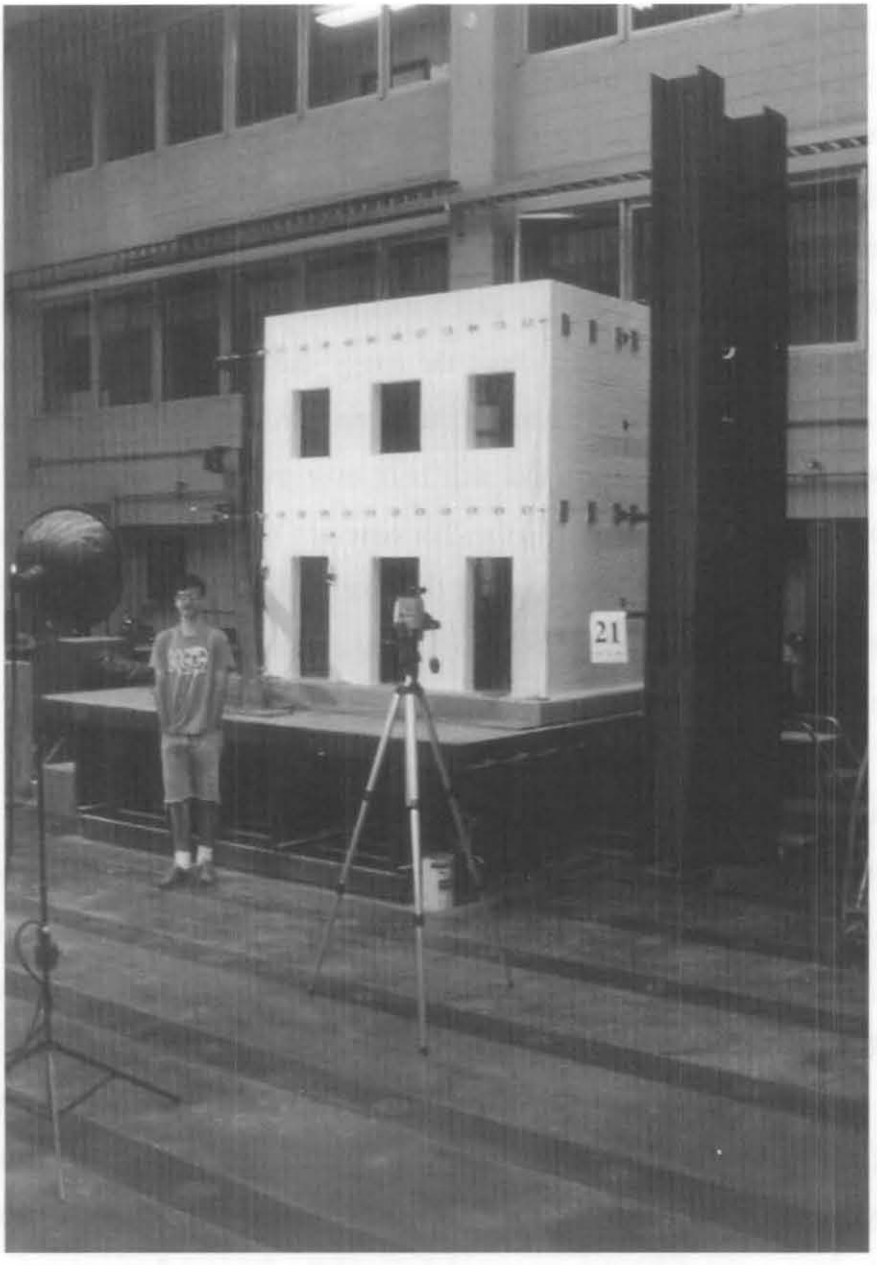

Figure 2.2 Second Test Structure (S2) on the Earthquake Simulator

2.2.1 Test Structure S1

In the first building, S1, the north shear wall, or door wall, had two equally-sized door openings in the first story and two equally-sized window openings in the second story (Figure 2.3). The door openings were labeled as such since the opening went down to the top of the footing. The south shear wall, or window wall, had three window openings on the first and second stories (Figure 2.4). The right and left windows were equal in size while the middle window was slightly larger. Both the transverse walls, east and west, were solid. All four walls measured 3.7" thick. Table 2.1 summarizes the pier sizes for S1.

Above each window and door opening was a lintel consisting of 28 bricks, 30 bricks for the middle windows (Figures 2.5a and 2.5b). The bricks in these ten lintels alternated in pairs, two horizontal and two vertical. Six courses above the lintels, the floor beams framed in, resulting in floor heights of 42.7" and 86.0" from the top of the footing. More detail about the floor systems is given in Section 2.3. A six-course parapet was built over the second-story floor beams to help solidify the floor beams in the masonry. In the plan view, the two transverse walls and the window wall were continuous, forming a C-shape, while the door wall was separated by a full-height joint the width of one mortar joint (Figure 2.6). This design resulted in shear walls both with and without flanges.

2.2.2 Test Structure S2

The second test structure, S2, was primarily based on S1 with the idea of testing different pier aspect ratios in the ground story. By effectively weakening one shear wall and strengthening the other shear wall from the design of S1, S2 could also be viewed as a rehabilitation of S1. In S2, the south shear wall, or door wall, had three door openings in the first story and three window openings in the second story (Figure 2.7). As in S1, the right and left openings were the same size with the middle opening slightly larger. The north shear wall, or window wall, had two equally-sized window openings in both stories (Figure 2.8). The two transverse walls, east and west, were again solid. The four walls of S2 also measured 3.7" thick. Table 2.2 summarizes the pier sizes for S2.

Table 2.1 Pier Sizes and Aspect Ratios for S1

Pier	Size (hxL) (Ext, Int)	Aspect Ratio (h/L) (Ext, Int)
Door 1st story	32.0"x17.3" 32.0"x27.0"	1.85:1 1.19:1
Door 2nd story	18.0"x17.3" 18.0"x27.0"	1.04:1 0.67:1
Window 1st story	18.0"x9.5" 18.0"x13.4"	1.89:1 1.34:1
Window 2nd story	18.0"x9.5" 18.0"x13.4"	1.89:1 1.34:1

Table 2.2 Pier Sizes and Aspect Ratios for S2

Pier	Size (hxL) (Ext, Int)	Aspect Ratio (h/L) (Ext, Int)
Door 1st story	32.0"x9.5" 32.0"x13.4"	3.37:1 2.39:1
Door 2nd story	18.0"x9.5" 18.0"x13.4"	1.89:1 1.34:1
Window 1st story	18.0"x17.3" 18.0"x27.0"	1.04:1 0.67:1
Window 2nd story	18.0"x17.3" 18.0"x27.0"	1.04:1 0.67:1

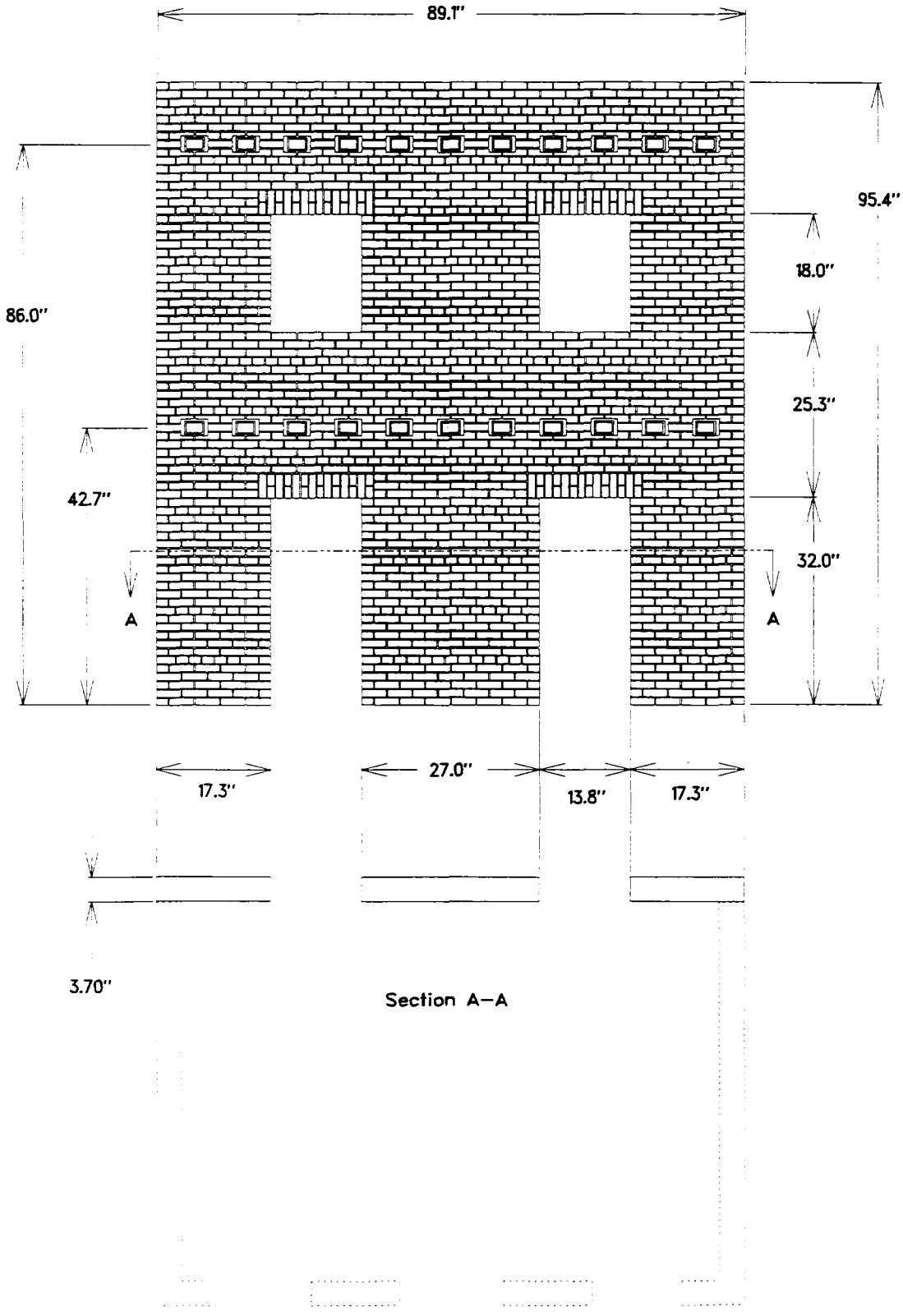

Figure 2.3 S1 Door Wall, Elevation and Plan

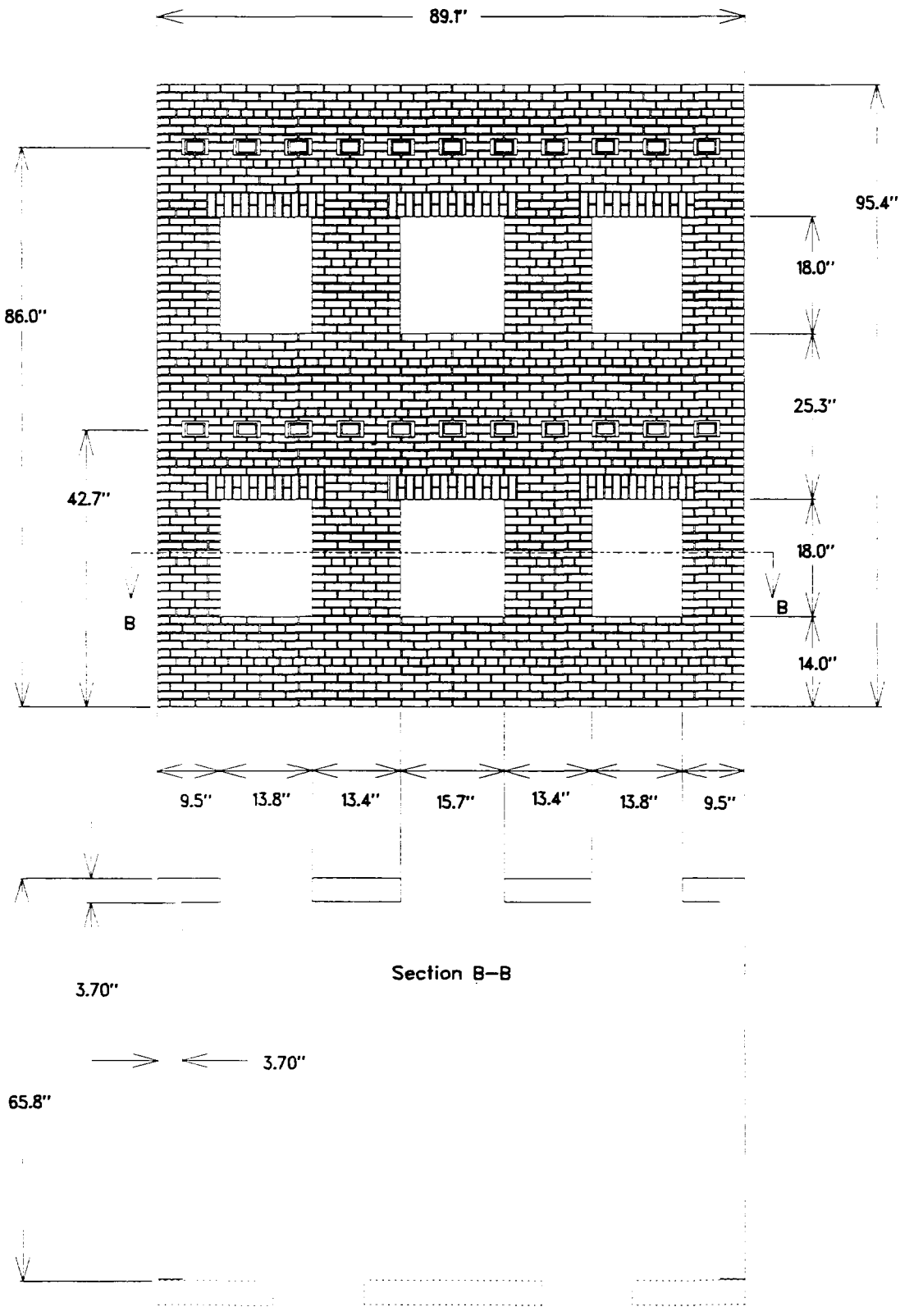

Figure 2.4 S1 Window Wall, Elevation and Plan

Figure 2.5a Typical Lintel (installed)

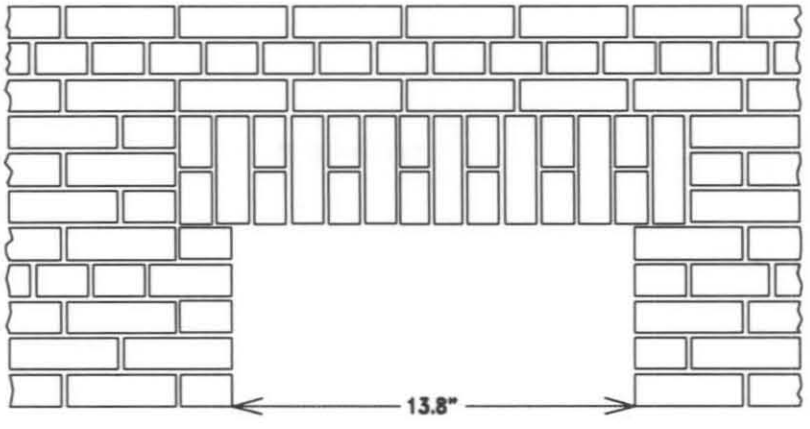

Figure2.5b Detail of Lintel Area

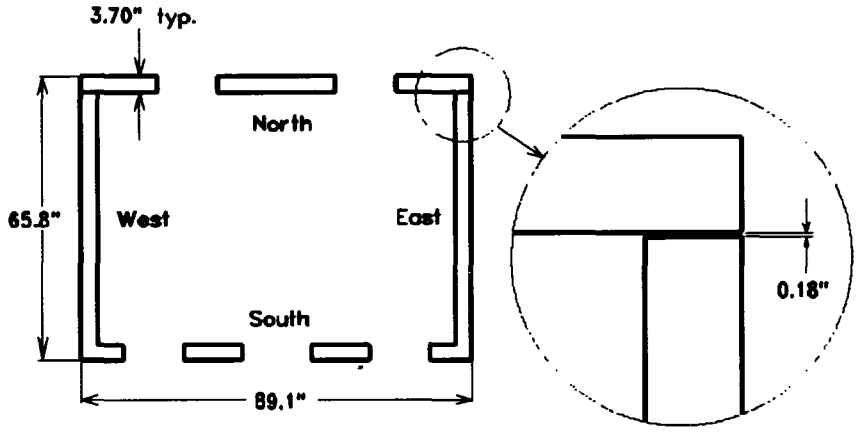

Figure2.6 Plan View of S1 and S2 Through the Openings

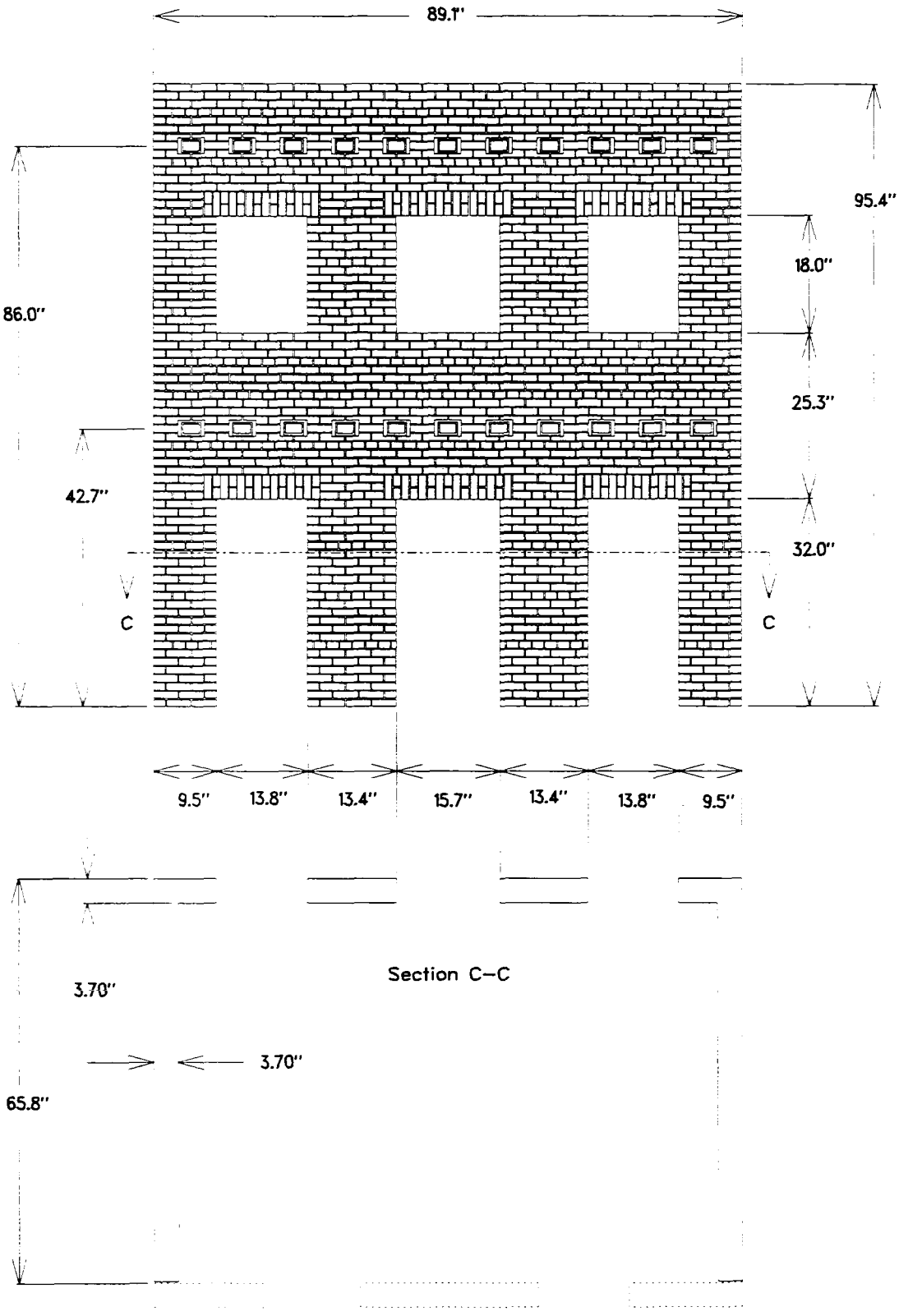

Figure 2.7 S2 Door Wall, Elevation and Plan

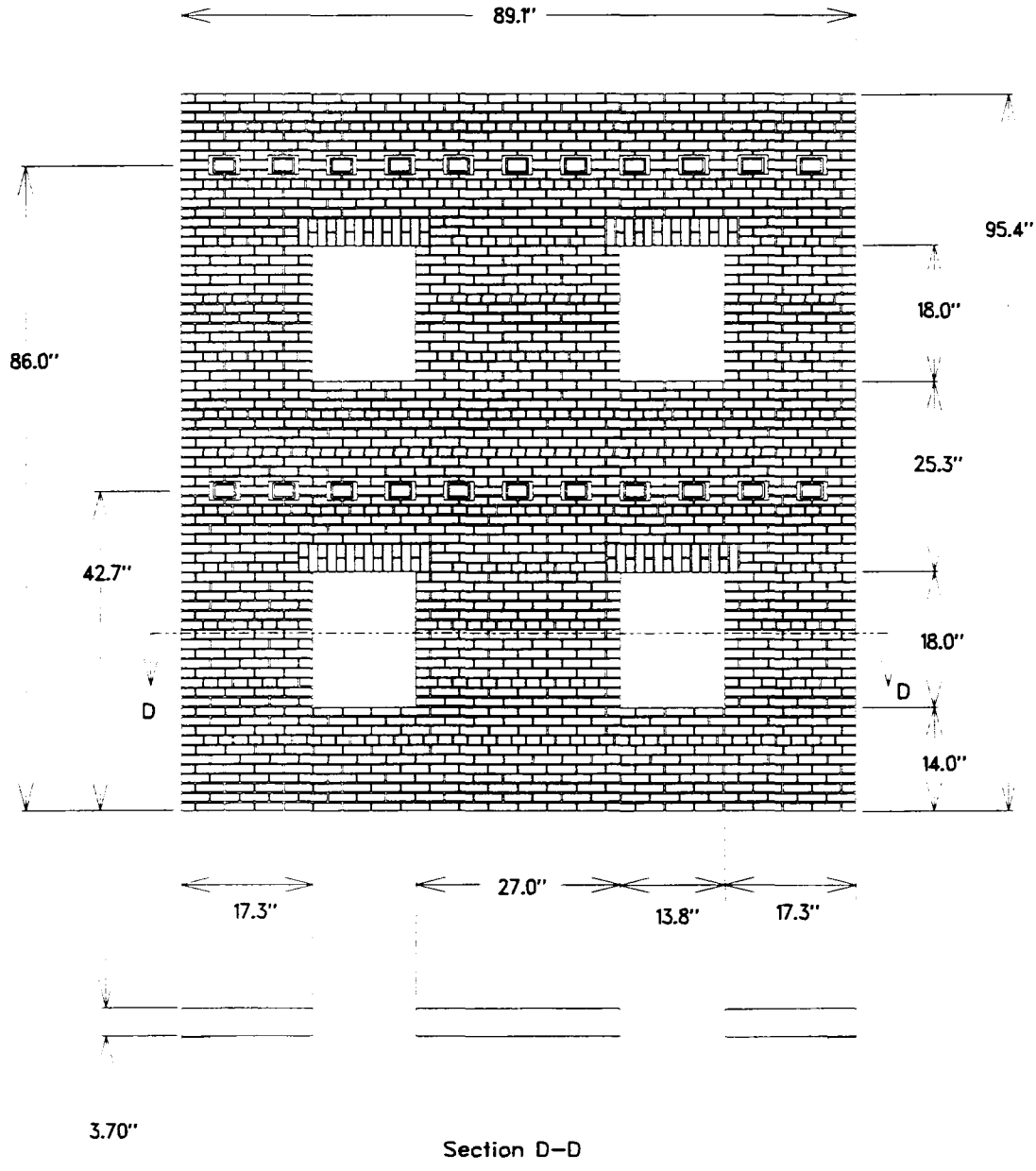

Figure 2.8 S2 Window Wall, Elevation and Plan

S2 had the same type of lintels, the same floor heights, and the same parapet sizes as S1. In plan, the two transverse walls and the door wall were continuous, forming a C-shape, while the window wall was separated by a full height joint (Figure 2.6).

2.3 Diaphragm Design

The original intent of the research program was to study the dynamic response of unreinforced brick buildings with timber floor/roof diaphragms. To facilitate the study, the isolated diaphragms should have a natural frequency well separated ($\leq {}^{1}/_{3}$) from that of the equivalent masonry structure with a rigid diaphragm. Finite element models and frame analyses confirmed simple hand calculations that the equivalent structure with rigid diaphragms had a fundamental mode near 30 Hz in the longitudinal direction (E-W), the direction of testing. A timber diaphragm flexible enough to resonate horizontally below 10 Hz and strong enough to support the 5 kips per story necessary to achieve realistic gravity stresses was difficult to design since strength demands resulted in overly large and stiff members. Furthermore, timber members do not have uniform material properties, making them hard to strain gauge and model analytically. The large timber members required also presented some construction problems. Therefore, a system using steel bars framed into the masonry with pinned ends was developed to satisfy all the design requirements. This steel diaphragm system represented similar relative flexibilities as would a longer span timber diaphragm system.

The floor/roof diaphragm system used in both S1 and S2 was partly comprised of eleven steel bars 1.75"x1.25"x65.8" spanning between the two shear/bearing walls and spaced 7.76" apart (Figures 2.9a and 2.9b). The bars were oriented with the weak axis reacting gravity loads. The estimated lateral stiffness of the system of bars was .00603 lb/in^2 for a loading applied uniformly along the beam span. Each beam end was connected inside a 3.7" long section of 2"x3"x¼" steel box section by a ¼" diameter pin that penetrated the bar and both faces of the box section (Figure 2.10). The pin was welded top and bottom to the box section. Two washers (1½"x0.05") were placed between the bottom of the beam and the bearing surface inside the box section to facilitate

Figure 2.9a Aerial View of Second-level Diaphragm (in S2)

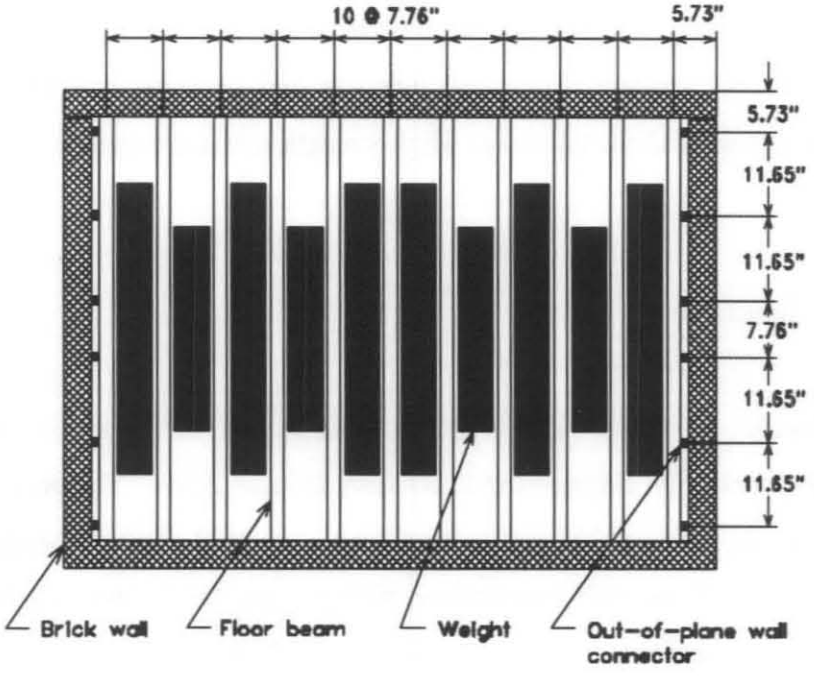

Figure2.9b Plan View of Diaphragm

end rotations of the beams. By using a set of specially cut step-shaped bricks, each box section (with the floor beams inside them) was built into the wall roughly replacing two bricks.

The other primary component of each floor system was ten steel weights, totalling 5 kips, that were hung vertically between the eleven floor beams. Of the twenty weights used, twelve were rectangular in shape (type H) and nominally weighed 525 pounds each, and eight were T-shaped (type L) and nominally weighed 455 pounds each (Figure 2.11). The weights were arranged H-L-H-L-H-H-L-H-L-H to provide a near uniform load on each beam. Each weight, made up of several steel plates welded together, had four drilled clip angles welded to two opposite faces. Each beam had four holes drilled through it for bolting the clip angles to the beams (Figure 2.12).

In addition to the floor beams being connected to the shear/bearing walls, the floor system was also tied to the transverse walls. Each end beam, the ones closest to the transverse walls, was connected to these two walls by six ¼" high-strength (H.S.) threaded rods. The end beams were tapped through horizontally and the rods were threaded in and nutted on either end (Figures 2.13a and 2.13b). The rods were positioned to line up with six mortar joints in the brick walls and extended from the inside face of the end beam to the outside face of the building. The rods were sleeved in plastic tubes inside the wall and were nutted on 3"x5"x¼" bearing plates on both faces of the wall. Split ring washers maintained tightness and hydrocal provided uniform bearing between the bearing plates and the masonry. High-strength nuts were used in all four positions per rod.

2.4 Earthquake Simulator

The earthquake simulator used in the dynamic testing of S1 and S2 (Section 2.12) is resident in the Newmark Civil Engineering Laboratory (Figure 2.14). The platform measures 12' by 12' and is supported by four, 32" high rocker arms for a total platform height of 36" (Figures 2.15 and 2.16). The platform itself is a shallow, multiple bay, box section comprised of two steel plates sandwiching steel sections. Incorporated in the platform are threaded inserts which form a

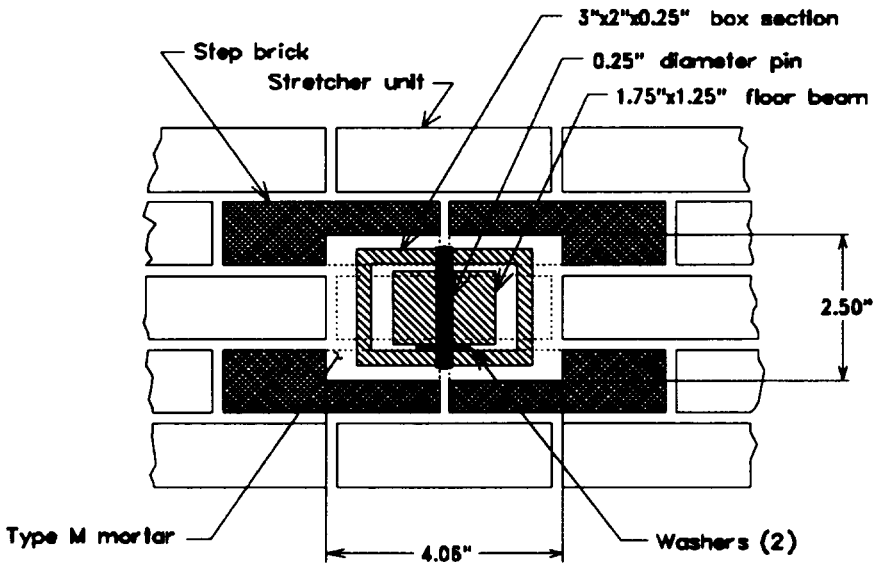

Figure2.10 Beam/In-plane Wall Connection Detail

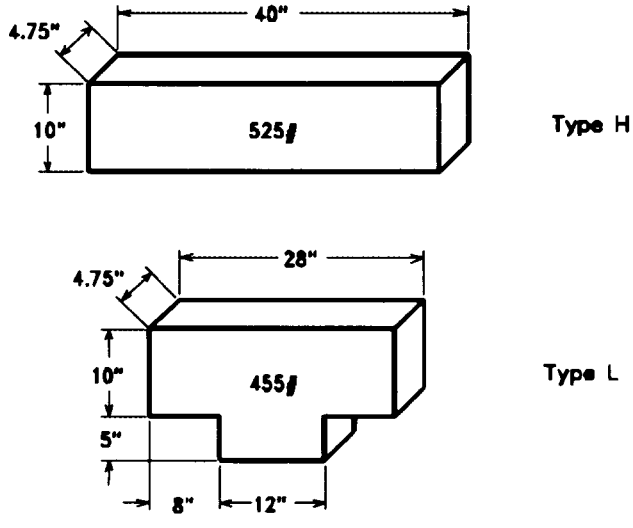

Figure2.11 Two Types of Weights Used in the Diaphragms

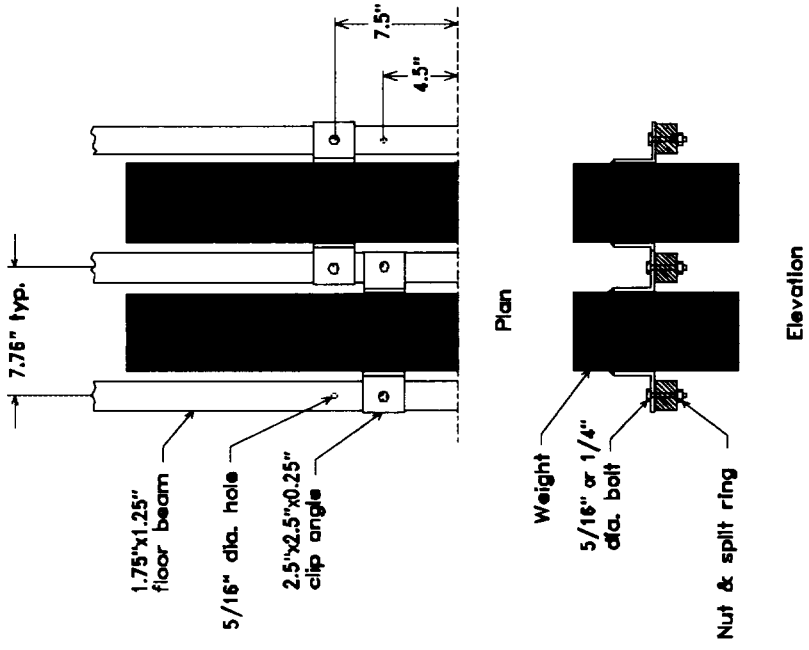

Figure2.12 Plan and Elevation Details of Weight to Floor Beam Connection

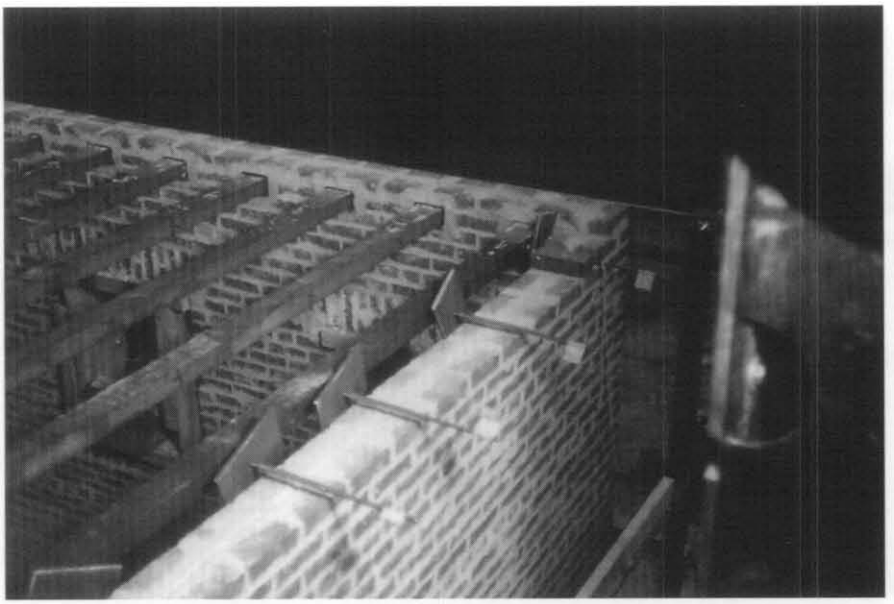

Figure 2.13a Out-of-plane Wall Connection Before Laying the Masonry

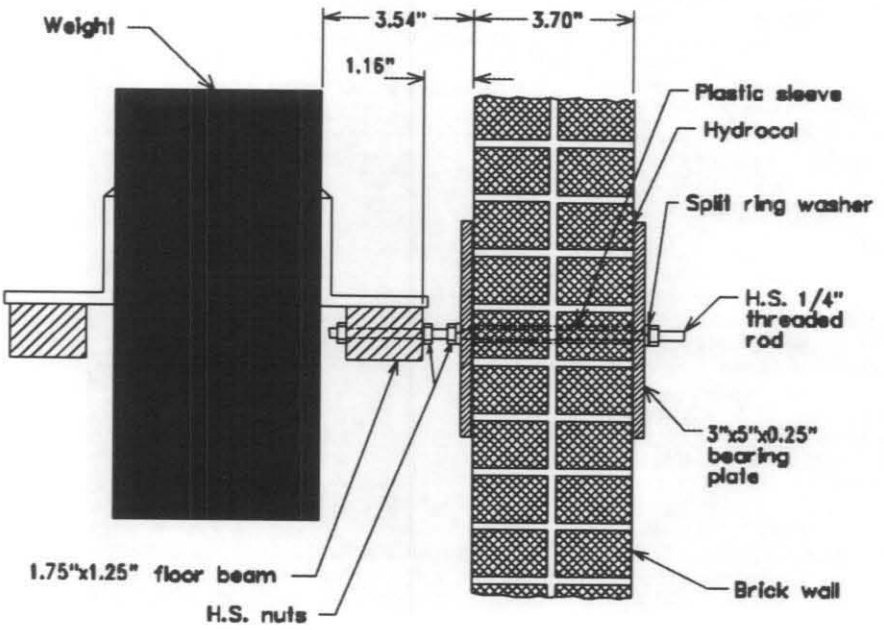

Figure2.13b Beam/Out-of-plane Wall Connection Detail

Fig 2.14 Newmark Civil Engineering Laboratoy Earthquake Simulator

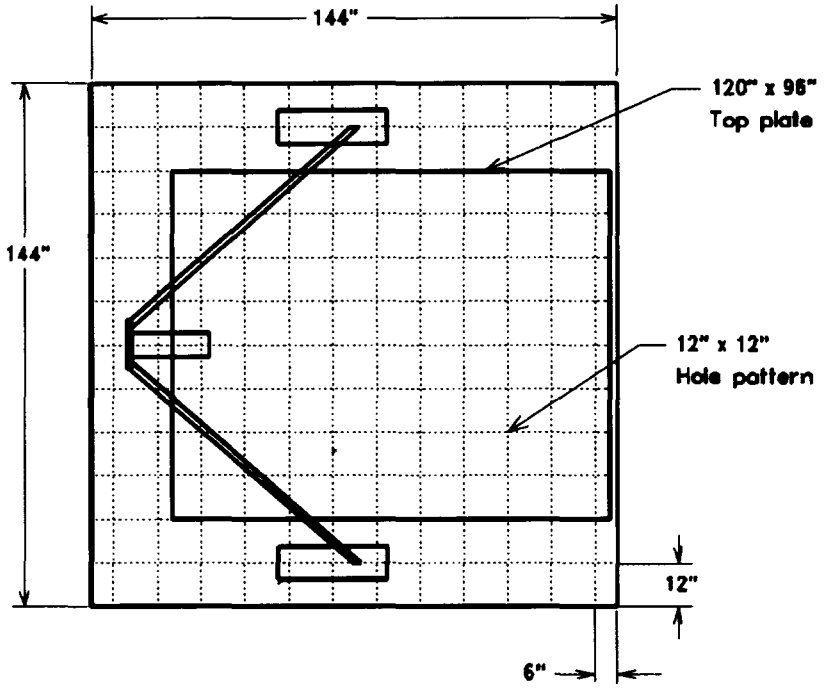

Figure2.15 Plan View of Earthquake Simulator Platform

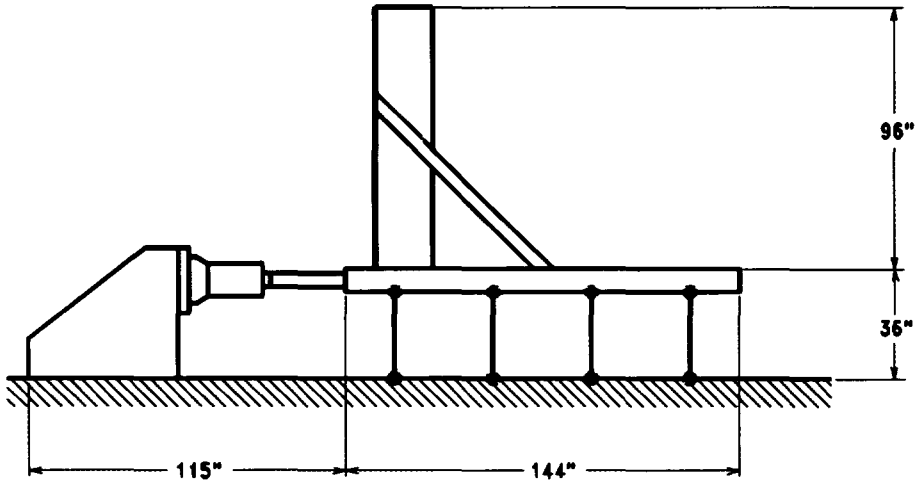

Figure2.16 Elevation of Earthquake Simulator

12" by 12" bolting pattern. An instrumentation datum is attached to one end of the simulator platform for collecting measurements relative to the platform base. Two large, steel braces support the datum against excessive movements during dynamic tests. The simulator is driven by a 75 kip hydraulic actuator supplied by two 3000 psi hydraulic pumps with a total capacity of 90 gpm. The displacement limit of the simulator is ± 2" while the velocity limit is approximately 13.5 in/sec. The simulator is controlled via MTS's Seismic Test EXecution (STEX) software which runs on a DEC Vaxstation II/GPX. A list of equipment is provided in Appendix A. More information about the Newmark Civil Engineering Laboratory earthquake simulator can be found in a paper by Sozen, et al, 1969.

2.5 Foundation Pad

A reinforced concrete foundation pad was designed and constructed on which to build S1 and S2. The pad was intended to serve two major functions: a) to interface between the earthquake simulator platform and the structures, and b) to provide a lifting element for transportation of the structures via the overhead crane. The pad formed the shape of a rectangular ring and had dimensions of 104" long by 80" wide by 5" thick. The ring was 20" wide (Figures 2.17a and 2.17b). To serve the interface requirements, the pad had 39 holes sleeved through it for bolting to the simulator platform, had four shear studs cast into its bottom face to prevent any pad motion relative to the simulator during dynamic tests, and was roughed on its top surface along the footprint of the structures to increase the bond with the base mortar joint. The pad was cast on the simulator platform to provide precise positioning of the sleeves and shear studs, which were bolted into the platform before the concrete was placed, so that the pad was custom fit to the top surface of the simulator platform. To meet strength requirements, which were to provide a four-point lift of the completed S1 or S2, heavy reinforcement was used in the pad. The longer sides of the ring had 3 #3 bars top and 3 #4 bars bottom with #3 hoops at 12" and the shorter sides of the ring had 3 #4 bars top and bottom with #3 hoops at 12". Four #4 loops positioned near the inside corners provided means for lifting.

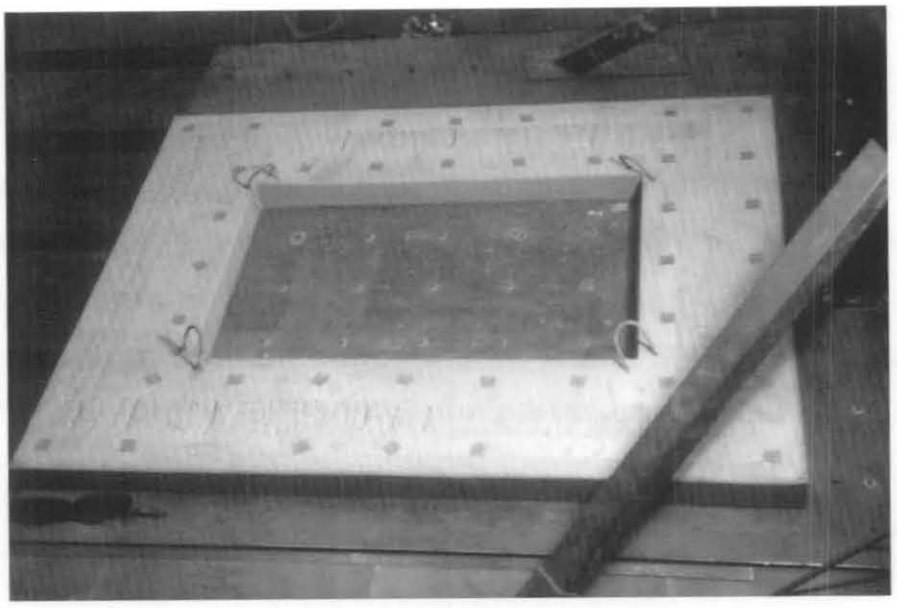

Figure 2.17a Reinforced Concrete Foundation Pad

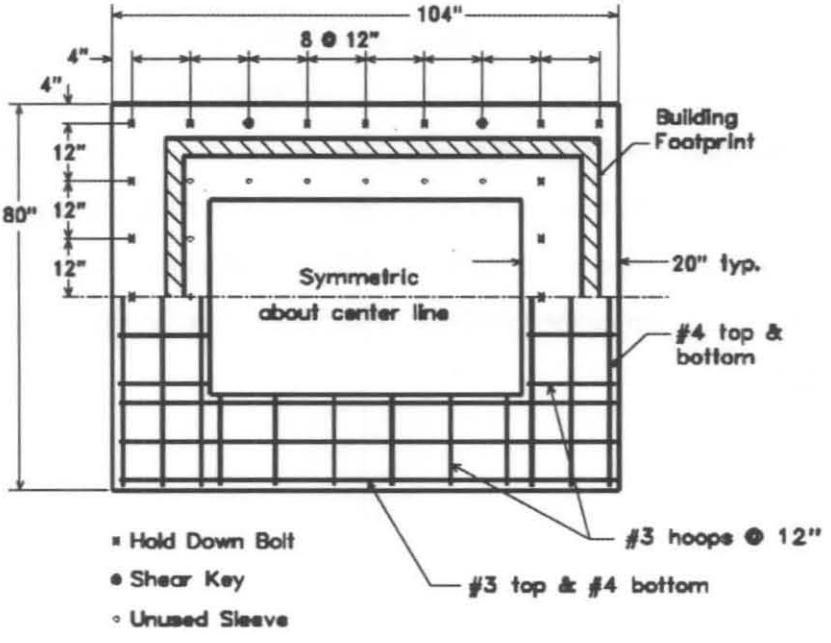

Figure2.17b Plan View of Foundation Pad Showing Hole Patterns and Reinforcement

2.6 Materials

2.6.1 Bricks

The bricks used in the two test structures were sized to be one-half scale of a standard U.S. clay masonry unit, taken as 7 5/8"x3 5/8"x2¼". This resulted in a scale brick nominally measuring 3.70"x1.76"x1.09" (Figures 2.18a and 2.18b). These scale bricks were saw cut from pavers which measured 7½"x3½"x1½", enabling four scale bricks to be produced from a single paver (Figure 2.19). Each scale brick had three sawn faces and three original faces. Other specially-shaped bricks were cut for use in the header courses and for framing in the floor beams. All the brick types used are detailed in Figure 2.20.

2.6.2 Mortar

The mortar used was Type O mortar with cement:lime:sand in 1:2:9 proportions. This weak type of mortar was representative of older construction and still produced a minimally strong structure for construction. Preliminary laboratory work done with a sand/lime mortar showed that this mortar had insufficient strength to be practical for construction. The sand that was used in the mortar was sifted to half-size particles to be consistent with the half-size bricks. Hydrated lime and Type I Portland cement made up the balance of the components. A few areas of the building required a stronger mortar, so Type M mortar made in a 4:1:14 mix of the same cement, lime and sand was also used. One of these areas was between the concrete footing and the base course. Type M mortar was also used surrounding the beam boxes (Figure 2.10). Bed and head joints were nominally 3/16", again to be consistent with the half-scale masonry. Collar joints were completely filled.

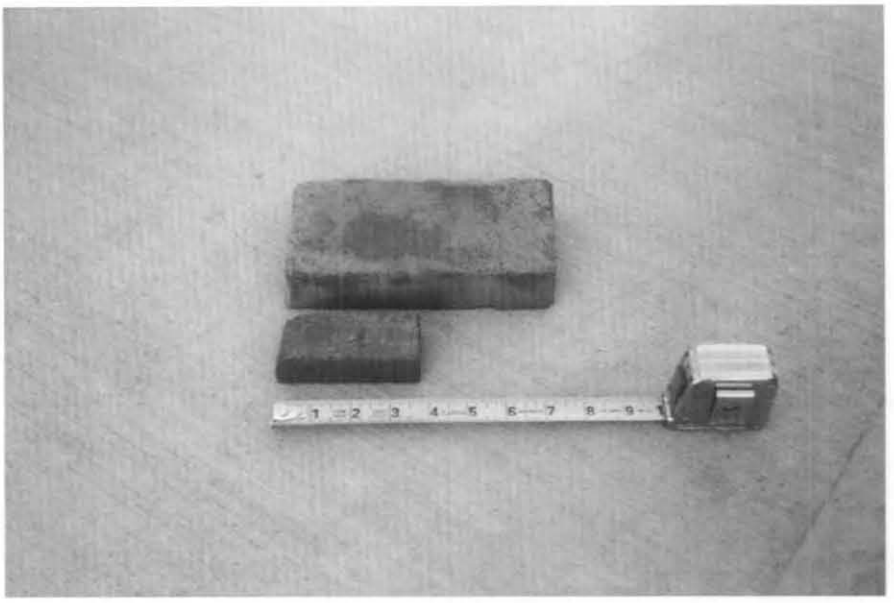

Figure 2.18a Original Paver and Reduced-Scale Clay Unit (brick)

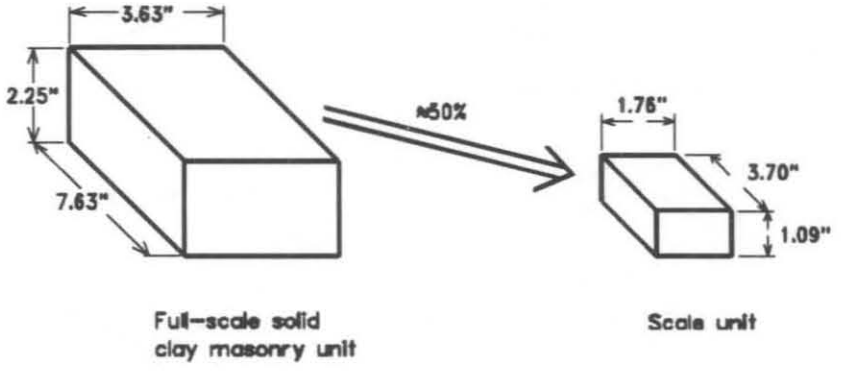

Figure 2.18b Dimensions of Full-scale and Reduced-scale Clay Masonry Unit

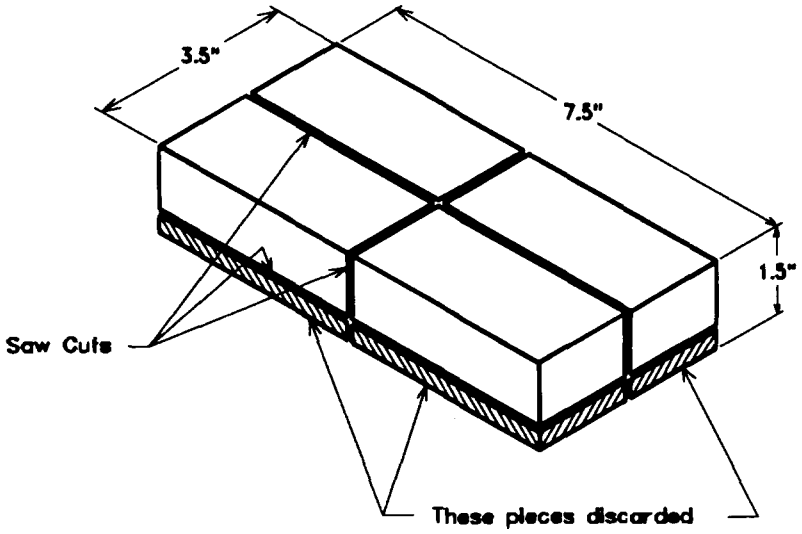

Figure 2.19 Cut Plan for Producing Reduced-scale Units from Pavers

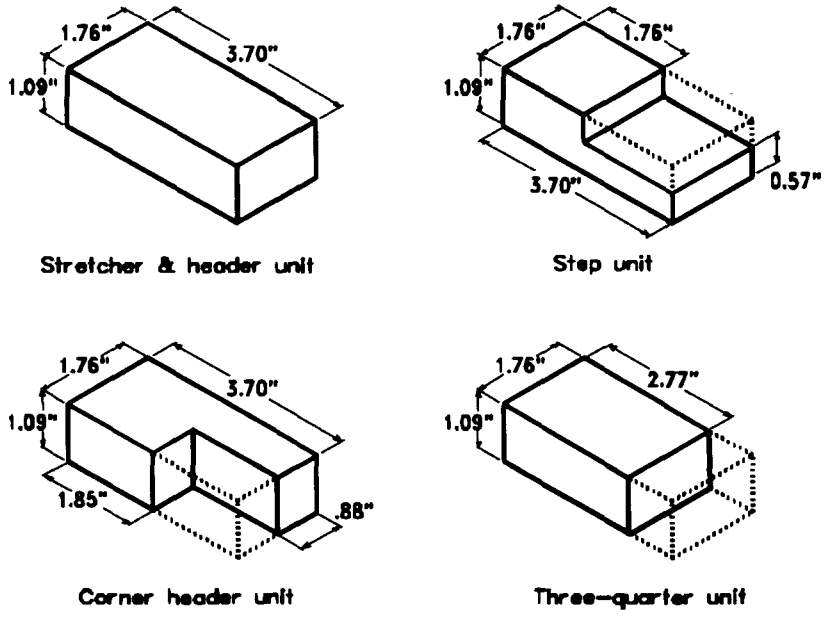

Figure 2.20 Four Brick Shapes Used in S1 and S2

2.7 Material Tests

2.7.1 Prism Tests

During construction of S1 and S2, brick prisms were constructed. These prisms consisted of five bricks stacked with four mortar (bed) joints in between (Figures 2.21a and 2.21b). After each series of dynamic tests was finished, the prisms were tested in compression to determine the strength of the masonry. Each end of the prism was coated with hydrocal to provide a uniform bearing surface. The prisms were then compressed until failure, with the highest load resisted recorded. The failure mode for the prisms was typical compression splitting of the masonry units. This load was divided by the plan area of the prism to determine the strength. The average compressive strength of 38 prisms from both S1 and S2 was 1960 psi with a coefficient of variation (COV) of 0.15.

An attempt was made during one set of prism tests to measure the elastic modulus of the masonry prism. Size constraints made instrumenting the prism difficult and the modulus measurement attempt was unsuccessful. The UBC (commentary to Chapter 21, 1995) recommendation for the elastic modulus of masonry is 750 times the prism compressive strength. Early prism tests indicated a compressive strength of 1900 psi, so a value of 1425 ksi (750*1900 psi) was used for the elastic modulus of masonry throughout the study.

2.7.2 Brick Compression Tests

Bricks collected from the two buildings during demolition were also tested for their compressive strength. Six undamaged bricks from each building were subjected to flatwise compression. The peak compressive force was divided the plan area of the brick to give the brick compressive strengths. The average compressive strength for eleven bricks was 6730 psi with a COV of 0.22. One brick (from S1) failed prematurely as a corner crushed and was excluded from the average. The ratio of the unit strength to the prism strength was typical of full scale construction.

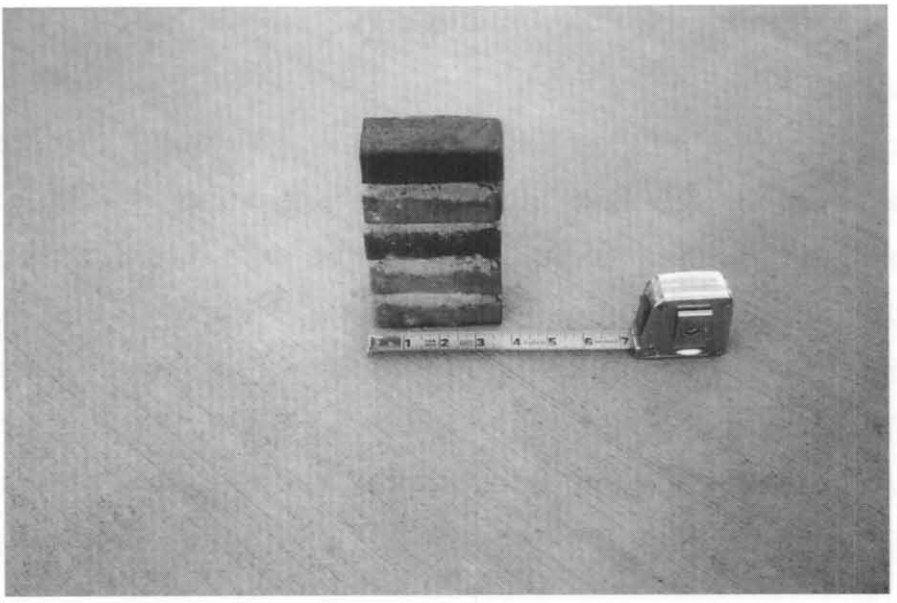

Figure 2.21a Typical Prism Constructed from Reduced-scale Bricks

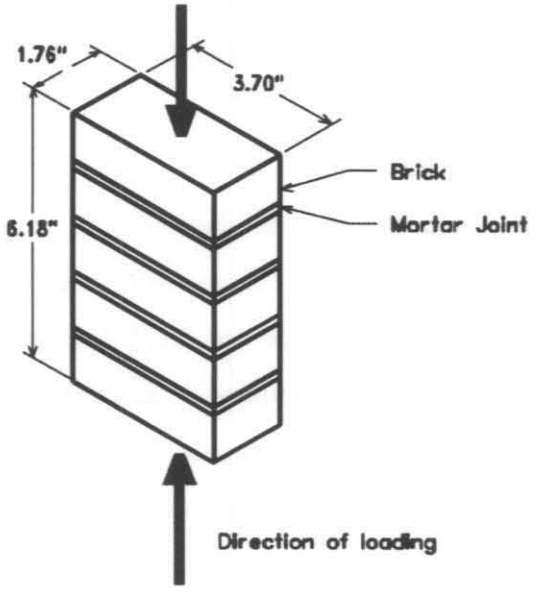

Figure 2.21b Direction of Loading for Prism Tests

2.7.3 Diagonal Compression Tests

Prior to construction of S1, tests were performed to help determine which type of mortar to use. One of these tests was the diagonal compression test, in which a square masonry panel is loaded in compression between two opposite corners (Figures 2.22a and 2.22b). This type of test provides a measure of the shear strength of the masonry. The panels were two foot square and were single wythe. Although the diagonal compression test is normally performed with the panels oriented vertically, the panels tested were resting on a horizontal surface. This was due to the fragility of an unreinforced masonry panel 24" high and only 1.7" thick. The peak load was recorded and divided by the product of the length of the diagonal and the thickness of the panel. For the three panels tested, the average strength was 46.5 psi with a COV of 0.15.

2.7.4 Flexural Tension Tests

Another material test conducted to provide information on which mortar to use was the flexural tension test. This test consisted of a horizontal masonry beam, simply supported, loaded vertically by a two point load application system (Figures 2.23a and 2.23b). The load was gradually increased until the beam failed. The beams consisted of twenty bricks and formed a column ten brick thicknesses high and two brick widths wide before they were rotated to the horizontal test position. The tensile stress reported, F_t, is calculated using Equation 2.1,

$$F_t = (P + 0.75 P_s) L / b d^2 \tag{2.1}$$

where P is the applied load, P_s is the weight of the beam, L is the distance between supports, and b and d are the width and depth of the beam, respectively. The average of three tests gave F_t as 40.6 psi with a COV of 0.09.

2.7.5 Initial Rate of Absorption Tests

The initial rate of absorption (IRA) test determines how much water a brick absorbs over a one minute period in a shallow (0.125") water bath. The weight of the water absorbed, in grams, is normalized by multiplying by $30in^2/A_{brick}$ for comparison between bricks of different sizes. If a

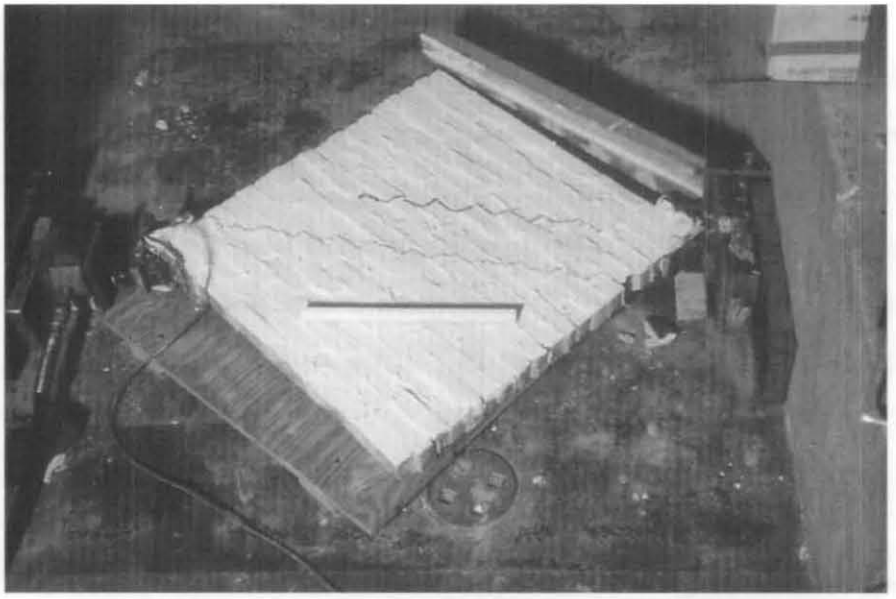

Figure 2.22a Diagonal Compression Test

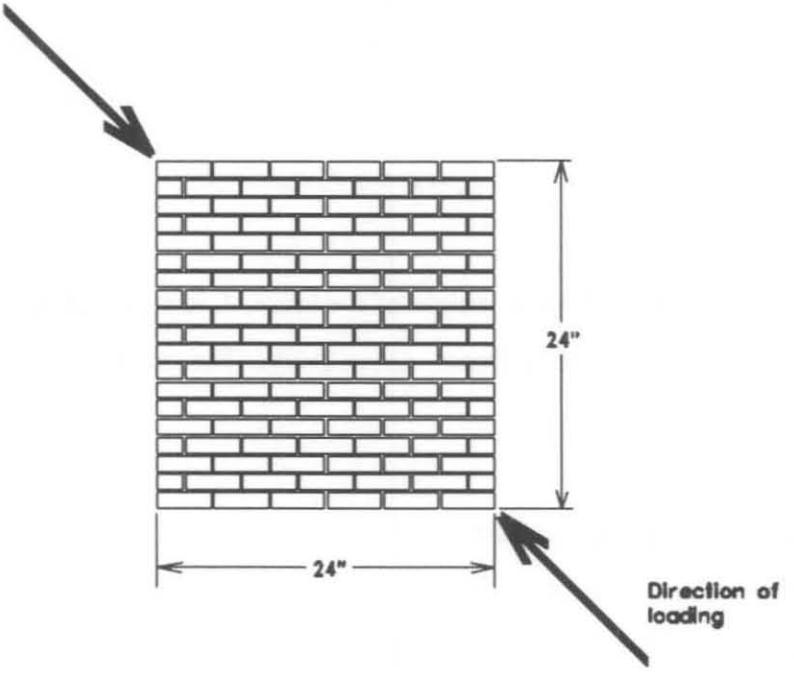

Figure 2.22b Direction of Loading for Diagonal Compression Tests

Figure 2.23a Flexural Tension Test Showing Mode of Failure

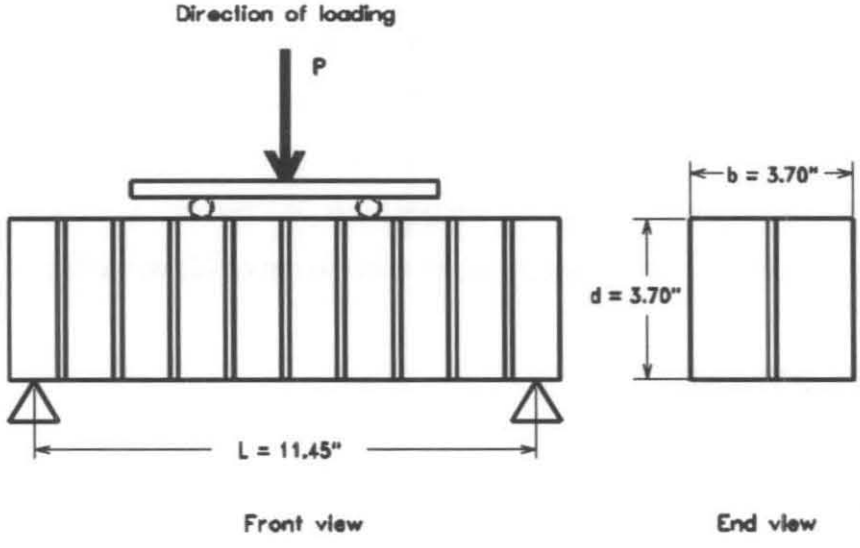

Figure 2.23b Direction of Loading for Flexural Tension Tests

brick's normalized IRA is too high, usually 30g/minute is considered the limit, poor bond with the mortar may occur, unless prewetting of the bricks is practiced. Before construction of S1 and S2 commenced, the IRA test was performed on four of the reduced-scale bricks. The average normalized IRA was 32.8g with a COV of 0.10.

2.7.6 In-Place Shear Tests

The last material test performed, this one after the dynamic testing of S1 and again after S2, was the in-place shear test, or shove test. This test usually requires the removal of a single brick and a head joint one brick away on the same course (Figure 2.24a). A loading device is placed in the cavity and the brick between the cavity and the missing head joint is forced towards the missing head joint until slip is achieved. The load at first movement of the test brick is divided by the surface area of both bed joints to produce a shear strength. The sum of the gravity stresses at the point of the test brick is subtracted from this shear strength to produce the reported test value. Due to the size of the bricks used in S1 and S2, removal of more than a single brick was necessary in order to insert the loading device, a small hydraulic piston. (Figures 2.24b and 2.24c). Although the shove test is normally a non-destructive test, the removal of the extra bricks tended to make these shove tests moderately destructive. This was the reason that the tests were performed after the dynamic testing was concluded on each structure. Vertical stress concentrations around the test brick resulting from the removal of 2-3 adjacent bricks likely led to strengths higher than those that would have been recorded had only one brick been removed. Regardless, the average shear strength of 12 tests, adjusted for vertical stresses, was 361 psi with a COV of 0.20. The shear strength value exceeded by eighty percent of the tests (10 out of 12) was 299 psi.

2.8 Construction Procedures

2.8.1 Bricks

As was mentioned in Section 2.6.1, the bricks used in S1 and S2 were cut from pavers. A jig was developed for use on a stationary wet brick saw that enabled the scale bricks to be produced

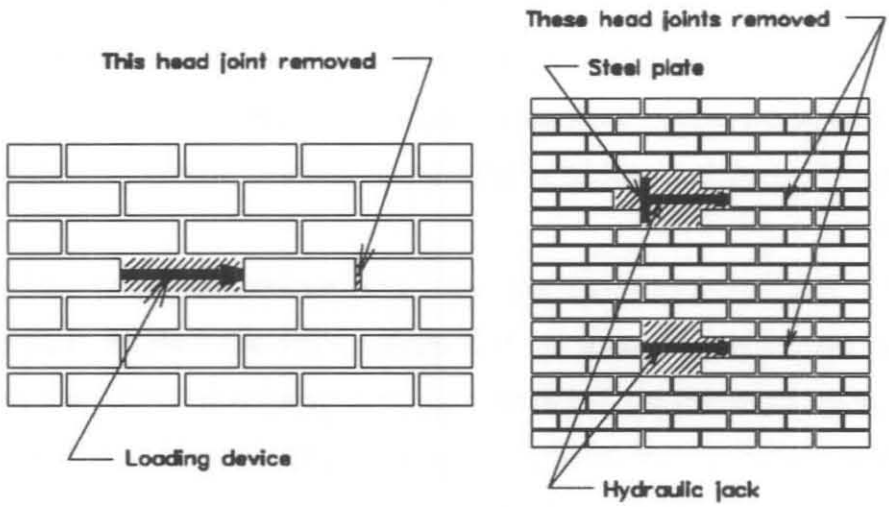

Figures 2.24 (a) Detail of Full-scale Shove Test; and (b) Detail of Reduced-scale Shove Tests

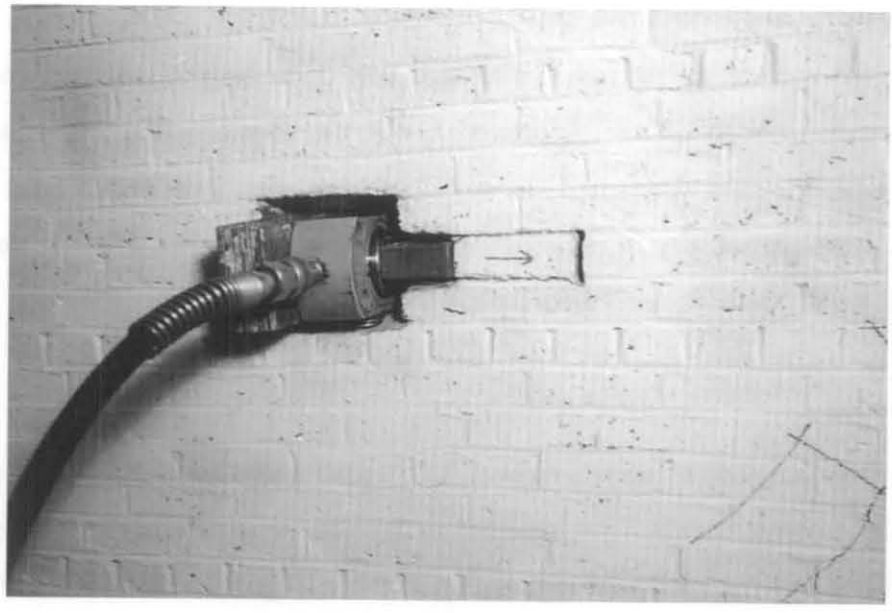

Figure 2.24c Typical Reduced-scale Shove Test

(all three cuts) without any adjustments. The jig had three movable stops that were set for length, width and thickness of the scale bricks. The paver was first crosscut to produce the 3.70" length and the two halves were then split lengthwise for the 1.76" width. The four quarters were then sliced to the 1.09" thickness, removing the uneven bottom face of the paver (Figure 2.19). Four bricks could thus be cut from a single paver, with seven passes of the saw, in almost an assembly line procedure. Nevertheless, at least an hour was required to produce 100 bricks once the setup was complete.

Prior to use, the bricks were soaked and lightly scrubbed to remove sand and residue from sawing. The fairly high IRA value of 32.8 g/min., combined with the relatively dry working environment of the structures lab, led to the practice of dunking the bricks in a pail of water prior to laying them in the walls. Furthermore, the individual attention paid to the bricks during the light scrubbing enabled for the rejection of bricks that had chips, cracks, or were improperly sized or shaped.

2.8.2 Sand

The sand used in the mortar was sifted, primarily from mason sand, to roughly half-size particles. As such, all particles had to pass through a #30 screen (600μ), although a #16 screen (1190μ) was also used as a first pass. The sand was dried both in a drying room and in the structures lab itself prior to sifting. Approximately five gallons of sifted sand could be produced per hour. Once the sand was sifted, it was combined with lime and cement in the proper proportions and was mixed dry in roughly five-gallon quantities. The dry mix was combined in smaller amounts with water as needed during the brick laying.

2.8.3 String Line

A specially designed string line rig was put together to enable bricklayers to lay each course straight and at the correct height. The cage had four vertical legs, graduated for the tops of the 75 courses, and eight horizontal straps tieing the legs together (Figure 2.25). The assembled cage was clamped to a rigid column for lateral stability and levelled using a surveyors level. Wooden blocks

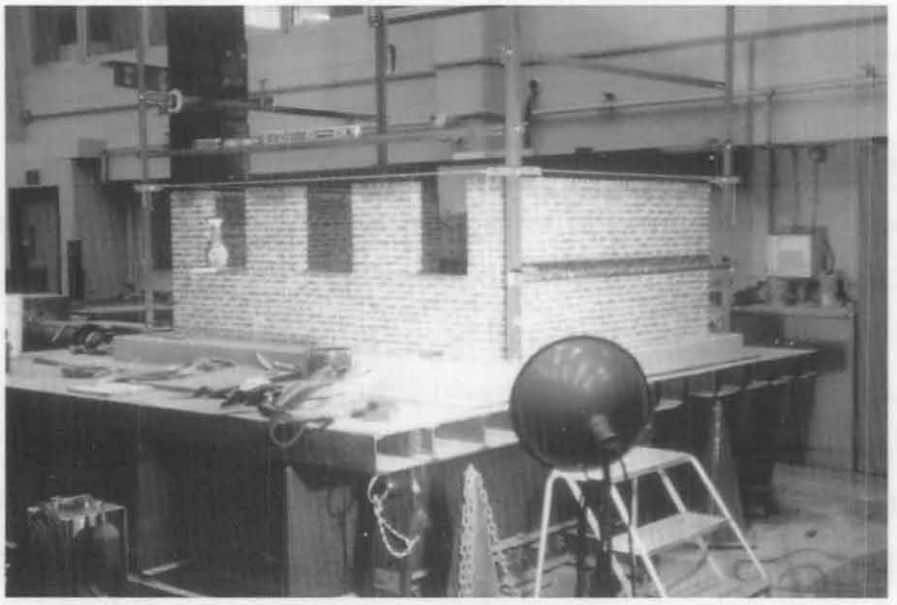

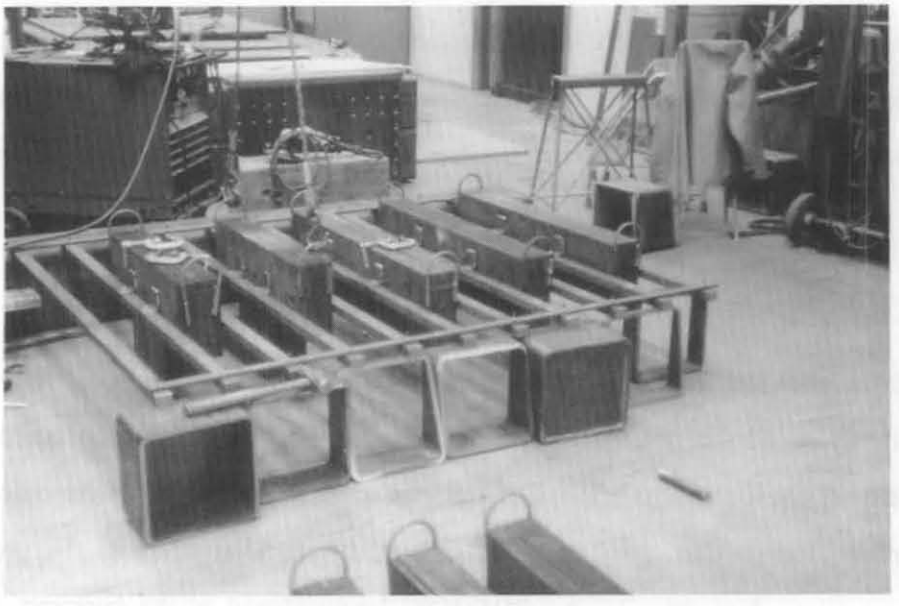

Figure 2.26 Prefabrication of One of the Diaphragms

held the string lines and slid up the legs to the various graduations. The wooden blocks were designed to provide horizontal adjustability of the string line, resulting in more variability in positioning the cage legs.

2.8.4 Test Structure S1

Once materials were prepared and the line cage was assembled, the brick laying proceeded in an orderly fashion at an average rate of one course per day. The first story of S1 was built with bricklayers working from inside the confines of the walls. Starting at one corner, one bricklayer would lay the outer wythe, working his way around the building, while another bricklayer would follow and lay the inner wythe. Two-wythe American bond was laid, with one header course after every five stretcher courses. This bond pattern continued through the piers and floor levels to the top course. The bricks were laid so that the cut faces would be exposed on the stretcher courses and the cut ends would be exposed on the header courses. After a day's work was completed, the bed and head joints were struck with a circular strike.

The second story of S1 was started in a manner similar to the first, with bricklayers working around the building, except that they worked from the outside of the walls. By this time, scaffolding was required. Near the end of constructing S1, the order of brick laying was altered slightly to increase efficiency and safety while working on the higher scaffolding levels. At this point, rather than work on one course per day, bricklayers worked on one wall per day, thus reducing the time spent climbing up and down the scaffolding and transporting materials around the building.

2.8.5 Lintels

Construction and installation of the lintels over the window and door openings were performed differently from the normal daily bricklaying. The lintels were premade vertically much like the flexural-tension beams. Pairs of bricks were laid on top of one another, this time alternating the orientation so that every pair was crossed by its adjacent pairs (Figures 2.5a and 2.5b). They were allowed to dry (2-3 weeks) before being placed in the building. Adjustable

formwork was made out of wooden 2x6s to support the lintels vertically while the surrounding masonry cured. Each lintel occupied the equivalent of three courses over the openings and was recessed into each pier half a brick length. The recessed piers were built up to two of the three courses before the lintels were inserted. The lintels were placed into fresh mortar on the pier tops and carefully pressed down to the top of the wooden formwork which was adjusted to the proper height for that opening. After placing the lintels, the third recessed course, equally the top of lintels, was immediately laid between the lintels to provide closure for the lintels.

2.8.6 Floor Beams

Installation of the floor system provided another break in the regular bricklaying. The courses on which the floor system rested, 33 and 67 from the bottom, were laid (door and window walls) using the step bricks. The entire floor system, beams and weights, was previously fabricated away from the building and then disassembled (Figure 2.26). The eleven beam/box assemblies were reconnected using a pair of template bars with holes at the proper beam spacing (7.76"). The beam/box/template assembly was then placed into the building as a single unit, using the overhead crane, to ensure the correct beam spacing. The boxes were set in Type M mortar on the lower portion of the step bricks. The next course, 34 or 68, was immediately laid between the beam boxes to provide support for the boxes. The closing course of the upside-down step bricks was laid later.

2.8.7 Floor Weights

Once several courses had been laid above the floor beam courses, and roughly a month had passed since placing the floor beams, the floor weights were installed. The weights, like the beam assemblies, were put in with the aid of the overhead crane. Each weight was lifted into a position over its place between the beams and four bolts were inserted through the clip angles. The weight was then lowered, guiding the four bolts through the four holes in the beams. The original design of the floor system called for ¼" diameter bolts to connect the clip angles to the floor beams, both angles and beams being drilled $^{5}/_{16}$" diameter, to guarantee that all the weights would be able to be

hung. S1 was initially constructed using this design. Since placing the eleven beams as a unit into the building provided a more accurate positioning of the beams than had been expected, prior to testing S1 approximately half of the ¼" diameter bolts on both floors were replaced with $^5/_{16}$" diameter bolts. When installing the weights in S2, *all* the bolts used to hang the weights were $^5/_{16}$" diameter, although the last one or two per floor required hammering. Another slight difference between S1 and S2 regarding the bolting of the clip angles to the beams concerns the tightness of the nuts. For S1, the nuts were fastened finger tight while for S2, the nuts were cinched tight with a wrench.

2.8.8 Test Structure S2

The construction of S2 proceeded in a slightly different fashion than that of S1. Whereas S1 was built from new masonry from the foundation up, S2 reused a significant portion of S1. After testing was completed on S1, the building was sawn along the mortar joint between the 36th and 37th course with a portable masonry saw. Prior to sawing, steel brackets were installed to connect the two transverse walls to the detached door wall. Once the brackets were attached, wedges were driven into the gaps between the door wall and the transverse walls to minimize relative movement of the walls. The undamaged second story was strapped through its window openings and was carefully lifted off and placed aside using the overhead crane. Two new courses were laid on top of the same reinforced concrete footing used under S1. The salvaged S1 second story was set down in a fresh mortar bed (on the two new courses) to become the new first story of S2. The new second story was then built from this point (Figure 2.27) utilizing the one wall per day method of bricklaying described in Section 2.8.4. The three window openings from the second story of S1 were later sawn into door openings using a portable masonry saw. Steel guides were clamped to the piers aligned with the window openings to provide for a straight, vertical cut. Since the saw could not cut down all the way through the first course, a hammer and chisel were used to remove the remaining masonry in the new door openings.

2.9 Instrumentation

A total of 39 channels of accelerometers, linear variable displacement transducers (LVDTs), and strain gauges were collected during the dynamic testing of S1 and S2. The instrumentation plan was designed to record a thorough description of the buildings' behavior, with an emphasis on the response of the two diaphragms. An overview of the instrumentation wiring is shown in Figure 2.28 while details regarding the three different types of instruments used are outlined in Sections 2.9.1, 2.9.2, and 2.9.3. A thorough list of equipment is given in Appendix A.

2.9.1 Accelerometers

Eighteen Endevco piezoresistive accelerometers ($\pm$25g) and one Kulite accelerometer ($\pm$10g) were used during the dynamic testing of S1. The Kulite accelerometer is a reference, or feedback, accelerometer mounted to the earthquake simulator while the eighteen Endevcos were attached to S1. The Endevco accelerometers were calibrated to a range of $\pm$2½g, resulting in an initial resolution of 0.0012g. During the later tests, some of the ranges were increased to prevent clipping. The accelerometers were positioned to record motions not only in the direction of testing, but also in the vertical direction and the plan direction perpendicular to the direction of testing. Table 2.3 summarizes the accelerometer locations and their sign conventions while Figure 2.29 illustrates their locations. The same accelerometers and locations were also used for the dynamic testing of S2, with two exceptions, channel 1 was used to record the acceleration of an LVDT support arm and channel 4 was not used. During the free vibration testing of S1 and S2, only ten accelerations were recorded, those from channels 2, 3, 5, 6, 7, 8, 13, 14, 16, and 17.

The accelerometers were attached to the various parts of the building using small, 1" cubes of aluminum (Figure 2.30). These blocks were machined orthogonal and had tapped holes in several faces. Each accelerometer also had a tapped hole in its base which allowed it to be firmly attached to the cube using a short piece of threaded rod. The cubes were epoxied to the walls, beams, or weights and the accelerometers were screwed in after the epoxy cured.

Table 2.3 Accelerometer Locations and Sign Conventions

Accelerometer No.	Location	Direction of Positive Acceleration
1*	Base of door wall	East
2	1st level door wall	East
3	2nd level door wall	East
4*	Base of window wall	East
5	1st level window wall	East
6	2nd level window wall	East
7	Mid 1st story west wall	East
8	Mid 2nd story west wall	East
9	1st level window wall west	North
10	2nd level window wall west	North
11	1st level window wall east	North
12	2nd level window wall east	North
13	1st level diaphragm beam #4	East
14	1st level diaphragm weight #3	East
15	1st level diaphragm beam #4	Down
16	2nd level diaphragm beam #4	East
17	2nd level diaphragm weight #3	East
18	EQ simulator platform	Down
19	EQ simulator platform	West

*S1 only.

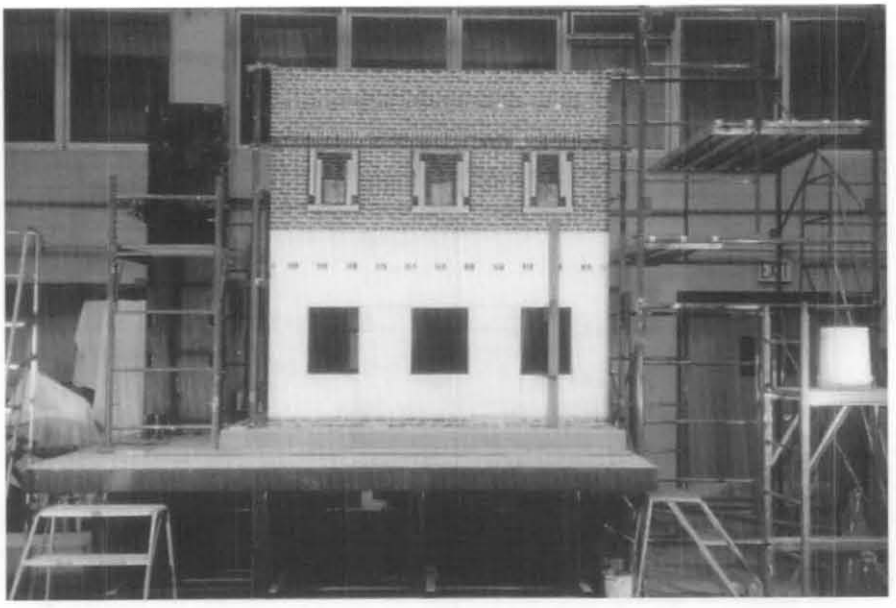

Figure 2.27 S2 Under Construction.

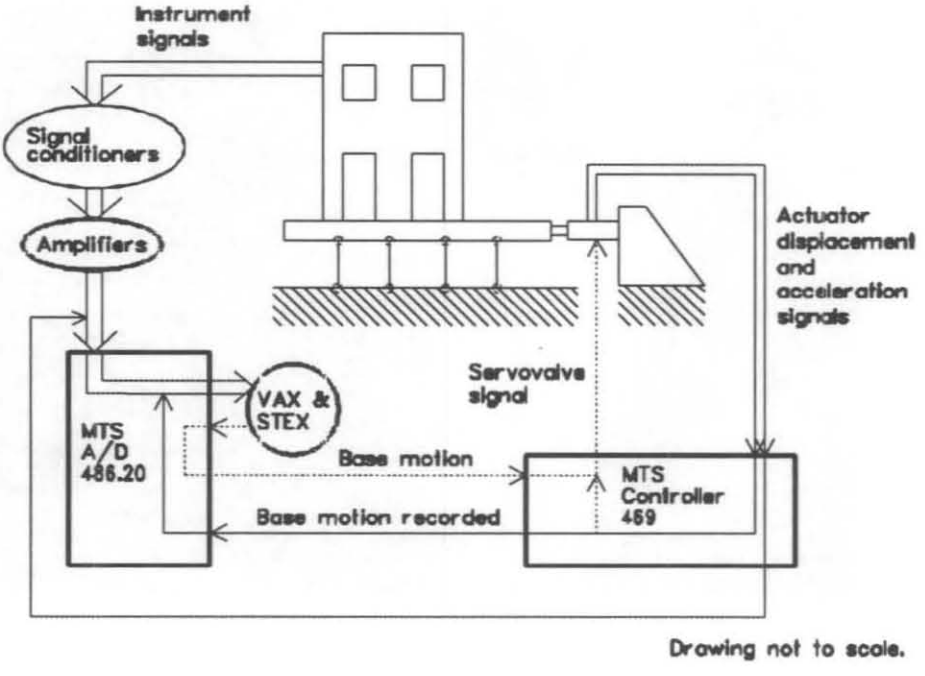

Figure 2.28 Wiring Diagram of the Experimental Setup

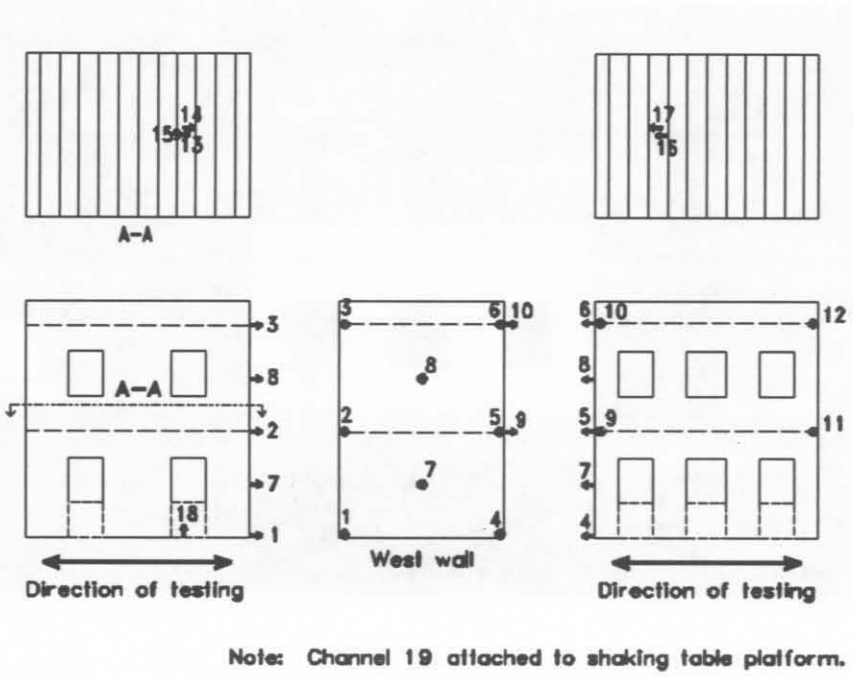

Figure 2.29 Location of Accelerometers on S1 and S2

Figure 2.30 Close-up of a Mounted Accelerometer

Each accelerometer signal needed to be conditioned and amplified before being sent to the analog/digital (A/D) converter. The eighteen Endevco accelerometers were wired to eighteen Vidar signal conditioners and eighteen Dana amplifiers which in turn were wired to the MTS A/D converters. The signal from the Kulite accelerometer is directly connected into the MTS controller where it is conditioned and amplified before being sent to the A/D converter.

2.9.2 LVDTs

A total of fifteen LVDTs were used during the dynamic testing of S1 and S2. One LVDT was built into the hydraulic actuator that drove the earthquake simulator. Twelve others were positioned around S1 and S2 to record motions in the direction of testing while two additional LVDTs were added for the testing of S2 to measure vertical displacements across cracks. The eight Schaevitz LVDTs on the west transverse wall measured relative deflection via a reference column bolted to the earthquake simulator. These 2" LVDTs were calibrated to $\pm$2" resulting in a resolution of 0.0010" for S1 and were calibrated to $\pm$1" with a resolution of 0.0005" for S2. The four Collins 5" LVDTs used on the east transverse wall measured absolute deflection and were calibrated to $\pm$4" with a 0.0020" resolution for S1 and $\pm$1" with a 0.0005" resolution for S2. Finally, the two ½" Schaevitz LVDTs used for vertical displacements on the door wall of S2 were calibrated to $\pm$½" resulting in a resolution of 0.0002". Table 2.4 summarizes the locations, ranges, and sign conventions of the LVDTs while Figure 2.31 illustrates their locations.

Mounting the LVDTs required considerably more hardware than was required to mount the accelerometers (Figure 2.32). Two vertical reference datums, one fixed to the earthquake simulator platform (moving) and one fixed to the laboratory floor (fixed) were used. The moving datum required diagonal bracing to stiffen it. The two datums each had four horizontal arms fastened to them for positioning of the LVDTs. The LVDT cores were attached to the building using small metal plates with circular mounting holes normal to the plate. The plates were epoxied to the masonry walls and the cores were fastened via a locking screw. LVDTs 5, 6, 7, and 8 required the use of offset cores due to the fact that the moving datum was on line with the axis of the building. Special blocks held the LVDT bodies to the horizontal arms. During the testing of

Table 2.4 LVDT Locations, Ranges, and Sign Conventions

LVDT No.	Location	Range S1, S2 (in.)	Positive Deflection
1	1st level door wall	2", 1"	East
2	2nd level door wall	2", 1"	East
3	1st level window wall	2", 1"	East
4	2nd level window wall	2", 1"	East
5	Mid 1st story west wall	2", 1"	East
6	1st level west wall	2", 1"	East
7	Mid 2nd story west wall	2", 1"	East
8	2nd level west wall	2", 1"	East
9	Mid 1st story east wall	4", 1"	East
10	1st level east wall	4", 1"	East
11	Mid 2nd story east wall	4", 1"	East
12	2nd level east wall	4", 1"	East
13*	1st story door wall west pier	½"	Crack closing
14*	1st story door wall west central pier	½"	Crack closing
15	Actuator	2"	East

*S2 only.

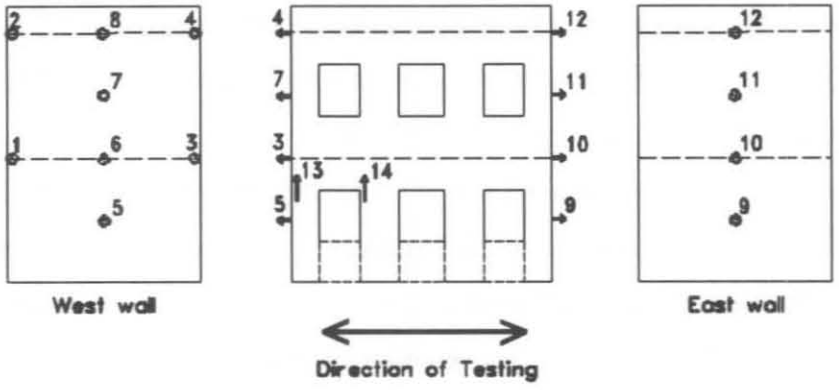

Figure 2.31 Location of LVDTs on S1 and S2

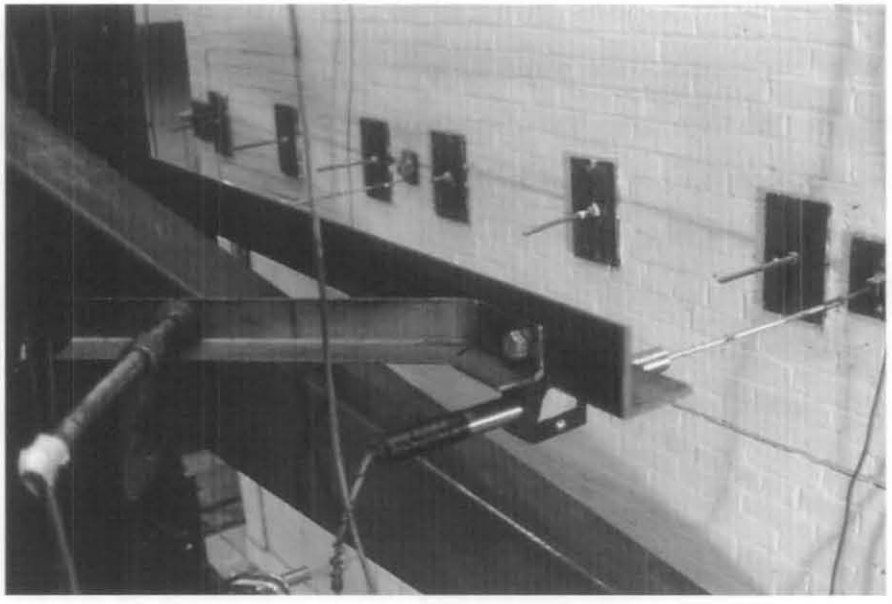

Figure 2.32 Close-up of a Mounted LVDT

S1, these blocks were clamped to the arms using C-clamps. This attachment method provided problems (see Appendix 4), so the blocks were epoxied to the arms and diagonal bracing was added to the arms before the testing of S2. The fixed datum remained the same for both series of tests. Since the two vertical LVDTs were measuring displacement within a pier, they were attached slightly differently. The special blocks were epoxied directly to the piers and the core was nutted to a small piece of angle also epoxied to the pier.

The LVDT signals also required conditioning and amplifying prior to being converted to digital form. The ten Schaevitz and four Collins LVDTS were wired into fourteen Endevco signal conditioners and fourteen Endevco amplifiers. The LVDT signals then were sent to the MTS A/D converters. The actuator LVDT, being a control signal, was wired directly into the MTS controller where it was conditioned and amplified.

2.9.3 Strain Gauges

Four strain gauge channels monitored the horizontal behavior of the diaphragms during the dynamic testing of S1 and S2. Each channel consisted of four Measurements Group 120Ω strain gauges and measured the strain of a single floor beam. Beams 5 and 7 from both diaphragms were gauged. Each beam had two gauges mounted on each side, one above the other, along the beam centerline. The four gauges were wired to form a full bridge. The gauges were attached to measure strain resulting from deflection of the beams in the direction of testing, but were calibrated to provide the horizontal reaction forces at the beam ends. As the strain gauges were glued directly to the beams, no other mounting hardware was required.

The four strain gauge channels, like the accelerometers and LVDTS, required conditioning and amplifying before sent to the MTS A/D converters. Here, four Neff signal conditioners and four Endevco amplifiers were used.

2.10 Ground Motion

The ground motion used as the basis for the input to the earthquake simulator came from the Nahanni earthquake of December 23, 1985. This event occurred at 5:16 AM in the Northwest Territories of Canada and had a body wave magnitude M_b=6.4 and a surface wave magnitude M_s=6.9. Of the records available for this event, the one from the Battlement Creek site was used. The Nahanni earthquake motion was used in the testing of S1 and S2 because it has a number of characteristics common to eastern United States earthquakes, including, (a) large magnitude, (b) shallow depth (18 km), (c) response spectrum shifted toward higher frequencies, and (d) intraplate center.

The records of the ground motion were received in an ASCII text format with a time step of 0.005 seconds and units in cm/sec^2, cm/sec, and cm for acceleration, velocity, and displacement, respectively. A modified version of the acceleration record was used during the dynamic testing. The first modification made to the record was a time compression to be consistent with the reduced scale of the test structures. Since the story heights of S1 and S2 were roughly $^3/_8$ that for a full size building (45"x$^8/_3$=10'), the relationship

$$\tau_{rs} = \sqrt{\frac{3}{8}}\,\tau_{fs} \tag{2.2}$$

was used to compress the record, where τ_{rs} is the time step for the reduced-scale structure and τ_{fs} is the time step for the full-scale structure. This resulted in a time step of 0.0031 seconds instead of the original 0.005 seconds. The second modification made to the record involved filtering out frequencies that were well below any natural frequencies of either S1 or S2. This was done primarily to reduce the displacement and velocity demands on the earthquake simulator which were limited to ±2" and 13.5 in/sec. To filter the record, a Fourier transform was taken of the acceleration history, frequency components below 3.8 Hz were set to 10^{-6}, several orders of magnitude below the original components, and the transform was inverse transformed to reproduce an acceleration history. Figure 2.33 shows the Fourier transforms of the acceleration history

before and after filtering. This filtered acceleration history was integrated twice to produce a displacement time history which was balanced to end at zero. Balancing was accomplished by subtracting a ramp function which started at zero and ended at the displacement of the twice integrated acceleration record.

The program that runs the earthquake simulator (STEX) required two slight modifications be made to the displacement history. First, the first and last 0.5 seconds of the record were multiplied by ramps to smooth the transitions and second, zeros were added to the beginning and end of the time history to produce a test duration with a convenient memory allocation. This time history, shown in Figure 2.34 normalized to its maximum value, was used to control the earthquake simulator. The magnitude was adjusted to produce base motions of varying intensities.

Prior to beginning the construction of S1, the earthquake simulator was calibrated to determine the acceleration levels which would result from various magnitudes of the input motion. Over 11.5 kips of steel plates were bolted to the platform surface to represent the load of the test structure. Using a square wave input, the feedback controls were tuned to produce the fastest response time with the minimum overshoot. Then, using the Nahanni time history as the input, the input magnitude was varied and the peak acceleration and displacement levels were recorded to produce a calibration curve. This curve would be used in selecting the input levels during the dynamic testing.

2.11 Free Vibration Testing

Prior to the dynamic testing, a free vibration test was conducted on both S1 and S2 to characterize the buildings' natural frequencies. After each dynamic test run of S1 and S2, an additional free vibration test was performed to determine if the resonant frequencies had changed. The buildings were displaced laterally by a large weight attached to the end of a cable which hung over a pulley. The 455 pound weight, Type L from Section 2.3, was released by a quick-release link which connected the weight to the cable. The other end of the cable was attached to one of the second-floor weights. A schematic of the free vibration setup is shown in Figure 2.35. The quick

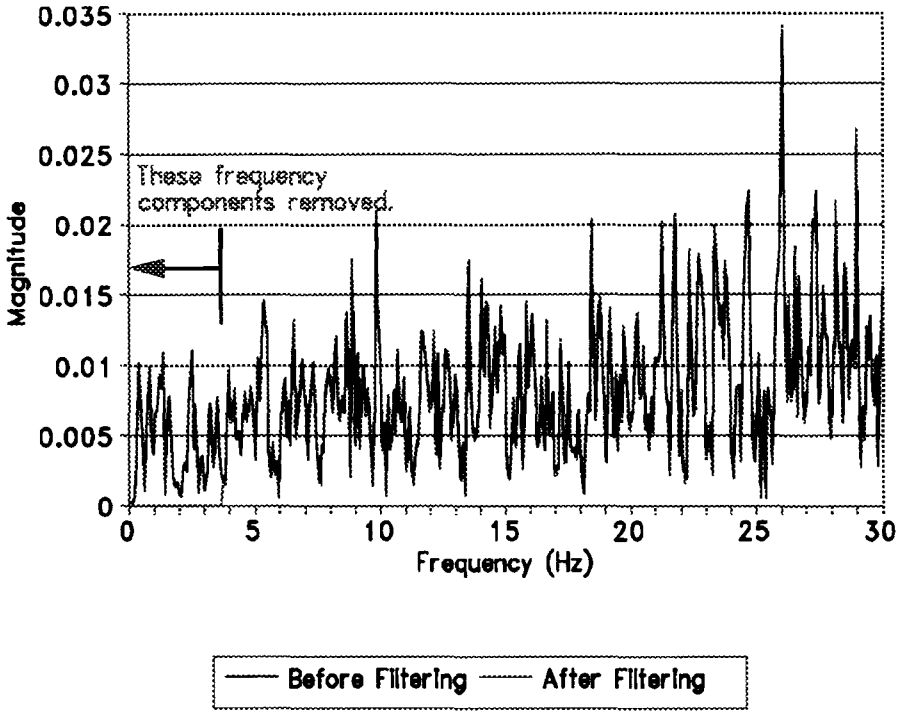

Figure 2.33 FFT of Acceleration History Before and After Filtering

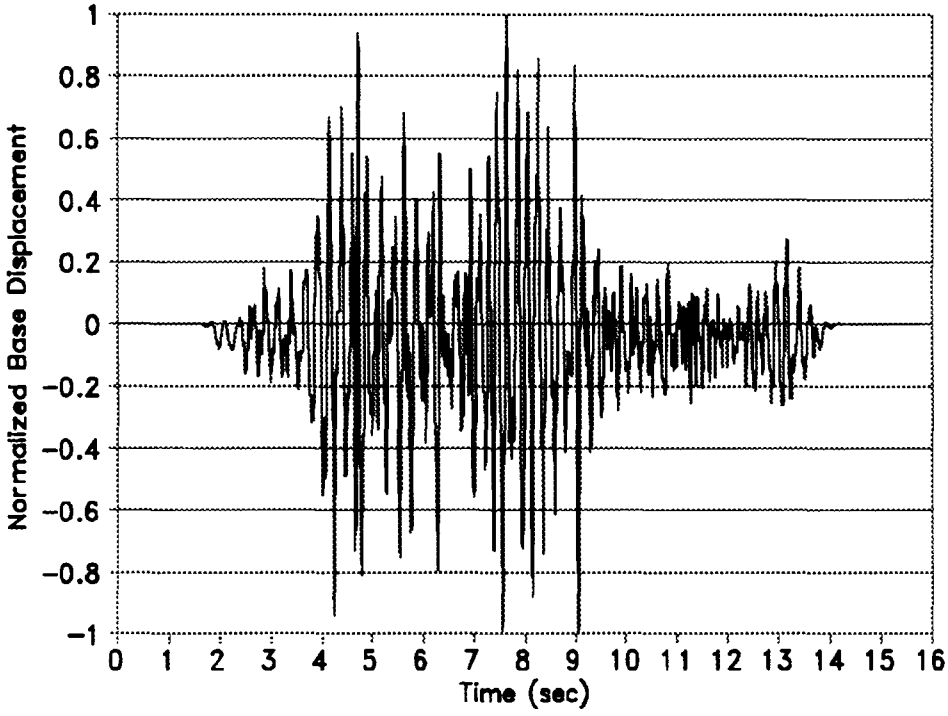

Figure 2.34 Normalized Base Displacement Distory

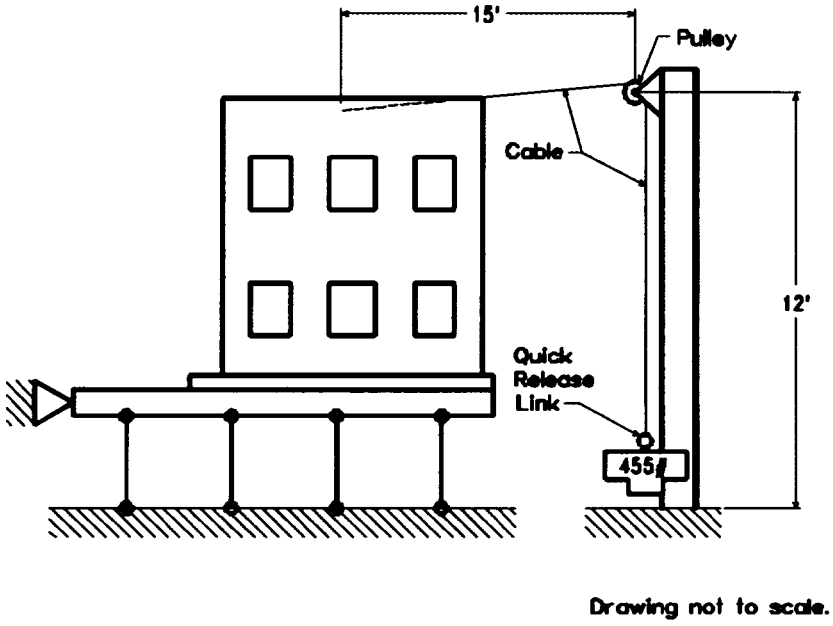

Figure 2.35 Experimental Setup for the Free Vibration Tests

release of the tension on the building allowed the building to oscillate freely from the initial displaced condition to its rest position.

During the free-vibration oscillations, ten channels of accelerometer data were collected. These channels are listed in Section 2.9.1 and included the first- and second-floor window- and door-wall accelerometers, in the test direction, and the four test-direction diaphragm accelerometers. Since the excitation levels during the free vibration tests were much lower than those during the dynamic tests, the gains on the accelerometer amplifiers were increased by 2½ times. The accelerometers were not recalibrated for these levels since the relative magnitudes within one test were important, rather than the absolute amplitude of the signals across tests.

2.12 Dynamic Testing

The complete experimental setup for S1 is shown in Figures 2.36a and 2.36b. A total of twelve earthquake simulations were performed with S1, although only the last five are reported here. The first seven runs used an unfiltered version of the Nahanni earthquake which had low frequency components large enough to maximize the earthquake simulator's displacement range without damaging the structure. The last five runs used the filtered displacement time history shown in Figure 2.34. These runs are labeled 11 through 15, referring to S1, runs 1 through 5. Each earthquake simulation increased the intensity of the base motion with respect to the previous simulation, with peak base accelerations ranging from 0.15g for run 11 to 1.8g for run 15. Four earthquake simulations were performed with S2, these being labeled 21 through 24, i.e., S2, runs 1 through 4. These runs also used the history shown in Figure 2.34 and had increasing base motion intensities with peak base accelerations ranging from 0.2g to 1.1g.

Between each earthquake simulation, visible damage was noted and recorded. Prior to their testing, both S1 and S2 were painted white to facilitate crack identification and marking. Cracks were marked with colored pens, with a different color used for each run that induced new cracks. After the cracks were marked on the buildings, their locations were also marked on detailed drawings of the buildings. These crack patterns are discussed in Section 4.2. In addition to

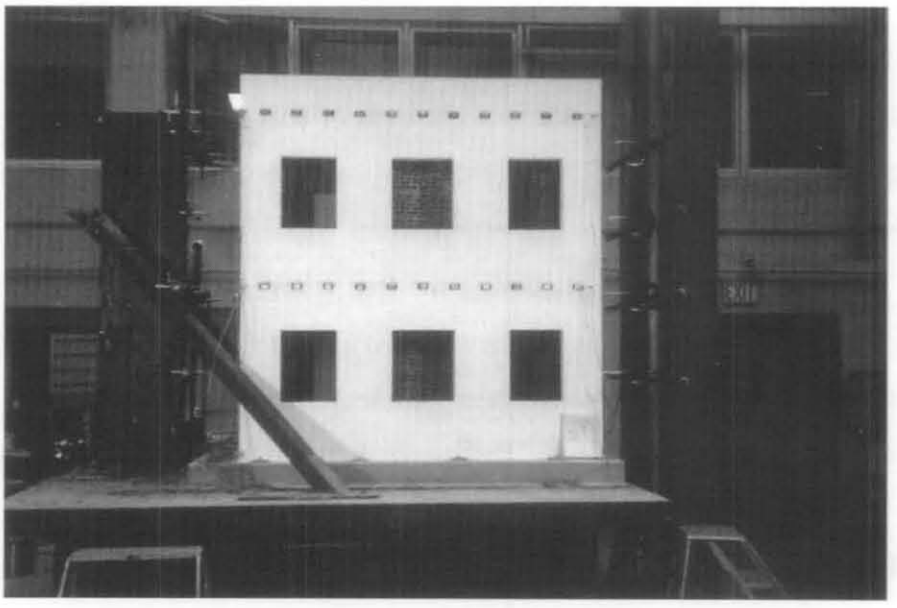

Figure 2.36a Experimental Setup Showing S1 Instrumented on the Earthquake Simulator

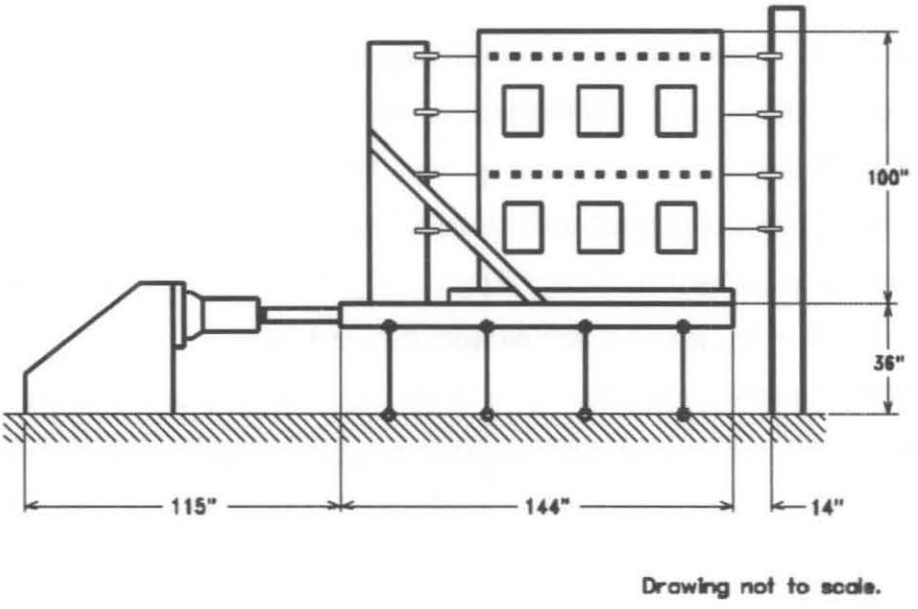

Figure 2.36b Experimental Setup for the Dynamic Test Runs

recording the cracks on paper drawings, a large number of photographs were taken between tests to record characteristics such as dislodged bricks, missing mortar, misalignment across cracks, and out-of-plumbness of the walls.

2.13 Data Collection and Reduction

The heart of the data acquisition was the MTS STEX (Seismic Test EXecution) software package resident on a DEC Vaxstation. This program was used extensively in the preparation of the input motion described in Section 2.10 and also served as an interface to the MTS (hydraulic) controller which drives the earthquake simulator. The STEX program collects the data by way of a "test definition" which specifies the active channels along with their calibrated ranges and appropriate units. STEX is also capable of providing rapid graphical display of the data once the test is complete.

After a test had been completed, the data from the various channels was exported in a text format from the STEX program to the VAX/VMS operating system environment. Each file, one per channel per test run, was transferred to another network before being downloaded to floppy disks in a DOS format. At this point, the data was still in "digital" form, i.e., values from $-(2^{15})$ to 2^{15} (in increments of 2^4), from the A/D converters. Each file header possessed the appropriate conversion factor and units declaration to convert from the "digital" form to inches, g's, and μstrains. The converted data files were given a new header with information pertaining to the structure number, test run number, instrument type, instrument location, time step, and the absolute data maximum. Further information regarding the collected and reduced data can be found in Appendix 2.

SECTION 3
RESPONSE CALCULATED WITH CONVENTIONAL METHODS

3.1 Overview

Prior to dynamic testing of S1 and S2, several building codes were reviewed and several structural analysis models were developed to predict the strength and behavior of the two buildings. Both static and dynamic methods were examined. This section will review the various methods used to predict the lateral strength and dynamic behavior of the test buildings. The methods used for the analysis represent methodologies and techniques currently available for the analysis of unreinforced masonry structures. The purpose of this exercise is to demonstrate the variations in building response, as determined using conventional methods, rather than to endorse any one particular method.

Two design codes, the commentary to Chapter 21, Masonry, of the 1994 Uniform Building Code (UBC) and the Building Code Requirements for Masonry Structures ACI 530-95/ASCE 5-95/TMS 402-95 Code (referred to hereafter as MSJC), were used to determine the allowable base shear. Two rehabilitation codes, the 1994 Uniform Code for Building Conservation (UCBC) and the NEHRP Handbook for the Seismic Evaluation of Existing Buildings (FEMA 178), were used to evaluate the lateral resistance of the two buildings as built. A linear, elastic finite element model was also developed to determine an allowable base shear.

Several dynamic models were used to determine natural frequencies, mode shapes, and response histories of S1 and S2. An equivalent frame analysis (two degrees of freedom) was first used to estimate the frequency of the building with a rigid diaphragm. The second analysis included a six-degree-of-freedom model. Using anticipated base accelerations, predicted displacement, velocity, and acceleration histories were produced using a time-step integration. Natural frequencies and mode shapes were also derived from this second model. The third dynamic model was a variation of the finite element model used for the static analysis. This model was used to determine the natural frequencies which were used in a response spectrum analysis.

3.2 Static Methods

3.2.1 UBC

The 1994 UBC was used to determine the strengths of the masonry shear walls for S1 and S2 when subjected to earthquake-type loadings. Each shear wall was analyzed independently for potential compression, shear, and tension failures. Equivalent lateral loads were applied at the two floor heights using an inverted triangular load distribution, resulting in a 2:1 ratio between the second- and first-floor loads (Figures 3.1 and 3.2).

Most of the allowable stresses defined by the UBC are based on the masonry compressive strength, f_m. For this analysis, f_m was estimated to be 1900 psi based on tests of prisms (Section 2.7.1). Using this value, the allowable compressive axial stresses, F_a, were 468 psi for the shorter, window piers and 453 psi for the longer, door piers. The allowable flexural compressive stress, F_b, was determined to be 633 psi. The allowable shear stress value, F_v, varied between 13.1 psi and 20.2 psi depending on the vertical stress in the pier being analyzed. Dead load stresses in the first-story piers (Table 3.1) were based on tributary areas. These values were reduced when piers were subjected to tensile forces from the overturning moment. The masonry tensile strength, F_t, was assumed equal to 40 psi based on flexural tension specimens (Section 2.7.4). The $^1/_3$ increase in the allowable stresses, F_a, F_b, F_v, and F_t, was taken into account for the earthquake load combinations. Lastly, to simplify the analysis, the flange effects from the out-of-plane walls on the window wall of S1 and the door wall of S2 were not included.

With the allowable stresses given above, both first-floor shear walls from both buildings were analyzed to determine the base shear. The horizontal floor loadings were distributed to the piers based on their relative stiffness within a given wall. With the assumption that the piers were fixed at both ends, each pier shear force also resulted in a pier moment. The global overturning moment was transformed into tensile and compressive axial pier forces at the tops of the piers. The load combination of $0.9D+0.75E<F_t$, where D is the dead load stress and E is stresses resulting from earthquake loads, provided the critical case of tensile failure for each of the four

Table 3.1 Dead Load Stresses Used in the Static Analyses

Shear Wall	Dead Load Stress (psi)	
	Outer Piers	Inner Pier(s)
S1 door wall	33.1	35.7
S1 window wall	39.8	48.4
S2 door wall	39.8	48.4
S2 window wall	33.1	35.7

Table 3.2 Displacement and Acceleration Maxima and Occurrence Times for MDOF Model with Flexible Diaphragms Simulation of Test Runs 11 and 21 (See Figure 3.8 for description of DOFs.)

S1 DOF #	Displacement (in) (Time (sec))	Acceleration (g) (Time (sec))
1	0.00135 (7.511)	0.060 (9.150)
2	0.00162 (7.511)	0.074 (9.150)
3	0.0618 (7.514)	0.439 (7.329)
4	0.0639 (7.514)	0.446 (7.329)
5	0.00101 (7.542)	0.060 (4.922)
6	0.00151 (7.542)	0.090 (9.209)
S2 DOF #		
1	0.00064 (4.996)	0.193 (4.928)
2	0.00097 (4.996)	0.293 (4.928)
3	0.0748 (4.931)	0.633 (4.928)
4	0.0748 (7.446)	0.624 (4.928)
5	0.00521 (5.048)	0.582 (5.048)
6	0.00594 (5.048)	0.654 (5.048)

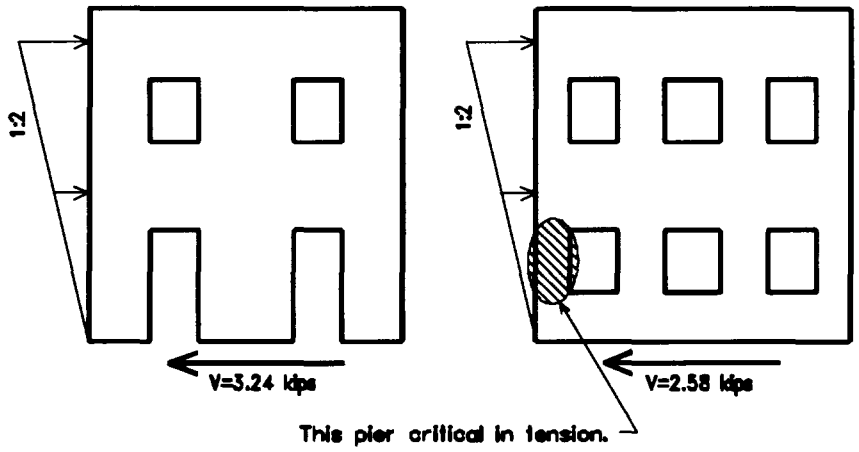

Figure 3.1 Critical Base Shears for S1 Using the UBC

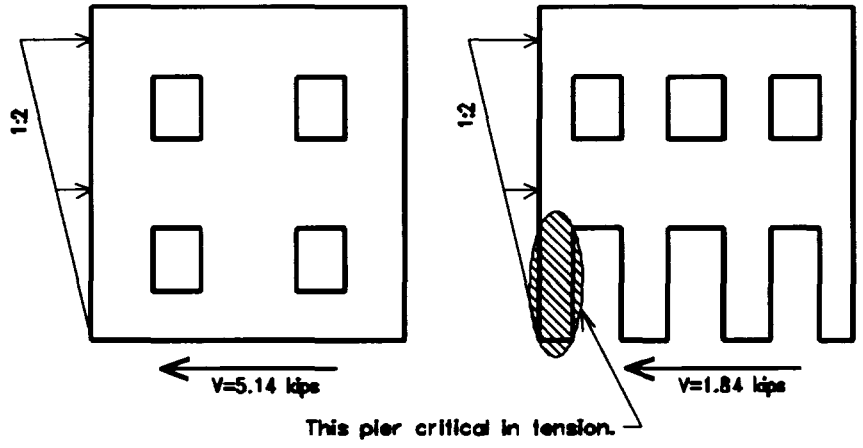

Figure 3.2 Critical Base Shears for S2 Using the UBC

walls. The *0.75* multiplier for E was used instead of the $^1/_3$ increase in allowable stress due to earthquake loading. The dead load term was not further reduced beyond the *0.9*.

For S1, the outer window pier would exceed the allowable 40 psi tension if the base shear was 2.6 kips while the outer door pier would exceed 40 psi in tension if the base shear was 3.2 kips (Figure 3.1). For S2, the outer door pier would exceed the allowable tensile stress if the base shear for that wall was 1.8 kips, whereas the window wall would not fail until a load of 5.1 kips (Figure 3.2). Since each wall was analyzed individually, the base shear values given are for a single wall. The walls were assumed to be equally loaded by the diaphragms, so the total base shear would be twice the base shear of the weaker wall, i.e., 5.2 kips and 3.7 kips, for S1 and S2, respectively.

3.2.2 MSJC

An analysis similar to the one described for the UBC was also conducted using the 1995 ACI/ASCE/TMS (MSJC) masonry code. The allowable axial compressive and bending stresses were the same as those determined using the UBC. Although peak shear stress is checked when using the MSJC code, instead of average shear stress as when using the UBC, the range of F_v from 37 psi to 53 psi more than accounted for this difference. Therefore, neither compressive nor shear stresses governed. The Commentary to the MSJC masonry code (1992 edition), however, infers zero tensile strength (i.e., F_t=0), for unreinforced masonry in-plane walls (Commentary Section 6.3.1.1). This resulted in very low base shear strengths for S1 and S2 since they are both tension critical.

Using the same loading, force distribution, and load combination as in 3.2.1, with the MSJC allowable stresses, the outer window pier of S1 would fail at a base shear of 1.2 kips while the outer door pier would crack at 1.4 kips. The outer door pier of S2 would exceed the allowable tensile stress at 0.9 kips and the outer window pier would crack in tension at 2.2 kips. Again, these computed base shears were for a single wall. Doubling the weaker wall shears produced total base shears of 2.4 kips for S1 and 1.7 kips for S2.

3.2.3 UCBC

One of the two rehabilitation codes used to determine the lateral strengths of S1 and S2 was the UCBC. The purpose of this code is to evaluate the resistance of an existing, usually older, structure whose material properties are essentially unknown. As such, the basis of lateral strengths is the in-place shear test, or shove test, described in Section 2.7.6. The UCBC details the required number and locations of these shove tests and prescribes the allowable shear stress, v_a, as

$$v_a = 0.1 v_t + 0.15 P_D / A \tag{3.1}$$

where v_t is the shear strength value exceeded by 80% of the test values and P_D/A is the average dead load stress across a pier or wall. The value of v_t is not allowed to exceed 100 psi. The allowable axial compressive stress is limited to 100 psi and unreinforced masonry is assumed to have no tensile strength. The $^1/_3$ increase for allowable stresses is permitted for the compressive stress, but does not apply to v_a.

The procedure for determining the lateral strength of a perforated shear wall involves a comparison of the pier shear capacity, V_a, calculated by

$$V_a = v_a A \tag{3.2}$$

where A is cross-sectional area of the pier, and the pier rocking shear capacity, V_r, calculated by

$$V_r = 0.5 P_D D / H \tag{3.3}$$

where P_D is the dead load on the pier and D/H is the pier aspect ratio, length over height. If $V_r < V_a$ for all piers on a given level then the shear forces are distributed proportional to $P_D D/H$. If $V_a < V_r$ in any one pier on a given level then the shear forces are proportioned according to D/H. For this second case, the code states that piers with assigned shears greater than V_r should be eliminated from the analysis.

The story shear capacity for each wall of S1 and S2 was calculated by summing the pier diagonal tension and pier rocking capacities. The strength of the weaker wall was tehn multiplied

by two to give the total strength of the pair of walls. Using the limit of 100 psi for the shove test values and the dead load stresses in Table 3.1 resulted in allowable stresses, v_a, ranging between 15.0 and 17.3 psi. These values, along with the dead load stresses, were used to analyze independently the first-story walls of S1 and S2 for rocking- or shear-controlled behaviors. For S1, the window wall was determined to be shear controlled with a base shear of 1.8 kips (using the force distribution according to *D/H*.) The S1 door wall was rocking controlled with a capacity of 2.7 kips. For S2, the door wall was rocking controlled with a base shear of 1.4 kips while the window wall had a shear-controlled behavior with a capacity of 3.4 kips. Thus, the total base shear for S1 was 3.6 kips and the total base shear for S2 was 2.8 kips.

3.2.4 FEMA 178

The second rehabilitation code used to determine the lateral strengths of S1 and S2 was FEMA 178. Like the UCBC, the purpose of this document is to assess the capacity of existing structures. Unlike the UCBC, however, which is based on allowable stresses, the FEMA 178 code is based on ultimate stresses. In an equation similar to the UCBC, shove tests form the basis of the masonry shear strength, v_m, calculated by

$$v_m = 0.56 v_t + 0.75 P_D / A \tag{3.4}$$

where v_t is the shear strength value exceeded by 80% of the test values and P_D/A is the average dead load stress. The value of v_t is not allowed to exceed 100 psi. The allowable axial compressive stress is limited to 300 psi and unreinforced masonry is assumed to have no tensile strength.

To determine the shear force distribution among the piers in a wall, the pier shear capacity is compared with the pier rocking capacity. In this case, the pier shear capacity, V_a, is calculated by

$$V_a = v_m D t / 1.5 \tag{3.5}$$

where D and t are the pier length and thickness, respectively. The pier rocking shear capacity, V_r, is determined as

$$V_r = 0.9 P_D D/H \tag{3.6}$$

where P_D is the dead load on the pier and D/H is the pier aspect ratio, length over height. If $V_r < V_a$ for all the piers at the level being considered, then the lateral loads are distributed proportional to $P_D D/H$. Furthermore, for the rocking-controlled case,

$$0.6 V_{wx} < \Sigma V_r \tag{3.7}$$

where V_{wx} is the total load resisted by the shear wall at that level. This condition effectively increases the calculated rocking capacity of a wall by 67% over the capacity determined by summing V_r in order to promote rocking over shear. If $V_a < V_r$ for a single pier at that level then the shear forces are proportioned according to D/H. For this shear-controlled case, piers with assigned shears greater than V_r should be eliminated from the analysis.

The maximum story shear capacity based on the V_r and V_a values was again determined. Using the maximum of 100 psi for v_t and the dead load stresses in Table 3.1, the masonry shear strengths, v_m, were calculated to be between 80.8 and 92.3 psi. These values, along with the dead load stresses, were used to determine the shear and rocking strengths of the first-story piers of S1 and S2. For S1, the window wall was critical with a rocking-controlled behavior at 7.6 kips when taking the 0.6 factor of Equation 3.7 into account. The door wall also had a rocking-controlled behavior at a wall base shear of 8.0 kips, again using the 0.6 factor. The door wall was rocking critical for S2 at a base shear of 4.3 kips. The window wall of S2 was also rocking-controlled at 14.1 kips. Note that using the 0.6 factor increased the total wall load beyond the shear-controlled mode (12.4 kips). The total base shears, again determined by doubling the strength of the weaker wall, were 15.2 kips for S1 and 8.5 kips for S2.

3.2.5 Finite Element Model - Linear Analysis

The final static analysis method consisted of using linear finite element models for determining stress distributions. The use of these models provided a finer refinement of the building's geometries and a more accurate assessment of stress distributions throughout the model than the code approaches. The three-dimensional geometry of the models was developed using Patran, a graphical interface program, while the models were solved using the finite element code Abaqus. Two translation programs, Pataba and Abapat, were used to convert files back and forth between Patran and Abaqus so that the same geometry models that were created for the Abaqus input could also be used to view the Abaqus output.

The linear finite element model attempted to mimic all the physical aspects of the actual test buildings (S1 and S2) before initial cracking. The undeformed geometries of the finite element models are shown in Figure 3.3 and 3.4. Each model consisted of four walls, with the two perforated in-plane shear walls connected by two floor systems each composed of eleven, rectangular beams. The two, solid, out-of-plane walls were joined to one of the shear walls (window wall for S1 and door wall for S2) while a gap was left between the transverse walls and the other shear wall. Dimensions of the models were the same as those in Figures 2.3, 2.4, 2.7, and 2.8.

To represent the masonry portion of S1 and S2, eight-node, three-dimensional, solid elements, or brick elements, were used. Material properties were assumed to be elastic with a modulus of 750 times the assumed prism strength (1900 psi), or 1425 ksi, a density of 125 pcf, and a Poisson's ratio of 0.3. The window and door walls were each discretized into a mesh 24 elements wide by 19 elements high while the two out-of-plane walls were each discretized into meshes of 5 by 19. All four walls were a single element thick. The meshes resulted in high element densities and element aspect ratios near 1:1:1 in the critical pier regions, and still gave enough resolution for the out-of-plane walls to deflect smoothly. Elements in the piers and the out-of-plane walls were rectangular, but those in the spandrels were slightly trapezoidal to enable uniform spacing of the floor beams.

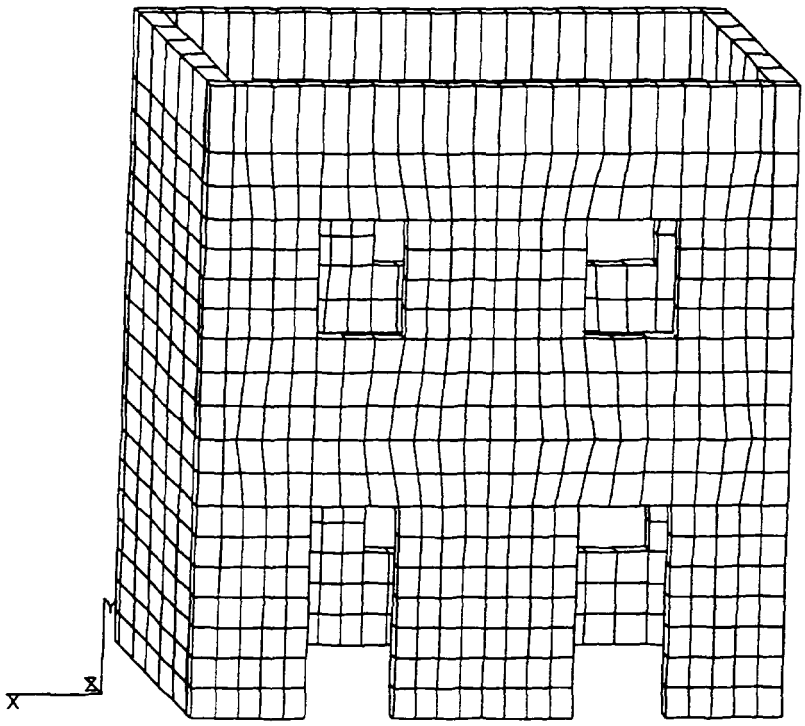

Figure 3.3 Finite Element Model of S1

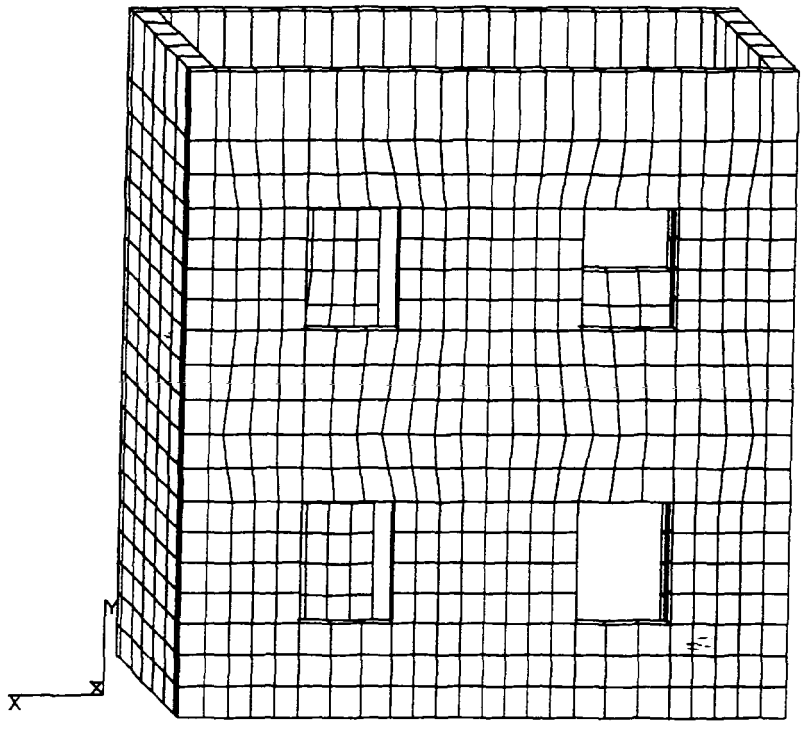

Figure 3.4 Finite Element Model of S2

The floor systems in the models were comprised of beam elements and point masses. Each floor beam spanned between the inner faces of the shear walls and was discretized into five rectangular beam elements. Material properties were elastic and consistent with those commonly assumed for steel. The middle two nodes of each beam were tied to adjacent beams. Horizontal deflections of the end beams were constrained to equal those of the out-of-plane walls at each level. The middle two nodes of each beam also had point masses with various magnitudes to recreate the actual placement of the floor weights (see Figure 2.9b). More detail on the floor system is given in Section 3.3.4.

Loading of the static model was similar to that of the UBC and MSJC code analyses. Horizontal loads were applied at the floor levels in a 2:1 ratio (second:first floor). Both shear walls were loaded equally. Each floor load was split between the two nodes defining the thickness of the shear walls and was applied as a nodal load. Gravity loads were included for the masonry, floor beam, and point mass elements. With the horizontal floor loadings and the gravity loads, the entire model was solved to determine element stresses. The magnitudes of the horizontal loads were increased, keeping the 2:1 ratio, until either a shear stress exceeded 46 psi or a tensile stress exceeded 40 psi. These values were determined from material tests described in Sections 2.7.3 and 2.7.4 and were not increased by $^1/_3$. For the S1 model, the toe of an outer, first-story, door-wall pier exceeded the 40 psi tensile stress at a total base shear of 4.8 kips (Figure 3.5). At this loading level, the maximum shear stress was 22 psi on an inner, first-story, window-wall pier. For the model of S2, a total base shear of 4.1 kips produced a tensile stress at the toe of an outer, first-story, door-wall pier that surpassed 40 psi (Figure 3.6). For this load, the maximum shear, 18 psi, was found in an inner, first-story, door-wall pier.

3.3 Dynamic Methods

3.3.1 Equivalent Frame Analysis

In conjunction with the design of S1, an elastic model was developed to predict the dynamic characteristics of the building. A PC-based modal and spectral analysis program called Sarsan was

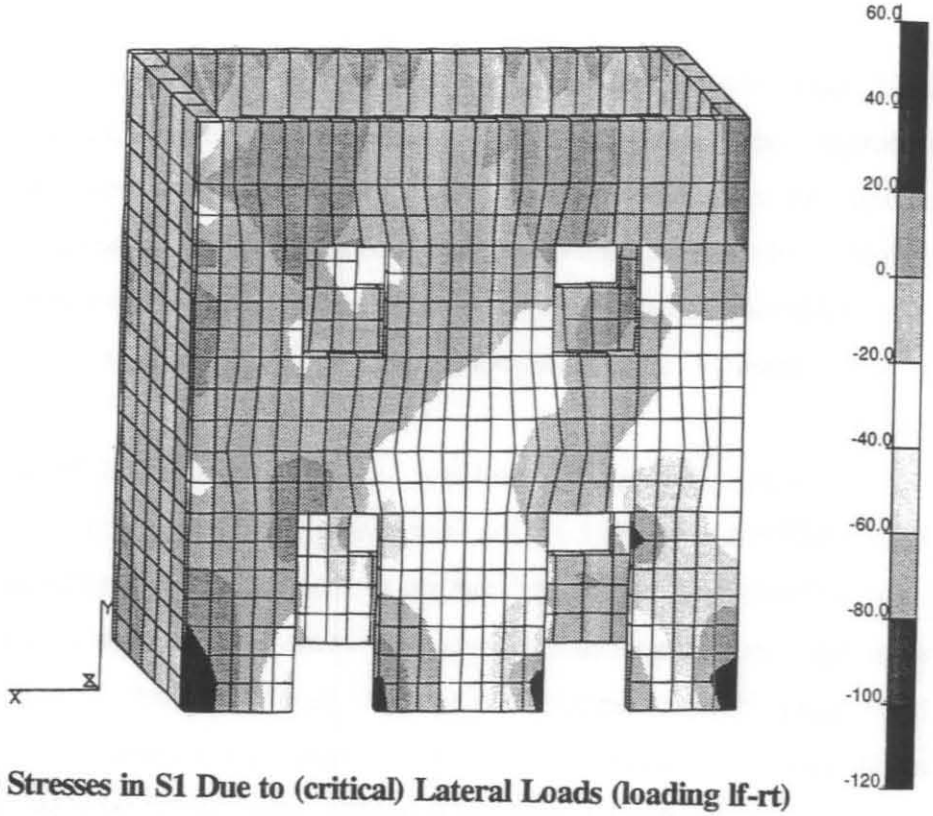

Figure 3.5 Vertical Stresses in S1 Due to (critical) Lateral Loads (loading lf-rt)

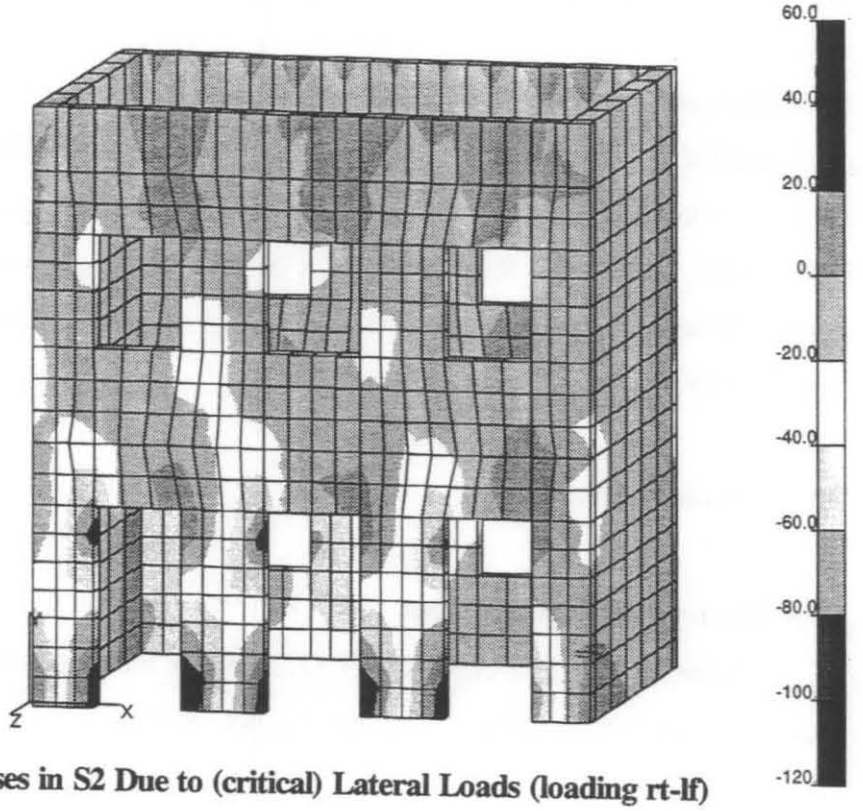

Figure 3.6 Vertical Stresses in S2 Due to (critical) Lateral Loads (loading rt-lf)

used to model a preliminary design of the building as if it had rigid diaphragms to help design the lateral stiffness of the flexible diaphragm system. Sarsan is a frame analysis program that links parallel frames so that each story is condensed to a single-degree-of-freedom lumped story weight. The model assumes that all lateral elements in a story undergo the same horizontal deformation. Beams, columns, and shear walls are input as the structural elements. Modal frequencies, shapes, and participation factors are among the values determined by the program.

To use Sarsan, the preliminary design of S1 had to be simplified to fit the program constraints. The fourteen piers were converted to equivalently-stiff columns based on gross section properties. The spandrels above the columns were converted to beams in a similar manner. The portions of the building where the beams and columns overlapped were considered to be rigid. The effect of the out-of-plane walls on the stiffness of the window wall was neglected. Finally, the total weight of each of the floor systems was lumped at the two story levels. Sarsan assumes fixed end conditions at the base. The elastic modulus was set to 750 times the prism strength. A schematic of the input structure defining equivalent beams and columns is shown in Figure 3.7. The first modal frequency determined for the model was 36 Hz, with a mode shape of {1.00, 0.55}. The 36 Hz frequency served as the basis for designing the lateral frequency of the flexible diaphragm below 10 Hz. When using the as-built geometry, Sarsan computed a 44 Hz frequency for S1 and a 47 Hz frequency for S2. Mode shapes of {1.00, 0.53} for S1 and {1.00, 0.49} for S2 were also determined.

3.3.2 MDOF Model with Flexible Diaphragms - Eigenvalues and Eigenvectors

Another, more complex, dynamic model was developed to better represent the behaviors of S1 and S2. This model had six degrees of freedom (DOF) per building, two for each in-plane wall, and an additional one for each floor system. The stiffnesses of the piers at a given level of a given wall were combined to form a story stiffness while the eleven floor beams were combined to form a floor stiffness. The stiffness of a pier, k_{pier}, was calculated by

$$k_{pier} = \frac{t E_m}{(H/D)[(H/D)^2 + 3]} \tag{3.8}$$

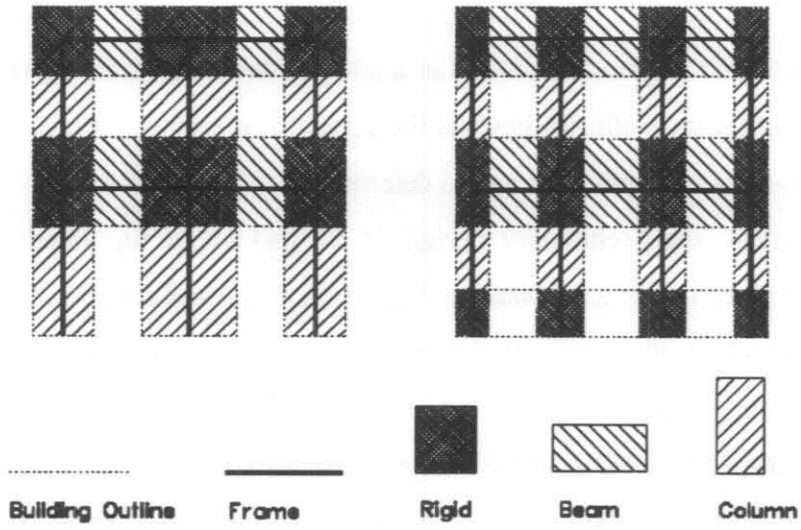

Figure 3.7 Equivalent Frame Representation of S1 for use with Sarsan

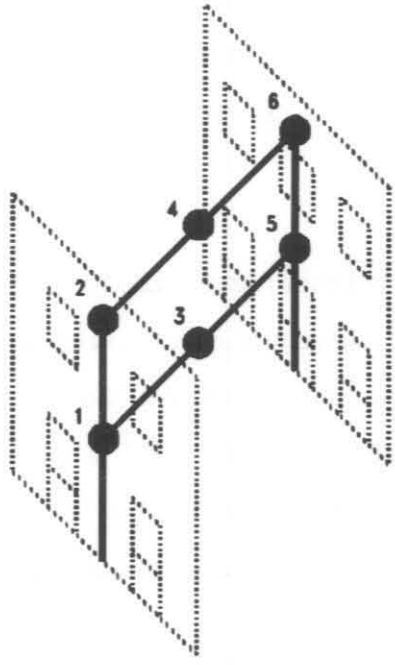

Figure 3.8 MDOF Model with Flexible Diaphragms

where t is the thickness of the pier, E_m is the elastic modulus, and H/D is the aspect ratio, height over length. This stiffness assumes both ends of the pier are fixed and includes both flexural and shear deformations. Equation 3.8 is only valid for piers with rectangular cross sections. Flange effects were not included. The stiffness of the floor beams was determined using a simply-supported beam with a midspan point load. A schematic of the model showing the lumped masses is given in Figure 3.8.

Modal frequencies and shapes were computed for S1 and S2 using this MDOF model. The first four natural frequencies for S1 were 8.3, 8.4, 80.2, and 87.8 Hz. For S2, the lowest four frequencies were 8.3, 8.4, 52.2, and 118.6 Hz. The degrees of freedom for each building are illustrated in Figure 3.8. Using these node numbers, the first mode shape for S1 was {0.115, 0.142, 5.15, 7.12, 0.088, 0.139} while for S2 the mode shape was {0.046, 0.072, 5.59, 6.78, 0.298, 0.345}.

3.3.3 MDOF Model with Flexible Diaphragms - Time-Step Integration

A second analysis was conducted using the same six-degree-of-freedom model described in Section 3.3.2. A computer program developed in a previous study[Tena-Colunga and Abrams, 1992a] was used to compute displacement, velocity, and acceleration histories for an input ground acceleration record. The solution scheme followed a direct solution (non-iterative) of the Newmark-Beta method. The analysis was restricted to linear behavior. Input parameters included the stiffness and mass matrices, damping coefficients, the ground acceleration history, and various time-step and integration constants. A combination of mass- and stiffness-proportional damping was used to provide as close to 2% damping as possible in the first four (of six) modes. A value of 2% was assumed as nominal amount representative of uncracked masonry for determining model characteristics. The key integration parameters of the method, γ, β, and Θ were set to ½, ¼, and 1, respectively. This combination represents an average acceleration during the time step and provides convergence and stability. More information about the program and its solution technique can be found in a report by Tena-Colunga and Abrams, 1992a.

The results of the integration were response histories of S1 and S2 for the ground accelerations of their first dynamic tests. Since the actual base accelerations of the two test buildings were available, they were used in the analyses. Table 3.2 lists the peak displacements and accelerations, as well as their occurrence times, for each degree of freedom, for both S1 and S2 during the computer simulation of Test Runs 11 and 21, respectively. Acceleration and displacement histories for S1 for the second-level diaphragm, DOF #4, are shown in Figures 3.9 and 3.10. For S2, the acceleration and displacement histories for DOF #4 are shown in Figures 3.11 and 3.12.

3.3.4 Finite Element Model

A third dynamic model was developed to determine the natural frequencies of S1 and S2. This dynamic model, similar to the one used for the linear, static analysis (Section 3.2.5), included flexible diaphragms. A separate model of just the diaphragm was also developed in conjunction with the full dynamic model. As with the static model, Abaqus was used to solve the three-dimensional dynamic models which were created using Patran. Pataba and Abapat were again used to translate the model and results back and forth between Abaqus and Patran.

Two slightly different models of the flexible diaphragm were developed, one which modeled an isolated diaphragm and one which modeled how the diaphragm would behave in the full dynamic model. The first model consisted of eleven floor beams, each with a two point vertical loading (point masses) based on the distribution of the floor weights. The two loads were spaced 12" apart and were centered along the length of the beams. The beams were 62.1" long, the actual span between the centers of the window and door walls. Each beam was discretized into five, two-node, linear, rectangular-section, beam elements, each approximately 12" long. The rectangular element cross section was set to 1.75" by 1.25". Beam ends were assumed pinned in the horizontal and vertical directions while the torsional rotation of the beams was restrained at all nodes. To promote a uniform dynamic behavior of the diaphragm model, the beams were linked together at the two central nodes with a tie-beam element. These massless elements were very stiff axially, very stiff against vertical bending, but flexible for in-plane bending. They were designed

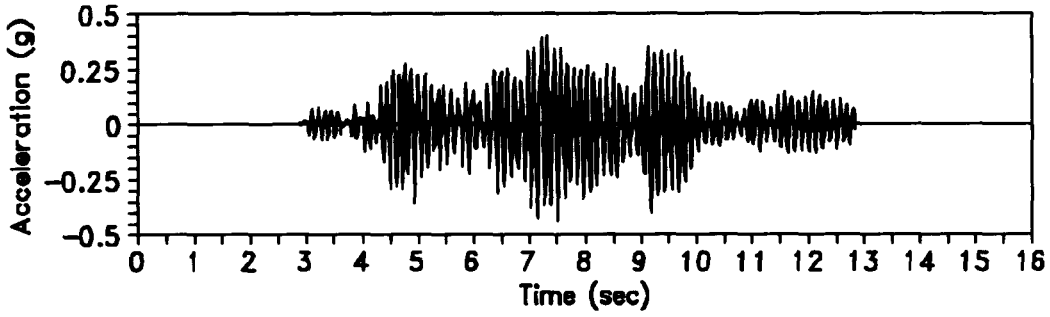

Figure 3.9 Second-level Diaphragm Acceleration for S1 Simulation of Test Run 11 with MDOF Model with Flexible Diaphragms

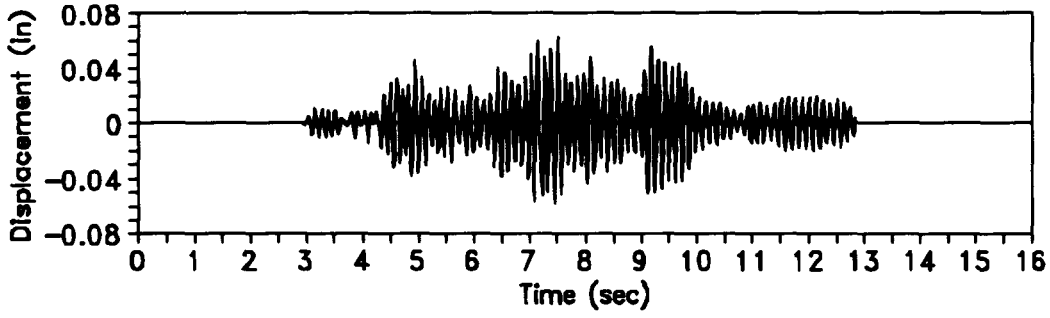

Figure 3.10 Second-level Diaphragm Displacement for S1 Simulation of Test Run 11 with MDOF Model with Flexible Diaphragms

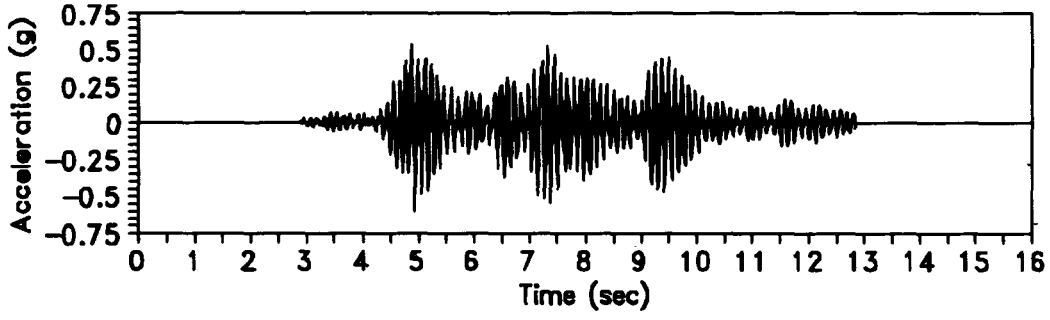

Figure 3.11 Second-level Diaphragm Acceleration for S2 Simulation of Test Run 21 with MDOF Model with Flexible Diaphragms

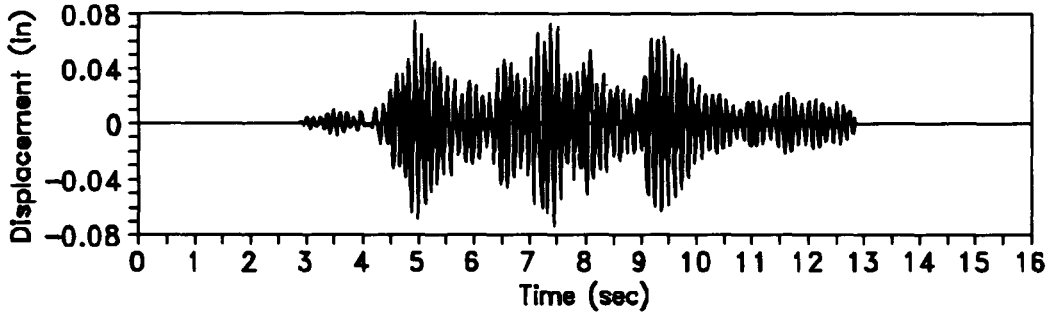

Figure 3.12 Second-level Diaphragm Displacement for S2 Simulation of Test Run 21 with MDOF Model with Flexible Diaphragms

to impose uniform deformations on the floor beams without increasing the floor system horizontal stiffness, representing the same effect as the floor weights tieing the beams together. Material properties for the floor-beam elements were assumed to be elastic with a modulus of 29,000 ksi and a density of 490 pcf. The point masses had various magnitudes to best represent the actual beam loads resulting from the placement of the floor weights (see Figure 2.9b). This model produced a lateral frequency of 8.6 Hz when solved using Abaqus. Figure 3.13 shows the modal deflection of this diaphragm model.

The diaphragm model had to be altered slightly when it was combined with the masonry portion of the model in order to keep its dynamic properties. The masonry part of the dynamic model was the same as for the static models and is discussed in Section 3.2.5. The first property that needed to be changed was the length of the beams. Since the masonry model had walls only one element thick, the beams would have to be attached at the inside faces of the walls and would therefore span only 58.4" instead of 62.1". The second change to the diaphragm model involved rediscretizing the two end beams to the same horizontal node spacing of the out-of-plane walls so the end beams could be linked to these walls. The third change involved removing the point masses and adding a mass density to the originally massless tie-beams. The altered tie-beam elements had the same stiffness properties, but now also uniformly simulated the total weight of the floor weights. The stiffnesses and density of the new tie-beams were adjusted, along with the elastic modulus of the floor beams, to maintain the original weight of the diaphragm and its 8.6 Hz lateral frequency. Thus, the elastic modulus of the floor-beam elements used was 23,500 ksi rather than the commonly assumed value of 29,000 ksi.

With the diaphragm model modified, it was combined (twice) with the masonry portion to produce the full dynamic model. Each beam end connected to an existing node in the window or door wall at the two floor heights. The same tie-beam elements used to link the floor beams together, except massless, were used to link the end beams to the out-of-plane walls at five places per beam. All the base nodes of the model were fixed against translation in three directions and the floor-beam elements were again prevented from rotating axially. Each dynamic model had more than 2300 nodes and over 1100 elements and required between 10 and 15 minutes to solve on a

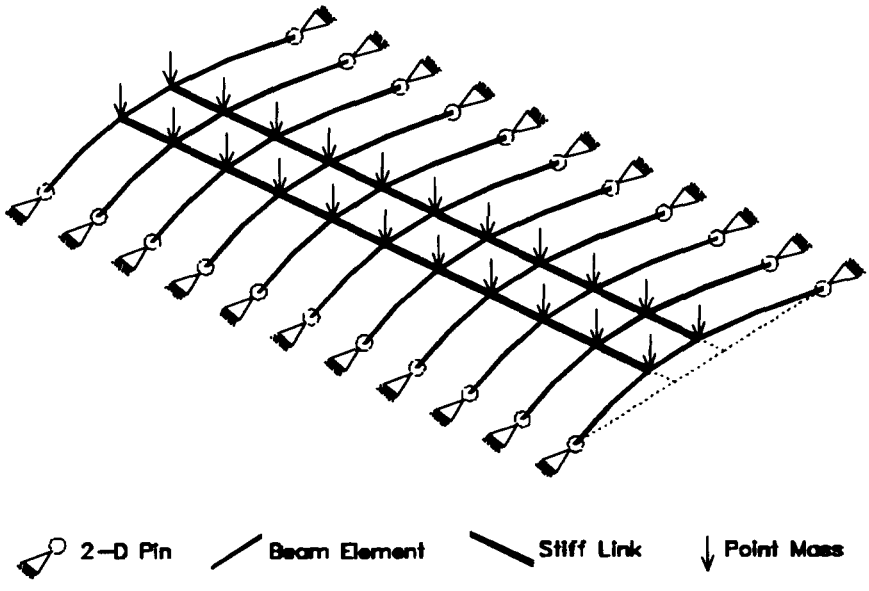

Figure 3.13 Modal Deformation of Finite Element Model of Diaphragm

Hewlett Packard Series 700 Workstation for the natural frequencies, mode shapes, and modal participation factors. The first lateral frequency determined by Abaqus for the entire S1 model was 21.5 Hz. The modal participation factor was 1.36. Figure 3.14 shows the modal deflection, exaggerated for clarity. For S2, the first horizontal frequency was 20.6 Hz and the participation factor was 1.38. The modal deflection is shown in Figure 3.15, again exaggerated for clarity.

The dynamic model with the flexible diaphragms was modified to produce a similar dynamic model with "rigid" diaphragms. The modifications consisted of changing the stiffness characteristics and increasing the elastic moduli of the floor-beam and tie-beam elements. Beam cross sectional areas were not altered so that the dynamic mass of the model was held constant. The beam element moduli were increased until a negligible change in frequency accompanied a substantial change in stiffness. The natural frequency of the "rigid" diaphragm model of S1 was 35 Hz while the frequency of S2 was 34 Hz.

3.3.5 Response Spectrum Analysis

The last dynamic analysis conducted was a response spectrum analysis of S1 and S2. Using anticipated ground accelerations, linear response spectra were produced. Both acceleration and relative displacement spectra were computed. Two percent critical damping was assumed for all spectra. Entering the spectral curves at the frequencies determined for S1 and S2 from the finite element eigenvalue extraction, 21.5 and 20.6 Hz, maximum accelerations and relative displacements were estimated. The acceleration spectra, in conjunction with the table calibration mentioned in Section 2.10, were used initially to set the intensity of the input motion to the earthquake simulator.

As in Section 3.3.3, where the actual base acceleration was used instead of an estimate for the time-step integration, the response spectra shown in Figures 3.16 (for S1) and 3.17 (for S2) also were computed using the base accelerations recorded during Test Runs 11 and 21. In these curves, the spectral acceleration is plotted as the ordinate while the abscissa is the spectral displacement. In this type of plot, lines radiating outward from the origin represent constant frequency, with frequency increasing counterclockwise. The lines representing 21.5 Hz and 20.6

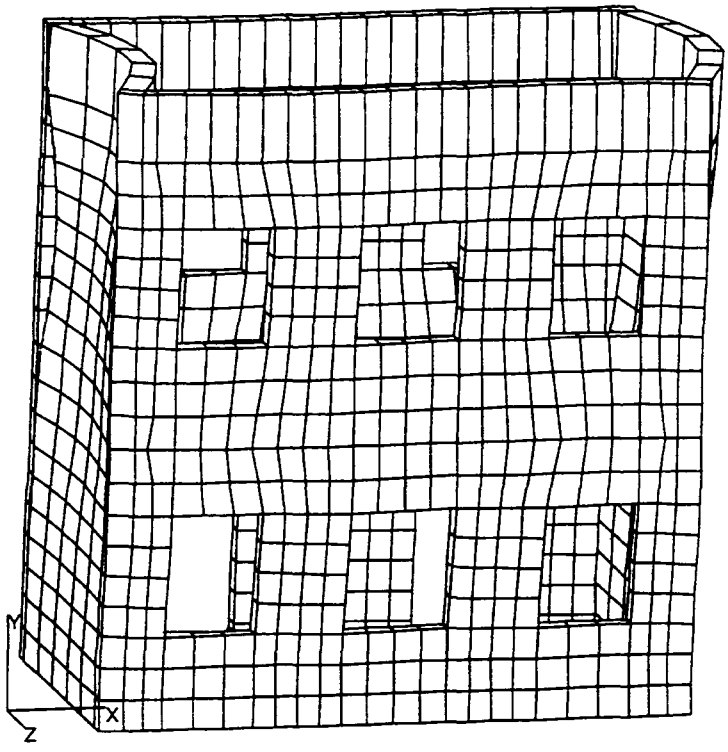

Figure 3.14 Modal Deformation of Finite Element Model of S1

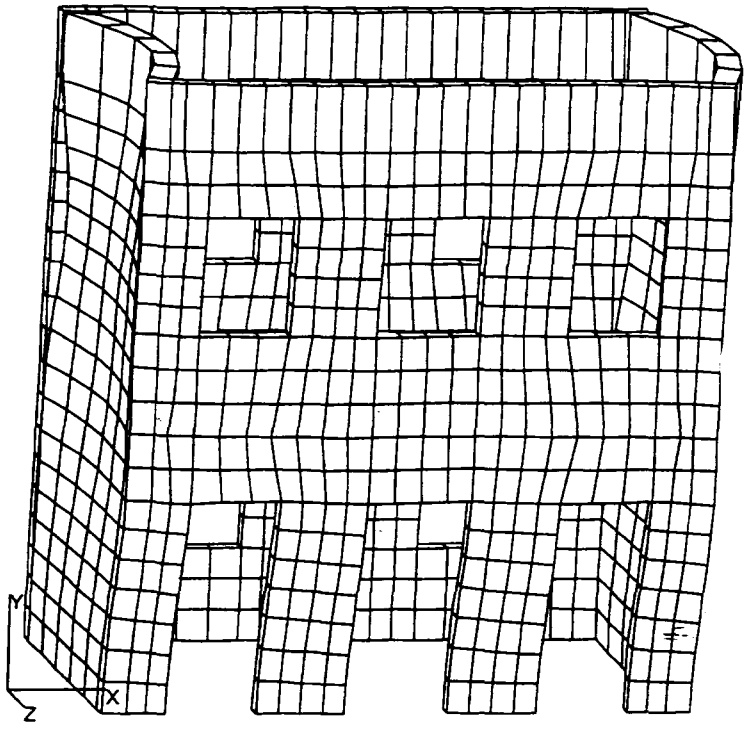

Figure 3.15 Modal Deformation of Finite Element Model of S2

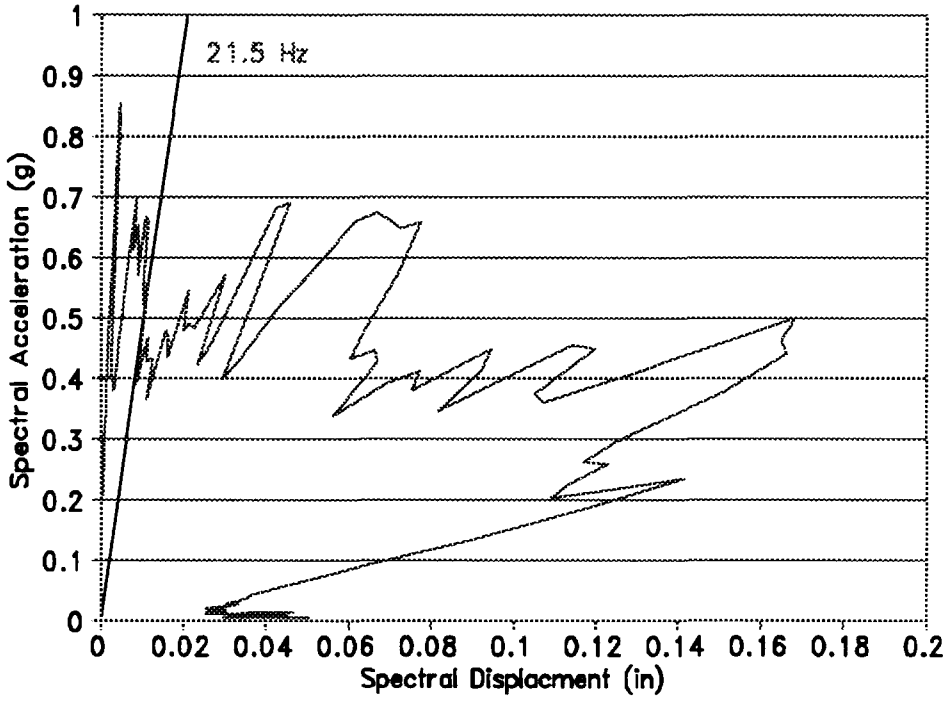

Figure 3.16 Response Spectra of S1 for Base Motion of Test Run 11 (2% damping)

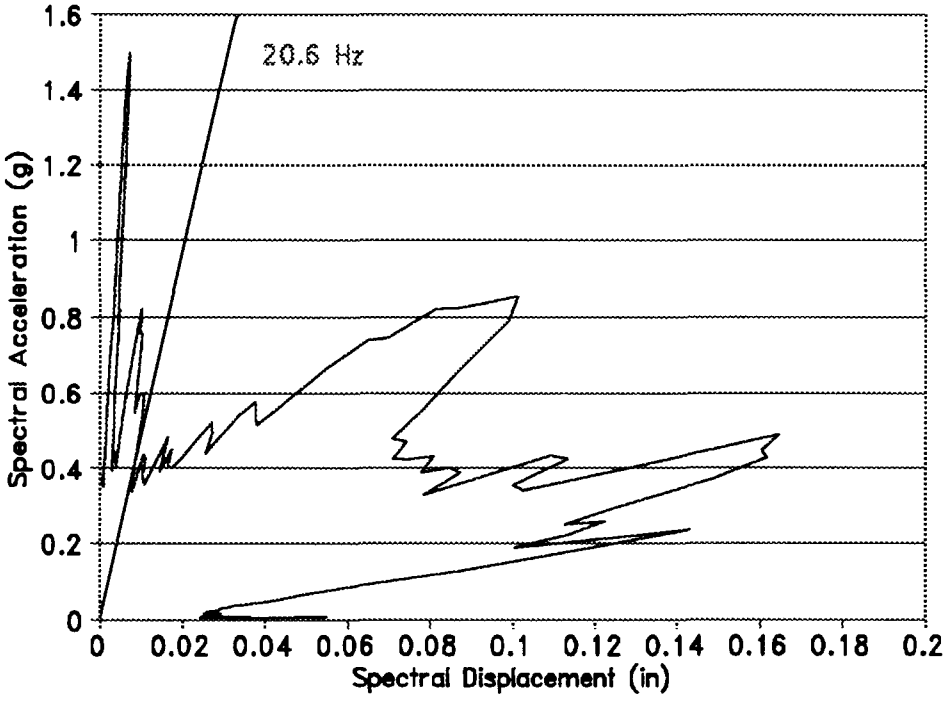

Figure 3.17 Response Spectra of S2 for Base Motion of Test Run 21 (2% damping)

Hz are shown on their respective graphs. Since the computed spectra did not have values exactly at 21.5 and 20.6 Hz, a linear interpolation of the two neighboring values was used to estimate the spectral values at the desired frequencies. The spectral values of relative displacement and acceleration for S1 were 0.0106" and 0.50g while the values for S2 were 0.0079" and 0.34g. The spectral values were converted to displacements and accelerations for the second-level diaphragm (see Section 5.2.1) by multiplying by the participation factors determined using the finite element models. This resulted in calculated values of displacement and acceleration of 0.014" and 0.68g for Test Run 11 and 0.011" and 0.47g for Test Run 21.

3.4 Summary of Calculated Response

A bar graph showing the range of strengths calculated using the static methods is given in Figure 3.18. Governing failure modes for the first-story walls of S1 and S2 are summarized in Table 3.3. Three of the static analysis methods used (UBC, UCBC, and finite element method) produced fairly consistent base shear estimates for S1 while the other two methods were either much higher (FEMA 178) or much lower (MSJC). The UBC and finite element methods both used the same allowable tensile stress and used the same inverted triangular force distribution. Although the base shear estimates were agreeable, 5.2 kips versus 4.8 kips, the UBC estimate was limited by tensile failure in the window wall while the finite element method estimate was limited by tensile failure in the door wall. The UCBC estimate indicated that the window wall was shear critical, but at a lower total base shear of 3.6 kips. Note that the UCBC and the FEMA 178 analyses used a totally different methodology than the other three static analyses. The high strength determined using FEMA 178, 15.2 kips, was due to the fact that it was based on ultimate strength while the other methods assumed working stress. The low value from the MSJC code, 2.4 kips, was attributable to neglecting the tensile capacity of masonry during in-plane flexure. Both of these two methods indicated that the window wall was weaker than the door wall.

A similar pattern was observed in the static analyses for S2 as was seen for S1. The UBC and finite element methods produced comparable results, 3.7 kips and 4.1 kips, while the UCBC

Table 3.3 Failure Modes for Static Analysis Methods of S1 and S2

S1 Analysis Method	Weaker Wall and Failure Mode	Stronger Wall and Failure Mode
UBC	Window - Tension	N.A.*
MSJC	Window - Tension	N.A.
UCBC	Window - Shear	Door - Rocking
FEMA 178	Window - Rocking	Door - Rocking
Finite Element Model	Door - Tension	N.A.
S2 Analysis Method		
UBC	Door - Tension	N.A.
MSJC	Door - Tension	N.A.
UCBC	Door - Rocking	Window - Shear
FEMA 178	Door - Rocking	Window - Rocking
Finite Element Model	Door - Tension	N.A.

*Not applicable.

Table 3.4 Summary of Results from Dynamic Analysis Models

Dynamic Model	S1 Result	S2 Result
	Natural Frequencies	Natural Frequencies
Equivalent Frame Analysis (rigid diaphragm)	44 Hz	47 Hz
Finite Element Model (rigid diaphragm)	35 Hz	34 Hz
MDOF w/ Flex. Diaphragm	11.8, 11.9, 80.2, 87.8 Hz	11.7, 11.9, 52.2, 118.6 Hz
Finite Element Model (flexible diaphragm)	21.5 Hz	20.6 Hz
	Acceleration, Displacement Simulation of Test Run 11	Acceleration, Displacement Simulation of Test Run 21
MDOF w/ Flex. Diaphragm (2nd Level Diaphragm)	0.45g, 0.064"	0.62g, 0.075"
Response Spectrum Analysis	0.68g, 0.014"	0.47g, 0.011"

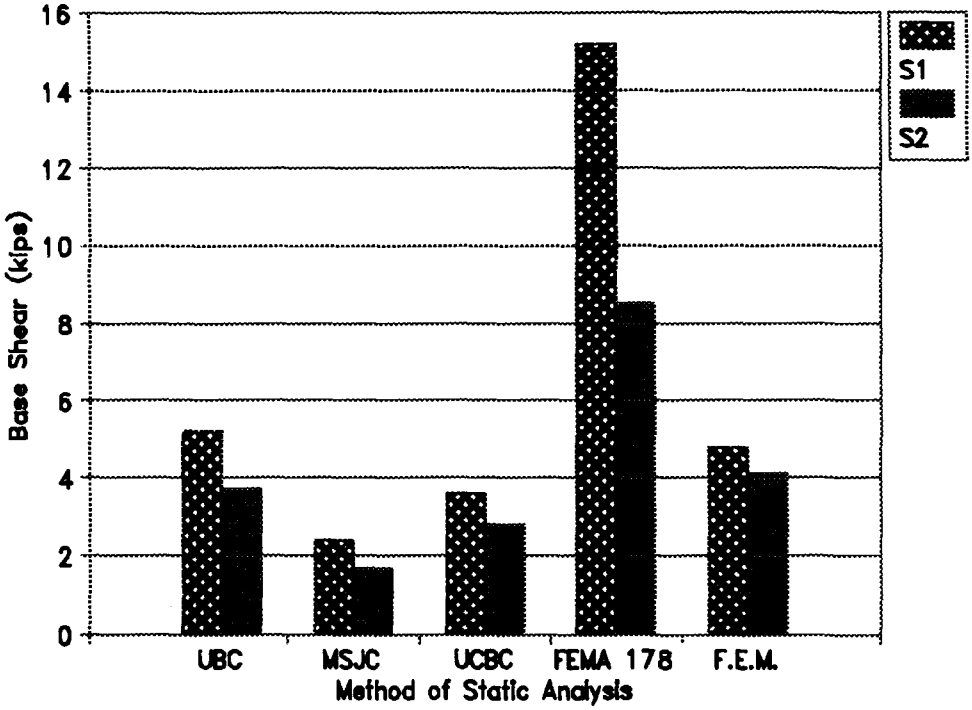

Figure 3.18 Comparison of Calculated Base Shears

was slightly lower at 2.8 kips. The ultimate capacity from the FEMA 178 analysis was much higher at 8.5 kips and the MSJC value, with no allowable tensile stress, was much lower at 1.7 kips. Unlike for S1, for S2 all five methods indicated that the door wall was weaker than the window wall.

For S1, the only method which determined that the window wall was stronger than the door wall was the only method that included the out-of-plane walls. The addition of the flanges to the exterior window piers may have strengthened these piers enough to cause the exterior door pier to exceed the allowable tensile stress first. The finite element method also produced the largest allowable shear for S2. The attached out-of-plane walls helped bear the vertical stresses in the exterior door piers, thus enabling higher forces to be resisted. Flange effects on the strengths of rocking piers will be discussed in Section 6.3.6.

A summary of the pertinent results from the dynamic analyses is presented in Table 3.4. Results from the different dynamic methods used to predict the natural frequencies of S1 and S2 are varied, but much of the disagreement can be explained by variations in the models. The finite element model's rigid diaphragm frequencies, 35 Hz and 34 Hz, are likely to be lower than those from Sarsan, 44 Hz and 47 Hz, since substantially more elements were used and there were no "rigid" joint zones. The natural frequencies computed for the MDOF model with flexible diaphragms, 11.8 Hz and 11.7 Hz, are probably best thought of as isolated frequencies of the floor systems since the first-mode eigenvectors indicated little participation of the walls. The lack of the stiffening effect of the out-of-plane walls on the floor-system DOFs partially accounts for the fact they are lower than the finite element model frequencies, 21.5 Hz and 20.6 Hz. Estimates of acceleration and displacement should be treated with caution as both methods used, time-step integration and spectral analysis, were sensitive to input parameters. Results from the time-step integration varied with the level of damping and the time step used while the spectral analysis was extremely sensitive to frequency and damping (see Section 5.2.1). As an example of this sensitivity, note that the spectral-based estimates of peak displacement, 0.014" and 0.011", are much lower than the time-step integration estimates, 0.064" and 0.075". The difference in

displacements is related to the difference in frequencies of the two models. Spectral displacements generally increase with decreasing frequency in Figures 3.16 and 3.17.

Based on the results presented in the previous sections a few general predictions can be made regarding the expected behavior of S1 and S2 during their dynamic tests.

1) Flexural tension is likely to be the primary failure experienced by most or all of the piers. Based on this, horizontal cracks should appear along the bases of the door and window piers. Due to the weak joint between courses 2 and 3 in S2, (see Section 2.8.8) base cracking should occur here.

2) Once flexural tension cracking does commence, a rocking-controlled behavior should dominate the response for both buildings.

3) The first natural frequencies of the buildings should fall between 11 and 22 Hz while the diaphragms should resonate near 9 Hz.

4) Peak accelerations of the second-level diaphragm are likely to range between 0.45 and 0.62g during the first test runs while maximum first-level drifts are expected to fall between 0.001% and 0.012%.

The static and dynamic methods described in the previous sections were reviewed to illustrate the variations inherent among commonly-used analysis methods. The calculations were performed to determine a range of values, strengths and frequencies, any one of which might be assigned to the test structures by an engineer. No one particular method is preferred or endorsed over the others as all have their limitations. As will be seen in Section 4, the experimental results were quite different than those presented in this Section.

SECTION 4 MEASURED DYNAMIC RESPONSE

4.1 Overview

This section will discuss the dynamic behavior of test structures S1 and S2 observed and recorded through a total of nine dynamic test runs and ten free vibration tests. Visual observations made, both through eyewitnesses and recording devices, will be described, followed by a detailed account of the recorded acceleration and displacement histories. Of the data channels collected, sixteen are used to describe the dynamic behavior of S1 and S2 in this section, as several channels were redundant, while others were used to monitor the performance of the experimental setup. These sixteen data channels, collected during each test run, will serve as the foundation for the analyses reviewed in Sections 4.3-4.9.

Estimates of the cracking shears and cracking drifts are made and are compared with those determined in Section 3 using conventional analysis methods. The force-displacement relationships are examined to verify the behaviors observed. Shifts in the natural frequencies of S1 and S2 are charted using both dynamic test run and free vibration data. The deflected shapes of the two test structures are investigated to determine the effects of cracking. Peak accelerations recorded during the test runs are examined to compare with full-size structures and to determine the effects of cracking on structural amplifications of base motions. Force distributions between the two floor levels of S1 and S2 will be examined. Lastly, horizontal displacements attributable to pier rocking will be investigated for two of the piers in the S2 door wall. Response spectra, in so much as spectral analysis is a form of modeling, will be discussed in Section 5.

4.2 Visually-Observed Response of S1 and S2

During the testing of S1 and S2, notes were made on the visually-observed behavior of the test structures. Notes on the initiation and development of cracking, residual deflections, and pier rocking were made. Cracks from each test run were marked on the test structures with different colored

marker pens so the progression could be analyzed later. Video cameras were used to record the action during the test runs and photographs were taken in between test runs.

4.2.1 Test Structure S1

The final crack patterns for S1 are shown in Figures 4.1-4.4. Prior to testing, a small crack (five brick lengths) was noticed near the bottom right of the east out-of-plane wall (Figure 4.3). Otherwise, Test Runs 11 and 12 produced no visible damage to S1.

Test Run 13 produced a small crack near the bottom right of the window wall which extended slightly into the east out-of-plane wall (Figures 4.2 and 4.3). In addition, the bottom left corner of the window wall and the entire west out-of-plane wall debonded from the concrete footing (Figures 4.2 and 4.4).

The greatest amount of cracking occurred during Test Run 14. All three, first-story, door-wall piers fully cracked across their bases and tops (Figure 4.1). Similar (horizontal) cracks appeared across some of the first-story, window-wall piers (Figure 4.2). A stair-stepped crack formed below the center, first-story, window and the west out-of-plane wall cracked full length just below the first-story beam connections (Figures 4.2 and 4.4). The two cracks near the bottom of the east out-of-plane wall were linked by a new crack during Test Run 14 (Figure 4.3).

During Test Run 15, further cracking occurred near both the bottom corners of the window wall, including cracking through bricks and spalling (Figure 4.2). These cracks extended into the east and west out-of-plane walls (Figures 4.3 and 4.4) The east out-of-plane wall suffered two additional full-length cracks (Figure 4.3). The left end of the door wall cracked again where the east out-of-plane wall appeared to ram into it (Figure 4.1). A second video camera was used to tape the left, first-story, door-wall pier. During Test Run 15, this pier could clearly be seen to be rocking. The central door-wall pier appeared not to rock, but rather to slide relative to the upper portion of the wall. The two outer, first-story, window-wall piers also rocked, but not as distinctly because cracks were not horizontal across the entire pier. During Test Run 15, the entire top portion of S1 appeared to be fixed in space as the earthquake simulator and the first-story piers travelled back and forth below.

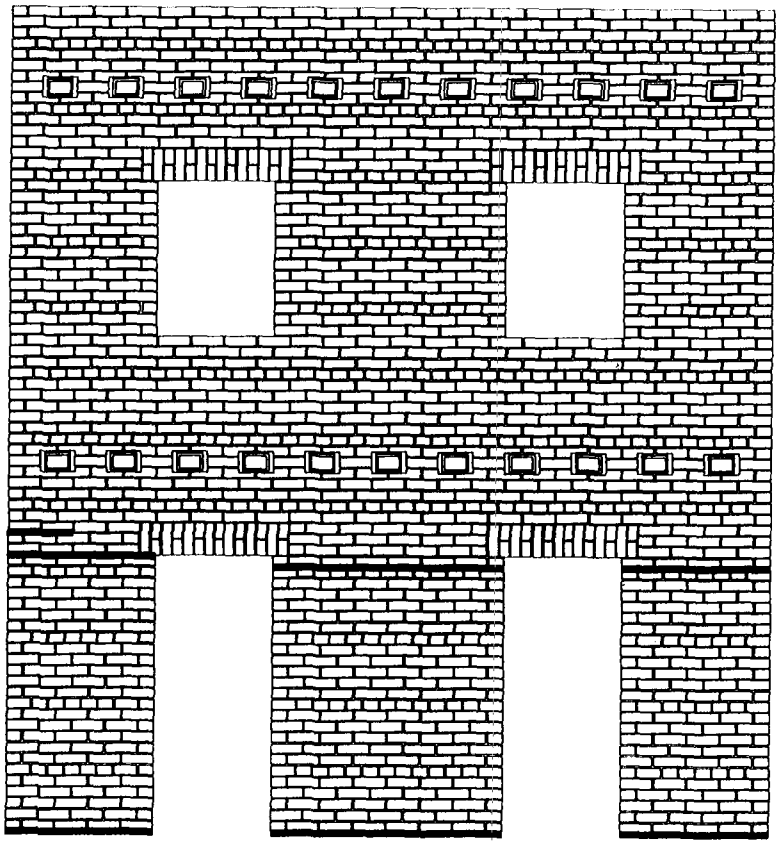

Figure 4.1 Final Crack Pattern of S1 Door-wall

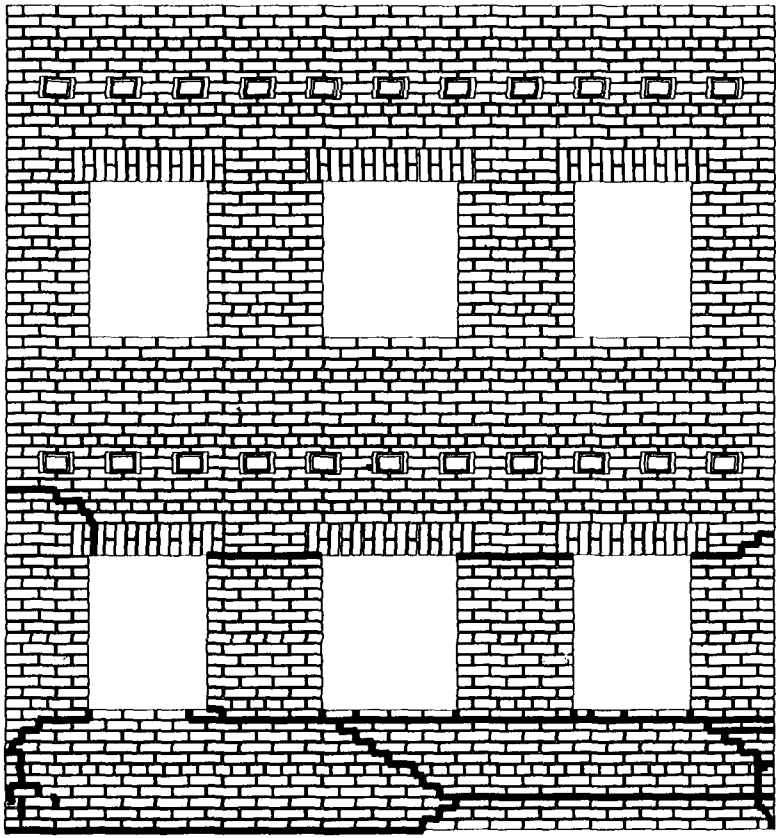

Figure 4.2 Final Crack Pattern of S1 Window-wall

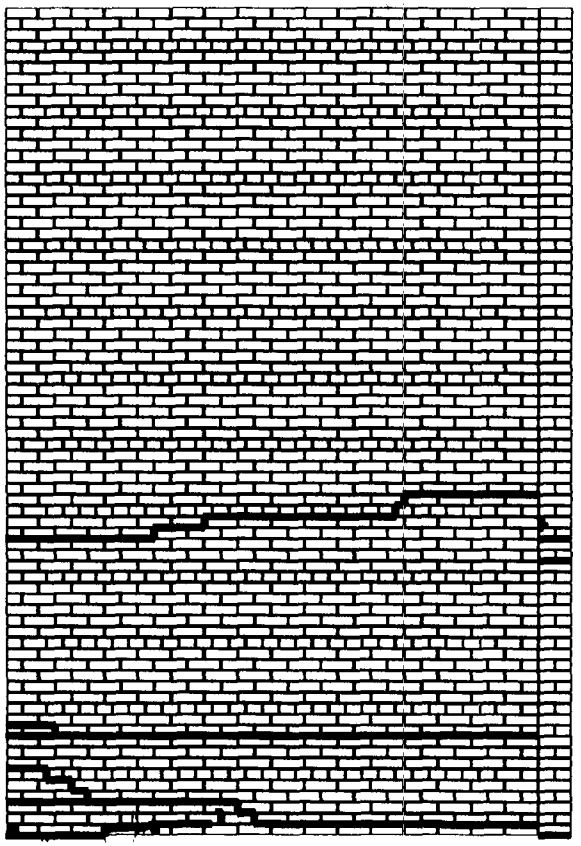

Figure 4.3 Final Crack Pattern of S1 East Out-of-plane Wall

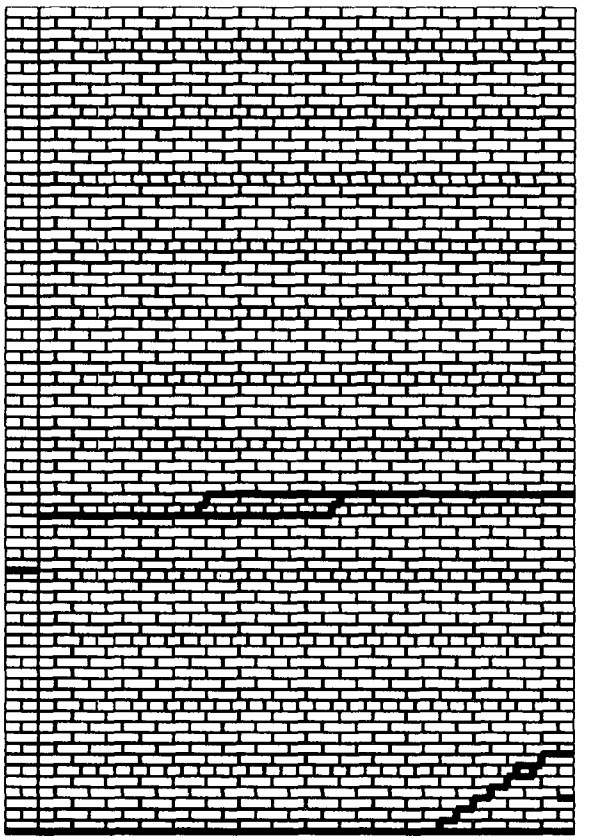

Figure 4.4 Final Crack Pattern of S1 West Out-of-plane Wall

After Test Run 15, both outer, first-story, window-wall piers (and the portions of the out-of-plane walls) had moved outward approximately $^1/_3$".

4.2.2 Test Structure S2

The final crack patterns for S2 are shown in Figures 4.5-4.8. Test Run 21 produced no visible damage to S2.

The method used to construct S2, (see Section 2.8.8) left a relatively weak joint between the second and third courses. During Test Run 22, all four walls fully cracked along this joint (Figures 4.5-4.8). In addition, horizontal cracks formed across the tops of the four, first-story, door-wall piers and spread into the out-of-plane walls (Figures 4.5, 4.7, and 4.8).

After Test Run 23, the out-of-plane walls had full length cracks emanating from those that had begun in Test Run 22 (Figures 4.7 and 4.8). Cracks continued to propagate in the top of the left, first-story, door-wall pier (Figure 4.5). No additional cracking occurred in the window wall during Test Run 23. The upper portion of S2 (including the entire window wall) moved slightly in the direction of the door wall. A video camera trained on the lower right portion of the door wall captured the rigid-body pier-rocking behavior for both the inner and outer piers during Test Run 23.

Test Run 24 produced no additional cracking in S2. The upper portion of the structure continued moving in the direction of the door wall. After Test Run 24, the first-story, door-wall piers were visibly out of plumb while the window wall had moved nearly 1" toward the door wall. Pier rocking was again observed for both the inner and outer, first-story, door-wall piers.

4.3 Wave Forms

Acceleration and displacement histories were recorded during the nine test runs as described in Section 2.13. The seven displacement and seven acceleration histories from each test run which are discussed in the subsequent sections are plotted versus time in Appendix C. All measurements are plotted with the convention that a positive acceleration from rest would produce a positive displacement of the test structures toward the east. The earthquake simulator acceleration was

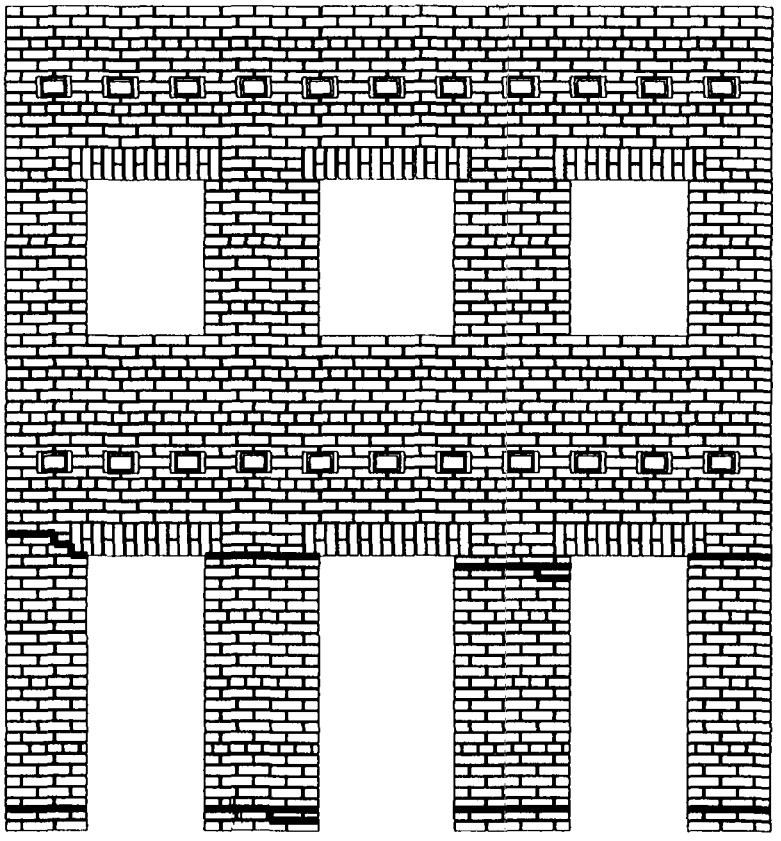

Figure 4.5 Final Crack Pattern of S2 Door-wall

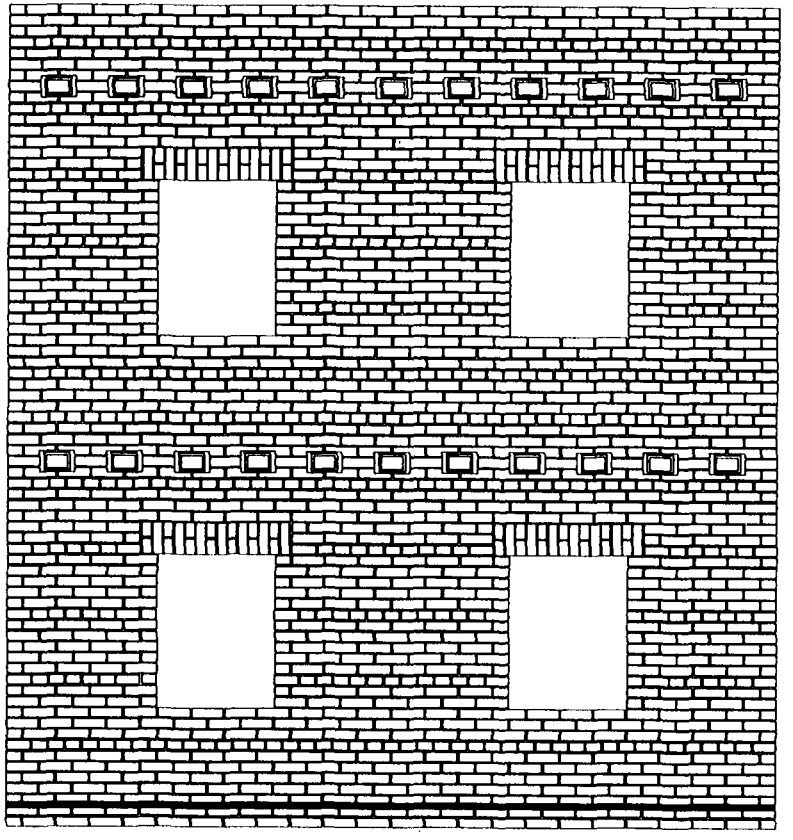

Figure 4.6 Final Crack Pattern of S2 Window-wall

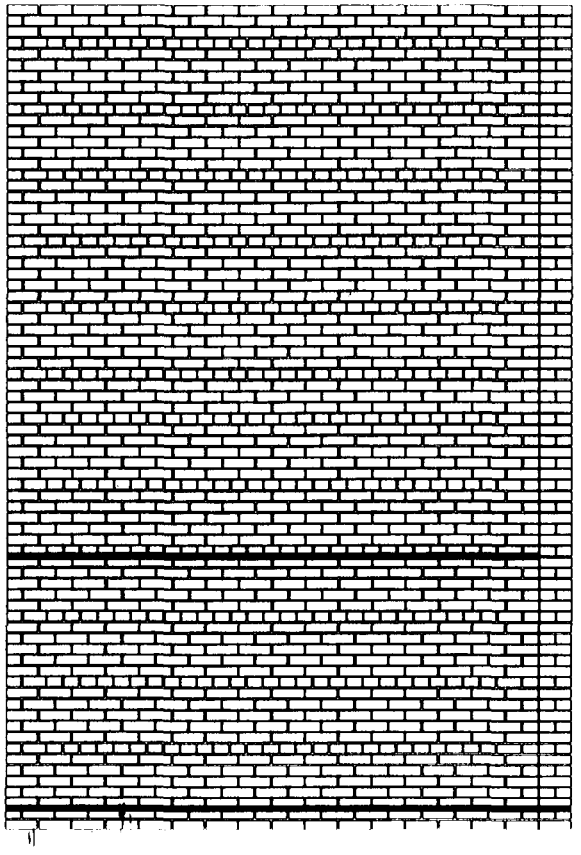

Figure 4.7 Final Crack Pattern of S2 East Out-of-plane Wall

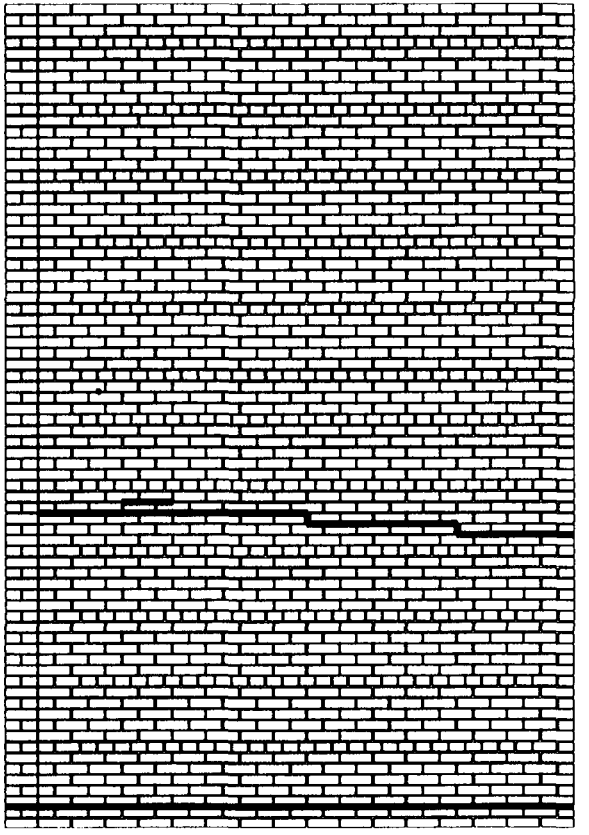

Figure 4.8 Final Crack Pattern of S2 West Out-of-plane Wall

multiplied by negative one to be consistent with the sense of the other accelerations. A sample acceleration history, from the second-level diaphragm, and a sample displacement history, from the second-level door wall, from Test Run 13 are presented in Figures 4.9 and 4.10, respectively. Note that no motion was recorded prior to 2.02 seconds, when the base motion began, but that some motion was recorded after 13.98 seconds even though the base motion had stopped.

Also plotted in Appendix C are dynamic base shear and overturning moment histories. The first- and second-level inertial forces were computed from six acceleration histories (two from each floor level and one from each diaphragm), multiplied by the masses associated with the regions of the structure where the accelerations were measured. The term base shear is used here to represent the sum of the inertial forces. This is the (horizontal) force that must be resisted, regardless of the resistance mechanisms. The term overturning moment is used here to be the sum of the products of the inertial forces and their respective heights. Tributary masses and heights used in the shear and moment calculations are summarized in Table 4.1. The base shear and moment computed for Test Run 13 are plotted in Figures 4.11 and 4.12, respectively, as examples. Note that these two curves have almost identical shapes, which is true for all test runs.

4.3.1 Test Structure S1

The two largest accelerations measured for each channel and the times for each of the peaks, for each test run of S1, are listed in Table 4.2. Note that nearly all of the peaks lie in two narrow time bands, 4.7-4.9 seconds and 7.6-7.9 seconds. Table 4.3 lists the two largest displacement peaks recorded for each LVDT during Test Runs 11-15, along with their occurrence times. Listed in Table 4.4 are the two largest dynamic base shear and overturning moment peaks and their corresponding times for the S1 test runs.

During Test Run 11 measured accelerations and displacements were quite small. Displacements of the door wall only reached 0.004" while displacements of the window wall reached 0.011". Though undamaged, the peak base shear of 3.63 kips was already larger than the MSJC cracking value of 2.4 kips. The maximum calculated second-level diaphragm displacement, 0.064", determined using the MDOF model with flexible diaphragms, was more than twice the measured

Table 4.1 Tributary Masses and Heights used in Base Shear and Moment Calculations

Test Structure Section	Tributary Mass (kips/g)	Height (in)
S1 door wall lower	1.6	42.7
S1 door wall upper	1.2	86.0
S1 window wall lower	1.5	42.7
S1 window wall upper	1.1	86.0
S2 door wall lower	1.5	42.7
S2 door wall upper	1.1	86.0
S2 window wall lower	1.6	42.7
S2 window wall upper	1.2	86.0
1st level diaphragm	5.0	42.7
2nd level diaphragm	5.0	86.0

Table 4.2 Largest Two Acceleration Peaks and Occurrence Times for S1

Channel	Test Run 11		Test Run 12		Test Run 13		Test Run 14		Test Run 15	
	Time (sec)	A (g)	Time (sec)	A (g)	Time (sec)	A (g)	Time (sec)	A (g)	Time (sec)	A (g)
Base	4.719	-0.153	4.752	0.436	4.756	0.641	4.709	-1.085	4.712	-1.781
	7.761	0.130	4.709	-0.408	4.706	-0.630	7.687	0.937	4.756	1.515
1st level door	7.674	0.161	4.749	0.460	7.646	-0.617	8.118	1.419	7.723	1.646
	4.752	0.157	4.706	-0.374	4.299	-0.615	8.324	1.364	5.686	1.583
2nd level door	7.674	0.190	4.749	0.528	7.646	-0.781	8.217	-1.937	9.129	-1.709
	4.752	0.183	4.731	-0.458	7.449	-0.761	7.609	-1.906	8.229	-1.669
1st level window	4.756	0.168	4.752	0.484	4.719	-0.658	7.699	0.957	5.714	1.715
	9.123	-0.138	4.299	-0.388	4.299	-0.641	4.764	0.939	4.962	1.512
2nd level window	4.756	0.187	4.728	-0.468	7.603	-0.735	7.702	1.223	5.714	1.426
	9.123	-0.146	9.113	-0.457	9.117	-0.709	4.302	-1.071	4.965	1.360
1st level diaphragm	4.799	0.352	4.796	1.043	4.796	1.817	4.796	3.031	4.697	1.576
	4.857	-0.324	9.138	-0.880	4.737	-1.637	4.743	-2.094	9.080	1.126
2nd level diaphragm	4.756	-0.373	9.144	-0.943	4.789	1.820	4.882	-2.435	7.474	-1.201
	4.931	0.350	7.517	0.928	4.879	-1.776	4.950	2.128	7.563	1.175

Table 4.3 Largest Two Displacement Peaks and Occurrence Times for S1

Channel	Test Run 11		Test Run 12		Test Run 13		Test Run 14		Test Run 15	
	Time (sec)	D (in)	Time (sec)	D (in)	Time (sec)	D (in)	Time (sec)	D (in)	Time (sec)	D (in)
Base	9.126	-0.018	7.616	-0.055	9.123	-0.092	9.123	-0.144	9.126	-0.210
	Various	±0.017	9.123	-0.055	7.619	-0.091	7.619	-0.140	7.619	-0.206
1st level door	4.913	0.004	4.746	-0.009	7.708	0.023	7.674	-0.356	4.712	0.437
	Various	±0.003	4.802	0.008	4.793	0.022	8.278	-0.327	4.580	-0.330
2nd level door	Various	±0.004	4.805	0.013	7.711	0.043	7.674	-0.382	4.709	0.474
			7.520	0.013	Various	0.033	8.275	-0.313	9.098	0.318
1st level window	4.796	0.006	7.523	0.016	7.727	0.031	8.257	-0.136	7.680	-0.394
	4.886	-0.006	7.699	0.015	4.808	0.030	8.053	-0.134	9.191	-0.365
2nd level window	4.799	0.011	7.526	0.032	7.714	0.063	7.665	-0.225	7.687	-0.470
	6.426	0.011	8.284	0.028	4.793	0.049	8.263	-0.204	9.178	-0.438
1st level diaphragm	4.796	0.019	7.690	0.033	7.702	0.061	7.665	-0.239	4.706	0.454
	4.913	0.018	9.178	0.033	9.184	0.052	8.170	-0.231	8.183	0.389
2nd level diaphragm	9.187	0.029	4.734	-0.066	7.702	0.091		No data	4.712	0.500
	4.746	-0.027	5.748	-0.048	9.120	-0.076		No data	7.683	-0.446

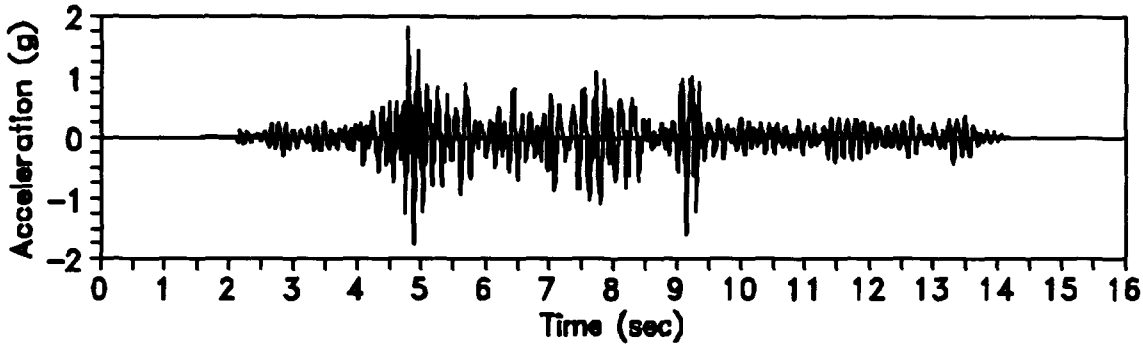

Figure 4.9 Measured Second-level Diaphragm Acceleration from Test Run 13

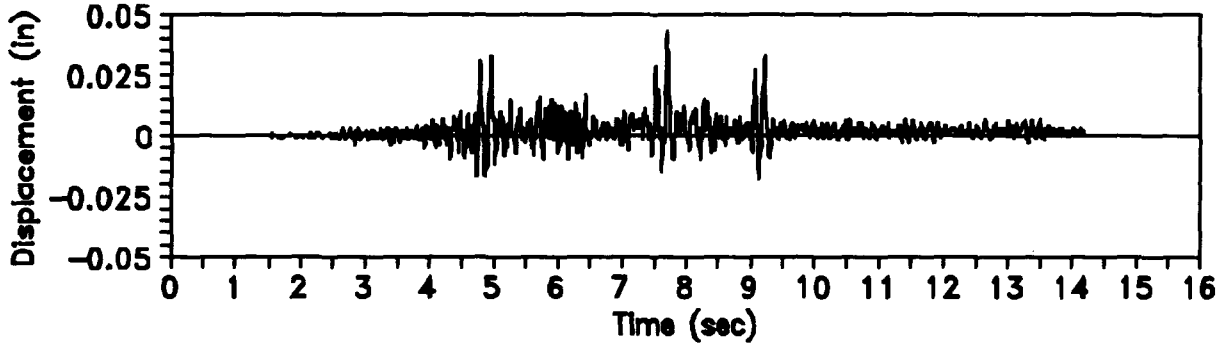

Figure 4.10 Measured Second-level Door-wall Displacement from Test Run 13

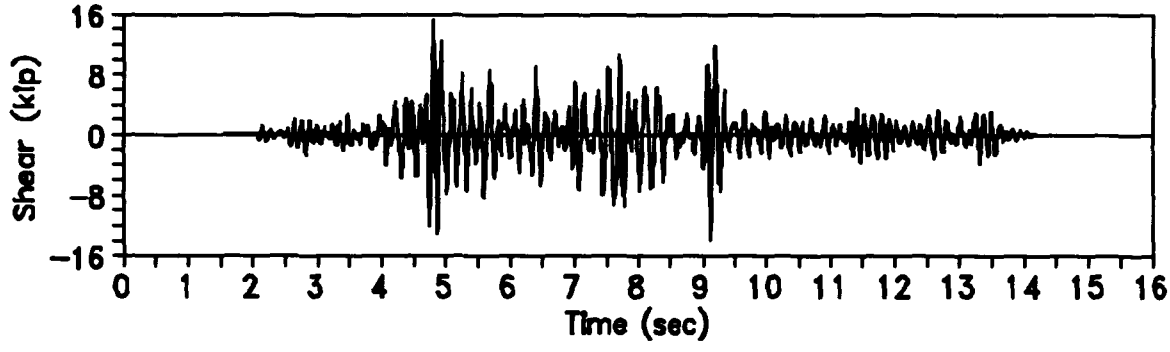

Figure 4.11 Measured Base Shear from Test Run 13

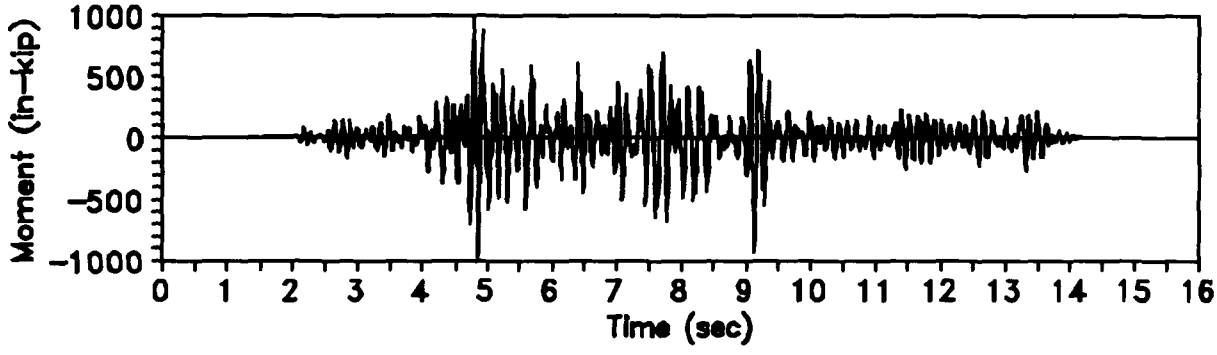

Figure 4.12 Measured Overturning Moment from Test Run 13

value of 0.029". The peak acceleration from the same model, 0.45g, was within 20% of the measured value, 0.37g.

S1 remained elastic during Test Run 12. The base motion was tripled, as were most of the measured accelerations and displacements. Both diaphragms had peak accelerations of approximately 1.0g. The maximum base shear measured, 8.97 kips, was almost twice as large as all of the cracking values calculated in Section 3, yet the structure remained undamaged.

The behavior of S1 during Test Run 13 was nearly linear relative to the prior two test runs. The peak base acceleration was 1.5 times greater than in Test Run 12 while the peak base displacement was almost doubled. Most measurements followed these increases, except the door wall, which tripled in displacement. Peak wall accelerations ranged between 0.74-0.78g. The peak base shear, 15.22 kips, was nearly three times the largest cracking shear, 5.2 kips, from Section 3.

Substantial cracking was observed in the first story during Test Run 14. As a result of this, measured displacements increased by a factor of 4 for the window wall and by a factor of 10 for the door wall. The base motion was only increased by a factor of 1.6. Diaphragm and window-wall accelerations followed this level of increase (1.6), but the door-wall accelerations increased by 2.3-2.5 times. The peak base shear, 17.97 kips, was 18% larger than the ultimate capacity determined, 15.2 kips, using the FEMA 178 analysis.

Two notes should be made regarding the displacements from Test Run 14. First, the second-floor diaphragm displacement was not recorded during this test run due to an instrument malfunction. Second, some of the displacement histories have offsets at the end because portions of the cracked test structure permanently shifted during the test run. These offsets were not removed prior to Test Run 15. An estimated offset was used for the second-floor diaphragm displacement in Test Run 15.

In Test Run 15, the base motion was increased 1.5 times over that used in Test Run 14. The peak diaphragm accelerations, however, decreased by 50%. Three of the wall accelerations increased while one decreased. Continued cracking in the first-story window wall was evidenced by these displacements nearly tripling. Door-wall displacements increased by only 20% as all three piers were fully cracked in the previous test run. Although the peak diaphragm accelerations were halved, increased wall accelerations kept the peak base shear high at 12.43 kips.

The peak base shears and overturning moments from each S1 test run are plotted against the average of the peak, first-level, wall drifts, i.e., $(\Delta_{door,max}/h_1+\Delta_{window,max}/h_1)/2$, in Figure 4.13. The peak shear values were normalized by 15.4 kips, the sum of the tributary weights, while the peak moment values were normalized by 1324 in-kips, the product of 15.4 kips and the height, 86.0". Observed damage states are noted in the figure. The most salient feature of the curves (Figure 4.13) was that the resistance values remained high well after cracking occurred. Also important was that the peak drift for Test Run 15 was over 10 times the drift for Test Run 13 while the shear value diminished only 20% between Test Runs 13 and 15.

It should be noted that most of the wave forms used in the analysis of S1 were filtered to remove unwanted noise. The filtering is described in detail in Appendix D.

4.3.2 Test Structure S2

The two largest acceleration peaks for each channel, measured during Test Runs 21-24, and the times for each of the peaks are listed in Table 4.5. Note again that most of the peaks lie in two narrow time bands, 4.7-4.9 seconds and 7.6-7.9 seconds. Table 4.6 lists the two largest displacement peaks recorded during the S2 test runs, for each LVDT, along with their occurrence times. The two largest dynamic base shear and overturning moment peaks and their corresponding times, for each test run of S2, are listed in Table 4.7.

Test Run 21 was the only elastic test run for S2. With a peak base acceleration of 0.20g, the second level diaphragm reached a peak of 0.79g. Door-wall displacements and accelerations were approximately 2-3 times those of the window wall. The peak base shear, 7.61 kips, was over 80% higher than the largest calculated cracking shear, 4.1 kips, from Section 3, and was already almost as large as the calculated ultimate shear, 8.5 kips.

Most of the cracks in S2 formed during Test Run 22. Although the base motion was 2.5-3 times that of Test Run 21, peak door-wall displacements were 4-5 times larger. Wall accelerations followed the increase of the base motion while diaphragm accelerations only increased by 40-50%. As a result of the damage to the first story, the base shear only increased 30% to 9.84 kips.

Table 4.4 Base Shear and Moment Peaks and Occurrence Times for S1

Test Run	Time (sec)	Base Shear (kips)	Time (sec)	Base Moment (in-kips)
11	4.857	-3.63	9.132	-229.7
	9.129	-3.50	4.857	-228.7
12	9.141	-8.97	9.141	-582.4
	7.517	7.90	7.517	553.7
13	4.793	15.22	4.789	997.4
	9.144	-13.78	4.876	-971.3
14	4.793	17.97	4.882	-1229.1
	4.822	-16.34	4.947	1139.1
15	4.697	12.43	7.563	778.9
	7.563	11.33	4.697	720.4

Table 4.5 Largest Two Acceleration Peaks and Occurrence Times for S2

Channel	Test Run 21		Test Run 22		Test Run 23		Test Run 24	
	Time (sec)	A (g)	Time (sec)	A (g)	Time (sec)	A (g)	Time (sec)	A (g)
Base	4.891	0.200	4.703	-0.522	4.752	0.693	4.706	-1.094
	4.811	-0.195	4.756	0.503	4.715	-0.669	4.765	1.030
1st level door	4.842	-0.535	4.777	1.091	4.552	-1.104	7.958	0.937
	4.774	0.326	4.759	-1.077	4.777	0.951	7.767	0.852
2nd level door	4.845	-0.657	4.777	1.459	7.680	-1.328	7.958	1.079
	4.789	0.491	4.762	-1.377	4.811	1.259	7.489	-1.025
1st level window	4.836	-0.253	4.715	-0.573	7.739	0.977	7.961	1.226
	4.777	0.227	4.826	-0.526	7.542	0.969	7.394	1.198
2nd level window	4.836	-0.385	4.826	-0.959	4.829	-1.404	4.780	1.674
	4.777	0.327	4.715	-0.927	7.739	1.346	7.964	1.248
1st level diaphragm	4.829	-0.647	4.740	-0.918	5.696	1.030	7.939	1.139
	4.891	0.488	4.799	0.848	5.225	0.988	7.187	1.001
2nd level diaphragm	4.836	-0.792	4.796	1.183	4.793	1.378	7.369	1.021
	4.777	0.780	4.746	-1.055	4.481	1.044	4.808	0.986

Table 4.6 Largest Two Displacement Peaks and Occurrence Times for S2

Channel	Test Run 21		Test Run 22		Test Run 23		Test Run 24	
	Time (sec)	D (in)	Time (sec)	D (in)	Time (sec)	D (in)	Time (sec)	D (in)
Base	9.123	-0.019	9.123	-0.057	7.619	-0.089	9.126	-0.145
	Various	±0.017	7.619	-0.056	9.123	-0.089	7.619	-0.140
1st level door	4.839	-0.025	9.138	-0.121	7.668	-0.242	9.175	-0.379
	Various	±0.016	9.212	0.101	7.563	0.240	7.979	0.309
2nd level door	4.839	-0.030	9.138	-0.129	7.563	0.275	9.178	-0.440
	4.885	0.024	4.805	0.119	7.674	-0.259	7.967	0.349
1st level window	4.897	0.008	9.215	0.042	7.742	0.110	7.970	0.178
	4.833	-0.007	Various	±0.030	8.352	0.108	8.177	0.166
2nd level window	4.894	0.014	9.215	0.075	7.742	0.168	7.967	0.253
	4.833	-0.014	4.814	0.060	8.352	0.162	8.177	0.246
1st level diaphragm	4.842	-0.031	9.135	-0.128	8.257	-0.263*	9.181	-0.527*
	4.731	-0.024	8.019	-0.100	7.668	-0.259*	8.075	-0.448*
2nd level diaphragm	4.833	-0.063	9.141	-0.137	8.263	-0.287*	9.172	-0.607*
	4.731	-0.043	4.746	-0.122	7.671	-0.279*	9.397	-0.489*

*Values unreliable due to out-of-plane motions.

Table 4.7 Base Shear and Moment Peaks and Occurrence Times for S2

Test Run	Time (sec)	Base Shear (kips)	Time (sec)	Base Moment (in-kips)
21	4.777	7.61	4.777	526.2
	4.836	-7.39	4.836	-516.4
22	4.743	-9.84	4.743	-664.9
	4.799	9.51	4.796	651.8
23	4.793	10.93	4.793	756.2
	5.696	9.82	5.696	595.3
24	7.939	9.40	4.749	-586.2
	5.723	9.16	7.939	571.3

Table 4.8 Measured Natural Frequencies of S1 and S2

	Test Run	Frequency During Test Run (Hz)	Frequency During Free Vibration After Test Run (Hz)
S1			10.0
	11	8.2	10.4
	12	8.2	9.9
	13	6.6	10.1
	14	5.3	9.0
	15	4.0	6.7
S2			12.1
	21	9.8	*
	22	8.2	9.6
	23	6.7	7.4
	24	5.1	5.8

*This free vibration test not performed.

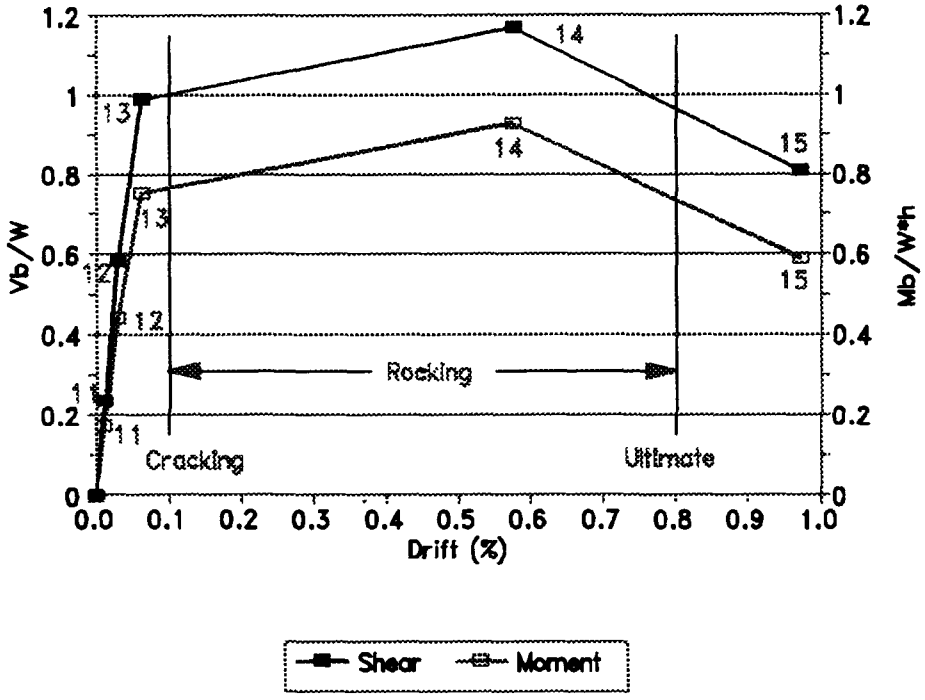

Figure 4.13 Base Shear and Moment Peaks versus First-level Drift for S1

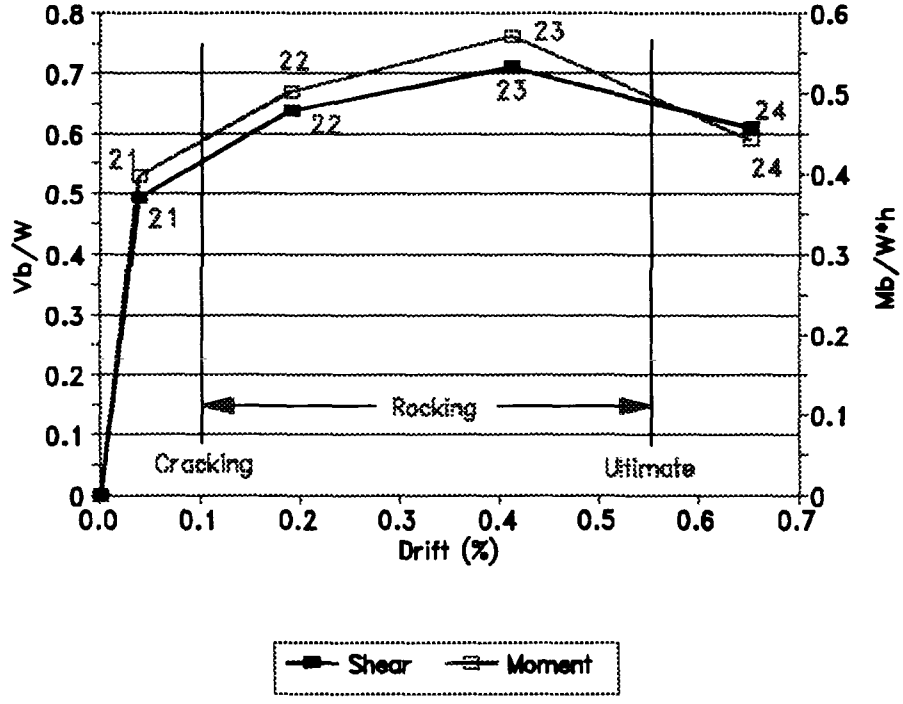

Figure 4.14 Base Shear and Moment Peaks versus First-level Drift for S2

Test Run 23 produced only a nominal increase in peak diaphragm and door-wall accelerations while the mostly undamaged window-wall accelerations continued increasing. Peak door- and window-wall displacements doubled those from Test Run 22. The peak base shear increased slightly to 10.93 kips, 29% higher than the ultimate capacity calculated, 8.5 kips, using the FEMA 178 analysis.

Out-of-plane motions observed during Test Run 23 (and Test Run 24) caused the first- and second-level diaphragm displacement histories to err. The out-of-plane translations were large enough that the LVDT cores became misaligned, producing a constant deviation away from the neutral position. Dead spots in the displacement histories also resulted from this misalignment.

For Test Run 24, the base motion was increased 60% over that of Test Run 23. Peak door- and window-wall displacements also increased by 60%. The peak window-wall accelerations increased by 20%, but the peak door-wall accelerations decreased by 20%. The peak base shear also declined slightly to 9.40 kips. Out-of-plane translations of the test structure continued to corrupt the measured diaphragm displacements.

As for S1, the peak base shear and overturning moments for S2 are plotted against the average of the peak, first-level, wall drifts in Figure 4.14. The shear and moment values were normalized by 15.4 kips and 1324 in-kips, as before. Damage states for S2 are noted in the figure. The ultimate drift for Test Run 24 was approximately 10 times that of Test Run 21 while the peak shear was larger in Test Run 24 than Test Run 21. As was the case for S1, resistance levels remained high, well beyond the point of considerable damage. The fact that the masonry could continue to resist loads after substantial cracking implies a form of ductility, which is contrary to the notion that unreinforced masonry follows a brittle behavior.

4.4 Cracking Strengths and Drifts

In Section 4.3, inertial forces were computed, using floor-level accelerations and tributary masses, and summed to produce a base shear history for the whole structure. Using the assumption that half of the inertial forces from each diaphragm are transferred to each in-plane wall, the base

shear for each shear wall can be computed in a similar way. These shear histories, along with the in-plane wall displacements measured, can be used to estimate the times of cracking, as well as the cracking loads and drifts. Drifts were calculated by dividing the measured first-level displacements by the first-story height.

Since it was known from visual observations that the S1 piers cracked during Test Run 14, the histories from this test run were examined. The base shears for the door and window walls, along with the first-level drifts of the two walls, are plotted versus time in Figure 4.15 and 4.16. First-level drifts were used since no cracking occurred in the second story. An examination of the proportionality between the force and drift in these curves indicated that cracking initiated during the negative half cycle at 4.75 seconds (labeled A). During this half cycle, the drifts were disproportionately large in relation to the forces. The next three half cycles (B, C, and D) showed an increase in drifts with little or no increase in force, indicating that the cracks continued to grow. The largest shear values during the previous test run, for each wall, were -6.9 kips and +7.6 kips. The peak values during the cracking period were -7.8 and +8.4 kips for the door wall and -7.6 and +9.6 kips for the window wall. Based on these values, an estimate of the cracking strengths of the two S1 shear walls would be 7.5 kips. Comparing the wall base shears with the first-level drifts showed that at the initiation of cracking the story drifts were approximately 0.1%.

A similar analysis was conducted using the data from Test Run 22. The door-wall base shear and the first-level drift are plotted against time in Figure 4.17. The S2 window wall did not crack other than between the second and third courses and will not be discussed. By again noting the relationship between force and drift, cracking was determined to have begun during the negative half cycle at 4.50 seconds (labeled A). This confirmed the finding in Section 4.10, which used the vertical LVDTs to determine the onset of cracking. Crack growth continued in the negative direction during half cycles B and D, as drifts increased faster than load. Cracking did not appear to start in the positive direction until half cycle C. Crack growth continued through half cycle E. The largest values of shear computed for the door wall during Test Run 21 were -3.8 and +3.8 kips. During half cycles A and C the peak shears were -4.4 and +4.5 kips, respectively. From these values, an estimate of the

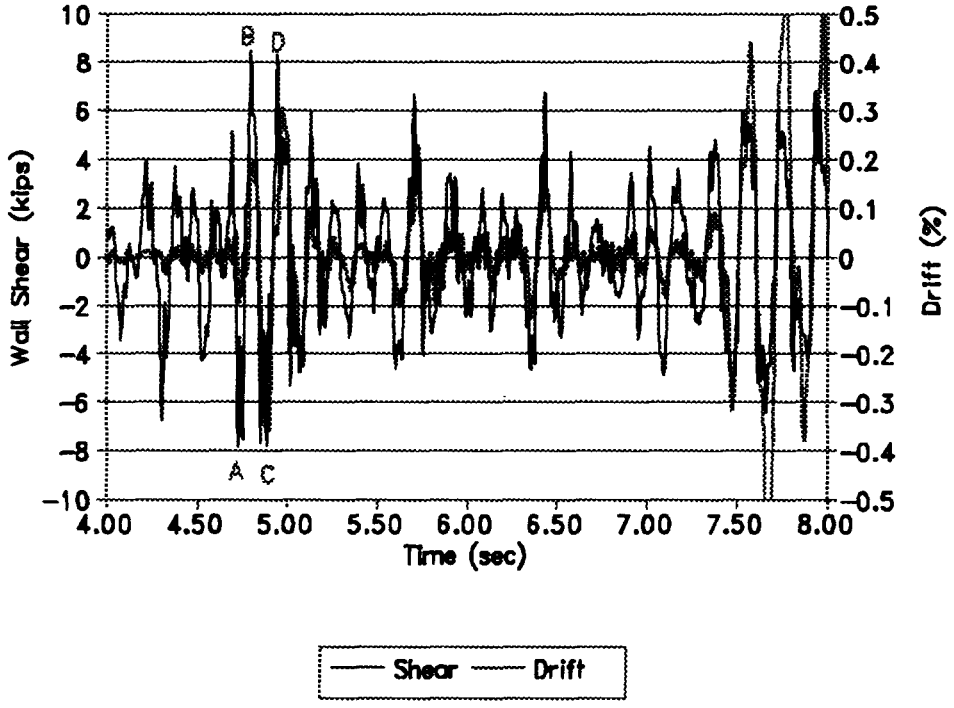

Figure 4.15 Door-wall Shear and First-level Door-wall Drift from Test Run 14

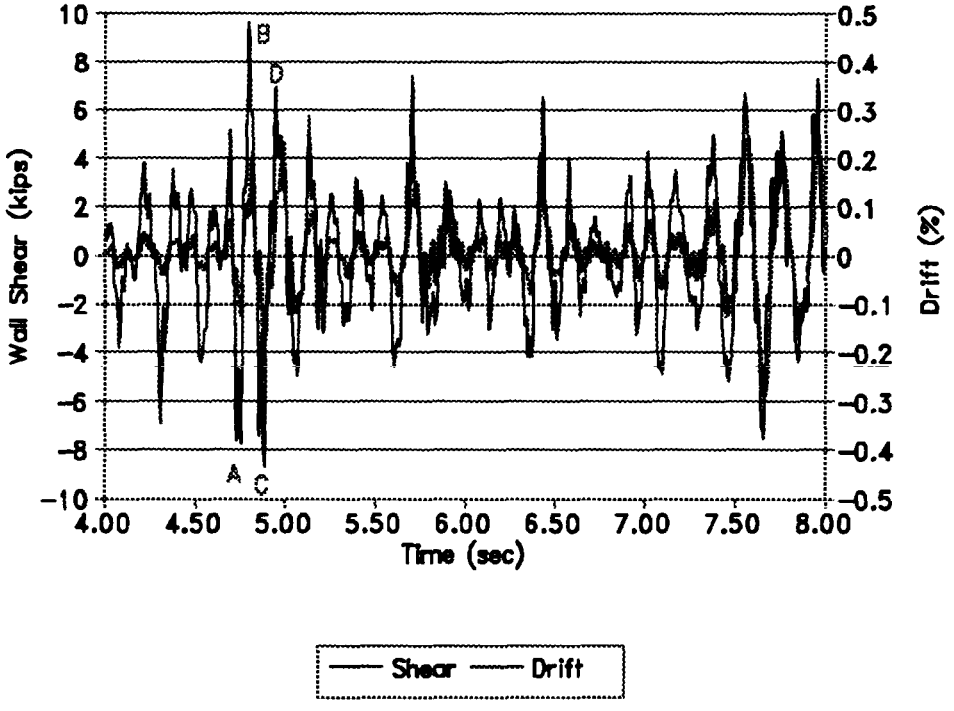

Figure 4.16 Window-wall Shear and First-level Window-wall Drift from Test Run 14

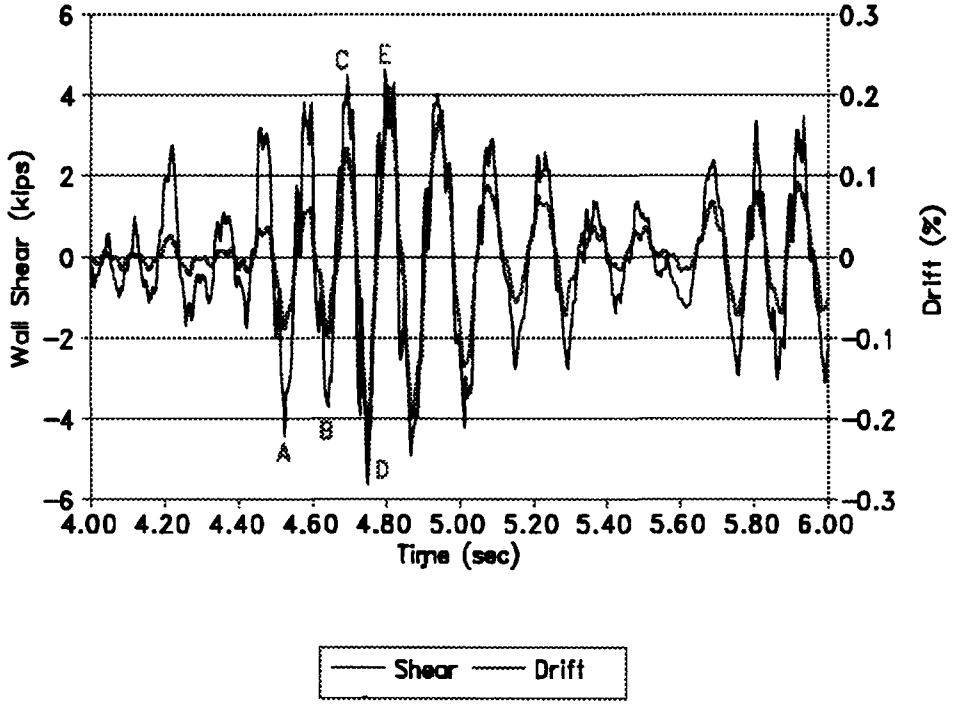

Figure 4.17 Door-wall Shear and First-level Door-wall Drift from Test Run 22

cracking strength of the S2 door wall would be 4.0 kips. The first-level drifts during the initial cracking again were near 0.1%.

4.5 Force-Displacement Relationships

Base shear histories were computed for each wall, door and window, for each test run of S1 and S2. These lateral force histories are plotted versus the measured first-level displacements of the walls in Figures 4.18-4.35 producing what are commonly referred to as hysteresis loops. By examining different aspects of the hysteresis loops, such as the slopes of the curves, the area enclosed by the loops, and the relative portions of linear and nonlinear behavior, many of the visual observations in Section 4.2 were confirmed. Note that different x- and y-scales are used in the figures.

Some of the hysteresis loops for Test Runs 11, 12, and 13, showed a predominantly linear behavior, as the test structure remained undamaged. This linear behavior was seen better in the window wall of S1 (Figures 4.19, 4.21, and 4.23), where larger displacements produced a clearer set of loops. Note that due to the predominance of the diaphragm component in the individual wall shears, both wall shears had similar magnitudes through the test runs.

The cracking experienced by S1 during Test Run 14, was clearly evidenced in the hysteresis loops for Test Runs 14 and 15. The force-displacement curves for both walls (Figures 4.24-4.27) showed a large amount of nonlinear behavior and an increase in the area enclosed by the loops. The almost bilinear nonlinear behavior exhibited, especially by the door wall, was indicative of pier rocking. This bilinear behavior was not as clearly evidenced in the window wall during Test Run 14 because cracks had not entirely developed across the piers. The amount of area enclosed by a hysteresis loop generally indicates a measure of energy dissipation from which an estimate of damping can be determined. For unreinforced masonry, energy dissipation is usually in the form of sliding across cracks, grinding of the mortar joints, and crushing of bricks. Due to the design of the flexible diaphragms (Section 2.3), a measure of structural damping from the hysteresis loops is unreliable since an unknown portion of the damping is attributable to the diaphragms.

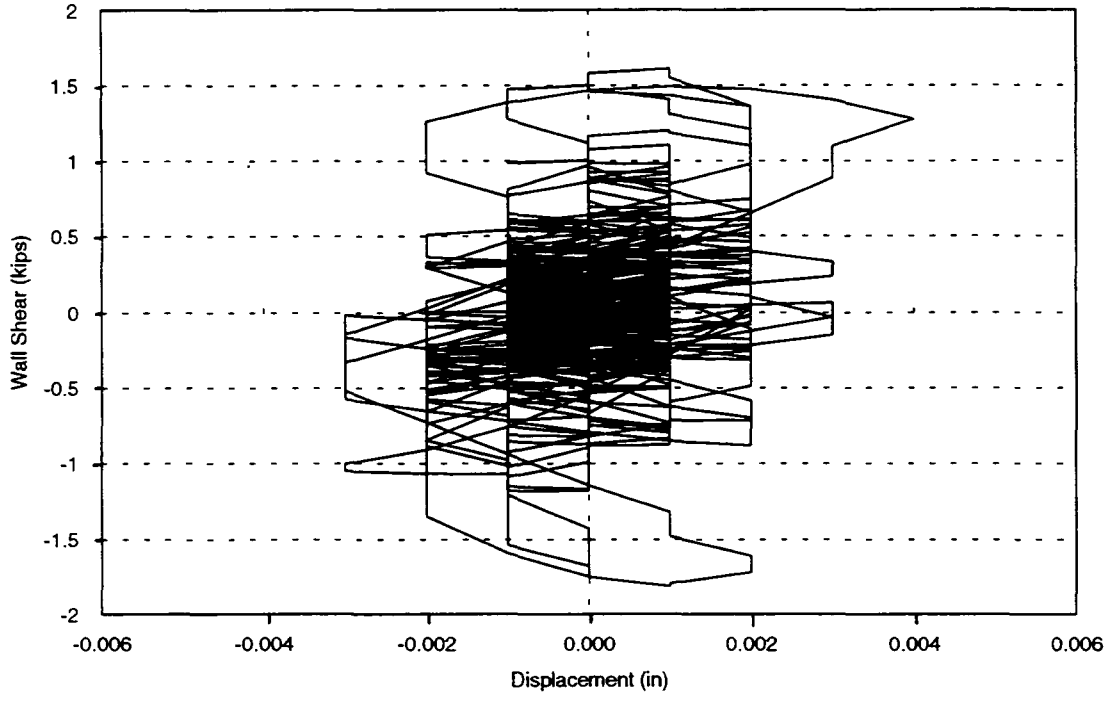

Figure 4.18 Door-wall Shear vs. First-level Door-wall Displacement from Test Run 11

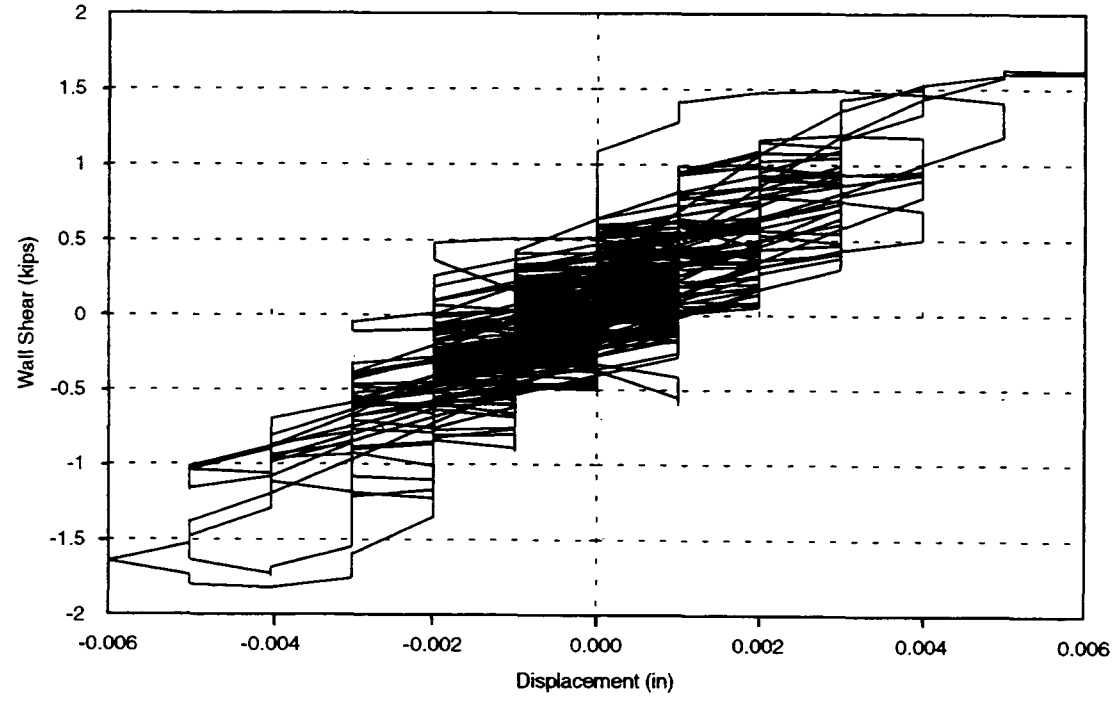

Figure 4.19 Window-wall Shear vs. First-level Window-wall Displacement from Test Run 11

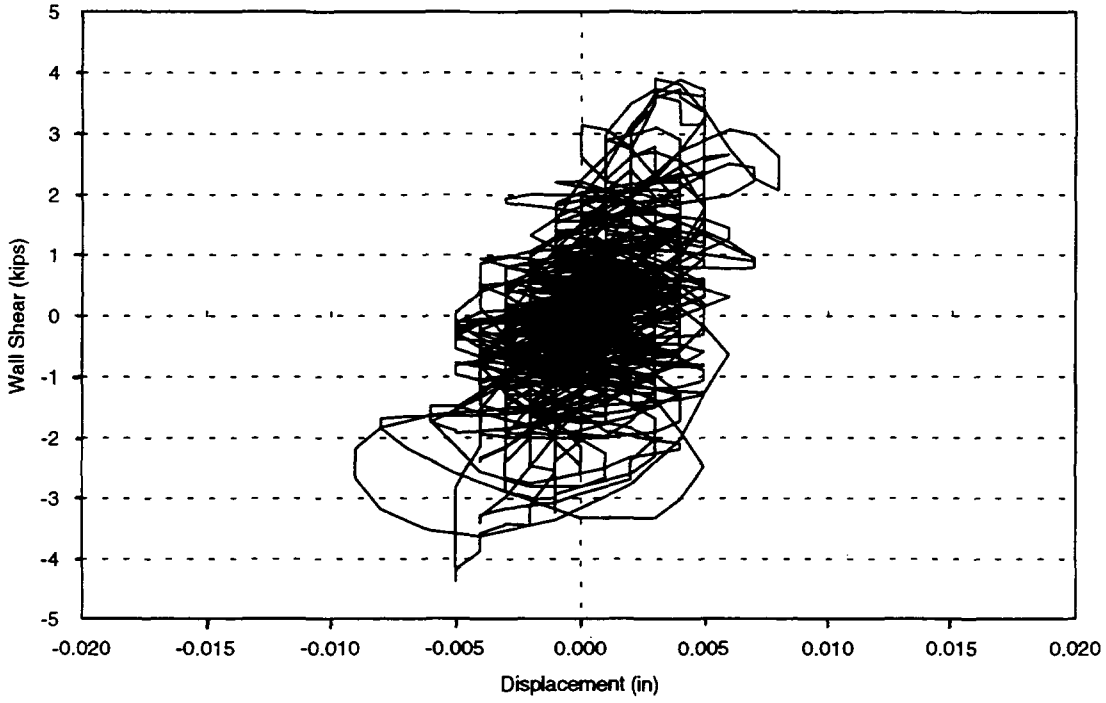

Figure 4.20 Door-wall Shear vs. First-level Door-wall Displacement from Test Run 12

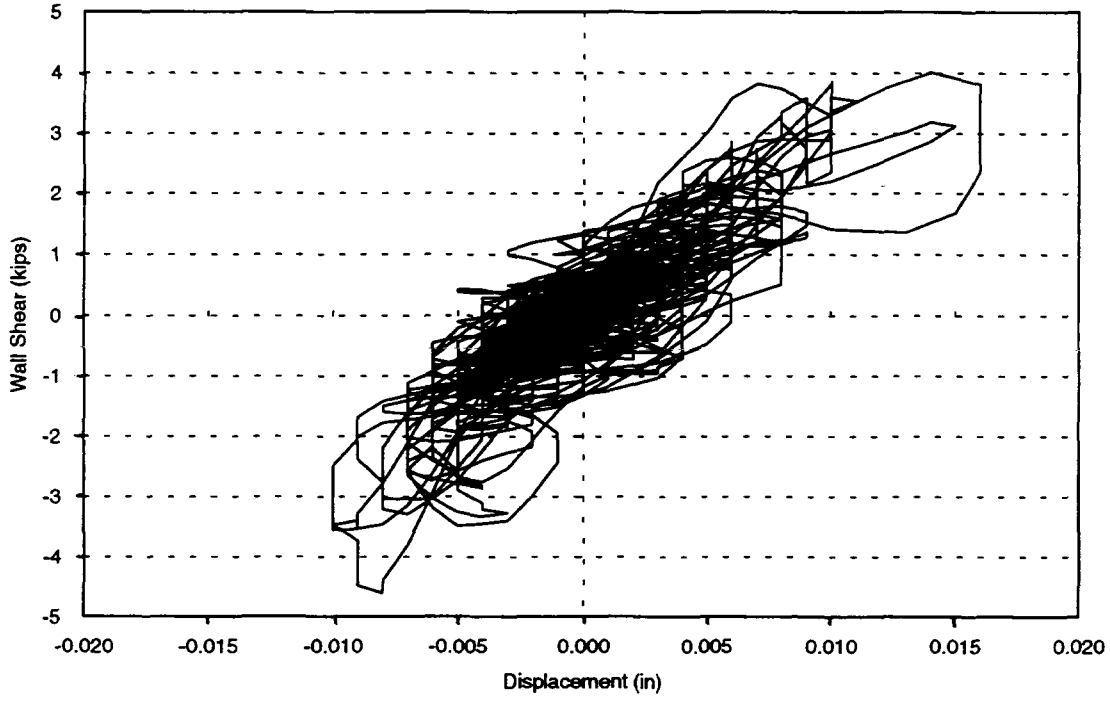

Figure 4.21 Window-wall Shear vs. First-level Window-wall Displacement from Test Run 12

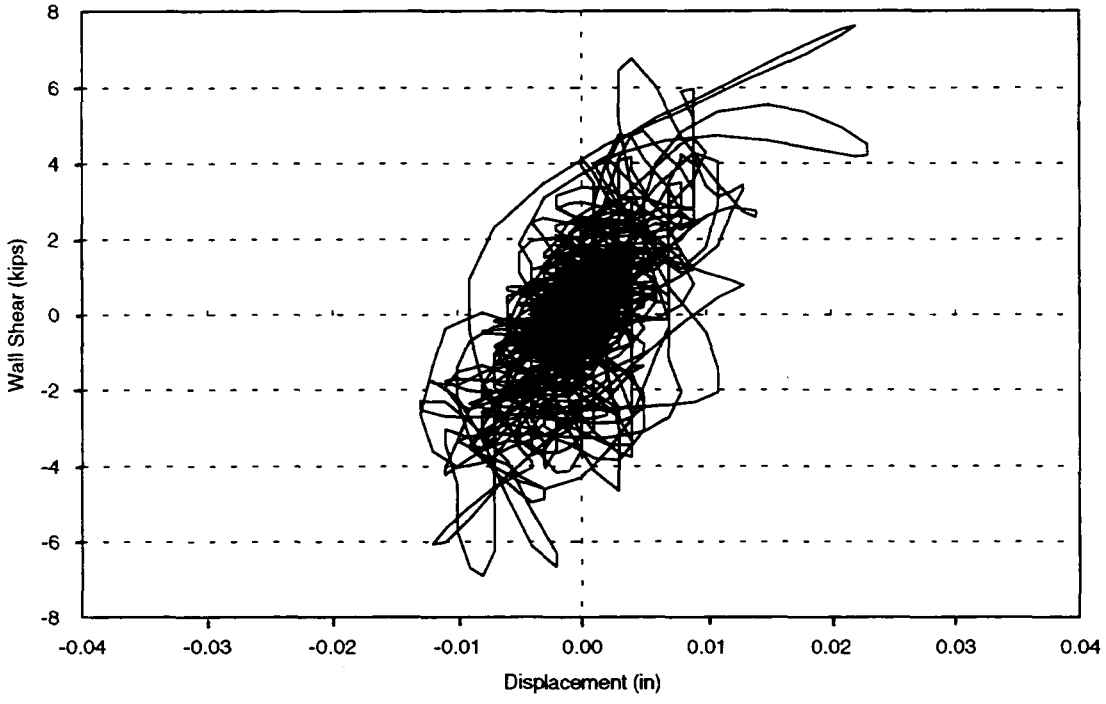

Figure 4.22 Door-wall Shear vs. First-level Door-wall Displacement from Test Run 13

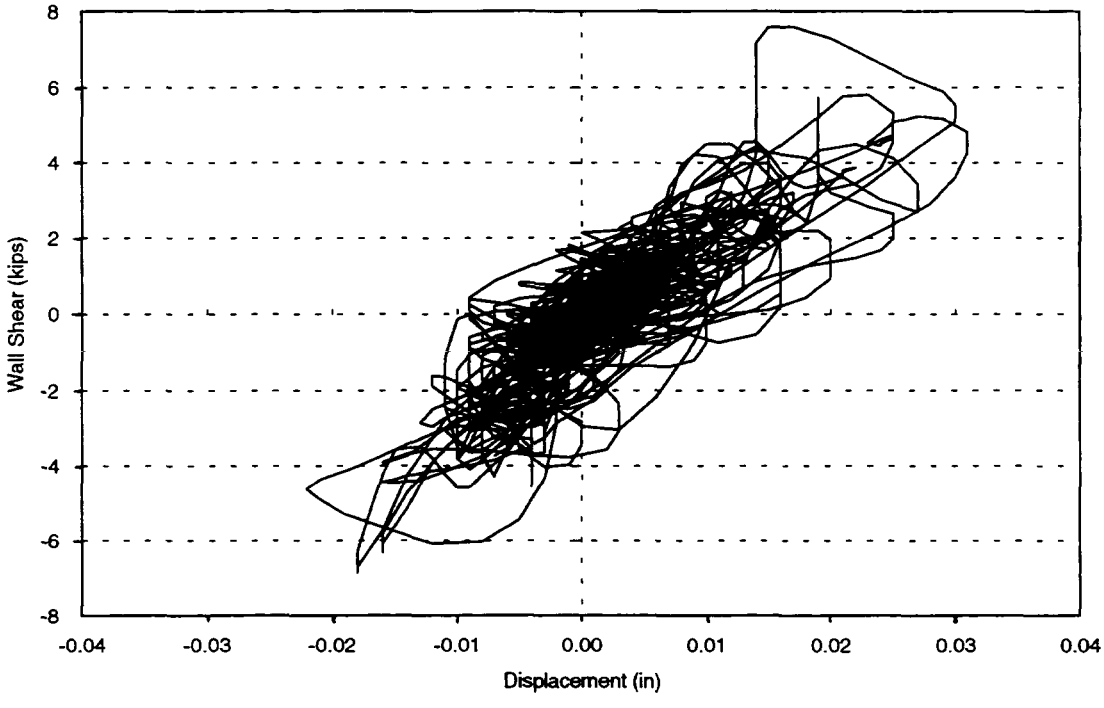

Figure 4.23 Window-wall Shear vs. First-level Window-wall Displacement from Test Run 13

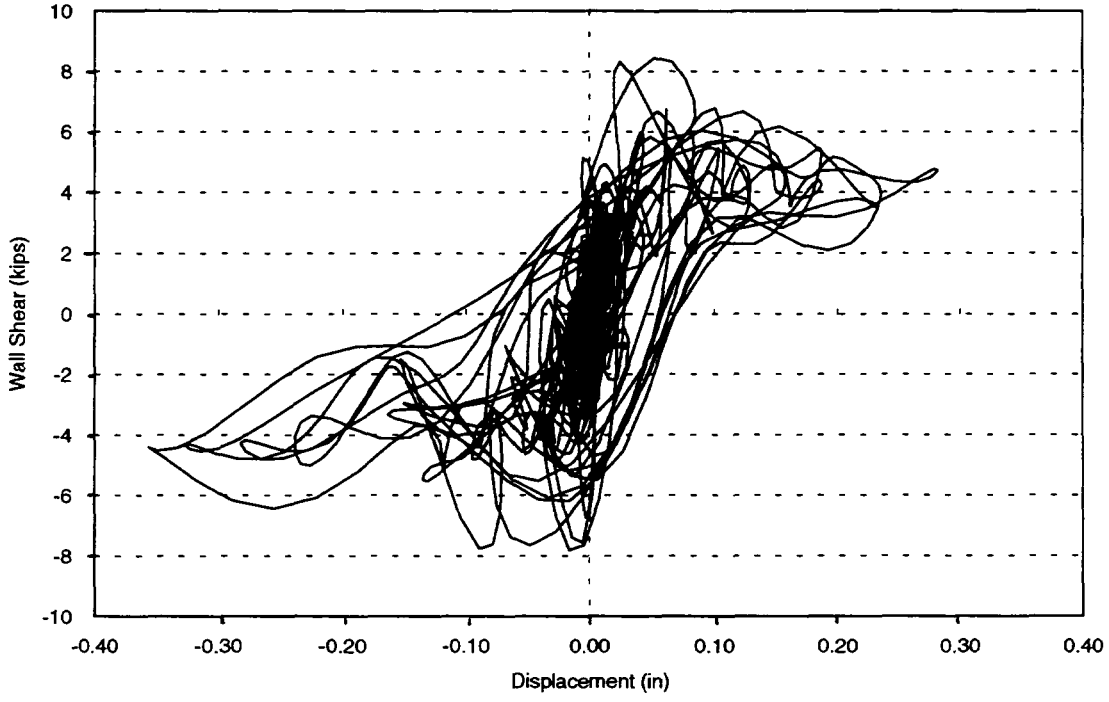

Figure 4.24 Door-wall Shear vs. First-level Door-wall Displacement from Test Run 14

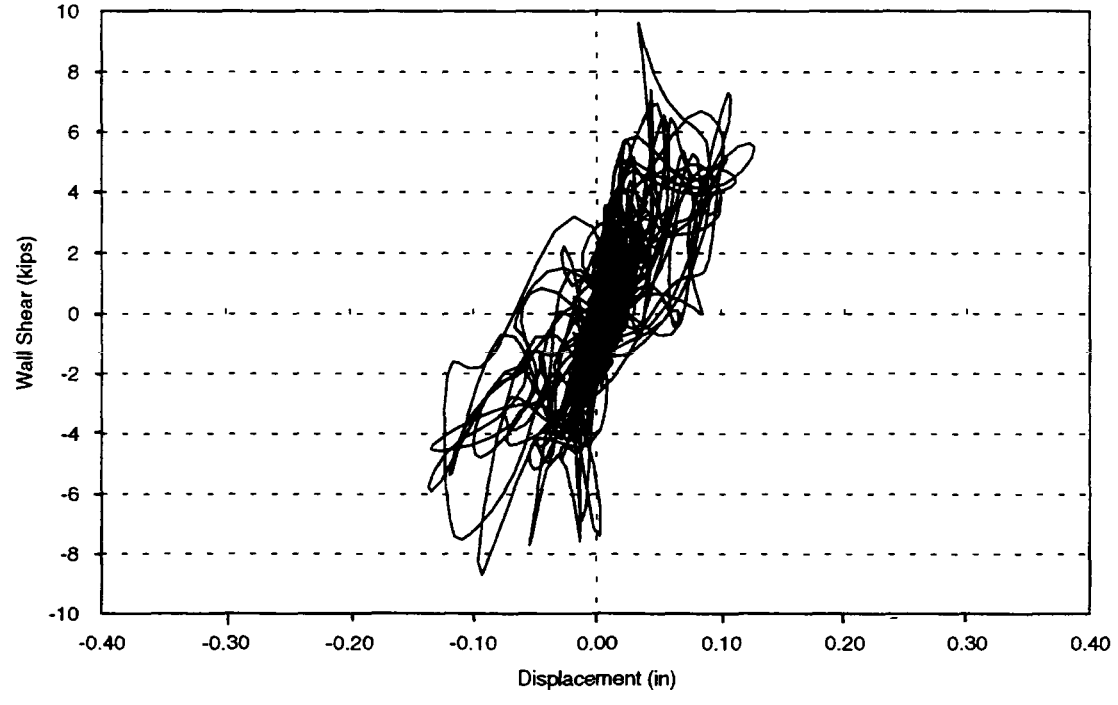

Figure 4.25 Window-wall Shear vs. First-level Window-wall Displacement from Test Run 14

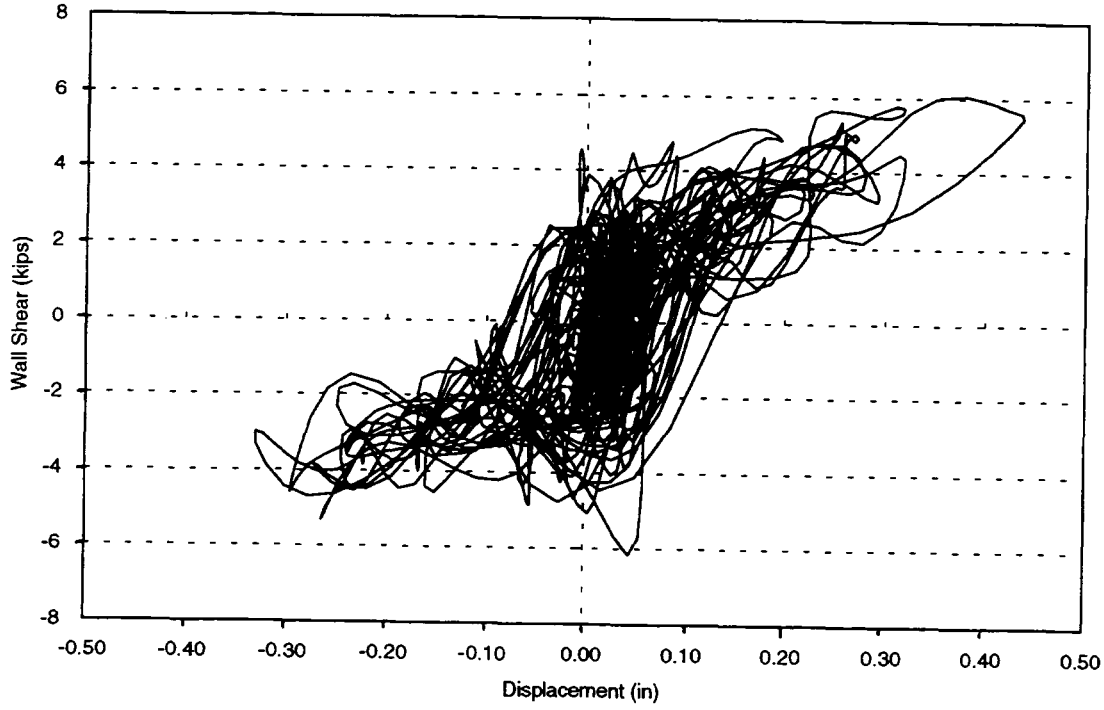

Figure 4.26 Door-wall Shear vs. First-level Door-wall Displacement from Test Run 15

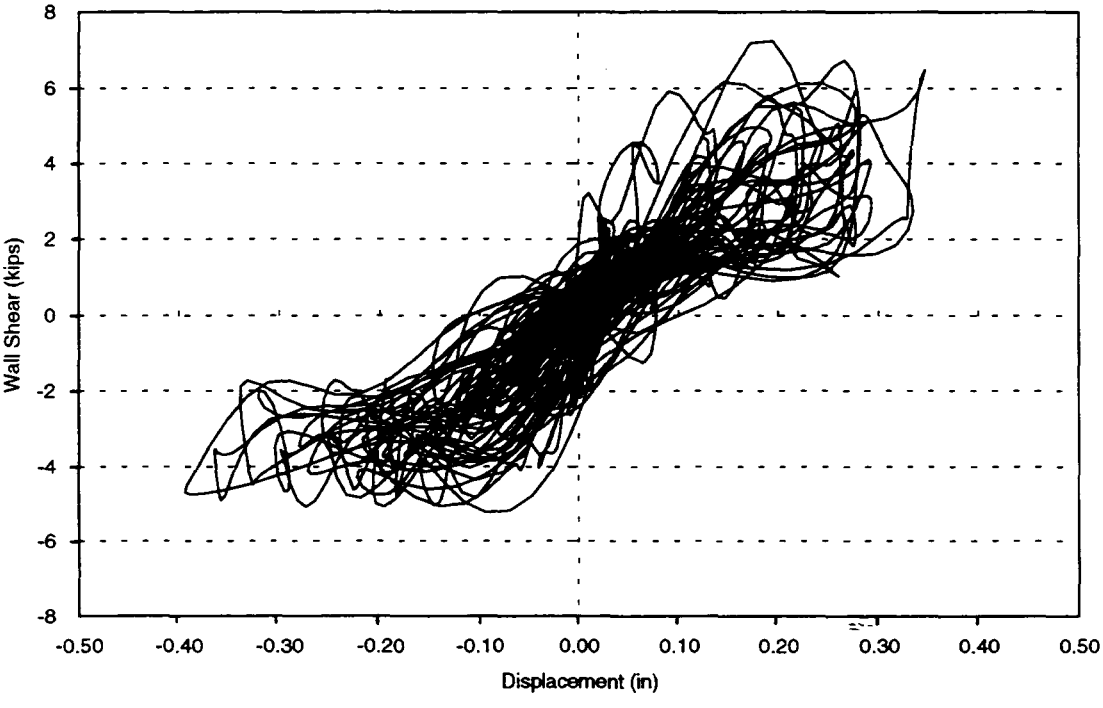

Figure 4.27 Window-wall Shear vs. First-level Window-wall Displacement from Test Run 15

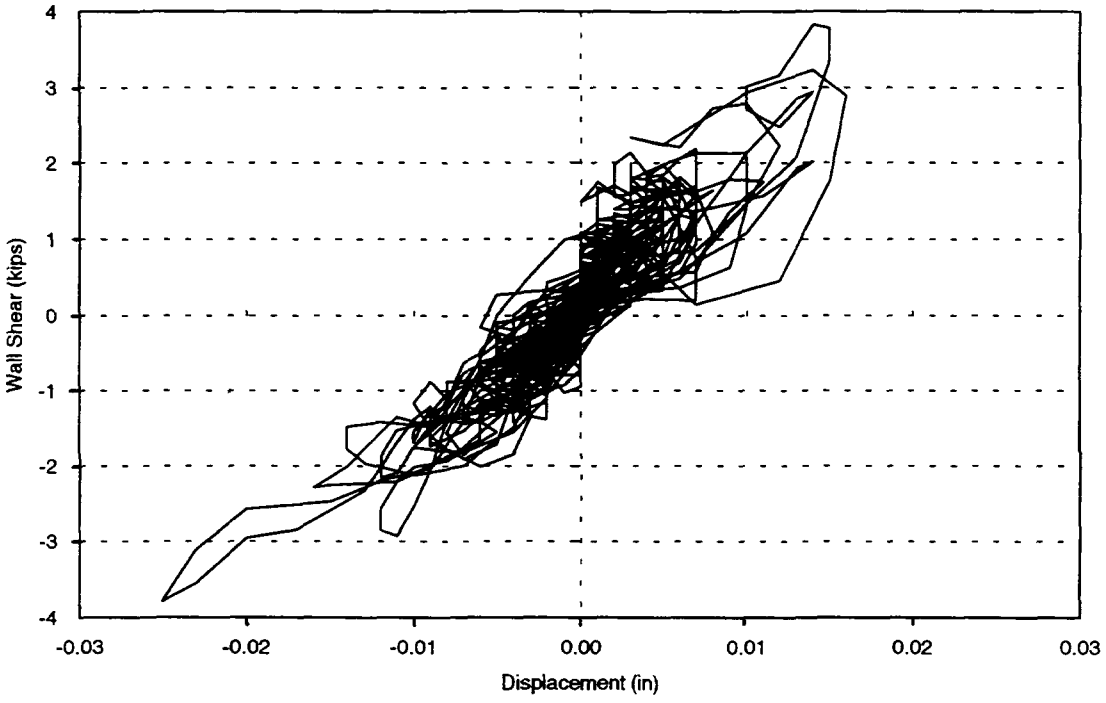

Figure 4.28 Door-wall Shear vs. First-level Door-wall Displacement from Test Run 21

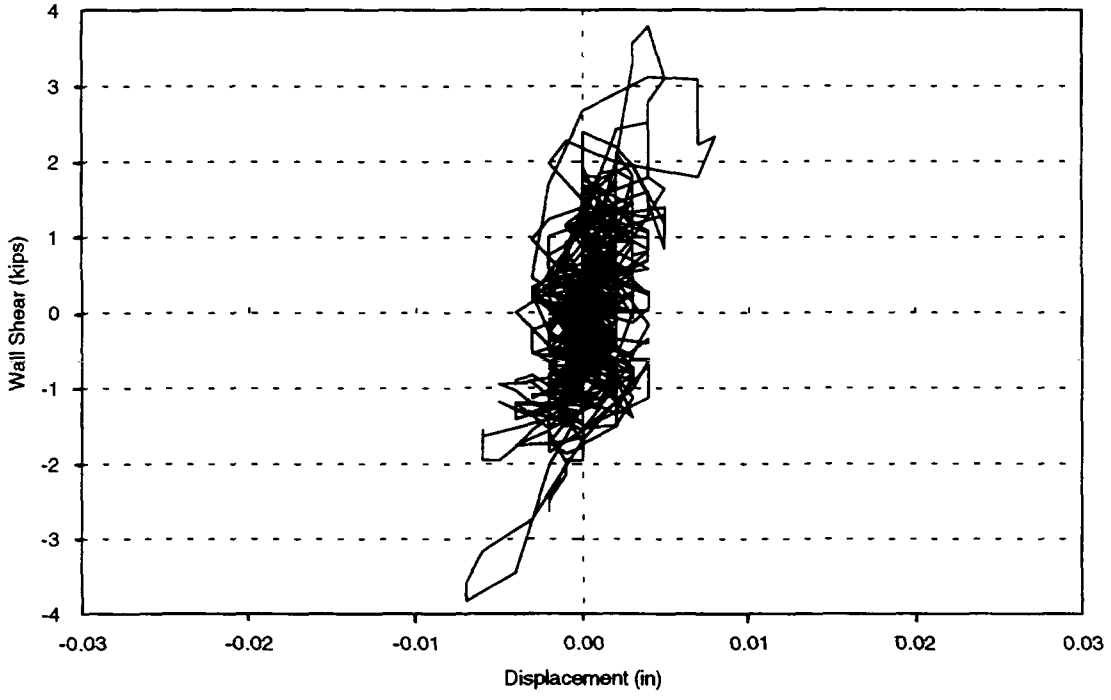

Figure 4.29 Window-wall Shear vs. First-level Window-wall Displacement from Test Run 21

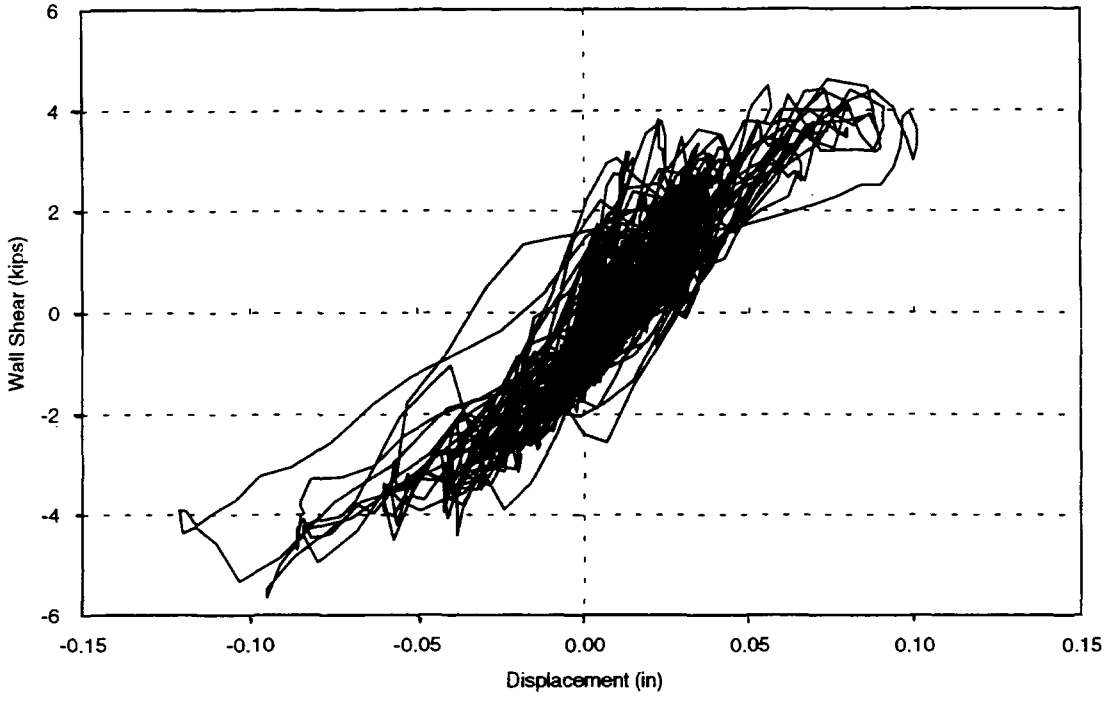

Figure 4.30 Door-wall Shear vs. First-level Door-wall Displacement from Test Run 22

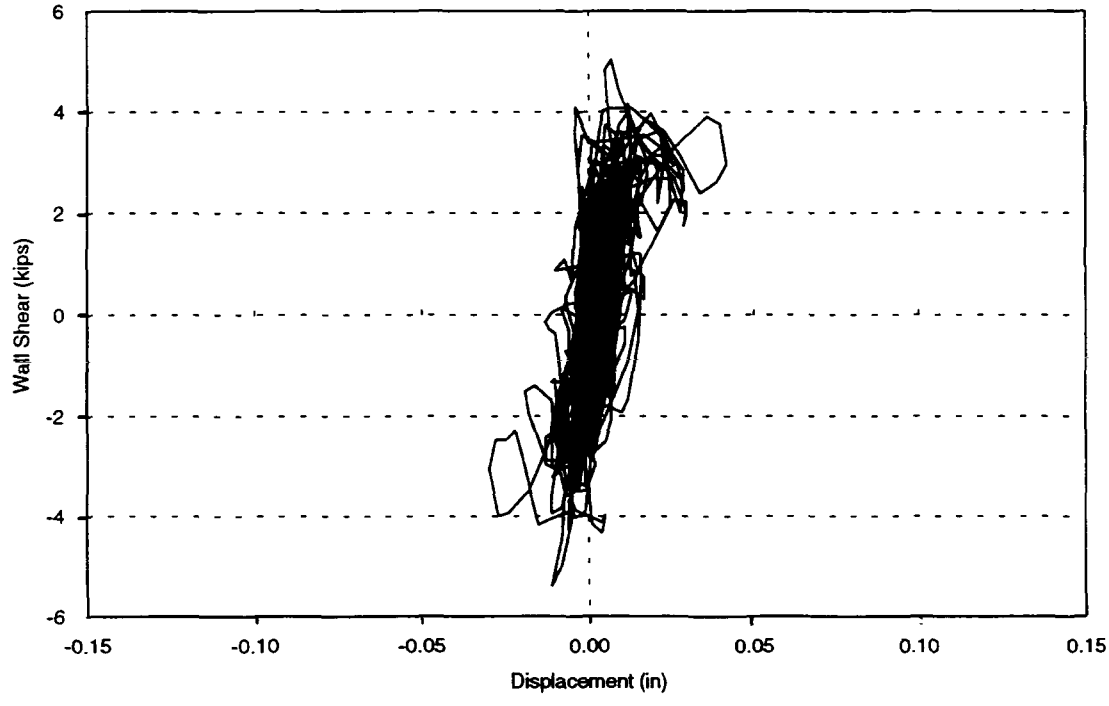

Figure 4.31 Window-wall Shear vs. First-level Window-wall Displacement from Test Run 22

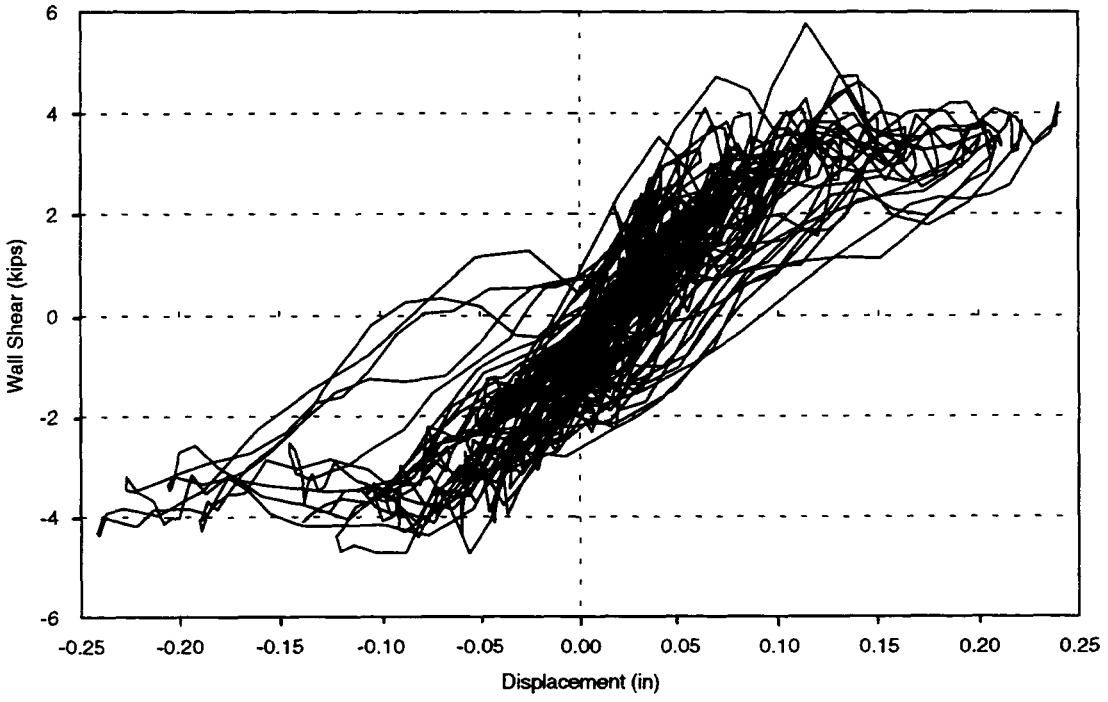

Figure 4.32 Door-wall Shear vs. First-level Door-wall Displacement from Test Run 23

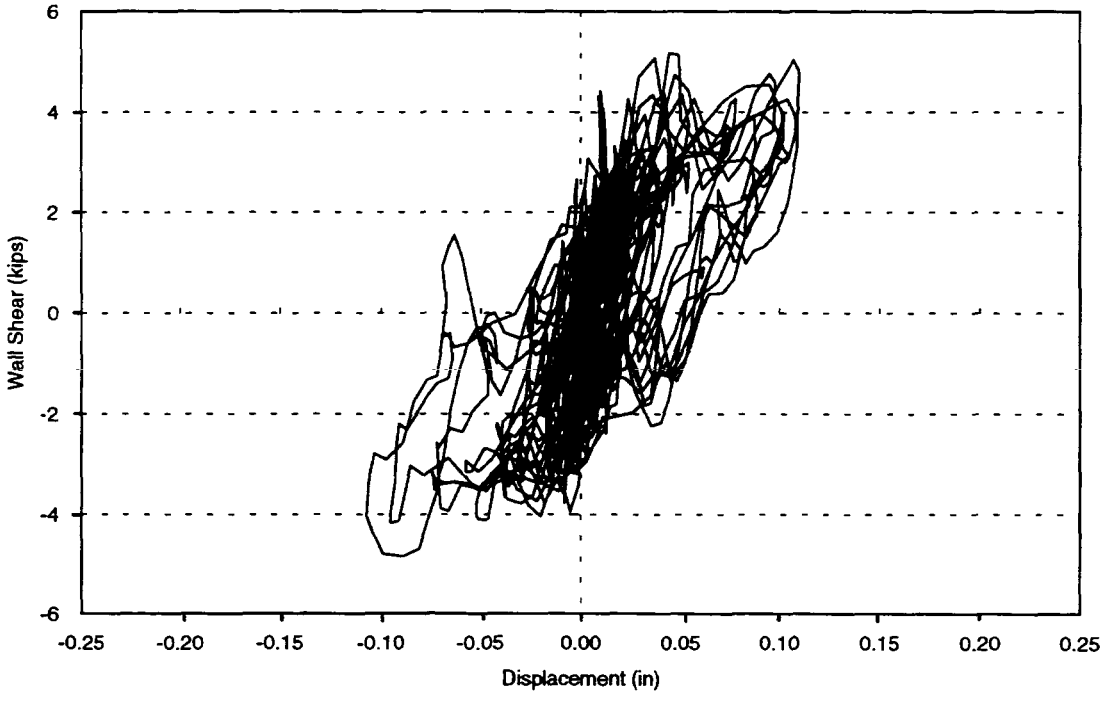

Figure 4.33 Window-wall Shear vs. First-level Window-wall Displacement from Test Run 23

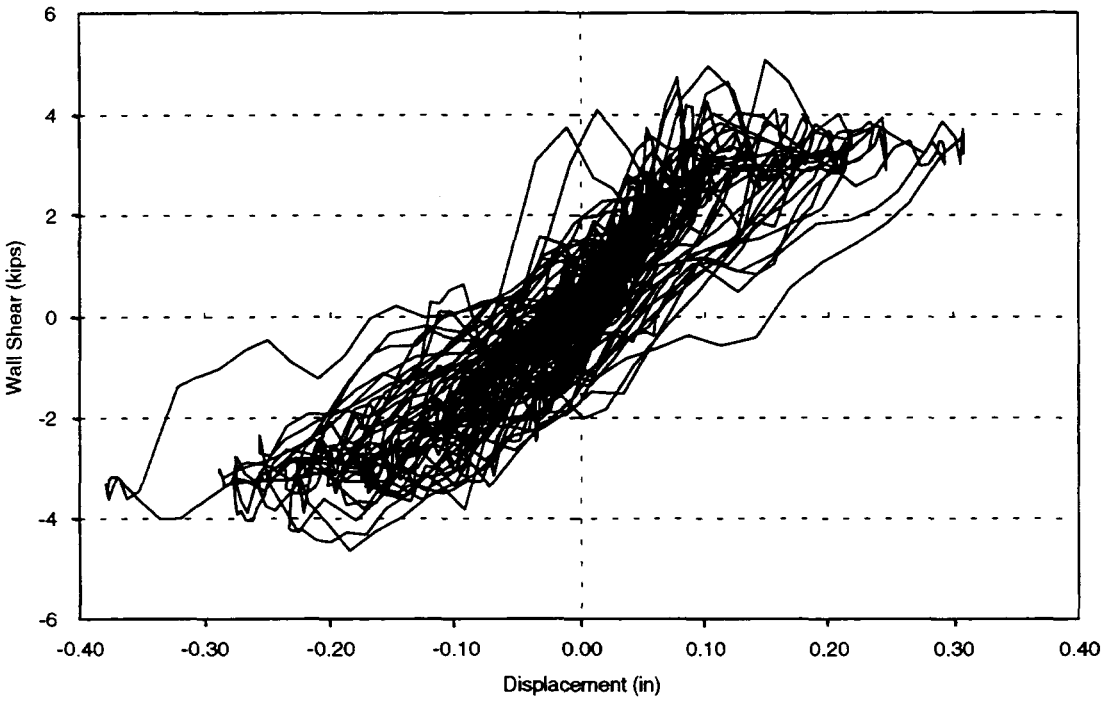

Figure 4.34 Door-wall Shear vs. First-level Door-wall Displacement from Test Run 24

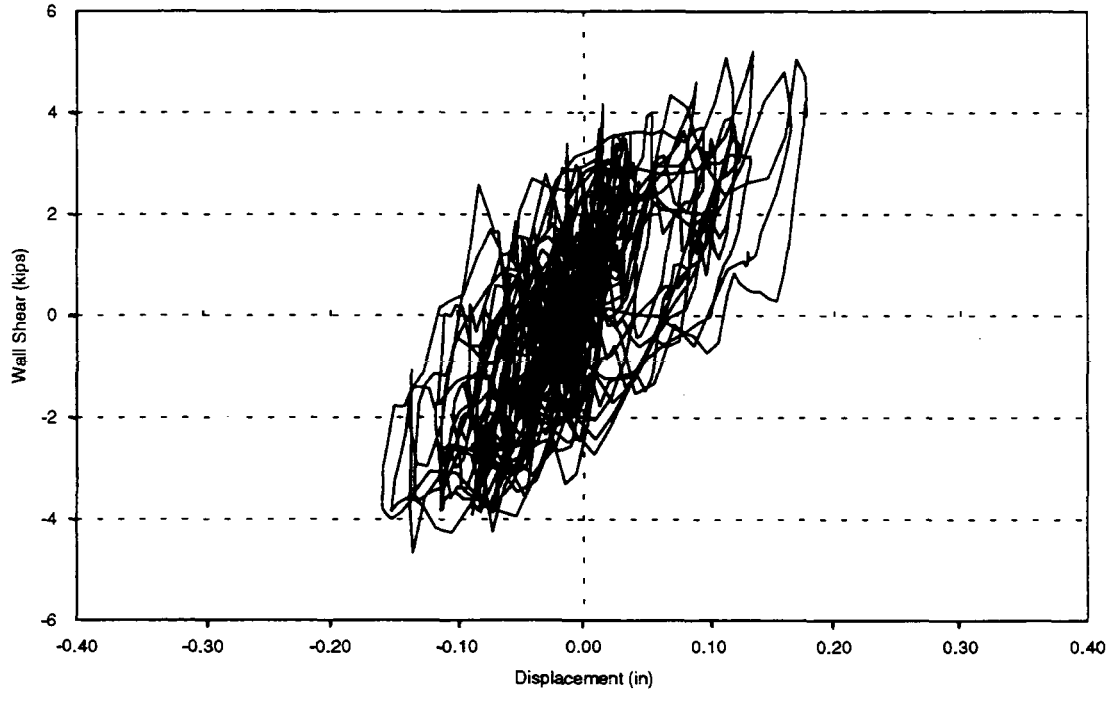

Figure 4.35 Window-wall Shear vs. First-level Window-wall Displacement from Test Run 24

Most of the same trends seen in the force-displacement curves for S1 were also seen for S2. A linear behavior was evident during Test Run 21, especially for the door wall (Figure 4.28), which was much more flexible. The bilinear shape was seen for the door wall in Test Runs 22, 23, and 24 (Figures 4.30, 4.32, and 4.34), again indicative of a pier-rocking behavior. Note that the rocking behavior for the S2 door wall was just as pronounced as it was for the S1 walls, even though only the door wall rocked. The hysteresis loops for the cracked test runs of the S2 window wall (Figures 4.31, 4.33, and 4.35) showed a shape similar to those of the rocking, S2 door wall even though the window wall did not rock. The behavior being exhibited was sliding across the full-length crack near the base of the wall. Although this sliding behavior looked similar to the rocking behavior in the hysteresis curves, as it should, it could be distinguished by the unloading portions of the curves. Whereas the rocking loops were mostly stationary and unloaded elastically through a single origin, the sliding loops shifted back and forth along the displacement axis and tended to unload immediately after the peak displacement.

4.6 Natural Frequencies

Fast Fourier transforms (FFTs) were computed from the response histories collected during both the dynamic testing and the free vibration testing. As an example, four FFTs, determined from the same data channel, for the four test runs of S2, are shown in Figure 4.36. By examining transforms from acceleration, displacement, and strain histories, the dominant frequencies were obtained for each test run of S1 and S2. The frequencies are listed in Table 4.8 while plots of natural frequency versus peak first-level drift are shown in Figures 4.37 and 4.38 for S1 and S2, respectively. Frequency values derived from the free vibration tests are plotted against the maximum drift of the preceding dynamic test. As an example, (see Figure 4.38) during Test Run 23, the dominant structural frequency was 6.7 Hz while for the free vibration test after Test Run 23, the natural frequency determined was 7.4 Hz.

An examination of Figures 4.37 and 4.38 revealed three items: (a) natural frequencies dropped as structural damage increased, (b) frequency measurements were dependent on the amplitude

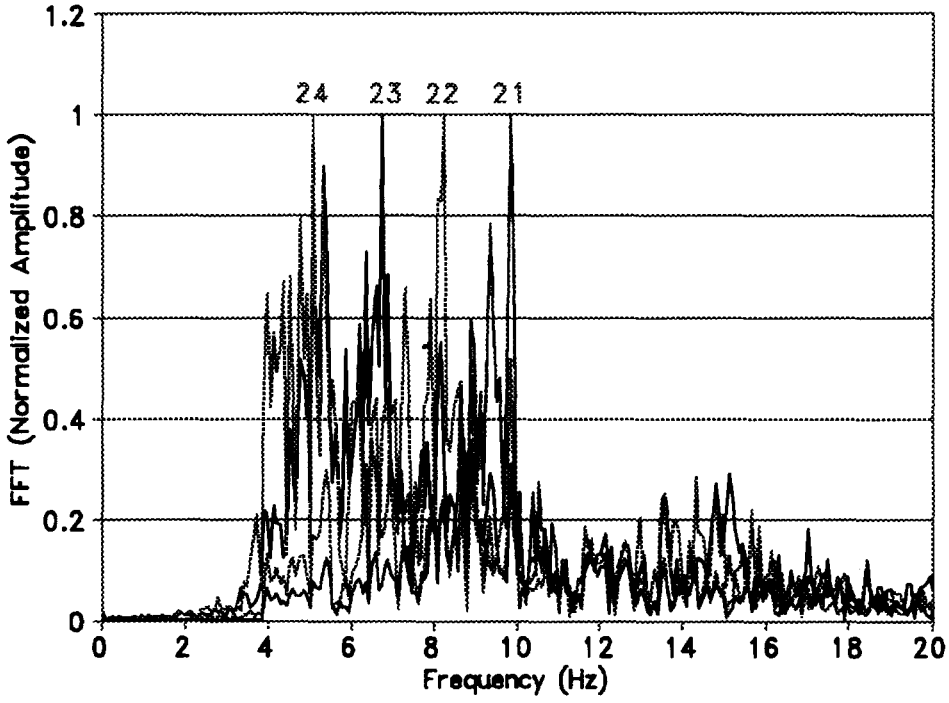

Figure 4.36 Fourier Transforms for Second-level Diaphragm Accelerations, Test Runs 21-24

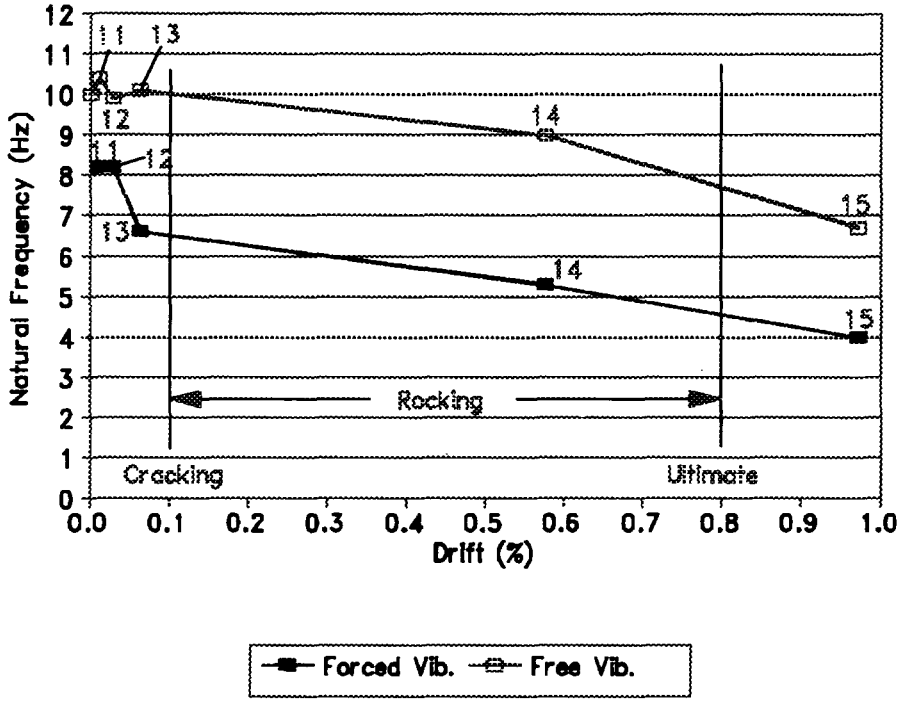

Figure 4.37 Measured Natural Frequencies versus Drift for S1

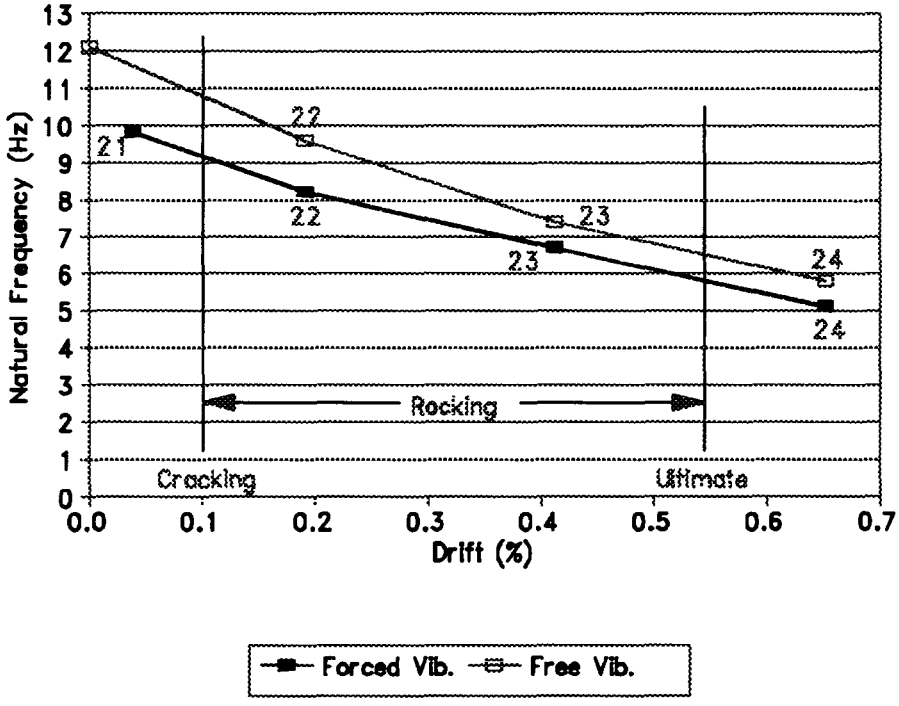

Figure 4.38 Measured Natural Frequencies versus Drift for S2

of the test, and (c) both S1 and S2 vibrated at much lower frequencies than determined by the numerical models.

As structural damage, in the form of cracking, increased, the natural frequencies of the structures decreased. This was due not only to a decreased stiffness directly caused by the cracking, but in the case of the dynamic testing measurements, was also due to the nonlinear behaviors of sliding across cracks and opening and closing of cracks. Sliding and rocking stiffnesses are essentially zero, so the presence of either behavior greatly reduces the effective structural stiffness. The more nonlinear behavior that is present, the lower the stiffness and natural frequency will be. This accounted for the continued decrease in natural frequency even after substantial cracking had occurred.

In the two graphs (Figures 4.37 and 4.38), the frequency determined from the free vibration testing was always higher than the corresponding frequency determined during the dynamic testing. The response amplitudes measured during the free vibration testing were essentially constant at levels much lower than those measured during the dynamic testing. Frequency determination must therefore be test amplitude dependent. During the later test runs, large-amplitude behaviors such as opening and closing of cracks and sliding across cracks were not accurately represented in the small-amplitude free vibration measurements. These nonlinear behaviors tended to lower natural frequencies, so the later dynamic testing frequencies (Test Runs 14, 15, 23, and 24) should be lower than the free vibration frequencies. The larger difference between forced and free vibration results exhibited in S1 was probably due to the greater damage (both walls) in S1.

A review of Table 3.4 shows that natural frequencies determined from the numerical models ranged between 12 and 47 Hz for S1 and S2. The measured initial natural frequencies, 8.2 Hz for S1 and 9.8 Hz for S2, were most closely approximated by the frequency determined by the finite element model of just the floor diaphragm, i.e., 8.6 Hz. The MDOF model with flexible diaphragms produced frequencies of 11.8 Hz for S1 and 11.7 Hz for S2 which were reasonable. Clearly, the rigid diaphragm models (34 to 47 Hz) did not accurately determine the natural frequencies of these flexible diaphragm structures.

4.7 Deflected Shapes

Eight displacements were measured relative to the base of the test structure: one at each floor level of the in-plane walls and four along the center of the west out-of-plane wall (Figure 2.31). The two floor-level displacements measured on the out-of-plane wall were considered to be equal to the displacements of the two diaphragms relative to the base. This assumption could be made because the end beams of the diaphragms were attached to the out-of-plane walls with axially rigid members (see Section 2.3). Deflected shapes for S1 and S2 were produced by plotting the measured displacements at the six floor-level instrument sites at the time of peak displacement of the second-level diaphragm. These shapes are shown in Figures 4.39-4.46, for Test Runs 12-15 and 21-24. Each of these deflected shapes is in essence a single frame, or "snapshot", of the test structures' displacement history. The shapes shown for Test Runs 14, 15, 22, 23, and 24 occurred after the initiation of cracking. The second-level diaphragm displacement was not recorded during Test Run 14, so the time of the peak first-level measurement was used for this graph. Note that all displacements were relative to the base of the structure and included any residuals from prior test runs. The deflected shapes for Test Runs 23 and 24 should be viewed with some caution as errors resulted from the out-of-plane motions.

A quick examination of the deflected shapes showed that the diaphragm deflections relative to the wall deflections appeared to decrease after cracking. Although the diaphragm *displacements* are plotted relative to the base of the structure, two small squares representing the average of the in-plane wall deflections are plotted to serve as a basis for estimating the diaphragm *deflection* relative to the walls. Diaphragm deflections relative to the average wall deflections, overlaid on average wall deflections, are plotted versus time in Figures 4.47-4.50 for uncracked and cracked test runs of S1 and S2. Prior to cracking, the relative diaphragm deflections were much greater than the wall deflections while after cracking, the wall deflections were many times greater than the relative diaphragm deflections. To quantify this trend, diaphragm displacements (relative to the base of the structure) were divided by the average wall deflections to produce a displacement amplification. Both histories were centered at zero (residuals removed) so that a meaningful ratio could be produced. The displacement ratios were averaged over the strong motion period of the records producing the values

——— Door Wall ····· Window Wall - - - - - - - - Diaphragm

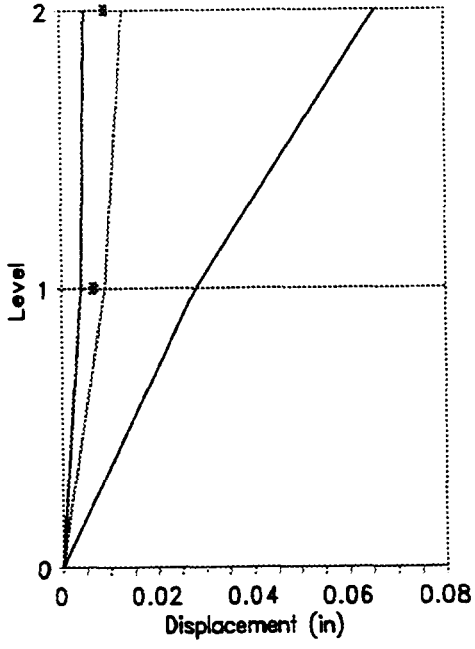

Figure 4.39 Measured Deflected Shape from Test Run 12

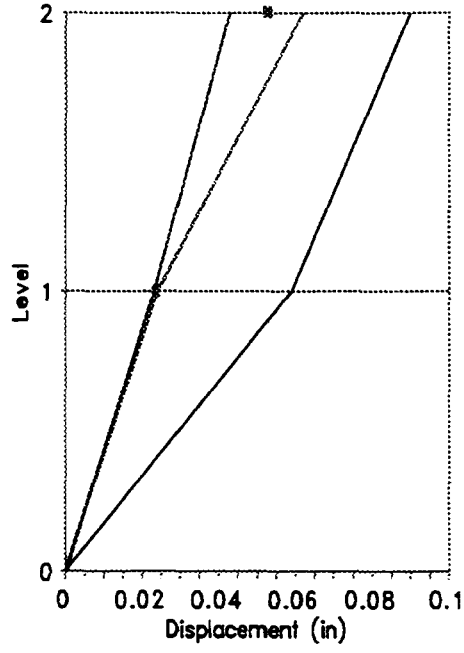

Figure 4.40 Measured Deflected Shape from Test Run 13

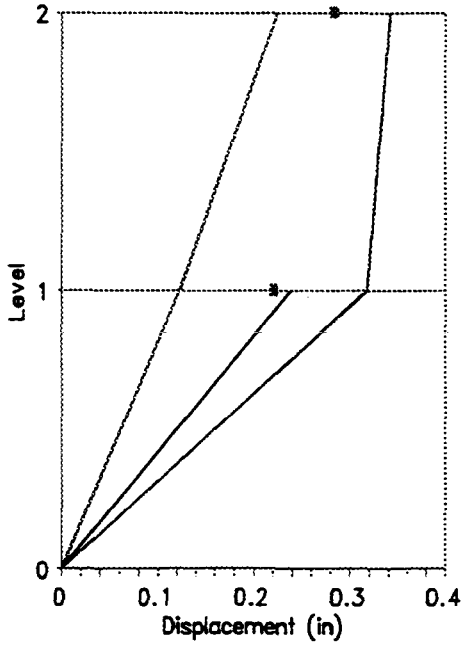

Figure 4.41 Measured Deflected Shape from Test Run 14

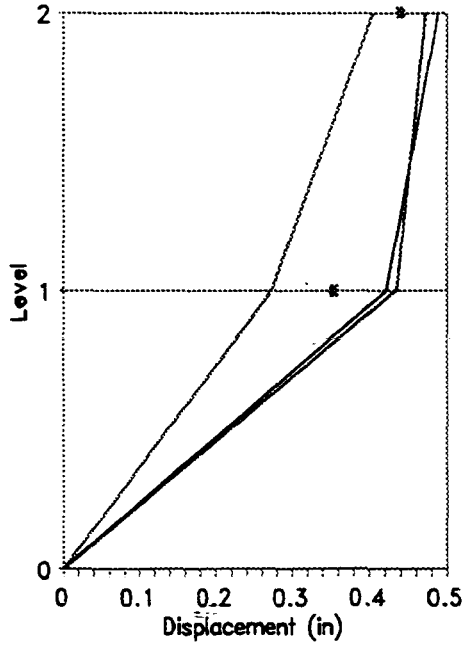

Figure 4.42 Measured Deflected Shape from Test Run 15

——— Door Wall ····· Window Wall - - - - - - - - Diaphragm

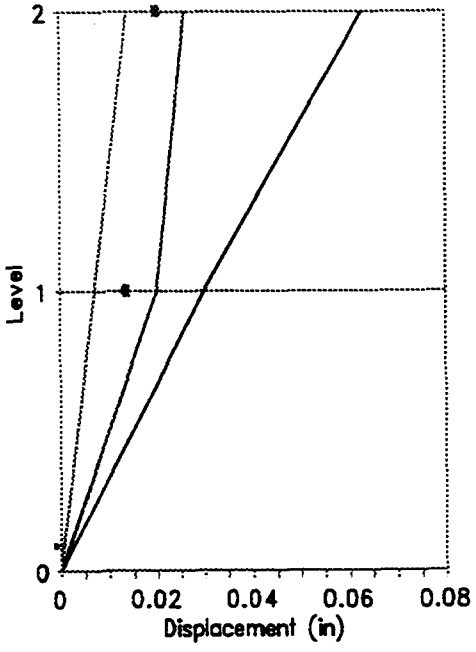

Figure 4.43 Measured Deflected Shape from Test Run 21

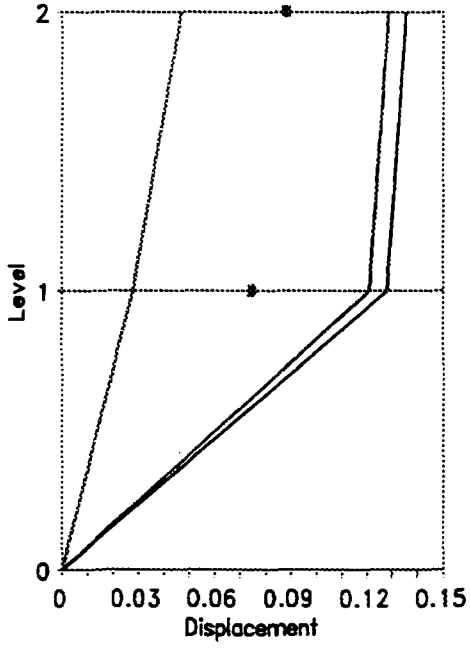

Figure 4.44 Measured Deflected Shape from Test Run 22

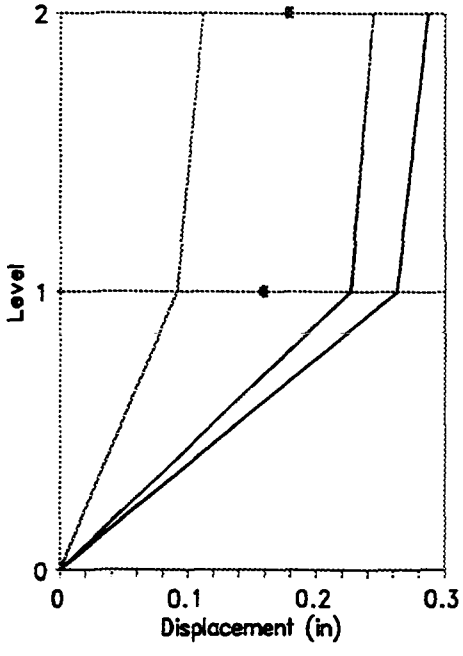

Figure 4.45 Measured Deflected Shape from Test Run 23

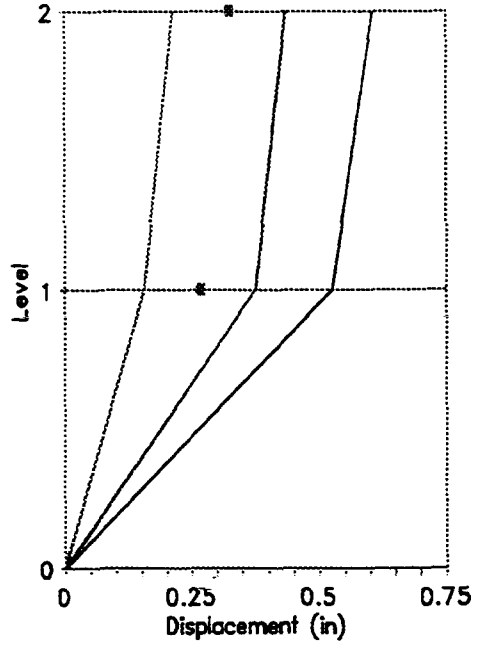

Figure 4.46 Measured Deflected Shape from Test Run 24

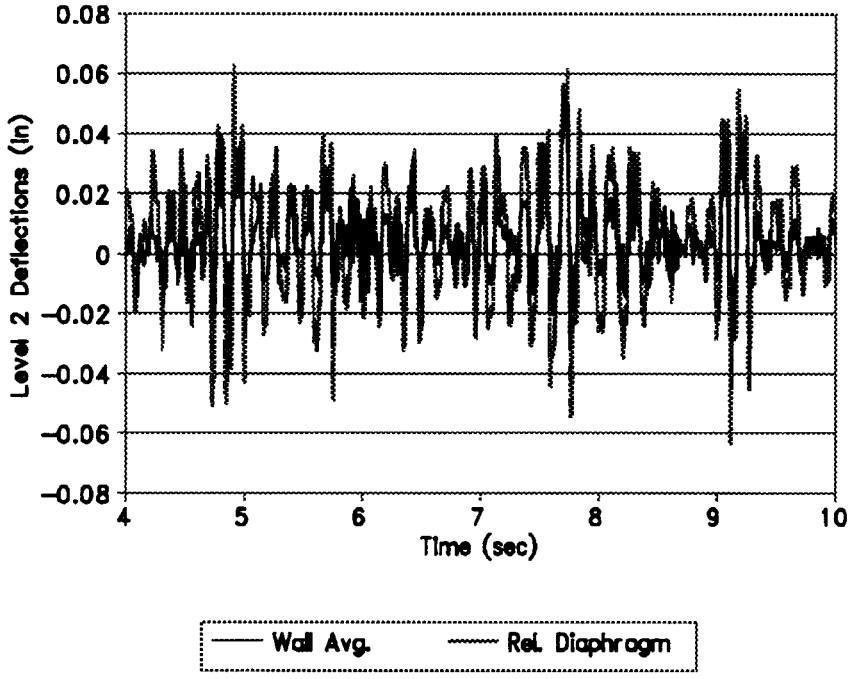

Figure 4.47 Average Second-level Wall and Relative Diaphragm Deflections from (uncracked) Test Run 13

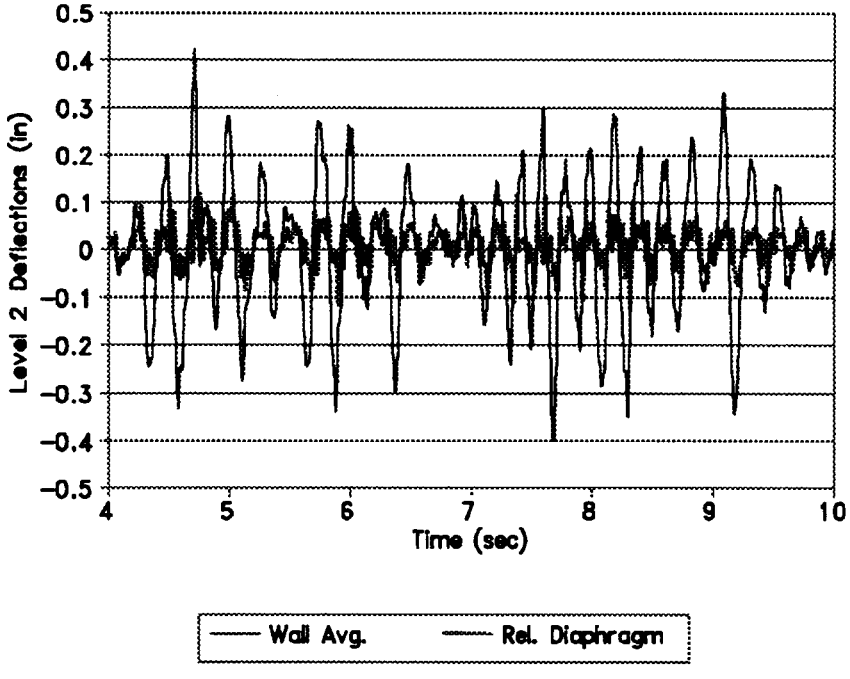

Figure 4.48 Average Second-level Wall and Relative Diaphragm Deflections from (cracked) Test Run 15

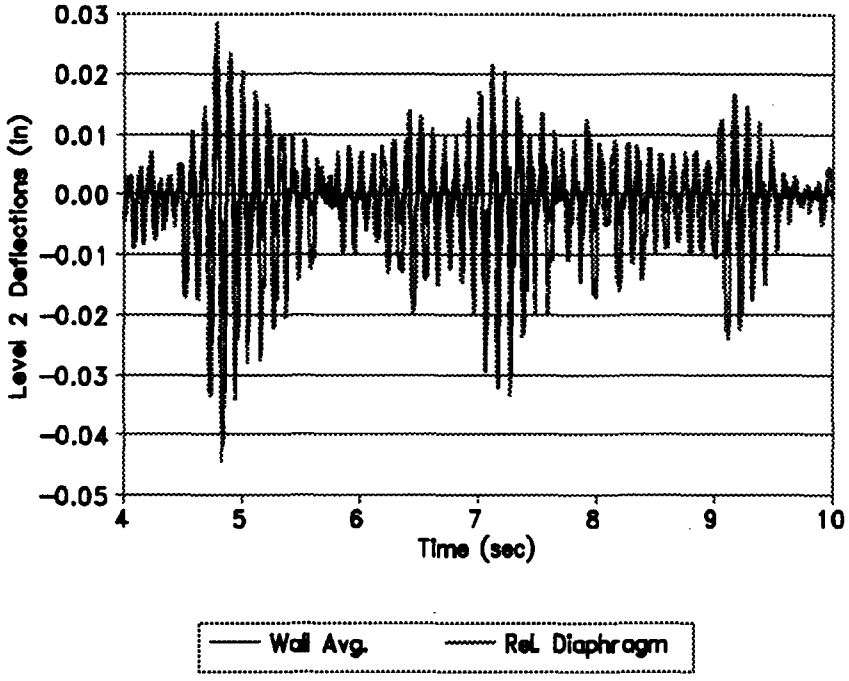

Figure 4.49 Average Second-level Wall and Relative Diaphragm Deflections from (uncracked) Test Run 21

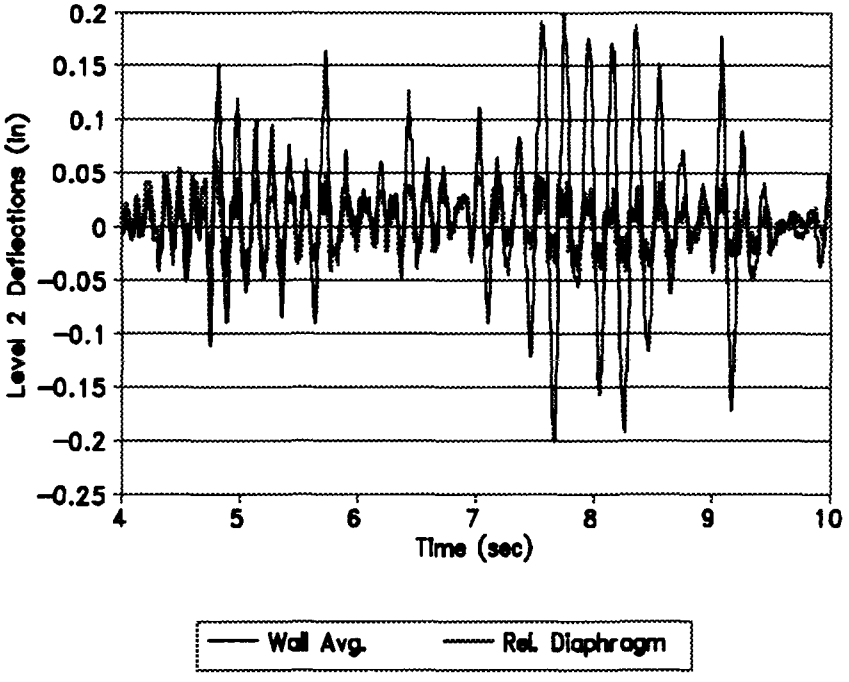

Figure 4.50 Average Second-level Wall and Relative Diaphragm Deflections from (cracked) Test Run 23 (Diaphragm deflection history balanced to zero inches.)

in Table 4.9. Ratios above 25 or below -25 were not included in the average. The time period used for each average is indicated in the table. Uncracked displacement ratios ranged from 2.5 to 4.0 for S1 and 4.1-4.5 for S2. Cracked displacement ratios ranged from 1.4-1.5 for S1 and 1.3-1.9 for S2. Values less than 2.0 indicated that the *relative* diaphragm deflection was less than the wall deflection. The displacement amplification effect of the flexible diaphragms diminished by at least a factor of two after substantial cracking had occurred below the diaphragms. This reduction was evident in S2 even though only the door wall experienced substantial cracking.

A second trend in the deflected shapes (Figures 4.39-4.46) was that the second-story drifts relative to first-story drifts also appeared to decrease after cracking. Interstory drifts for the door walls of S1 and S2, before and after cracking, are plotted in Figures 4.51-4.54. Before cracking (Figures 4.51 and 4.53), the drift levels for the first and second stories are comparable in magnitude. After cracking (Figures 4.52 and 4.54), the first-story drifts are much greater than the second-story drifts. Furthermore, the second-story drifts do not generally exceed the 0.1% level established as the cracking drift in Section 4.4. This behavior was also examined by computing another ratio, the average of second-floor wall displacements to the average of first-floor wall displacements. The histories were again balanced so that amplifications would be relative to zero. The ratios were computed and averaged as before over the strong motion period of the records. These averages are presented in Table 4.10 along with the time windows used. Second floor-level displacements were 1.7 times first floor-level displacements in S1 and S2 prior to cracking. After cracking, second-floor displacements averaged only 10% greater than those of the first floor. After the initiation of cracking, the interstory drift above the cracking was largely reduced. Most of the displacement occurred across the cracks while very little occurred in the undamaged masonry. This behavior can be represented by stretching two springs in series. If the first spring yields, almost all additional deformation will take place across that spring. This effect is more noticeable in S1, where both first story walls cracked.

By combining the ratios presented in Tables 4.9 and 4.10, a mode shape was computed for each test run. The four degrees of freedom for the mode shape are shown in Figure 4.55 while the modal coordinates are listed in Table 4.11. The mode shapes were scaled such that the second-floor diaphragm coordinate (DOF #4) was equal to 1.00. Also presented in Table 4.11 are the participation

Table 4.9 Average Ratios of Diaphragm-displacement-to-wall-deflection and Time Windows

Test Run	Condition	Diaphragm Displacement / Average Wall Deflection		Time Window (sec)
		2nd Level	1st Level	
12	Uncracked	2.50	4.04	4.0-9.5
13	Uncracked	2.72	3.52	4.0-13.0
14	Cracking	N.A.	1.85	4.0-9.0
15	Cracked	1.39	1.49	4.0-10.0
21	Uncracked	4.47	4.10	4.0-12.0, 4.0-10.0
22	Cracking	2.22	2.26	5.0-10.0, 4.0-8.0
23	Cracked	1.85	1.51	2.5-4.5 & 10.0-14.0, 2.5-4.5 & 10.0-14.0
24	Cracked	1.26	N.A.	2.5-4.5 & 10.0-14.0

Table 4.10 Average Ratios of Second-level-wall-displacement-to-first-level-wall-displacement and Time Windows

Test Run	Condition	Average Second Level Wall Displacement / Average First Level Wall Displacement	Time Window (sec)
12	Uncracked	1.83	4.0-9.5
13	Uncracked	1.79	4.0-13.0
14	Cracking	1.52	4.0-9.0
15	Cracked	1.07	4.0-10.0
21	Uncracked	1.67	4.0-10.0
22	Cracking	1.18	5.0-9.0
23	Cracked	1.18	4.0-13.0
24	Cracked	1.09	4.0-13.0

Table 4.11 Average Mode Shapes and Participation Factors for S1 and S2

Test Run	Condition	Mode Shape				Γ (mode shape)	Γ (deflected shape)
		1st Level Walls (ϕ_1)	1st Level Diaphragm (ϕ_2)	2nd Level Walls (ϕ_3)	2nd Level Diaphragm (ϕ_4)		
11	Uncracked	N.A.				N.A.	1.26
12	Uncracked	0.22	0.88	0.40	1.00	1.17	1.30
13	Uncracked	0.21	0.72	0.37	1.00	1.25	1.28
14	Cracking	N.A.				N.A.	1.2*
15	Cracked	0.67	1.00	0.72	1.00	1.09	1.12
21	Uncracked	0.13	0.55	0.22	1.00	1.30	1.35
22	Cracking	0.38	0.86	0.45	1.00	1.20	1.14
23	Cracked	0.45	0.69	0.54	1.00	1.27	1.15
24	Cracked	0.73	0.9*	0.79	1.00	1.12*	1.19

*Estimated.

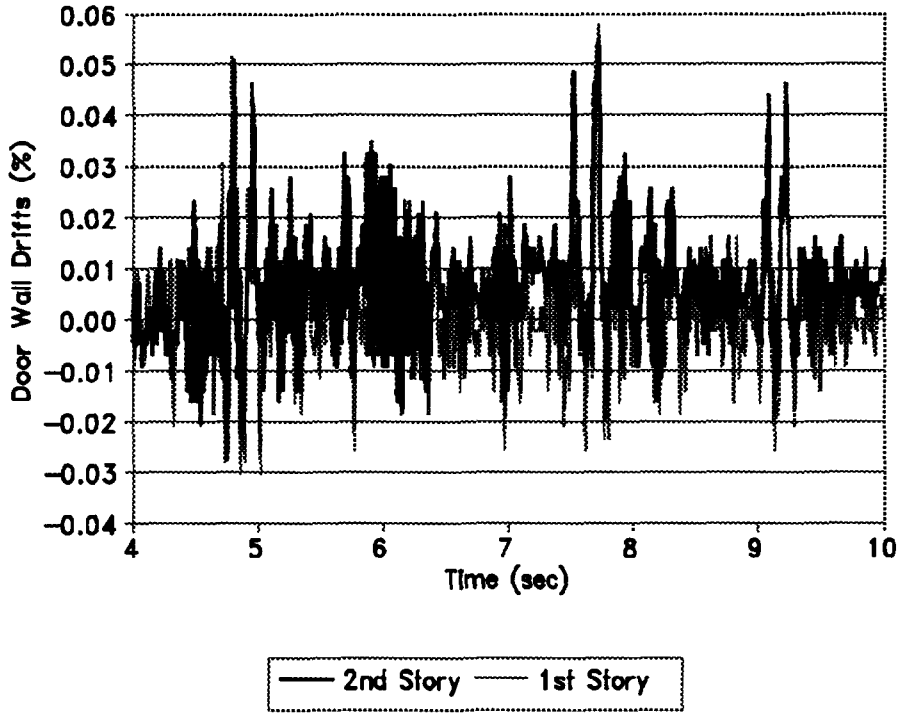

Figure 4.51 Story Drifts from the S1 Door Wall Before cracking (Test Run 13)

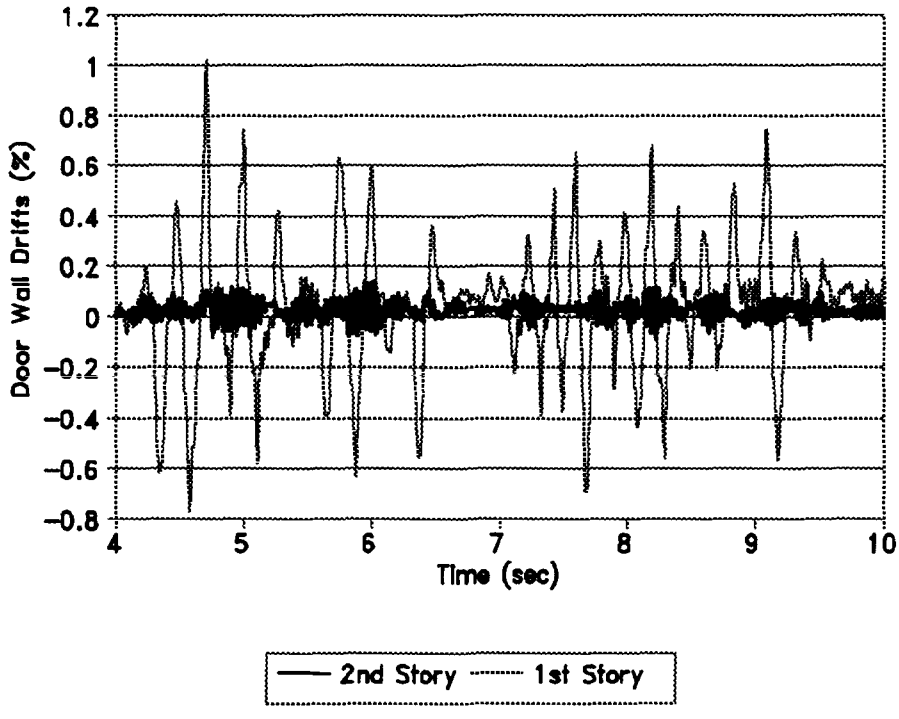

Figure 4.52 Story Drifts from the S1 Door Wall After cracking (Test Run 15)

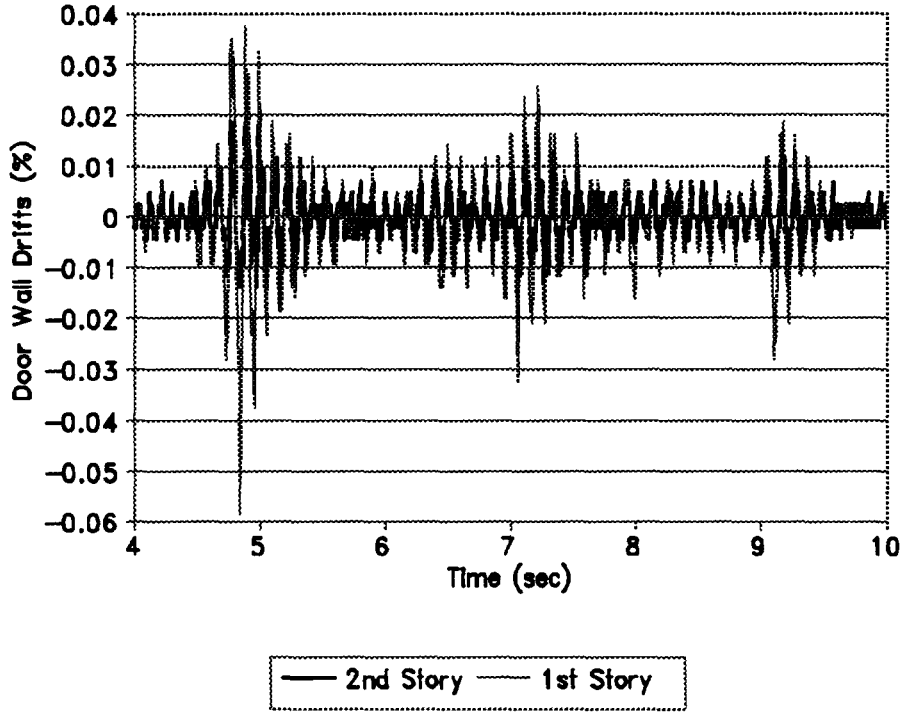

Figure 4.53 Story Drifts from the S2 Door Wall Before cracking (Test Run 21)

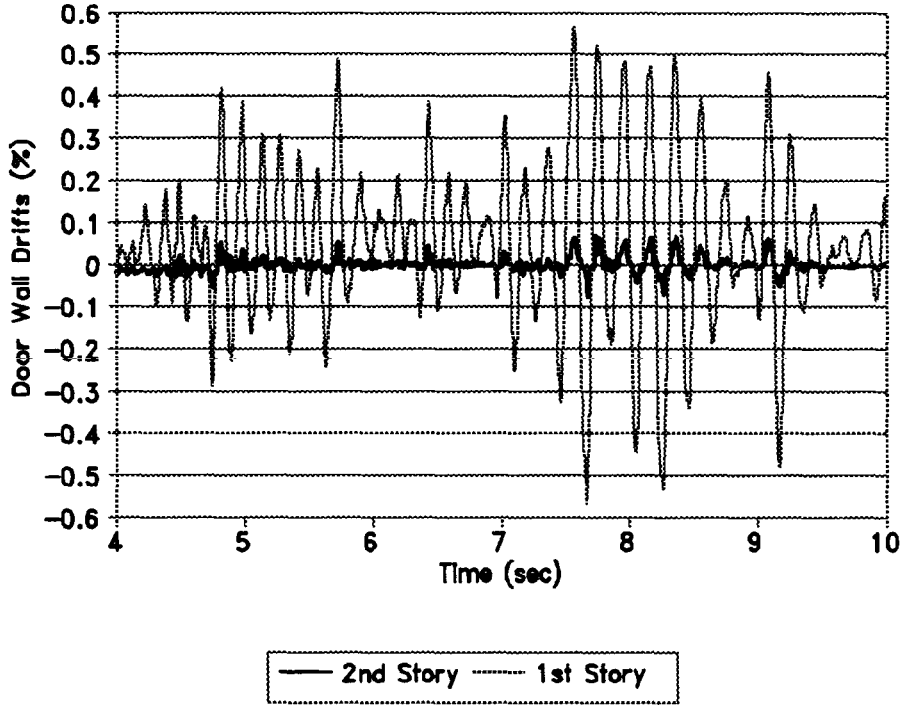

Figure 4.54 Story Drifts from the S2 Door Wall After cracking (Test Run 23)

factors calculated using these mode shapes, as well as the participation factors determined using the deflected shapes presented in Figures 4.39-4.46. The modal participation factor, Γ, was determined by

$$\Gamma = \frac{\sum_{i=1}^{4} m_i \phi_i}{\sum_{i=1}^{4} m_i \phi_i^2} \qquad 4.1$$

where m is the nodal mass and ϕ is the modal coordinate. Before cracking, Γ was generally 1.3 while after cracking Γ was approximated as 1.15.

Substantial cracking had two major effects on the diaphragm and wall deflections above the damaged zone. The first was that diaphragm deflections relative to the walls were greatly reduced and the second was that interstory drift above the cracking was also reduced.

4.8 Acceleration Amplifications

Using the peak values of accelerations reported in Tables 4.2 and 4.5, various ratios were produced to investigate the amplification of base and wall accelerations during dynamic testing. Of particular interest were the ratios of the wall acceleration to the base acceleration, diaphragm acceleration to the wall acceleration, and the diaphragm acceleration to the base acceleration. These three acceleration ratios, based on peak values, are presented in Figures 4.56-4.58, plotted against the peak base acceleration. Ratios for both S1 and S2 are plotted on the same graph. Also plotted are the same ratios computed from acceleration peaks recorded on masonry buildings with flexible diaphragms during the Loma Prieta earthquake in 1989 (Tena-Colunga and Abrams, 1992a and b).

Several items were noted upon examination of the three acceleration ratio plots. The first was that the ratios for S1 and S2, computed from the initial test runs, agreed well with the ratios from full-size buildings during real seismic events. This was especially important since the intent of the structural design was to model flexible diaphragm systems found in older, URM buildings. Also, the

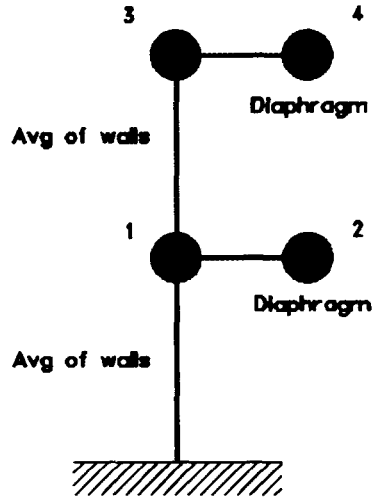

Figure 4.55 Four-degree-of-freedom Mode Shape

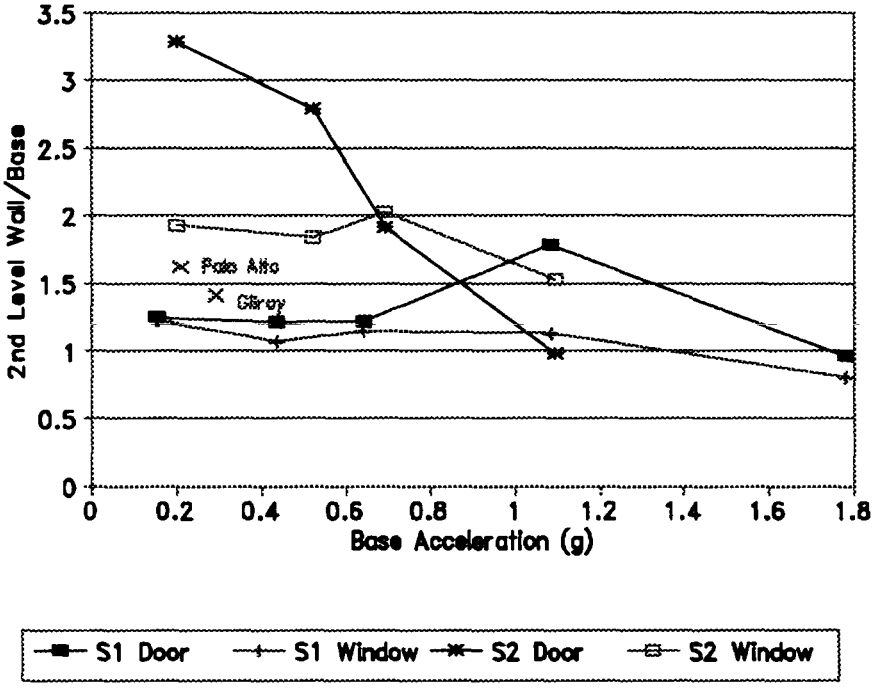

Figure 4.56 Peak Second-level Wall Acceleration to Peak Base Acceleration Ratios, vs Peak Base Acceleration

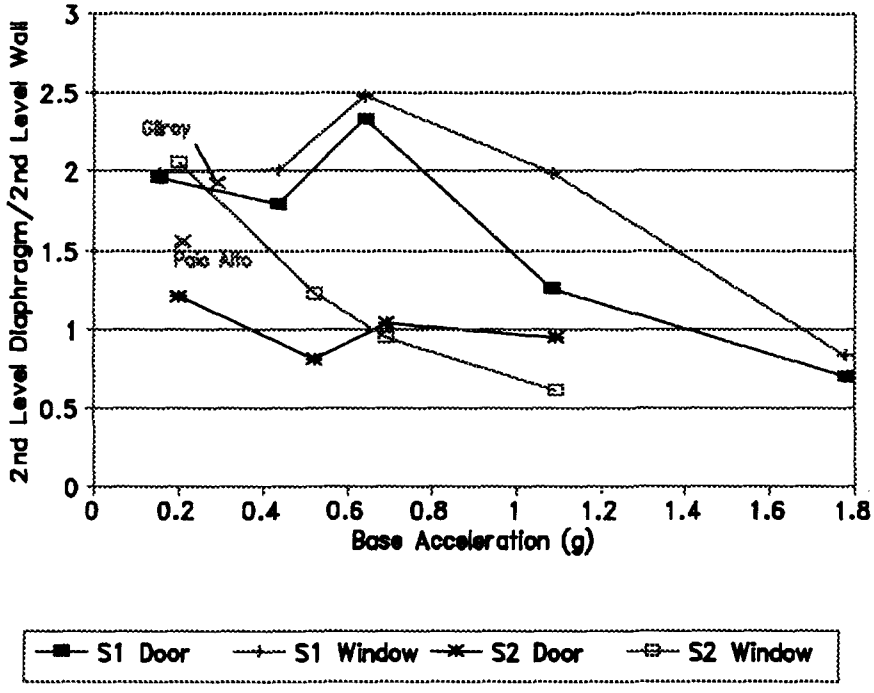

Figure 4.57 Peak Second-level Diaphragm Acceleration to Peak Second-level Wall Acceleration Ratios, vs Peak Base Acceleration

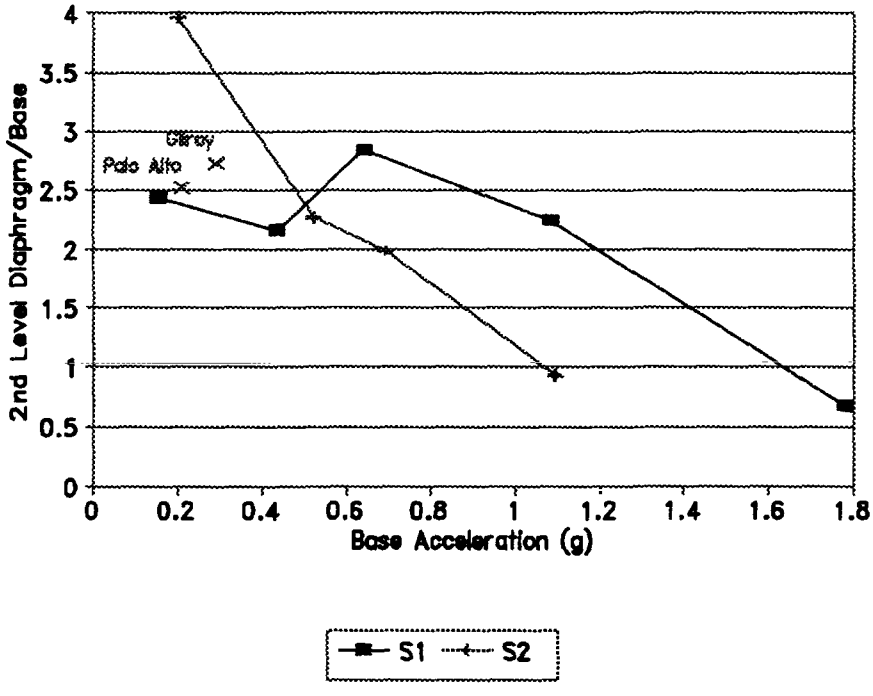

Figure 4.58 Peak Second-level Diaphragm Acceleration to Peak Base Acceleration Ratios, vs Peak Base Acceleration

fact that the plots from S2 were smoother than those from S1, suggested that the improvement in the diaphragm bolting connections was warranted.

Cracking during Test Runs 14 and 22 was described in Section 4.2 while the time of cracking was investigated in Section 4.4. During these two test runs, most of the peak values used in the acceleration ratios (Figures 4.56-4.58) occurred near the time that cracking was taking place. Therefore, only the last test run of S1 and the last two of S2 should be treated as cracked behavior. In Figure 4.56, the two S1 walls amplified the base acceleration at nearly a constant level until the walls cracked. After cracking, the acceleration ratios were less than all previous ratios and were very near 1.0. For S2, a decrease in base acceleration amplification with increasing base acceleration was observed for the door wall. The amplification was less after cracking (the last two points) and the final ratio was also near 1.0. For the S2 window wall, heavy cracking was not sustained and the acceleration ratios remained fairly constant. The decrease in the last value could have been due to sliding across the crack that formed or due to the reduction of the door-wall motions.

The diaphragm acceleration to wall acceleration ratios (Figure 4.57) showed similar trends as were discussed for the wall-to-base ratios. Prior to cracking, the ratios were fairly constant while after cracking, the ratios dropped below 1.0. This was evident in the three test runs where the test structure was substantially cracked. A similar trend, although not shown, existed for the first-floor diaphragm to first-floor wall acceleration ratios. The diaphragm to S2 window-wall ratio showed a gradual decrease. Even without substantial cracking in the window wall, the diaphragm could not exceed the window-wall acceleration once the door wall had cracked.

Combining the results from Figures 4.56 and 4.57 produced the second-level diaphragm to base acceleration ratios plotted in Figure 4.58. These three figures indicated that after cracking took place, two changes in behavior occurred. The first was that wall amplification of base accelerations decreased to the point of negligible amplification. More importantly, the second change in behavior was that after substantial cracking, the large amplification of either the wall or base accelerations by the flexible diaphragm diminished to the point where no amplification existed at all. This amplification reduction occurred even when only one supporting wall experienced major cracking.

4.9 Lateral Force Distributions

Floor-level forces were computed for S1 and S2 for each of the points in the histories. These (inertial) forces were determined by multiplying the diaphragm and two wall accelerations at a given level by the tributary masses listed in Table 4.1. Note that the mass distributions of S1 and S2 were approximately 3:5 for masonry mass : diaphragm mass. Thus, the diaphragm component of the forces was usually the dominant component. The total masonry mass is not fully reflected in Table 4.1 since half of the lower story was tributary to the base.

Floor-level force pairs, one for each test run, are plotted in Figures 4.59 and 4.60. Each force pair was concurrent in time from one of the largest base shear peaks of each test run. Clearly, these force pairs did not follow a linear, or inverted-triangular, force distribution. Rather, the two floor-level forces in each pair appeared to be nearly the same.

To determine whether the force pairs plotted in Figures 4.59 and 4.60 were representative of the behavior of the test structures, all the force pairs from each test run were examined. The first-level forces were divided into the second-level forces to produce force ratios for each point in the history. A representative set of force ratios is plotted versus time in Figure 4.61. The ratios for each test run were averaged between 2 and 14 seconds, the duration of ground motion. Spurious ratios, calculated when the first-level force was very small, were eliminated by not including ratios greater than 10 or less than -10 in the average. The average force ratios are plotted against peak base acceleration in Figure 4.62. From the data in Figures 4.59-4.62, the floor-level forces for S1 and S2 did not follow a linear distribution, as is commonly assumed for earthquake loadings. Instead, the floor-level forces were, on the average, almost equal through all test runs. This result might be expected for the cracked test runs since the upper portion (including both diaphragms) of S1 and S2 remained intact. For a system with rigid walls and equally-flexible diaphragms, this result should be expected since each diaphragm would receive the same input motion and would vibrate in the same manner. During the uncracked test runs, the masonry walls must have been stiff enough relative to the diaphragms to have produced this behavior.

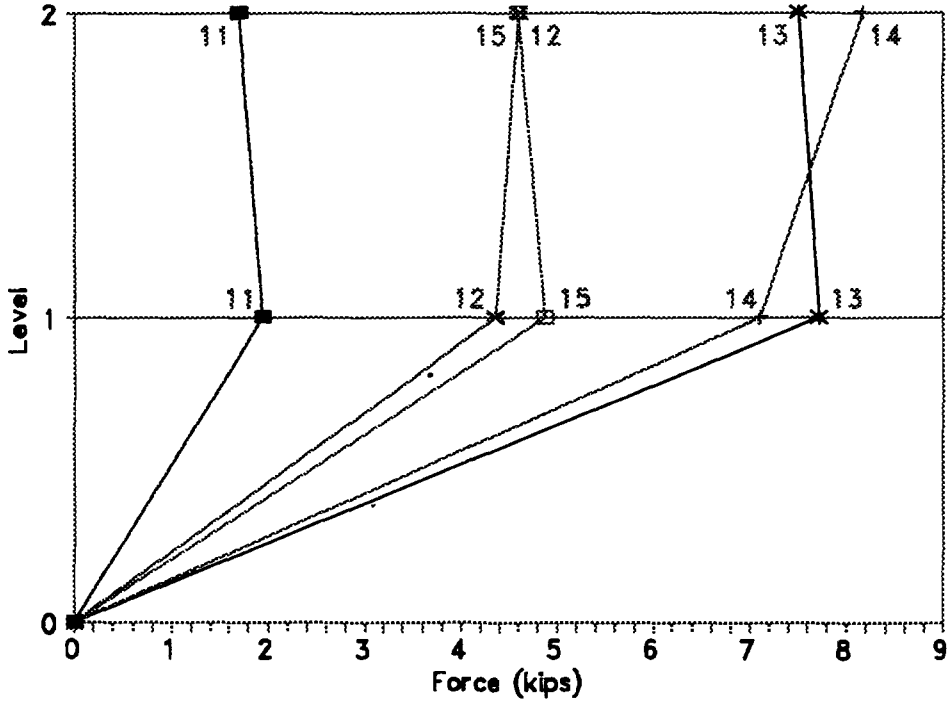

Figure 4.59 Representative Measured Force Pairs from S1 test runs

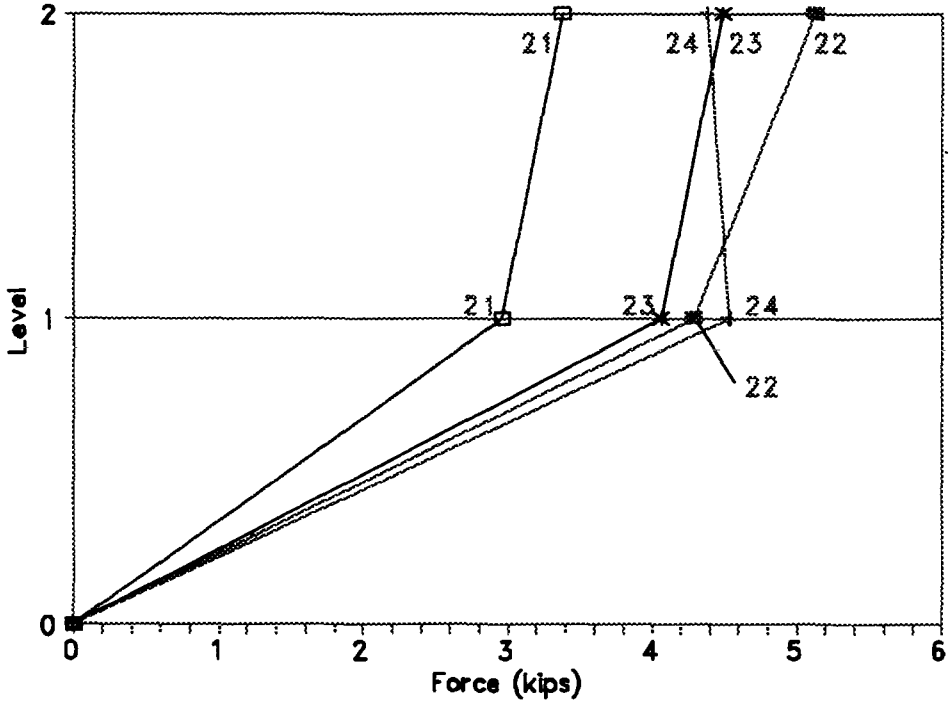

Figure 4.60 Representative Measured Force Pairs from S2 test runs

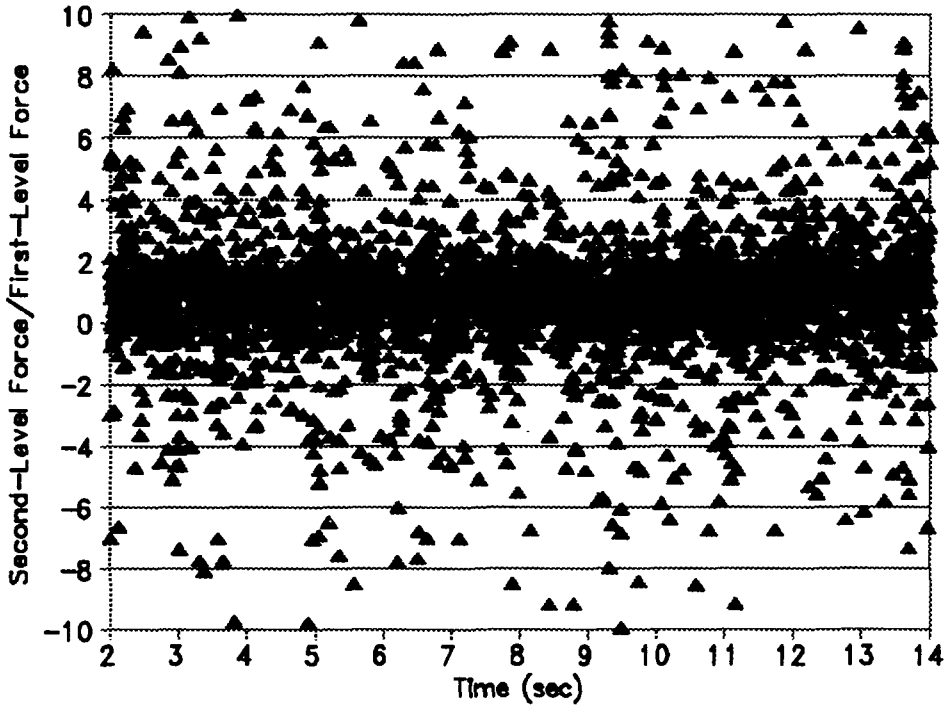

Figure 4.61 Sample History of Force Pairs (Test Run 13)

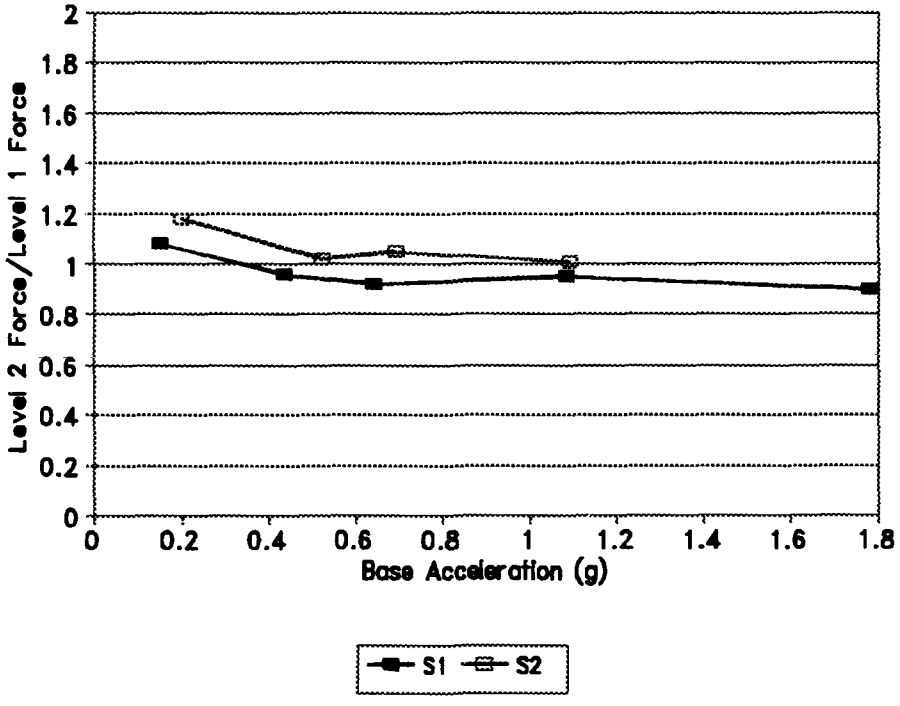

Figure 4.62 Average Force Ratios vs. Peak Base Acceleration for S1 and S2

4.10 Rocking Displacements

During the testing of S2, two LVDTs were used to measure the opening and closing of horizontal cracks at the top of the two, left (west), first-story, door-wall piers (see Figure 2.31 for location of LVDTs). The displacement histories from these two instruments are plotted in Appendix E. With these measurements, negative values represent an opening of the crack, which was caused by a negative displacement (west) of S2. By examining the two histories from Test Run 22, fairly accurate estimations were made as to when cracks first appeared along these specific bed joints. A blow-up of the two response histories, plotted from 4.4-5.0 seconds, is shown in Figure 4.63. From this figure, the left pier was likely to have started cracking at 4.51 seconds and was definitely cracked by 4.78 seconds, where the first residual occurred (the crack did not close completely). Similarly, the left central pier appeared to start cracking at 4.50 seconds and had its first residual displacement at 4.92 seconds.

Another feature of the crack opening/closing histories was the regular pattern that existed for the opening and closing of the horizontal cracks. This pattern was more clearly seen in the left central pier histories. This repetitive, regular opening and closing motion was indicative of a pier undergoing a rocking behavior. Although some horizontal sliding occurred across the cracks during Test Runs 23 and 24, a consistent sliding motion would have produced twice as many peaks in the record since sliding would have occurred in both directions, and would not have produced the "dead" spots in between the peaks, when the crack was mostly closed. Furthermore, large horizontal sliding oscillations, greater than 1", would have been required to withdraw the LVDT core enough to imitate the 0.1" level of vertical displacement measured across the cracks. A rocking behavior was the only explanation and was consistent with visual observations.

A rocking behavior was established for the left central door pier of S2 after horizontal cracks formed at its top and near its base. An examination of the crack opening history for this pier from Test Run 24 gave an indication of how much of the post-cracking horizontal displacements were due to the rocking motion. The rocking portion of the left central door pier was 29.3" high and 13.4" wide. By initializing the crack-opening displacement history to zero and multiplying by $^{29.3}/_{13.4}$, an

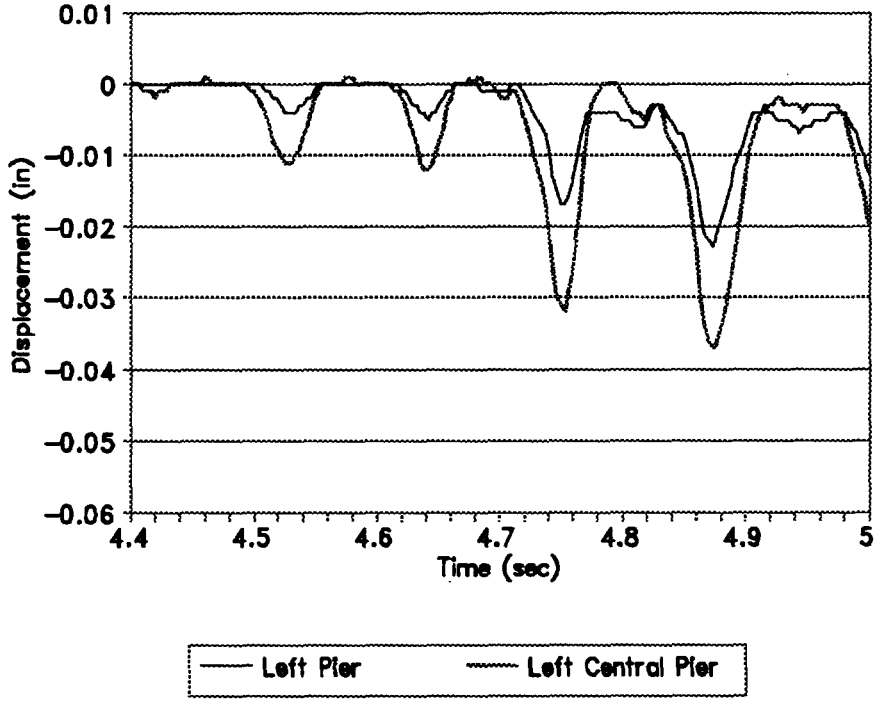

Figure 4.63 Blow-up of Vertical LVDT Measurements at Initiation of Cracking (Test Run 22)

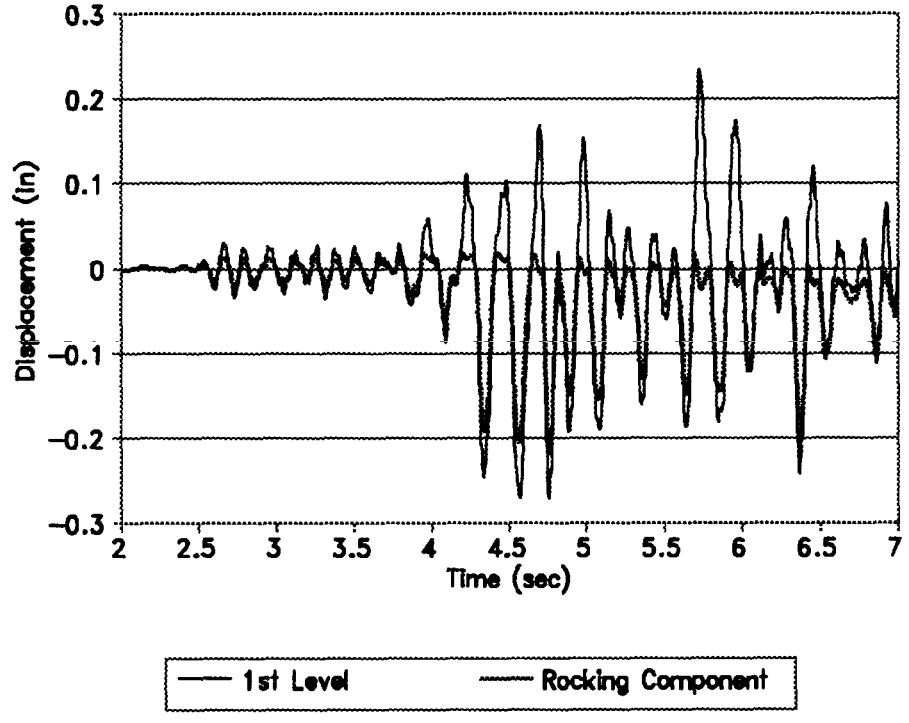

Figure 4.64 First-level Door-wall Displacement and Rocking Displacement from Test Run 24

estimate of the horizontal displacements caused by rocking was made. A portion of the rocking-induced horizontal displacement history is overlaid on the first-level displacement history, also initialized to zero, in Figure 4.64. Note that the rocking measurements were only made in one direction of building motion (west) since the crack (width) being measured was closed when the building rocked in the other direction (east). Ratios were made of the rocking component to the first-level displacement for all pairs of points below zero. The ratios between 2.0 and 7.0 seconds were averaged. Only ratios greater than zero and less than two were included in this average. The average indicated that approximately 80% of the first-level displacement was attributable to the rocking behavior. Comparable results were computed for a similar procedure using the data from Test Run 23. An overlay of measured first-level displacement and the computed rocking-induced horizontal displacement for Test Run 23 is shown in Figure 4.65.

4.11 Comparison of Measured Response to Conventional Methods

4.11.1 Static

The cracking loads calculated using the two design codes, UBC and MSJC (Sections 3.2.1 and 3.2.2), were quite conservative relative to those measured during Test Runs 14 and 22 (Figure 4.66). For S1, the measured value (15 kips) was three times higher than the UBC (5.2 kips) and six times higher than the MSJC (2.4 kips). For S2, the measured cracking load (8 kips) was more than twice the value calculated using the UBC (3.7 kips) and more than five times the value calculated using the MSJC (1.7 kips). The level of conservatism for the UBC values, ½ to $^1/_3$, implied a factor of safety of 2 to 3. This was consistent with the working stress approach used by the UBC. Since the MSJC allowed no tensile capacity for the masonry, the cracking loads calculated were twice as conservative as the UBC values. This factor of two was related to the fact that the dead load stress in the masonry was approximately equal to the value of the tensile capacity of the masonry.

Cracking loads were also calculated using the finite element method (Section 3.2.5). These values (4.8 and 4.1 kips, for S1 and S2, respectively) had similar levels of conservatism as the UBC values. This conservatism was primarily due to the high dependence of the calculated cracking loads

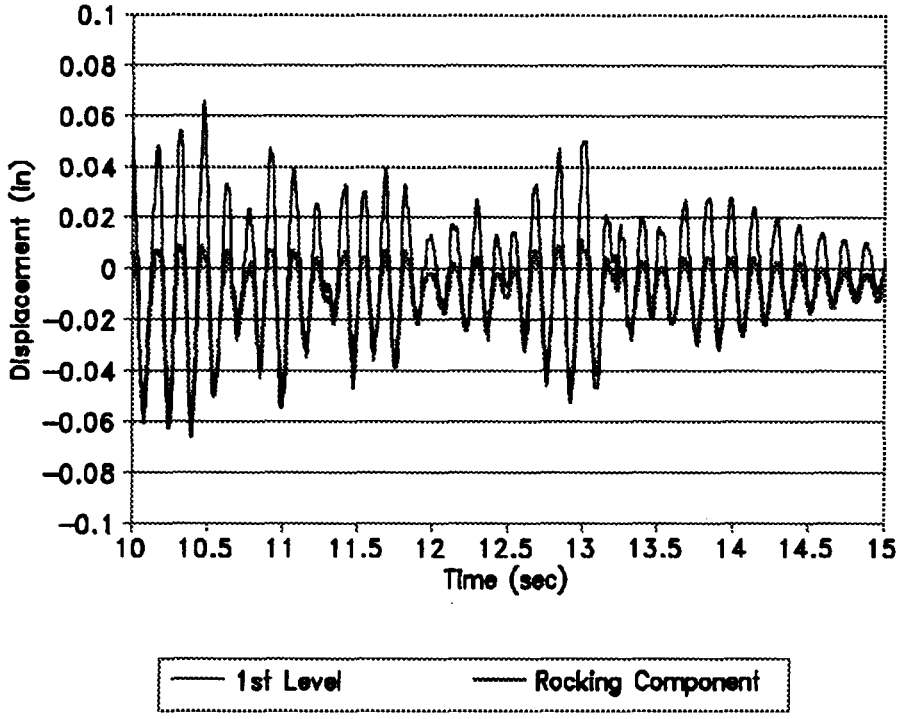

Figure 4.65 First-level Door-wall Displacement and Rocking Displacement from Test Run 23

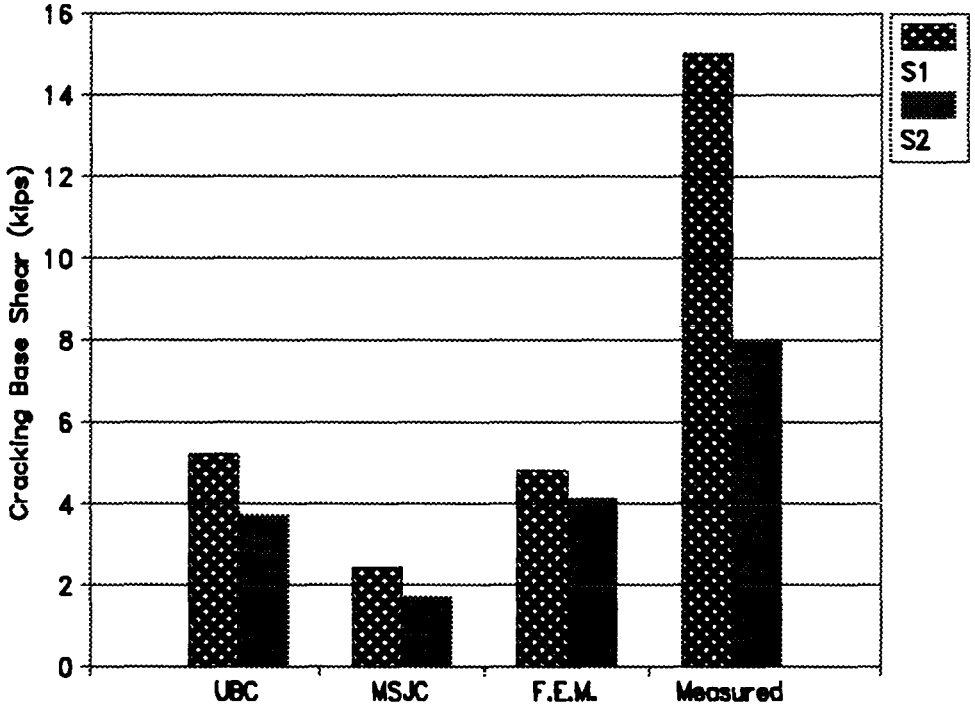

Figure 4.66 Comparison of Calculated and Measured Cracking Shears

on the tensile capacity used in the analysis. The dynamic tensile strength of the masonry was obviously much higher than that measured during the flexural tension tests.

The cracking loads were calculated using (lateral) floor-level loads based on an inverted-triangular distribution. During the dynamic tests, (lateral) floor-level loads were approximately equal, resulting in a uniform distribution (Section 4.9). For a two-story building, the difference in global overturning moment between the two force distributions is only 10%. Therefore, the static analyses were not very sensitive to the lateral force distribution.

The ultimate capacity of S1 and S2 were calculated using the FEMA 178 method (Section 3.2.4). The capacities of 15.2 kips and 8.5 kips, for S1 and S2 respectively, compared moderately well to the peak base shears measured during Test Runs 15 and 24, 12.4 kips and 9.4 kips respectively (Figure 4.67). In both buildings, the FEMA 178 methodology indicated a rocking-controlled behavior rather than a shear-controlled behavior. Experimental observations confirmed this. Higher base shear values were measured in previous test runs of both buildings, but since rocking was most prevalent during the final test runs, these base shears were used for comparison.

The UCBC analysis (Section 3.2.3) indicated that pier rocking would control over pier shear for S2, but that shear would control for S1. The calculated strengths, however, were a factor of $3^1/_3$ below the rocking strengths measured experimentally. This was because the UCBC method used a working stress approach even though the rocking and shear conditions were ultimate behaviors. Other than the difference in the coefficients in the equations, the UCBC and FEMA 178 approaches were the same and should have been expected to produce similar results, if properly scaled. In fact, multiplying the UCBC results by $3^1/_3$ gave almost exactly the measured results. Therefore, the UCBC strengths agreed with the experimental results when a factor of safety of $3^1/_3$ was included.

4.11.2 Dynamic

Agreement between the simple dynamic analyses examined (Sections 3.3.1-3.3.5) and measured dynamic results was generally poor (Table 4.12). An equivalent frame model was used to estimate natural frequencies (Section 3.3.1). Using the assumption of rigid diaphragms, the two in-plane walls were combined to form a model with one degree of freedom at each floor level. The rigid

Table 4.12 Comparison of Results from Dynamic Analysis Models with Measured Values

Dynamic Model	S1 Result	S2 Result
	Natural Frequencies	Natural Frequencies
Equivalent Frame Analysis (rigid diaphragm)	44 Hz	47 Hz
Finite Element Model (rigid diaphragm)	35 Hz	34 Hz
MDOF w/ Flex. Diaphragm	11.8, 11.9, 80.2, 87.8 Hz	11.7, 11.9, 52.2, 118.6 Hz
Finite Element Model (flexible diaphragm)	21.5 Hz	20.6 Hz
MEASURED	8.2 Hz	9.8 Hz
	Acceleration, Displacement Simulation of Test Run 11	Acceleration, Displacement Simulation of Test Run 21
MDOF w/ Flex. Diaphragm (2nd Level Diaphragm)	0.45g, 0.064"	0.62g, 0.075"
Response Spectrum Analysis (2nd Level Diaphragm)	0.50g, 0.011"	0.34g, 0.008"
MEASURED (2nd Level Diaphragm)	0.373g, 0.029"	0.792g, 0.063"

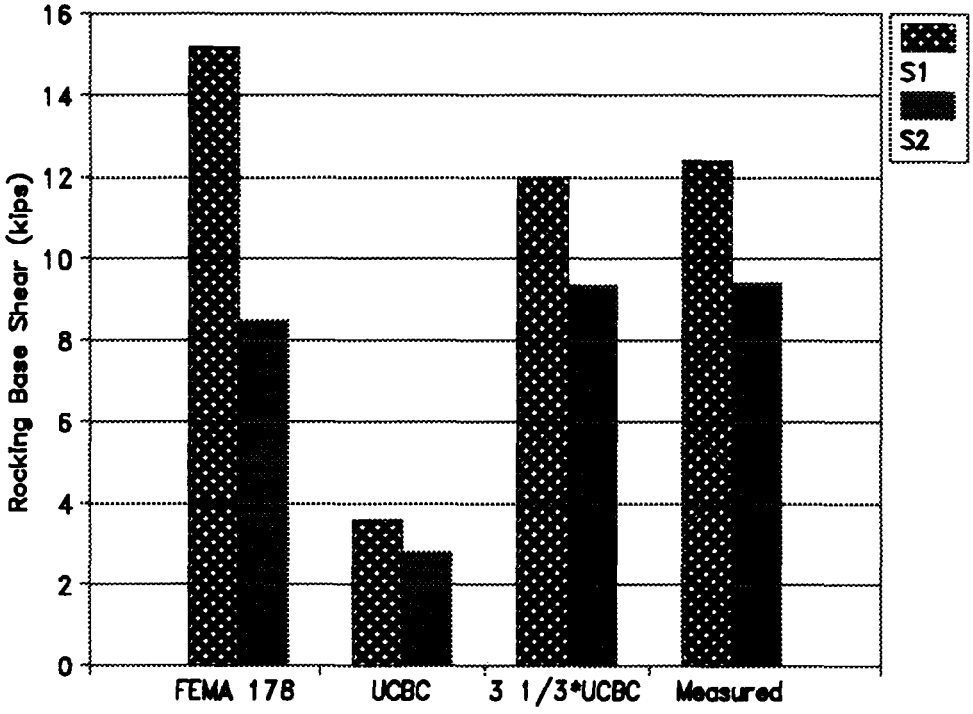

Figure 4.67 Comparison of Calculated and Measured Rocking Shears

diaphragm assumption resulted in natural frequencies which were 4½ to 5½ times higher than the frequencies measured during Test Runs 11 and 21.

Natural frequencies and mode shapes were calculated using the MDOF model with flexible diaphragms (Section 3.3.2). The mode shapes from this model showed almost no coupling between the walls or between either wall and the diaphragms. As a result, the first and second mode frequencies were essentially frequencies of just the diaphragms. Since the natural frequencies of S1 and S2 were dominated by the diaphragms, agreement between the calculated (11.8 and 11.7 Hz) and measured (8.2 and 9.8 Hz) values was fair.

Finite element models were also used to calculate natural frequencies and mode shapes (Section 3.3.4). Both flexible and nearly-rigid diaphragm models were used. These models produced mode shapes with diaphragms and walls vibrating in unison (Figures 3.14 and 3.15), but the natural frequencies (21.5 and 20.6 Hz for the flexible diaphragms) were more than twice those measured. Frequencies calculated with the nearly-rigid diaphragms (35 and 34 Hz) were half again greater.

Peak displacements calculated using the MDOF model with flexible diaphragms (Section 3.3.3) ranged from 14.4 times smaller than to 3.3 times larger than the measured peaks from Test Runs 11 and 21. Wall displacements were too low while diaphragm displacements were too high. Calculated accelerations also varied in comparison to measured values though not as widely as displacements. The variation was primarily due to the large difference in stiffnesses between the walls and the diaphragms in the MDOF model.

The spectral values determined in Section 3.3.5 were based on calculated natural frequencies much higher than those measured and are therefore erroneous. Spectral analysis will be discussed again in Section 5.2.

4.12 Summary of Measured Response

Based on the measured results of a total of nine test runs on two buildings, the following conclusions were drawn.

1) Diaphragm and wall amplifications of base accelerations compared well with results measured on full-size buildings during actual earthquakes. Prior to cracking, both walls and diaphragms amplified base accelerations at a constant level while after cracking, little to no amplification existed.

2) Flexible diaphragms amplified wall displacements prior to cracking in the walls. After cracking, diaphragm deflections relative to the walls were greatly diminished. Interstory drifts above the cracks also decreased after cracking.

3) As expected for a truely flexible diaphragm system, little or no coupling was observed between parallel shear walls. Individual walls vibrated independantly of each other with no torsion of the diaphragm. In some cases deflection of the door-walls was two times larger than that of the window-walls.

4) Lateral forces were distributed equally between the two floor levels, not by the inverted-triangular distribution normally assumed for rigid diaphragms.

5) Low masonry tensile strength resulted in horizontal cracks across the bases and tops of most of the piers.

6) Cracking loads were many times higher than those determined using design codes and a finite element model. First-story cracking drifts were approximately 0.1%.

7) Substantial strength and deformation capacity existed after cracking. This ductility resulted from pier rocking in the first story.

8) After cracking, up to 80% of first-story displacements were attributable to rocking.

9) Post-cracking force-displacement curves were bilinear in shape, which is indicative of rocking.

10) Natural frequencies decreased as structural damage, in the form of cracking, increased. Frequency measurements were dependent on the amplitude of the test. Calculated natural frequencies were much higher than measured frequencies.

11) Simple dynamic methods did a poor job at estimating the natural frequencies and peak displacements and accelerations.

SECTION 5. ANALYTICAL MODELING

5.1 Overview

Two common analysis methods were studied to determine if they could be used to model unreinforced masonry structures with flexible diaphragms. These two methods were (a) response spectrum (elastic dynamic with a single degree of freedom) and (b) pushover (inelastic static analysis with an equivalent frame). Based on response measured during the dynamic test runs, a third analysis (inelastic dynamic) was conducted that utilized a nonlinear time-step integration program to compute post-cracking displacements of a three-degree-of-freedom model. For this third type of analysis, pier rocking was modelled to compute displacements.

The purpose of this section is to apply the three analysis methods to the two structures tested and to illustrate the merits and shortcomings of the three methods relative to the results determined experimentally.

5.2 Response Spectrum Analysis

In Section 3, a linear response spectrum analysis was used to estimate likely peak accelerations and displacements for the first test runs of S1 and S2. This cursory analysis was based on calculated natural frequencies and was intended merely to demonstrate the method rather than to predict response values. This section investigates the response spectrum method more thoroughly as an analysis technique for unreinforced masonry structures with flexible diaphragms.

5.2.1 Analysis

Linear acceleration and displacement response spectra were calculated for each of the nine test runs using the measured base acceleration histories. Spectra were computed using several percentages of critical damping, 2%, 5%, and 10%. Samples of an acceleration spectrum and a displacement spectrum for Test Run 22 with 5% damping are shown in Figures 5.1 and 5.2.

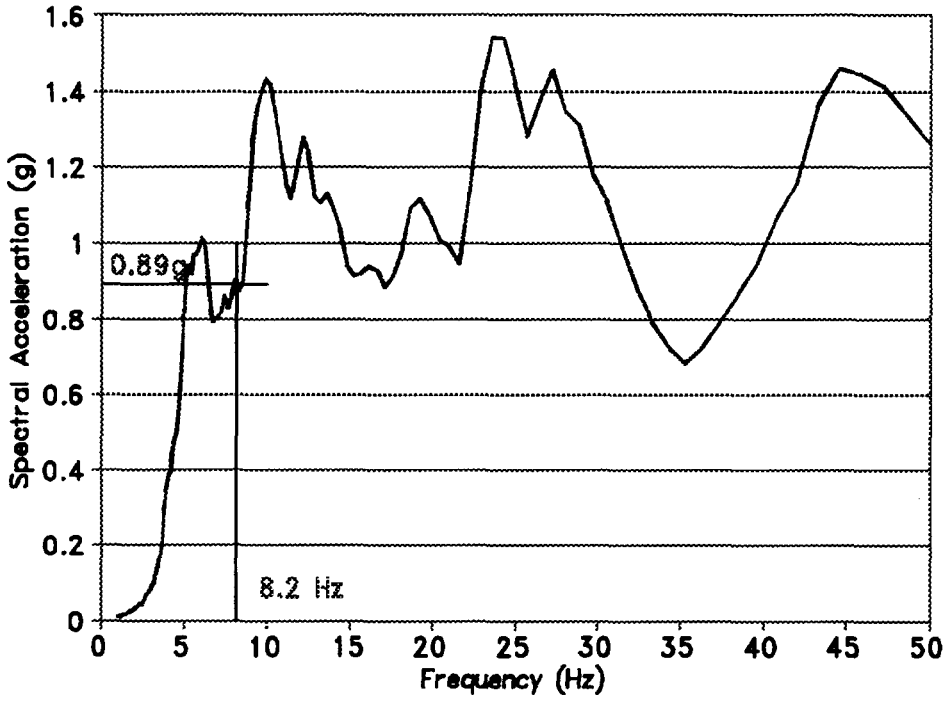

Figure 5.1 Acceleration Spectrum for Test Run 22 (5% damping)

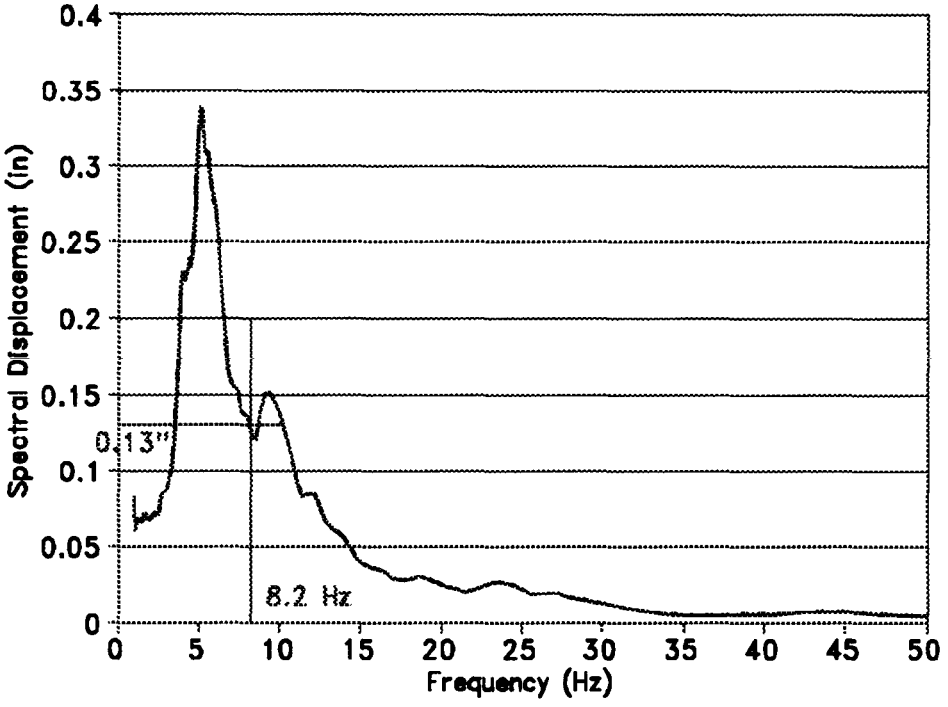

Figure 5.2 Displacement Spectra for Test Run 22 (5% damping)

Spectral accelerations and spectral displacements were extracted from each spectra (for each test run) at the natural frequency measured during the test run. Measured natural frequencies are plotted in Figures 4.37 and 4.38 and listed in Table 4.8. As an example, during Test Run 22, the measured natural frequency was 8.2 Hz. In Figures 5.1 and 5.2 this would correspond to a spectral acceleration of 0.89g and a spectral displacement of 0.13".

To convert spectral values to floor-level accelerations, the following equation was used,

$$a_{m_{ij}} = \Gamma_j \phi_{ij} S_{A_j} \tag{5.1}$$

where a_{mij} is the maximum acceleration at node i for mode j, Γ_j is the participation factor for mode j, ϕ_{ij} is the coordinate at node i for mode j, and S_{Aj} is the spectral acceleration for mode j. In this analysis, only one location, the second-level diaphragm, and only the first mode were considered ($j=1$). Furthermore, since the second-level diaphragm coordinate used to determine the modal participation factors was unity ($\phi_4=1.0$), Equation 5.1 reduced to

$$a_m = \Gamma S_A \tag{5.2}$$

where a_m is the maximum second-level diaphragm acceleration, Γ is the first-mode participation factor, and S_A is the first-mode spectral acceleration. Similarly, for displacements,

$$d_m = \Gamma S_D \tag{5.3}$$

where d_m is the maximum second-level diaphragm displacement, Γ is the first-mode participation factor, and S_D is the first-mode spectral displacement.

The spectral acceleration and displacement curves were converted into peak floor-level acceleration and displacement curves using Equations 5.2 and 5.3 for each point on the curve. A participation factor of 1.3 was used for uncracked test runs (11, 12, 13, 21) while 1.15 was used for cracked test runs (14, 15, 22, 23, 24). The second floor-level acceleration and displacement curves are plotted in Figures 5.3 to 5.12 for S1 and Figures 5.13 to 5.20 for S2. The percentage of critical damping used is noted by each curve. A vertical line in the figures indicates the natural frequency measured during each test run. A small, filled square is also plotted in each figure representing the value of acceleration or displacement measured during the test run. Note that in

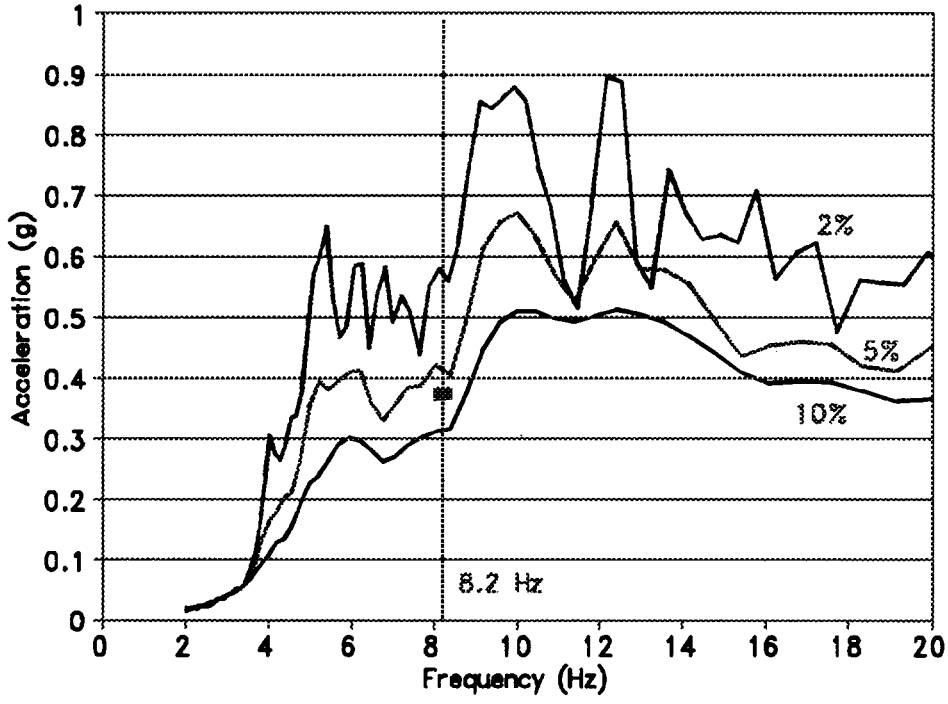

Figure 5.3 Spectrally-based Accelerations for Test Run 11

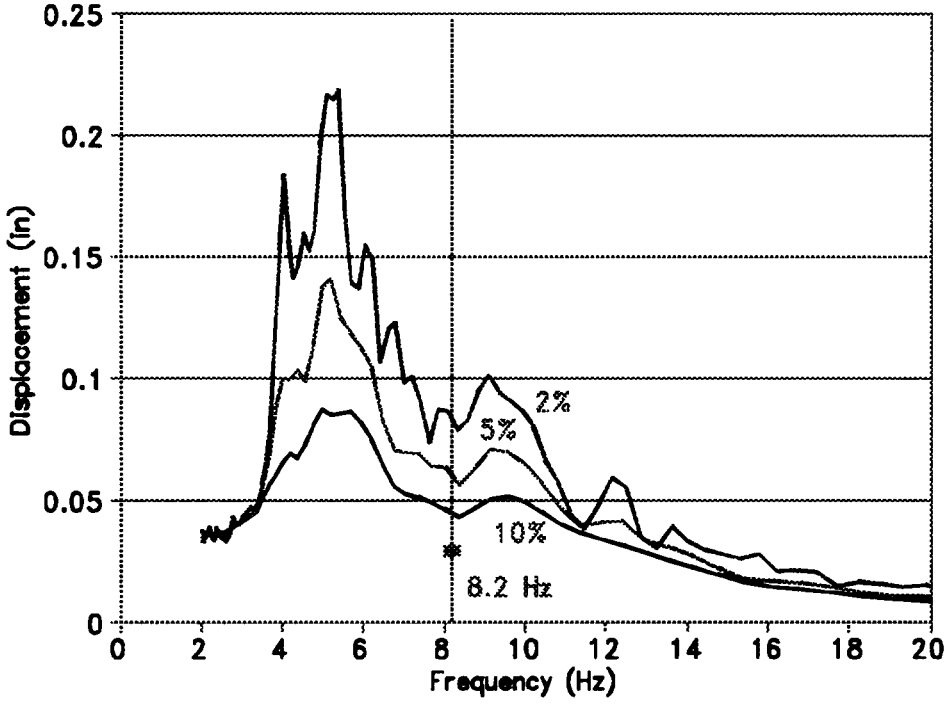

Figure 5.4 Spectrally-based Displacements for Test Run 11

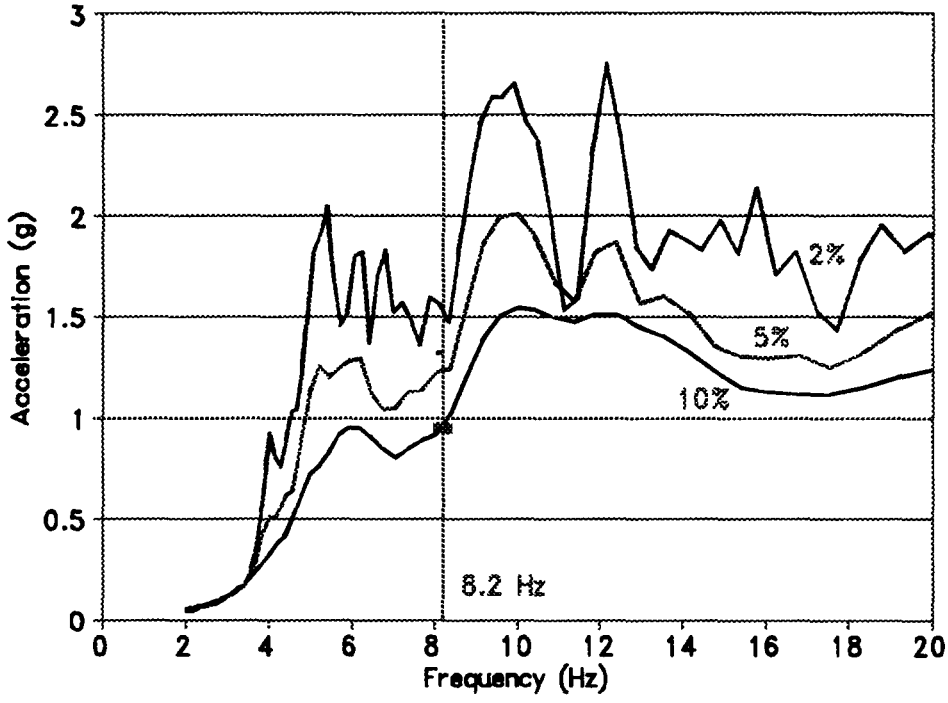

Figure 5.5 Spectrally-based Accelerations for Test Run 12

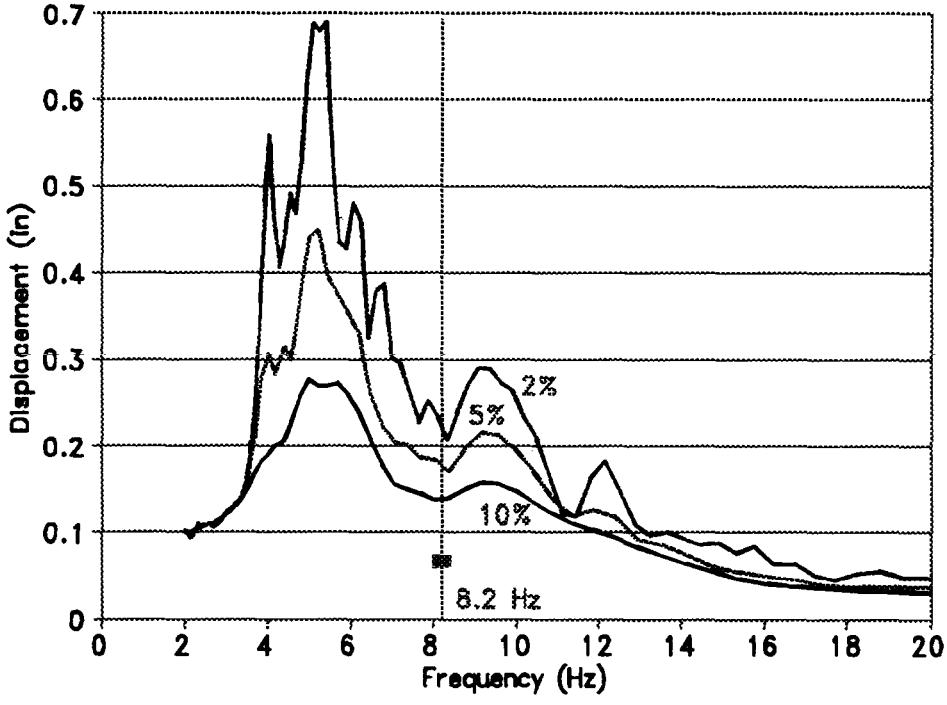

Figure 5.6 Spectrally-based Displacements for Test Run 12

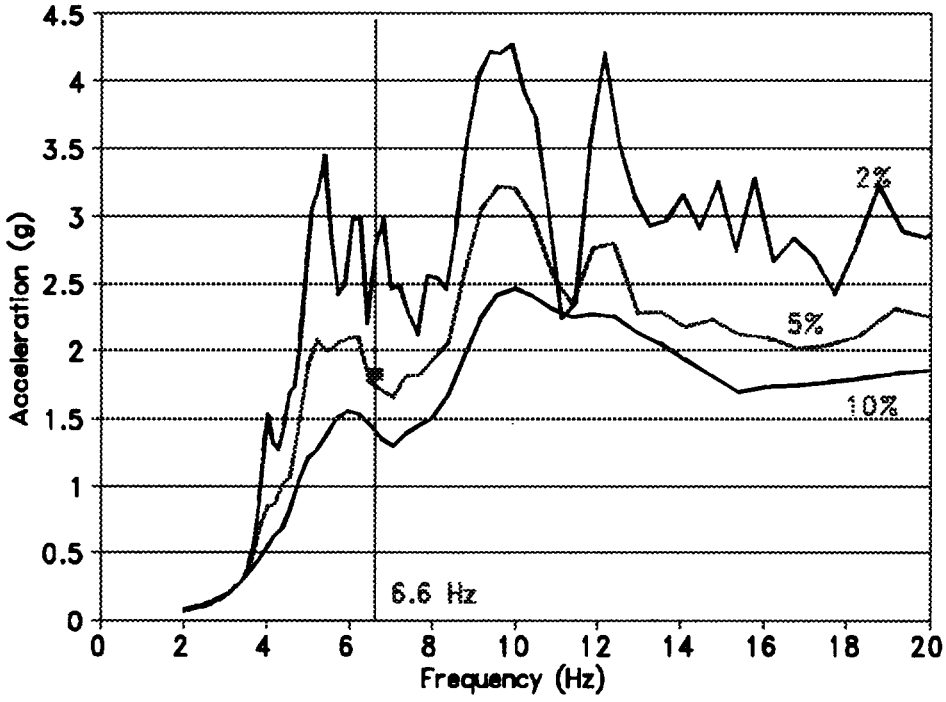

Figure 5.7 Spectrally-based Accelerations for Test Run 13

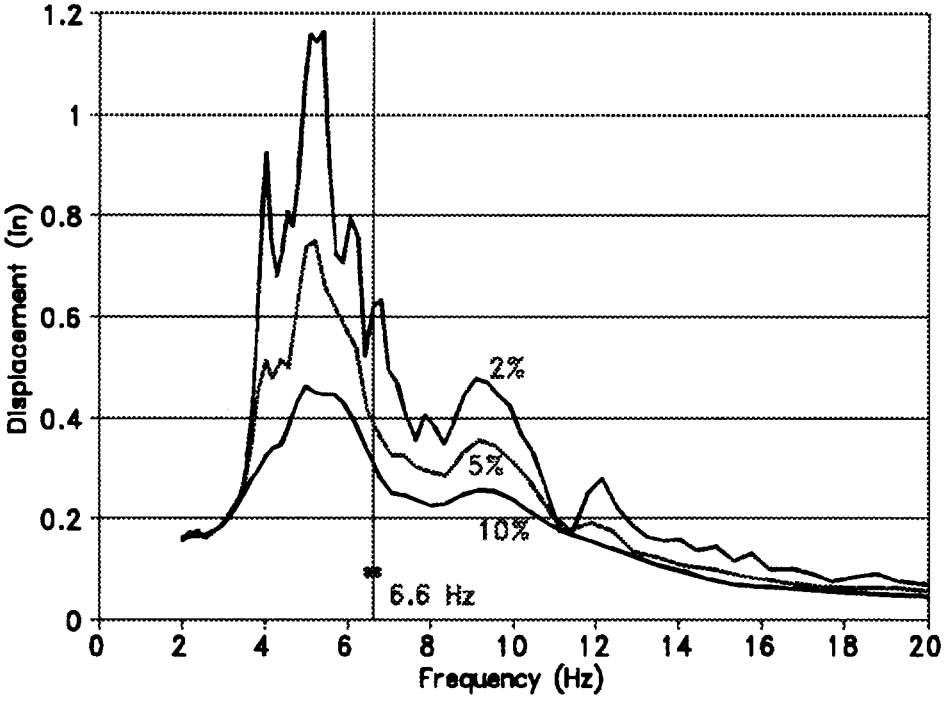

Figure 5.8 Spectrally-based Displacements for Test Run 13

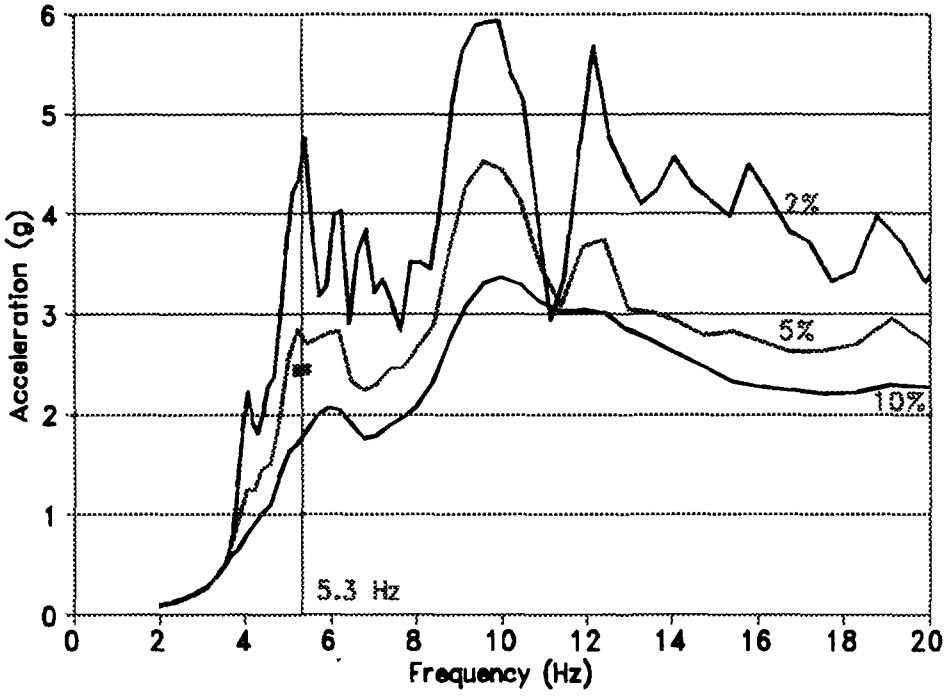

Figure 5.9 Spectrally-based Accelerations for Test Run 14

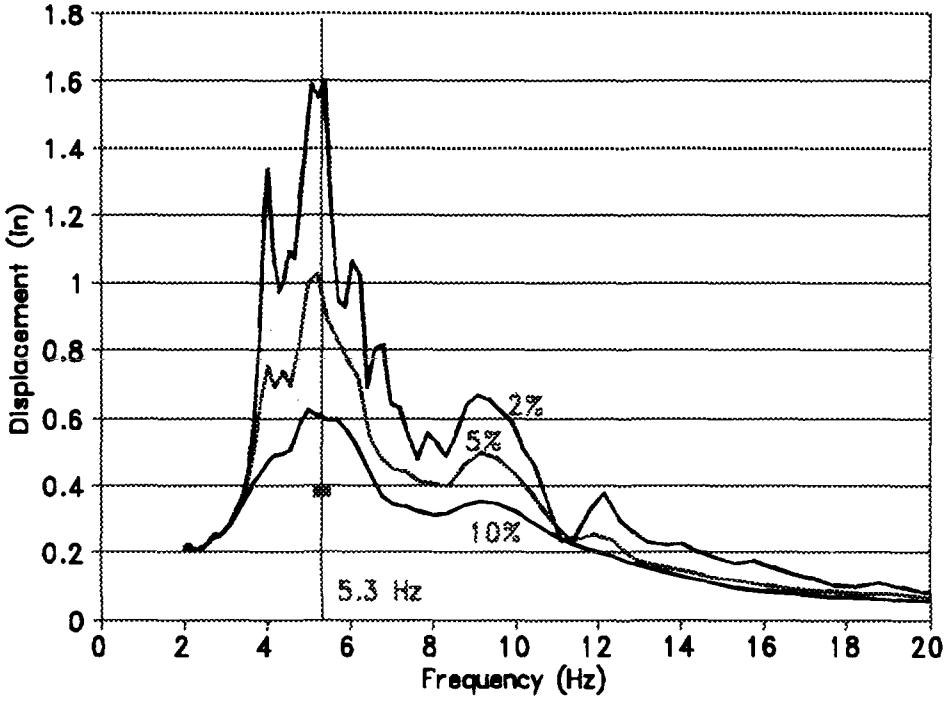

Figure 5.10 Spectrally-based Displacements for Test Run 14

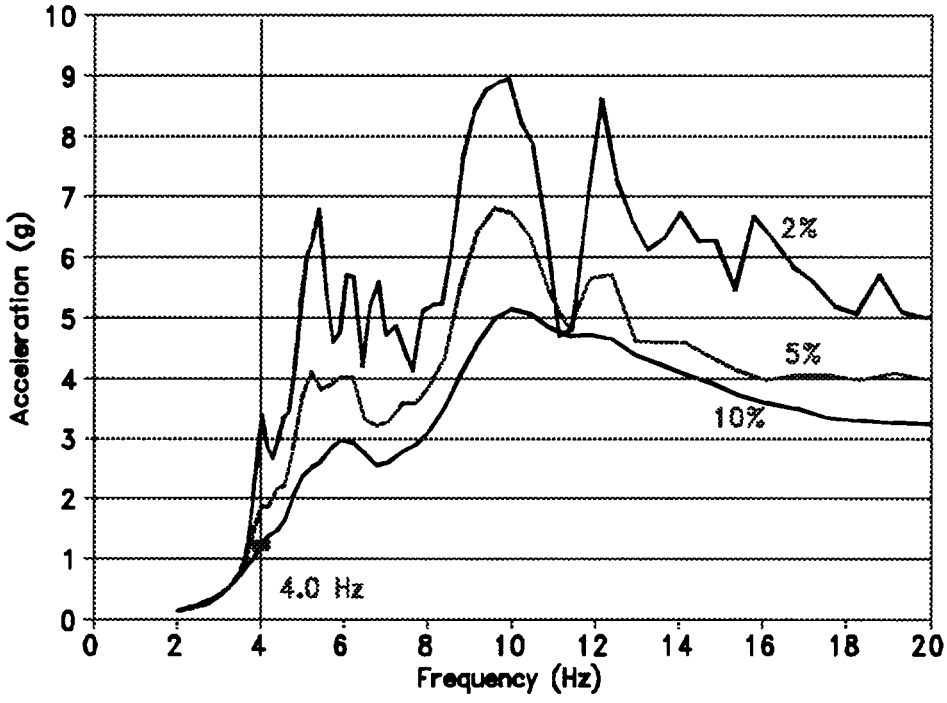

Figure 5.11 Spectrally-based Accelerations for Test Run 15

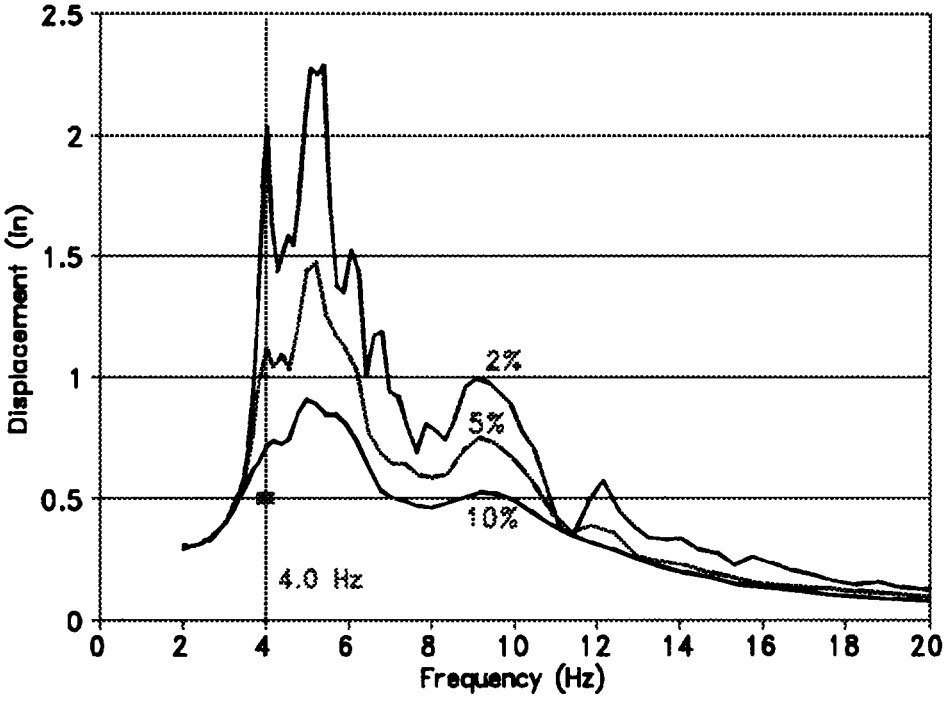

Figure 5.12 Spectrally-based Displacements for Test Run 15

Figure 5.10, the measured displacement for Test Run 14 was estimated. Of particular note in each pair of figures for a given test run is that the measured values correspond to different levels of damping for acceleration and displacement.

In Figures 5.3 to 5.20, spectrally-derived accelerations and displacements are plotted versus frequency. Since frequency is a common parameter to both curves, each pair of curves from a test run can be combined into one curve by parametrically plotting acceleration against displacement. Examples of such curves for Test Runs 12 and 13 are given in Figures 5.21 and 5.22. Note that in this type of plot, straight lines radiating from the origin are lines of constant frequency. Frequency decreases in a clockwise direction, from infinite along the y-axis to zero along the x-axis. The accelerations and displacements at the measured natural frequencies (represented by small filled squares) were extracted from the parametric plots (Figures 5.21 and 5.22) and replotted in Figures 5.23 and 5.24, forming a summary plot for S1 and S2. The level of damping is again noted by each curve. Each value plotted is the peak acceleration (a_m) and peak displacement (d_m) calculated for the test run using the measured base acceleration, the measured natural frequency, and the various levels of damping. Also plotted in Figures 5.23 and 5.24 are the peak accelerations and displacements of the second-level diaphragm measured during each test run. Note again that the displacement for Test Run 14 was estimated in Figure 5.23. Since the summary curves in Figures 5.23 and 5.24 are moderately complex, the measured values are replotted with a "best guess" estimate of the spectrally-derived accelerations and displacements in Figures 5.25 and 5.26, for S1 and S2, respectively.

5.2.2 Comparison with Measured Values

A comparison of the computed spectrally-derived peaks and the measured acceleration and displacement peaks gave mixed results. For most of the test runs, spectrally-derived accelerations were reasonably close to the measured ones, if the proper level of damping was assumed. As an example, in Figure 5.23, the measured acceleration for Test Run 14 (2.4g) fell between the 5% and 10% damping calculated values (2.8g and 1.7g, respectively). The measured acceleration from Test Run 24 (Figure 5.24) was the only significant deviation. Overall, however, spectrally-derived

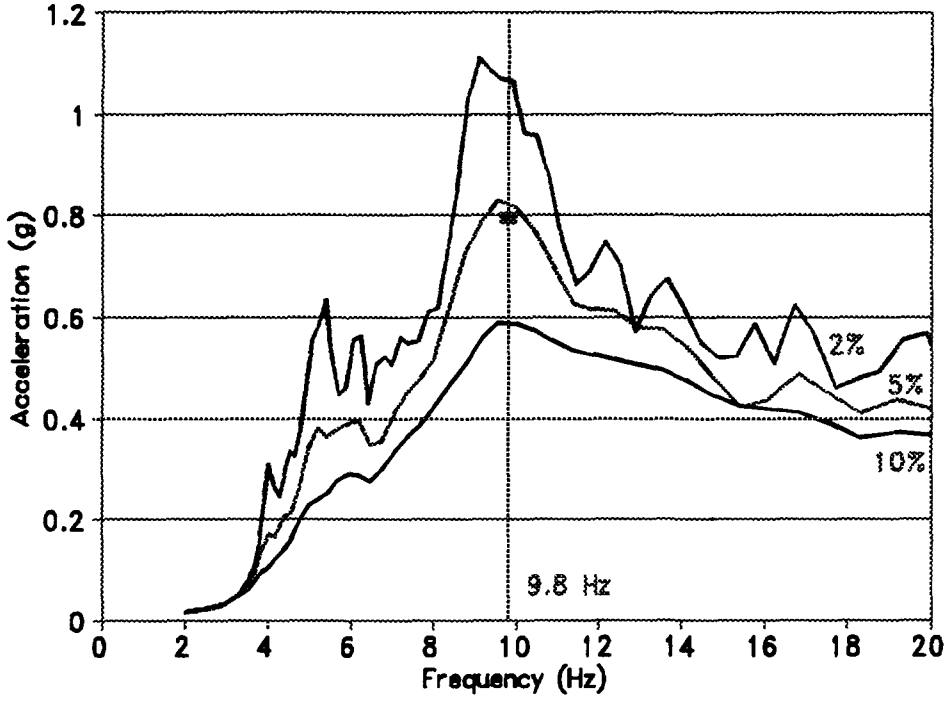

Figure 5.13 Spectrally-based Accelerations for Test Run 21

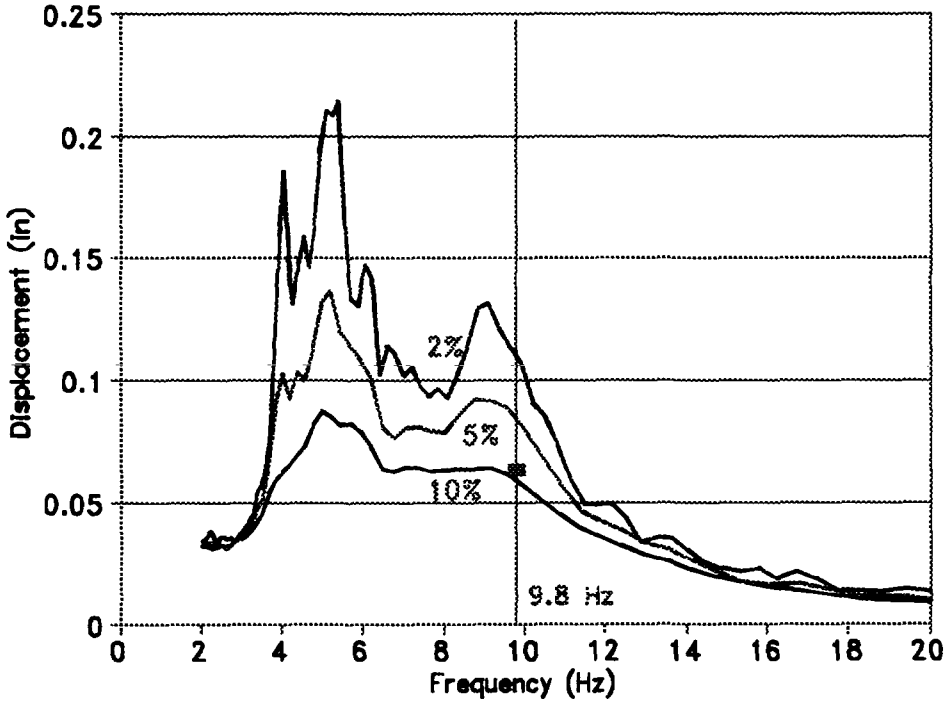

Figure 5.14 Spectrally-based Displacements for Test Run 21

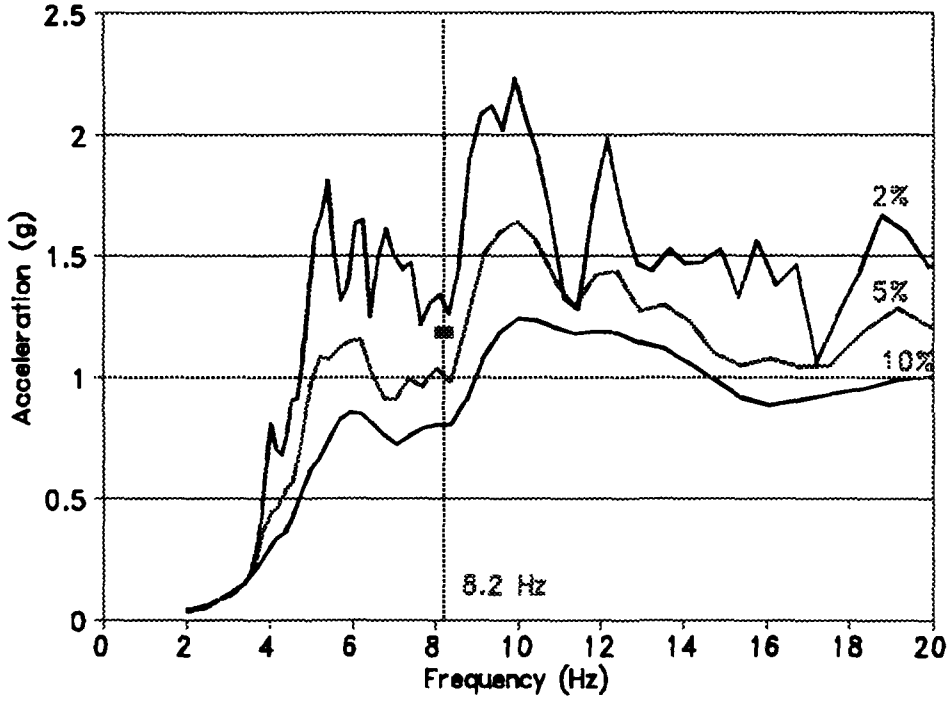

Figure 5.15 Spectrally-based Accelerations for Test Run 22

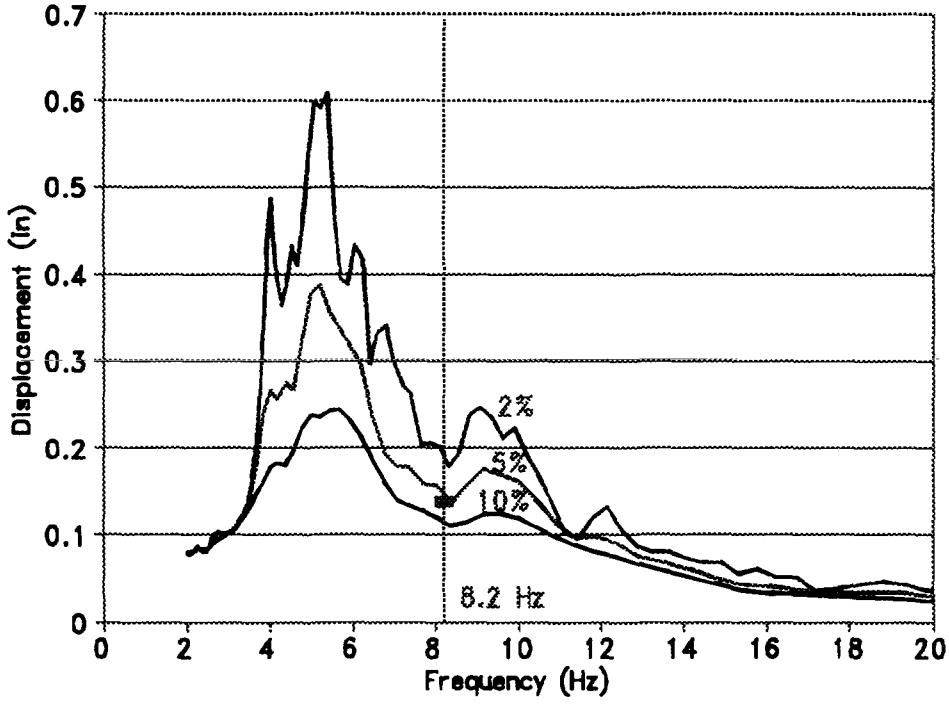

Figure 5.16 Spectrally-based Displacements for Test Run 22

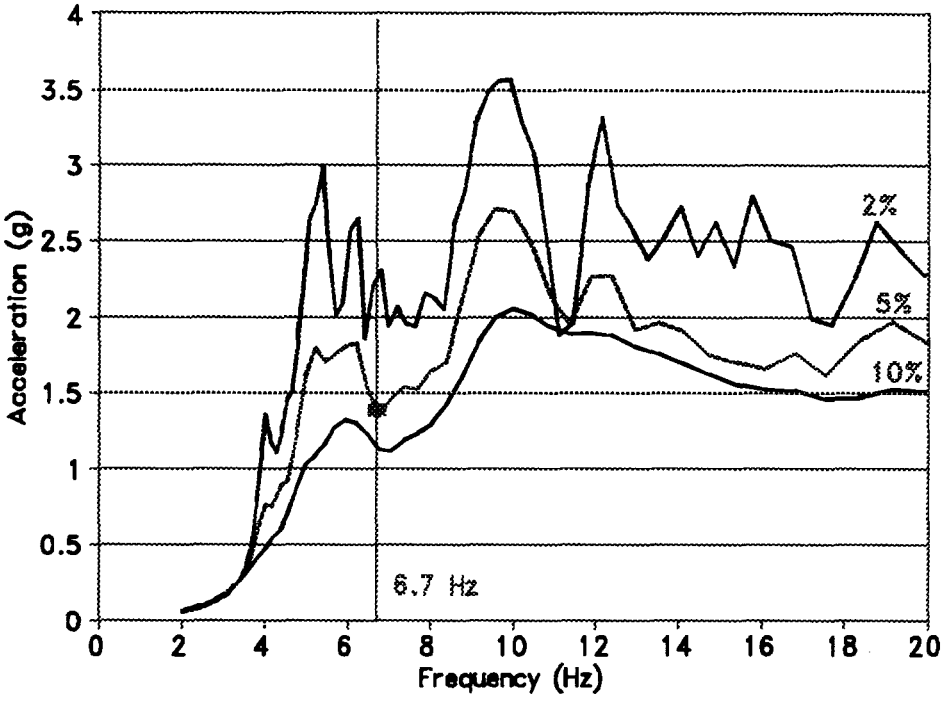

Figure 5.17 Spectrally-based Accelerations for Test Run 23

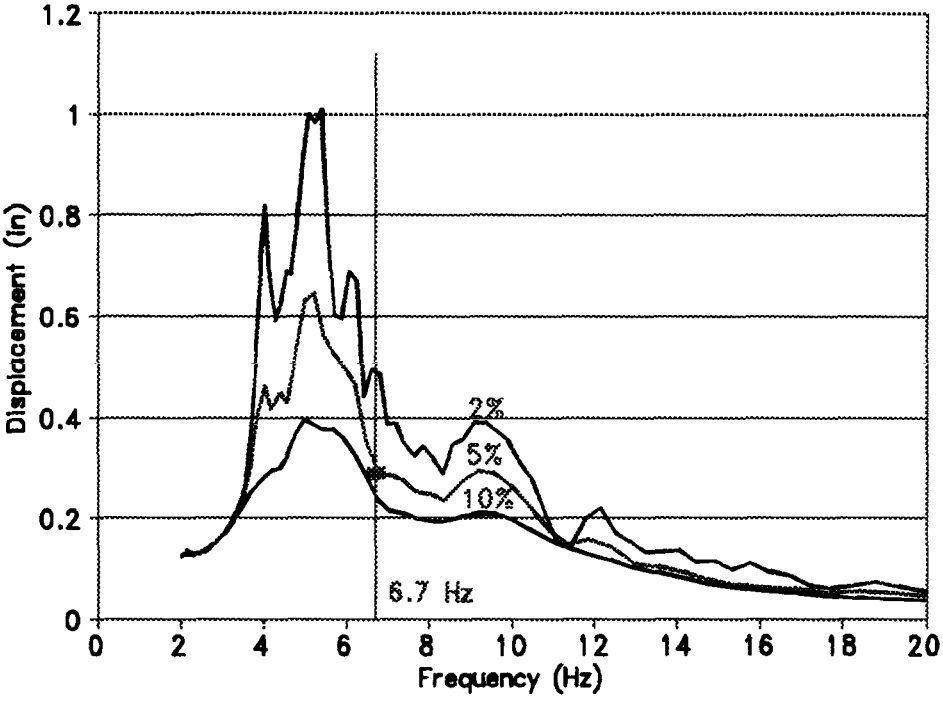

Figure 5.18 Spectrally-based Displacements for Test Run 23

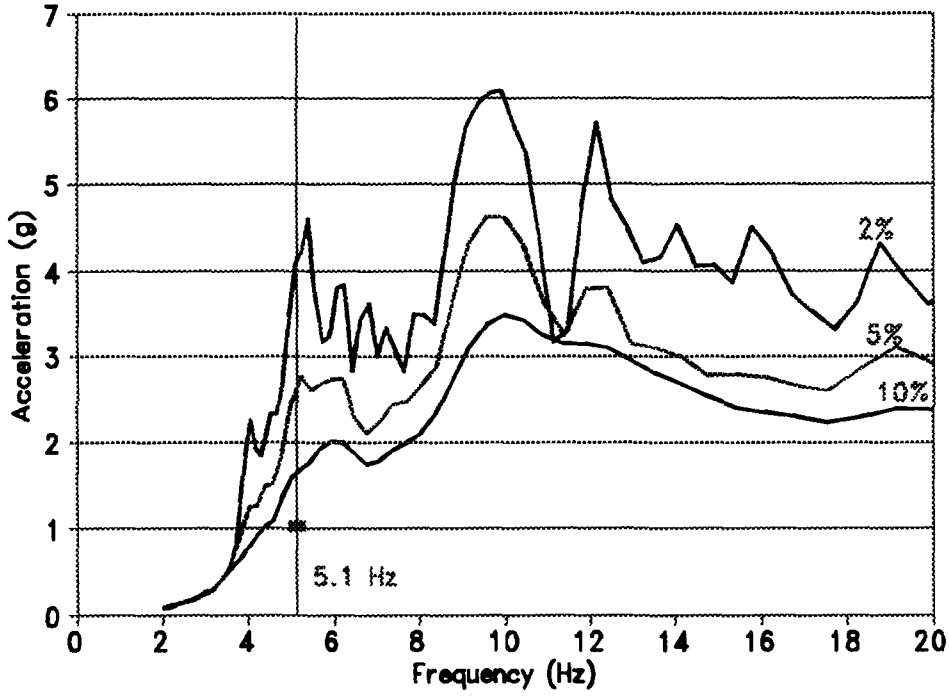

Figure 5.19 Spectrally-based Accelerations for Test Run 24

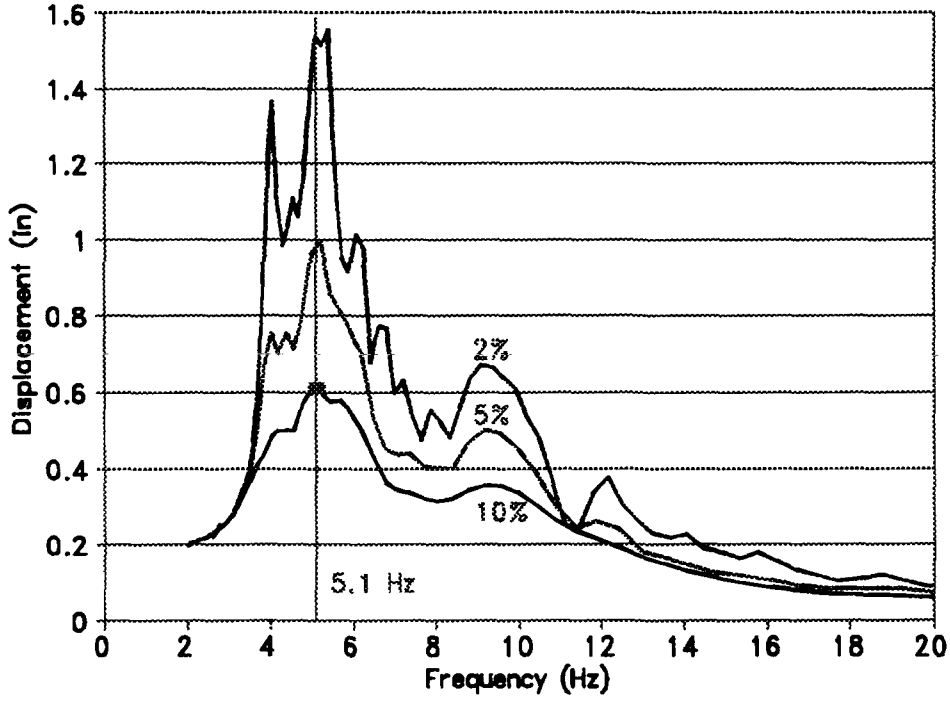

Figure 5.20 Spectrally-based Displacements for Test Run 24

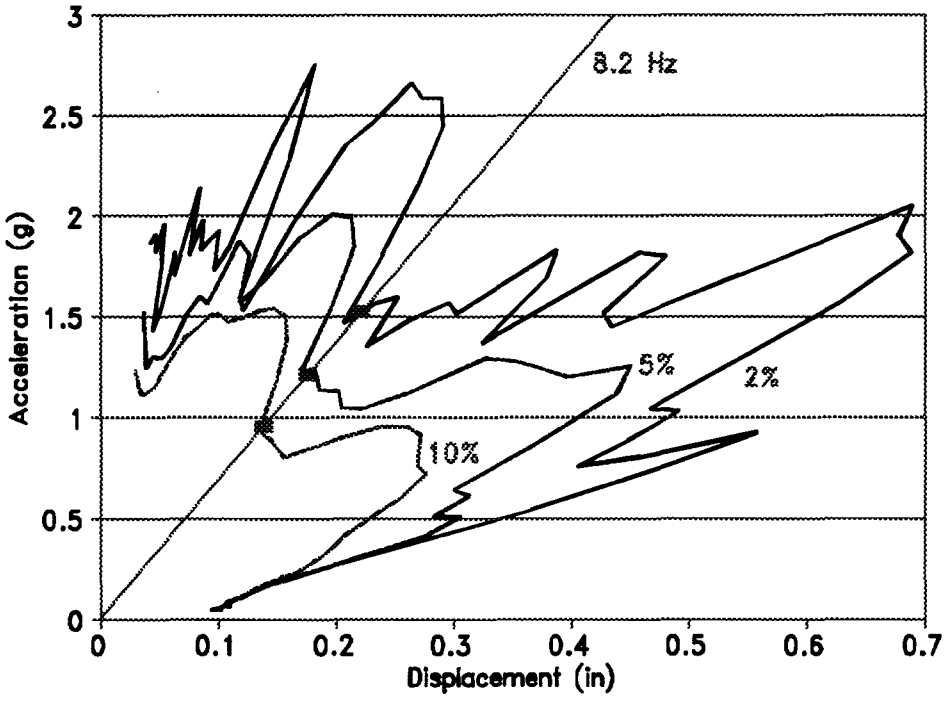

Figure 5.21 Parametric Plot of Acceleration versus Displacement for Test Run 12

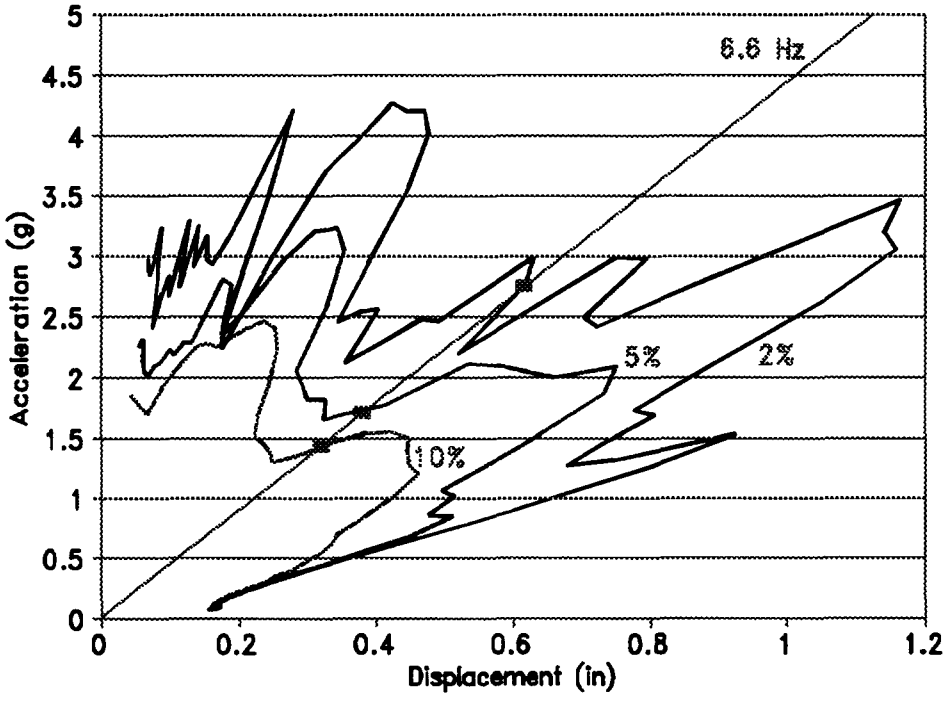

Figure 5.22 Parametric Plot of Acceleration versus Displacement for Test Run 13

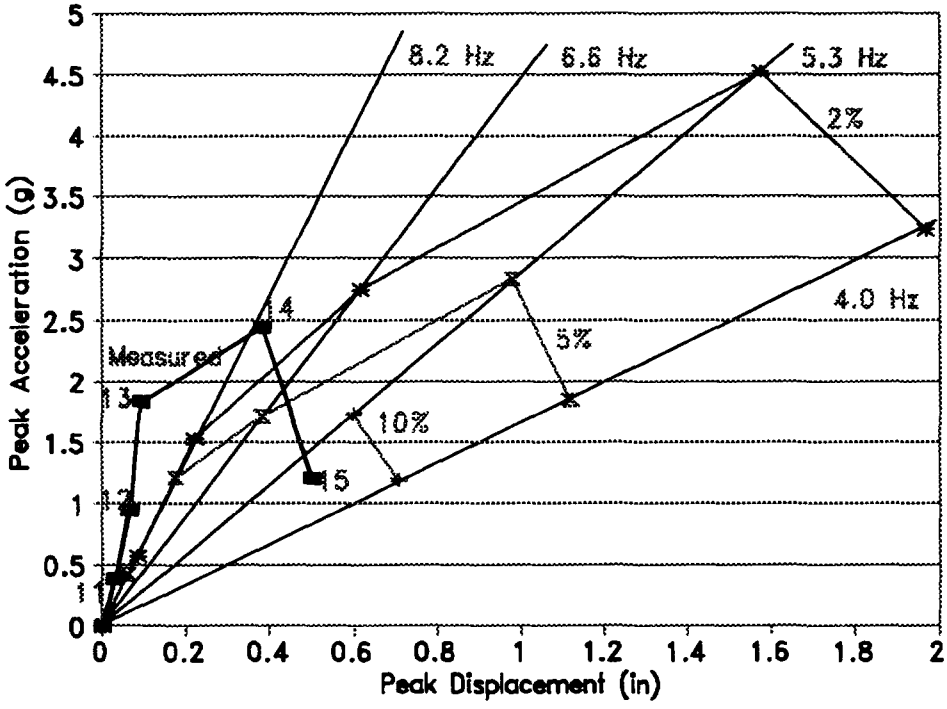

Figure 5.23 Parametric Summary Plot of Response Spectrum Analysis for S1 Test Runs

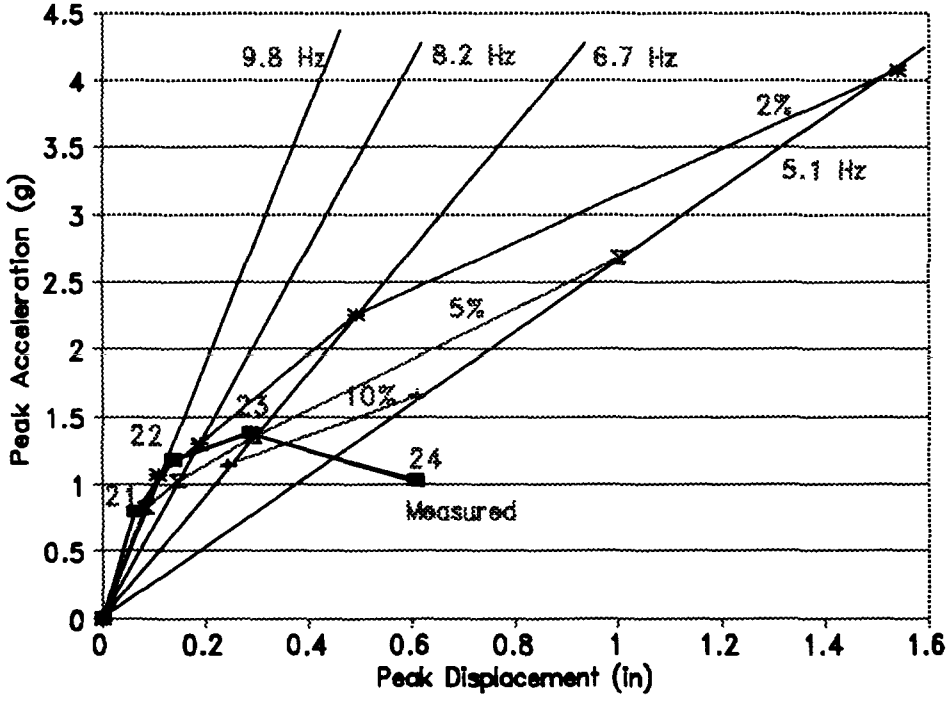

Figure 5.24 Parametric Summary Plot of Response Spectrum Analysis for S2 Test Runs

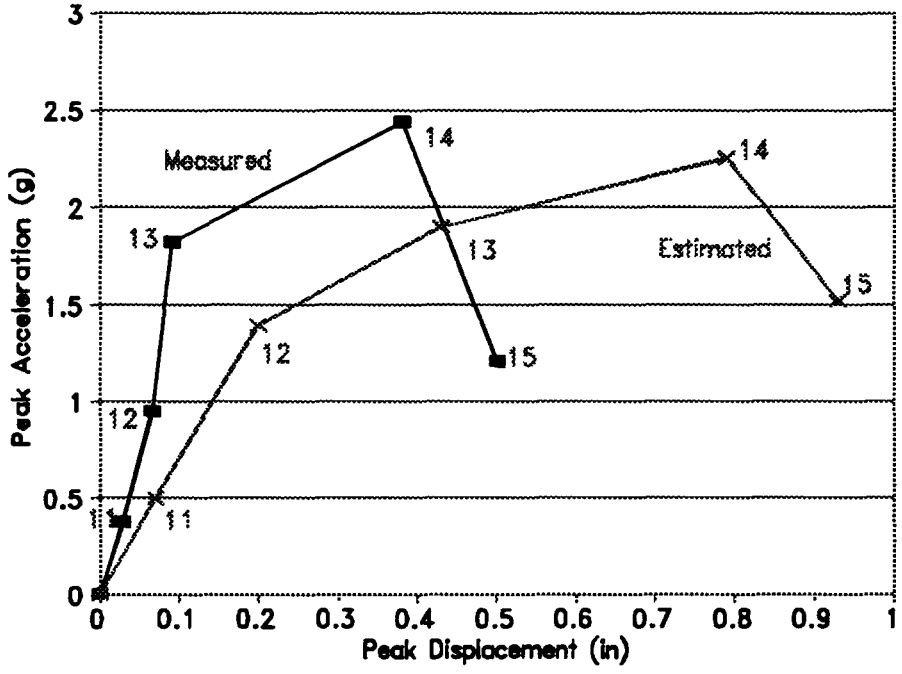

Figure 5.25 Comparison of Measured and Estimated Peak Accelerations and Displacements for S1 Test Runs

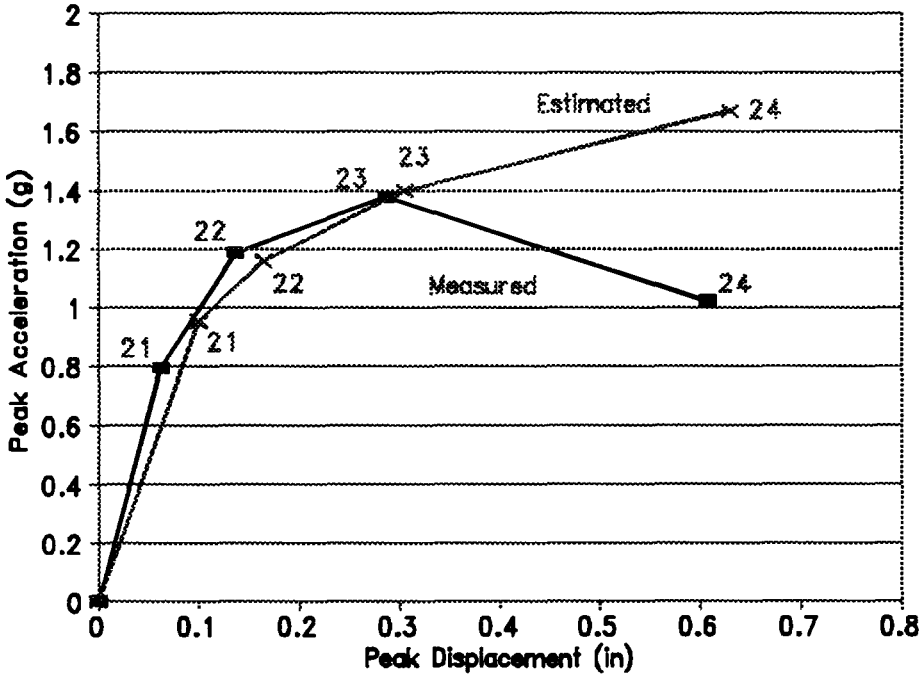

Figure 5.26 Comparison of Measured and Estimated Peak Accelerations and Displacements for S2 Test Runs

displacements were much higher than measured displacements, especially for S1. The displacements from the last two test runs of S2 appeared to be exceptions, but these measured values were too high due to the out-of-plane motions of S2. Also, the measured displacements from the later test runs (15, 23 and 24) included some permanent displacements. The response spectrum analysis was based on zero initial conditions, remained elastic throughout, and ended with zero relative displacement.

Recalling that radial lines represent lines of constant frequency, each point in Figures 5.23 and 5.24 represents not only an acceleration and a displacement, but a frequency. The mass is constant across all test runs, so each point (or radial line) also represents a stiffness. Frequency decreases clockwise, as does stiffness. All but one of the measured points in Figures 5.23 and 5.24 are to the left of their respective, spectral, frequency lines. Therefore, the SDOF model used in the response spectrum analysis was too flexible relative to the actual buildings. Surprisingly, better frequency correlation was achieved with the measured values from the cracked test runs than the values from the uncracked test runs. Since this response spectrum analysis used a linear SDOF, better correlation should have been expected with the undamaged test structures.

This apparent conflict was largely resolved through an investigation of the frequency components of the measured response histories. The basis of the SDOF response spectrum method is a single, exact natural frequency for each spectral value. For a single mode analysis, the SDOF oscillator is assumed to represent the entire structure, with all structural components always vibrating in exact phase with each other. An examination of acceleration and displacement records from the test runs indicated that all parts of the structure did not vibrate in phase with one another (Figure 5.27). Furthermore, the walls did not even vibrate at the same frequencies as the diaphragms, or each other, especially prior to rocking. Note that the frequency values reported in Section 4.6 were the dominant frequencies during each test run, but in no way were the only frequency components of the response histories. When rocking was occurring during the later test runs, much of the building did vibrate in phase, whereas during the uncracked test runs, very little phase agreement was found among the response histories. This was true for both S1 and S2, but

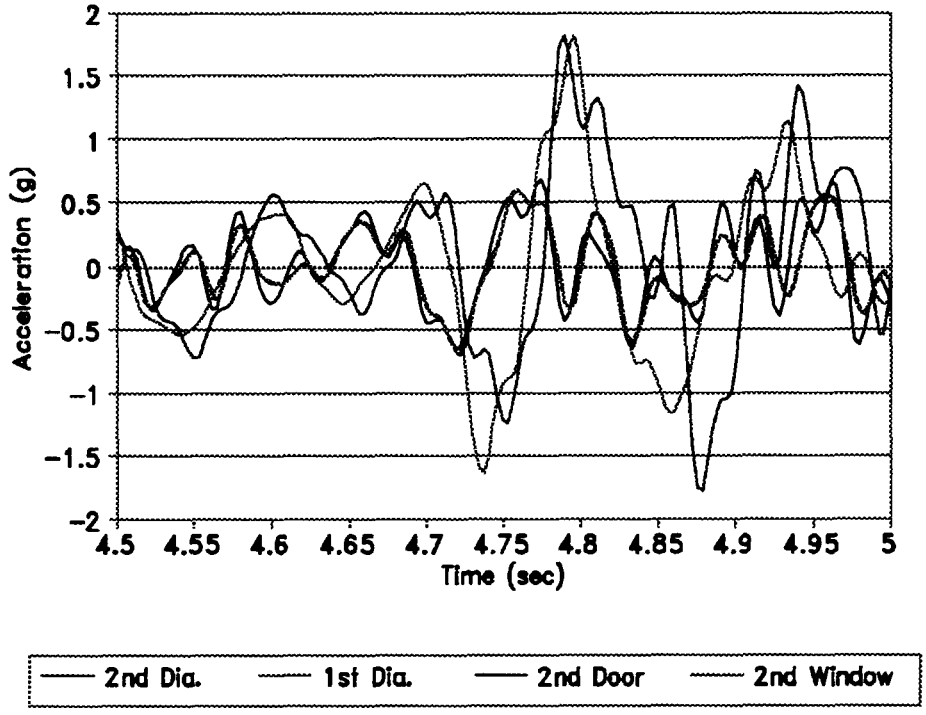

Figure 5.27 Measured Accelerations from Test Run 13 Showing out-of-phase Response

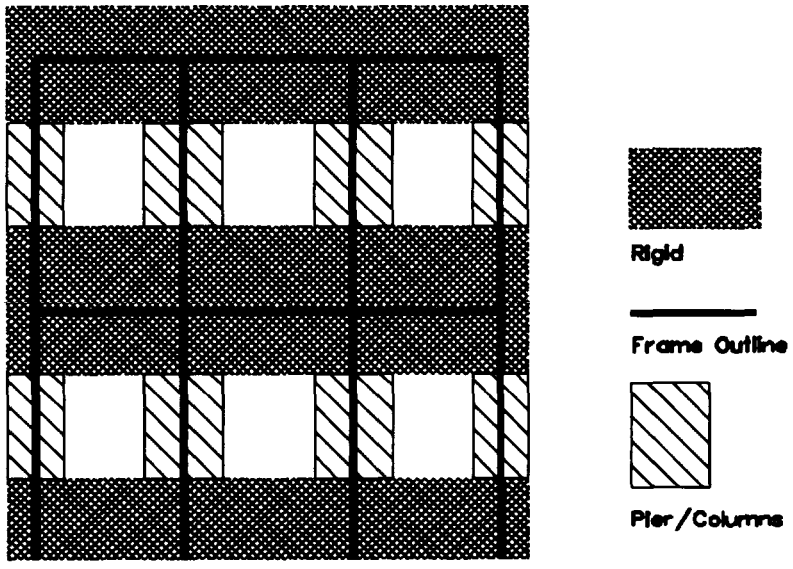

Figure 5.28 Frame Analog for S1 Window Wall Used in Pushover Analysis

more so for S1, probably due to the difference in diaphragm bolting. The conclusions of the frequency investigation were twofold:

1) Some of the discrepancy between measured and computed displacements could be attributed to the walls and diaphragms of S1 and S2 not vibrating at a single frequency or in phase with each other. If all structural components had vibrated in unison, displacements would undoubtedly have been higher.

2) The better agreement between the cracked test-run displacements and the (linear) spectral values was due to the rocking behavior unifying the frequency and phase of vibration. The cracked test runs, which had the first-story piers rocking below the undamaged upper portion of the building(s), were better modeled by a SDOF system than the uncracked test runs.

5.3 Pushover Analysis

A nonlinear, static analysis method, known as a "pushover" analysis, is being proposed by code-writing committees for the design and analysis of building structures. Briefly, this method involves a uni-directional, incremental, lateral loading of the lateral-force system. After each (linear) load step, member stiffnesses are adjusted to model yielding or plastic hinging. The loadings and stiffness reductions alternately continue until either a predetermined displacement is reached, or a collapse mechanism is identified, i.e., the system is "pushed over". The design of the frame can then be modified, if necessary, to improve behavior. The pushover analysis method is examined in this section for its applicability for unreinforced masonry wall structures with flexible diaphragms.

5.3.1 Background

The pushover analysis concept is not new. As early as the late sixties, researchers were using static, nonlinear analysis methods. Saiidi and Sozen, (1979) used a pushover-type analysis to create an equivalent, nonlinear stiffness curve for a SDOF representation of ten-story, reinforced concrete frames. More recently, in 1992, the JTCC-PRESSS[Otani, et al, 1992] proposed using static,

nonlinear analyses to determine ultimate response of concrete buildings idealized as a series of plane frames. In 1993, Section 4.6 of ATC-34 (Draft) suggested incorporating several new procedures for inelastic frame design and analysis. One of these described a "Static load-to-collapse analysis" as part of a procedure "suitable for analysis and design of all structural systems... irrespective of regularity and height." Finally, in 1995, ATC-33 - Simplified Nonlinear Method (75% Draft), described in detail the implementation and use of the static pushover analysis. A pushover analysis like the one described in ATC-33 is discussed in the next section (5.3.2).

5.3.2 Nonlinear Static Analysis

ATC-33 - Simplified Nonlinear Method was 75% drafted in January of 1995. The basic premise is that a static pushover analysis is performed on a structure until a predetermined target displacement is reached. The element forces and displacements are analyzed at the target displacement and compared with capacities to determine if individual elements need to be modified, or if the system as a whole needs to be altered. The draft emphasized that the pushover analysis is a static analysis and therefore cannot accurately represent all dynamic behavior. Also noted was that the pushover analysis is best used to estimate behavior at highly inelastic displacements.

To implement a pushover analysis, the first step is to create an analytical model of the structure. All structural elements that contribute to the lateral or gravity systems, as well as very stiff elements or elements with small displacement capacities, should be included. Each element should be modeled such that important elastic and inelastic stiffness and strength behaviors are represented. However, simpler models, such as bilinear and trilinear, are best. For each element, the deformation at which an acceptable damage state has been reached (for a given performance level) must be known.

Both gravity and lateral loadings are included in the analysis. Since the exact distribution of lateral loads is unknown, multiple lateral load patterns should be used. Gravity loads are applied to the model first and the lateral loads are then incrementally increased until a stiffness discontinuity is reached in an element. This stiffness is modified and the loads are again incremented (another

elastic analysis) until another stiffness discontinuity occurs. This stiffness is modified and the process repeats until the target displacement is met.

The determination of the target displacement can be accomplished in various ways. One way is the capacity spectrum method, which is not discussed in detail in ATC-33. A brief outline and references are given. A second method to determine the target displacement is called the coefficient method. The coefficient method is based on a response spectrum analysis with additional coefficients to account for behaviors associated with large displacements and different types of structural models. These coefficients were determined from statistical studies of the inelastic responses of SDOF and MDOF models[Lawson, et al, 1994 and Seneviratna, et al, 1994]. The fundamental period of the structure is used with the 5% damped response spectrum to determine a spectral acceleration. This acceleration is then modified by the various coefficients to produce the target displacement.

The acceptability of the structural elements is assessed in terms of the target displacement. Demand, stresses or deformations from the pushover analysis at the target displacement, is compared with capacity, which is dependent on the type of element, its importance to the structure, and the performance level being investigated.

5.3.3 Implementation of Nonlinear Static Analysis on S1 and S2

The first step in performing the pushover analysis was to convert the in-plane walls of S1 and S2 into analytical models. A frame analog was used with rigid beams and flexible columns. An example of a masonry frame for the S1 window wall is shown in Figure 5.28. The masonry piers were treated as equivalent (rectangular) column elements. Gross pier dimensions (Tables 2.1 and 2.2) were used to calculate the areas and moments of inertia of the column elements. Spandrels were considered to be rigid and were given very large areas and moments of inertia. Column and beam elements were aligned with the original pier axes (vertical) and floor levels (horizontal). Short "rigid" column elements were used to produce the proper floor heights. The elastic modulus used in the analysis was 750 times the prism strength, or 1425 ksi. The base of each wall was assumed to be fixed against translation and rotation. Column elements were

assumed to deform in flexure and shear. Gravity loads (Table 5.1) were based on dead load stresses (Table 3.1) and were applied as point loads at each of the two floor levels. Lateral loads were applied with a uniform distribution at the first and second floor levels.

In a pushover analysis, when an element yields, the element is removed and the incremental loadings continue with the reduced structure. Using this procedure inherently assumes that the yielding member(s) continue to provide resistance at their yield strength(s), i.e., a perfectly elasto-plastic behavior. However, for the unreinforced masonry buildings being analyzed here, this behavior was not entirely appropriate because once an unreinforced masonry element cracks, tensile forces cannot be transferred across the crack. As such, a new method of accounting seemed necessary to enable these brittle, element behaviors to be modeled. (Note that previous studies[Abrams and Shah, 1992 and Epperson and Abrams, 1989] have shown that cracked masonry walls can continue to resist loads after the initiation of cracking if they resist vertical compression forces.) Several methods of accounting for cracks in the model were examined, but these methods were needlessly complex and did not produce a noticeable difference in results from neglecting the effects of cracks altogether.

To take into account pier rocking in the pushover analysis of the buildings, one of two (lateral) force-displacement curves was used for each column element (Figures 5.29a and 5.29b). Which of the two curves, A or B, was used was dependent on the relative magnitudes of the cracking force and the rocking force for each element. Rocking cannot occur until the pier has cracked. Rocking forces (Table 5.2) were determined by PD/H, where P is the initial axial force, D is the pier length, and H is the pier height. Cracking was assumed to occur at a combined axial and flexural tension of 100 psi.

Gravity loads were applied to the frame model and lateral loads were increased until one of the column elements (piers) reached the break point in either curve A or B. If a column element followed the behavior of curve A, then at rocking, the shear at the top of the column element was released and replaced with a pair of opposing horizontal forces equal to the rocking strength. If a column element followed the behavior of curve B, then at cracking, the shear at the top of the column element was released and replaced with a pair of opposing horizontal forces equal to the rocking strength. After the internal forces were redistributed, the applied forces were increased or

Table 5.1 Gravity loads applied at each floor level in the pushover analysis.

Shear Wall	Pier Load (kips)	
	Outer Piers	Inner Pier(s)
S1 door wall	1.06	1.78
S1 window wall	0.70	1.20
S2 door wall	0.70	1.20
S2 window wall	1.06	1.78

Table 5.2 Rocking forces used in the pushover analysis and the 3-DOF model.

Shear Wall	Rocking Force (kips)	
	Outer Piers	Inner Pier(s)
S1 door wall	1.14	3.01
S1 window wall	0.74	1.79
S2 door wall	0.42	1.01
S2 window wall	2.03	5.35

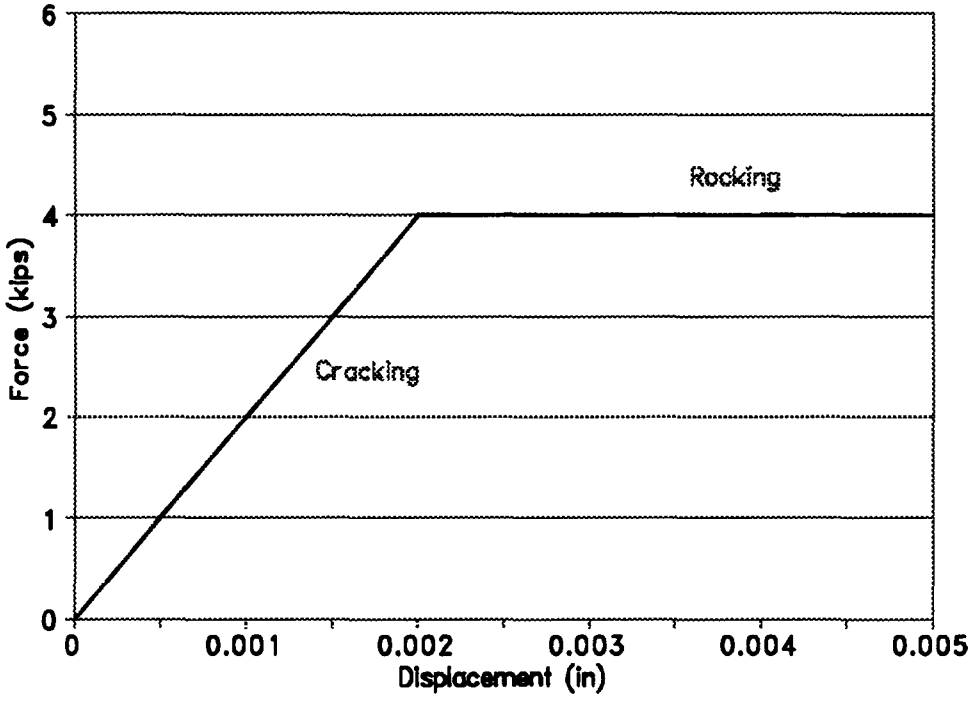

Figure 5.29a Example of Bilinear Force-displacement Curve "A" used in Pushover Analysis

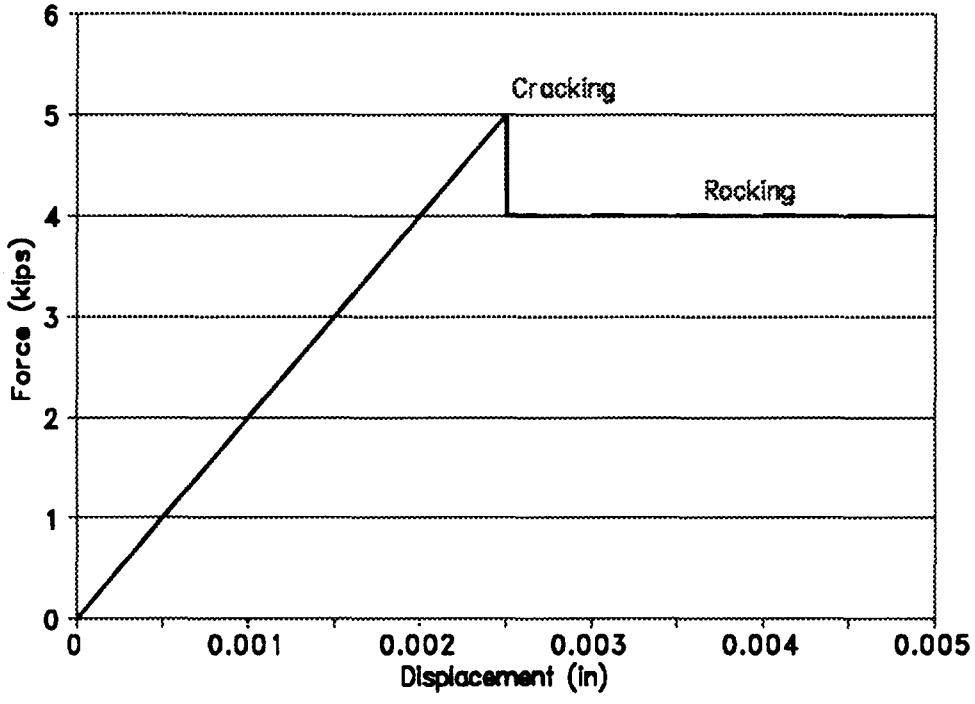

Figure 5.29b Example of Bilinear Force-displacement Curve "B" used in Pushover Analysis

decreased until another column element reached the break point in curve A or B. The process was repeated until a mechanism formed.

Lateral loads were assumed to be applied to the center of the flexible diaphragms and were assumed to be equally distributed between the two walls. As such, the two walls were analyzed separately, but simultaneously. The total lateral load is plotted against the average of the first-level drifts for S1 and S2 in Figure 5.30 and 5.31. Each point in the analysis is numbered in the figures. For S1, the numbers in Figure 5.30 are as follows: 1) exterior window column element cracks, 2) exterior door column element cracks, 3) interior window column element cracks, 4) exterior window column element rocks, 5) exterior door column element rocks, 6) interior window column element rocks, 7) second interior window column element cracks and rocks, 8) interior door column element cracks and rocks, and second exterior window column element cracks and rocks forming a mechanism in the window wall, and 9) ultimate capacity. For S2, the numbers in Figure 5.31 are as follows: 1) interior door column element cracks, 2) exterior door column element cracks, 3) interior door column element rocks, 4) second interior door column element cracks and rocks and exterior door column element rocks, 5) second exterior door column element cracks and rocks, forming a mechanism in the door wall, and 6) ultimate capacity. The S2 window wall experienced no damage in the pushover analysis.

5.3.4 Discussion

The pushover curves in Figure 5.30 and 5.31 did not compare well with measured results. Although the calculated capacity for S1, 10.1 kips, was close to the 12.4 kips measured, the S2 capacity of 5.7 kips was much lower than the 9.4 kips measured. Calculated wall drifts (0.01%) were 10 times lower than those measured for cracking (0.1%).

The pushover analysis can be greatly simplified for unreinforced masonry building models such as those used to analyze S1 and S2. For both models, the onset of cracking in the first column element was quickly followed by cracking and the subsequent rocking of all column elements along a wall. The resulting load-drift curves were essentially bilinear, with a brief elastic portion and a substantial flat (rocking) portion. Both the elastic stiffnesses and the rocking

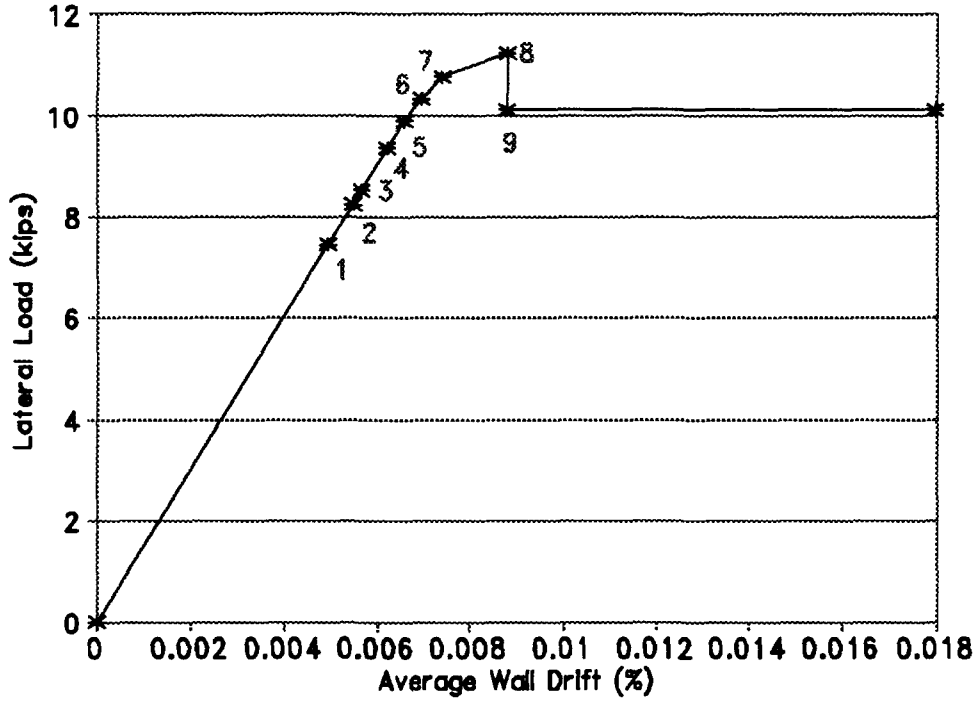

Figure 5.30 Pushover Curve for S1

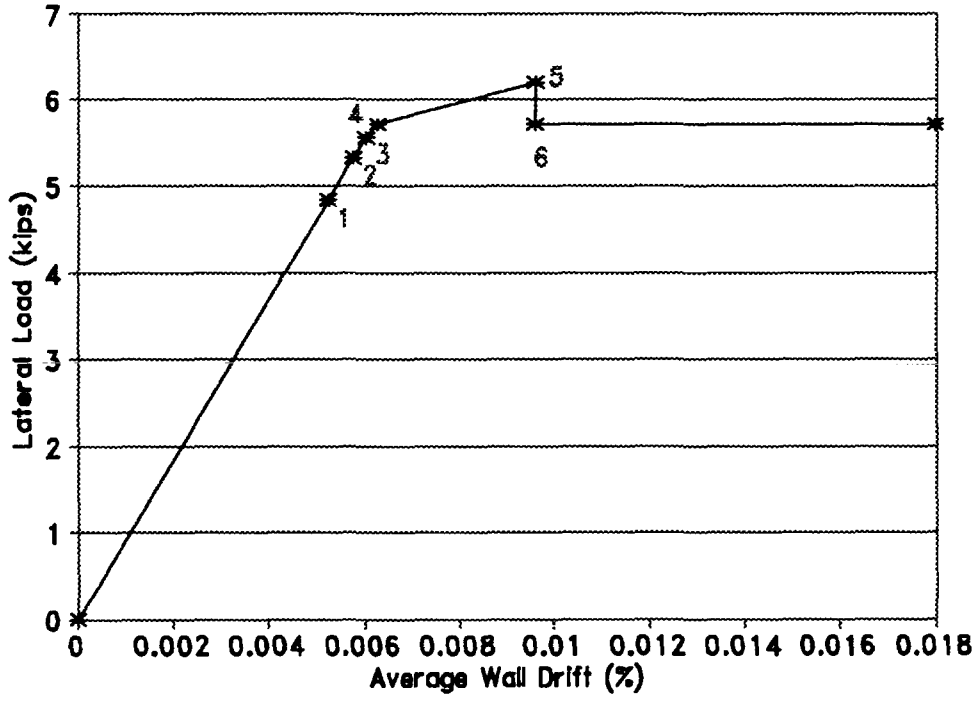

Figure 5.31 Pushover Curve for S2

strengths could have been calculated independently of the pushover analysis. For simple models in which a rocking mechanism is formed, rather than proceed through the incremental loading steps, the analyst could form the bilinear curve with just an estimate of the elastic stiffness and a computation of the sum of the rocking strengths.

One major reason that the pushover analysis is not suitable for unreinforced masonry buildings with flexible diaphragms is that the complex and changing frequency characteristics of the structures were not included. The pushover analysis was developed primarily on multi-story frame models where first-mode response dominated the behavior. Also inherent in these models was that the deflected shapes remained relatively constant throughout the pushover analysis. The two-story buildings tested in this study satisfied neither description. A unified building motion was not present during the dynamic tests (Figure 5.27). Also, post-cracking deflected shapes were substantially different from the pre-cracking deflected shapes (Section 4.7). Furthermore, experimental results indicated that the dominant response frequencies were controlled either by the diaphragms (precracking) or by rocking (post-cracking). Since the behavior of buildings like S1 and S2 is so dependent on dynamic properties, methods such as the pushover analysis cannot accurately determine their response.

Another reason why the pushover analysis is unsuitable for unreinforced masonry is related to the bilinear shape of the load-drift curve. The basis of the pushover analysis is analyzing structural elements at a target displacement to determine their acceptability. For the models analyzed here, once all the piers in one of the two walls started to rock, displacements (drifts) were effectively unbounded. Furthermore, additional displacements (after the formation of the rocking mechanism) did not produce additional stresses in the elements. Since any target displacement could be reached with the same capacity level (rocking), a target displacement becomes meaningless as an indication of the demand for a particular performance level.

5.4 Nonlinear Time-Step Integration

Neither of the two analysis methods discussed in Section 5.2 or 5.3, the response spectrum analysis or the pushover analysis, included the full nonlinear behavior of pier rocking. Since pier rocking was shown, in Chapter 4, to contribute so significantly to the inelastic response of S1 and S2, any accurate analysis method should include this behavior. As such, using experimental results from Chapter 4, a simple model was developed that takes pier rocking into account in determining the displacement histories of unreinforced masonry buildings with flexible diaphragms.

5.4.1 3-DOF Model

Three degrees of freedom (DOF) were used to represent S1 and S2 (Figure 5.32). One DOF was used for each of two in-plane, shear walls and the third DOF was used for the diaphragms. The post-cracking deflected shapes shown in Figures 4.41, 4.42, and 4.44-4.46, the drift plots in Figures 4.52 and 4.54, and the displacement ratios and modes shapes listed in Tables 4.10 and 4.11, all showed that after horizontal cracks had formed across the piers, second-level displacements were negligible when compared to first-level displacements. Therefore, in the model, the wall DOFs were located at the first level while the second-level masonry was assumed to be rigid. As a result of this assumption, both diaphragms received the same input motion, that of the two wall DOFs. Since both diaphragms also had equal stiffnesses and had equal masses, the two diaphragms were combined into one DOF. This again was consistent with the response observations.

The three DOFs used to model S1 and S2 were chosen for the particular buildings tested in this study. If the two diaphragms had had unequal stiffnesses or masses, one DOF could have been used for each. Each diaphragm DOF would have, however, still received the same input motions from the two wall DOFs. Also, in theory, additional wall DOFs could have been used if more than two shear walls had existed in one of the buildings.

The diaphragm DOF was assumed to remain linear throughout the analysis. The two wall DOFs, however, used bilinear force-displacement curves (Figure 5.33). The first portion of the curve was computed by summing the pier stiffnesses (see Equation 3.8). The second portion of the curve, which had zero slope, represented the rocking behavior. A simple statics study suggested

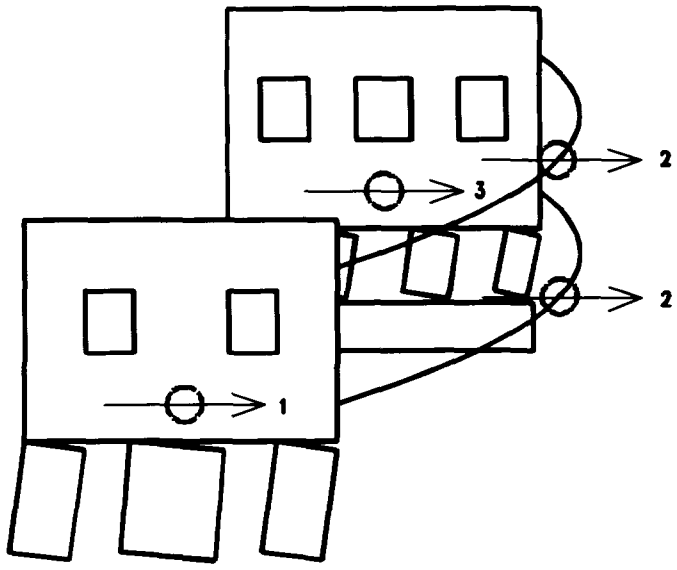

Figure 5.32 Description of the Degrees of Freedom (for S1) in the 3-DOF Model

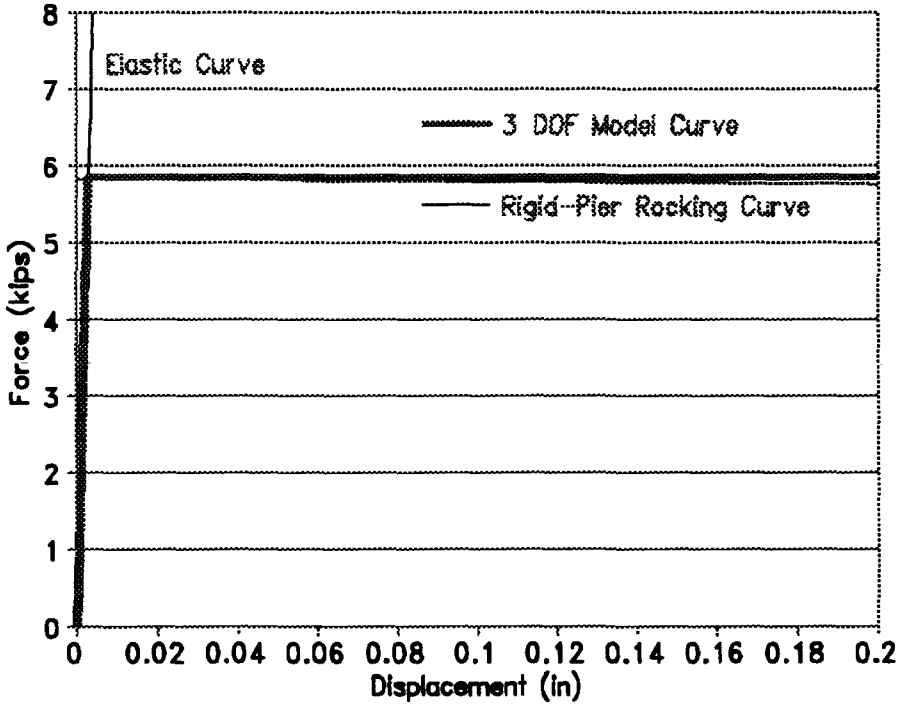

Figure 5.33 Assumed Bilinear Rocking Behavior and Actual Rigid-pier Rocking Behavior

that the force-displacement curve for a rocking rigid body actually has a slightly negative slope (Figure 5.33). Under normal circumstances, a curve with zero slope models rocking extremely well. The force value of the second portion was the sum of *PD/H* for each pier, where *P* is the axial load in the pier, and *D/H* is the aspect ratio, length over height. The rocking strengths calculated in this way were within about 20% of the measured base shear values during the post-cracking test runs. With this bilinear force-displacement curve, all piers in each wall were assumed to rock in unison, and were assumed to have constant rocking strengths. This assumption may not be valid for walls with a wide range of pier aspect ratios or walls which are highly asymmetric. Neither description fit S1 or S2.

5.4.2 Integration Program

A time-step integration program was written to compute the response of the nonlinear, 3-DOF model to base accelerations. A listing can be found in Appendix F. The program uses the Newmark-Beta method to solve displacements, velocities, and accelerations at each time step. Because of the discontinuity in the wall DOF force-displacement curves, an iterative approach was used rather than a closed-form solution. A second program was written to compute the elastic stiffnesses and rocking strengths of the walls while a third program was written to interpolate an acceleration history to a different time increment. Listings of these two programs are also in Appendix F.

The integration program was run using input parameters from S1 and S2 and base acceleration histories from Test Runs 14, 15, 23, and 24. Slight variations among the calculated results were evident with different integration time steps, levels of damping, and elastic stiffnesses, but this is to be expected. Results from the simulations are summarized in Table 5.3. Plots of the computed door- and window-wall displacements, overlain with the measured door- and window-wall displacements, are presented in Figures 5.34-5.41. Results from the S2 window wall are not presented since this wall did not rock. For these results, the integration parameters were, $\alpha=1/2$, $\beta=1/6$, time step=0.001 seconds, and the relative convergence limit ($|1-a_{i+1}/a_i|$) $< 10^{-4}$ for each

Table 5.3 Comparison of calculated and measured wall displacements and base shears.

	Test Run 14		Test Run 15		Test Run 23			Test Run 24		
	Meas.	Calc.	Meas.	Calc.	Meas.	Calc.	Calc.	Meas.	Calc.	Calc.
Door-wall displacement (in)	0.356	0.340	0.437	0.444	0.242	0.172	0.245	0.379	0.372	0.350
Window-wall displacement (in)	0.136	0.353	0.394	0.462	0.110*	0.0019	0.214	0.178*	0.204	0.322
Base shear (kips)	17.97**	14.53	12.43	16.77	10.93	12.17	8.13	9.40	15.49	11.78
Calculated Rocking Strengths										
Sum (kips)		10.36		10.36		12.27	5.70		12.27	7.85
Door wall (kips)		5.30		5.30		2.85	2.85		2.85	2.85
Window wall (kips)		5.06		5.06		9.42	2.85		9.42	5.00

*This wall did not rock.
**Prior to cracking (and rocking).

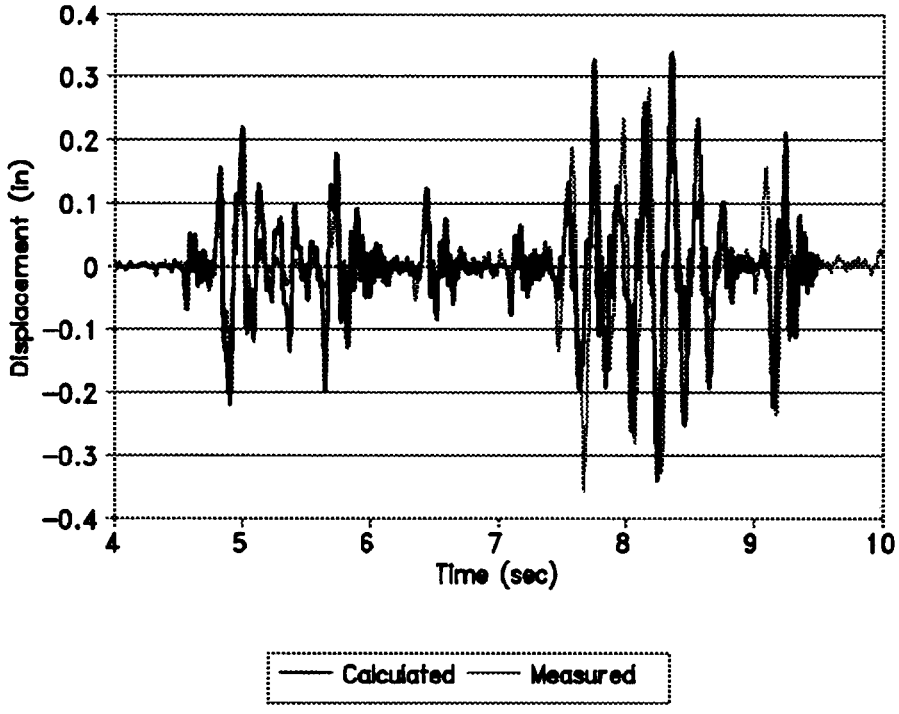

Figure 5.34 Calculated and Measured Door-wall Displacements for Test Run 14

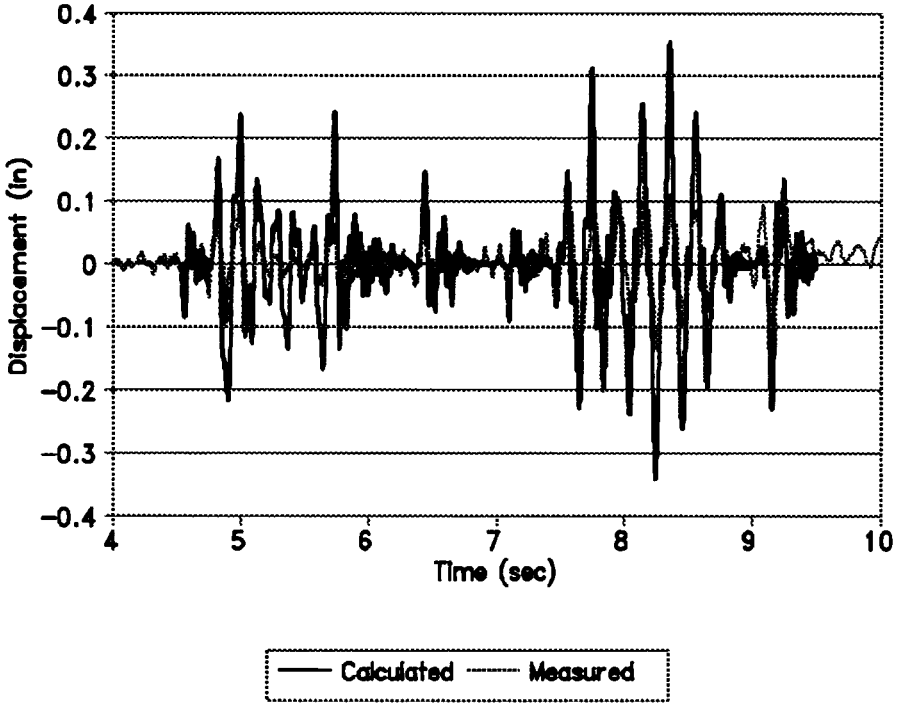

Figure 5.35 Calculated and Measured Window-wall Displacements for Test Run 14

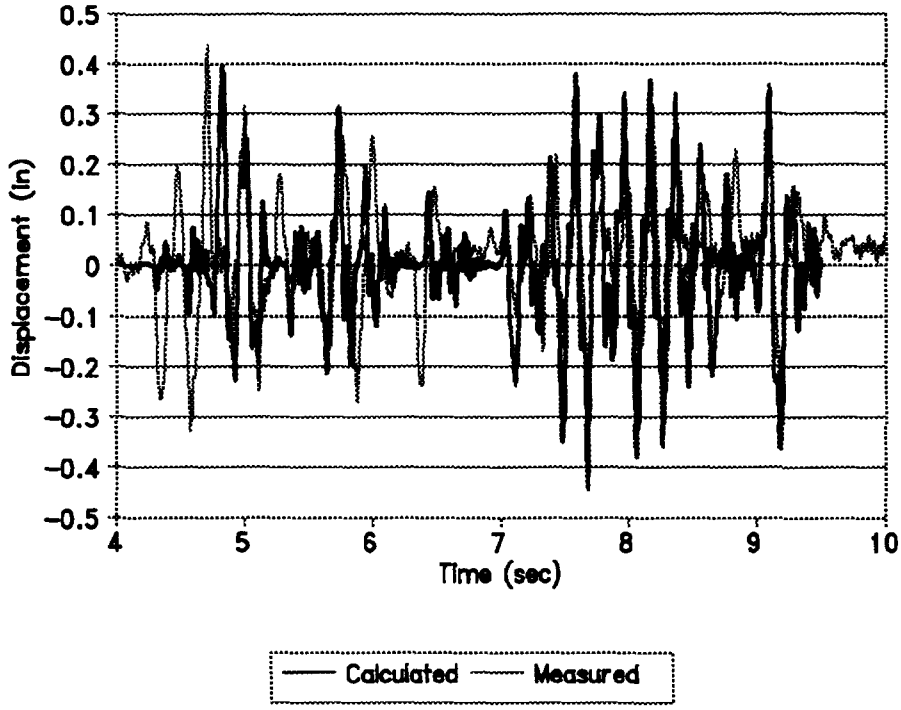

Figure 5.36 Calculated and Measured Door-wall Displacements for Test Run 15.

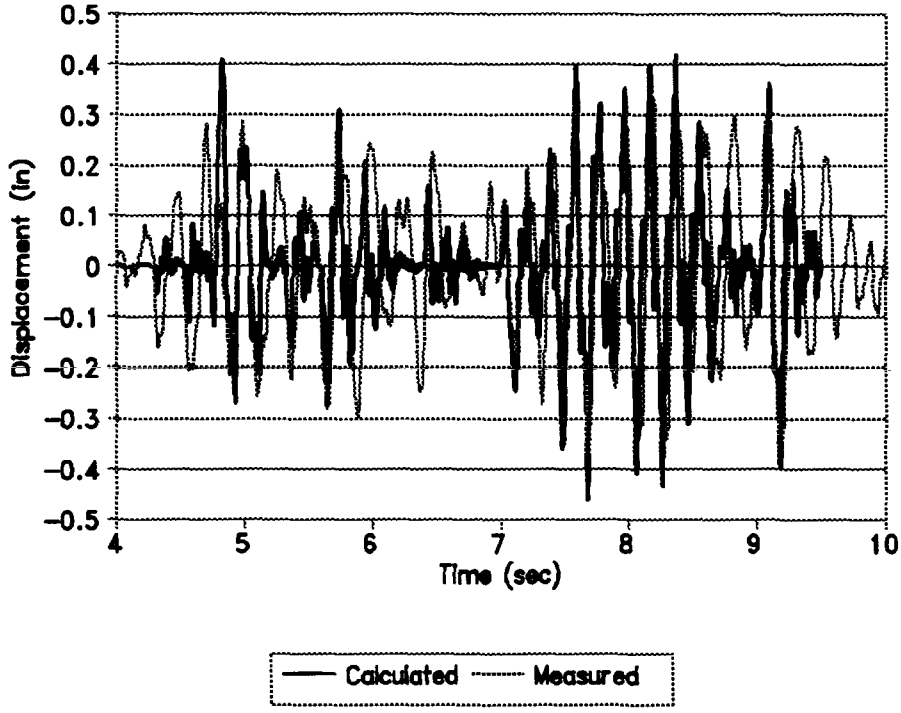

Figure 5.37 Calculated and Measured Window-wall Displacements for Test Run 15.

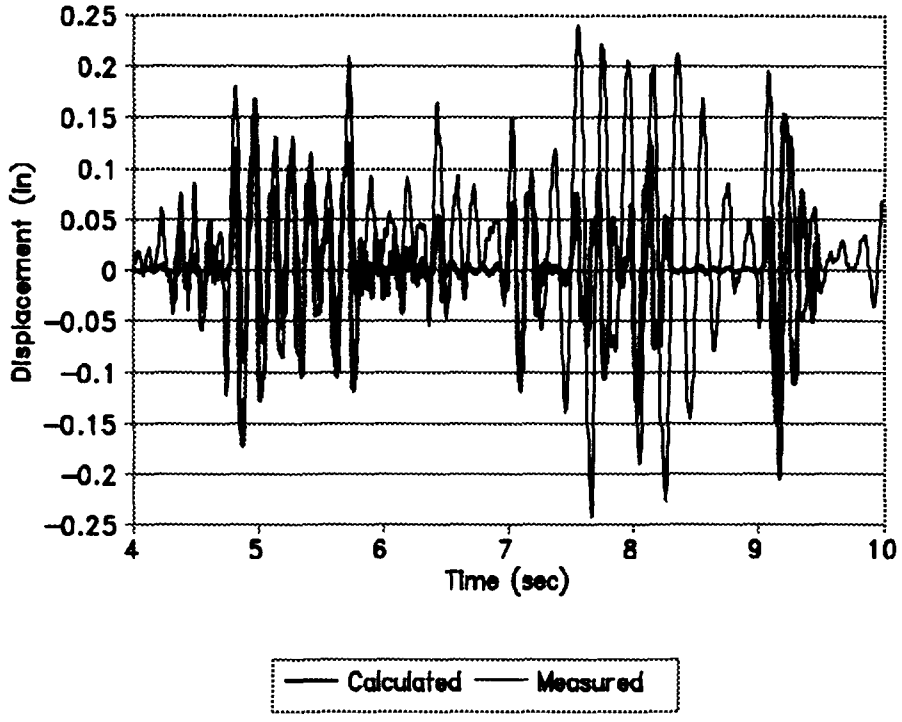

Figure 5.38 Calculated and Measured Door-wall Displacements for Test Run 23

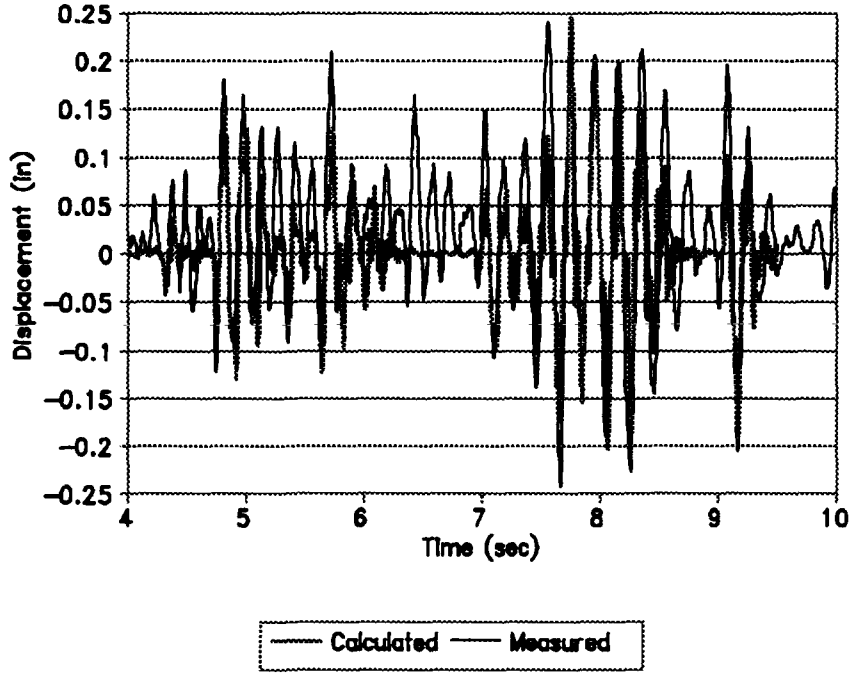

Figure 5.39 Calculated and Measured Door-wall Displacements for Test Run 23 (with reduced window-wall strength)

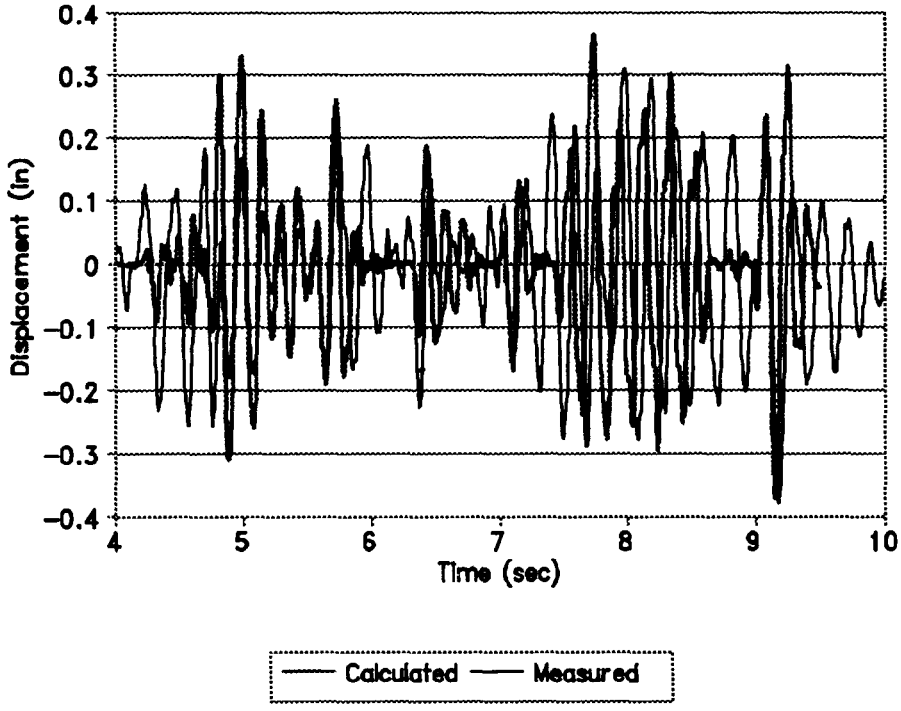

Figure 5.40 Calculated and Measured Door-wall Displacements for Test Run 24

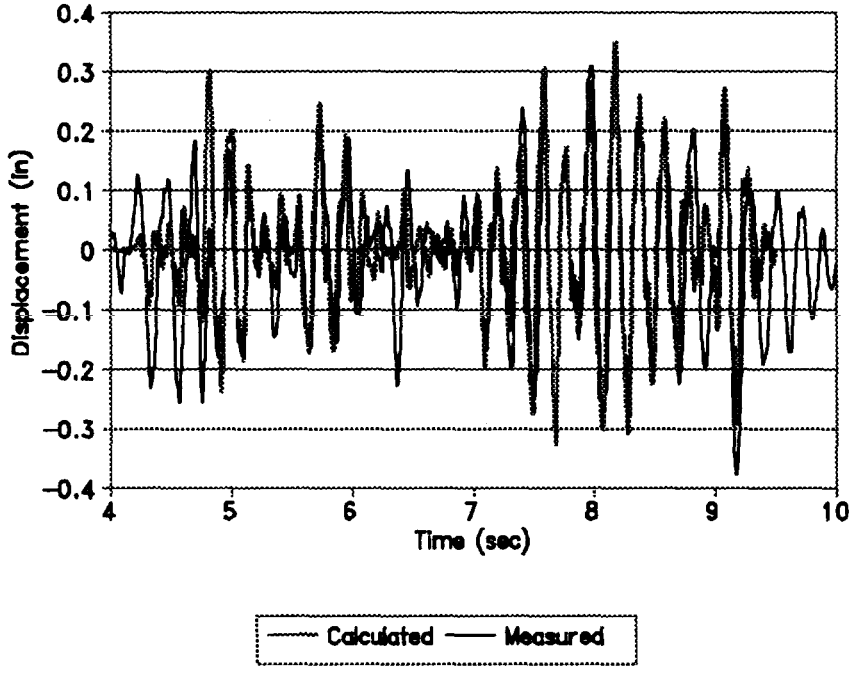

Figure 5.41 Calculated and Measured Door-wall Displacements for Test Run 24 (with reduced window-wall strength)

of the three accelerations. Pier dimensions are given in Figures 2.3, 2.4, 2.7, and 2.8, and the elastic modulus used was 1425 ksi. Calculated rocking forces are listed in Table 5.2.

5.4.3 Correlation Between Calculated and Measured Results

The correlation between calculated and measured displacements for Test Run 14 was good (Figures 5.34 and 5.35). For both walls, the periods were matched almost exactly. The window-wall calculated peak was only one-half cycle away from the measured peak (at 8.3 seconds) while the door-wall peaks were within 5%. For the window wall, the calculated amplitudes were higher than those measured because the S1 window wall had not cracked enough to promote full rocking.

For Test Run 15, the correlation between calculated and measured displacements was also good (Figures 5.36 and 5.37). The portions of the history when rocking occurred during the experiments were identified by the model for both walls and the periods were matched quite well. Although the measured displacement peak for the door wall occurred well before the calculated peak, the magnitudes agreed to within 1.5%. Several variations of the input parameters were tried, but the measured door-wall displacement peak (at 4.7 seconds) could not be recreated with the computer model. For the window wall, both calculated and measured peaks occurred simultaneously (at 7.7 seconds), but the magnitudes were 17% off.

For Test Run 23, the correlation between the calculated door-wall displacements and the measured displacements (Figure 5.38) was good for the first part of the history (4-6 seconds), but not good through the latter part of the history (6-10 seconds). Inelastic displacements in the measured results were partially responsible for the discrepancies. The lack of agreement was largely due to the fact that no rocking occurred in the computer-model window-wall DOF while during the actual test run, significant sliding took place near the base of the window wall. The 0.0019" peak displacement calculated for the window wall was below the initiation of rocking. In an effort to model the sliding using the bilinear rocking curve, the window-wall rocking strength was reduced to the door-wall rocking strength (2.85 kips). This reduction gave better magnitude and phase agreement with the latter portion of the measured displacements, but gave poorer agreement with the earlier portion of the measured displacement history (Figure 5.39). The sliding

resistance of the window wall must have decreased during Test Run 23. By using the reduced window-wall rocking strength, the calculated and measured door-wall displacement peaks were within one-half cycle of each other (at 7.7 seconds) and were only different by 1%.

The calculated displacement history for the door wall during Test Run 24 also had poor phase correlation with the measured displacements (Figure 5.40) during the latter part of the history (7-10 seconds). This was again largely due to the sliding of the wall during the laboratory experiment which was not properly modeled by the bilinear, rocking, force-displacement curve. However, the calculated door-wall peak occurred during the same cycle as the measured peak (at 9.2 seconds) and the magnitudes were within 2%. To account for the poor phase agreement, the window-wall rocking strength was again lowered, this time to 5.0 kips. This change resulted in a calculated door-wall displacement history with a much better phase correlation with the measured displacements (Figure 5.41) throughout the history. The calculated peak displacement did not, however, occur simultaneously with the measured peak, nor were the magnitudes as close, with the reduced window-wall strength.

In comparison to the generally good correlation between calculated and measured displacements, agreement between the calculated and measured base shears, both inertial-based, was not nearly as good. Note that the program calculates *relative* acceleration and that calculated base shears are computed from *absolute* acceleration (relative + base). Some of the discrepancies can be explained by the inability of the model to represent or accumulate any form of damage. The force-displacement curves remained unchanged and elastic. Some of the disagreement can also be rationalized as inherent to the solution method. Acceleration was the highest order derivative calculated and tended to vary widely, especially near the abrupt change in stiffness of the wall DOFs. These variances produced the high, calculated accelerations and base shears.

Since the calculated base shears presented in Table 5.3 are based on inertial forces, these shears can (and do) exceed the sum of the rocking strengths of the two walls. However, with the bilinear force-displacement curve used for the walls, the force transmitted to the "foundation" of the model can never exceed the sum of the rocking strengths. The force balance is maintained with the velocity-dependent damping forces.

Clearly evident of the calculated base shears was that an increase in nonlinear response resulted in a relative decrease in the acceleration-based base shear. Even though the amplitude of the base motion was increased by 50% between Test Run 14 and 15, the calculated base shear increased only 15%. The amplitude of the base motion was increased by 60% between Test Run 23 and 24, yet the calculated base shear increased only 27%.

The purpose for developing the model was to estimate wall displacements resulting from a rocking-dominant behavior. The model was never intended to accurately determine accelerations or base shears. Overall, agreement between calculated results and measured results was surprisingly good considering the simplicity of the model. The model was able to

- estimate the peak wall displacements due to rocking
- determine the times when rocking occurred
- demonstrate the reduction of relative diaphragm displacements during rocking (not shown here)
- demonstrate the shift in frequency from before to during rocking
- estimate the rocking frequency
- demonstrate increases in base shear not proportional to increases in base excitations.

The model was not able to

- consistently determine the time of (measured) peak displacements
- accumulate inelastic displacements or other damage
- accurately match measured inertial-based base shears.

SECTION 6
COMMENTS ON EVALUATION AND REHABILITATION OF URM STRUCTURES

6.1 Overview

The differences between the measured response of S1 and S2 are discussed and are related to physical differences in the configuration and construction of the two buildings. Comments on the merits and shortcomings of evaluation methods presented in Sections 3 and 5 are made. Linear and nonlinear static and dynamic methods are covered. Recommendations for modeling, and the best uses for different models are given. Suggestions for rehabilitation relating to rocking, pier aspect ratios, strong wall/weak wall systems, and out-of-plane bending of out-of-plane walls are made based on measured results.

6.2 Comparison of Measured Response of S1 with S2

In prior sections, the responses of S1 and S2 were discussed in terms of their similarities as two, two-story, unreinforced masonry structures. Although similar in many ways, the two structures had some differences. The most significant difference was the relative lateral strengths of the two shear walls. The two in-plane walls of S1 had nearly equal strengths while those of S2 had vastly different strengths. The S2 shear walls were designed by strengthening one S1 wall and weakening the other while leaving the pier and opening cross sections unchanged. S2 can, therefore, be viewed not only as a second test structure, but also as an altered or rehabilitated version of S1. Similarly, S1 can be viewed as a rehabilitated version of S2. Other, less important differences between S1 and S2 were, the existence of a weak bed joint between the second and third course of S2 (Section 2.8.8), and the bolting of the weights to the floor beams (Section 2.8.7). By comparing the responses of S1 and S2 against each other, and correlating the similarities and differences to the differences between the structures, additional information can be derived from the laboratory data.

Overall, both S1 and S2 performed well while uncracked and cracked. After initial cracking, both structures were subjected to at least one additional test run with a higher intensity base motion than the previous run. Pier rocking was a reliable, repeatable behavior that resulted in only minor damage to the structure as a whole. Out-of-plane motions experienced by S2 led the two inner door-wall piers to end up slightly out of plumb. The stockier piers of S1 did not have this problem, but they also did not undergo as many rocking cycles as those of S2. Although rocking is initially a stable behavior, alignment problems can occur after a large number of cycles. Severe alignment problems could result in the loss of a pier if subjected to several earthquakes. Even though both buildings in this study were tested repeatedly, a real building should not be allowed to experience a second seismic event while severely damaged.

The difference in the diaphragm boltings was evidenced by increased displacements, increased accelerations, and a slightly higher natural frequency for S2 during the first test runs. The more uniform diaphragm behavior, coupled with the more flexible door wall, resulted in higher displacements and accelerations in Test Run 21 than in Test Run 11. The S2 diaphragm bolt plan also had a stiffening effect on the diaphragm when compared to that of S1. The stiffer diaphragm produced slightly higher natural frequencies for the uncracked S2.

The most significant differences in response between S1 and S2 resulted primarily from the difference in the relative lateral strengths of the two shear walls. The weak bed joint in S2 also played a minor role. Although the S2 door wall, and the S1 door and window walls, initially cracked at approximately 0.1% story drift, the weak joint possibly led to premature cracking in the S2 window wall. The weak bed joint forced a horizontal crack near the bottom of the S2 window wall which prevented any further damage in this wall. Whether or not this crack (or others) would have occurred in the absence of a weak joint is not known. Note that in S1, the bed joint below the base course was the weakest. Regardless, S2 was weaker than S1 and should have cracked at lower force levels.

Due to several factors, S2 cracked during the second test run while S1 did not start cracking until the fourth test run. As a result of the early cracking in S2, and the ensuing departure from linear response, measured displacements were generally higher, and measured accelerations were

generally lower, than in S1 for equivalent base motions. The lower accelerations produced lower inertial forces which resulted in lower total base shears for S2. The fact that lower base shears were measured for S2 (after cracking) than for S1 is important since the total weight, weight distribution, and base motions were the same for S1 and S2. The implication here is that the weaker structure had a lower demand under otherwise equal conditions. After cracking, the three peak base shears for S2, from Test Runs 22, 23, and 24, varied by only 15%, even though the base motion was increased by 60% between each test. This implies that there was a limit to the demand that the rocking-pier building needed to resist. This demand limit was set by the capacity of the structure, not visa versa.

6.3 Recommendations for Evaluation

6.3.1 Linear Elastic Analyses

All linear elastic analyses of URM buildings will have the handicap of large uncertainties in the elastic modulus of the masonry. Note also that masonry is not isotropic. Since for stocky piers, aspect ratios less than 1.0, shear deformations can exceed flexural deformations, shear deformations should be included in determining elastic stiffnesses. Thus, an estimate of the shear modulus is also required. If the elastic modulus is not well known, it is likely that the shear modulus is not known at all.

Determination of tensile, compressive, and shear stress distributions are perhaps the best use for linear elastic analyses of URM structures. Overstressed structural elements can be identified for rehabilitation. To determine stress distributions in an elastic model, the magnitude of the elastic and shear moduli are not critical as long as each can be assumed to be constant and are in proper proportion to each other. An accurate analysis should include all load resisting elements. For simplicity, most of the analyses discussed in Section 3 did not include the out-of-plane walls. These "pier models" assumed that no out-of-plane walls existed for either gravity or lateral loads. Only the finite element models included the transverse walls and stress distributions from these models showed that the transverse walls did participate slightly in resisting horizontal and vertical

forces. For an elastic stress distribution, a model that includes transverse walls is likely to be more accurate though it need not be as complex as the ones used in this study. Ignoring transverse walls will be quicker, but may be too conservative in some cases.

Another facet of performing a linear elastic analysis is the application of loads. Gravity loads are generally known and can easily be applied to a model. Equivalent seismic loads, however, are much more difficult to determine accurately. Experimental results from Section 4.9 indicated that seismically-induced, floor-level, inertial loads were proportional to the mass at each floor level, not proportional to the mass multiplied by the height. In Section 3, the two-story models were analyzed with loads proportional to the mass times the heights. Had they been analyzed with loads proportional to just the mass, global overturning moments would have been reduced by 10%. Global moment reductions for three-, four-, and five-story models would be 14%, 17%, and 18%, respectively, (assuming equal floor heights and masses) for mass-proportional loadings from mass-times-height-proportional loadings.

The last parameters needed for a linear elastic analysis are assessments of tensile, shear, and compressive strengths. Flexural tension tests (Section 2.7.4) gave conservative results (by a factor of 4½ times lower) compared to the dynamic tensile strengths inferred from the test runs. Diagonal compression tests (Section 2.7.3) gave shear strengths much weaker than the in-place shear tests performed on S1 and S2 (Section 2.7.6). The underestimation of strengths from the static component tests resulted in conservative estimates of the loads that would initially crack the test structures.

With relative stiffnesses and estimates of material strengths, a linear elastic model can be used to determine a range of initial cracking loads for URM structures. Several different lateral force distributions should be used to identify all possible critical regions of the structure. All load-carrying elements should be included in the model. Elastic displacements will have large inaccuracies due to uncertainties in the elastic and shear moduli. However, for many masonry buildings, the linear elastic displacement under assumed loads may not be a critical parameter if a stable nonlinear behavior, such as rocking, is expected.

6.3.2 Linear Static Analyses - Reduction Factors

Current force-based design philosophies rely heavily on the reduction of lateral loads derived from linear analyses. One simplistic approach is to assume the level of reduction, R, is equal to the ductility factor, μ, as defined in Figure 6.1 The reduction factors typically are specified in design codes for structural systems as a whole, but can also be specified for each element in a structural system. Referring back to the force-displacement curves for the cracked test runs, in particular Figures 4.24-4.27, 4.32, and 4.34, a conservative estimate of ductility in the walls would be two. The S1 door wall actually reached ductility levels of between four and six. Since the wall behavior is directly related to the pier behaviors, these wall ductilities can also be used for the individual piers. The base shear versus drift curves presented in Figures 4.13 and 4.14 suggest an ultimate ductility of nearly ten for S1 and more than six for S2. Note that the gravity stresses in the piers in this study were low to moderate for a two-story building. Estimated reduction factors (R) for various performance levels and aspect ratios are summarized in Table 6.1.

6.3.3 Nonlinear Analyses - FEMA 178 and UCBC

Rocking strengths of S1 and S2 were determined using the FEMA 178 procedure. Within the accuracy of the parameters used in the analysis, the calculated ultimate strengths were within 20% of those measured during the final test runs (15 and 24) of each building. The UCBC approach was much the same and produced comparable results, with, in this case, a factor of safety of $3^1/_3$. Both documents promoted rocking as the preferred response over a shear-controlled behavior. The FEMA 178 document seemed to overpromote rocking by reducing the forces applied to the rocking-controlled walls (Equation 3.7). Calculated rocking strengths presented in Table 5.2 included no reduction or enhancement coefficients and were as accurate as those determined using FEMA 178. For simple structures like the ones tested here, both documents were fairly straightforward and easy to implement. However, calculated capacities of walls that are shear controlled can be much lower than either the rocking or shear capacities. This was the case for the S1 window wall. In this instance, lowering the assumed axial stresses would have increased the calculated capacity which is contrary to the fact that both rocking and shear strengths

Table 6.1 Estimated reduction factors (*R*) for various performance levels.

Vertical Stress	Aspect Ratio (height/length)	Performance Level		
		Immediate Occupancy	Life Safety	Collapse Prevention
Low	0.5	1.0	3.0	3.0
Low	1.0	1.2	4.0	4.0
Low	2.0	1.5	6.0	6.0
Low	3.0	1.0	3.0	3.0
Moderate, High	Any	N.A.*	N.A.	N.A.

*Not available.

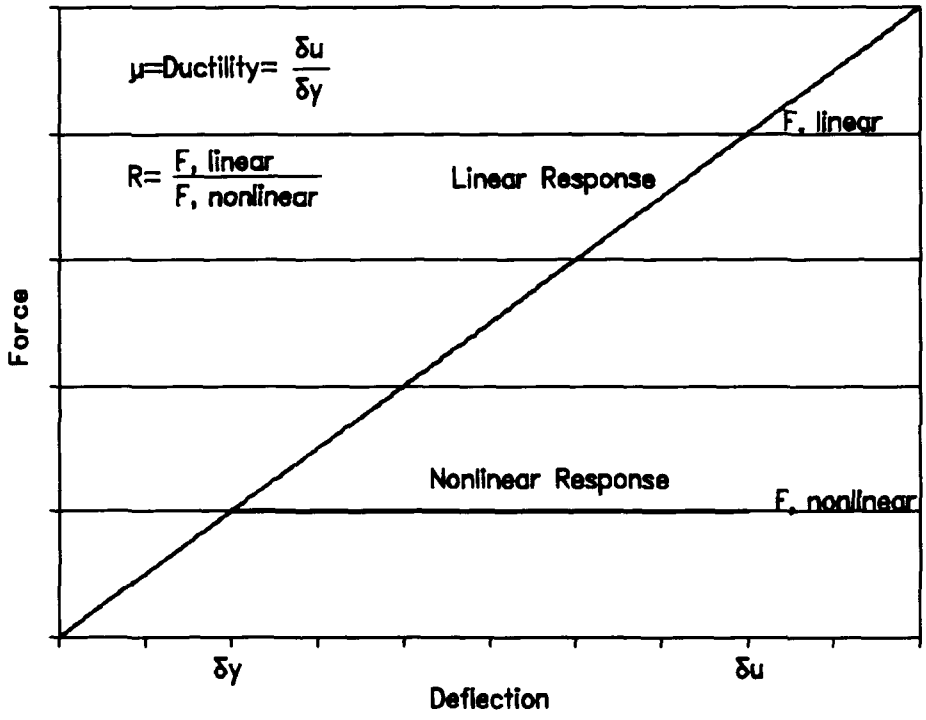

Figure 6.1 Force-deflection Curve Showing Definition of Reduction Factor, *R*

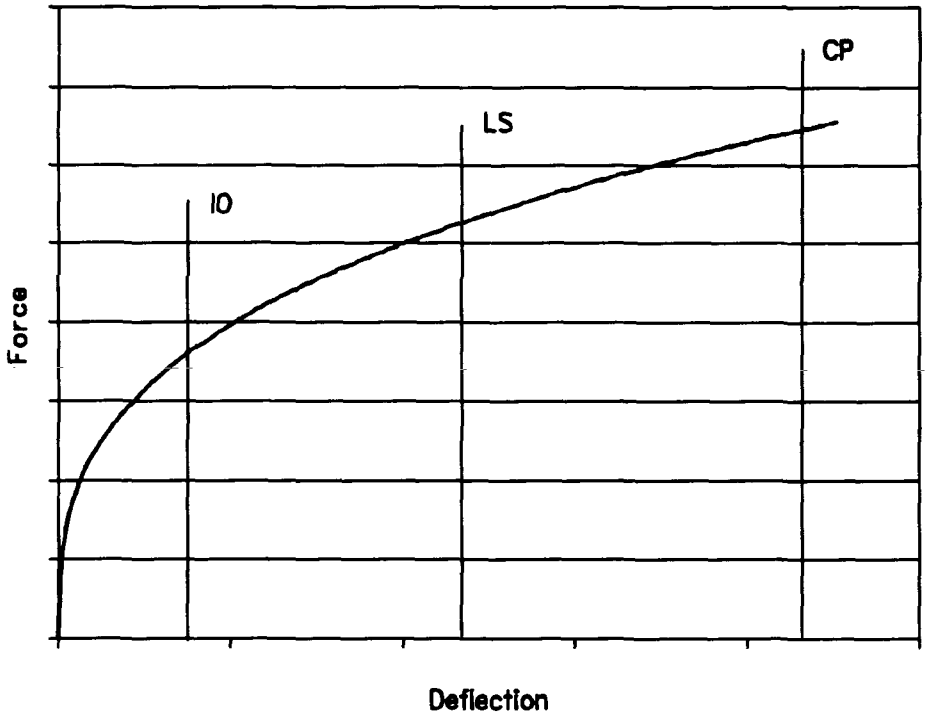

Figure 6.2 Sample Force-deflection Curve Showing Performance Levels

decrease with decreased axial stress. No comments can be made regarding shear strengths per FEMA 178 and UCBC since both buildings tested were rocking controlled. Research on this topic is suggested in Section 7.

The main drawback to FEMA 178 and UCBC was that each prescribed a method to estimate pier (and wall) rocking capacity without specifying conditions necessary for piers to withstand the potentially large rocking displacements. Although in Section 6.2, demand was determined to be unable to exceed capacity while the buildings were rocking, one can not conclude that every rocking-controlled masonry building will withstand any earthquake. Other requirements such as minimum tensile strengths and maximum aspect ratios are needed to ensure that rocking piers will not degrade or topple.

Unlike for the linear elastic models, applying equivalent seismic loads was not an issue for these two methods. Wall strengths were based on pier capacities and were independent of lateral force distributions.

6.3.4 Nonlinear Static Analysis - Pushover Method

The pushover method described in Section 5.3 produced pushover curves (Figures 5.30 and 5.31) for rocking-controlled structures that can be simplified to bilinear curves. These bilinear curves can be created in a manner much easier than by using the incremental pushover approach, as both the elastic stiffness and rocking capacity can be estimated without using the pushover method. The bilinear shape of the curve, however, presents a problem in that once a rocking mechanism forms in one of the walls, drifts become unbounded. Increased target displacements (demand) will not result in any change in the capacity level. Various levels of demand can be met with the same (rocking) capacity while stress distributions through the model remain constant through extensive deformations. In order to use the pushover analysis, and other performance-based approaches for evaluation of rocking-controlled buildings, additional information, such as story drifts, must be included (see Section 6.3.7).

6.3.5 Nonlinear Dynamic Analysis - 3-DOF Model

Simple multi-degree-of-freedom models can be used to fairly accurately estimate dynamic behavior of URM buildings. The 3-DOF model described in Section 5.4, with the assumed bilinear rocking behavior, was used to determine displacement histories for S1 and S2 using the base accelerations recorded during the rocking test runs. Peak calculated displacements compared favorably with measured values (Table 5.3), although the incidence time was not always correct. The simple model developed in this study can be expanded to analyze URM buildings with different configurations. By varying the intensity of the base motion, and the base motion itself, a performance curve for the structure can easily be developed. However, given the simplicity of the current model, results should not be treated as more than *estimates* of response.

6.3.6 Out-of-Plane Walls - Flange Effects

The (linear elastic) finite element analysis indicated that transverse, or out-of-plane, walls shared some of the stresses of the piers to which they were adjoined. Dead load stresses and stresses due to global overturning were slightly shared by the out-of-plane walls (Figures 3.5 and 3.6) while horizontal shear stresses were resisted by the in-plane piers only.

Out-of-plane walls also played a role in the post-cracking behavior of the URM test structures. Recall that after Test Run 24, the interior door-wall piers were out of plumb due to transverse (perpendicular to the direction of testing) motions of S2. The exterior door-wall piers were still plumb due to the connection to the out-of-plane walls. Conversely, after Test Run 15, the exterior window-wall piers of S1 were leaning slightly outward (permanent in-plane displacements), possibly due to the inertial effects of the out-of-plane walls. Qualitatively, transverse walls can provide a stabilization against out-of-plane movements of in-plane piers. At the same time, long transverse walls may induce in-plane displacements of in-plane piers because of inertial effects.

Fair agreement (20%) was found between the measured rocking strengths and those calculated using the FEMA 178 method (Section 4.11.1). Taking into account a factor of $3^1/_3$, excellent agreement between measured and UCBC rocking strengths was found (Section 4.11.1).

Neither method explicitly stated that flange effects of out-of-plane walls should be considered while calculating the rocking strength of an adjoing (in-plane) pier. Therefore, the presence of out-of-plane walls was not included in the calculations. Since calculated strengths agreed with measured values *without* the inclusion of flange effects from the out-of-plane walls, the flange effects on rocking piers, if any, are minimal. Further research on this topic is suggested in Section 7 to quantify any flange effects.

6.3.7 Performance-Based Design Approaches

The problems in applying the pushover analysis to rocking-controlled structures were mentioned in Section 6.3.4. Some of the problems relate to performance-based design approaches in general, namely, how to define different levels of seismic performance when capacity is essentially constant and seemingly unlimited. Typical damage states might include no to light damage, moderate damage, and severe damage without collapse. Performance levels that are associated with these damage states are immediate occupancy (IO) after an earthquake, and life safety (LS) and collapse prevention (CP) during an earthquake. A sample force-deflection curve showing different performance levels is shown in Figure 6.2. A sample force-displacement curve for a rocking-controlled element showing arbitrarily-placed performance levels is shown in Figure 6.3. In structural systems where increasing deflections produce increasing stress demands, performance levels can be assigned on these bases. For rocking-controlled elements, however, stress distributions are constant once rocking has begun. In order to apply performance-based design (or evaluation) approaches to rocking-controlled systems, a different means of relating performance levels to damage states must be developed.

One way to define performance levels for rocking systems would be to use story drift as the bounding parameter. The use of story drift as the bounding parameter has the advantage of not requiring the calculation of cracking or "yielding" displacements of the walls. Since these displacements can be very small relative to rocking displacements, and have large uncertainties, using them as the basis for estimating ductility (and in turn damage states) can produce erroneous results. As an example of how story drifts could be used to define performance levels, a peak drift

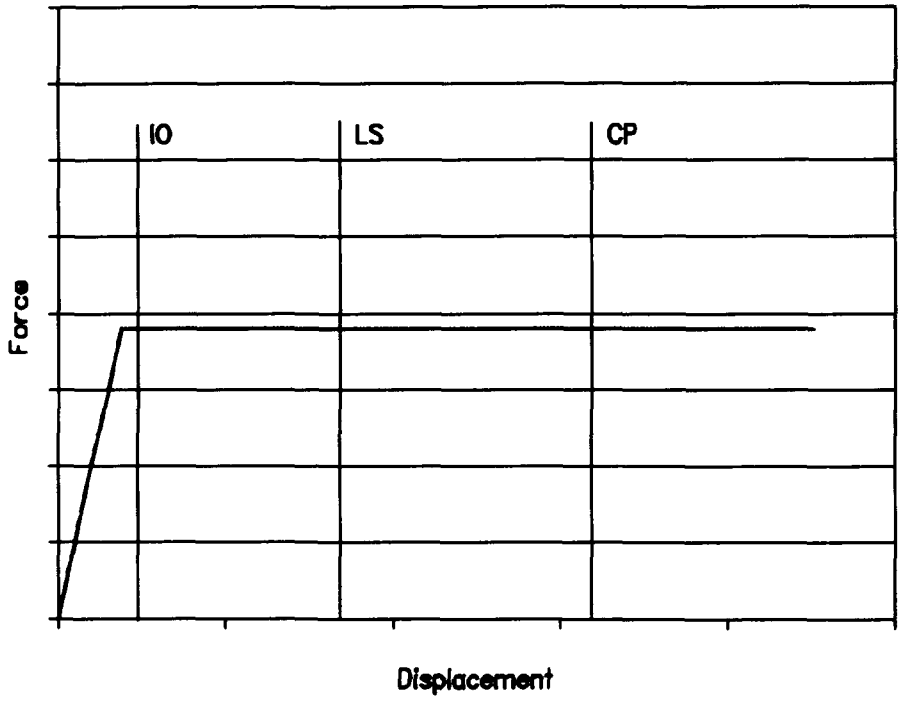

Figure 6.3 Force-displacement Curve for Rocking System Showing Performance Levels

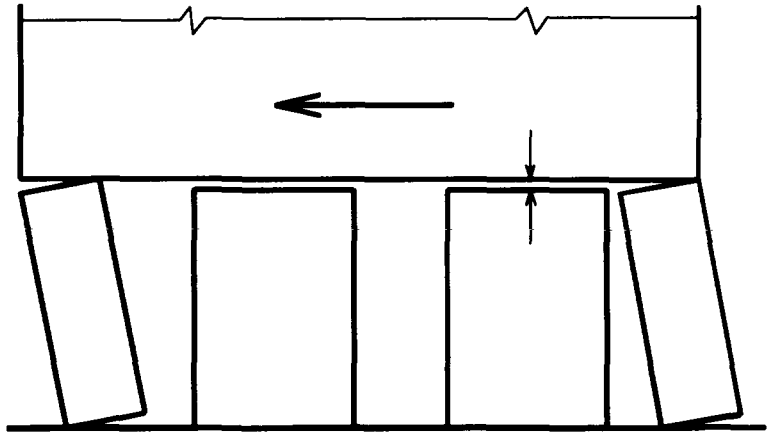

Figure 6.4 Rocking Wall with Widely-varied Pier Aspect Ratios

of less than 0.1% could be considered as producing no to light damage, and could be related to the immediate occupancy performance level. However, since pier rocking can produce large (story) drifts with little damage, the life safety and collapse prevention performance levels become indistinguishable. Peak drifts between 0.1% and 0.5% could then relate to a combined life safety/collapse prevention performance level. Factors such as the importance of the pier to the gravity or lateral system, the redundancy in the systems, the level of vertical stress in the pier, and the pier aspect ratio should all characterize the allowable story drift for each performance level. Although the drifts used in this example are fictitious, the example serves to illustrate how performance-based approaches may be used for rocking-controlled systems.

6.4 Recommendations for Rehabilitation

6.4.1 Rocking

Pier rocking during the dynamic tests has been clearly established (Sections 4.2.1, 4.2.2, 4.5, and 4.10). Based on the fact that both test structures were able to withstand displacements several times greater than the cracking displacements, and the fact that neither structure collapsed, even after numerous rocking cycles, rocking can be classified as stable and reliable. Therefore, rocking is a recommended post-cracking behavior for URM structures. Note that a minimum mortar strength is required to maintain pier integrity during repeated rocking cycles.

6.4.2 Pier Aspect Ratios

Numerous pier aspect ratios (height/length) were present in the two test structures, ranging from 0.67:1 to 3.37:1 (Tables 2.1 and 2.2). The stockiest pier that rocked was the middle door-wall pier of S1 with an aspect ratio of 1.19:1. Piers stockier than this (0.67:1 and 1.04:1) did not rock, as they did not crack. If piers are too stocky, they will likely be shear-critical. Since S2, with its relatively slender door-wall piers (2.39:1 and 3.37:1), did not achieve the same level of ductility as S1, S1 could be viewed as performing "better" in the nonlinear range. Therefore, there is a limit to how slender rocking piers should be. Based on the pier aspect ratios tested in this

study, piers that are expected to rock should have aspect ratios between 1:1 and 2:1. Furthermore, pier aspect ratios along a single wall should not be too dissimilar from one another. Purely geometric considerations indicate that if very stocky and very slender piers are mixed in a single wall, then the stocky piers may not rock (Figure 6.4). In such cases, the stocky piers may not attract lateral force because of the "lifting" of the story level by the (more slender) rocking piers. Additional studies to examine this behavior are suggested in Section 7.

The recommendation for limiting the aspect ratios of rocking piers to between 1:1 and 2:1 implies that existing URM buildings may be rehabilitated by *increasing* the size of existing openings, rather than by infilling them. The rehabilitated structure may be weaker, but the nonlinear response will be predictable and stable. Furthermore, since for rocking-controlled buildings demand cannot exceed capacity, seismic forces will actually be lowered. If existing piers are too slender, then partially infilling an adjacent opening would be recommended. However, the infill masonry and the original piers should be made integral.

6.4.3 Strong Wall/Weak Wall Systems

One of the primary differences between S1 and S2 was the relative lateral strengths of the two in-plane (shear) walls. In S1, the two walls had approximately the same strength while in S2, the window wall was much stronger than the door wall. Thus S2 could be classified as a strong wall/weak wall system. Since S1 exhibited more ductility than S2, had a more uniform distribution of cracking, and was in generally better shape after the fourth test run than S2, the strong wall/weak wall system of S2 is not recommended over the equal wall strength system of S1. Note that the sum of the rocking strengths of the two shear walls was actually higher for S2 than for S1 (Table 5.3). The code strengths reported (Sections 3.2.1-3.2.4) were double the weaker-wall strength and were therefore lower for S2 than S1.

For shear walls with piers, strength and stiffness are both related to the aspect ratios of the piers. As the aspect ratio (height/length) increases, both strength and stiffness decrease. As such, a strong wall/weak wall system is also likely to be a stiff wall/flexible wall system. For systems with rigid diaphragms, the strong, stiff wall will attract the majority of the load. For systems with

flexible diaphragms, however, the diaphragm loads are more evenly distributed between the two walls. The capacity of the strong wall is not fully utilized while the weak wall might experience substantial nonlinear displacements. Within the limits for aspect ratios set in Section 6.4.2, the two walls should be brought to more equal strengths to reduce the displacement requirements of the weaker wall.

6.4.4 Out-of-Plane Walls - Out-of-Plane Bending

Post-earthquake reconnaissance teams frequently categorize different types of failures in URM buildings during their studies. One such category is "out-of-plane failure"[(Bruneau, 1994b)]. Among other reasons, these out-of-plane failures can sometimes be attributed to long-span, flexible diaphragms driving the out-of-plane walls beyond their capacity. Although the two buildings tested in this study had out-of-plane walls and flexible diaphragms, no out-of-plane failures were noted. All four out-of-plane walls developed horizontal cracks which initiated in the in-plane piers, but none suffered any diaphragm-induced damage.

The absence of out-of-plane failures during the earthquake simulations can be attributed to several factors. Probably the most important factors were the relatively short horizontal span of the out-of-plane walls coupled with the full-height vertical joint along one edge of the out-of-plane walls. The vertical joint acted as a moment release at one end of the out-of-plane wall (horizontal) span. The horizontal cracks that formed across the out-of-plane walls prevented further damage in these walls along their vertical span. The diaphragm/out-of-plane wall connection detail (Figure 2.13b) prevented the diaphragm from pounding against the out-of-plane walls during dynamic excitation, thus eliminating another source of damage.

By incorporating a few details into a rehabilitation scheme, the occurrence of out-of-plane failures can be minimized. Reducing the horizontal span of masonry elements is one of the easiest ways to reduce out-of-plane damage. Making sure the diaphragm and masonry walls are positively-connected is also recommended.

SECTION 7 SUMMARY AND CONCLUSIONS

7.1 Objectives of Study

Three primary objectives were followed throughout the course of the study. The first was to investigate the dynamic behavior of two, reduced-scale, URM buildings with flexible diaphragms. The second objective was to develop a simple analytical model to estimate dynamic response maxima of URM buildings. The third primary objective was to examine various static and dynamic methods of analyzing URM buildings to determine their applicability and accuracy. The end result of the study was to provide recommendations for the evaluation and rehabilitation of URM buildings with flexible diaphragms.

7.2 Summary of Experimental and Analytical Work

Two reduced-scale unreinforced masonry buildings were designed and constructed. Each two-story building had four walls, two perforated, in-plane, shear walls and two, solid, out-of-plane walls. The two shear walls were coupled by two flexible diaphragm systems designed with a natural frequency well below that of an equivalent rigid-diaphragm structure. The two buildings were instrumented with over thirty channels of accelerometers, strain gauges and LVDTs. Using a modified version of the 1985 Nahanni earthquake, the two test structures were tested dynamically on the Newmark Civil Engineering Laboratory earthquake simulator. Detailed results of the dynamic tests were presented in Section 4.

Several conventional methods, both static and dynamic, were used to estimate the response of the two test structures. The static analyses included both working stress methods, UBC, MSJC, and UCBC, and an ultimate strength method, FEMA 178. Static analyses were also performed using finite element models. Some linear elastic dynamic methods, equivalent frame, MDOF with flexible diaphragms, and finite elements, were used to estimate natural frequencies while others,

time-step integration and response spectrum analysis, were used to estimate displacement and accelerations likely in the early test runs.

Three analysis models were used to try to simulate the measured response. The three models were linear dynamic (response spectrum analysis), nonlinear static (pushover analysis), and nonlinear dynamic (time-step integration of a nonlinear 3-DOF model).

7.3 Summary of Measured Response

Based on the results of a total of nine test runs on two buildings, the following conclusions are drawn.

1) Diaphragm and wall amplifications of base accelerations compared well with results measured on full-size buildings during actual earthquakes. Prior to cracking, both walls and diaphragms amplified base accelerations at a constant level while after cracking, little to no amplification existed.

2) Flexible diaphragms amplified wall displacements prior to cracking in the walls. After cracking, diaphragm displacements relative to the walls were greatly diminished. Interstory drifts above the cracks also decreased after cracking.

3) Lateral forces were distributed equally between the two floor levels, not by the inverted-triangular distribution normally assumed for rigid diaphragms.

4) Low masonry tensile strength resulted in horizontal cracks across the bases and tops of most of the piers.

5) First-story cracking drifts were approximately 0.1%.

6) Substantial strength and deformation capacity existed after cracking. This ductility resulted from pier rocking in the first story.

7) After cracking, up to 80% of first-story displacements were attributable to rocking.

8) Post-cracking force-displacement curves were bilinear in shape which is indicative of rocking.

9) Natural frequencies decreased as structural damage, in the form of cracking, increased. Frequency measurements were dependent on the amplitude of the test. Calculated natural frequencies were much higher than measured frequencies.

7.4 Comparison of Measured Response to Conventional Methods (Section 3)

7.4.1 Static

The cracking loads calculated using the design codes and the finite element models were conservative relative to those measured. Measured loads were generally 2-3 times higher than those calculated. This conservatism was due to the direct dependence of the calculated cracking loads on the masonry tensile capacity used in the analysis. The value measured during the (static) flexural tension tests did not accurately represent the dynamic tensile strength of the masonry.

The FEMA 178 methodology indicated a rocking-controlled behavior for both buildings while the UCBC indicated a shear-controlled behavior for S1 and a rocking-controlled behavior for S2. Experimental observations indicated both S1 and S2 were controlled by rocking. The ultimate capacity of S1 and S2 determined using the FEMA 178 method compared moderately well to the peak base shears measured during Test Runs 15 and 24. The UCBC strengths, however, were much lower (3-4 times) than the measured rocking strengths. These working stress force levels, derived from the ultimate behavior of rocking, had a safety factor of $3^1/_3$, whereas the force levels from the FEMA 178 analysis were true ultimate strengths.

7.4.2 Dynamic

Agreement between the measured dynamic behaviors and the results from the simple dynamic analyses (Sections 3.3.1 to 3.3.5) was generally poor. Rigid diaphragm models produced natural frequencies much higher than those determined experimentally. Large differences between wall and diaphragm stiffnesses in the MDOF model with flexible diaphragms produced mode shapes and natural frequencies indicating almost independent diaphragm and wall behaviors. The finite element models produced mode shapes with uniform diaphragm and wall motions, but the

natural frequencies were nearly twice those measured. Peak displacements and accelerations calculated using the MDOF model with flexible diaphragms ranged from several times higher to many times lower than experimental values. This wide variation was also attributable to the large difference between wall and diaphragm stiffnesses. The estimated natural frequencies, mode shapes, accelerations, and displacements were all related to the elastic modulus of the masonry used in the analyses.

7.5 Comparison of Measured Response to Analytical Models (Section 5)

Three analytical models were examined to determine their applicability to unreinforced masonry buildings with flexible diaphragms. The response spectrum method used measured base accelerations, measured natural frequencies, and modal participation factors based on measured displacements to estimate peak accelerations and displacements. Compared with measured acceleration and displacement peaks, the spectral results were mixed. In general, spectrally-based accelerations were close to measured peaks, if the proper level of damping was assumed. Spectrally-based displacements were, however, much higher than measured displacements, especially for S1. Better correlation was achieved with the measured values from the cracked test runs than the values from the uncracked test runs due to the uniform motion induced by pier rocking.

The pushover analysis is a stiffness/strength approach that produces a force-deflection curve leading to mechanism. Normally during the analysis, force distributions throughout the model are analyzed to determine potential weak points at different target displacements. However, when applied to the models of S1 and S2, the pushover analysis resulted in a rapid, sequential cracking and rocking of all the piers in a wall. This behavior produced a nearly bilinear force-displacement curve which is more easily obtainable by other methods. The bilinear behavior also negated the use of various target displacements, representing different performance levels, since capacity was constant with increasing displacement.

The third model examined, time-step integrated, nonlinear, 3-DOF model, was developed as a result of the measured data. This model was used with recorded base accelerations from the post-cracking test runs to determine first-story displacement histories of the two walls. A bilinear force-displacement curve was used to model rocking. Considering the simplicity of the model, the correlation between measured and calculated displacements was excellent. Peak displacements were closely estimated, the change in frequency during rocking was accurately determined, and the portions of the history when rocking occurred were identified. The only major drawback was that the model was inconsistent at determining the time of peak displacement.

7.6 Recommendations

Recommendations for the analysis and rehabilitation of unreinforced masonry buildings with flexible diaphragms were discussed in Section 6. Based on these discussions, the following recommendations are made.

1) Linear elastic analyses of URM structures should be used only to produce stress distributions. Large uncertainties in the elastic modulus of the masonry limit the effectiveness of these types of analysis in estimating accelerations, displacements, and natural frequencies.

2) A conservative estimate of ductility for rocking piers is two. This value of two can be used as a reduction factor for equivalent seismic forces derived from linear static analyses. Reduction factors of 1.0-6.0 were suggested for different performance levels, based on pier aspect ratio, for performance-based analysis approaches.

3) FEMA 178 and UCBC can be used to estimate the rocking capacities of URM buildings, but with some caution. The force reduction for rocking-controlled walls in FEMA 178 can produce unconservative results while the force distribution among piers for the shear-controlled behavior in both codes can produce overly-conservative results.

4) The pushover analysis (nonlinear static) for rocking-controlled walls can be simplified to a single elastic analysis and a summing of the pier rocking strengths. More information about pier behavior is necessary to apply different performance levels to the bilinear pushover curve.

5) Simple dynamic models can be used to estimate peak displacements of rocking-controlled walls.

6) While useful in linear elastic analyses, flange effects of out-of-plane walls need not be included in calculating the rocking strengths of adjoining (in-plane) piers.

7) Story drifts can be used to define different performance levels for rocking-controlled systems in performance-based design approaches.

8) Pier rocking is recommended as a stable, repeatable nonlinear behavior in URM structures.

9) Piers that are expected to rock should have aspect ratios (height/length) from 1:1 to 2:1. Also, pier aspect ratios along a given wall should not vary widely.

10) Strong wall/weak wall systems are not recommended over systems with near equal strength walls due to large displacement demands placed on the weak wall.

11) The occurrence of out-of-plane failures in out-of-plane walls can be reduced by limiting the horizontal and vertical spans of these walls and by positively connecting the out-of-plane walls to the diaphragms.

7.7 Future Research

There is a need for further investigations of the dynamic response of unreinforced masonry buildings with flexible floor and roof diaphragms. In the current study, eight different pier aspect ratios were used in two test buildings. Both buildings had the same diaphragms and were subjected to amplified versions of the same base motions. Additional studies should investigate similar structures with two different diaphragms and/or different base motions. Shear walls with stockier piers, approaching solid shear walls, should be studied to examine dynamic response and the various code provisions for shear-controlled behavior.

The effect of the out-of-plane walls on the rocking and shear strengths of corner piers should also be examined. A possible configuration would be one similar to the buildings tested in this study except with equal openings in both shear walls. This way, one shear wall would have

two flanges and the other would have no flanges. The response of the two walls should be compared against each other to determine the effect of the out-of-plane walls.

Another suggested investigation is to test buildings with an unsymmetric layout of openings. Both buildings tested in this study had a symmetric opening layout. Mixing stocky and slender piers in an unsymmetric arrangement could provide information regarding pier rocking strengths not obtainable from this study.

There is also a need for full-scale dynamic testing of unreinforced masonry structures. Full-scale test structures would have a truer mass distribution between the walls and the diaphragms since additional mass would not be necessary to achieve realistic gravity stresses in the piers. Also, with full-scale dynamic tests, a direct comparison between base shear and structural weight would be possible.

Any additional dynamic studies on unreinforced masonry structures with flexible diaphragms would be beneficial to either confirm or contradict the conclusions reached in this study. Additional test results are also needed to further validate the proposed 3-DOF model and to provide insight on possible modifications to the model.

Static tests of rocking piers are needed to identify the force-deflection relationships. Such tests would also provide information for improved elastic analyses of URM buildings with perforated bearing walls. A parallel study would be to use cyclic static tests of rocking piers to determine the minimum mortar strength necessary to hold the pier together during repeated cycles of rocking.

Finally, there is a need for improved simplified models for estimating response maxima of URM buildings. Simple models which can estimate limit states for performance-based design methodologies are also needed.

SECTION 8 REFERENCES

ABK, "Methodology for Mitigation of Seismic Hazards in Existing Unreinforced Masonry Buildings: The Methodology", Topical Report 08, El Segundo, CA, 1984.

Abrams, D., "Dynamic and Static Testing of Reinforced Concrete Masonry Structures", *TMS Journal*, v. 7, #1, Jan-Jun 1988, pp. T18-T22.

Abrams, D., *A Set of Classnotes for a Course in: Masonry Structures*, The Masonry Society, 1991, pp. 140.

Abrams, D., and N. Shah, "Cyclic Load Testing of Unreinforced Masonry Walls", ACTC No. 92-26-10, UILU-ENG-92-1938, December 1992, pp. 46.

Abrams, D., "Seismic Evaluation and Rehabilitation of Unreinforced Masonry Buildings in the United States", presented at First Pan American Masonry Symposium, Bogota, Colombia, October 1993, pp. 11.

Adham, S. and R. Ewing, "Interaction Between Unreinforced Masonry Structures and Their Roof Diaphragms During Earthquakes", *Proceedings, North American Masonry Conference*, 1978, pp. 57-1--57-16.

Alcocer, S., and R. Meli, "Experimental Program on the Seismic Behavior of Confined Masonry Structures", *Proceedings, The Sixth North American Masonry Conference*, v. 2, 1993, pp. 693-704.

Anthoine, A., Gu. Magenes, and G. Magonette, "Shear-compression testing and analysis of brick masonry walls", *Proceedings, Tenth European Conference on Earthquake Engineering* (Vienna), 1994.

ASTM, *Annual Book of ASTM Standards*, Part 16, C67-78, ASTM, Philadelphia, PA, 1979.

ATC-33 - Simplified Nonlinear Method, (Draft by H. Krawinkler), 1/14/95.

ATC-34 Project: Study of Critical Code Issues, (Draft), 11/29/93.

Bariola, J., J. Ginocchio, and D. Quiun, "Out-of-Plane Seismic Response of Brick Walls", *Proceedings, Fifth North American Masonry Conference*, v. I, 1990, pp. 429-439.

Beall, C., *Masonry Design and Detailing: For Architects, Engineers, and Builders*, Second Edition, McGraw-Hill Book Company, New York, 1987, pp. 491.

Bermudez, J., "Structural Masonry in Costa Rica", *Masonry in the Americas*, ACI (SP-147), 1994, pp. 263-281.

Bruneau, M., "Assessing The Seismic Performance of Existing Buildings in Canada", *Masonry in the Americas*, ACI (SP-147), 1994, pp. 171-203.

Bruneau, M., "State-of-the-Art Report on Seismic Performance of Unreinforced Masonry Buildings", *Journal of Structural Engineering*, v. 120, No. 1, Jan. 1994, ASCE, pp. 230-251.

Bruneau, M., "Damage to Masonry Buildings from the 1995 Hanshin-Awaji (Kobe, Japan) Earthquake - Preliminary Report", *Proceedings of the Seventh Canadian Masonry Symposium*, v.1, 1995, pp. 84-98.

Building Code Requirements for Masonry Structures (ACI 530-95/ASCE 5-95/TMS 402-95) and Commentary, The Masonry Standards Joint Committee, ACI/ASCE/TMS, 1995.

Calvi, M., Gi. Magenes, Gu. Magenes, and A. Pavese, "Experimental and numerical investigation on a brick masonry building prototype: Design of the experimental tests", Dipartimento di Meccanica Strutturale, Università di Pavia, February, 1992, pp. 61.

Calvi, M., Gu. Magenes, A. Pavese, and D. Abrams, "Large Scale Seismic Testing of an Unreinforced Brick Masonry Building", *Proceedings, Fifth U.S. National Conference on Earthquake Engineering*, v. I, 1994, pp. 137-146.

Chopra, A., *Dynamics of Structures: A Primer*, EERI, 1982, pp. 126.

Clough, R., R. Mayes, and P. Gülkan, "Shaking Table Study of Single-Story Masonry Houses, Volume 3: Summary, Conclusions, and Recommendations", UCB/EERC-79/25, September 1979, pp. 96.

Clough, R., and J. Penzien, *Dynamics of Structures*, McGraw-Hill Book Company, New York, 1975, pp. 634.

Commentary to Chapter 21, Masonry, of the Uniform Building Code, 1994 Edition, The Masonry Society Codes and Standards Committee, TMS, 1995.

EERI, *Northridge Earthquake January 17, 1994 Preliminary Reconnaissance Report*, EERI, Oakland, CA, 1994, pp. 42-44.

El-Mustapha, A., and J. Kariotis, "The Inelastic Response of Masonry Structures Free to Uplift on their Bases", *Proceedings, Fifth North American Masonry Conference*, v. I, 1990, pp. 249-260.

Epperson, G., and D. Abrams, "Nondestructive Evaluation of Masonry Buildings", ACTC No. 89-26-03, October 1989, pp. 208.

Ewing, R., J. Kariotis, R. Englekirk, and G. Hart, "Analytical Modelling for Reinforced Masonry Buildings and Components - TCCMAR Category 2 Program", *Proceedings, Fourth North American Masonry Conference*, v. II, 1987, pp. 39-1--39-41.

Feng, J., "The Seismic Shear Strength of Masonry Wall", *Proceedings of US-PRC Joint Workshop on Seismic Resistance of Masonry Structures*, 1986, pp. II-4-1--II-4-12.

Gallegos, H., "Masonry in Peru", *Masonry in the Americas*, ACI (SP-147), 1994, pp. 307-331.

Garcia, L., and L. Yamin, "A Review of Masonry Construction in Colombia", *Masonry in the Americas*, ACI (SP-147), 1994, pp. 283-305.

Gergely, P., and R. Hamburger, "Simplified Methods for Evaluation of Rehabilitated Buildings", *Proceedings of the U.S.-Italy Workshop on Guidelines for Seismic Evaluation and Rehabilitation of Unreinforced Masonry Buildings*, NCEER-94-0021, 1994, pp. 4-3--4-16.

Hamid, A., S. Magd, and A. Salama, "Performance of Loadbearing Masonry Buildings During the October 1992 Earthquake in Cairo, Egypt", *Proceedings, The Sixth North American Masonry Conference*, v. 2, 1993, pp. 717-726.

Healey T., and M. Sozen, "Experimental Study of the Dynamic Response of a Ten-Story Reinforced Concrete Frame With a Tall First Story", SRS No. 450, UILU-78-2012, August 1978, pp. 120.

Heidebrecht, A. and N. Naumoski, "Engineering Implications of the 1985 Nahanni Earthquakes", *Earthquake Engineering and Structural Dynamics*, v. 16, No. 5, July 1988, pp. 675-690.

Housner, G., and P. Jennings, *Earthquake Design Criteria*, EERI, 1982, pp. 126.

Jalil, I., W. Kelm, and R. Klingner, "The Performance of Masonry and Masonry Veneer Buildings in the 1989 Loma Prieta Earthquake", *Proceedings, The Sixth North American Masonry Conference*, v. 2, 1993, pp. 681-692.

Jurukovski, D., L. Krstevska, R. Alessi, P. Diotallevi, M. Merli, and F. Zarri, "Shaking table tests of three four-storey brick masonry models: Original and strengthened by RC core and by RC jackets", *Proceedings of the Tenth World Conference on Earthquake Engineering*, v. 5, 1992, pp. 2795-2800.

Kariotis, J., R. Ewing, and A. Johnson, "Methodology for Mitigation of Earthquake Hazards in Unreinforced Brick Masonry Buildings", *Proceedings of US-PRC Joint Workshop on Seismic Resistance of Masonry Structures*, 1986, pp. I-1-1--I-1-12.

Krawinkler, H., "Possibilities and Limitations of Scale-Model Testing in Earthquake Engineering", *Proceedings of the 2nd U.S. National Conference on Earthquake Engineering*, 1979, pp. 283-292.

Langenbach, R., "Earthquakes: A New Look at Cracked Masonry", *Civil Engineering*, November, 1992, ASCE, pp. 56-58.

Lawson, R., V. Vance, and H. Krawinkle, "Nonlinear Static Push-Over Analysis - Why, When, and How?", *Proceedings, Fifth U.S. National Conference on Earthquake Engineering*, v. I, 1994, pp. 283-292.

Magenes, Gu., and G. Calvi, "Shaking table tests on brick masonry walls", *Proceedings, Tenth European Conference on Earthquake Engineering* (Vienna), 1994.

Mahmoud, A., A. Hamid, and S. El Magd, "Lateral Response of Unreinforced Solid Masonry Shear Walls: An Experimental Study", *Proceeding of the Seventh Canadian Masonry Symposium*, v. 1, 1995, pp. 110-125.

Manos, G., R. Clough, and R. Mayes, "Shaking Table Study of Single-Story Masonry Houses: Dynamic Performance Under Three Component Seismic Input and Recommendations", UCB/EERC-83/11, July 1983, pp. 156.

Manos, G., "Earthquake Performance of Masonry Structures During the Thessaloniki 1978 Earthquake", *Proceedings, 4th Canadian Masonry Symposium*, v. 1, 1986, pp. 426-437.

McCabe, S., and M. McMahon, "Seismic Evaluation of an Unreinforced Masonry Fire Station", *Proceedings, Fifth North American Masonry Conference*, v. II, 1990, pp. 759-770.

Mengi, Y., and H. McNiven, "A Mathematical Model for Predicting the Nonlinear Response of Unreinforced Masonry Walls to In-Plane Earthquake Excitations", UCB/EERC-86/07, May 1986, pp. 113.

Modena, C., P. La Mendola, and A. Terrusi, "Shaking table study of a reinforced masonry building model", *Proceedings of the Tenth World Conference on Earthquake Engineering*, v. 6, 1992, pp. 3523-3526.

NEHRP Handbook for the Seismic Evaluation of Existing Buildings (FEMA 178), Building Seismic Safety Council, Washington, D.C., 1992, Appendix C.

Newmark, N. and W. Hall, *Earthquake Spectra and Design*, EERI, 1982, pp. 103.

Otani, S., et al., "Design Guidelines (Draft) for Reinforced Concrete Buildings", Notes from The Third Meeting of the U.S.-Japan Joint Technical Coordinating Committee on Precast Seismic Structural Systems (JTCC-PRESSS), October 18-20, 1992, Chapter 4.

Paulson, T., and D. Abrams, "Measured Inelastic Response of Reinforced Masonry Building Structures to Earthquake Motions", SRS No. 555, UILU-ENG-90-2013, October 1990, pp. 290.

Paz, M., *Structural Dynamics: Theory and Computation*, Second Edition, Van Nostrand Reinhold Company, New York, 1985, pp. 561.

Pomonis, A., R. Spence, A. Coburn, and C. Taylor, "Shaking table tests on strong motion damagingness upon unreinforced masonry", *Proceedings of the Tenth World Conference on Earthquake Engineering*, v. 6, 1992, pp. 3533-3538.

Saiidi, M., and M. Sozen, "Simple and Complex Models for Nonlinear Seismic Response of Reinforced Concrete Structures", SRS No. 465, UILU-ENG-79-2013, August 1979, pp. 188.

San Bartolomé, A. and D. Torrealva, "A New Approach for Seismic Design of Confined Masonry Buildings in Peru", *Proceedings, Fifth North American Masonry Conference*, v. I, 1990, pp. 37-44.

San Bartolomé, A., D. Quiun, and D. Torrealva, "Seismic behaviour of a three-story half scale confined masonry structure", *Proceedings of the Tenth World Conference on Earthquake Engineering*, v. 6, 1992, pp. 3527-3531.

Scawthorn, C., and A. Becker, "Relative Benefits of Alternative Strengthening Methods for Low Strength Masonry Buildings", *Proceedings, Third U.S. National Conference on Earthquake Engineering*, V. III, 1986, pp. 2023-2034.

Schultz, A., "Performance of Masonry Structures During Extreme Lateral Loading Events", *Masonry in the Americas*, ACI (SP-147), 1994, pp. 85-125.

Seible, F., et. al., "Preliminary Results from the TCCMAR 5-Story Full-Scale Reinforced Masonry Research Building Test", *Proceedings, Sixth North American Masonry Conference*, v. 1, 1993, pp. 173-184.

Seneviratna, G., and H. Krawinkler, "Strength and Displacement Demands for Seismic Design of Structural Walls", *Proceedings, Fifth U.S. National Conference on Earthquake Engineering*, v. II, 1994, pp. 181-190.

Shing, P. B., J. Brunner, and H. Lotfi, "Analysis of Shear Strength of Reinforced Masonry Walls", *Proceedings, The Sixth North American Masonry Conference*, v. 2, 1993, pp. 1133-1144.

Sozen, M., S. Otani, P. Gulkan, and N. Nielsen, "The University of Illinois Earthquake Simulator", *Proceedings, Fourth World Conference on Earthquake Engineering*, v. III, 1969, Session B-5, pp. 139-150.

Specifications for Masonry Structures (ACI 530.1-95/ASCE 6-95/TMS 602-95) and Commentary, The Masonry Standards Joint Committee, ACI/ASCE/TMS, 1995.

Sucuoglu, H., Y. Mengi, and H. McNiven, "A Mathematical Model for the Response of Masonry Walls to Dynamic Excitations", UCB/EERC-82/24, November 1982, pp. 121.

Tena-Colunga, A., and D. Abrams, "Response of an Unreinforced Masonry Building During the Loma Prieta Earthquake", SRS No. 576, UILU-ENG-92-2024, December 1992, pp. 288.

Tena-Colunga, A., and D. Abrams, "Response of an Instrumented Masonry Shear Wall Building with Flexible Diaphragms During the Loma Prieta Earthquake", SRS No. 577, UILU-ENG-92-2025, December 1992, pp. 114.

Tolles, E. C. Thiel, F. Webster, and W. Ginell, "Advances in the Seismic Retrofitting of Adobe Buildings", *Proceedings, Fifth U.S. National Conference on Earthquake Engineering*, v. III, 1994, pp. 717-726.

Tomazevic, M., "Dynamic Modelling of Masonry Buildings: Storey Mechanism Model as a Simple Alternative", *Earthquake Engineering and Structural Dynamics*, v. 15, No. 6, August 1987, pp. 731-749.

Tomazevic, M., C. Modena, T. Velechovsky, and P. Weiss, "The Influence of Structural Layout and Reinforcement on the Seismic Behavior of Masonry Buildings: An Experimental Study", *The Masonry Society Journal*, v. 9, No. 1, August 1990, pp. 26-50.

Tomazevic, M., M. Lutman, P. Weiss, and T. Velechovsky, "The Influence of Rigidity of Floors on the Seismic Resistance of Old Masonry Buildings: Shaking-Table Tests of Stone-Masonry Houses - Summary Report", ZRMK/PI-92/04, Ljubljana, 1992, pp. 117.

Tomazevic, M., and T. Velechovsky, "Some Aspects of Testing Small-Scale Masonry Building Models on Simple Earthquake Simulators", *Earthquake Engineering and Structural Dynamics*, v. 21, No. 11, November 1992, pp. 945-963.

Tomazevic, M., P. Weiss, M. Lutman, and L. Petkovi_, "Influence of Floors and Connection of Walls on Seismic Resistance of Old Brick Masonry Houses: Part One: Shaking Table Tests of Model Houses A and B", ZRMK/PI-93/04, Ljubljana, 1993, pp. 119.

Tomazevic, M., M. Lutman, and P. Weiss, "The Seismic Resistance of Historical Urban Buildings and the Interventions in Their Floor Systems: An Experimental Study", *The Masonry Society Journal*, v. 12, No. 1, August 1993, pp. 77-86.

Tomazevic, M., and P. Weiss, "Seismic Behavior of Plain- and Reinforced-Masonry Buildings", *Journal of Structural Engineering*, v. 120, No. 2, February 1994, ASCE, pp. 323-338.

Tomazevic, M., P. Weiss, M. Lutman, and L. Petkovi_, "Influence of Floors and Connection of Walls on Seismic Resistance of Old Brick Masonry Houses: Part One: Shaking Table Tests of Model Houses C and D", ZRMK/PI-94/06, Ljubljana, 1994, pp. 146.

Uniform Code for Building Conservation, 1994 Edition, International Conference of Building Officials, Whittier, CA, Appendix Chapter 1.

Weaver, W., and P. Johnston, *Finite Elements for Structural Analysis*, Prentice-Hall, Inc., Englewood Cliffs, NJ, 1984, pp. 403.

Xia, J., Z. Wei, Q. Huang, and L. Gao, "Shaking Table Test of Multi-Story Masonry Building with Coal-Slag-Gas-Concrete Blocks", *Proceedings, Fifth North American Masonry Conference*, v. I, 1990, pp. 165-176.

Xu, W., and D. Abrams, "Evaluation of Lateral Strength and Deflection for Cracked Unreinforced Masonry Walls", ACTC No. 92-26-11, UILU-ENG-92-1939, December 1992, pp. 177.

Yamazaki, Y., F. Seible, H. Mizuno, T. Kaminosono, and M. Teshigawara, "The Japanese 5-Story Full Scale Reinforced Concrete Masonry Test - Forced Vibration and Cyclic Load Test Results", *TMS Journal*, v. 7, #1, Jan-Jun 1988, pp. T1-T17.

Yamazaki, Y., T. Kaminosono, M. Teshigawara, and F. Seible, "The Japanese 5-Story Full Scale Reinforced Concrete Masonry Test - Pseudo Dynamic and Ultimate Load Test Results", *TMS Journal*, v. 7, #2, Jul-Dec 1988, pp. T1-T18.

Zhu, B., "A Review of Aseismic Test for Masonry Structures in China", *Proceedings of US-PRC Joint Workshop on Seismic Resistance of Masonry Structures*, 1986, pp. III-5-1--III-5-12.

Zhu, B., M. Wu, and D. Zhou, "Shaking Table Study of a Five-Story Unreinforced Block Masonry Model Building Strengthened with Reinforced Concrete Columns and Tie Bars", *Proceedings of US-PRC Joint Workshop on Seismic Resistance of Masonry Structures*, 1986, pp. IV-11-1--IV-11-11.

APPENDIX A

LIST OF EQUIPMENT

Eight ±2" Schaevitz Engineering, Pennsauken, NJ, LVDT Type 2000HR
Four ±5" G.L. Collins Corp., Long Beach, CA, LMA-71184T
Two ±.5" Schaevitz Engineering, Pennsauken, NJ, LVDT Type 500HR
Fourteen Endevco Model 4470 Signal Conditioners
Fourteen Endevco Model 4478-1A Carrier Amplifiers
One MTS LVDT (internal to the hydraulic actuator)

Eighteen ± 25g Endevco, San Juan Capistrano, CA, Piezoresistive
Accelerometer Model 2262C-25
Eighteen Vidar 611 (signal conditioners)
Two Vidar 111 Power Modules
Eighteen Dana Model 3500 D.C. Amplifiers
One ±10g Kulite Semiconductor Accelerometer Model GAD-813-10

Sixteen Measurements Group Inc. Micro-Measurements Division,
Raleigh, NC, EA-06-250BG-120 120Ω ¼" strain gauges
Four Endevco Model 4470 Signal Conditioners
Four NEFF Model 122 DC Amplifiers

MTS 468.20 Test Processor (analog/digital (A/D) converters)
MTS 469 Controller (actuator control and feedback settings)
MTS 436 Control Unit (hydraulic pumps)
DEC Vaxstation II/GPX w/ VMS operating system
MTS STEX (Seismic Test EXecution) software c. 1990.

One 70 gpm hydraulic pump (3000 psi)
One 20 gpm hydraulic pump (3000 psi)
MTS 75 kip actuator
Various small capacity hydraulic accumulators
12'x12' Ormond Inc. Earthquake Simulator (rocker type w/ 32" arms)

APPENDIX B

FORMAT OF COLLECTED DATA

The data measured during the earthquake simulations and free vibration tests were collected using the MTS STEX program. From this program, data was output to the VMS operating system and subsequently transferred to a PC computing environment. The output from the STEX program, or the raw data, is not very meaningful without performing the scaling necessary to convert the recorded values to either g's, inches, or microstrains. The top portion of a raw data file (EQ11XNW2) follows.

```
"seconds                "        Independent Units
 0.00000E+00                       Minimum
 1.57768E+01                       Maximum
EVEN_TABULATED                     Representation
 3.08200E-03                       Resolution
      5120                         Values count
"g                      "        Dependent Units
WORD_TYPE                          Data type
 7.62939E-05                       Scale
 0.00000E+00                       Offset
  1024                             Points per frame
   -32
   -32
   -16
   -32
   -32
   -32
   -32
   -32
   -32
   -32
   -16
   -32
   -48
```

The important items to note in the header of the raw data file, the top eleven lines, are the resolution, or time step, of 0.003082 seconds, the number of values, 5120, the units of the dependent (measured) values, g, and the scale, 7.62939×10^{-5}. This scale is used to convert the values, i.e., -32, -32, -16, -32, -32, etc., to (in this case) acceleration measurements in units of g. While each earthquake data file has 5120 values, or 15.7768 seconds of data, the free vibration data files contain only 4096 values, or 12.6208 seconds of data.

The first test structure, S1, had 36 data channels and five test runs. The second test structure, S2, had 37 data channels and four test runs. Ten channels of data were recorded during a total of ten free vibration tests. All the raw data from the nine earthquake test runs and the ten free vibration tests, 428 data files in total, were converted to engineering units using a popular spreadsheet program. The top portion of a converted data file, (also EQ11XNW2) follows.

```
"EQ 11"
"Accel (g)"
"NW 2nd Floor"
"Time Step ="
     0.003082
"(seconds)"
"End Time ="
      15.7768
"Max Value ="
        0.220


0.000
0.000
0.001
0.000
0.000
0.000
0.000
0.000
0.000
0.000
0.000
0.001
0.000
```

Note that the header of the converted data file, the top twelve lines, contains some of the same information of the raw data file, i.e., the units of the measurement, g, the time step of 0.003082 seconds, and the end time of 15.7768 seconds. Additional information has also been included, namely, the top three lines and the maximum measured value of the history, 0.220g. In addition to scaling the raw data to the proper units, offsets were removed from the data files such that all converted data files begin with approximately zero initial conditions. As a example of this balancing, note that in the *raw* data file above, the starting values are mostly -32. For this channel and test run, 32 was added to all of the 5120 values in the history prior to multiplying by the scale. Note that $(-16+32)*7.62939\text{x}10^{-5}=0.001$ for the third and eleventh values in the history.

The top three lines of each converted data file contain all the information necessary to identify from where and when the data was measured. The same information is also coded into the name of each data file. Both raw and converted data files use the same name, so both names possess the same information. Each file name contains seven or eight characters or numbers in a fixed format. The first two characters, either EQ or FV, designate whether the data was collected during an EarthQuake simulation or during a Free Vibration test. For the earthquake files, the next two numbers indicate the structure number, 1 or 2, and the test number, 1-5 or 1-4. The two numbers together form the test run numbers, 11-15 and 21-24. For the free vibration files, three numbers are used to indicate when the test took place according to the following:

(S1)

101	Prior to Test Run 11
112	Between Test Run 11 and 12
123	Between Test Run 12 and 13
134	Between Test Run 13 and 14
145	Between Test Run 14 and 15
15N	After Test Run 15

(S2)

201	Prior to Test Run 21
223	Between Test Run 22 and 23
234	Between Test Run 23 and 24
24N	After Test Run 24

Note that a free vibration test was not performed between Test Runs 21 and 22.

For the earthquake files, the fifth position of the filename is one of five letters, L, X, T, V, or S. L represents (LVDT) displacement, X represents longitudinal acceleration, T represents transverse acceleration, V represents vertical acceleration, and S represents strain gauge.

For both the earthquake and free vibration files, the last two or three positions of the filename determine the location of the instrument. Most of the letters refer to compass bearings, N, S, W, or E. For S1, the door wall was North and the window wall was South, while for S2, the window wall was North and the door wall was South. For both structures, relative displacements were measured on the West out-of-plane wall and absolute displacements were measured on the East out-of-plane wall. The letter code is as follows:

NW	Door wall of S1 and window wall of S2 (west end)
SW	Window wall of S1 and door wall of S2 (west end)
SE	Window wall of S1 and door wall of S2 (east end)
W	West out-of-plane wall of S1 or S2
E	East out-of-plane wall of S1 or S2
ACH	Earthquake simulator LVDT (achieved motion)
R	LVDT used to measure crack openings of S2 (rocking)
B	Accelerometer mounted on one of the floor beams
D	Accelerometer mounted on one of the floor weights (diaphragm)
TAB	Accelerometer mounted on the earthquake simulator (table)
NWA	Accelerometer mounted on a NW LVDT support arm (S2 only)
ED	Strain gauges on eastern beam of diaphragm (east of other)
WD	Strain gauges on western beam of diaphragm (west of other)

Numbers in the location refer to the vertical position of the instrument:

0	Base (S1 only)
01	Midway between base and 1st level
1	1st level
12	Midway between 1st and 2nd level
2	2nd level

EXCEPT for the LR files. Here LR1 is the left (exterior), first-story, door-wall pier and LR2 is the left-central, first-story, door-wall pier. LR measurements were only made on S2. For the free vibration files, all of the measurements are longitudinal accelerations and the files use the same three digit location codes as the earthquake files.

Several examples of the file naming convention follow.

EQ11XNW2 Earthquake simulation, structure 1, run #1, longitudinal acceleration of door wall at the second level.

EQ12LSW1 Earthquake simulation, structure 1, run #2, displacement measurement of the window wall at the first level.

EQ13XTAB Earthquake simulation, structure 1, run #3, longitudinal acceleration of the simulator platform.

EQ22VD1 Earthquake simulation, structure 2, run #2, vertical acceleration of the first-level diaphragm (floor weight).

EQ23SWD2 Earthquake simulation, structure 2, run #3, strain gauge reading of the western instrumented beam at the second level.

FV201B2 Free vibration test, structure 2, prior to run #1, longitudinal acceleration of the floor beam at the second level.

FV134W01 Free vibration test, structure 1, between runs #3 and #4, longitudinal acceleration of the west out-of-plane wall midway between the base and the first level.

FV15ND2 Free vibration test, structure 1, after run #5, longitudinal acceleration of second-level diaphragm (floor weight).

EQ24LR2 Earthquake simulation, structure 2, run #4, vertical crack opening displacement of the west-central, first-story, door-wall pier.

The raw and converted data files have been stored on a data tape in a QIC-80 format using "Gateway Tape System". The directory structure of the material on the tape is illustrated below. Subdirectory names use the same conventions as filenames.

DATA

RAW

EQ11
EQ12
EQ13
EQ14
EQ15
EQ21
EQ22
EQ23
EQ24
FV101
FV112
FV123
FV134
FV145
FV15N
FV201
FV223
FV234
FV24N

CONV

(same as for RAW)

For completeness, some of the test run subdirectories contain files in addition to those described above. For instance, the subdirectories EQ11-EQ15 contain files with .25, .30, and .45 extensions. These files contain the filtered versions of the records with the same base names. The extension is the cutoff frequency, in Hz, used in the low pass filter. The filtered records contain 4096 data points instead of 5120, due to the use of a Fast Fourier Transform (FFT), and start at time=1.553328 seconds instead of 0.000 seconds. The end time for these filtered records is 14.1741 seconds. Note also that some of the filtered displacement records from the later test runs include residual displacements from previous test runs while the unfiltered records have zero initial conditions.

Subdirectories EQ21-EQ24 also contain some additional displacement files. These files end with a .ABS extension and include residual displacements from previous test runs. The files without the extensions have zero initial conditions.

APPENDIX C

MEASURED RESPONSE HISTORIES

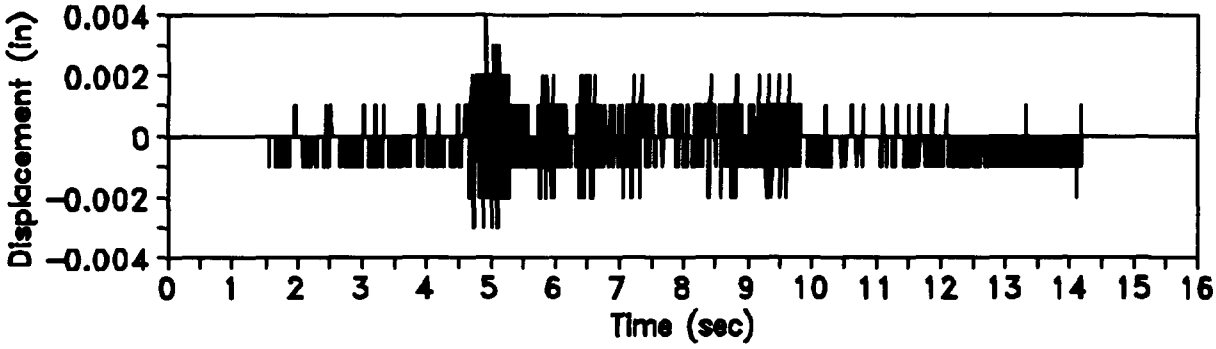

Figure C.1 First-level Door-wall Displacement for Test Run 11

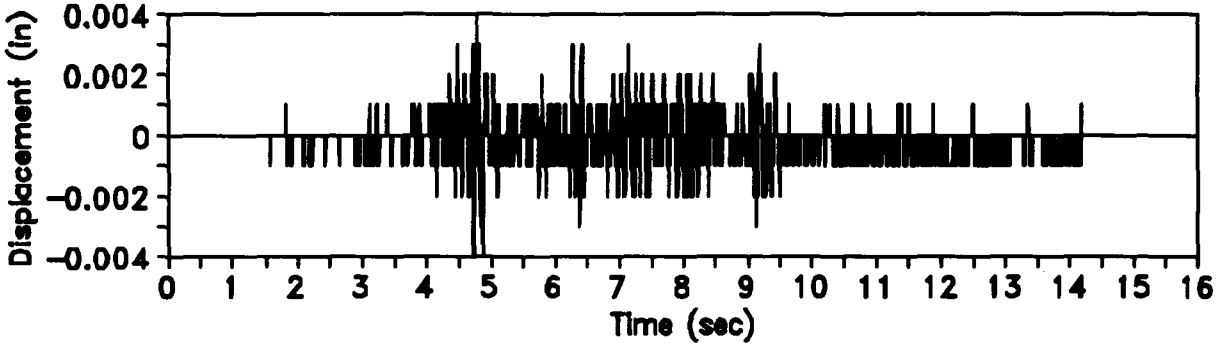

Figure C.2 Second-level Door-wall Displacement for Test Run 11

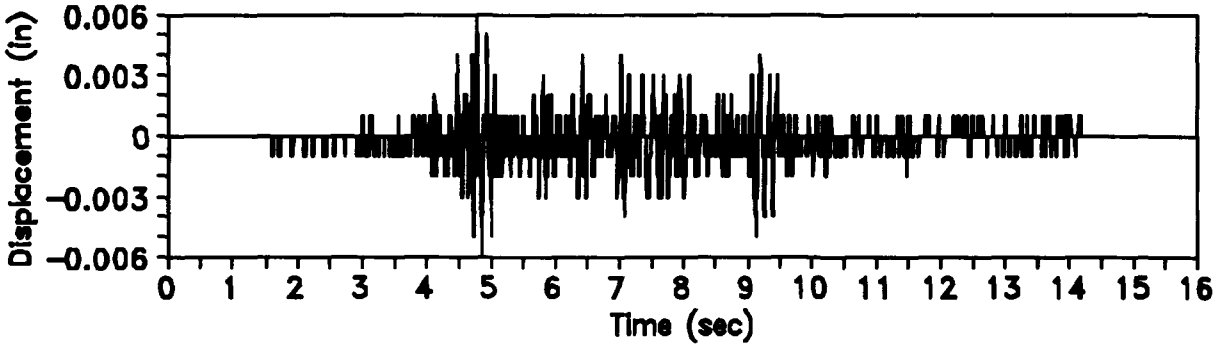

Figure C.3 First-level Window-wall Displacement for Test Run 11

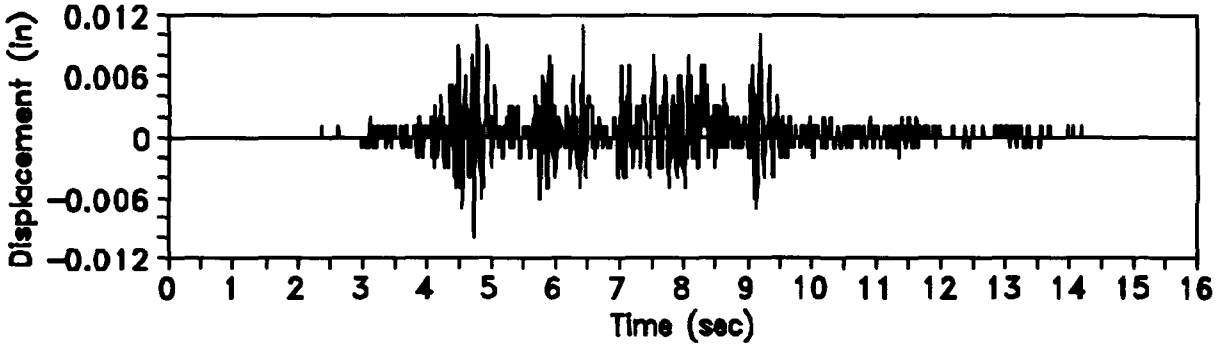

Figure C.4 Second-level Window-wall Displacement for Test Run 11

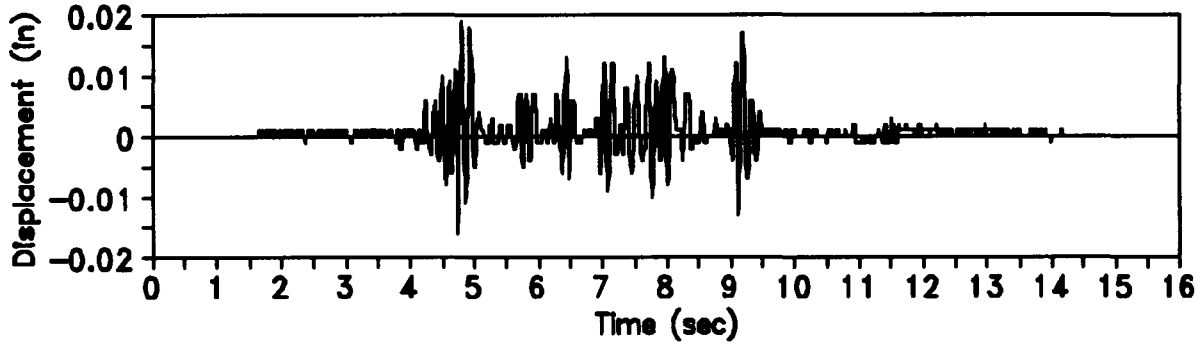

Figure C.5 First-level Diaphragm Displacement for Test Run 11

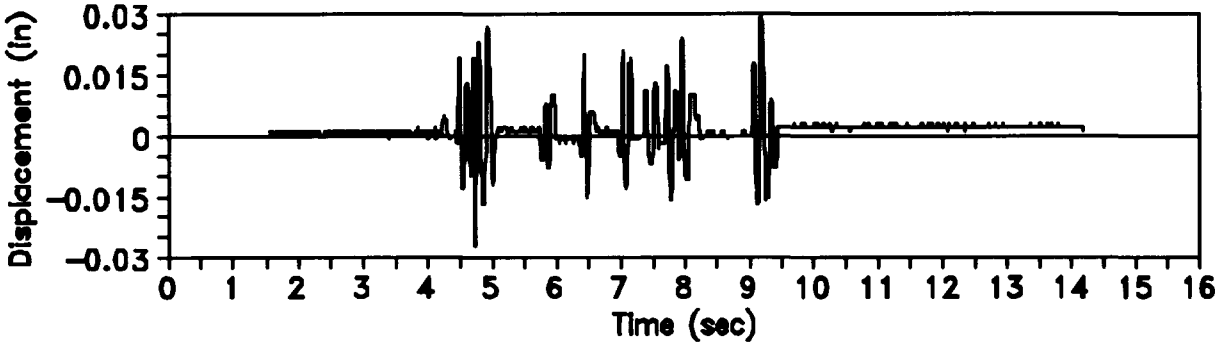

Figure C.6 Second-level Diaphragm Displacement for Test Run 11

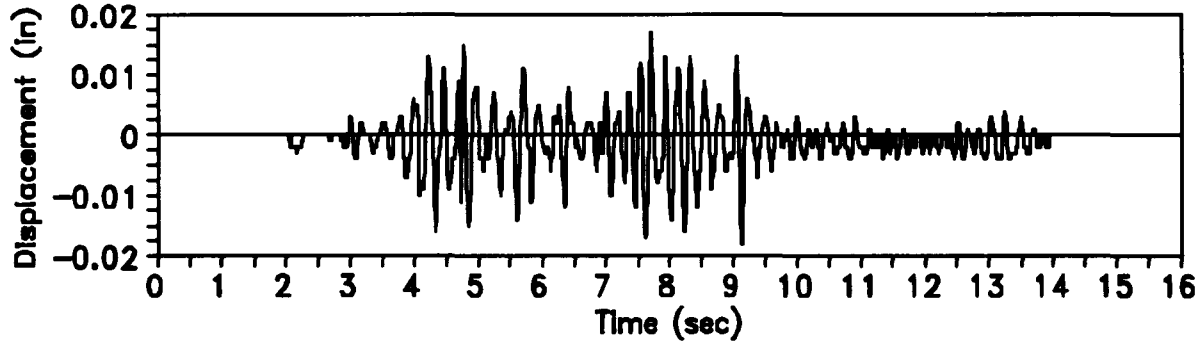

Figure C.7 Absolute Base Displacement for Test Run 11

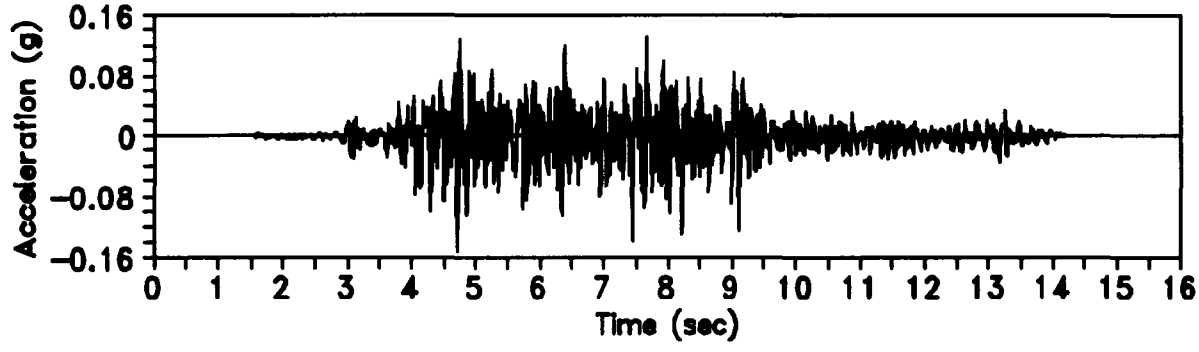

Figure C.8 Base Acceleration for Test Run 11

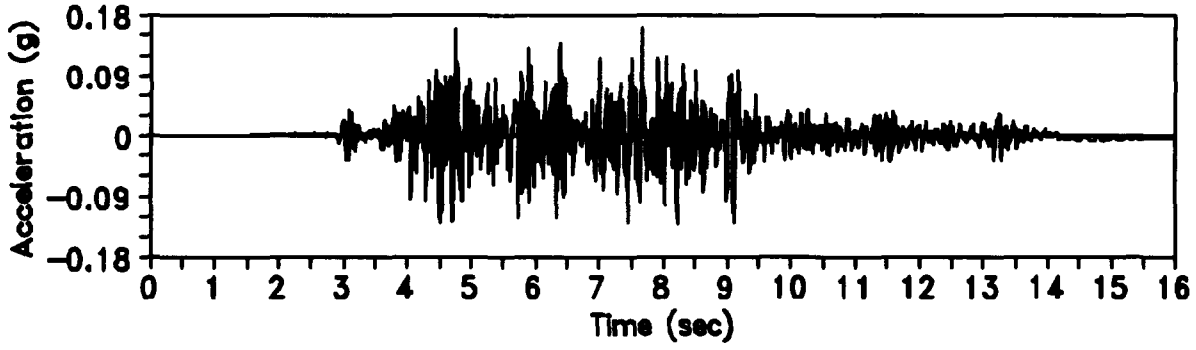

Figure C.9 First-level Door-wall Acceleration for Test Run 11

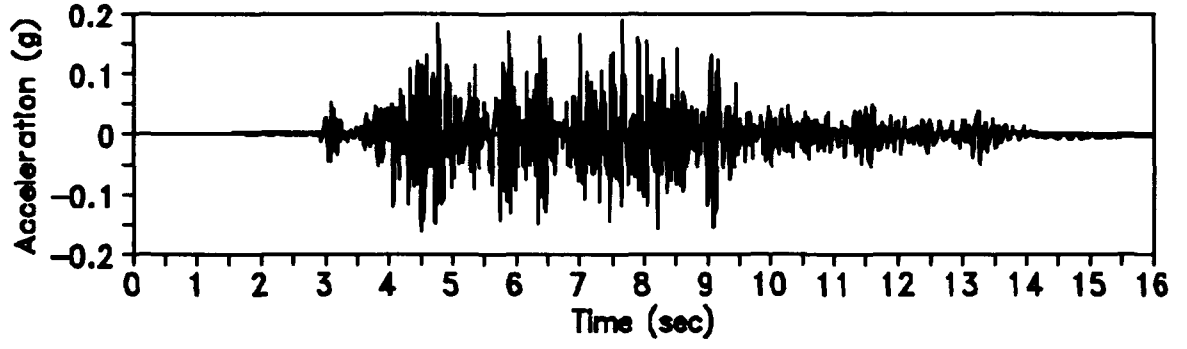

Figure C.10 Second-level Door-wall Acceleration for Test Run 11

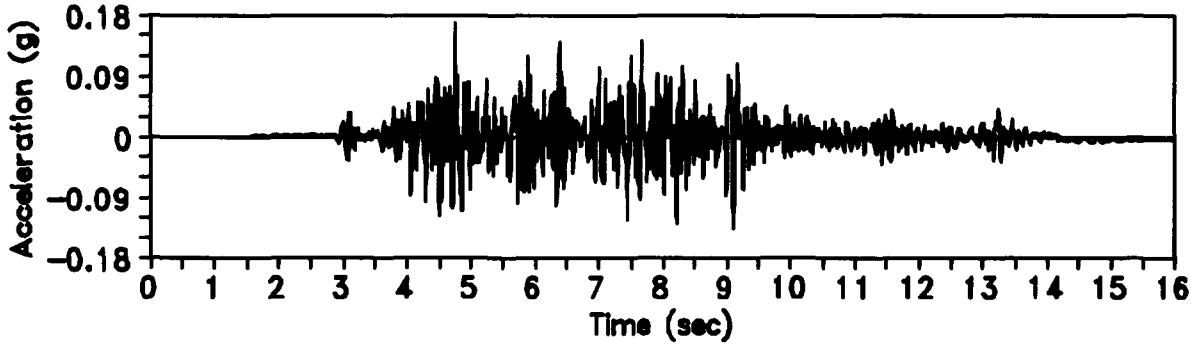

Figure C.11 First-level Window-wall Acceleration for Test Run 11

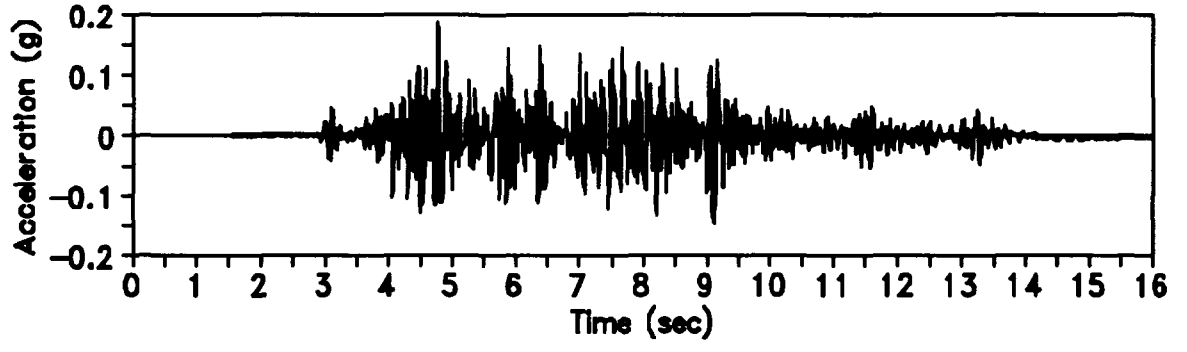

Figure C.12 Second-level Window-wall Acceleration for Test Run 11

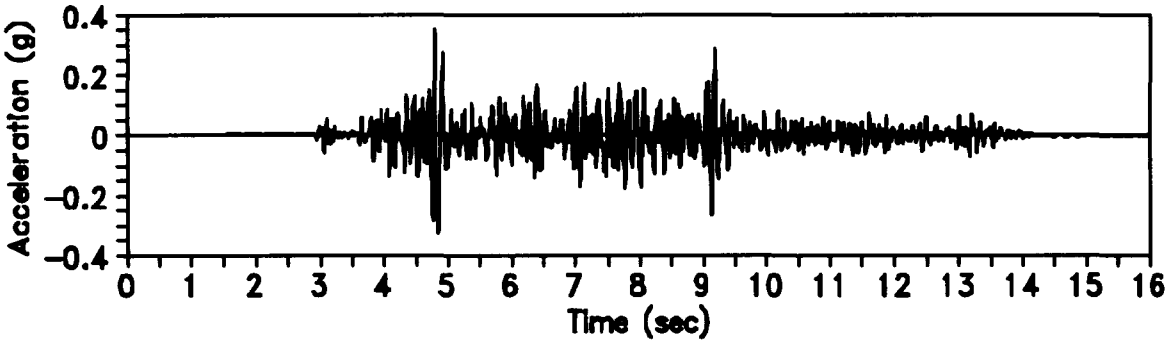

Figure C.13 First-level Diaphragm Acceleration for Test Run 11

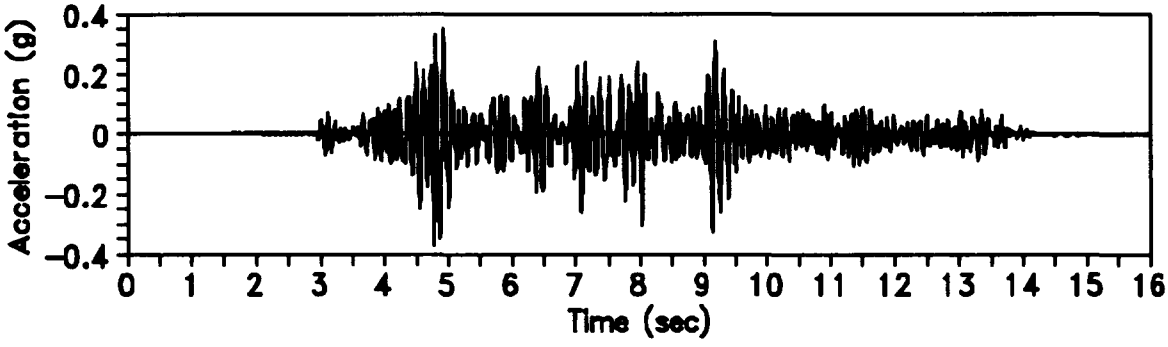

Figure C.14 Second-level Diaphragm Acceleration for Test Run 11

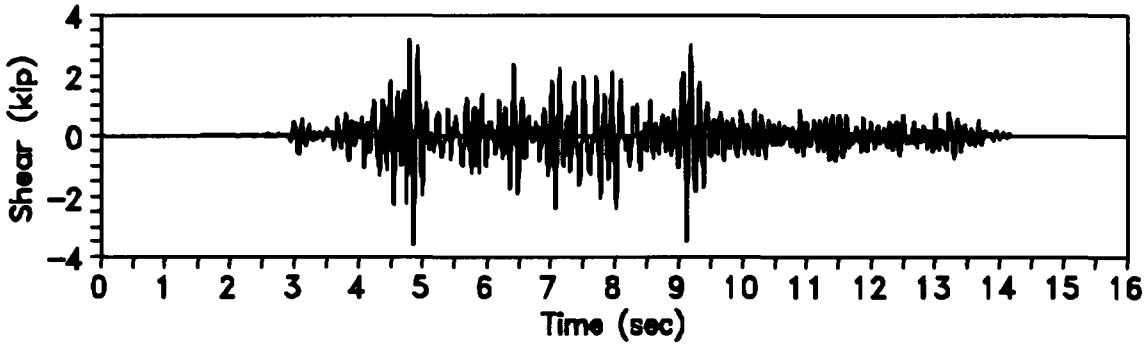

Figure C.15 Base Shear for Test Run 11

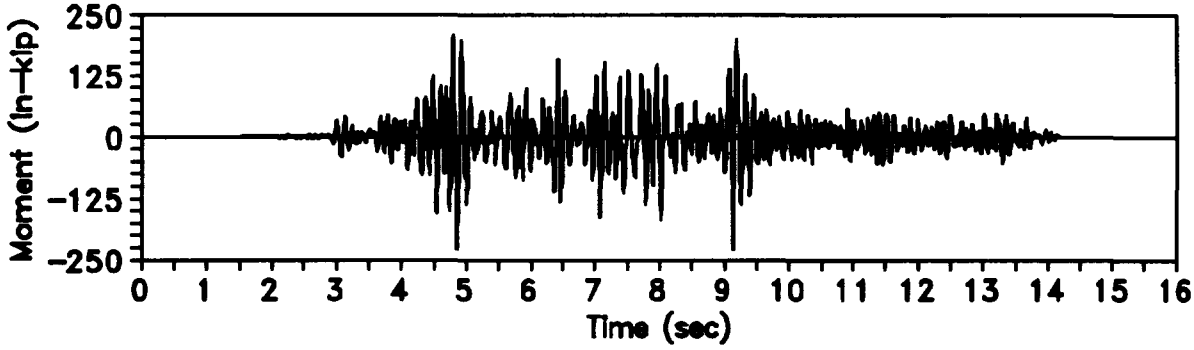

Figure C.16 Base Moment for Test Run 11

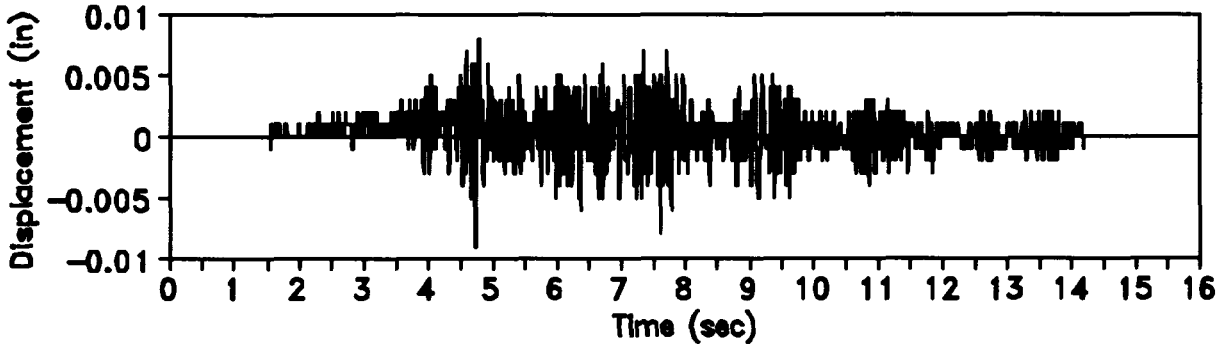

Figure C.17 First-level Door-wall Displacement for Test Run 12

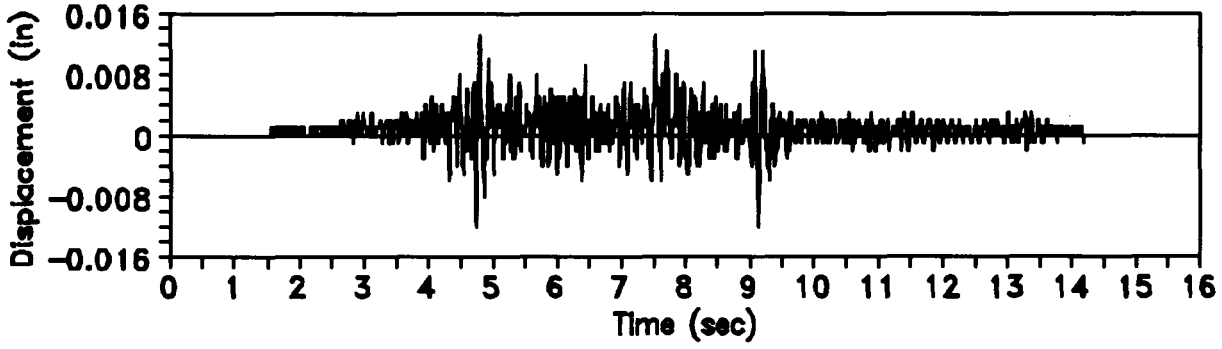

Figure C.18 Second-level Door-wall Displacement for Test Run 12

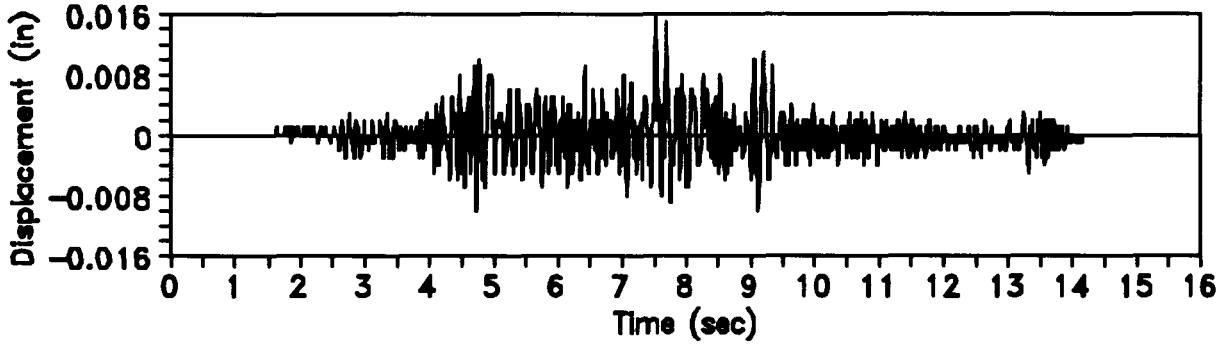

Figure C.19 First-level Window-wall Displacement for Test Run 12

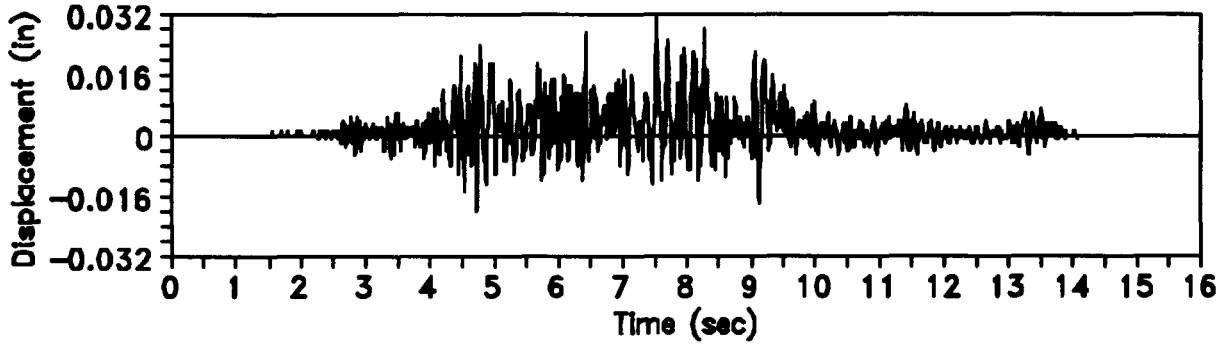

Figure C.20 Second-level Window-wall Displacement for Test Run 12

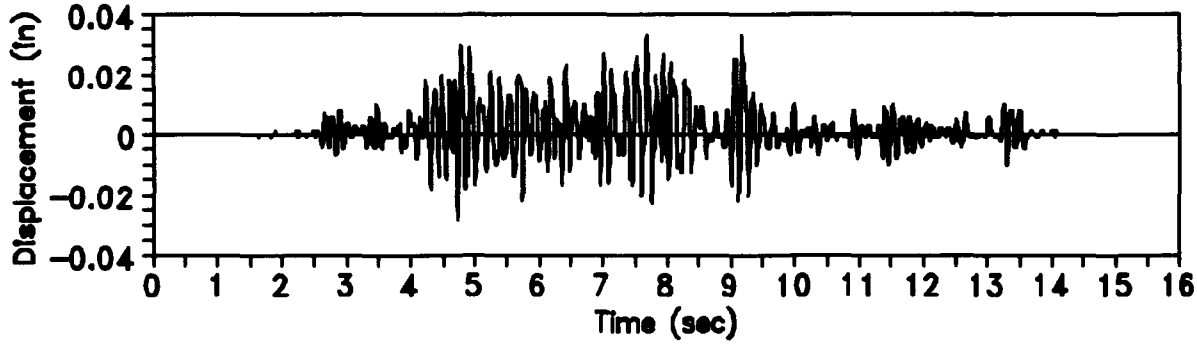

Figure C.21 First-level Diaphragm Displacement for Test Run 12

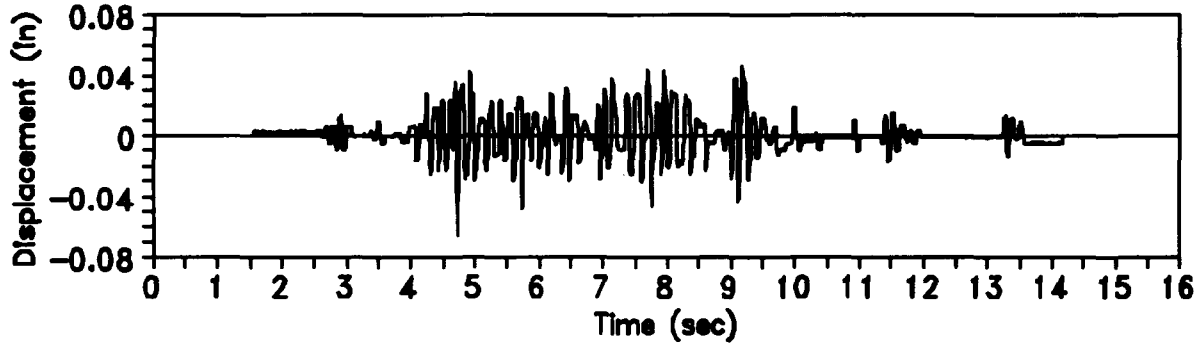

Figure C.22 Second-level Diaphragm Displacement for Test Run 12

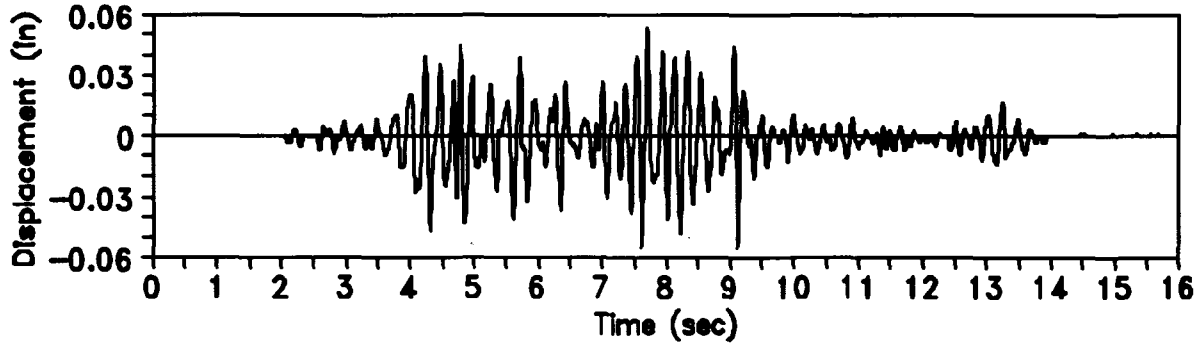

Figure C.23 Absolute Base Displacement for Test Run 12

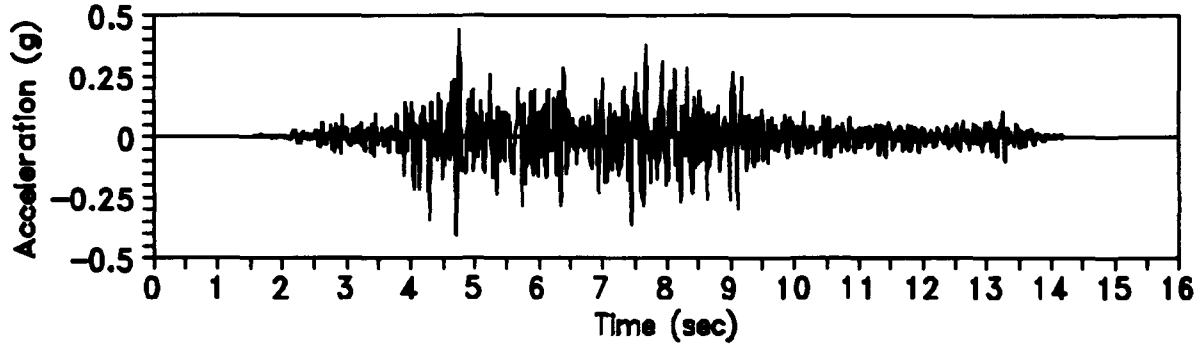

Figure C.24 Base Acceleration for Test Run 12

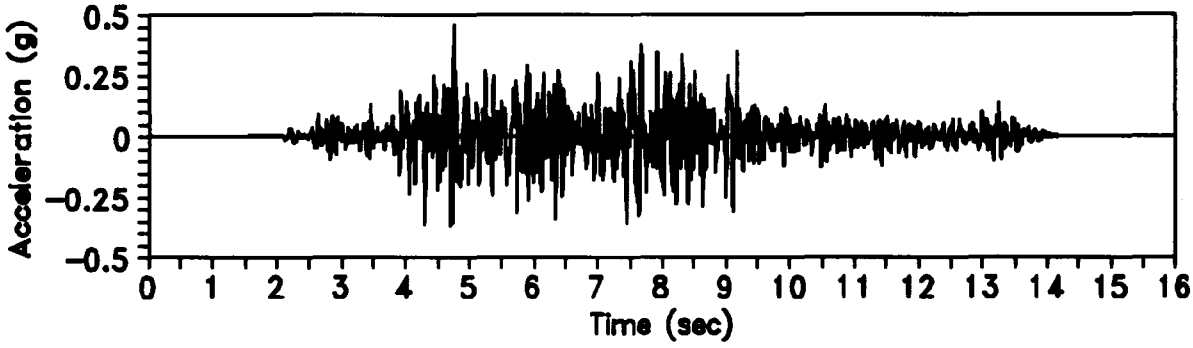

Figure C.25 First-level Door-wall Acceleration for Test Run 12

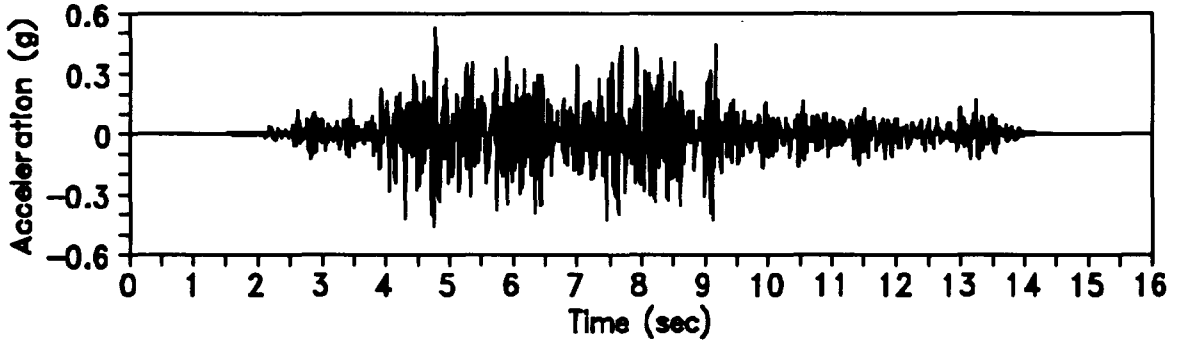

Figure C.26 Second-level Door-wall Acceleration for Test Run 12

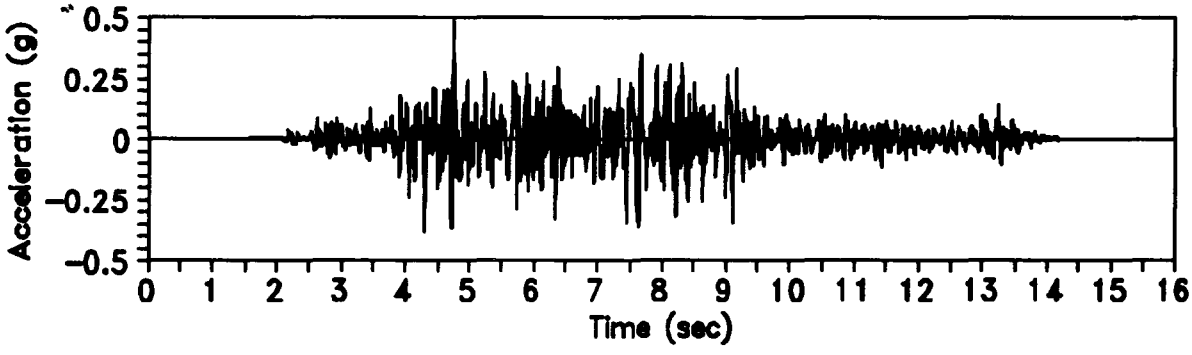

Figure C.27 First-level Window-wall Acceleration for Test Run 12

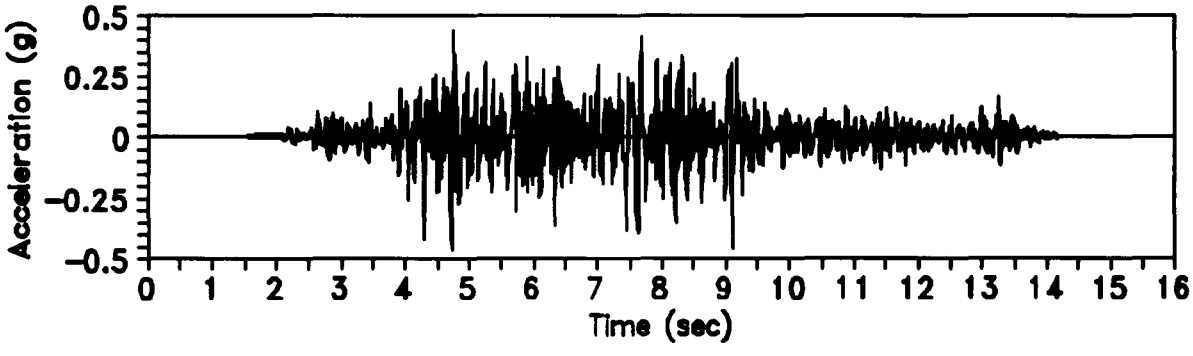

Figure C.28 Second-level Window-wall Acceleration for Test Run 12

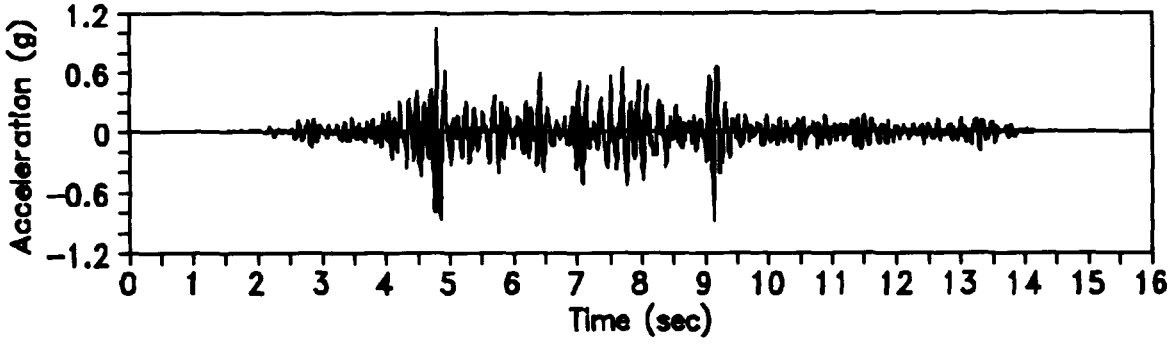

Figure C.29 First-level Diaphragm Acceleration for Test Run 12

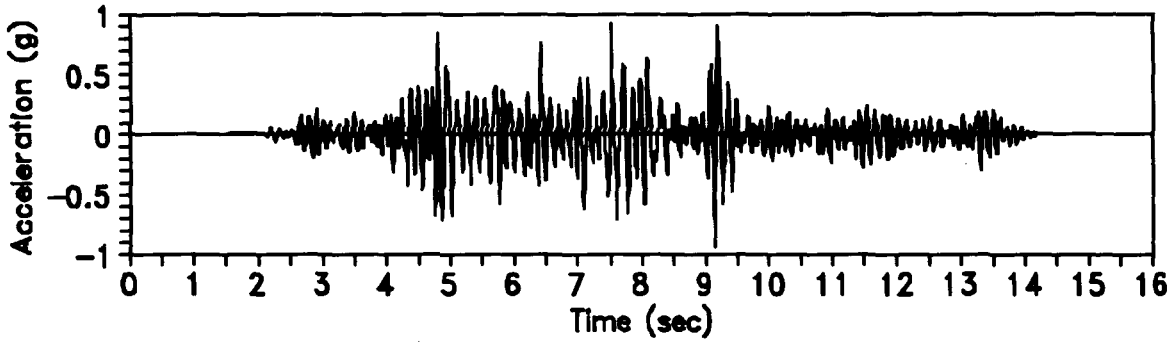

Figure C.30 Second-level Diaphragm Acceleration for Test Run 12

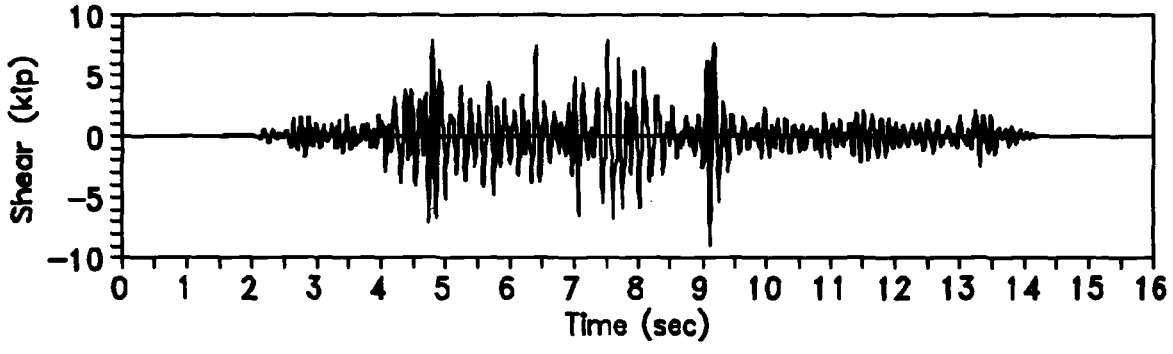

Figure C.31 Base Shear for Test Run 12

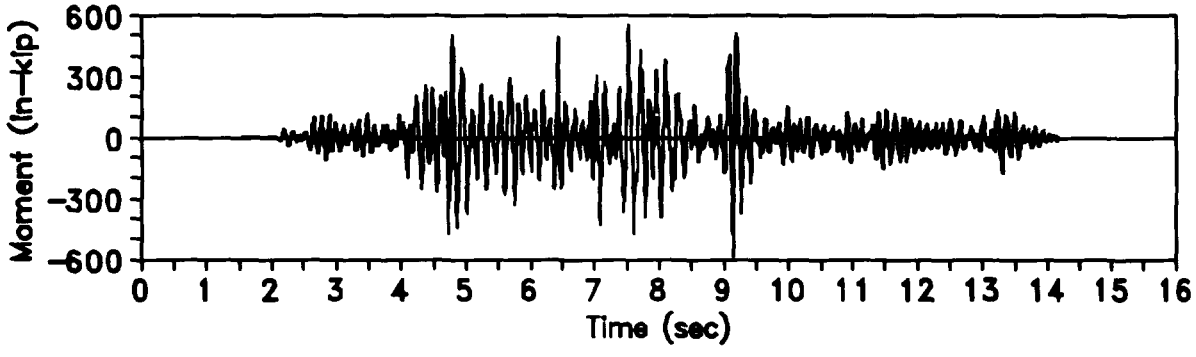

Figure C.32 Base Moment for Test Run 12

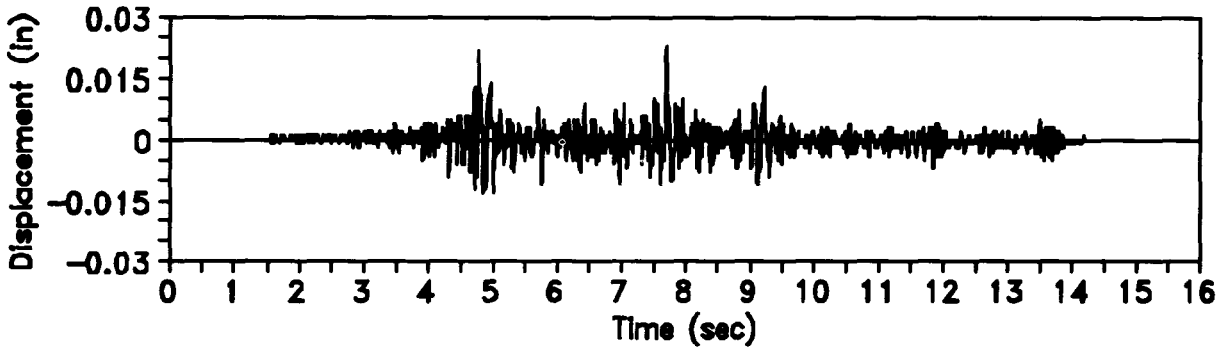

Figure C.33 First-level Door-wall Displacement for Test Run 13

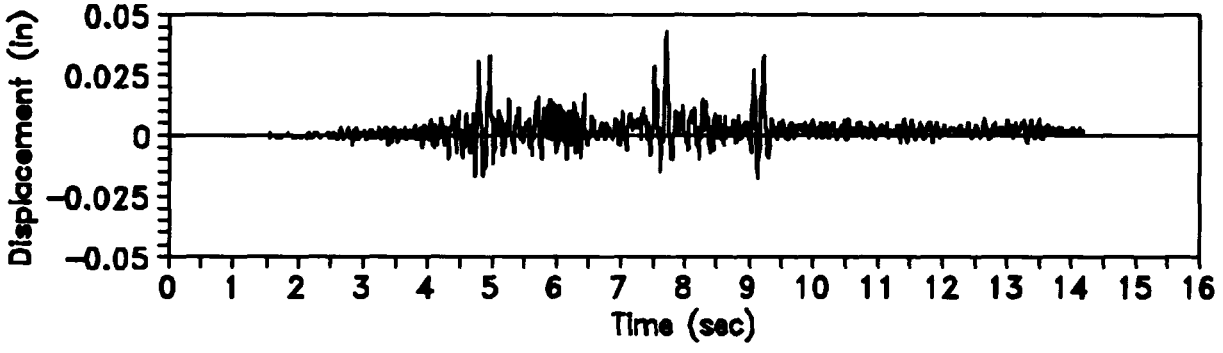

Figure C.34 Second-level Door-wall Displacement for Test Run 13

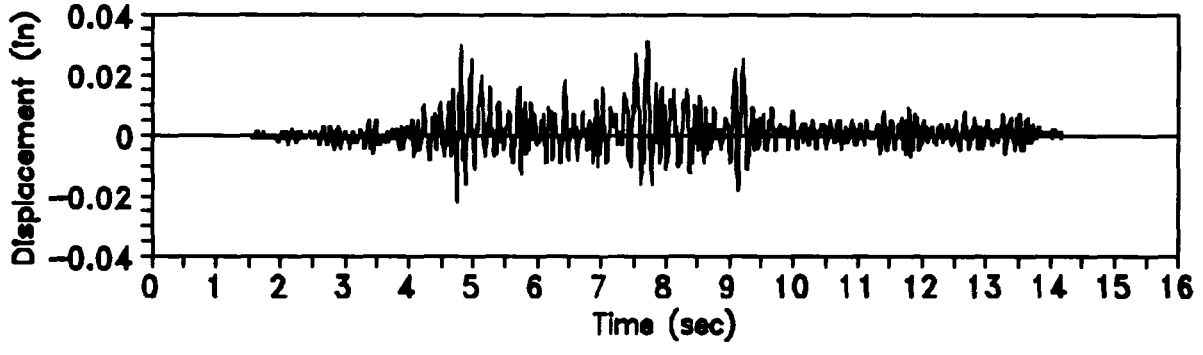

Figure C.35 First-level Window-wall Displacement for Test Run 13

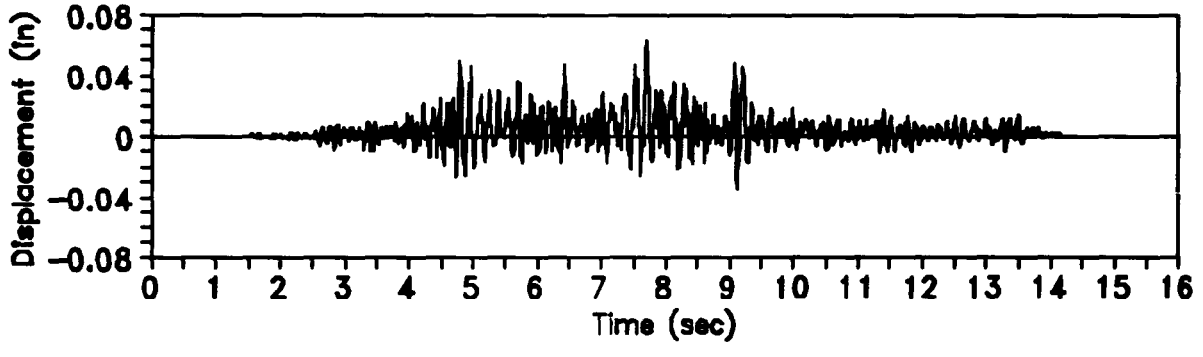

Figure C.36 Second-level Window-wall Displacement for Test Run 13

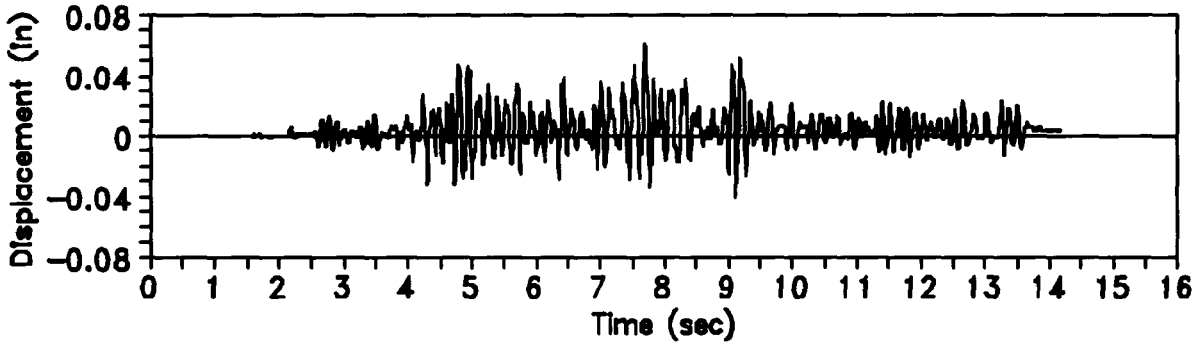

Figure C.37 First-level Diaphragm Displacement for Test Run 13

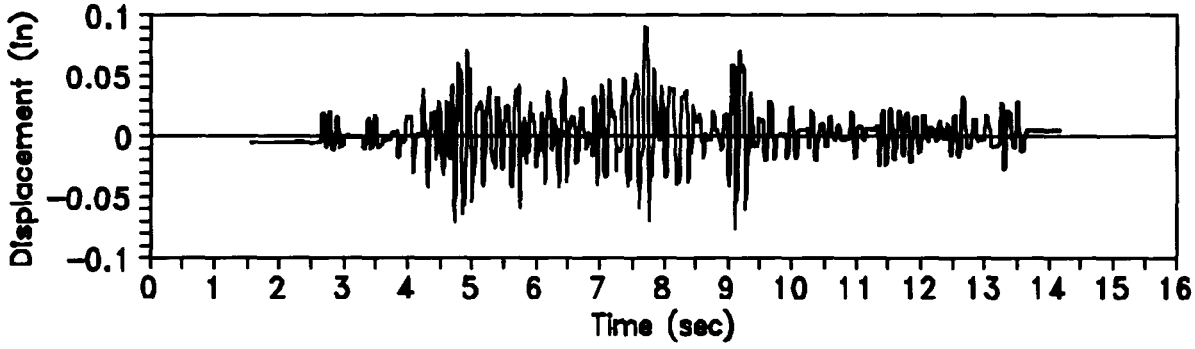

Figure C.38 Second-level Diaphragm Displacement for Test Run 13

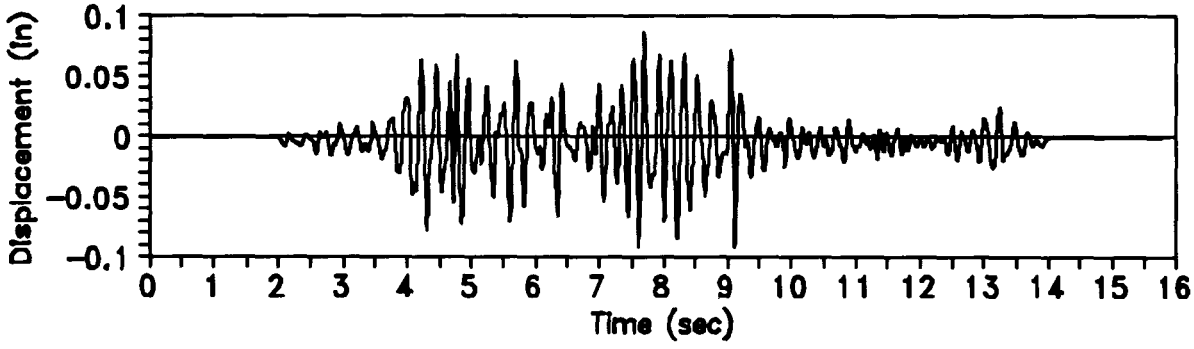

Figure C.39 Absolute Base Displacement for Test Run 13

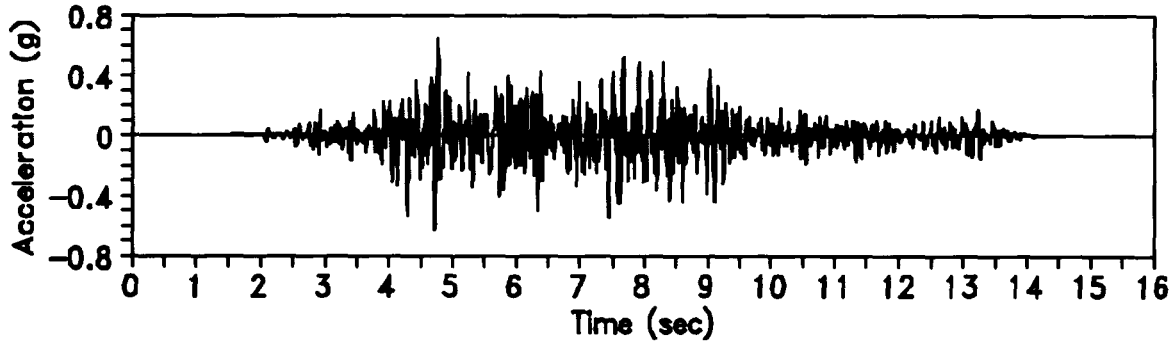

Figure C.40 Base Acceleration for Test Run 13

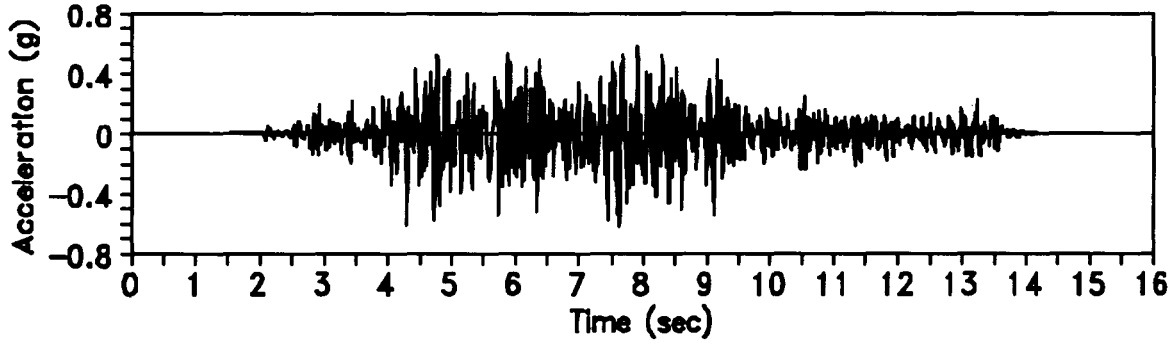

Figure C.41 First-level Door-wall Acceleration for Test Run 13

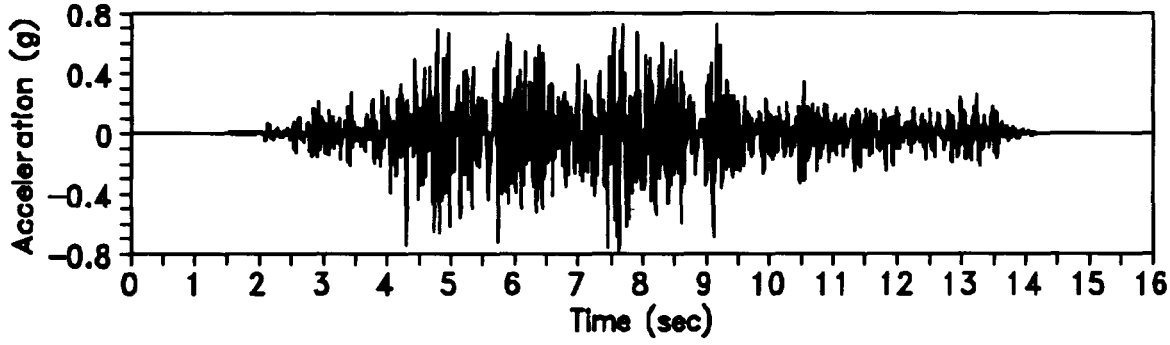

Figure C.42 Second-level Door-wall Acceleration for Test Run 13

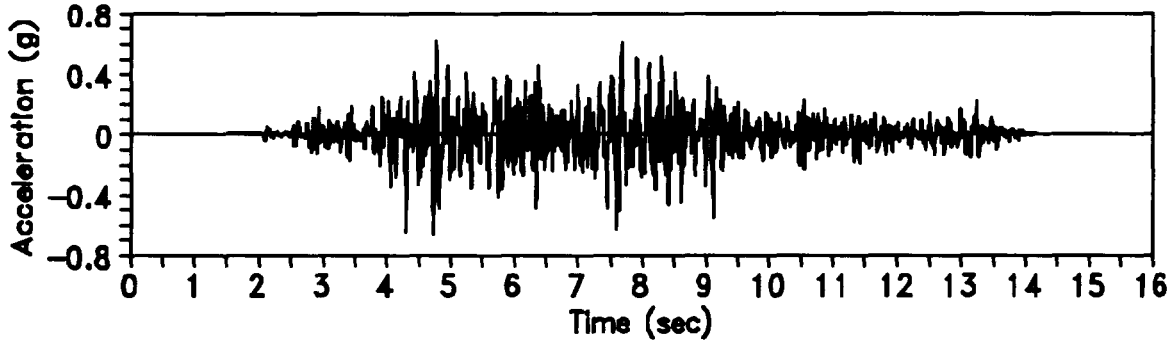

Figure C.43 First-level Window-wall Acceleration for Test Run 13

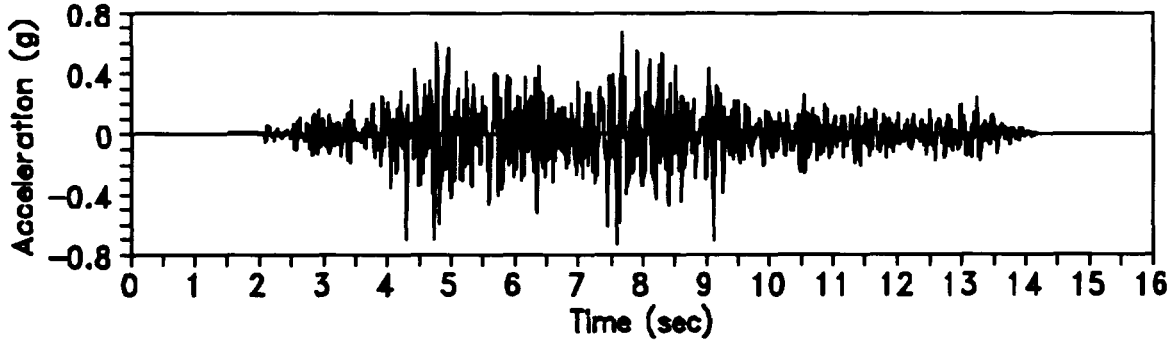

Figure C.44 Second-level Window-wall Acceleration for Test Run 13

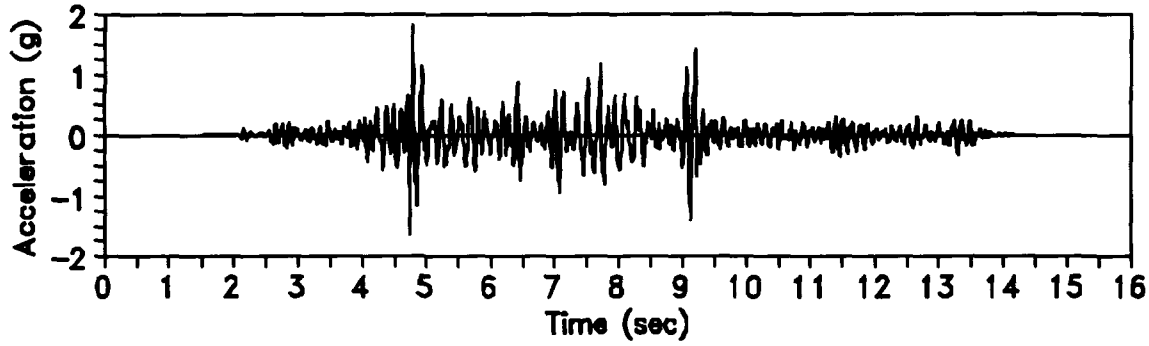

Figure C.45 First-level Diaphragm Acceleration for Test Run 13

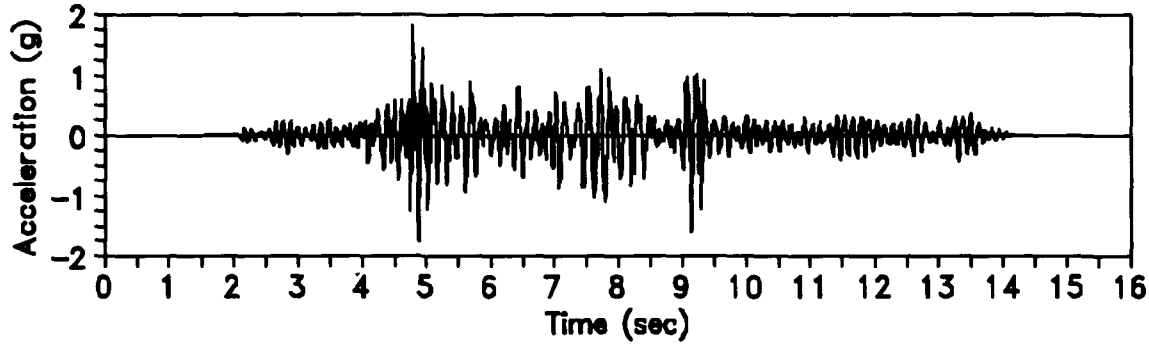

Figure C.46 Second-level Diaphragm Acceleration for Test Run 13

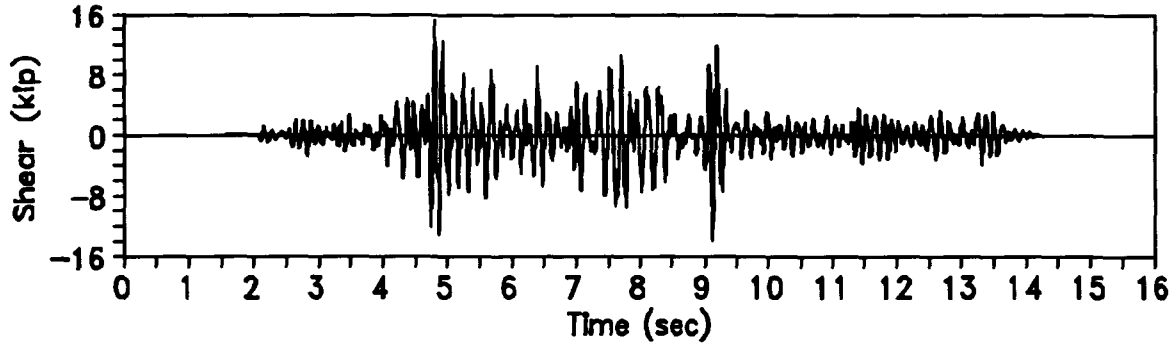

Figure C.47 Base Shear for Test Run 13

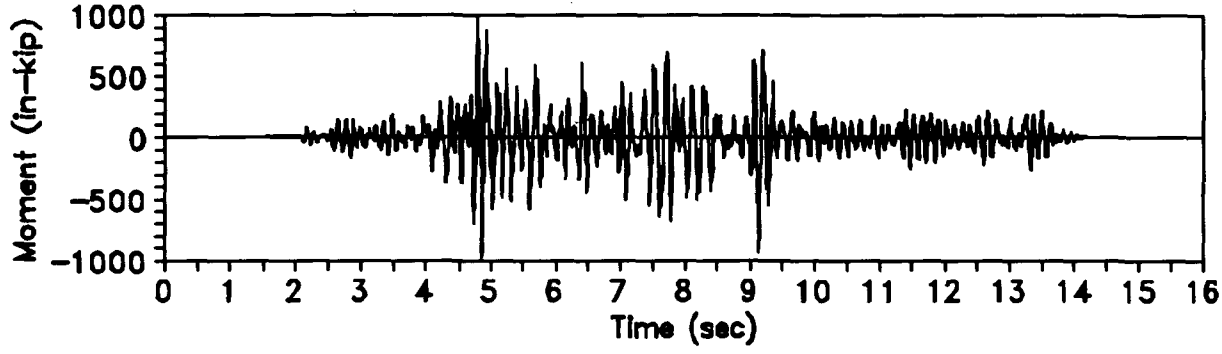

Figure C.48 Base Moment for Test Run 13

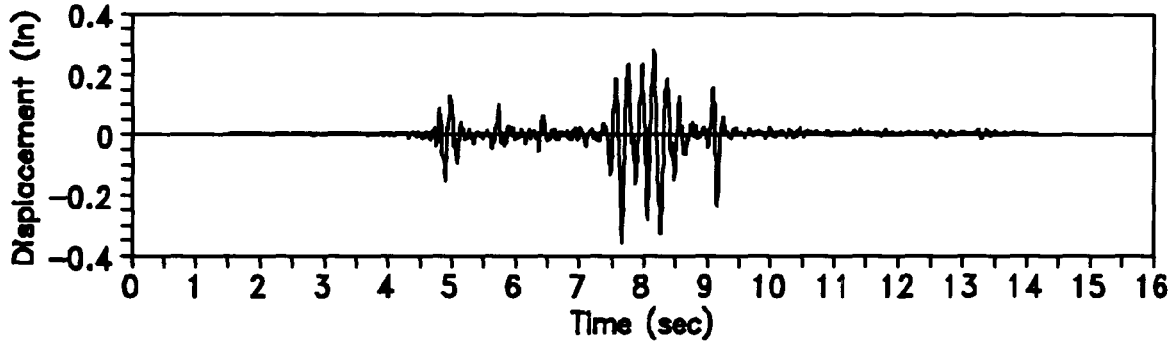

Figure C.49 First-level Door-wall Displacement for Test Run 14

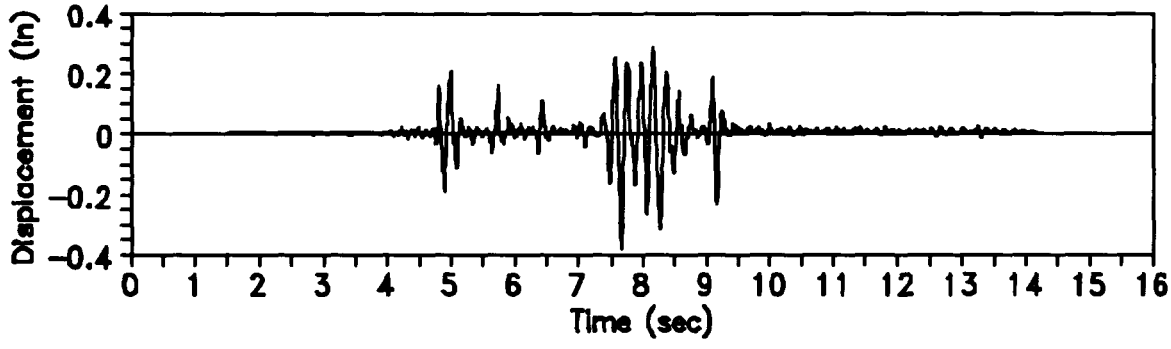

Figure C.50 Second-level Door-wall Displacement for Test Run 14

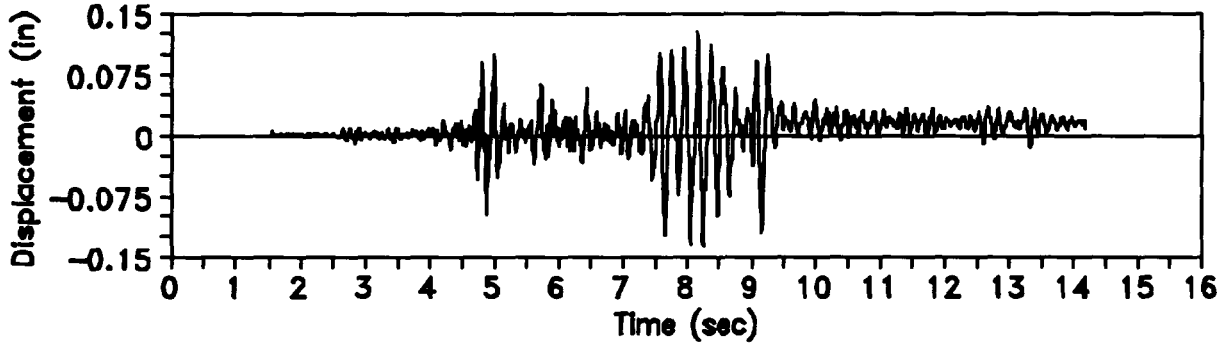

Figure C.51 First-level Window-wall Displacement for Test Run 14

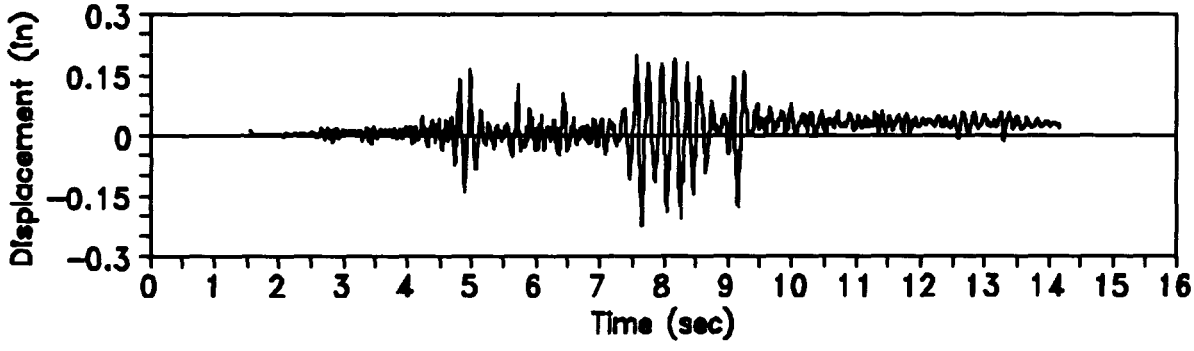

Figure C.52 Second-level Window-wall Displacement for Test Run 14

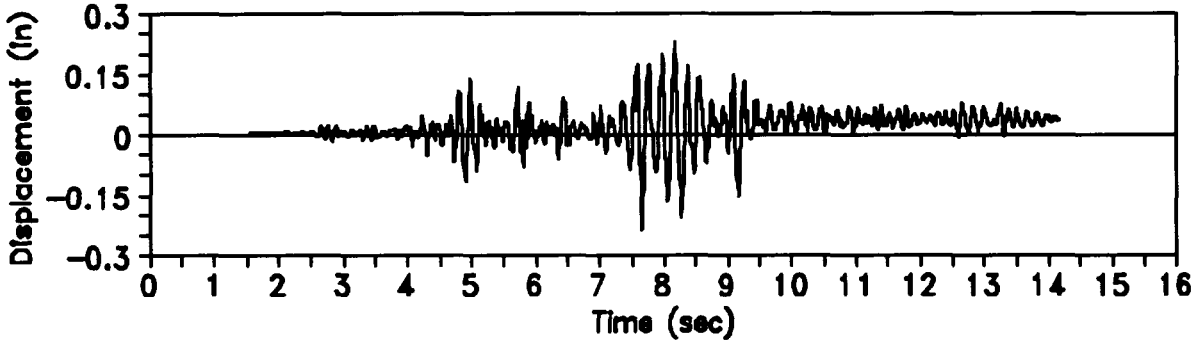

Figure C.53 First-level Diaphragm Displacement for Test Run 14

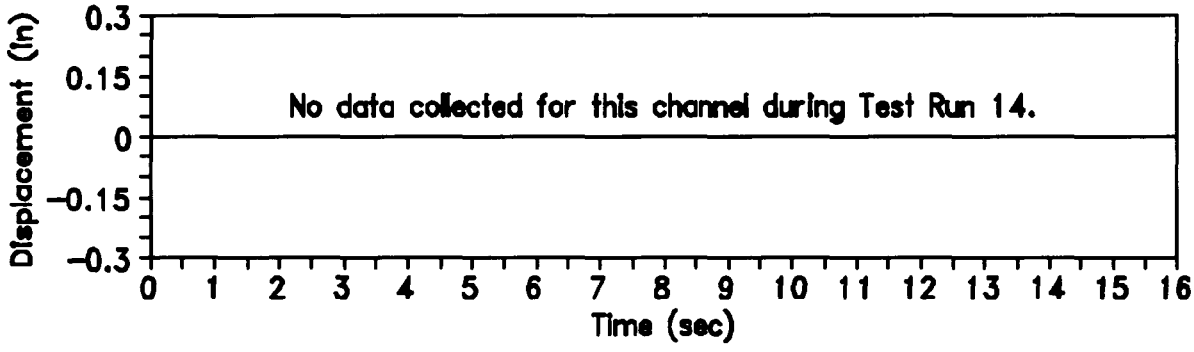

Figure C.54 Second-level Diaphragm Displacement for Test Run 14

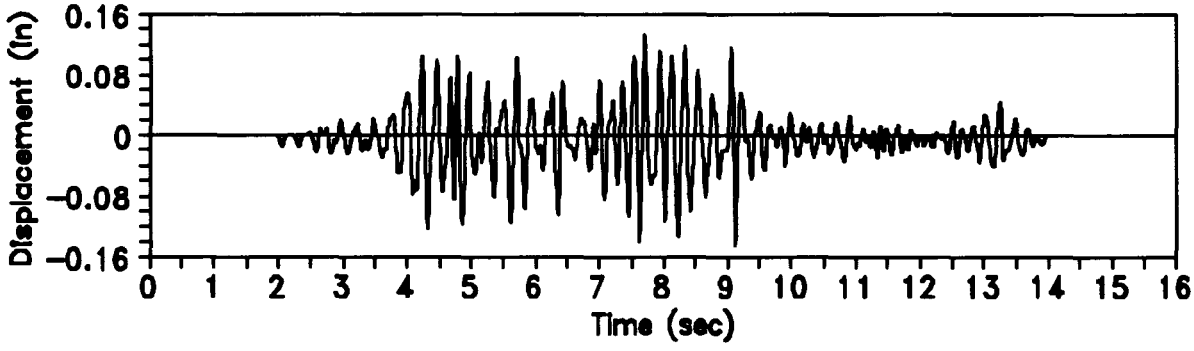

Figure C.55 Absolute Base Displacement for Test Run 14

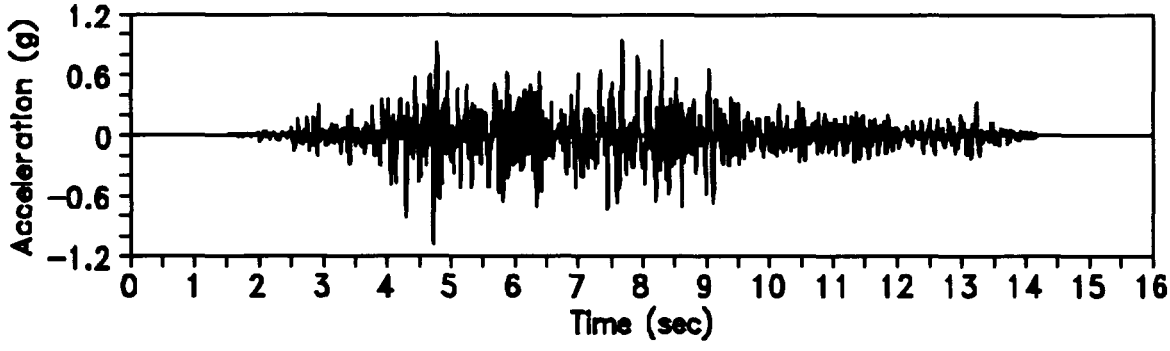

Figure C.56 Base Acceleration for Test Run 14

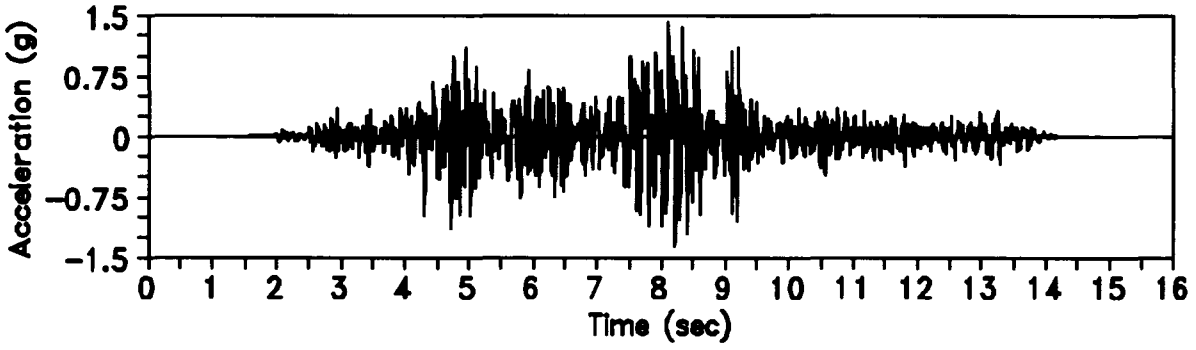

Figure C.57 First-level Door-wall Acceleration for Test Run 14

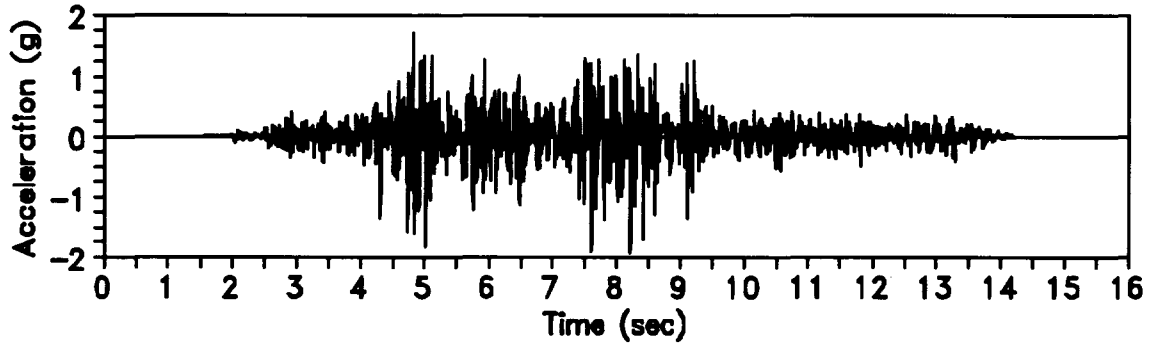

Figure C.58 Second-level Door-wall Acceleration for Test Run 14

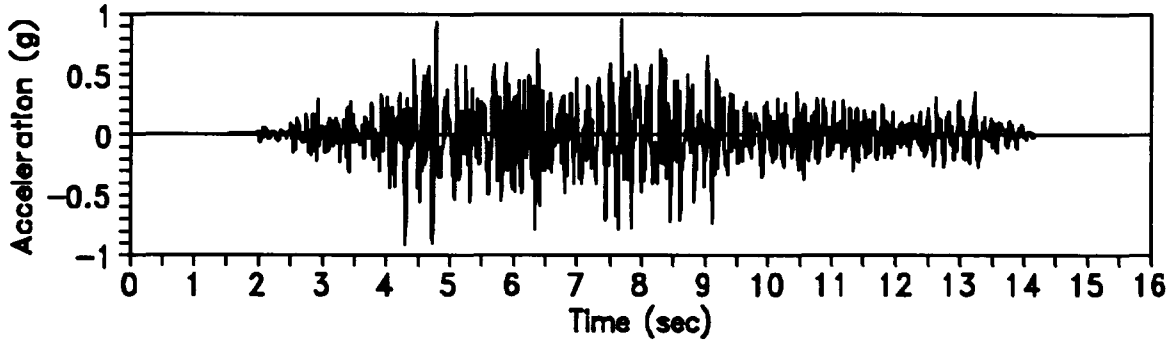

Figure C.59 First-level Window-wall Acceleration for Test Run 14

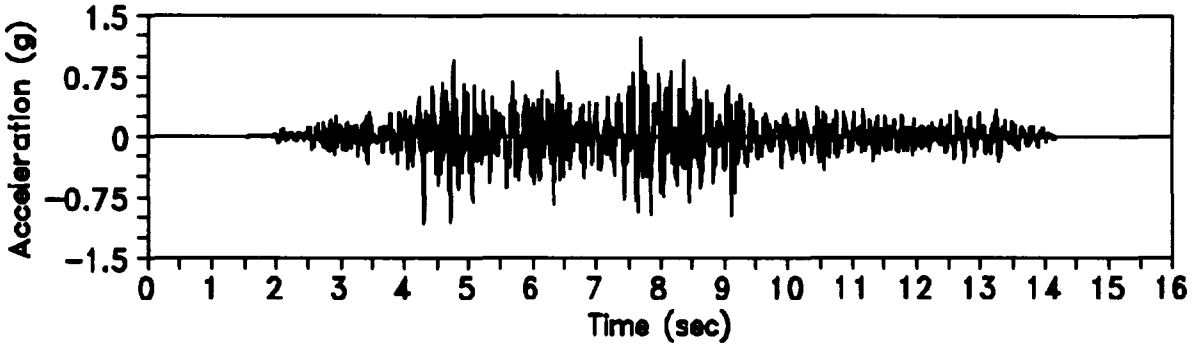

Figure C.60 Second-level Window-wall Acceleration for Test Run 14

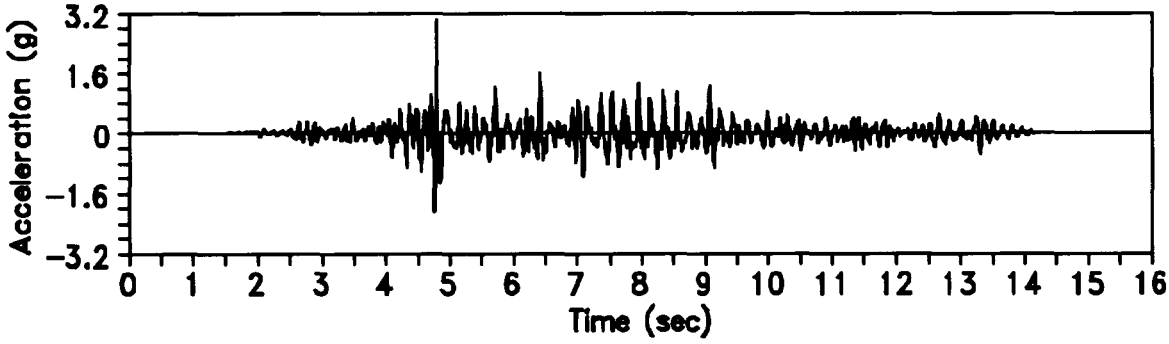

Figure C.61 First-level Diaphragm Acceleration for Test Run 14

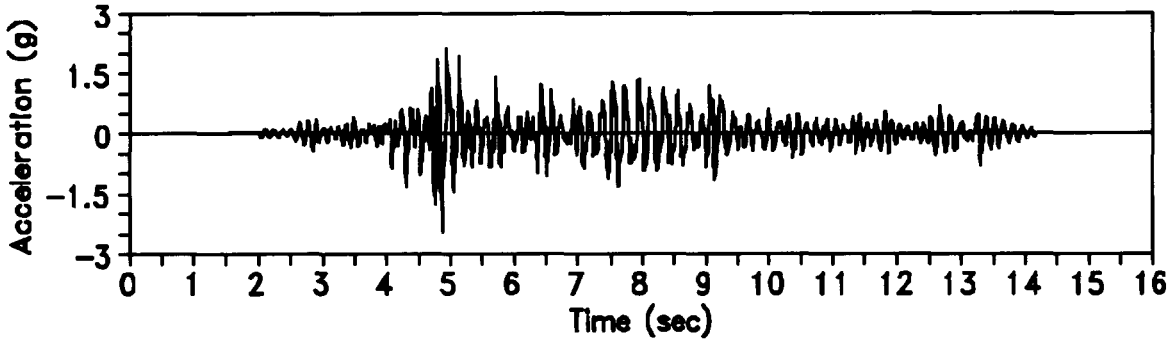

Figure C.62 Second-level Diaphragm Acceleration for Test Run 14

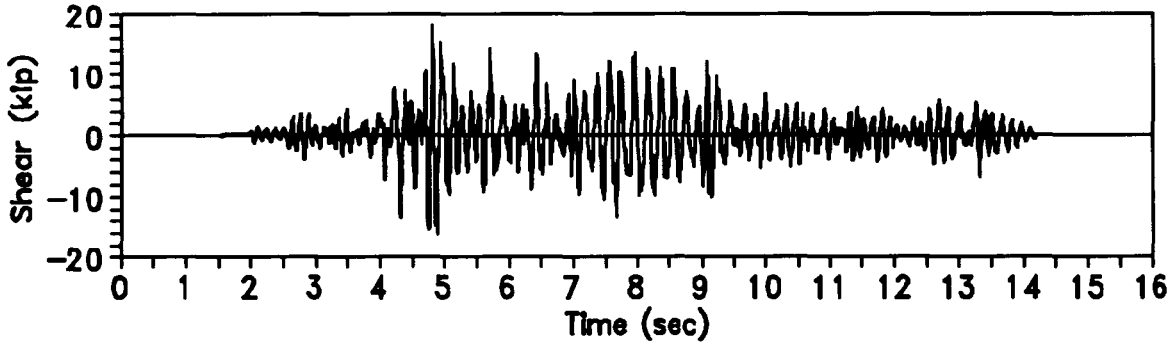

Figure C.63 Base Shear for Test Run 14

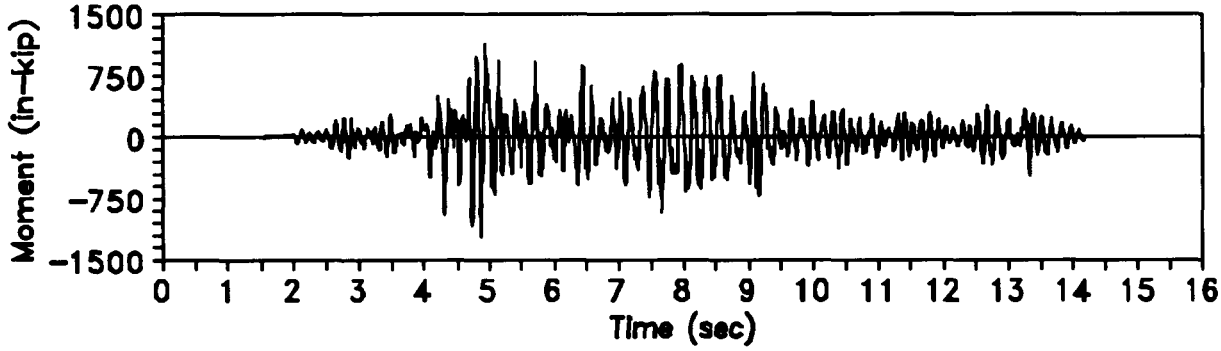

Figure C.64 Base Moment for Test Run 14

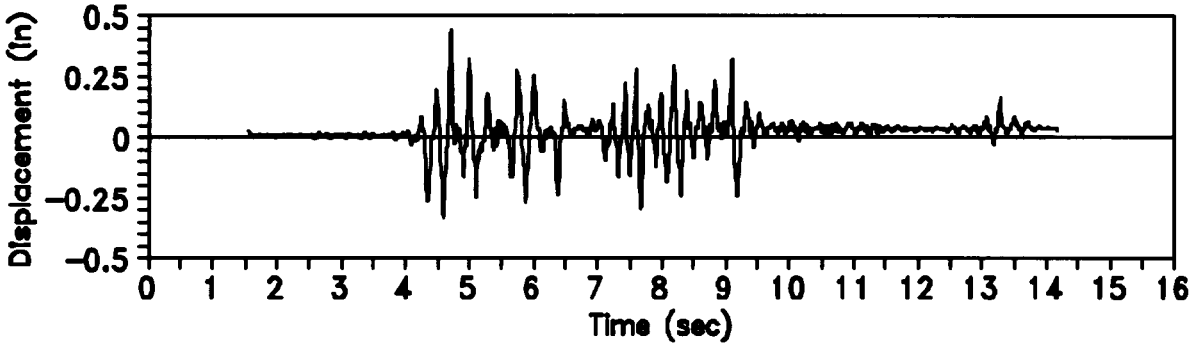

Figure C.65 First-level Door-wall Displacement for Test Run 15

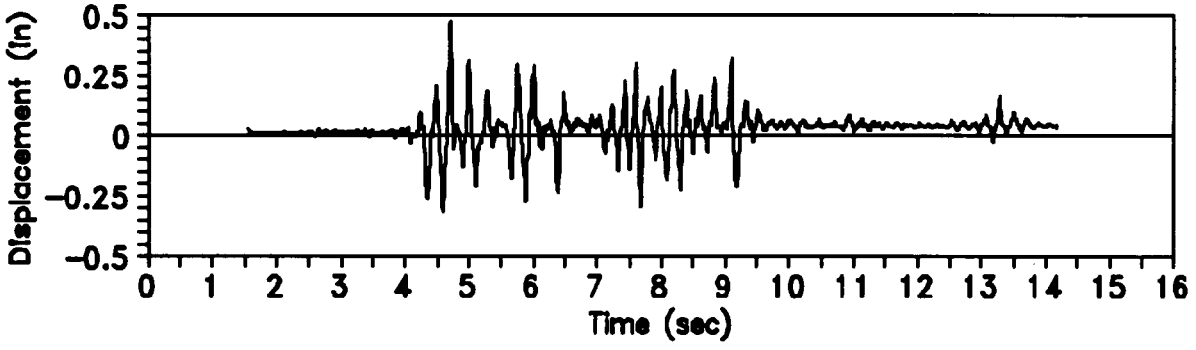

Figure C.66 Second-level Door-wall Displacement for Test Run 15

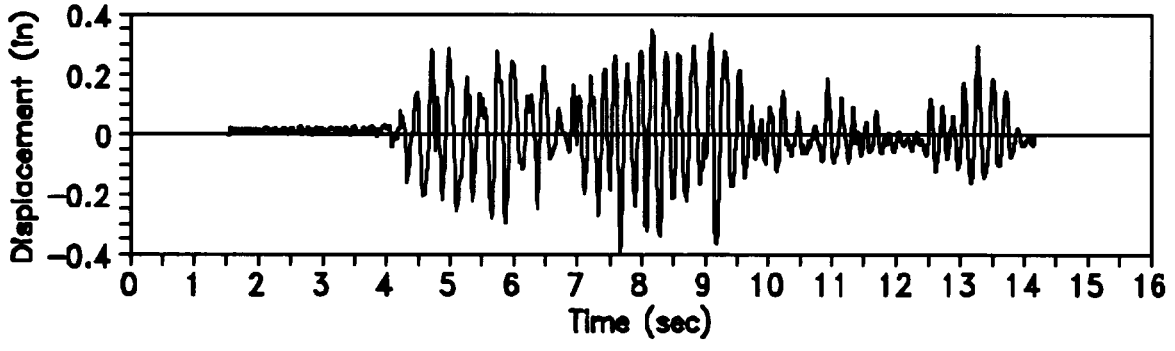

Figure C.67 First-level Window-wall Displacement for Test Run 15

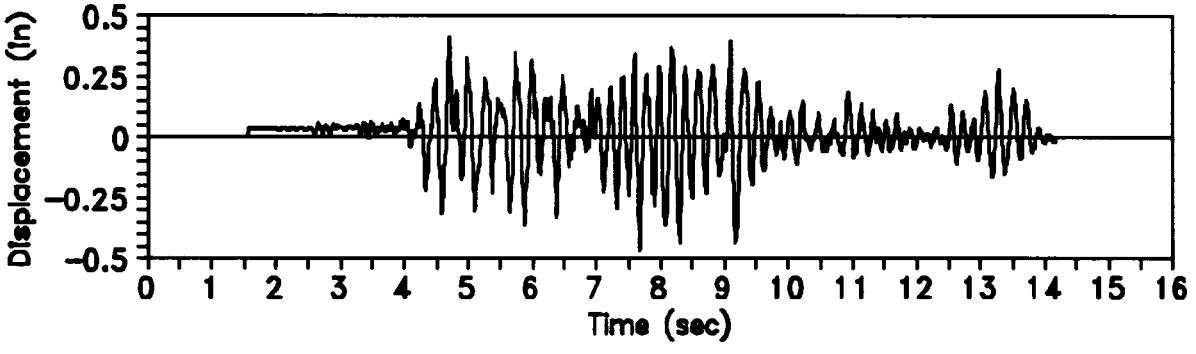

Figure C.68 Second-level Window-wall Displacement for Test Run 15

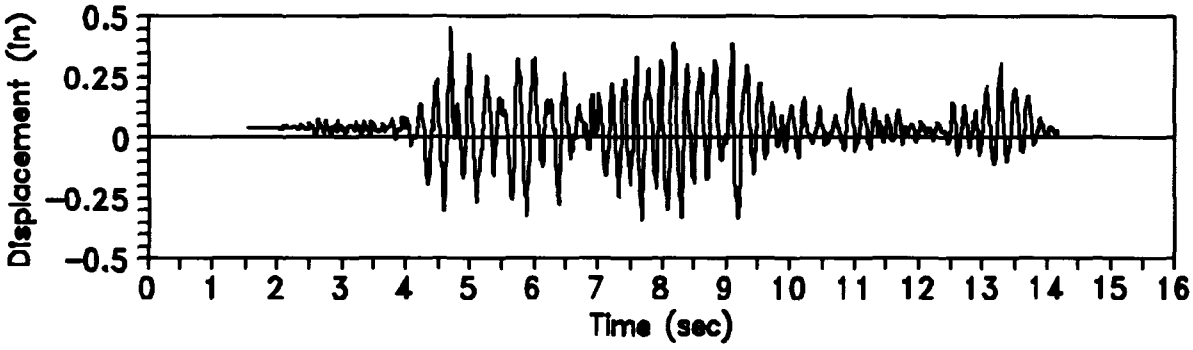

Figure C.69 First-level Diaphragm Displacement for Test Run 15

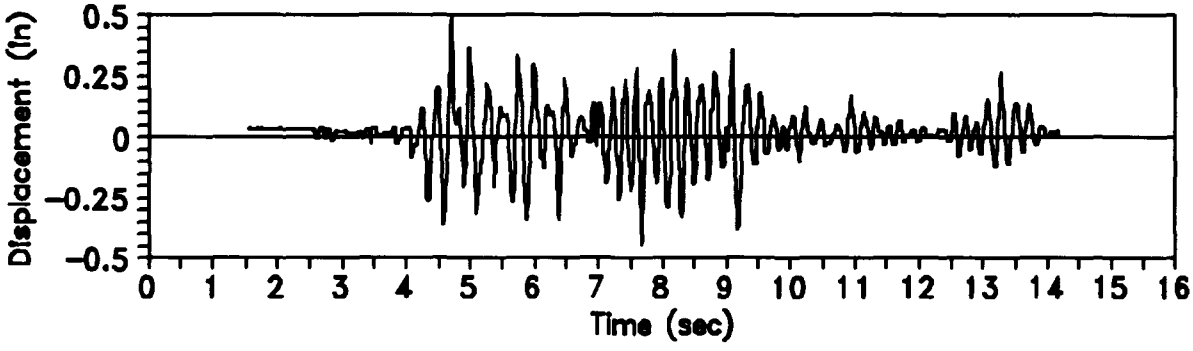

Figure C.70 Second-level Diaphragm Displacement for Test Run 15

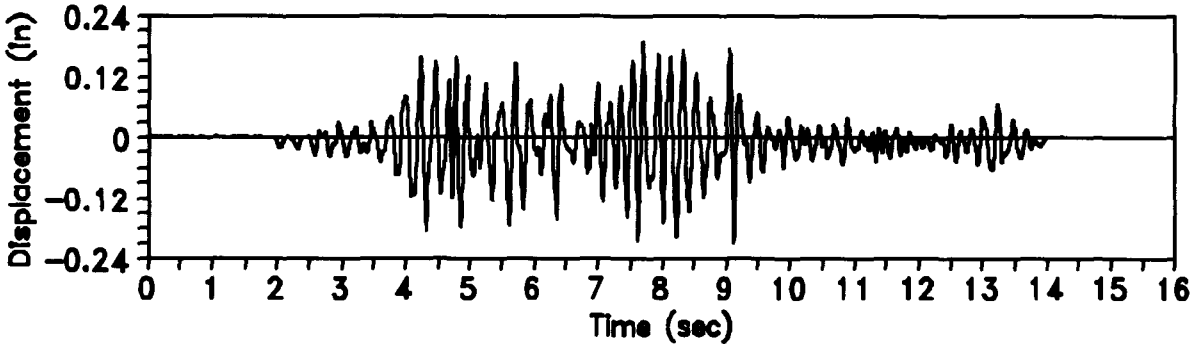

Figure C.71 Absolute Base Displacement for Test Run 15

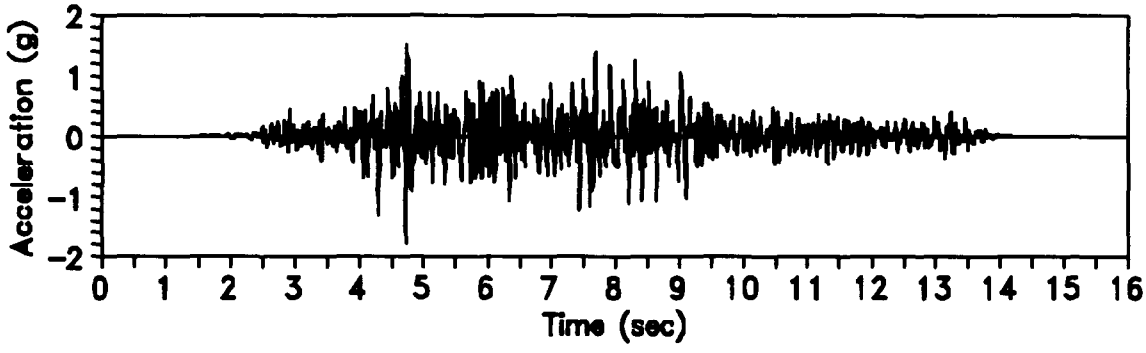

Figure C.72 Base Acceleration for Test Run 15

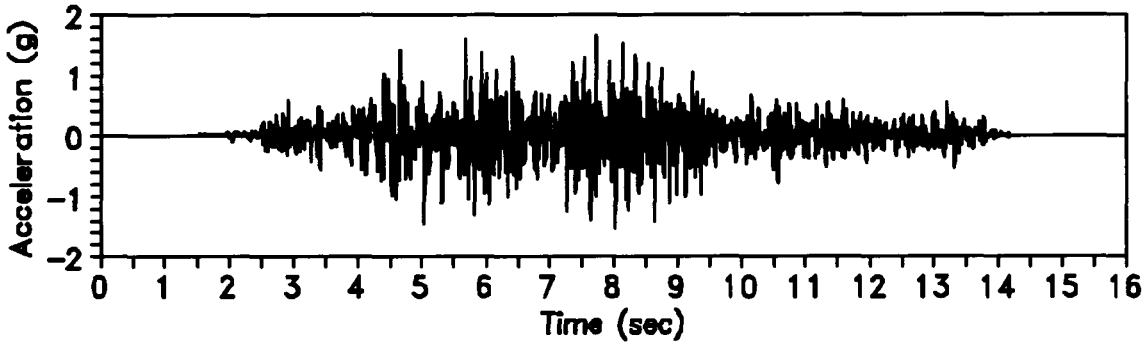

Figure C.73 First-level Door-wall Acceleration for Test Run 15

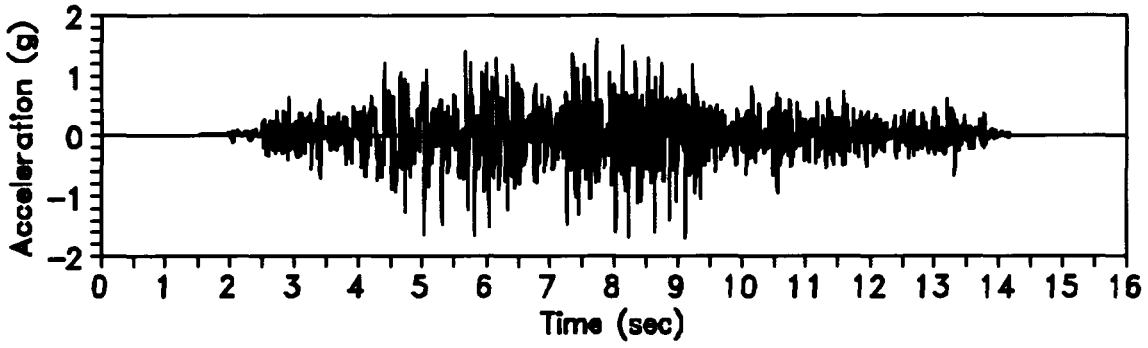

Figure C.74 Second-level Door-wall Acceleration for Test Run 15

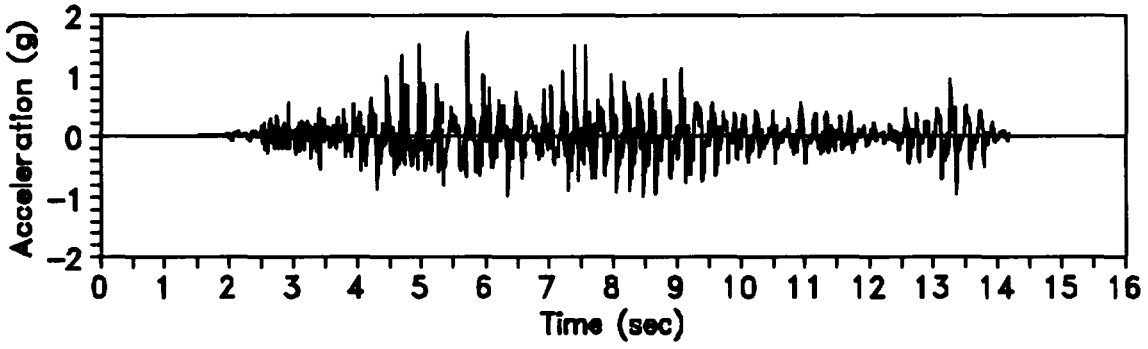

Figure C.75 First-level Window-wall Acceleration for Test Run 15

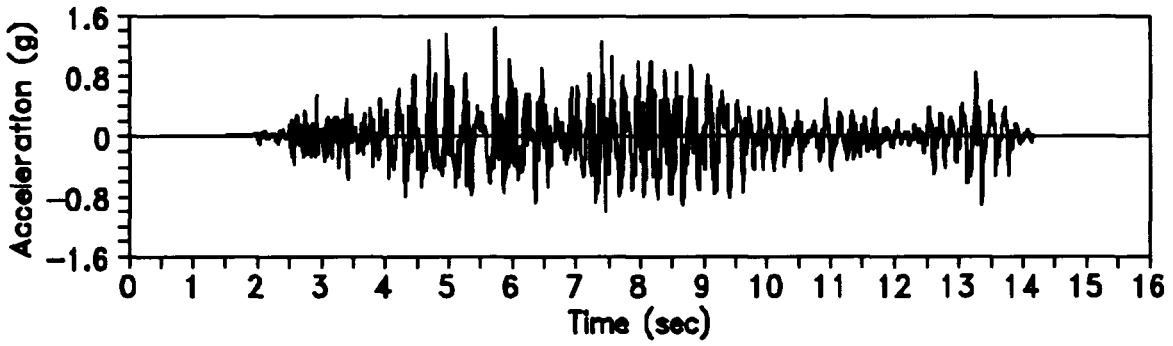

Figure C.76 Second-level Window-wall Acceleration for Test Run 15

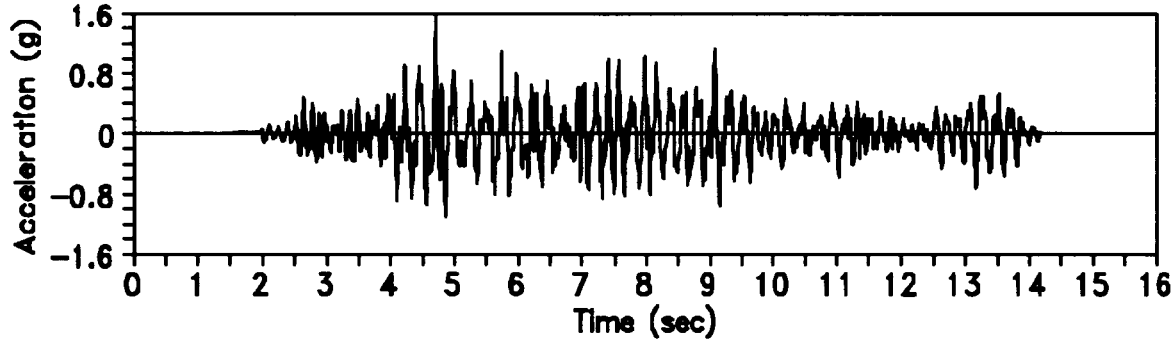

Figure C.77 First-level Diaphragm Acceleration for Test Run 15

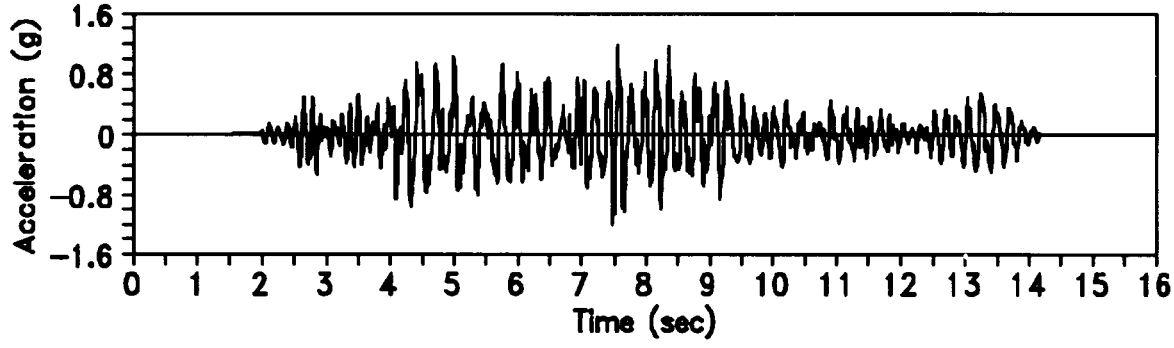

Figure C.78 Second-level Diaphragm Acceleration for Test Run 15

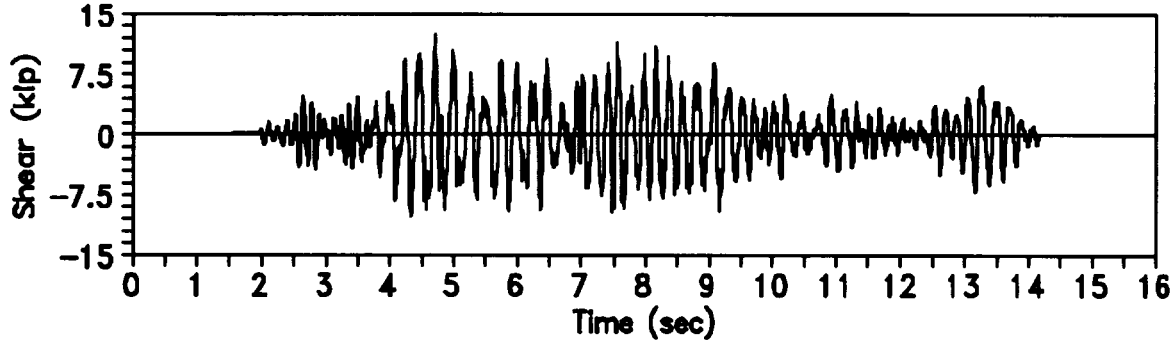

Figure C.79 Base Shear for Test Run 15

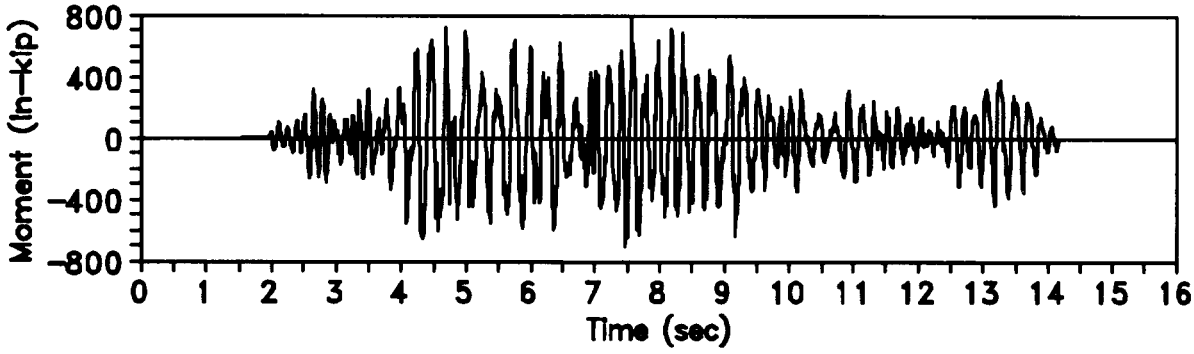

Figure C.80 Base Moment for Test Run 15

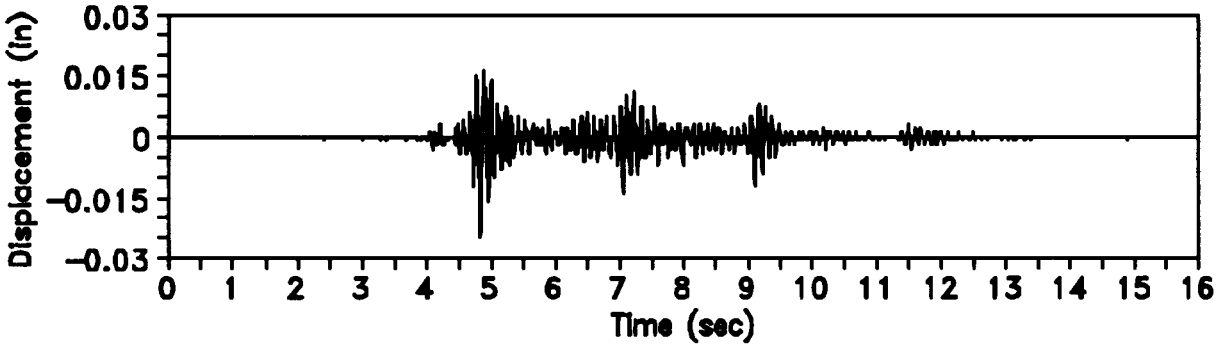

Figure C.81 First-level Door-wall Displacement for Test Run 21

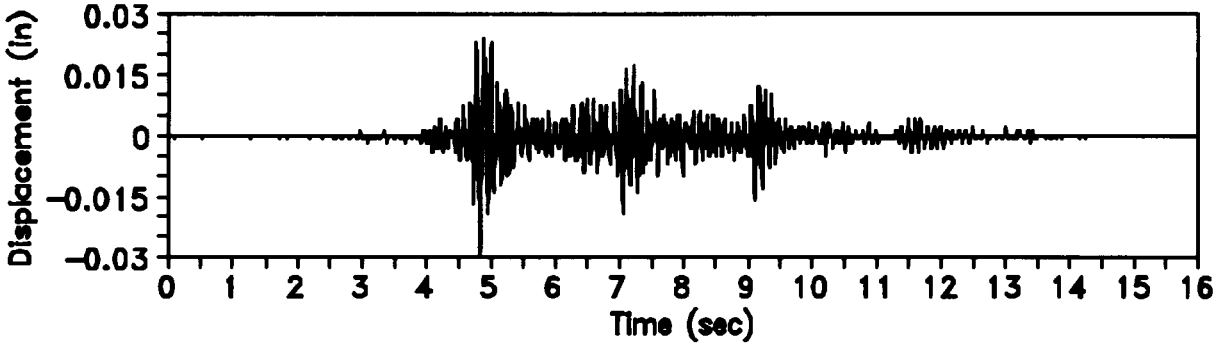

Figure C.82 Second-level Door-wall Displacement for Test Run 21

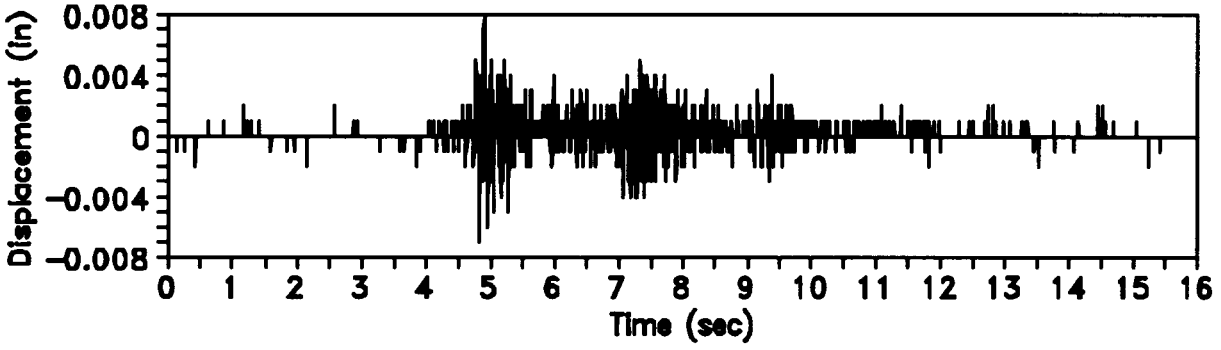

Figure C.83 First-level window-wall Displacement for Test Run 21

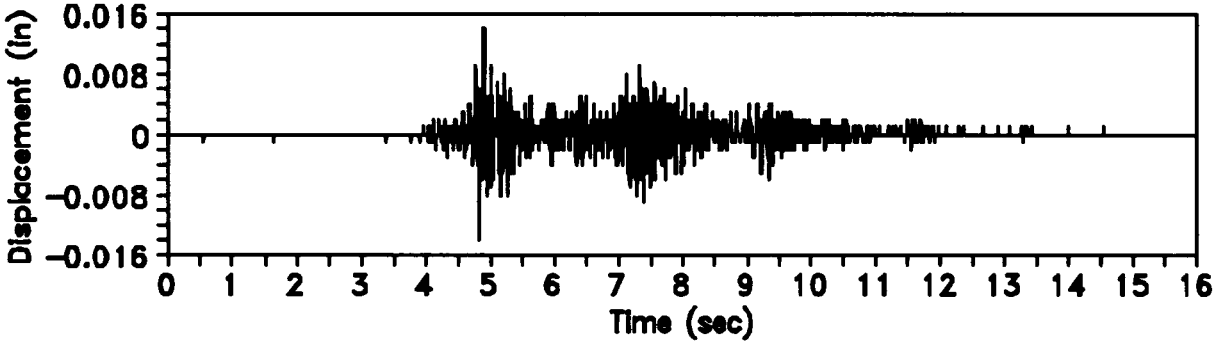

Figure C.84 Second-level window-wall Displacement for Test Run 21

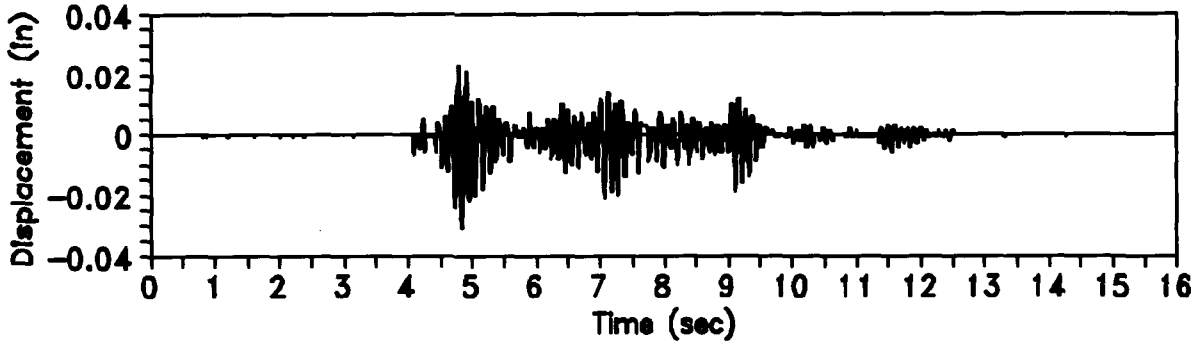

Figure C.85 First-level diaphragm Displacement for Test Run 21

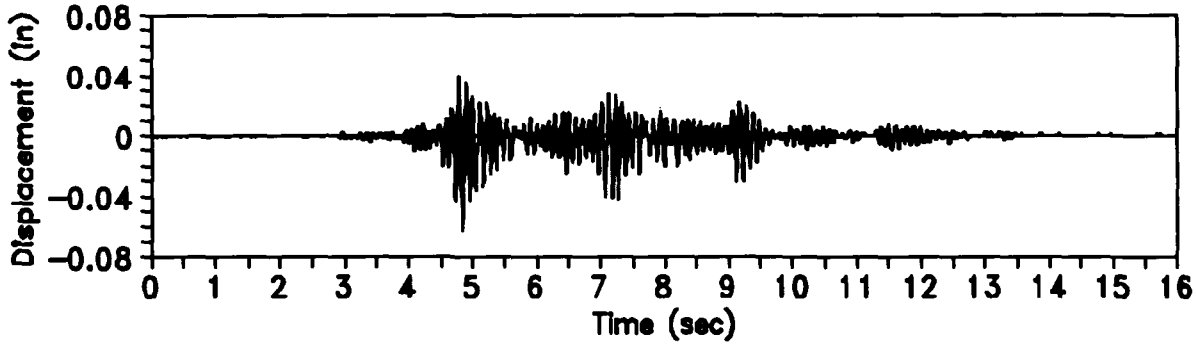

Figure C.86 Second-level diaphragm Displacement for Test Run 21

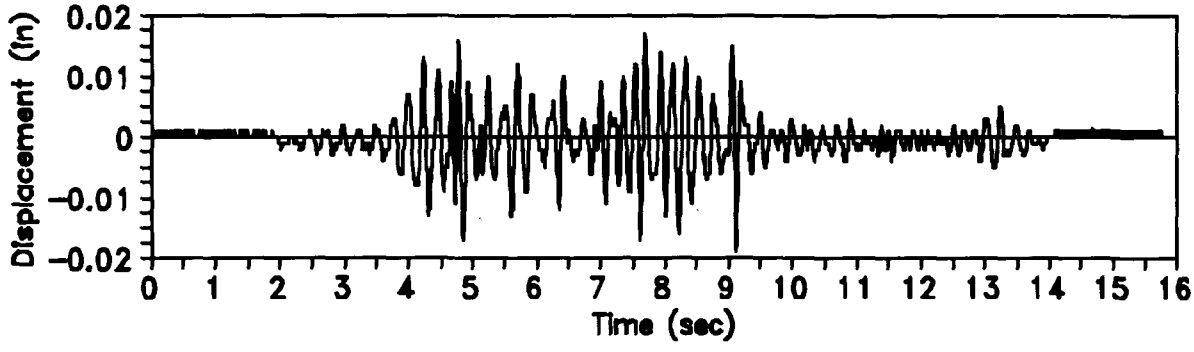

Figure C.87 Absolute Base Displacement for Test Run 21

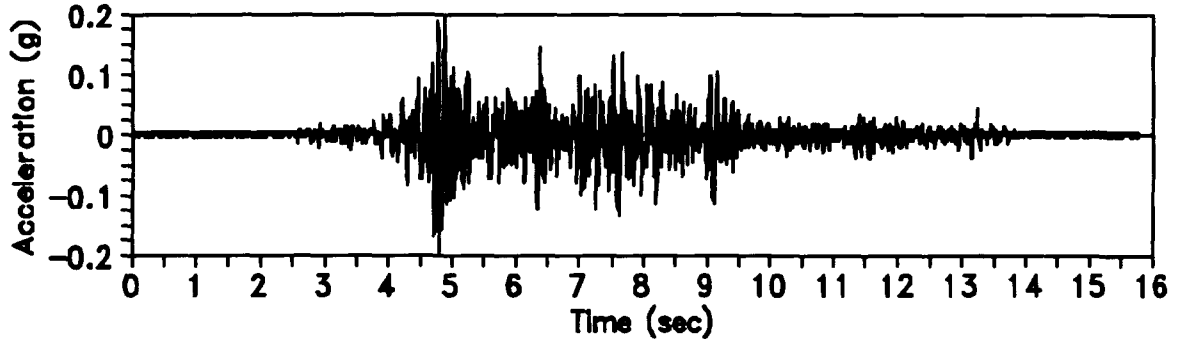

Figure C.88 Base Acceleration for Test Run 21

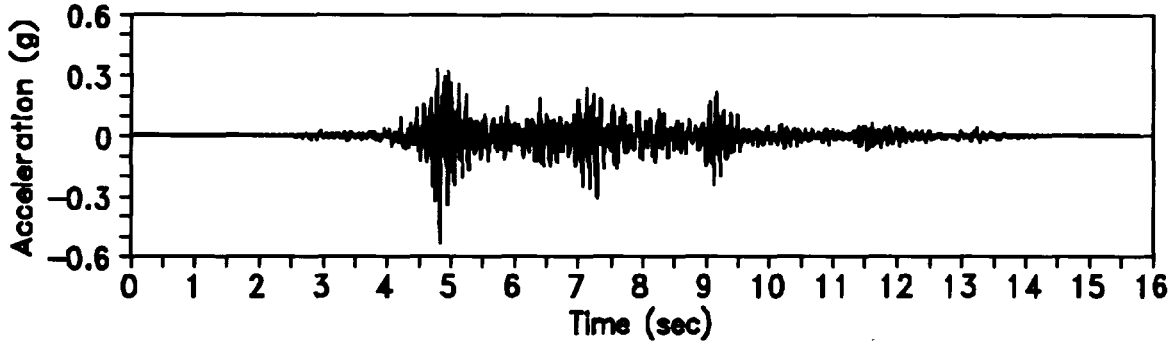

Figure C.89 First-level Door-wall Acceleration for Test Run 21

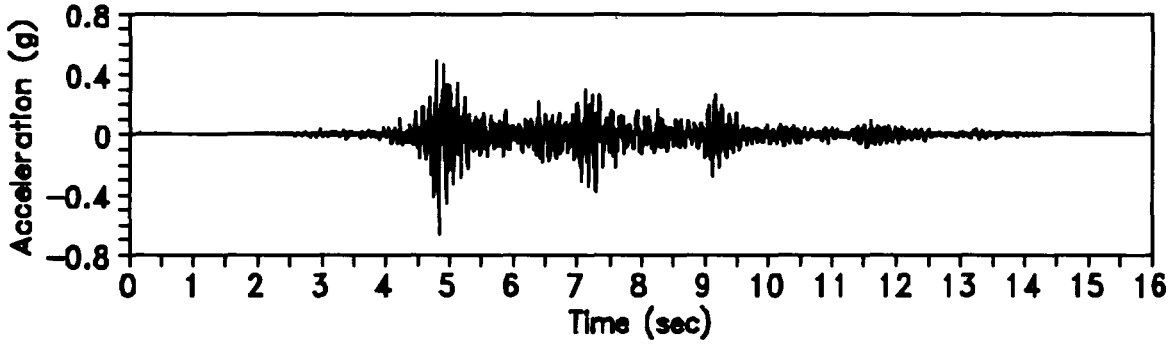

Figure C.90 Second-level Door-wall Acceleration for Test Run 21

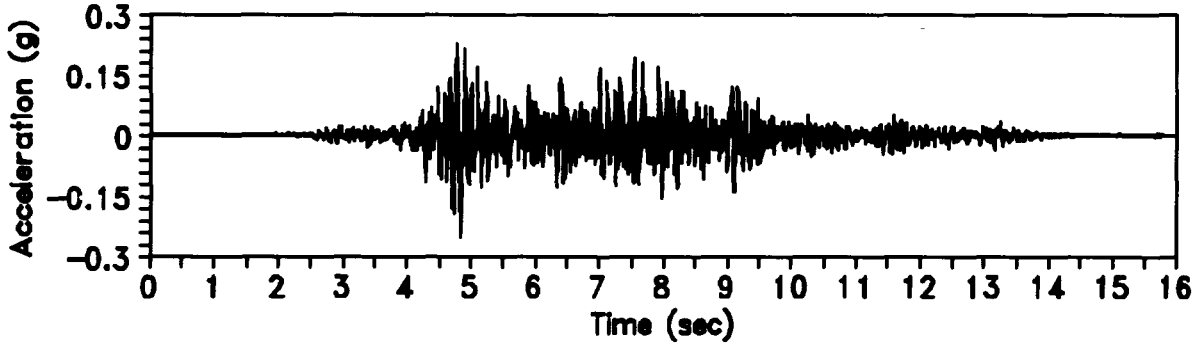

Figure C.91 First-level window-wall Acceleration for Test Run 21

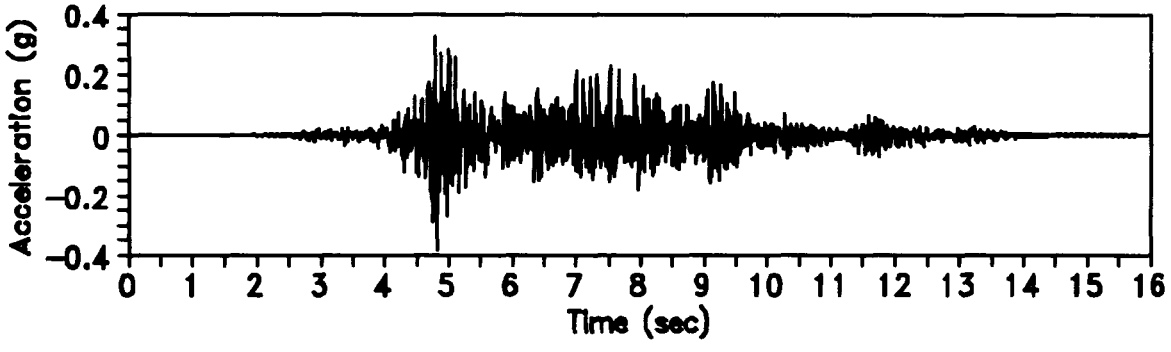

Figure C.92 Second-level window-wall Acceleration for Test Run 21

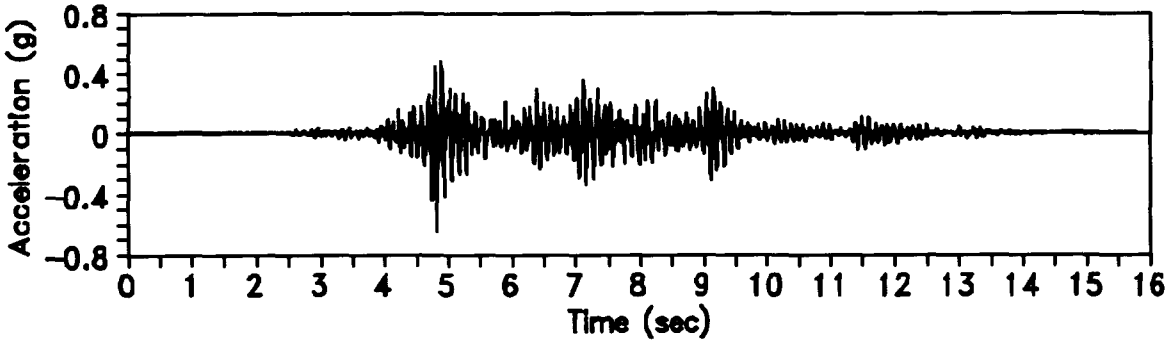

Figure C.93 First-level diaphragm Acceleration for Test Run 21

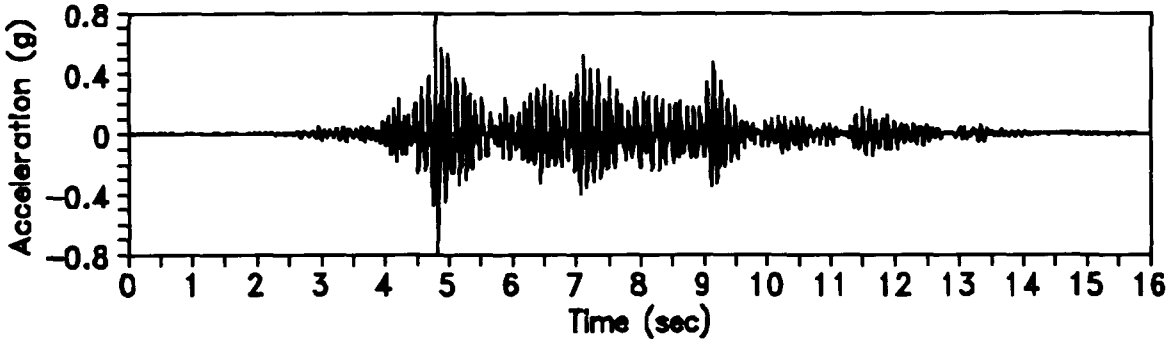

Figure C.94 Second-level diaphragm Acceleration for Test Run 21

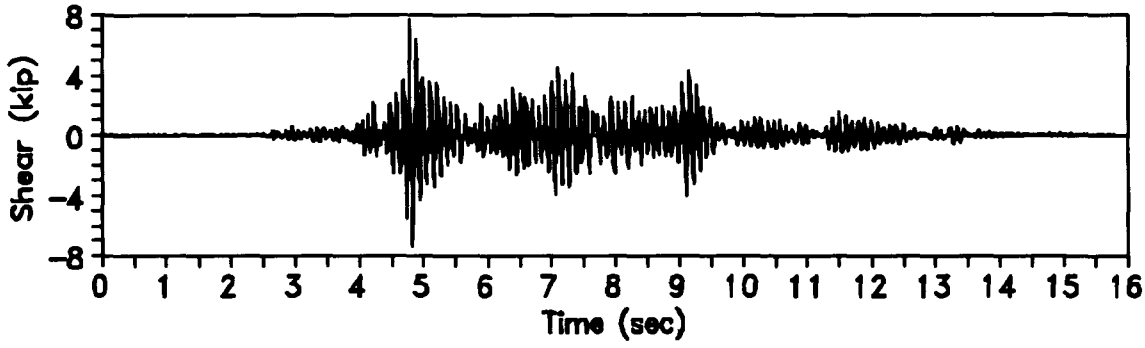

Figure C.95 Base Shear for Test Run 21

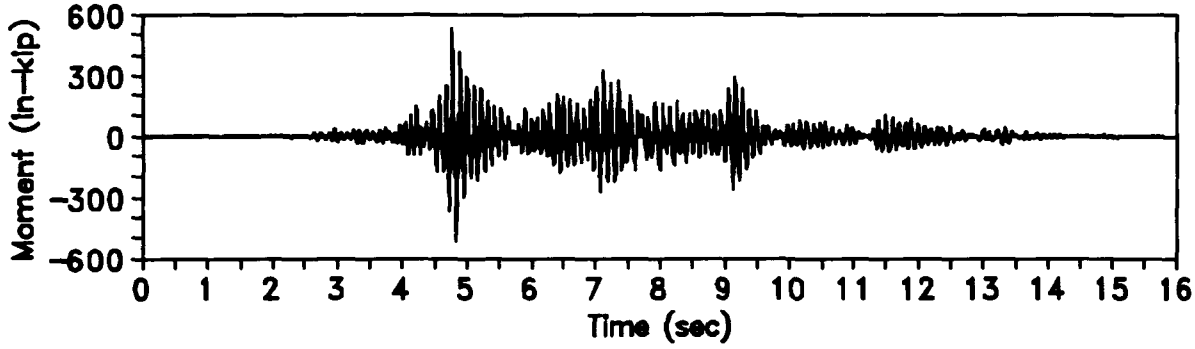

Figure C.96 Base Moment for Test Run 21

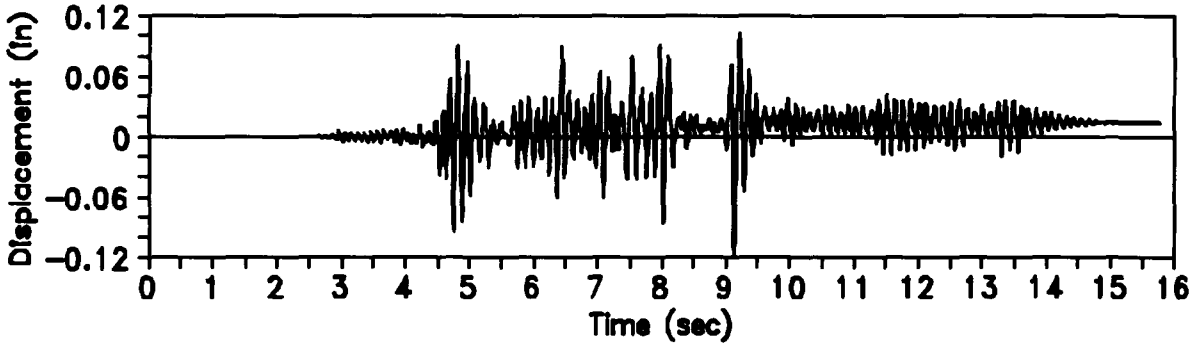

Figure C.97 First-level Door-wall Displacement for Test Run 22

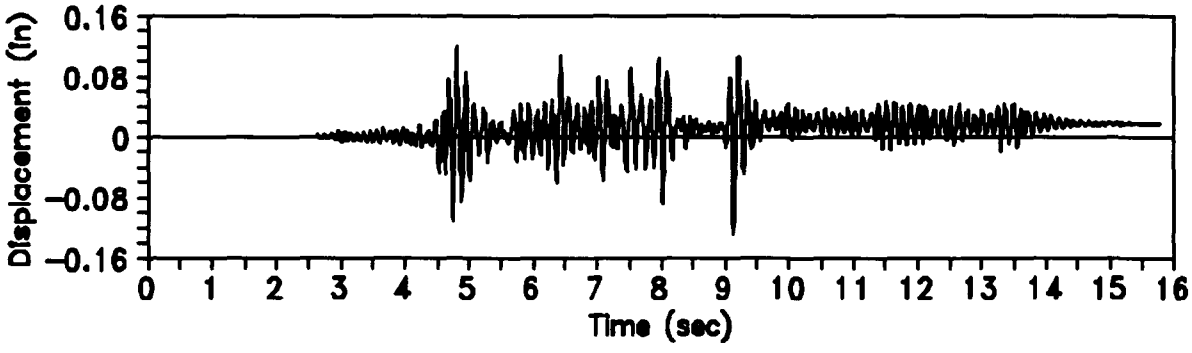

Figure C.98 Second-level Door-wall Displacement for Test Run 22

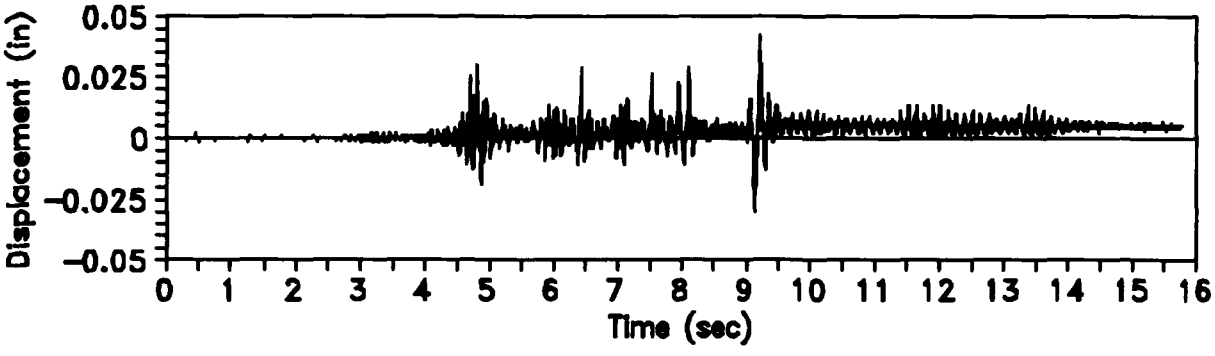

Figure C.99 First-level window-wall Displacement for Test Run 22

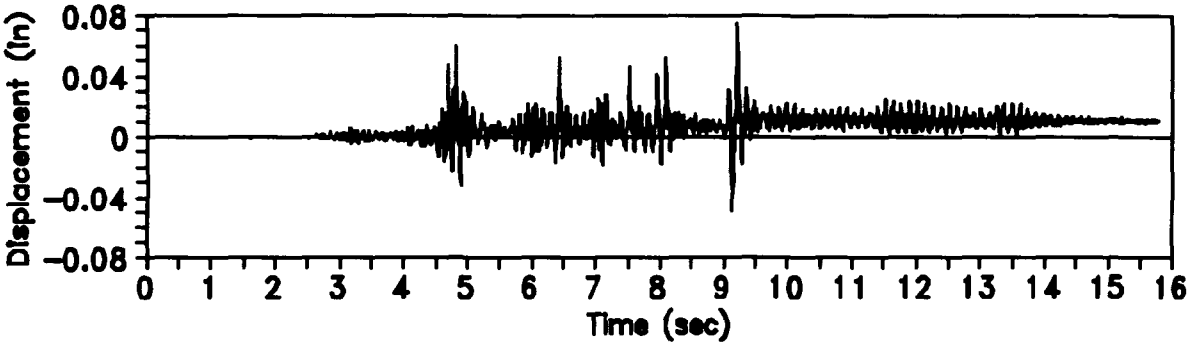

Figure C.100 Second-level window-wall Displacement for Test Run 22

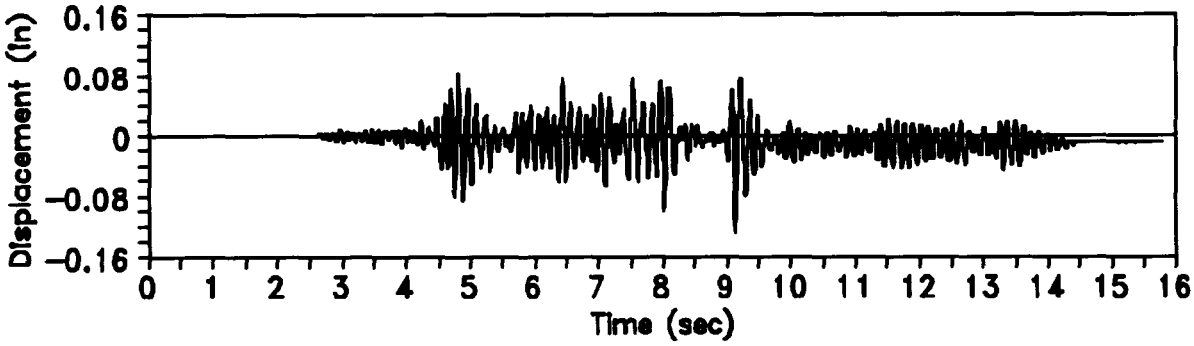

Figure C.101 First-level diaphragm Displacement for Test Run 22

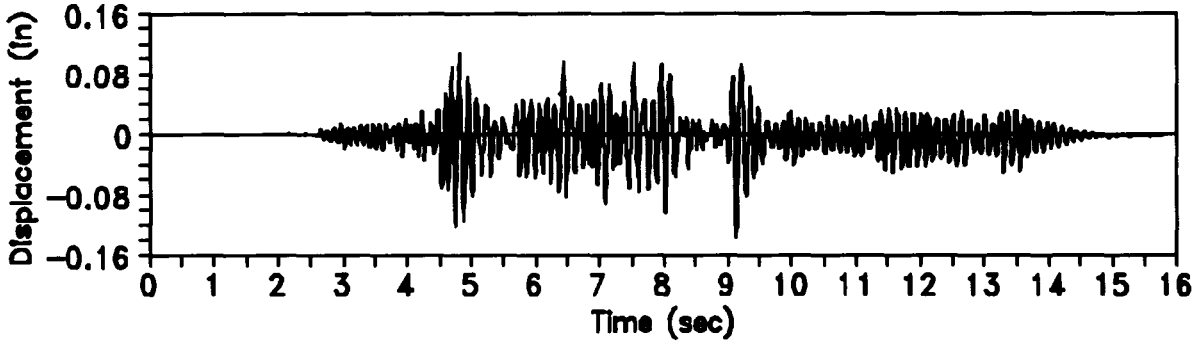

Figure C.102 Second-level diaphragm Displacement for Test Run 22

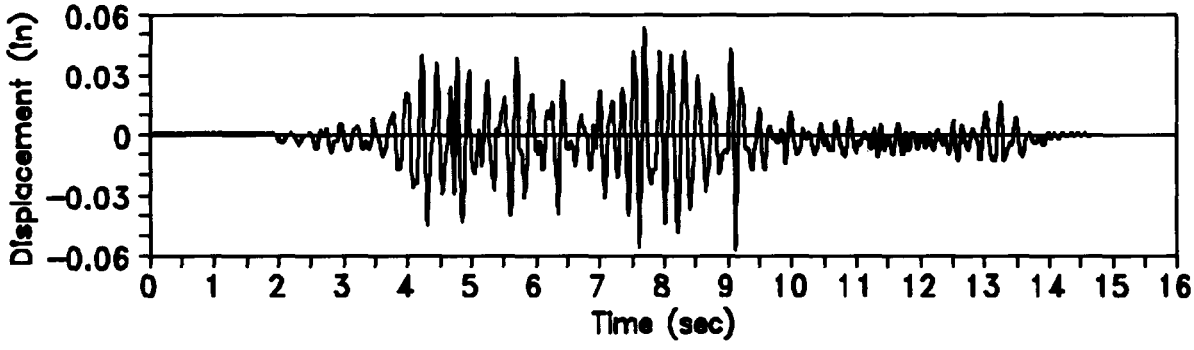

Figure C.103 Absolute Base Displacement for Test Run 22

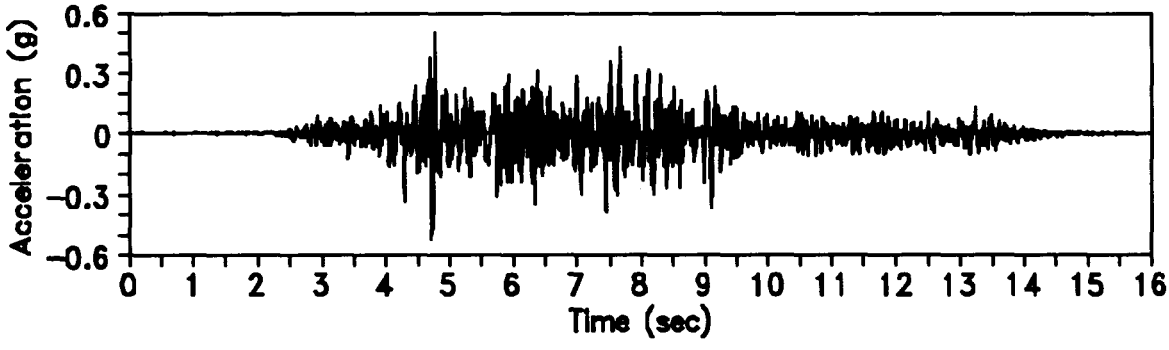

Figure C.104 Base Acceleration for Test Run 22

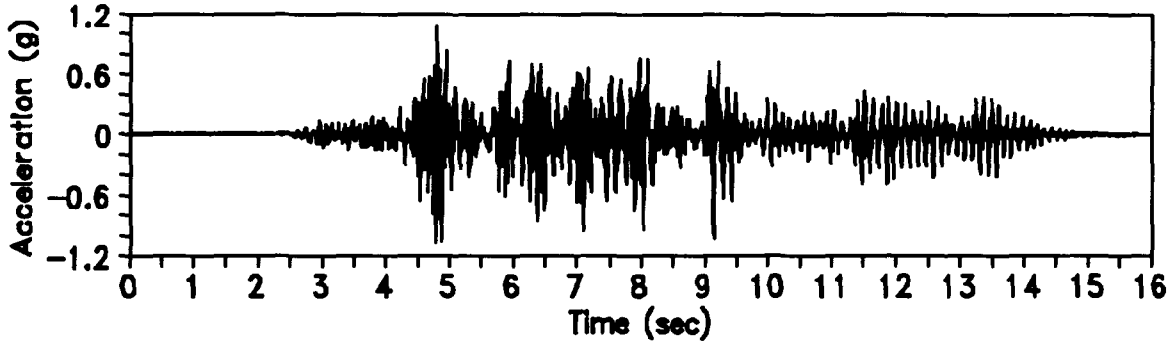

Figure C.105 First-level Door-wall Acceleration for Test Run 22

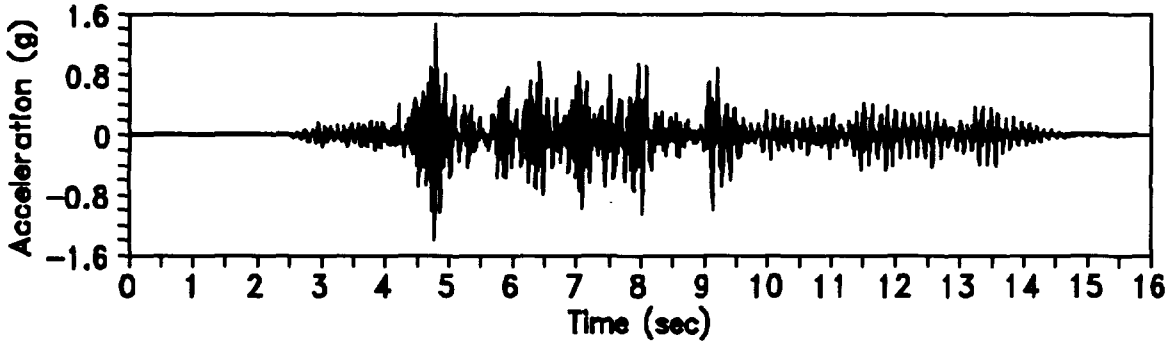

Figure C.106 Second-level Door-wall Acceleration for Test Run 22

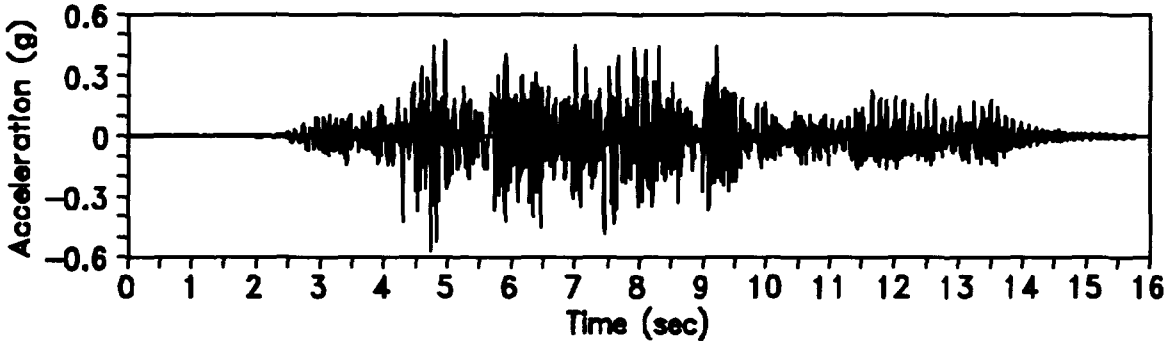

Figure C.107 First-level window-wall Acceleration for Test Run 22

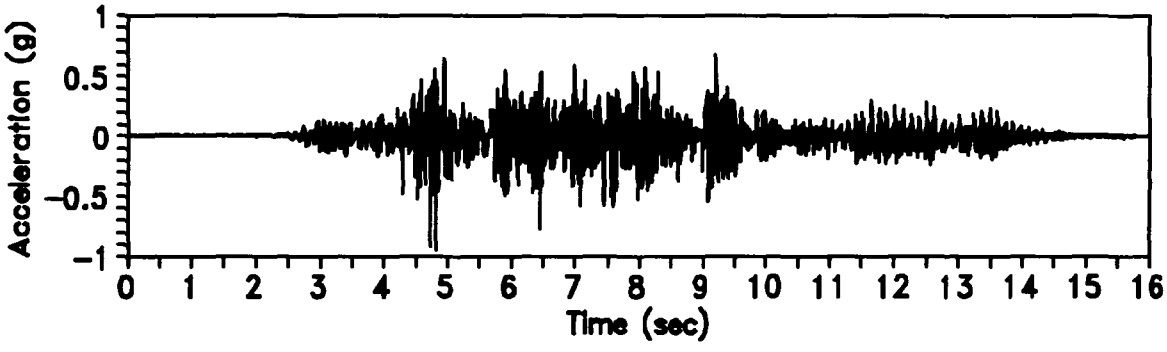

Figure C.108 Second-level window-wall Acceleration for Test Run 22

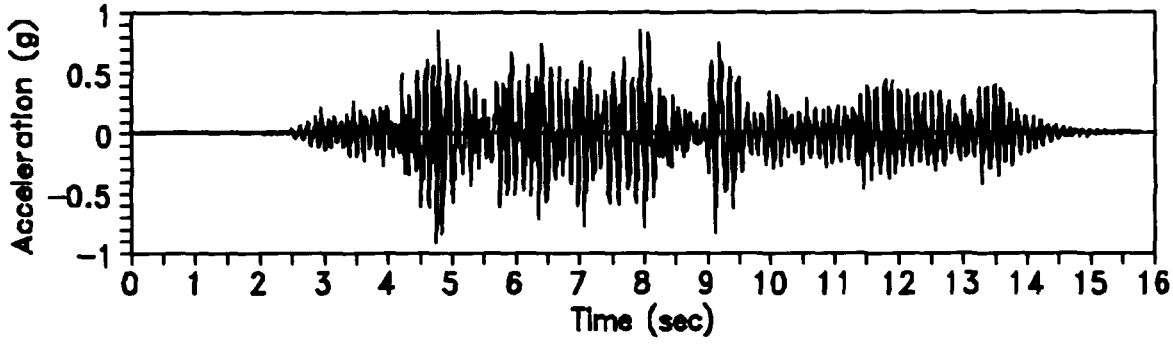

Figure C.109 First-level diaphragm Acceleration for Test Run 22

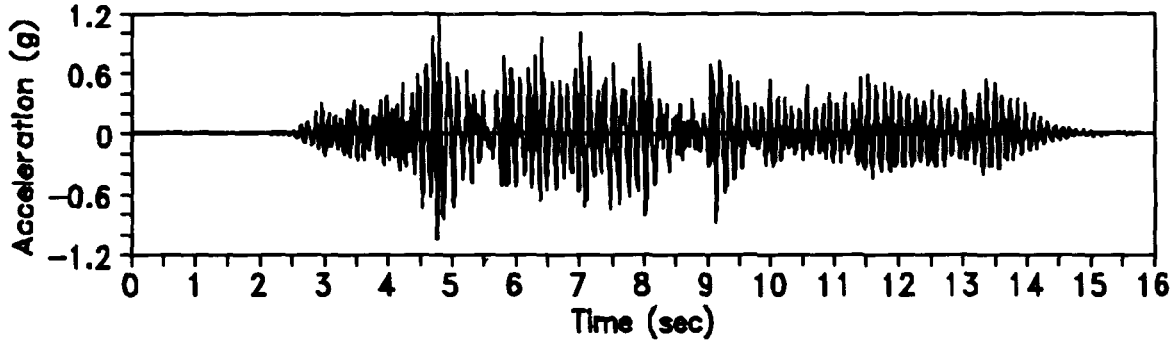

Figure C.110 Second-level diaphragm Acceleration for Test Run 22

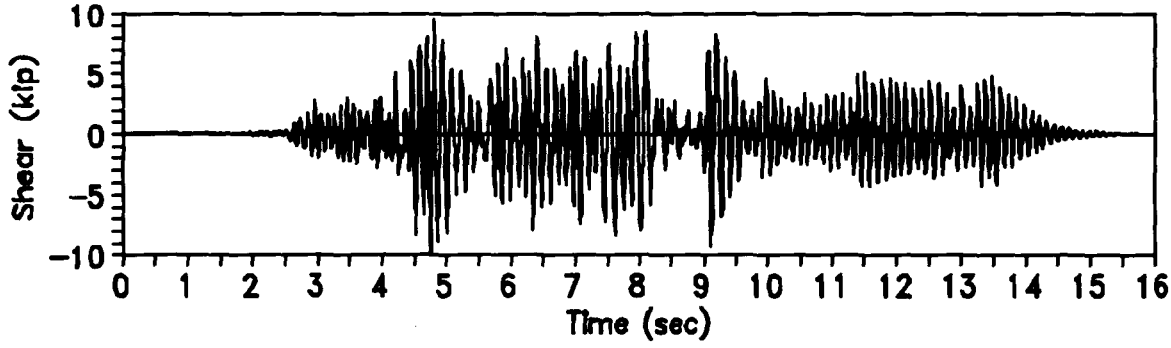

Figure C.111 Base Shear for Test Run 22

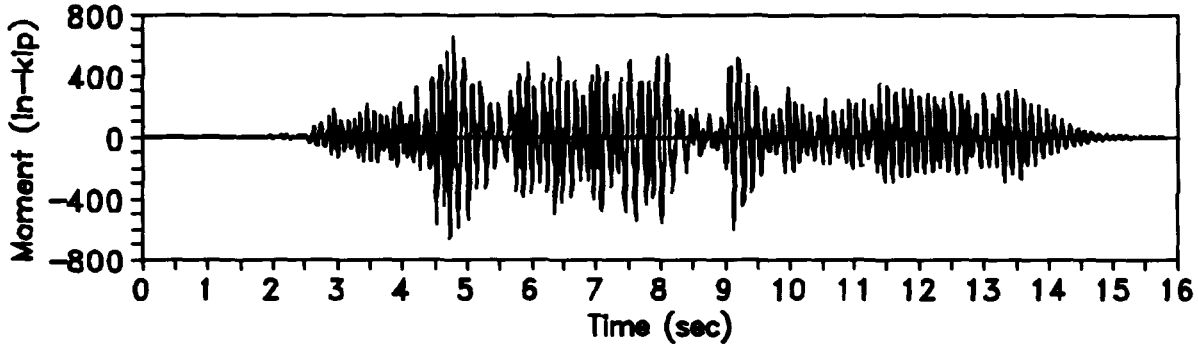

Figure C.112 Base Moment for Test Run 22

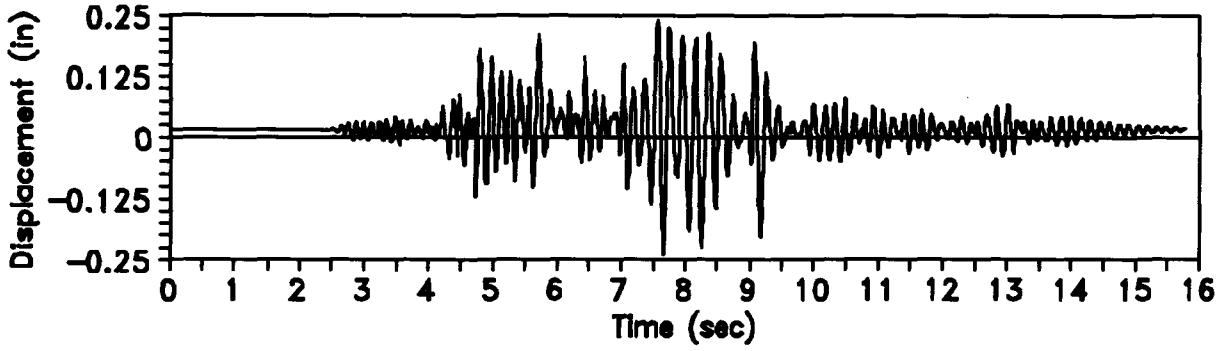

Figure C.113 First-level Door-wall Displacement for Test Run 23

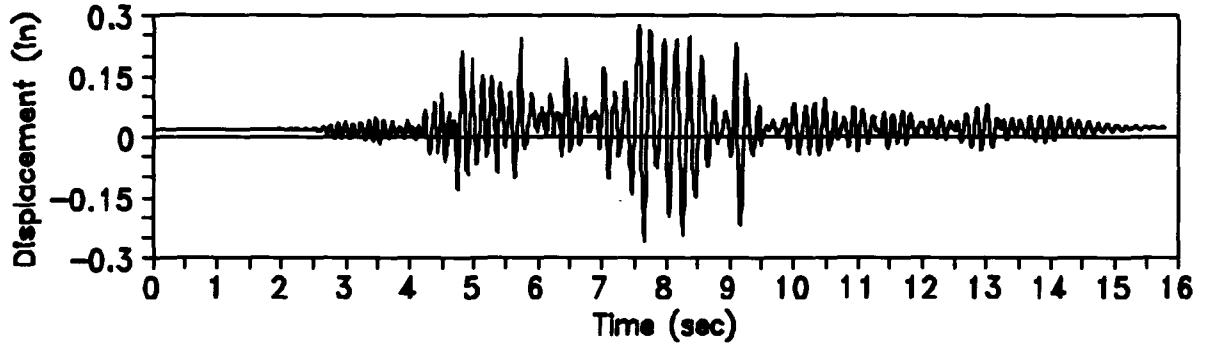

Figure C.114 Second-level Door-wall Displacement for Test Run 23

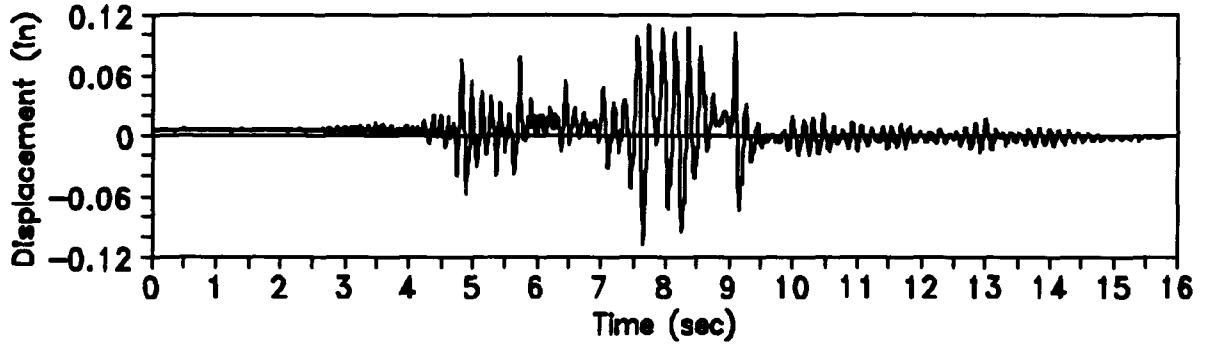

Figure C.115 First-level window-wall Displacement for Test Run 23

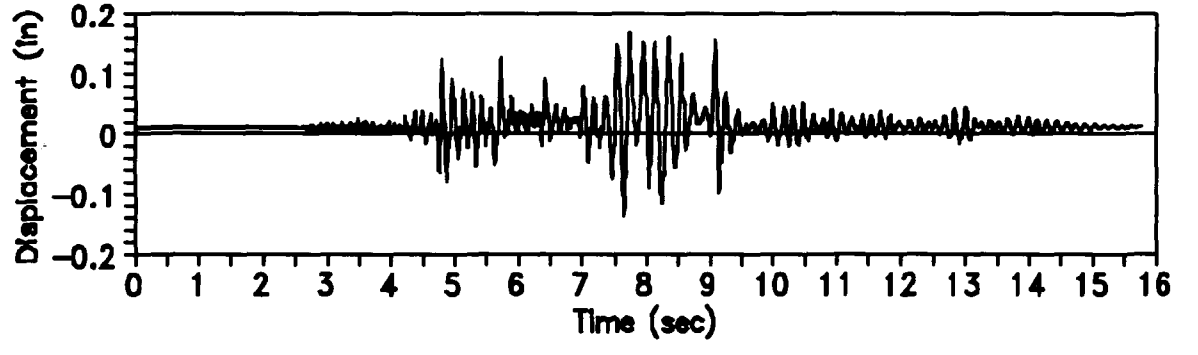

Figure C.116 Second-level window-wall Displacement for Test Run 23

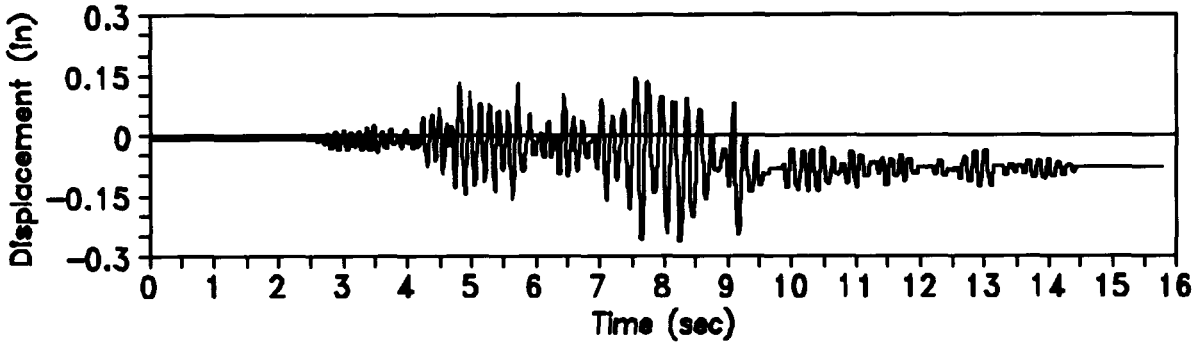

Figure C.117 First-level diaphragm Displacement for Test Run 23

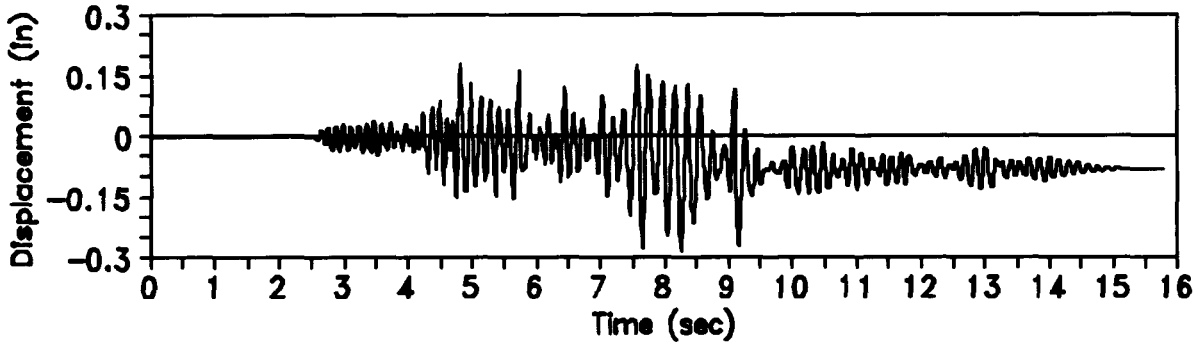

Figure C.118 Second-level diaphragm Displacement for Test Run 23

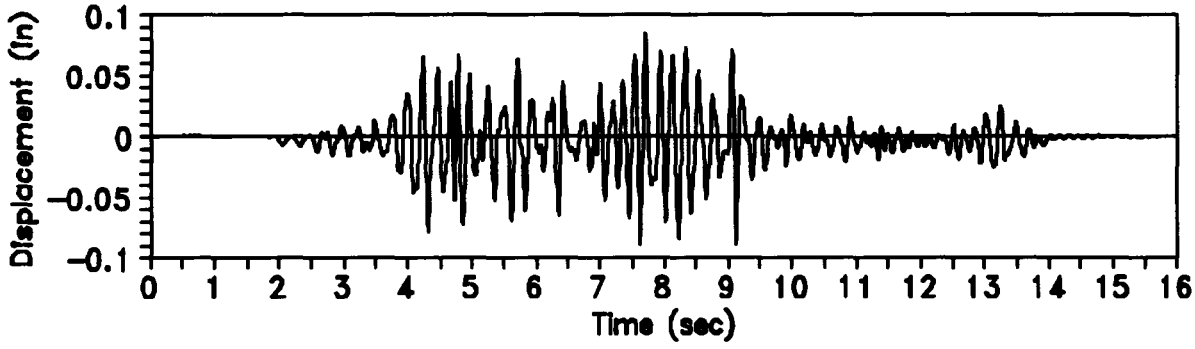

Figure C.119 Absolute Base Displacement for Test Run 23

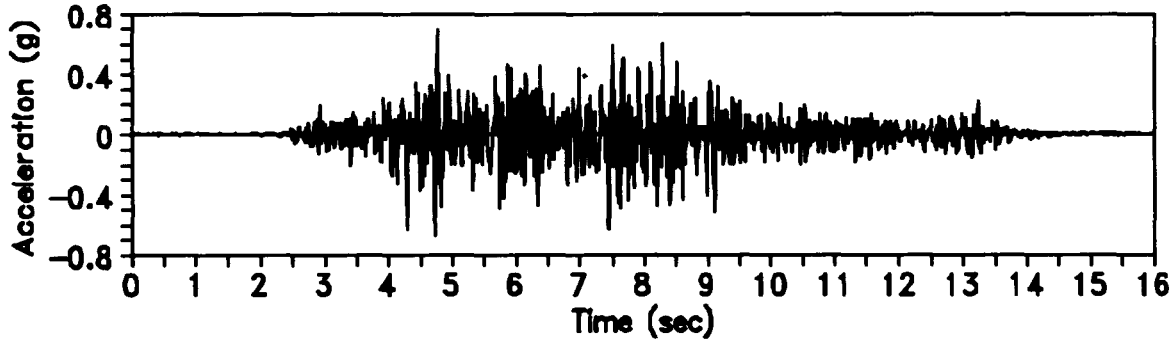

Figure C.120 Base Acceleration for Test Run 23

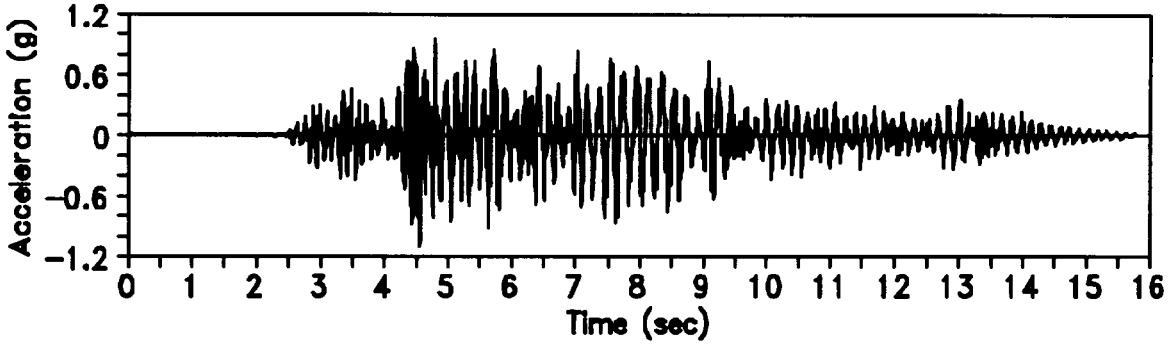

Figure C.121 First-level Door-wall Acceleration for Test Run 23

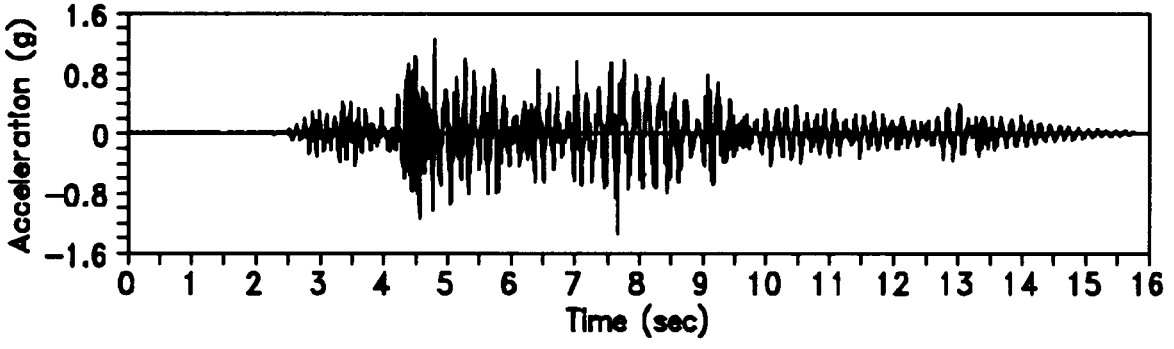

Figure C.122 Second-level Door-wall Acceleration for Test Run 23

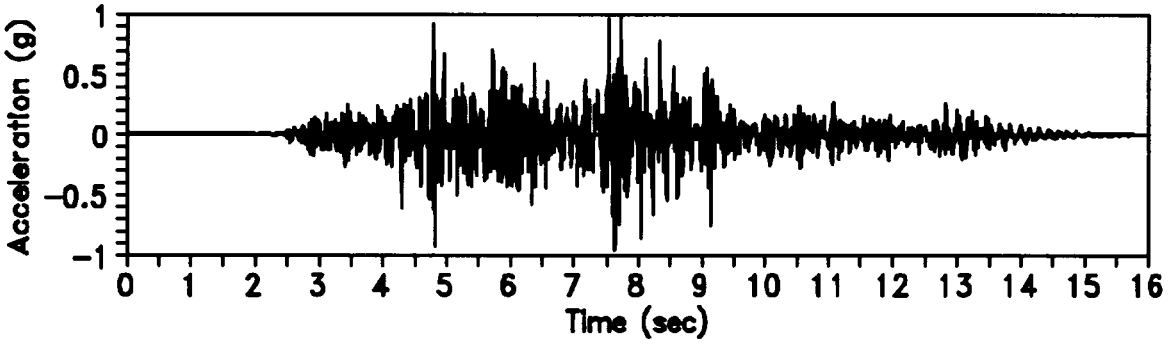

Figure C.123 First-level window-wall Acceleration for Test Run 23

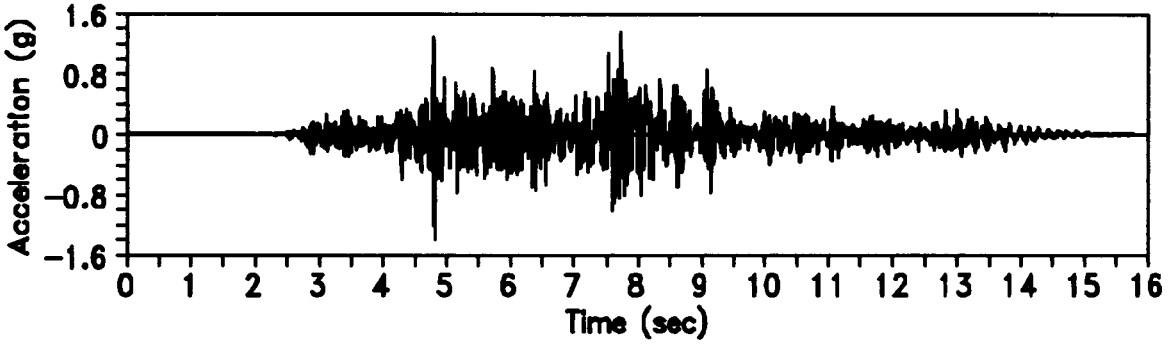

Figure C.124 Second-level window-wall Acceleration for Test Run 23

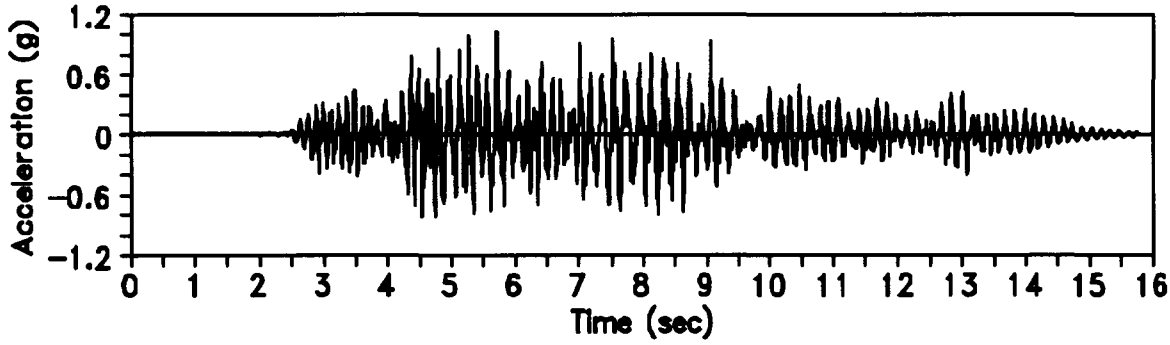

Figure C.125 First-level diaphragm Acceleration for Test Run 23

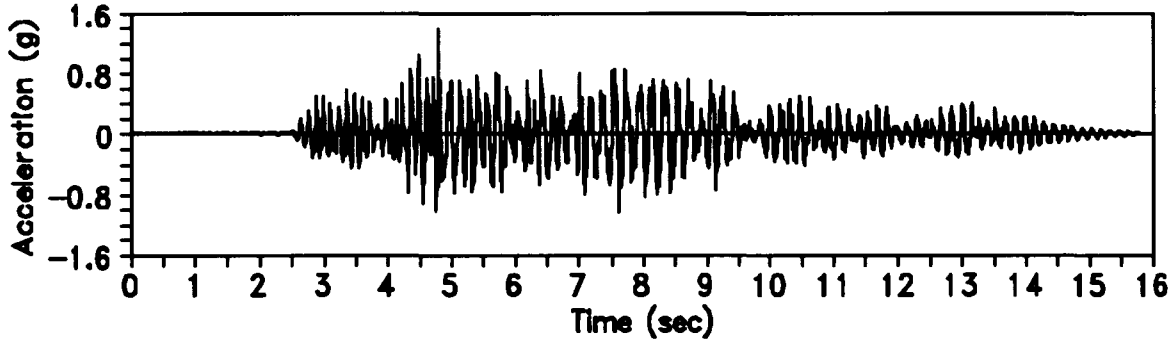

Figure C.126 Second-level diaphragm Acceleration for Test Run 23

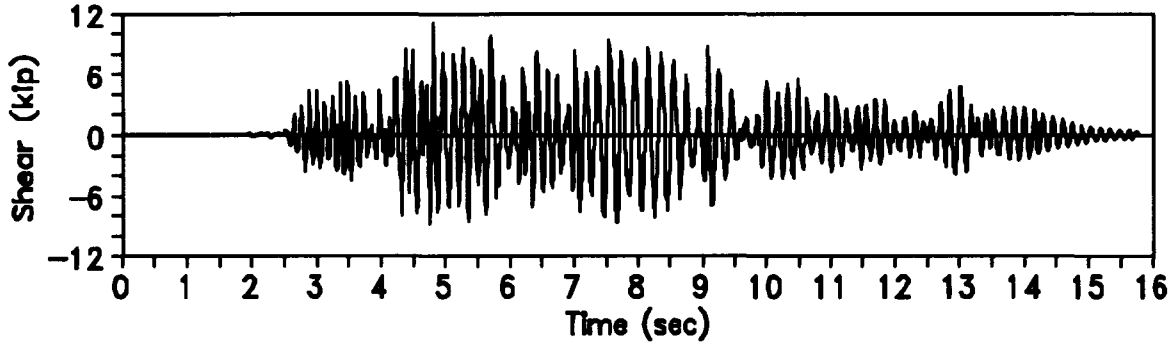

Figure C.127 Base Shear for Test Run 23

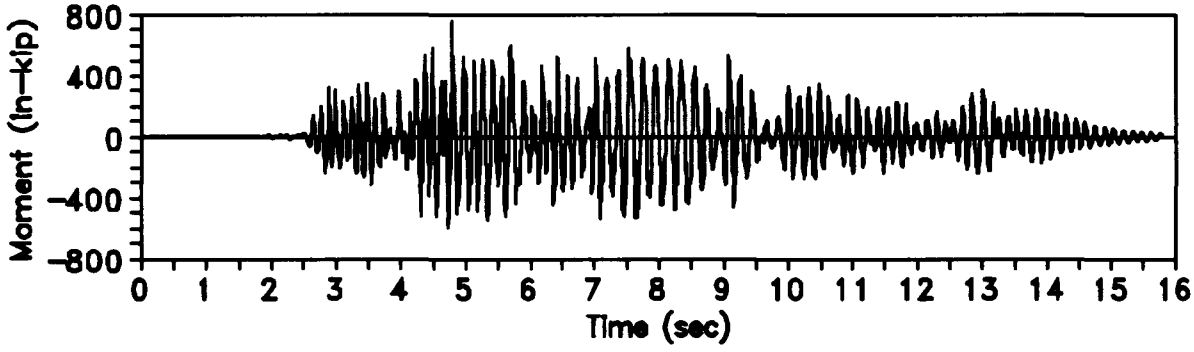

Figure C.128 Base Moment for Test Run 23

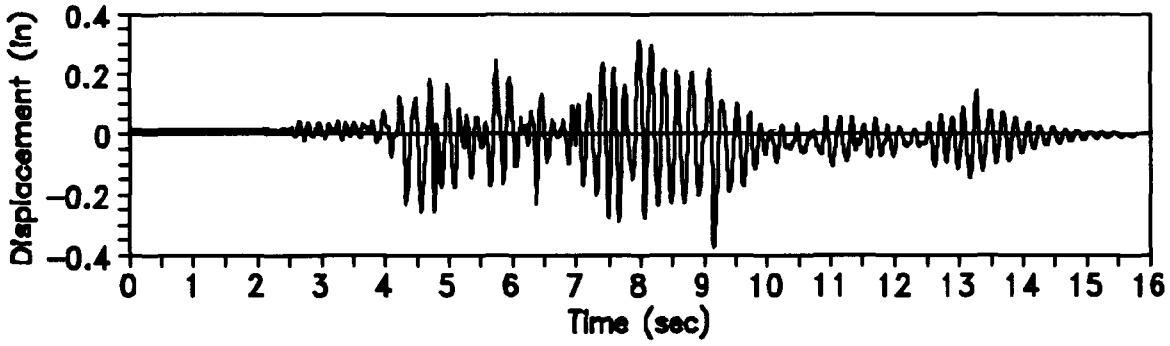

Figure C.129 First-level Door-wall Displacement for Test Run 24

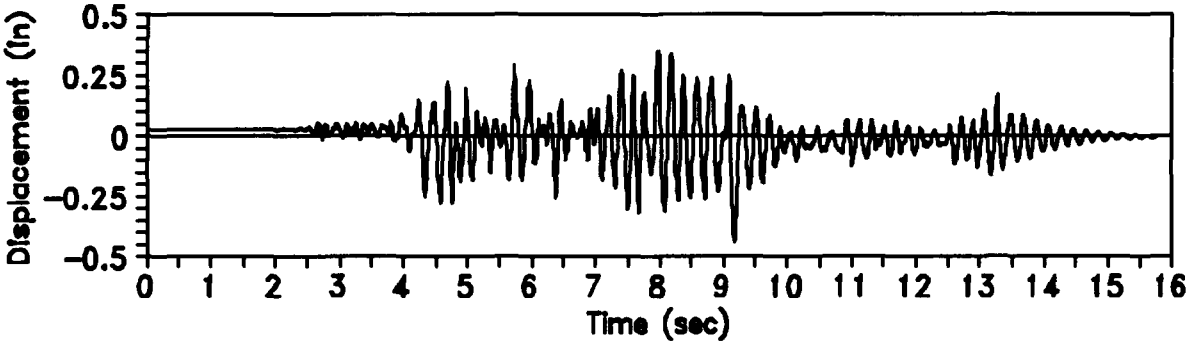

Figure C.130 Second-level Door-wall Displacement for Test Run 24

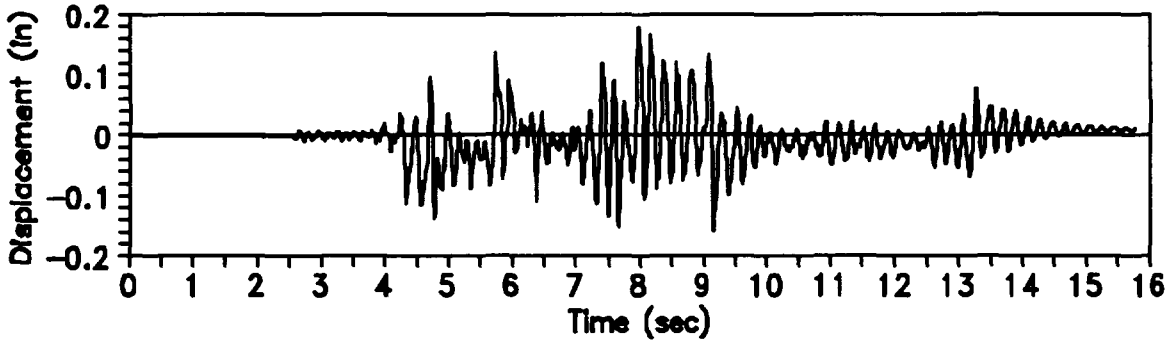

Figure C.131 First-level window-wall Displacement for Test Run 24

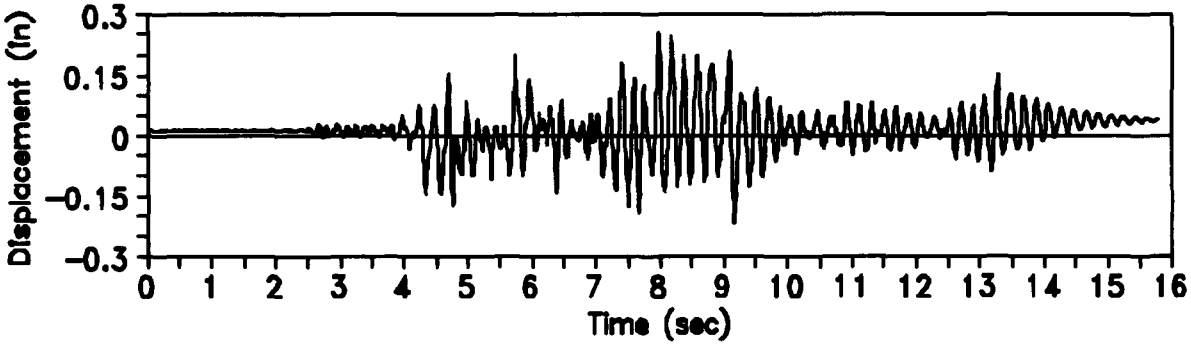

Figure C.132 Second-level window-wall Displacement for Test Run 24

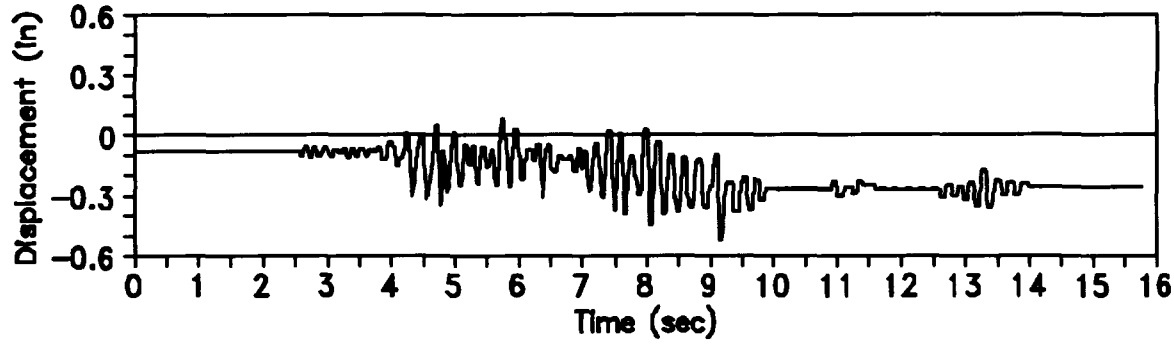

Figure C.133 First-level diaphragm Displacement for Test Run 24

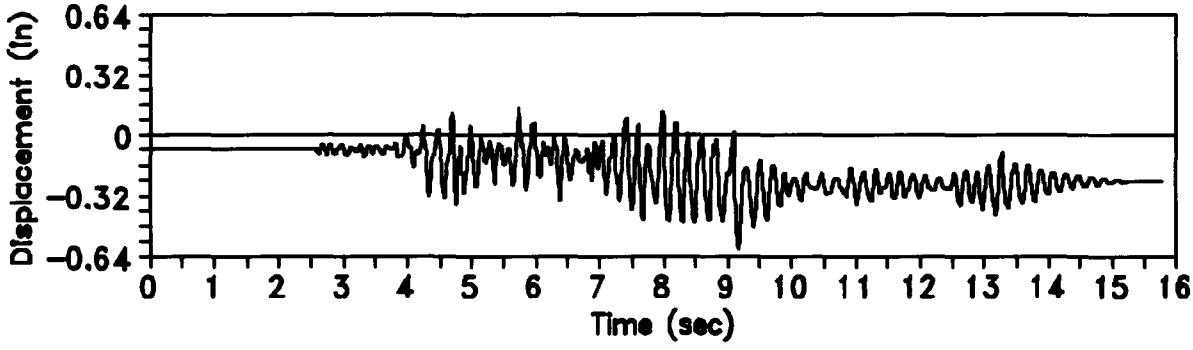

Figure C.134 Second-level diaphragm Displacement for Test Run 24

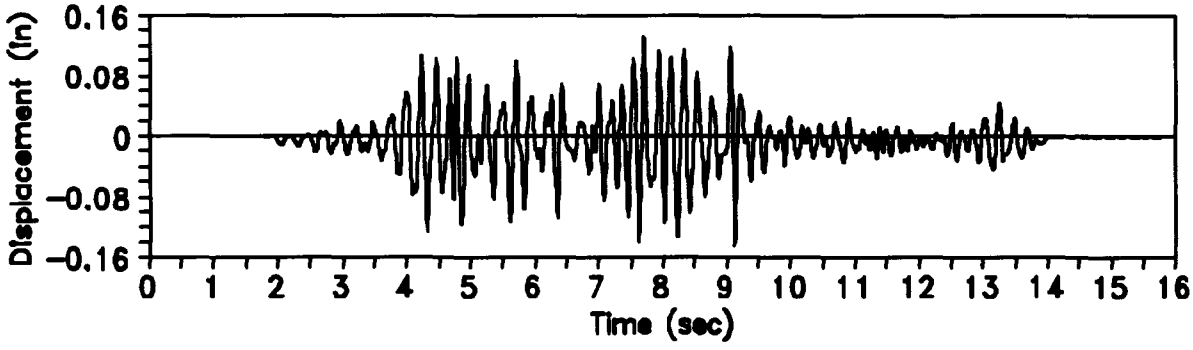

Figure C.135 Absolute Base Displacement for Test Run 24

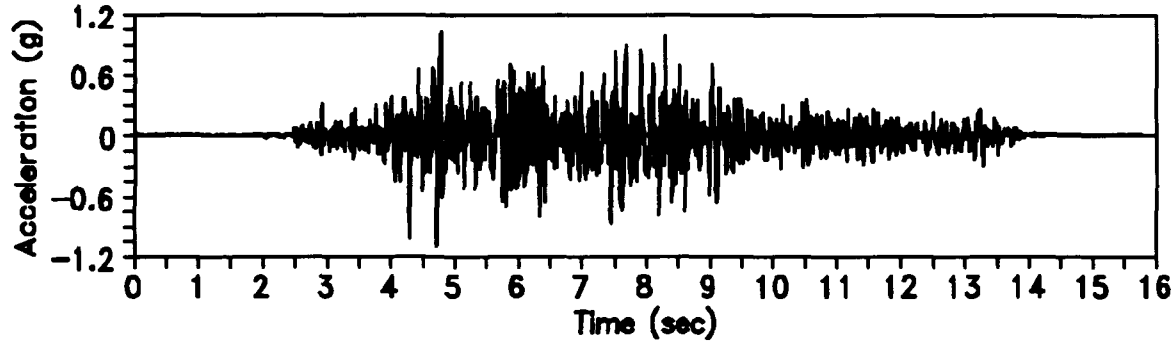

Figure C.136 Base Acceleration for Test Run 24

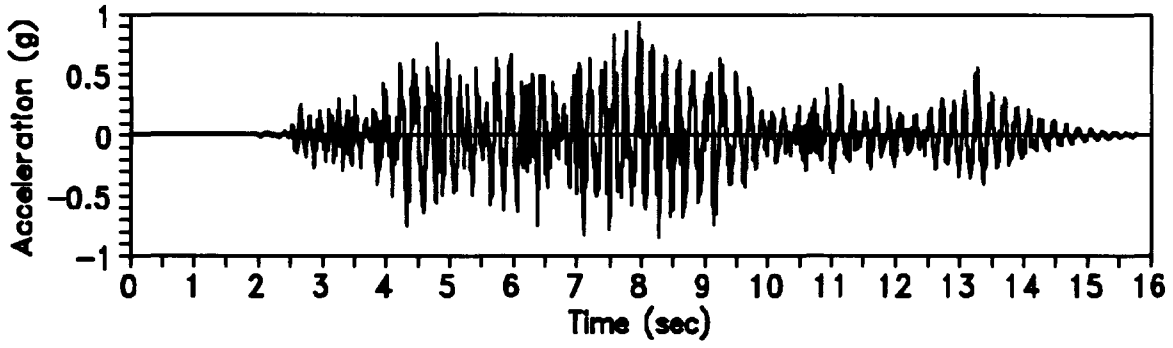

Figure C.137 First-level Door-wall Acceleration for Test Run 24

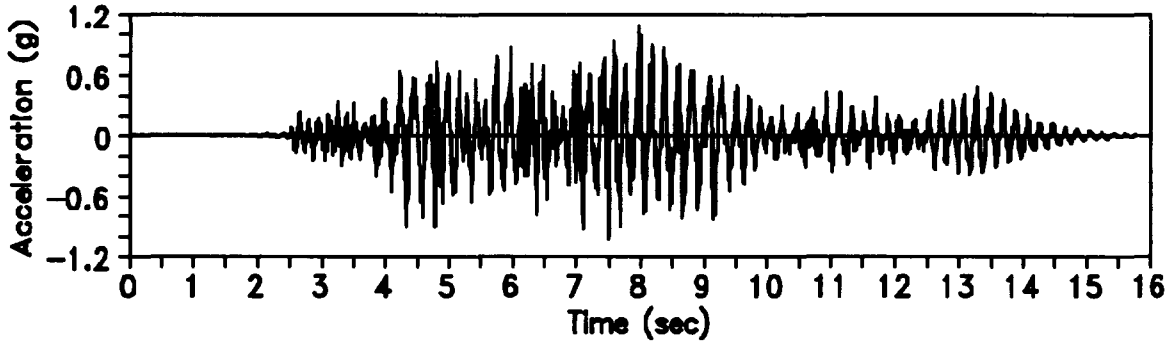

Figure C.138 Second-level Door-wall Acceleration for Test Run 24

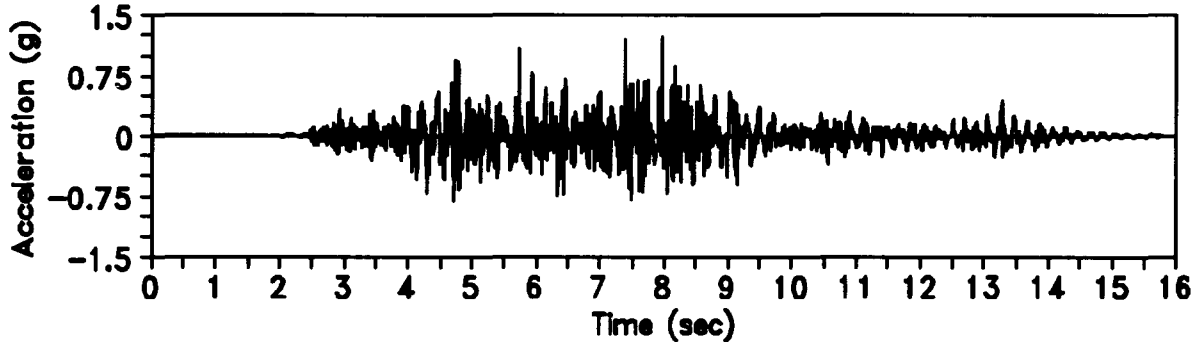

Figure C.139 First-level window-wall Acceleration for Test Run 24

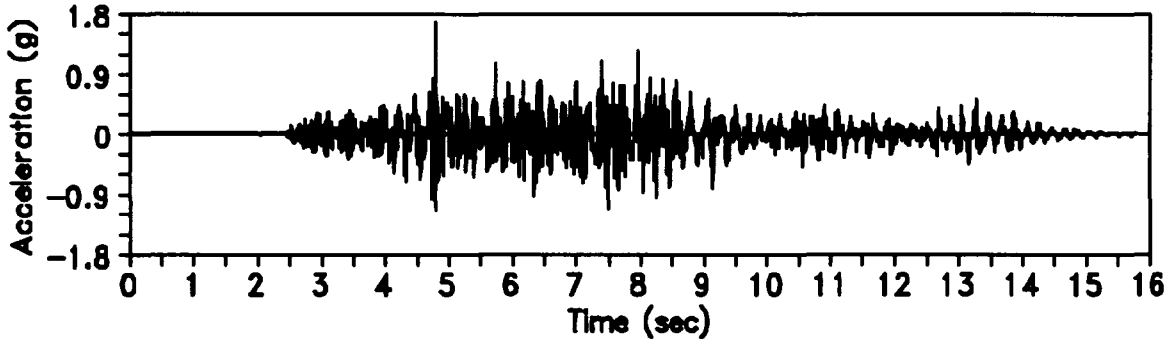

Figure C.140 Second-level window-wall Acceleration for Test Run 24

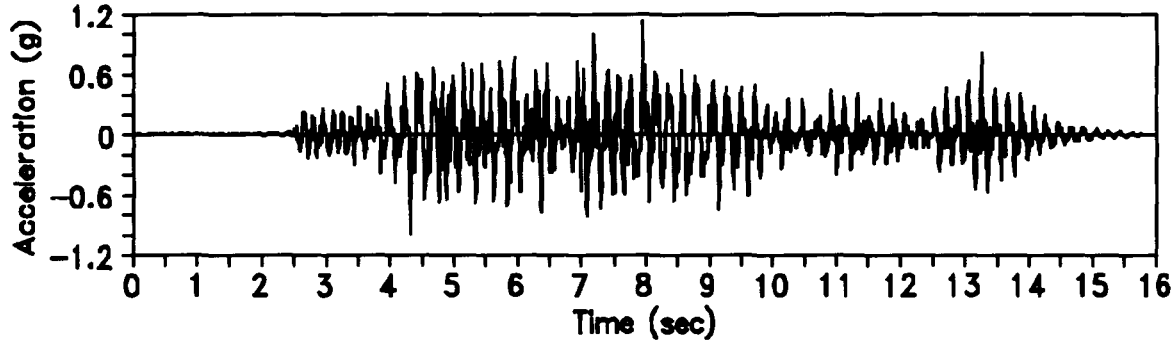

Figure C.141 First-level diaphragm Acceleration for Test Run 24

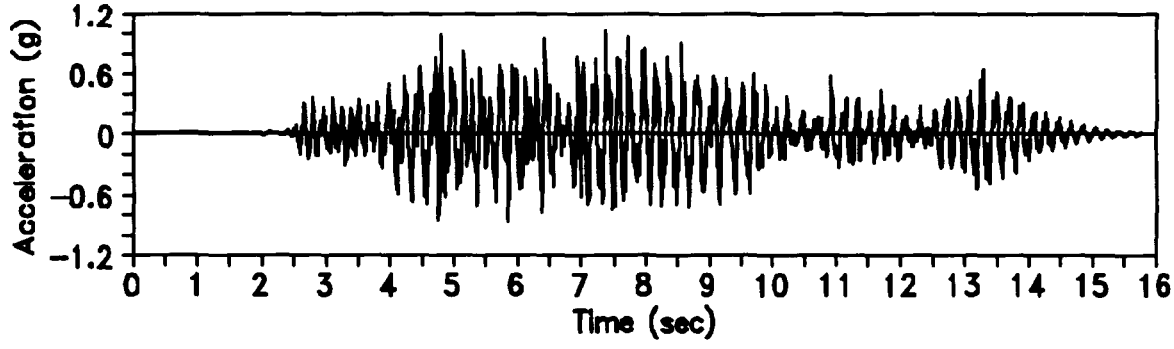

Figure C.142 Second-level diaphragm Acceleration for Test Run 24

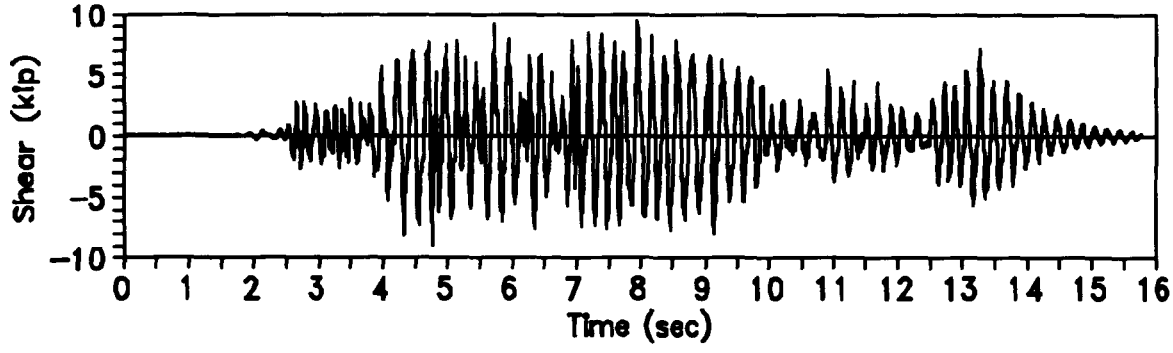

Figure C.143 Base Shear for Test Run 24

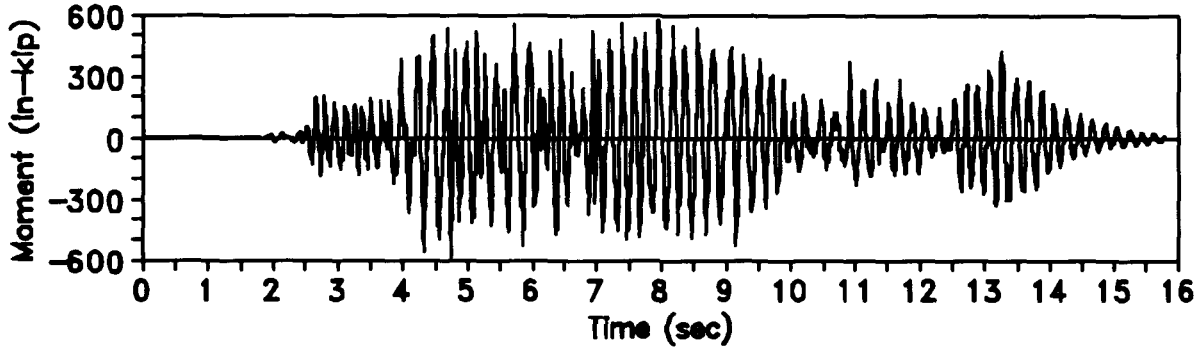

Figure C.144 Base Moment for Test Run 24

APPENDIX D

DESCRIPTION OF FILTERING

Most of the data collected during Test Runs 11 through 15 (for S1) were filtered. This filtering was necessitated by two unwanted phenomenon that occurred during testing. The first was an excessive vibration of the support arms for the LVDTs that measured relative displacements of the first- and second-floor in-plane (door and window) walls. The vibrational frequency was much lower than was anticipated while the dynamic deflection of the arms was much higher. An independent study of the support arms determined that the arms for the first-floor LVDTs had a natural frequency near 26-28 Hz while the arms for the second-floor LVDTs had a natural frequency just greater than 30 Hz. Therefore, the displacement histories from the first-floor LVDTs were filtered to remove all vibrational components above 25 Hz. Similarly, the histories from the second-floor LVDTs were filtered to remove all components above 30 Hz.

The second unwanted phenomena observed during Test Runs 11 through 15 was a banging of the floor weights against the bolts that connected them to the floor beams. As was described in Section 2.8.7, only approximately half of the ¼" dia. bolts were replaced with $^5/_{16}$" dia. bolts. This over-tolerance led to the banging of the weights during the dynamic tests. It should be noted, however, that the weights were not banging against each other, nor were they striking the beams, rather the clip angles were striking the ¼" dia. bolts as some of the weights slid across the floor beams. As a result of this banging, high frequency spikes were present in the acceleration and displacement histories. To remove this noise, the histories were filtered to remove all vibrational components above 45 Hz. This limit was set by examining the pre- and post-filtered records and determining at what frequency limit the spikes could be minimized without affecting the magnitude of the underlying record.

The filtering process was briefly described in Section 2.10 for a high-pass filter. A similar method, again involving a forward and an inverse Fourier transform, was used for the low-pass filters here. The only difference was that instead of removing low-frequency components from the transforms, high-frequency components were removed. The high-frequency components were removed by setting the magnitudes equal to zero. Due to the use of the Fast Fourier Transform (FFT), only 4096 of the 5120 collected data points were used per history. Since the input motion (to the earthquake simulator) contained a few seconds of zero at both ends of the record, the time window, 4095*0.003082 = 12.6 seconds, was sufficient to capture the strong motion of the structure. Samples of unfiltered and filtered LVDT and accelerometer signals are shown in Figures D.1 and D.2.

Note that while the filtered time histories were used in the analysis of S1, and are plotted in Appendix C, the data stored on the tape archive are in both the unfiltered and filtered form. In this way, future users may analyze the raw data and, if desired, may filter the signals in ways different than those conducted here.

For Test Runs 21 through 24 (of S2), the LVDT arms were stiffened to virtually eliminate all unwanted vibrations. Also, by using all $^5/_{16}$" dia. bolts with the floor weights, the banging of the weights was eliminated. Therefore, no filtering was performed on any of the histories recorded during Test Runs 21 through 24.

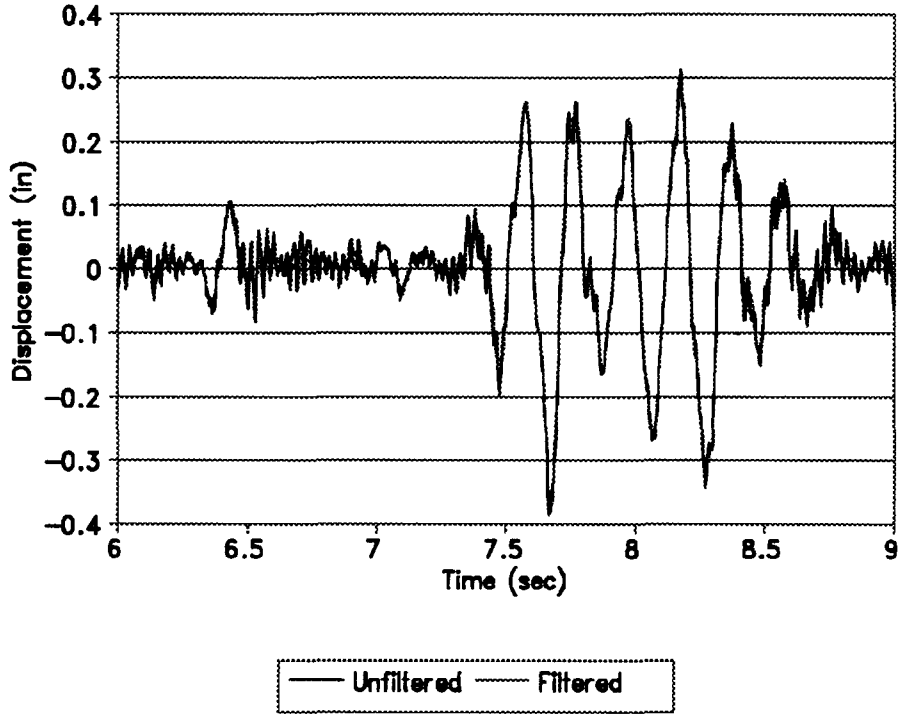

Figure D.1 Unfiltered and Filtered Displacement Histories (EQ14LNW2)

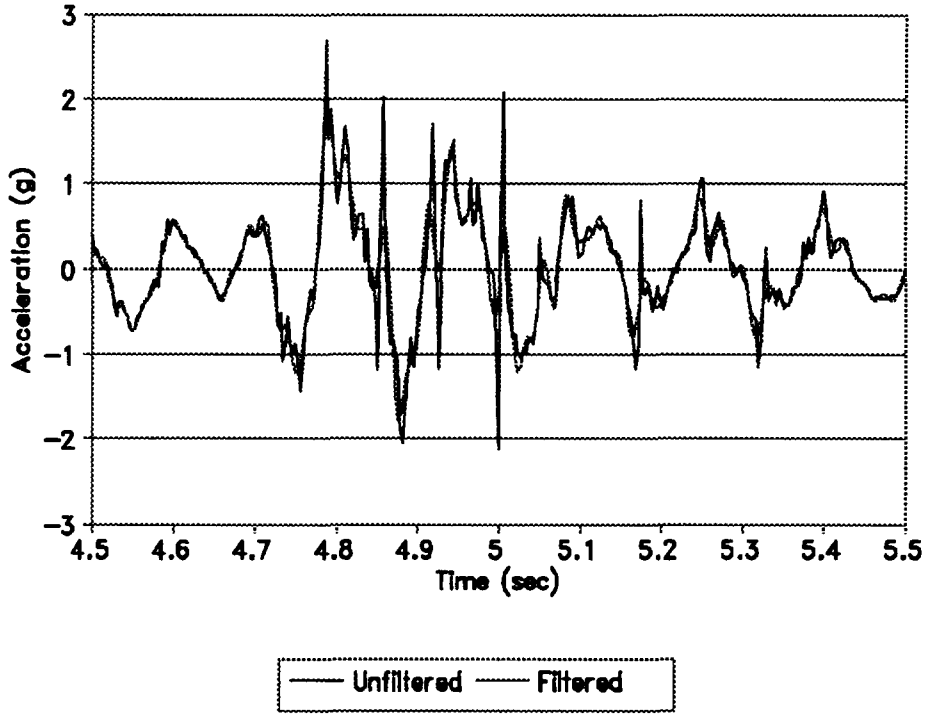

Figure D.2 Unfiltered and Filtered Acceleration Histories (EQ13XB2)

APPENDIX E

ROCKING DISPLACEMENT (VERTICAL) HISTORIES

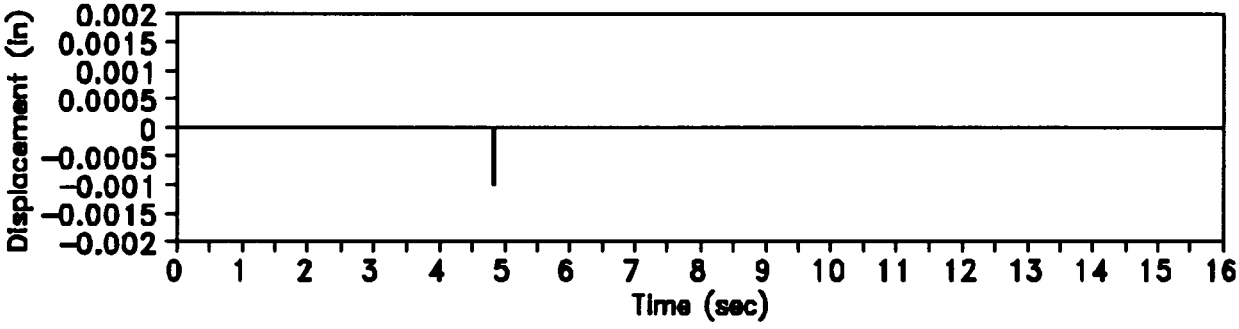

Figure E.1 Top of Left Door-wall Pier, Test Run 21

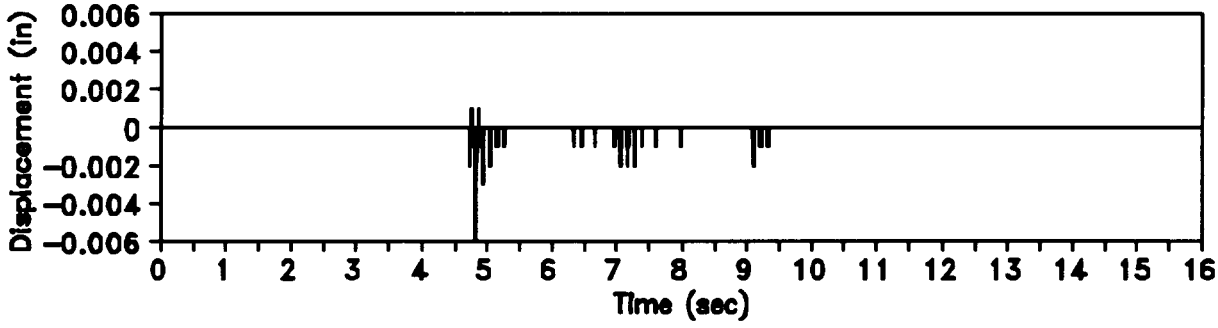

Figure E.2 Top of Left-central Door-wall Pier, Test Run 21

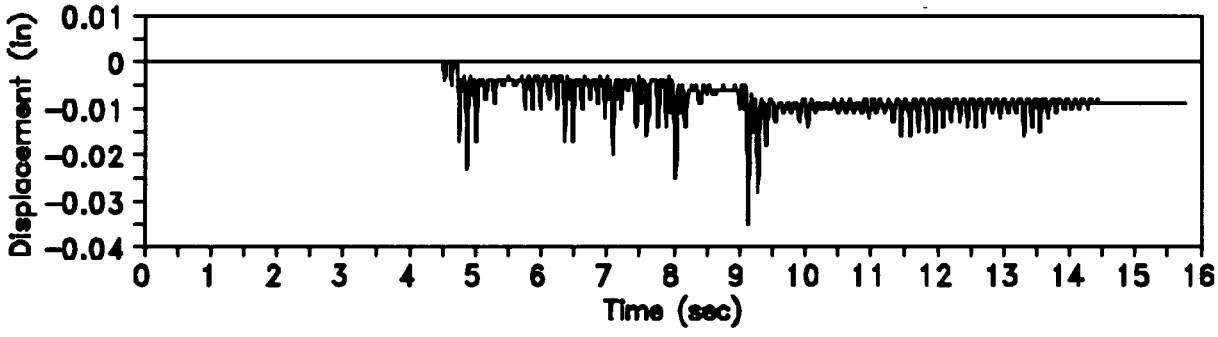

Figure E.3 Top of Left Door-wall Pier, Test Run 22

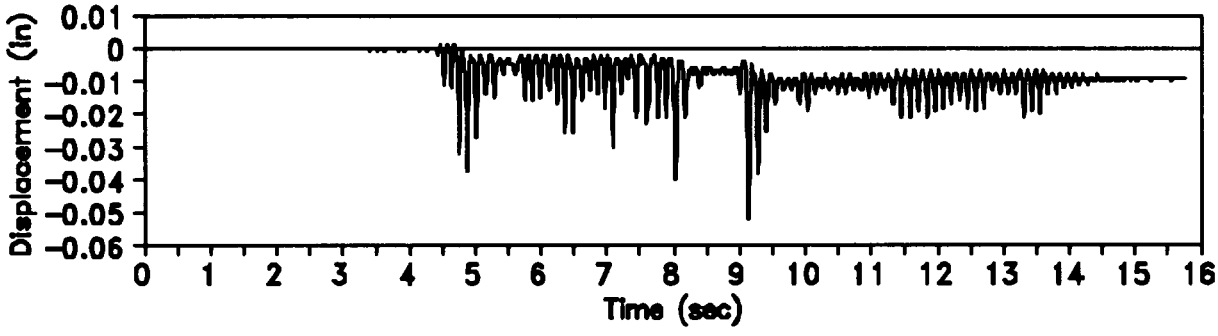

Figure E.4 Top of Left-central Door-wall Pier, Test Run 22

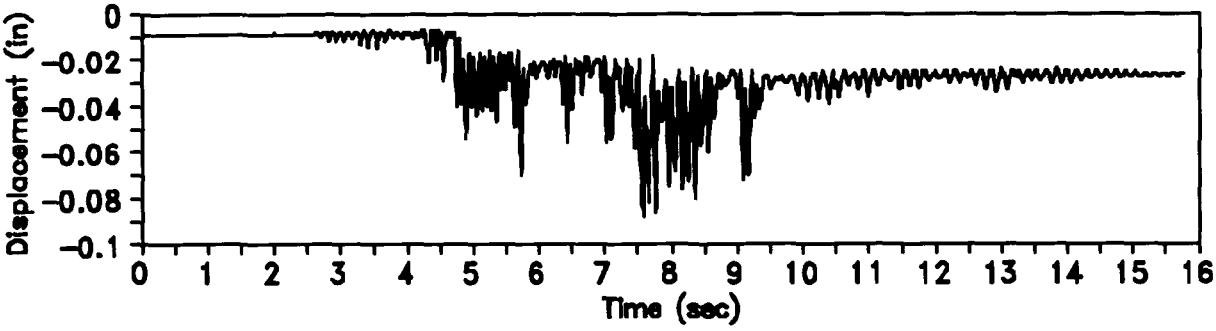

Figure E.5 Top of Left Door-wall Pier, Test Run 23

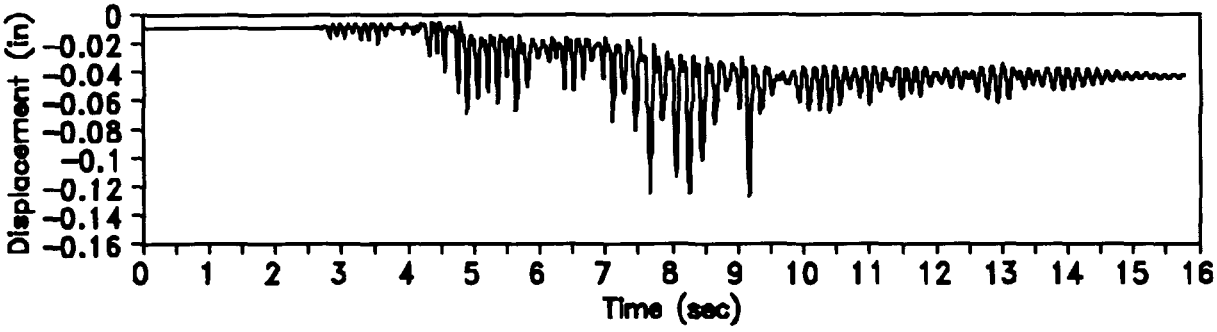

Figure E.6 Top of Left-central Door-wall Pier, Test Run 23

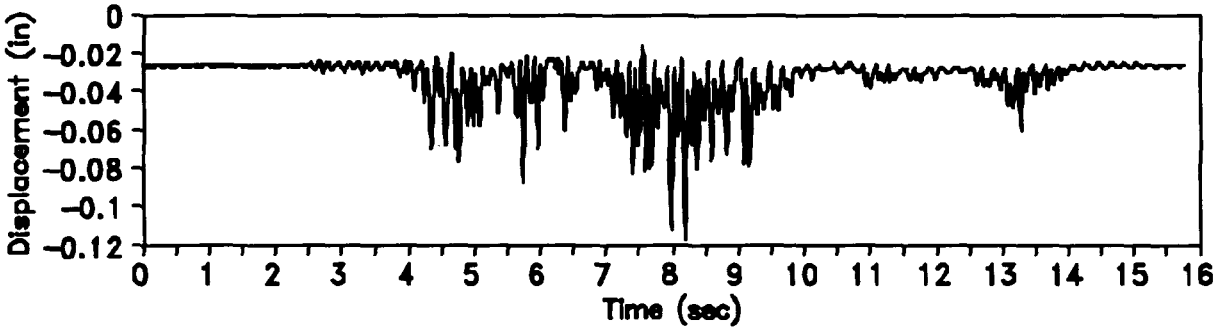

Figure E.7 Top of Left Door-wall Pier, Test Run 24

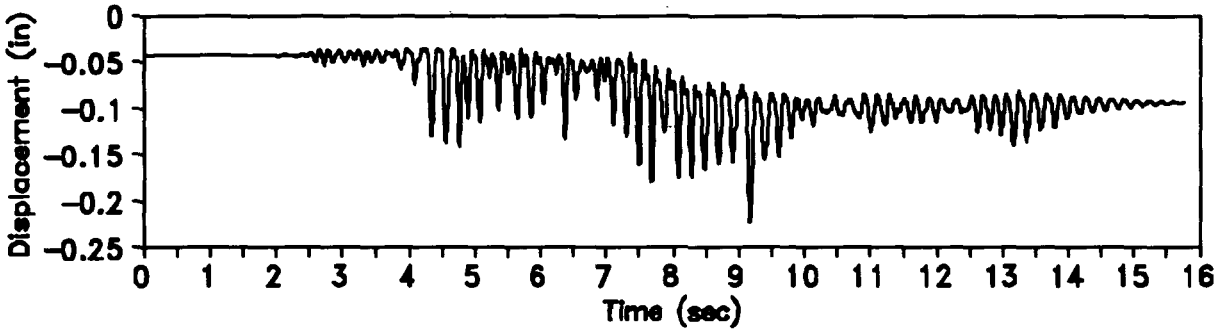

Figure E.8 Top of Left-central Door-wall Pier, Test Run 24

APPENDIX F

NONLINEAR ELASTIC TIME-STEP INTEGRATION

F.1 3-DOF Model

The model that was developed used three degrees of freedom (DOF) to represent S1 and S2 (Figure F.1). One DOF was used for each of two, in-plane, shear walls and the third DOF was used for the diaphragms. The wall DOFs were located at the first level while the second-level masonry was assumed to be rigid. As a result of this assumption, both model diaphragms would receive the same input motion, that of the two wall DOFs. Since both diaphragms also had equal stiffnesses and had equal masses, the two diaphragms were combined in one DOF.

The three DOFs used to model S1 and S2 were chosen for these particular buildings and the programs written were tailormade as well. If the two diaphragms had had unequal stiffnesses or masses, one DOF could have been used for each. Each diaphragm DOF would have, however, still received the same input motions from the two wall DOFs. Also, in theory, additional wall DOFs could have been used if more than two shear walls had existed in one of the buildings.

The diaphragm DOF (#2) was assumed to remain linear throughout the analysis. The two wall DOFs (#1 and #3) used bilinear force-displacement curves (Figure F.2).

- The first portion of the curve was computed by summing the pier stiffnesses from a given wall. Individual pier stiffnesses, k_{pier}, were calculated by

$$k_{pier} = \frac{t E_m}{(H/D)[(H/D)^2 + 3]} \qquad \text{F.1}$$

where t is the thickness of the pier, E_m is the elastic modulus, and H/D is the aspect ratio, height over length. This stiffness assumed both ends of the pier were fixed and included both flexural and shear deformations. Equation F.1 is only valid for piers with rectangular cross sections.

- The second portion of the curve, which had zero slope, represented the rocking behavior. A simple statics study suggested that the force-displacement curve for a rocking, rigid body actually has a slightly negative slope (Figure F.2). Under normal circumstances, a curve with zero slope models rocking extremely well. The force value of the second portion was the sum of PD/H for each pier, where P is the axial load in the pier, and D/H is the aspect ratio, length over height. With this bilinear force-displacement curve, all piers in each wall were assumed to both rock in unison and to have constant rocking strengths. This assumption may not be valid for walls with a wide range of pier aspect ratios or walls which are highly asymmetric.

F.2 Integration Program

A time-step integration program (NLEL) was written to compute the response of the nonlinear elastic, 3-DOF model to base accelerations. A documented Fortran listing of NLEL.FOR follows. The program uses the Newmark-Beta method to solve displacements, velocities, and accelerations at each time step. It should be noted that the program calculates

relative accelerations and that inertial forces are computed from *absolute* accelerations (relative + base). Because of the discontinuity in the wall DOF force-displacement curves, an iterative approach was used rather than a closed-form solution. A second program was written to compute the elastic stiffnesses and rocking strengths of the wall DOFs while a third program was written to interpolate an acceleration history to different time increment (if desired). Documented listings of these two programs, PIER.FOR and INTP.FOR, also follow. Samples of input and output files for PIER and NLEL, along with descriptive information, are given after the program listings.

The integration program (NLEL) was run using input parameters from S1 and S2 and base acceleration histories from Test Runs 14, 15, 23, and 24. Slight variations among the calculated results were evident with different integration time steps, levels of damping, and elastic stiffnesses, but this is to be expected. An average of 10-20 iterations per time step was common. For these runs, the integration parameters were, $\alpha=1/2$, $\beta=1/6$, time step=0.001 seconds, and the relative convergence limit ($|1-a_{i+1}/a_i|$) < 10^{-4} for each of the three accelerations. Note that α, β, and the relative convergence limit (TOL) are fixed within the program, whereas the time step (H) is set by the user in the input file (IN.IN). Currently, the damping coefficient (C) in PIER.FOR is set at 0.1 for all three DOFs. Light damping is recommended for all degrees of freedom.

The purpose for developing the model was to estimate wall displacements resulting from a rocking-dominant behavior. The model was never intended to accurately determine accelerations or base shears. Overall, agreement between calculated results and measured results was surprisingly good considering the simplicity of the model. The program was able to

- estimate the peak wall displacements due to rocking
- determine the times when rocking occurred
- demonstrate the reduction of relative diaphragm displacements during rocking
- demonstrate the shift in frequency from before to during rocking
- estimate the rocking frequency
- demonstrate increases in base shear not proportional to increases in base excitations.

The program was not able to

- consistently determine the time of (measured) peak displacements
- accumulate inelastic displacements or other damage
- accurately match measured inertial-based base shears.

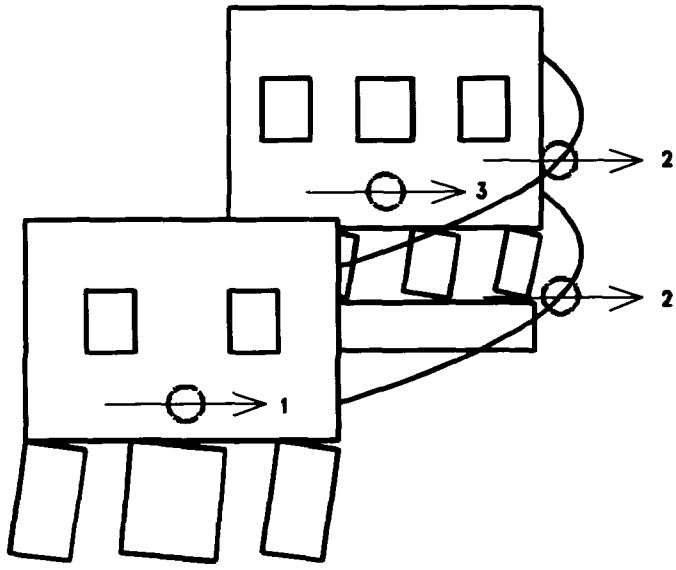

Figure F.1 The 3-DOF Model Used in the Nonlinear Time-step Lntegration.

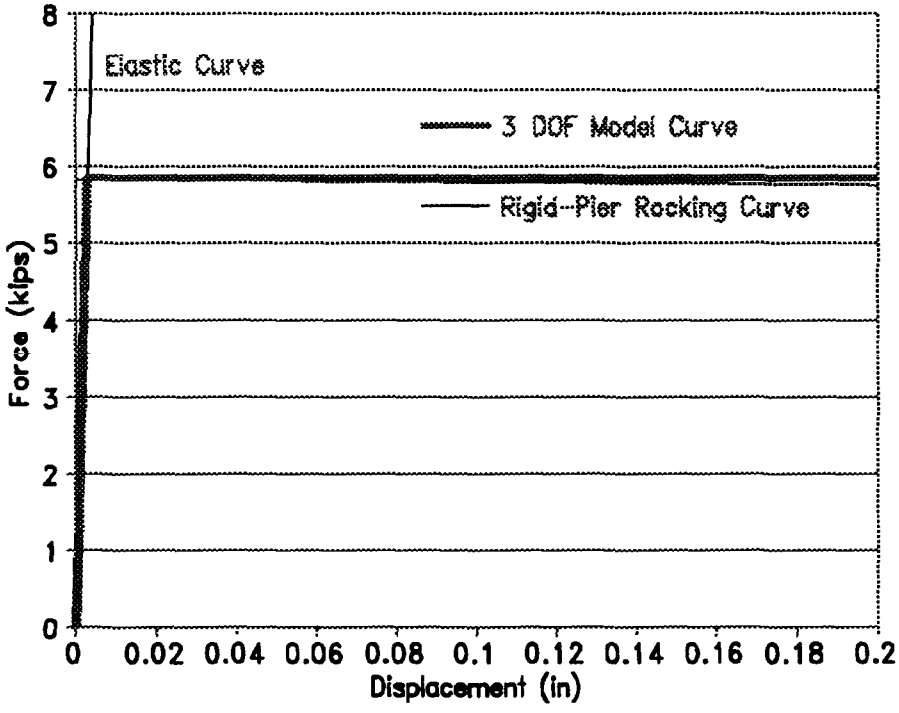

Figure F.2 Theoretical and Approximate (bilinear) Force-displacement Curves for Rocking

```
C NLEL.FOR by Andrew C. Costley

C This program is designed to determine the nonlinear displacements of
C a three degree of freedom system.  An iterative version of the Newmark
C Beta Method is used.  PIER.FOR is intended to complement this program.

C DOF's 1 and 3 are nonlinear elastic and represent the two in-plane,
C rocking, shear walls, while DOF 2 is linear elastic and represents
C the flexible diaphragm(s).

C File ACC.IN is the base acceleration history.
C File IN.IN is the program input file.
C Files DIS.OUT, VEL.OUT, and ACC.OUT are the relative displacement,
C velocity, and acceleration output histories.  Note that relative accel
C must be converted to absolute accel for inertial force calculations.

C Paragraph 1 is variable declaration and array sizing.
C Paragraph 2 opens the appropriate input and output files.
C Paragraph 3 inputs the mass, stiffness, and damping properties from IN.IN.
C Paragraph 4 inputs the ground motion from ACC.IN into an array called XG.
C Paragraph 5 initializes the working disp, vel, and acc arrays.
C Note that XI=disp, XDOTI=vel, and XDDOTI=accel of the ith time step
C and XIPO=disp, XDOTIPO=vel, and XDDOTIP=accel of the i plus one time
C step.  After each time step has converged, values are written to output
C files and are not stored by the program.

C M, C, and K, are mass, damping and stiffess values.
C LIMIT(I) is the rocking strengths of the walls.
C ERR(I) is the relative error used to judge convergence and TOL is the
C convergence limit.
C T is the sum of the time increments.

C H is the time step or increment.  To change the integration time step,
C interpolate the base accel history to the desired integration time step.
C A lightly documented example of an interpolation program is given
C in INTP.FOR.

C ICOUNT is the convergence check variable for the iterative method.  If
C convergence at any time step is not achieved in 100 iterations, the
C programs aborts "goto 999".  KOUNT keeps track of the total number of
C iterations performed through all time steps.

C The program actually starts with the "do 900 while" line.
C Line "do 200" calculates the i plus one estimates of the disp and vel,
C based on the ith values of disp, vel, and the ASSUMED i plus one values
C of accel.

C Lines "keff(1)= etc" determine the linear values of the k[11]*x[1] and
C k[33]*x[3] terms of the equation of motion.  The next lines
C "if (keff(1).gt. etc" check to see if either spring is in the nonlinear
C range.  If so, LIMIT(1) or LIMIT(3) is assigned to KEFF(1) or KEFF(3).
C LIMIT(1) and LIMIT(3) are the rocking strengths of the two shear walls.

C The next three lines, "xddotip(1)= etc" calculate the ACTUAL i plus one
C value of accel by solving the equation of motion using the i plus one
C values of disp and vel, the current XG, and the current KEFF.

C The ACTUAL and ASSUMED values of accel are compared in "do 330".

C If the ACTUAL i plus one values of accel are within the tolerance of the
C ASSUMED values (stored in TEMP) then the disp, vel, and accel are written
C to the appropriate output files.  The disp are checked for being a
```

```
C maxima by "do 350".  The i plus one values of disp, vel, and accel are put
C into the i values "do 400" and the program increments one time step
C at line 900.  The ASSUMED accel values for the new time step are the
C converged accel values from the previous time step "temp(i)=xddotip(i)".
C For the first time step, the ASSUMED accel values are initially 0.00001.

C If the ACTUAL i plus one values of accel are NOT within the tolerance of
C the ASSUMED values, then the ASSUMED values are replaced with the ACTUAL
C i plus one values "do 320" and another iteration is performed by
C "goto 150".

C The relative error between the ASSUMED and ACTUAL accels is used and
C all three accels must be within tolerance or the time step will be
C iterated again.  The use of double precision variables was necessary
C to prevent the accel values from flip-flopping back and forth just
C outside the tolerance.

C The program ends by displaying the three displacement maxima calculated.
C Iteration data is also displayed to determine if the entire history was
C computed.  L is the number of time steps that converged and should be
C roughly (TEND/H)+1 for a successful program run.

C Note that NLEL.FOR was intended for a pair of specific structural
C models (3DOF) and cannot, in its current form, model everything.
C Slight modifications should be able to be made to extend the program
C for larger models.


c234567
      parameter(nsteps=8000)
      double precision xddoti(3),xddotip(3),temp(3),
     2 xi(3),xipo(3),xdoti(3),xdotipo(3),keff(3)
      real t,h,tol,err(3),k(3,3),m(3),c,xg(nsteps),
     2 limit(3),max(3)
      integer i,j,kount,l,ndof,ncount
c
      open(unit=20,file='acc.in')
      open(unit=25,file='in.in')
      open(unit=30,file='dis.out')
      open(unit=40,file='vel.out')
      open(unit=50,file='acc.out')
c
      NDOF=3
      read(25,*) m(1),m(2),m(3),c,k(1,1),k(2,2),
     2          k(3,3),k(1,2),k(2,3)
      k(2,1)=k(1,2)
      k(3,2)=k(2,3)
      read(25,*) tend,h,limit(1),limit(3)
      TOL=0.0001
      BETA=0.166667
c
      ncount=int(tend/h)
      xg(1)=0.0001
      do 90 i=1,ncount
         read(20,*) xg(i+1)
         xg(i+1)=xg(i+1)*386.4
  90    continue
c
      do 100 i=1,ndof
        temp(i)=0.00001
        xi(i)=0.0
        xdoti(i)=0.0
```

```
        xddoti(i)=0.0
 100    continue
      l=0
      kount=0
      t=0.0
c
      do 900 while (t.lt.tend)
        l=l+1
        icount=0
c
  150   icount=icount+1
        if (icount.gt.99) goto 999
        do 200 i=1,ndof
          xipo(i)=xi(i)+h*xdoti(i)+h*h*((0.5-beta)*
     2           xddoti(i)+beta*temp(i))
          xdotipo(i)=xdoti(i)+h*(0.5*xddoti(i)+0.5*temp(i))
  200     continue
c
         keff(1)=k(1,1)*xipo(1)
         keff(3)=k(3,3)*xipo(3)
c
         if (keff(1).gt.limit(1)) then
             keff(1)=limit(1)
             else
             if (keff(1).lt.-limit(1)) then
                 keff(1)=-limit(1)
             endif
             endif
c
         if (keff(3).gt.limit(3)) then
             keff(3)=limit(3)
             else
             if (keff(3).lt.-limit(3)) then
                 keff(3)=-limit(3)
             endif
             endif
c
        xddotip(1)=-xg(1)-keff(1)/m(1)-xipo(1)/m(1)*k(1,2)+
     2             k(1,2)/m(1)*xipo(2)-c*xdotipo(1)/m(1)
c
        xddotip(2)=-xg(1)-k(2,2)/m(2)*xipo(2)+k(2,1)/m(2)*
     2     xipo(1)+k(2,3)/m(2)*xipo(3)-c*xdotipo(2)/m(2)
c
        xddotip(3)=-xg(1)-keff(3)/m(3)-xipo(3)/m(3)*k(3,2)+
     2             k(3,2)/m(3)*xipo(2)-c*xdotipo(3)/m(3)
c
        kount=kount+1
c
        do 330 i=1,ndof
          err(i)=abs(1-(xddotip(i)/temp(i)))
          if (err(i).gt.tol) then
            do 320 j=1,ndof
              temp(j)=xddotip(j)
 320          continue
            goto 150
            endif
 330      continue
c
         write(30,301) (xipo(i),i=1,ndof),xg(1)
         write(40,301) (xdotipo(i),i=1,ndof),xg(1)
         write(50,301) (xddotip(i),i=1,ndof),xg(1)
c
```

```
 301     format(4f15.6)
c
         do 350, i=1,ndof
           if (abs(xipo(i)).gt.abs(max(i))) then
             max(i)=xipo(i)
             endif
 350       continue
c
         do 400 i=1,ndof
           xi(i)=xipo(i)
           xdoti(i)=xdotipo(i)
           xddoti(i)=xddotip(i)
           temp(i)=xddotip(i)
 400       continue
c
        t=t+h
 900    continue
 999   write(*,*) '# of iterations = ',icount,'   ',l,kount
 410   format(3f9.5)
       write(*,410) (max(i), i=1,ndof)
       stop
       end
```

```
C PIER.FOR by Andrew C. Costley

C This program is designed to create the bulk of the input file
C required to run NLEL.FOR for the three DOF system used to model two
C specific test structures.  Currently, PIER.FOR is set up for
C 2 walls (with a total of 7 piers) and two levels of equivalent
C diaphragms spanning the 2 walls.

C Material and geometric properties of the first story piers and the
C diaphragm are read into the program via PIER.IN.

C The main purpose of the program is to estimate an elastic stiffness and
C a rocking strength for each shear wall.  Mass and diaphragm stiffness
C properties are input from PIER.IN and output to PIER.OUT in a form
C appropriate to be used by NLEL.FOR (for the 3DOF system).  After running
C PIER.FOR, TEND and H must be added to the beginning of line 2 in
C PIER.OUT.  PIER.OUT can then be renamed IN.IN for use with NLEL.FOR.
C Time parameters were not included in PIER.FOR so that the structural
C model could stand alone.

C E is the elastic modulus of the piers and NWALL is the number of walls
C in the model.
C KDIA and MDIA are the elastic stiffness and mass of one diaphragm.
C NPIER is the number of piers in a wall.  T is the thickness of the wall.
C M is the total mass tributary to the wall DOF.
C L and H are the length and height of each pier.  DL is the dead load
C stress attributable to each pier.

C Elastic wall stiffnesses are calculated assuming fixed pier ends and both
C shear and flexural deformations.  KPIER is the elastic stiffness of each
C pier save T and E. TEMP2 sums the KPIERs for each wall while K(I,I)
C multiplies the final sum by T and E.
C The stiffness components are organized in PIER.OUT so that the diaphragm
C degree of freedom is #2.

C Rocking strengths are determined using P*L/H.  P is estimated using an
C input vertical stress (DL) over the area of the pier (L*T). TEMP1 adds
C the rocking strengths of the piers within a wall and the sum is saved
C as ROCKSUM.

C Within the loops "do 30" and "do 25", the variable INDEX increments
C toward the total number of piers, while the J variable increments the
C number of piers in a given wall.

C The program ends by writing a two line output file PIER.OUT.

C Note that PIER.FOR was intended for a pair of specific structural
C models (3DOF) and cannot, in its current form, model everything.
C Slight modifications should be able to be made to extend the program
C for larger models.



c234567
      parameter(maxwall=2, maxpier=7)
      real dl(maxpier), t(maxwall), h(maxpier), l(maxpier),
     2 ver(maxpier), E, rock(maxpier), rocksum(maxwall),
     3 kpier(maxpier), k(3,3), kdia, mdia, m(3), temp1, temp2
      integer npier(maxwall), index, i, j, isum, nwall
c
```

```
      open(unit=20, file='pier.in')
      open(unit=30, file='pier.out')
c
      read(20,*) E, nwall
      read(20,*) kdia, mdia
      do 5 i=1,nwall
        read(20,*) npier(i), t(i), m(i)
    5   continue
      isum=0
      do 10 i=1,nwall
        isum=isum+npier(i)
   10   continue
      do 20 i=1,isum
        read(20,*) l(i), h(i), dl(i)
   20   continue
c
      index=0
      do 30 i=1,nwall
        temp1=0.0
        temp2=0.0
        do 25 j=1,npier(i)
          index=index+1
          ver(index)=dl(index)*t(i)*l(index)
          rock(index)=ver(index)*l(index)/h(index)
          temp1=temp1+rock(index)
          kpier(index)=(h(index)/l(index))*
     2             ((h(index)/l(index))**2+3.)
          temp2=temp2+1./kpier(index)
   25     continue
        rocksum(i)=temp1
        k(i,i)=temp2*t(i)*E
   30   continue
c
      m(3)=m(2)
      m(2)=2*mdia
      k(3,3)=k(2,2)
      k(2,2)=kdia*2.0
      k(1,2)=kdia
      k(2,3)=kdia
c
      c=.1
      write(30,100) m(1),m(2),m(3),c,k(1,1),k(2,2),
     2 k(3,3),k(1,2),k(2,3)
      write(30,110) rocksum(1),rocksum(2)
  100 format(3f8.5,f4.2,5f7.0)
  110 format(2f8.3)
      stop
      end
```

```
C INTP.FOR by Andrew C. Costley

C This program reads a column of numbers from a file called ACC.OLD with a
C time step of DTOLD and interpolates them to a time step of DTNEW and
C writes the new series to ACC.NEW, in a single column.  Also required is
C NOLD, the number of values in the original series.

C OLD stores the original series, while NEW stores the new series.
C IOLD and INEW are array indicies for the two arrays.
C TOLD and TNEW are the current times in the respective series.
C DX is the difference between values in the OLD series.

C The body of the program is contained between lines 150 and 900 in two
C nested do while loops "do 900" and "do 800".  NEW increments within
C OLD "inew=inew+1" (linear interpolation) until TNEW exceeds TOLD.
C OLD then increments "iold=iold+1" and an updated DX is calculated.

C At the end of the program NEW is written to ACC.NEW.


c234567
      real old(3000),new(10000),dtold,dtnew,told,tnew,dx
      integer nold,iold,inew
c
      open(unit=20,file='acc.old')
      open(unit=30,file='acc.new')
c
      write(*,*) 'how many old data points, dt-old, dt-new'
      read(*,*) nold, dtold, dtnew
      do 100 i=1,nold
        read(20,*) old(i)
 100    continue
c
      iold=1
      inew=1
      told=0.0
      tnew=dtnew
      new(1)=old(1)
c
 150  do 900 while (iold.lt.nold)
        told=told+dtold
        dx=old(iold+1)-old(iold)
c
 200    do 800 while (tnew.le.told)
          inew=inew+1
c
          new(inew)=old(iold)+(tnew-(told-dtold))/dtold*dx
          tnew=tnew+dtnew
c
 800      continue
        iold=iold+1
 900    continue
c
      do 950 i=1,inew
        write(30,*) new(i)
 950    continue
c
      stop
      end
```

```
 0.015
-0.014
-0.029
-0.031
-0.025
```

(==========)

(The following is an example of an output file "DIS.OUT". Only the top eleven lines are presented. Note that zeros are assumed for the initial conditions (assumed by NLEL.FOR). The last ten XG values correspond with the XG values listed above in ACC.IN. "VEL.OUT" and "ACC.OUT" have similar formats. Everything enclosed by parentheses is for explanation only.)

(Displacements (in)			XG
DOF #1	DOF #2	DOF #3	(in/sec^2))
.000000	.000000	.000000	.000100
.000011	.000016	.000010	-10.046400
.000040	.000085	.000032	6.182400
-.000037	.000098	-.000047	18.933600
-.000158	-.000057	-.000121	23.184000
-.000136	-.000414	-.000056	17.388000
.000006	-.000912	.000020	5.796000
.000064	-.001436	-.000013	-5.409600
-.000012	-.001874	-.000035	-11.205600
-.000058	-.002160	.000024	-11.978400
.000005	-.002279	.000029	-9.660000

(==========)

(The following is an example of an input file for PIER.FOR, "PIER.IN".
MDIA and M(I) are mass units. Other units are kips and in. Everything
enclosed by parentheses is for explanation only.)

```
1425. 2                    (E, NWALL)
36. .01294                 (KDIA, MDIA)
3 3.7 .00707               (NWALL(1), T(1), M(1))
4 3.7 .00676               (NWALL(2), T(2), M(2))
17.29 31.98 .0331          (L(1), H(1), DL(1))    (Wall #1)
26.99 31.98 .0357                  .
17.29 31.98 .0331                  .
9.52 17.99 .0398                   .              (Wall #2)
13.41 17.99 .0484                  .
13.41 17.99 .0484                  .
9.52 17.99 .0398           (L(7), H(7), DL(7))
```

(==========)

(The following is an example of an output file from PIER.FOR, "PIER.OUT".
Everything enclosed by parentheses is for explanation only. Note that
the diaphragm is now DOF #2.)

```
  .00707  .02588  .00676 .10  1898.    72.  2487.    36.    36.
   5.298   5.064

( M(1)    M(2)    M(3)   C    K(1,1) K(2,2) K(3,3)   K(1,2) K(2,3)
   ROCKSUM(1) ROCKSUM(2) )
```

(==========)

(The following is an example of an input file for NLEL.FOR, "IN.IN"
Everything enclosed by parentheses is for explanation only.)

```
.00707 .02588 .00676 .10 1898 72 2487 36 36
7.49 .003082 5.298 5.064

(M(1)  M(2)   M(3)   C   K(1,1) K(2,2) K(3,3) K(1,2) K(2,3)
TEND H       ROCKSUM(1) ROCKSUM(2) )
```

(==========)

(The following is an example of the input file "ACC.IN". Only the top ten
lines are presented. ACC.IN should be a single column of values, in terms
of g. Format of each value is left to the user. Everything enclosed
by parentheses is for explanation only.)

```
      -0.026
       0.016
       0.049
        0.06
       0.045
```

NATIONAL CENTER FOR EARTHQUAKE ENGINEERING RESEARCH
LIST OF TECHNICAL REPORTS

The National Center for Earthquake Engineering Research (NCEER) publishes technical reports on a variety of subjects related to earthquake engineering written by authors funded through NCEER. These reports are available from both NCEER Publications and the National Technical Information Service (NTIS). Requests for reports should be directed to NCEER Publications, National Center for Earthquake Engineering Research, State University of New York at Buffalo, Red Jacket Quadrangle, Buffalo, New York 14261. Reports can also be requested through NTIS, 5285 Port Royal Road, Springfield, Virginia 22161. NTIS accession numbers are shown in parenthesis, if available.

NCEER-87-0001 "First-Year Program in Research, Education and Technology Transfer," 3/5/87, (PB88-134275, A04, MF-A01).

NCEER-87-0002 "Experimental Evaluation of Instantaneous Optimal Algorithms for Structural Control," by R.C. Lin, T.T. Soong and A.M. Reinhorn, 4/20/87, (PB88-134341, A04, MF-A01).

NCEER-87-0003 "Experimentation Using the Earthquake Simulation Facilities at University at Buffalo," by A.M. Reinhorn and R.L. Ketter, to be published.

NCEER-87-0004 "The System Characteristics and Performance of a Shaking Table," by J.S. Hwang, K.C. Chang and G.C. Lee, 6/1/87, (PB88-134259, A03, MF-A01). This report is available only through NTIS (see address given above).

NCEER-87-0005 "A Finite Element Formulation for Nonlinear Viscoplastic Material Using a Q Model," by O. Gyebi and G. Dasgupta, 11/2/87, (PB88-213764, A08, MF-A01).

NCEER-87-0006 "Symbolic Manipulation Program (SMP) - Algebraic Codes for Two and Three Dimensional Finite Element Formulations," by X. Lee and G. Dasgupta, 11/9/87, (PB88-218522, A05, MF-A01).

NCEER-87-0007 "Instantaneous Optimal Control Laws for Tall Buildings Under Seismic Excitations," by J.N. Yang, A. Akbarpour and P. Ghaemmaghami, 6/10/87, (PB88-134333, A06, MF-A01). This report is only available through NTIS (see address given above).

NCEER-87-0008 "IDARC: Inelastic Damage Analysis of Reinforced Concrete Frame - Shear-Wall Structures," by Y.J. Park, A.M. Reinhorn and S.K. Kunnath, 7/20/87, (PB88-134325, A09, MF-A01). This report is only available through NTIS (see address given above).

NCEER-87-0009 "Liquefaction Potential for New York State: A Preliminary Report on Sites in Manhattan and Buffalo," by M. Budhu, V. Vijayakumar, R.F. Giese and L. Baumgras, 8/31/87, (PB88-163704, A03, MF-A01). This report is available only through NTIS (see address given above).

NCEER-87-0010 "Vertical and Torsional Vibration of Foundations in Inhomogeneous Media," by A.S. Veletsos and K.W. Dotson, 6/1/87, (PB88-134291, A03, MF-A01). This report is only available through NTIS (see address given above).

NCEER-87-0011 "Seismic Probabilistic Risk Assessment and Seismic Margins Studies for Nuclear Power Plants," by Howard H.M. Hwang, 6/15/87, (PB88-134267, A03, MF-A01). This report is only available through NTIS (see address given above).

NCEER-87-0012 "Parametric Studies of Frequency Response of Secondary Systems Under Ground-Acceleration Excitations," by Y. Yong and Y.K. Lin, 6/10/87, (PB88-134309, A03, MF-A01). This report is only available through NTIS (see address given above).

NCEER-87-0013 "Frequency Response of Secondary Systems Under Seismic Excitation," by J.A. HoLung, J. Cai and Y.K. Lin, 7/31/87, (PB88-134317, A05, MF-A01). This report is only available through NTIS (see address given above).

NCEER-87-0014 "Modelling Earthquake Ground Motions in Seismically Active Regions Using Parametric Time Series Methods," by G.W. Ellis and A.S. Cakmak, 8/25/87, (PB88-134283, A08, MF-A01). This report is only available through NTIS (see address given above).

NCEER-87-0015 "Detection and Assessment of Seismic Structural Damage," by E. DiPasquale and A.S. Cakmak, 8/25/87, (PB88-163712, A05, MF-A01). This report is only available through NTIS (see address given above).

NCEER-87-0016 "Pipeline Experiment at Parkfield, California," by J. Isenberg and E. Richardson, 9/15/87, (PB88-163720, A03, MF-A01). This report is available only through NTIS (see address given above).

NCEER-87-0017 "Digital Simulation of Seismic Ground Motion," by M. Shinozuka, G. Deodatis and T. Harada, 8/31/87, (PB88-155197, A04, MF-A01). This report is available only through NTIS (see address given above).

NCEER-87-0018 "Practical Considerations for Structural Control: System Uncertainty, System Time Delay and Truncation of Small Control Forces," J.N. Yang and A. Akbarpour, 8/10/87, (PB88-163738, A08, MF-A01). This report is only available through NTIS (see address given above).

NCEER-87-0019 "Modal Analysis of Nonclassically Damped Structural Systems Using Canonical Transformation," by J.N. Yang, S. Sarkani and F.X. Long, 9/27/87, (PB88-187851, A04, MF-A01).

NCEER-87-0020 "A Nonstationary Solution in Random Vibration Theory," by J.R. Red-Horse and P.D. Spanos, 11/3/87, (PB88-163746, A03, MF-A01).

NCEER-87-0021 "Horizontal Impedances for Radially Inhomogeneous Viscoelastic Soil Layers," by A.S. Veletsos and K.W. Dotson, 10/15/87, (PB88-150859, A04, MF-A01).

NCEER-87-0022 "Seismic Damage Assessment of Reinforced Concrete Members," by Y.S. Chung, C. Meyer and M. Shinozuka, 10/9/87, (PB88-150867, A05, MF-A01). This report is available only through NTIS (see address given above).

NCEER-87-0023 "Active Structural Control in Civil Engineering," by T.T. Soong, 11/11/87, (PB88-187778, A03, MF-A01).

NCEER-87-0024 "Vertical and Torsional Impedances for Radially Inhomogeneous Viscoelastic Soil Layers," by K.W. Dotson and A.S. Veletsos, 12/87, (PB88-187786, A03, MF-A01).

NCEER-87-0025 "Proceedings from the Symposium on Seismic Hazards, Ground Motions, Soil-Liquefaction and Engineering Practice in Eastern North America," October 20-22, 1987, edited by K.H. Jacob, 12/87, (PB88-188115, A23, MF-A01).

NCEER-87-0026 "Report on the Whittier-Narrows, California, Earthquake of October 1, 1987," by J. Pantelic and A. Reinhorn, 11/87, (PB88-187752, A03, MF-A01). This report is available only through NTIS (see address given above).

NCEER-87-0027 "Design of a Modular Program for Transient Nonlinear Analysis of Large 3-D Building Structures," by S. Srivastav and J.F. Abel, 12/30/87, (PB88-187950, A05, MF-A01). This report is only available through NTIS (see address given above).

NCEER-87-0028 "Second-Year Program in Research, Education and Technology Transfer," 3/8/88, (PB88-219480, A04, MF-A01).

NCEER-88-0001 "Workshop on Seismic Computer Analysis and Design of Buildings With Interactive Graphics," by W. McGuire, J.F. Abel and C.H. Conley, 1/18/88, (PB88-187760, A03, MF-A01). This report is only available through NTIS (see address given above).

NCEER-88-0002 "Optimal Control of Nonlinear Flexible Structures," by J.N. Yang, F.X. Long and D. Wong, 1/22/88, (PB88-213772, A06, MF-A01).

NCEER-88-0003 "Substructuring Techniques in the Time Domain for Primary-Secondary Structural Systems," by G.D. Manolis and G. Juhn, 2/10/88, (PB88-213780, A04, MF-A01).

NCEER-88-0004 "Iterative Seismic Analysis of Primary-Secondary Systems," by A. Singhal, L.D. Lutes and P.D. Spanos, 2/23/88, (PB88-213798, A04, MF-A01).

NCEER-88-0005 "Stochastic Finite Element Expansion for Random Media," by P.D. Spanos and R. Ghanem, 3/14/88, (PB88-213806, A03, MF-A01).

NCEER-88-0006 "Combining Structural Optimization and Structural Control," by F.Y. Cheng and C.P. Pantelides, 1/10/88, (PB88-213814, A05, MF-A01).

NCEER-88-0007 "Seismic Performance Assessment of Code-Designed Structures," by H.H-M. Hwang, J-W. Jaw and H-J. Shau, 3/20/88, (PB88-219423, A04, MF-A01). This report is only available through NTIS (see address given above).

NCEER-88-0008 "Reliability Analysis of Code-Designed Structures Under Natural Hazards," by H.H-M. Hwang, H. Ushiba and M. Shinozuka, 2/29/88, (PB88-229471, A07, MF-A01). This report is only available through NTIS (see address given above).

NCEER-88-0009 "Seismic Fragility Analysis of Shear Wall Structures," by J-W Jaw and H.H-M. Hwang, 4/30/88, (PB89-102867, A04, MF-A01).

NCEER-88-0010 "Base Isolation of a Multi-Story Building Under a Harmonic Ground Motion - A Comparison of Performances of Various Systems," by F-G Fan, G. Ahmadi and I.G. Tadjbakhsh, 5/18/88, (PB89-122238, A06, MF-A01). This report is only available through NTIS (see address given above).

NCEER-88-0011 "Seismic Floor Response Spectra for a Combined System by Green's Functions," by F.M. Lavelle, L.A. Bergman and P.D. Spanos, 5/1/88, (PB89-102875, A03, MF-A01).

NCEER-88-0012 "A New Solution Technique for Randomly Excited Hysteretic Structures," by G.Q. Cai and Y.K. Lin, 5/16/88, (PB89-102883, A03, MF-A01).

NCEER-88-0013 "A Study of Radiation Damping and Soil-Structure Interaction Effects in the Centrifuge," by K. Weissman, supervised by J.H. Prevost, 5/24/88, (PB89-144703, A06, MF-A01).

NCEER-88-0014 "Parameter Identification and Implementation of a Kinematic Plasticity Model for Frictional Soils," by J.H. Prevost and D.V. Griffiths, to be published.

NCEER-88-0015 "Two- and Three- Dimensional Dynamic Finite Element Analyses of the Long Valley Dam," by D.V. Griffiths and J.H. Prevost, 6/17/88, (PB89-144711, A04, MF-A01).

NCEER-88-0016 "Damage Assessment of Reinforced Concrete Structures in Eastern United States," by A.M. Reinhorn, M.J. Seidel, S.K. Kunnath and Y.J. Park, 6/15/88, (PB89-122220, A04, MF-A01). This report is only available through NTIS (see address given above).

NCEER-88-0017 "Dynamic Compliance of Vertically Loaded Strip Foundations in Multilayered Viscoelastic Soils," by S. Ahmad and A.S.M. Israil, 6/17/88, (PB89-102891, A04, MF-A01).

NCEER-88-0018 "An Experimental Study of Seismic Structural Response With Added Viscoelastic Dampers," by R.C. Lin, Z. Liang, T.T. Soong and R.H. Zhang, 6/30/88, (PB89-122212, A05, MF-A01). This report is available only through NTIS (see address given above).

NCEER-88-0019 "Experimental Investigation of Primary - Secondary System Interaction," by G.D. Manolis, G. Juhn and A.M. Reinhorn, 5/27/88, (PB89-122204, A04, MF-A01).

NCEER-88-0020 "A Response Spectrum Approach For Analysis of Nonclassically Damped Structures," by J.N. Yang, S. Sarkani and F.X. Long, 4/22/88, (PB89-102909, A04, MF-A01).

NCEER-88-0021 "Seismic Interaction of Structures and Soils: Stochastic Approach," by A.S. Veletsos and A.M. Prasad, 7/21/88, (PB89-122196, A04, MF-A01). This report is only available through NTIS (see address given above).

NCEER-88-0022 "Identification of the Serviceability Limit State and Detection of Seismic Structural Damage," by E. DiPasquale and A.S. Cakmak, 6/15/88, (PB89-122188, A05, MF-A01). This report is available only through NTIS (see address given above).

NCEER-88-0023 "Multi-Hazard Risk Analysis: Case of a Simple Offshore Structure," by B.K. Bhartia and E.H. Vanmarcke, 7/21/88, (PB89-145213, A05, MF-A01).

NCEER-88-0024 "Automated Seismic Design of Reinforced Concrete Buildings," by Y.S. Chung, C. Meyer and M. Shinozuka, 7/5/88, (PB89-122170, A06, MF-A01). This report is available only through NTIS (see address given above).

NCEER-88-0025 "Experimental Study of Active Control of MDOF Structures Under Seismic Excitations," by L.L. Chung, R.C. Lin, T.T. Soong and A.M. Reinhorn, 7/10/88, (PB89-122600, A04, MF-A01).

NCEER-88-0026 "Earthquake Simulation Tests of a Low-Rise Metal Structure," by J.S. Hwang, K.C. Chang, G.C. Lee and R.L. Ketter, 8/1/88, (PB89-102917, A04, MF-A01).

NCEER-88-0027 "Systems Study of Urban Response and Reconstruction Due to Catastrophic Earthquakes," by F. Kozin and H.K. Zhou, 9/22/88, (PB90-162348, A04, MF-A01).

NCEER-88-0028 "Seismic Fragility Analysis of Plane Frame Structures," by H.H-M. Hwang and Y.K. Low, 7/31/88, (PB89-131445, A06, MF-A01).

NCEER-88-0029 "Response Analysis of Stochastic Structures," by A. Kardara, C. Bucher and M. Shinozuka, 9/22/88, (PB89-174429, A04, MF-A01).

NCEER-88-0030 "Nonnormal Accelerations Due to Yielding in a Primary Structure," by D.C.K. Chen and L.D. Lutes, 9/19/88, (PB89-131437, A04, MF-A01).

NCEER-88-0031 "Design Approaches for Soil-Structure Interaction," by A.S. Veletsos, A.M. Prasad and Y. Tang, 12/30/88, (PB89-174437, A03, MF-A01). This report is available only through NTIS (see address given above).

NCEER-88-0032 "A Re-evaluation of Design Spectra for Seismic Damage Control," by C.J. Turkstra and A.G. Tallin, 11/7/88, (PB89-145221, A05, MF-A01).

NCEER-88-0033 "The Behavior and Design of Noncontact Lap Splices Subjected to Repeated Inelastic Tensile Loading," by V.E. Sagan, P. Gergely and R.N. White, 12/8/88, (PB89-163737, A08, MF-A01).

NCEER-88-0034 "Seismic Response of Pile Foundations," by S.M. Mamoon, P.K. Banerjee and S. Ahmad, 11/1/88, (PB89-145239, A04, MF-A01).

NCEER-88-0035 "Modeling of R/C Building Structures With Flexible Floor Diaphragms (IDARC2)," by A.M. Reinhorn, S.K. Kunnath and N. Panahshahi, 9/7/88, (PB89-207153, A07, MF-A01).

NCEER-88-0036 "Solution of the Dam-Reservoir Interaction Problem Using a Combination of FEM, BEM with Particular Integrals, Modal Analysis, and Substructuring," by C-S. Tsai, G.C. Lee and R.L. Ketter, 12/31/88, (PB89-207146, A04, MF-A01).

NCEER-88-0037 "Optimal Placement of Actuators for Structural Control," by F.Y. Cheng and C.P. Pantelides, 8/15/88, (PB89-162846, A05, MF-A01).

NCEER-88-0038 "Teflon Bearings in Aseismic Base Isolation: Experimental Studies and Mathematical Modeling," by A. Mokha, M.C. Constantinou and A.M. Reinhorn, 12/5/88, (PB89-218457, A10, MF-A01). This report is available only through NTIS (see address given above).

NCEER-88-0039 "Seismic Behavior of Flat Slab High-Rise Buildings in the New York City Area," by P. Weidlinger and M. Ettouney, 10/15/88, (PB90-145681, A04, MF-A01).

NCEER-88-0040 "Evaluation of the Earthquake Resistance of Existing Buildings in New York City," by P. Weidlinger and M. Ettouney, 10/15/88, to be published.

NCEER-88-0041 "Small-Scale Modeling Techniques for Reinforced Concrete Structures Subjected to Seismic Loads," by W. Kim, A. El-Attar and R.N. White, 11/22/88, (PB89-189625, A05, MF-A01).

NCEER-88-0042 "Modeling Strong Ground Motion from Multiple Event Earthquakes," by G.W. Ellis and A.S. Cakmak, 10/15/88, (PB89-174445, A03, MF-A01).

NCEER-88-0043 "Nonstationary Models of Seismic Ground Acceleration," by M. Grigoriu, S.E. Ruiz and E. Rosenblueth, 7/15/88, (PB89-189617, A04, MF-A01).

NCEER-88-0044 "SARCF User's Guide: Seismic Analysis of Reinforced Concrete Frames," by Y.S. Chung, C. Meyer and M. Shinozuka, 11/9/88, (PB89-174452, A08, MF-A01).

NCEER-88-0045 "First Expert Panel Meeting on Disaster Research and Planning," edited by J. Pantelic and J. Stoyle, 9/15/88, (PB89-174460, A05, MF-A01). This report is only available through NTIS (see address given above).

NCEER-88-0046 "Preliminary Studies of the Effect of Degrading Infill Walls on the Nonlinear Seismic Response of Steel Frames," by C.Z. Chrysostomou, P. Gergely and J.F. Abel, 12/19/88, (PB89-208383, A05, MF-A01).

NCEER-88-0047 "Reinforced Concrete Frame Component Testing Facility - Design, Construction, Instrumentation and Operation," by S.P. Pessiki, C. Conley, T. Bond, P. Gergely and R.N. White, 12/16/88, (PB89-174478, A04, MF-A01).

NCEER-89-0001 "Effects of Protective Cushion and Soil Compliancy on the Response of Equipment Within a Seismically Excited Building," by J.A. HoLung, 2/16/89, (PB89-207179, A04, MF-A01).

NCEER-89-0002 "Statistical Evaluation of Response Modification Factors for Reinforced Concrete Structures," by H.H-M. Hwang and J-W. Jaw, 2/17/89, (PB89-207187, A05, MF-A01).

NCEER-89-0003 "Hysteretic Columns Under Random Excitation," by G-Q. Cai and Y.K. Lin, 1/9/89, (PB89-196513, A03, MF-A01).

NCEER-89-0004 "Experimental Study of `Elephant Foot Bulge' Instability of Thin-Walled Metal Tanks," by Z-H. Jia and R.L. Ketter, 2/22/89, (PB89-207195, A03, MF-A01).

NCEER-89-0005 "Experiment on Performance of Buried Pipelines Across San Andreas Fault," by J. Isenberg, E. Richardson and T.D. O'Rourke, 3/10/89, (PB89-218440, A04, MF-A01). This report is available only through NTIS (see address given above).

NCEER-89-0006 "A Knowledge-Based Approach to Structural Design of Earthquake-Resistant Buildings," by M. Subramani, P. Gergely, C.H. Conley, J.F. Abel and A.H. Zaghw, 1/15/89, (PB89-218465, A06, MF-A01).

NCEER-89-0007 "Liquefaction Hazards and Their Effects on Buried Pipelines," by T.D. O'Rourke and P.A. Lane, 2/1/89, (PB89-218481, A09, MF-A01).

NCEER-89-0008 "Fundamentals of System Identification in Structural Dynamics," by H. Imai, C-B. Yun, O. Maruyama and M. Shinozuka, 1/26/89, (PB89-207211, A04, MF-A01).

NCEER-89-0009 "Effects of the 1985 Michoacan Earthquake on Water Systems and Other Buried Lifelines in Mexico," by A.G. Ayala and M.J. O'Rourke, 3/8/89, (PB89-207229, A06, MF-A01).

NCEER-89-R010 "NCEER Bibliography of Earthquake Education Materials," by K.E.K. Ross, Second Revision, 9/1/89, (PB90-125352, A05, MF-A01). This report is replaced by NCEER-92-0018.

NCEER-89-0011 "Inelastic Three-Dimensional Response Analysis of Reinforced Concrete Building Structures (IDARC-3D), Part I - Modeling," by S.K. Kunnath and A.M. Reinhorn, 4/17/89, (PB90-114612, A07, MF-A01).

NCEER-89-0012 "Recommended Modifications to ATC-14," by C.D. Poland and J.O. Malley, 4/12/89, (PB90-108648, A15, MF-A01).

NCEER-89-0013 "Repair and Strengthening of Beam-to-Column Connections Subjected to Earthquake Loading," by M. Corazao and A.J. Durrani, 2/28/89, (PB90-109885, A06, MF-A01).

NCEER-89-0014 "Program EXKAL2 for Identification of Structural Dynamic Systems," by O. Maruyama, C-B. Yun, M. Hoshiya and M. Shinozuka, 5/19/89, (PB90-109877, A09, MF-A01).

NCEER-89-0015 "Response of Frames With Bolted Semi-Rigid Connections, Part I - Experimental Study and Analytical Predictions," by P.J. DiCorso, A.M. Reinhorn, J.R. Dickerson, J.B. Radziminski and W.L. Harper, 6/1/89, to be published.

NCEER-89-0016 "ARMA Monte Carlo Simulation in Probabilistic Structural Analysis," by P.D. Spanos and M.P. Mignolet, 7/10/89, (PB90-109893, A03, MF-A01).

NCEER-89-P017 "Preliminary Proceedings from the Conference on Disaster Preparedness - The Place of Earthquake Education in Our Schools," Edited by K.E.K. Ross, 6/23/89, (PB90-108606, A03, MF-A01).

NCEER-89-0017 "Proceedings from the Conference on Disaster Preparedness - The Place of Earthquake Education in Our Schools," Edited by K.E.K. Ross, 12/31/89, (PB90-207895, A012, MF-A02). This report is available only through NTIS (see address given above).

NCEER-89-0018 "Multidimensional Models of Hysteretic Material Behavior for Vibration Analysis of Shape Memory Energy Absorbing Devices, by E.J. Graesser and F.A. Cozzarelli, 6/7/89, (PB90-164146, A04, MF-A01).

NCEER-89-0019 "Nonlinear Dynamic Analysis of Three-Dimensional Base Isolated Structures (3D-BASIS)," by S. Nagarajaiah, A.M. Reinhorn and M.C. Constantinou, 8/3/89, (PB90-161936, A06, MF-A01). This report has been replaced by NCEER-93-0011.

NCEER-89-0020 "Structural Control Considering Time-Rate of Control Forces and Control Rate Constraints," by F.Y. Cheng and C.P. Pantelides, 8/3/89, (PB90-120445, A04, MF-A01).

NCEER-89-0021 "Subsurface Conditions of Memphis and Shelby County," by K.W. Ng, T-S. Chang and H-H.M. Hwang, 7/26/89, (PB90-120437, A03, MF-A01).

NCEER-89-0022 "Seismic Wave Propagation Effects on Straight Jointed Buried Pipelines," by K. Elhmadi and M.J. O'Rourke, 8/24/89, (PB90-162322, A10, MF-A02).

NCEER-89-0023 "Workshop on Serviceability Analysis of Water Delivery Systems," edited by M. Grigoriu, 3/6/89, (PB90-127424, A03, MF-A01).

NCEER-89-0024 "Shaking Table Study of a 1/5 Scale Steel Frame Composed of Tapered Members," by K.C. Chang, J.S. Hwang and G.C. Lee, 9/18/89, (PB90-160169, A04, MF-A01).

NCEER-89-0025 "DYNA1D: A Computer Program for Nonlinear Seismic Site Response Analysis - Technical Documentation," by Jean H. Prevost, 9/14/89, (PB90-161944, A07, MF-A01). This report is available only through NTIS (see address given above).

NCEER-89-0026 "1:4 Scale Model Studies of Active Tendon Systems and Active Mass Dampers for Aseismic Protection," by A.M. Reinhorn, T.T. Soong, R.C. Lin, Y.P. Yang, Y. Fukao, H. Abe and M. Nakai, 9/15/89, (PB90-173246, A10, MF-A02).

NCEER-89-0027 "Scattering of Waves by Inclusions in a Nonhomogeneous Elastic Half Space Solved by Boundary Element Methods," by P.K. Hadley, A. Askar and A.S. Cakmak, 6/15/89, (PB90-145699, A07, MF-A01).

NCEER-89-0028 "Statistical Evaluation of Deflection Amplification Factors for Reinforced Concrete Structures," by H.H.M. Hwang, J-W. Jaw and A.L. Ch'ng, 8/31/89, (PB90-164633, A05, MF-A01).

NCEER-89-0029 "Bedrock Accelerations in Memphis Area Due to Large New Madrid Earthquakes," by H.H.M. Hwang, C.H.S. Chen and G. Yu, 11/7/89, (PB90-162330, A04, MF-A01).

NCEER-89-0030 "Seismic Behavior and Response Sensitivity of Secondary Structural Systems," by Y.Q. Chen and T.T. Soong, 10/23/89, (PB90-164658, A08, MF-A01).

NCEER-89-0031 "Random Vibration and Reliability Analysis of Primary-Secondary Structural Systems," by Y. Ibrahim, M. Grigoriu and T.T. Soong, 11/10/89, (PB90-161951, A04, MF-A01).

NCEER-89-0032 "Proceedings from the Second U.S. - Japan Workshop on Liquefaction, Large Ground Deformation and Their Effects on Lifelines, September 26-29, 1989," Edited by T.D. O'Rourke and M. Hamada, 12/1/89, (PB90-209388, A22, MF-A03).

NCEER-89-0033 "Deterministic Model for Seismic Damage Evaluation of Reinforced Concrete Structures," by J.M. Bracci, A.M. Reinhorn, J.B. Mander and S.K. Kunnath, 9/27/89, (PB91-108803, A06, MF-A01).

NCEER-89-0034 "On the Relation Between Local and Global Damage Indices," by E. DiPasquale and A.S. Cakmak, 8/15/89, (PB90-173865, A05, MF-A01).

NCEER-89-0035 "Cyclic Undrained Behavior of Nonplastic and Low Plasticity Silts," by A.J. Walker and H.E. Stewart, 7/26/89, (PB90-183518, A10, MF-A01).

NCEER-89-0036 "Liquefaction Potential of Surficial Deposits in the City of Buffalo, New York," by M. Budhu, R. Giese and L. Baumgrass, 1/17/89, (PB90-208455, A04, MF-A01).

NCEER-89-0037 "A Deterministic Assessment of Effects of Ground Motion Incoherence," by A.S. Veletsos and Y. Tang, 7/15/89, (PB90-164294, A03, MF-A01).

NCEER-89-0038 "Workshop on Ground Motion Parameters for Seismic Hazard Mapping," July 17-18, 1989, edited by R.V. Whitman, 12/1/89, (PB90-173923, A04, MF-A01).

NCEER-89-0039 "Seismic Effects on Elevated Transit Lines of the New York City Transit Authority," by C.J. Costantino, C.A. Miller and E. Heymsfield, 12/26/89, (PB90-207887, A06, MF-A01).

NCEER-89-0040 "Centrifugal Modeling of Dynamic Soil-Structure Interaction," by K. Weissman, Supervised by J.H. Prevost, 5/10/89, (PB90-207879, A07, MF-A01).

NCEER-89-0041 "Linearized Identification of Buildings With Cores for Seismic Vulnerability Assessment," by I-K. Ho and A.E. Aktan, 11/1/89, (PB90-251943, A07, MF-A01).

NCEER-90-0001 "Geotechnical and Lifeline Aspects of the October 17, 1989 Loma Prieta Earthquake in San Francisco," by T.D. O'Rourke, H.E. Stewart, F.T. Blackburn and T.S. Dickerman, 1/90, (PB90-208596, A05, MF-A01).

NCEER-90-0002 "Nonnormal Secondary Response Due to Yielding in a Primary Structure," by D.C.K. Chen and L.D. Lutes, 2/28/90, (PB90-251976, A07, MF-A01).

NCEER-90-0003 "Earthquake Education Materials for Grades K-12," by K.E.K. Ross, 4/16/90, (PB91-251984, A05, MF-A05). This report has been replaced by NCEER-92-0018.

NCEER-90-0004 "Catalog of Strong Motion Stations in Eastern North America," by R.W. Busby, 4/3/90, (PB90-251984, A05, MF-A01).

NCEER-90-0005 "NCEER Strong-Motion Data Base: A User Manual for the GeoBase Release (Version 1.0 for the Sun3)," by P. Friberg and K. Jacob, 3/31/90 (PB90-258062, A04, MF-A01).

NCEER-90-0006 "Seismic Hazard Along a Crude Oil Pipeline in the Event of an 1811-1812 Type New Madrid Earthquake," by H.H.M. Hwang and C-H.S. Chen, 4/16/90, (PB90-258054, A04, MF-A01).

NCEER-90-0007 "Site-Specific Response Spectra for Memphis Sheahan Pumping Station," by H.H.M. Hwang and C.S. Lee, 5/15/90, (PB91-108811, A05, MF-A01).

NCEER-90-0008 "Pilot Study on Seismic Vulnerability of Crude Oil Transmission Systems," by T. Ariman, R. Dobry, M. Grigoriu, F. Kozin, M. O'Rourke, T. O'Rourke and M. Shinozuka, 5/25/90, (PB91-108837, A06, MF-A01).

NCEER-90-0009 "A Program to Generate Site Dependent Time Histories: EQGEN," by G.W. Ellis, M. Srinivasan and A.S. Cakmak, 1/30/90, (PB91-108829, A04, MF-A01).

NCEER-90-0010 "Active Isolation for Seismic Protection of Operating Rooms," by M.E. Talbott, Supervised by M. Shinozuka, 6/8/9, (PB91-110205, A05, MF-A01).

NCEER-90-0011 "Program LINEARID for Identification of Linear Structural Dynamic Systems," by C-B. Yun and M. Shinozuka, 6/25/90, (PB91-110312, A08, MF-A01).

NCEER-90-0012 "Two-Dimensional Two-Phase Elasto-Plastic Seismic Response of Earth Dams," by A.N. Yiagos, Supervised by J.H. Prevost, 6/20/90, (PB91-110197, A13, MF-A02).

NCEER-90-0013 "Secondary Systems in Base-Isolated Structures: Experimental Investigation, Stochastic Response and Stochastic Sensitivity," by G.D. Manolis, G. Juhn, M.C. Constantinou and A.M. Reinhorn, 7/1/90, (PB91-110320, A08, MF-A01).

NCEER-90-0014 "Seismic Behavior of Lightly-Reinforced Concrete Column and Beam-Column Joint Details," by S.P. Pessiki, C.H. Conley, P. Gergely and R.N. White, 8/22/90, (PB91-108795, A11, MF-A02).

NCEER-90-0015 "Two Hybrid Control Systems for Building Structures Under Strong Earthquakes," by J.N. Yang and A. Danielians, 6/29/90, (PB91-125393, A04, MF-A01).

NCEER-90-0016 "Instantaneous Optimal Control with Acceleration and Velocity Feedback," by J.N. Yang and Z. Li, 6/29/90, (PB91-125401, A03, MF-A01).

NCEER-90-0017 "Reconnaissance Report on the Northern Iran Earthquake of June 21, 1990," by M. Mehrain, 10/4/90, (PB91-125377, A03, MF-A01).

NCEER-90-0018 "Evaluation of Liquefaction Potential in Memphis and Shelby County," by T.S. Chang, P.S. Tang, C.S. Lee and H. Hwang, 8/10/90, (PB91-125427, A09, MF-A01).

NCEER-90-0019 "Experimental and Analytical Study of a Combined Sliding Disc Bearing and Helical Steel Spring Isolation System," by M.C. Constantinou, A.S. Mokha and A.M. Reinhorn, 10/4/90, (PB91-125385, A06, MF-A01). This report is available only through NTIS (see address given above).

NCEER-90-0020 "Experimental Study and Analytical Prediction of Earthquake Response of a Sliding Isolation System with a Spherical Surface," by A.S. Mokha, M.C. Constantinou and A.M. Reinhorn, 10/11/90, (PB91-125419, A05, MF-A01).

NCEER-90-0021 "Dynamic Interaction Factors for Floating Pile Groups," by G. Gazetas, K. Fan, A. Kaynia and E. Kausel, 9/10/90, (PB91-170381, A05, MF-A01).

NCEER-90-0022 "Evaluation of Seismic Damage Indices for Reinforced Concrete Structures," by S. Rodriguez-Gomez and A.S. Cakmak, 9/30/90, PB91-171322, A06, MF-A01).

NCEER-90-0023 "Study of Site Response at a Selected Memphis Site," by H. Desai, S. Ahmad, E.S. Gazetas and M.R. Oh, 10/11/90, (PB91-196857, A03, MF-A01).

NCEER-90-0024 "A User's Guide to Strongmo: Version 1.0 of NCEER's Strong-Motion Data Access Tool for PCs and Terminals," by P.A. Friberg and C.A.T. Susch, 11/15/90, (PB91-171272, A03, MF-A01).

NCEER-90-0025 "A Three-Dimensional Analytical Study of Spatial Variability of Seismic Ground Motions," by L-L. Hong and A.H.-S. Ang, 10/30/90, (PB91-170399, A09, MF-A01).

NCEER-90-0026 "MUMOID User's Guide - A Program for the Identification of Modal Parameters," by S. Rodriguez-Gomez and E. DiPasquale, 9/30/90, (PB91-171298, A04, MF-A01).

NCEER-90-0027 "SARCF-II User's Guide - Seismic Analysis of Reinforced Concrete Frames," by S. Rodriguez-Gomez, Y.S. Chung and C. Meyer, 9/30/90, (PB91-171280, A05, MF-A01).

NCEER-90-0028 "Viscous Dampers: Testing, Modeling and Application in Vibration and Seismic Isolation," by N. Makris and M.C. Constantinou, 12/20/90 (PB91-190561, A06, MF-A01).

NCEER-90-0029 "Soil Effects on Earthquake Ground Motions in the Memphis Area," by H. Hwang, C.S. Lee, K.W. Ng and T.S. Chang, 8/2/90, (PB91-190751, A05, MF-A01).

NCEER-91-0001 "Proceedings from the Third Japan-U.S. Workshop on Earthquake Resistant Design of Lifeline Facilities and Countermeasures for Soil Liquefaction, December 17-19, 1990," edited by T.D. O'Rourke and M. Hamada, 2/1/91, (PB91-179259, A99, MF-A04).

NCEER-91-0002 "Physical Space Solutions of Non-Proportionally Damped Systems," by M. Tong, Z. Liang and G.C. Lee, 1/15/91, (PB91-179242, A04, MF-A01).

NCEER-91-0003 "Seismic Response of Single Piles and Pile Groups," by K. Fan and G. Gazetas, 1/10/91, (PB92-174994, A04, MF-A01).

NCEER-91-0004 "Damping of Structures: Part 1 - Theory of Complex Damping," by Z. Liang and G. Lee, 10/10/91, (PB92-197235, A12, MF-A03).

NCEER-91-0005 "3D-BASIS - Nonlinear Dynamic Analysis of Three Dimensional Base Isolated Structures: Part II," by S. Nagarajaiah, A.M. Reinhorn and M.C. Constantinou, 2/28/91, (PB91-190553, A07, MF-A01). This report has been replaced by NCEER-93-0011.

NCEER-91-0006 "A Multidimensional Hysteretic Model for Plasticity Deforming Metals in Energy Absorbing Devices," by E.J. Graesser and F.A. Cozzarelli, 4/9/91, (PB92-108364, A04, MF-A01).

NCEER-91-0007 "A Framework for Customizable Knowledge-Based Expert Systems with an Application to a KBES for Evaluating the Seismic Resistance of Existing Buildings," by E.G. Ibarra-Anaya and S.J. Fenves, 4/9/91, (PB91-210930, A08, MF-A01).

NCEER-91-0008 "Nonlinear Analysis of Steel Frames with Semi-Rigid Connections Using the Capacity Spectrum Method," by G.G. Deierlein, S-H. Hsieh, Y-J. Shen and J.F. Abel, 7/2/91, (PB92-113828, A05, MF-A01).

NCEER-91-0009 "Earthquake Education Materials for Grades K-12," by K.E.K. Ross, 4/30/91, (PB91-212142, A06, MF-A01). This report has been replaced by NCEER-92-0018.

NCEER-91-0010 "Phase Wave Velocities and Displacement Phase Differences in a Harmonically Oscillating Pile," by N. Makris and G. Gazetas, 7/8/91, (PB92-108356, A04, MF-A01).

NCEER-91-0011 "Dynamic Characteristics of a Full-Size Five-Story Steel Structure and a 2/5 Scale Model," by K.C. Chang, G.C. Yao, G.C. Lee, D.S. Hao and Y.C. Yeh," 7/2/91, (PB93-116648, A06, MF-A02).

NCEER-91-0012 "Seismic Response of a 2/5 Scale Steel Structure with Added Viscoelastic Dampers," by K.C. Chang, T.T. Soong, S-T. Oh and M.L. Lai, 5/17/91, (PB92-110816, A05, MF-A01).

NCEER-91-0013 "Earthquake Response of Retaining Walls; Full-Scale Testing and Computational Modeling," by S. Alampalli and A-W.M. Elgamal, 6/20/91, to be published.

NCEER-91-0014 "3D-BASIS-M: Nonlinear Dynamic Analysis of Multiple Building Base Isolated Structures," by P.C. Tsopelas, S. Nagarajaiah, M.C. Constantinou and A.M. Reinhorn, 5/28/91, (PB92-113885, A09, MF-A02).

NCEER-91-0015 "Evaluation of SEAOC Design Requirements for Sliding Isolated Structures," by D. Theodossiou and M.C. Constantinou, 6/10/91, (PB92-114602, A11, MF-A03).

NCEER-91-0016 "Closed-Loop Modal Testing of a 27-Story Reinforced Concrete Flat Plate-Core Building," by H.R. Somaprasad, T. Toksoy, H. Yoshiyuki and A.E. Aktan, 7/15/91, (PB92-129980, A07, MF-A02).

NCEER-91-0017 "Shake Table Test of a 1/6 Scale Two-Story Lightly Reinforced Concrete Building," by A.G. El-Attar, R.N. White and P. Gergely, 2/28/91, (PB92-222447, A06, MF-A02).

NCEER-91-0018 "Shake Table Test of a 1/8 Scale Three-Story Lightly Reinforced Concrete Building," by A.G. El-Attar, R.N. White and P. Gergely, 2/28/91, (PB93-116630, A08, MF-A02).

NCEER-91-0019 "Transfer Functions for Rigid Rectangular Foundations," by A.S. Veletsos, A.M. Prasad and W.H. Wu, 7/31/91, to be published.

NCEER-91-0020 "Hybrid Control of Seismic-Excited Nonlinear and Inelastic Structural Systems," by J.N. Yang, Z. Li and A. Danielians, 8/1/91, (PB92-143171, A06, MF-A02).

NCEER-91-0021 "The NCEER-91 Earthquake Catalog: Improved Intensity-Based Magnitudes and Recurrence Relations for U.S. Earthquakes East of New Madrid," by L. Seeber and J.G. Armbruster, 8/28/91, (PB92-176742, A06, MF-A02).

NCEER-91-0022 "Proceedings from the Implementation of Earthquake Planning and Education in Schools: The Need for Change - The Roles of the Changemakers," by K.E.K. Ross and F. Winslow, 7/23/91, (PB92-129998, A12, MF-A03).

NCEER-91-0023 "A Study of Reliability-Based Criteria for Seismic Design of Reinforced Concrete Frame Buildings," by H.H.M. Hwang and H-M. Hsu, 8/10/91, (PB92-140235, A09, MF-A02).

NCEER-91-0024 "Experimental Verification of a Number of Structural System Identification Algorithms," by R.G. Ghanem, H. Gavin and M. Shinozuka, 9/18/91, (PB92-176577, A18, MF-A04).

NCEER-91-0025 "Probabilistic Evaluation of Liquefaction Potential," by H.H.M. Hwang and C.S. Lee," 11/25/91, (PB92-143429, A05, MF-A01).

NCEER-91-0026 "Instantaneous Optimal Control for Linear, Nonlinear and Hysteretic Structures - Stable Controllers," by J.N. Yang and Z. Li, 11/15/91, (PB92-163807, A04, MF-A01).

NCEER-91-0027 "Experimental and Theoretical Study of a Sliding Isolation System for Bridges," by M.C. Constantinou, A. Kartoum, A.M. Reinhorn and P. Bradford, 11/15/91, (PB92-176973, A10, MF-A03).

NCEER-92-0001 "Case Studies of Liquefaction and Lifeline Performance During Past Earthquakes, Volume 1: Japanese Case Studies," Edited by M. Hamada and T. O'Rourke, 2/17/92, (PB92-197243, A18, MF-A04).

NCEER-92-0002 "Case Studies of Liquefaction and Lifeline Performance During Past Earthquakes, Volume 2: United States Case Studies," Edited by T. O'Rourke and M. Hamada, 2/17/92, (PB92-197250, A20, MF-A04).

NCEER-92-0003 "Issues in Earthquake Education," Edited by K. Ross, 2/3/92, (PB92-222389, A07, MF-A02).

NCEER-92-0004 "Proceedings from the First U.S. - Japan Workshop on Earthquake Protective Systems for Bridges," Edited by I.G. Buckle, 2/4/92, (PB94-142239, A99, MF-A06).

NCEER-92-0005 "Seismic Ground Motion from a Haskell-Type Source in a Multiple-Layered Half-Space," A.P. Theoharis, G. Deodatis and M. Shinozuka, 1/2/92, to be published.

NCEER-92-0006 "Proceedings from the Site Effects Workshop," Edited by R. Whitman, 2/29/92, (PB92-197201, A04, MF-A01).

NCEER-92-0007 "Engineering Evaluation of Permanent Ground Deformations Due to Seismically-Induced Liquefaction," by M.H. Baziar, R. Dobry and A-W.M. Elgamal, 3/24/92, (PB92-222421, A13, MF-A03).

NCEER-92-0008 "A Procedure for the Seismic Evaluation of Buildings in the Central and Eastern United States," by C.D. Poland and J.O. Malley, 4/2/92, (PB92-222439, A20, MF-A04).

NCEER-92-0009 "Experimental and Analytical Study of a Hybrid Isolation System Using Friction Controllable Sliding Bearings," by M.Q. Feng, S. Fujii and M. Shinozuka, 5/15/92, (PB93-150282, A06, MF-A02).

NCEER-92-0010 "Seismic Resistance of Slab-Column Connections in Existing Non-Ductile Flat-Plate Buildings," by A.J. Durrani and Y. Du, 5/18/92, (PB93-116812, A06, MF-A02).

NCEER-92-0011 "The Hysteretic and Dynamic Behavior of Brick Masonry Walls Upgraded by Ferrocement Coatings Under Cyclic Loading and Strong Simulated Ground Motion," by H. Lee and S.P. Prawel, 5/11/92, to be published.

NCEER-92-0012 "Study of Wire Rope Systems for Seismic Protection of Equipment in Buildings," by G.F. Demetriades, M.C. Constantinou and A.M. Reinhorn, 5/20/92, (PB93-116655, A08, MF-A02).

NCEER-92-0013 "Shape Memory Structural Dampers: Material Properties, Design and Seismic Testing," by P.R. Witting and F.A. Cozzarelli, 5/26/92, (PB93-116663, A05, MF-A01).

NCEER-92-0014 "Longitudinal Permanent Ground Deformation Effects on Buried Continuous Pipelines," by M.J. O'Rourke, and C. Nordberg, 6/15/92, (PB93-116671, A08, MF-A02).

NCEER-92-0015 "A Simulation Method for Stationary Gaussian Random Functions Based on the Sampling Theorem," by M. Grigoriu and S. Balopoulou, 6/11/92, (PB93-127496, A05, MF-A01).

NCEER-92-0016 "Gravity-Load-Designed Reinforced Concrete Buildings: Seismic Evaluation of Existing Construction and Detailing Strategies for Improved Seismic Resistance," by G.W. Hoffmann, S.K. Kunnath, A.M. Reinhorn and J.B. Mander, 7/15/92, (PB94-142007, A08, MF-A02).

NCEER-92-0017 "Observations on Water System and Pipeline Performance in the Limón Area of Costa Rica Due to the April 22, 1991 Earthquake," by M. O'Rourke and D. Ballantyne, 6/30/92, (PB93-126811, A06, MF-A02).

NCEER-92-0018 "Fourth Edition of Earthquake Education Materials for Grades K-12," Edited by K.E.K. Ross, 8/10/92, (PB93-114023, A07, MF-A02).

NCEER-92-0019 "Proceedings from the Fourth Japan-U.S. Workshop on Earthquake Resistant Design of Lifeline Facilities and Countermeasures for Soil Liquefaction," Edited by M. Hamada and T.D. O'Rourke, 8/12/92, (PB93-163939, A99, MF-E11).

NCEER-92-0020 "Active Bracing System: A Full Scale Implementation of Active Control," by A.M. Reinhorn, T.T. Soong, R.C. Lin, M.A. Riley, Y.P. Wang, S. Aizawa and M. Higashino, 8/14/92, (PB93-127512, A06, MF-A02).

NCEER-92-0021 "Empirical Analysis of Horizontal Ground Displacement Generated by Liquefaction-Induced Lateral Spreads," by S.F. Bartlett and T.L. Youd, 8/17/92, (PB93-188241, A06, MF-A02).

NCEER-92-0022 "IDARC Version 3.0: Inelastic Damage Analysis of Reinforced Concrete Structures," by S.K. Kunnath, A.M. Reinhorn and R.F. Lobo, 8/31/92, (PB93-227502, A07, MF-A02).

NCEER-92-0023 "A Semi-Empirical Analysis of Strong-Motion Peaks in Terms of Seismic Source, Propagation Path and Local Site Conditions, by M. Kamiyama, M.J. O'Rourke and R. Flores-Berrones, 9/9/92, (PB93-150266, A08, MF-A02).

NCEER-92-0024 "Seismic Behavior of Reinforced Concrete Frame Structures with Nonductile Details, Part I: Summary of Experimental Findings of Full Scale Beam-Column Joint Tests," by A. Beres, R.N. White and P. Gergely, 9/30/92, (PB93-227783, A05, MF-A01).

NCEER-92-0025 "Experimental Results of Repaired and Retrofitted Beam-Column Joint Tests in Lightly Reinforced Concrete Frame Buildings," by A. Beres, S. El-Borgi, R.N. White and P. Gergely, 10/29/92, (PB93-227791, A05, MF-A01).

NCEER-92-0026 "A Generalization of Optimal Control Theory: Linear and Nonlinear Structures," by J.N. Yang, Z. Li and S. Vongchavalitkul, 11/2/92, (PB93-188621, A05, MF-A01).

NCEER-92-0027 "Seismic Resistance of Reinforced Concrete Frame Structures Designed Only for Gravity Loads: Part I - Design and Properties of a One-Third Scale Model Structure," by J.M. Bracci, A.M. Reinhorn and J.B. Mander, 12/1/92, (PB94-104502, A08, MF-A02).

NCEER-92-0028 "Seismic Resistance of Reinforced Concrete Frame Structures Designed Only for Gravity Loads: Part II - Experimental Performance of Subassemblages," by L.E. Aycardi, J.B. Mander and A.M. Reinhorn, 12/1/92, (PB94-104510, A08, MF-A02).

NCEER-92-0029 "Seismic Resistance of Reinforced Concrete Frame Structures Designed Only for Gravity Loads: Part III - Experimental Performance and Analytical Study of a Structural Model," by J.M. Bracci, A.M. Reinhorn and J.B. Mander, 12/1/92, (PB93-227528, A09, MF-A01).

NCEER-92-0030 "Evaluation of Seismic Retrofit of Reinforced Concrete Frame Structures: Part I - Experimental Performance of Retrofitted Subassemblages," by D. Choudhuri, J.B. Mander and A.M. Reinhorn, 12/8/92, (PB93-198307, A07, MF-A02).

NCEER-92-0031 "Evaluation of Seismic Retrofit of Reinforced Concrete Frame Structures: Part II - Experimental Performance and Analytical Study of a Retrofitted Structural Model," by J.M. Bracci, A.M. Reinhorn and J.B. Mander, 12/8/92, (PB93-198315, A09, MF-A03).

NCEER-92-0032 "Experimental and Analytical Investigation of Seismic Response of Structures with Supplemental Fluid Viscous Dampers," by M.C. Constantinou and M.D. Symans, 12/21/92, (PB93-191435, A10, MF-A03).

NCEER-92-0033 "Reconnaissance Report on the Cairo, Egypt Earthquake of October 12, 1992," by M. Khater, 12/23/92, (PB93-188621, A03, MF-A01).

NCEER-92-0034 "Low-Level Dynamic Characteristics of Four Tall Flat-Plate Buildings in New York City," by H. Gavin, S. Yuan, J. Grossman, E. Pekelis and K. Jacob, 12/28/92, (PB93-188217, A07, MF-A02).

NCEER-93-0001 "An Experimental Study on the Seismic Performance of Brick-Infilled Steel Frames With and Without Retrofit," by J.B. Mander, B. Nair, K. Wojtkowski and J. Ma, 1/29/93, (PB93-227510, A07, MF-A02).

NCEER-93-0002 "Social Accounting for Disaster Preparedness and Recovery Planning," by S. Cole, E. Pantoja and V. Razak, 2/22/93, (PB94-142114, A12, MF-A03).

NCEER-93-0003 "Assessment of 1991 NEHRP Provisions for Nonstructural Components and Recommended Revisions," by T.T. Soong, G. Chen, Z. Wu, R-H. Zhang and M. Grigoriu, 3/1/93, (PB93-188639, A06, MF-A02).

NCEER-93-0004 "Evaluation of Static and Response Spectrum Analysis Procedures of SEAOC/UBC for Seismic Isolated Structures," by C.W. Winters and M.C. Constantinou, 3/23/93, (PB93-198299, A10, MF-A03).

NCEER-93-0005 "Earthquakes in the Northeast - Are We Ignoring the Hazard? A Workshop on Earthquake Science and Safety for Educators," edited by K.E.K. Ross, 4/2/93, (PB94-103066, A09, MF-A02).

NCEER-93-0006 "Inelastic Response of Reinforced Concrete Structures with Viscoelastic Braces," by R.F. Lobo, J.M. Bracci, K.L. Shen, A.M. Reinhorn and T.T. Soong, 4/5/93, (PB93-227486, A05, MF-A02).

NCEER-93-0007 "Seismic Testing of Installation Methods for Computers and Data Processing Equipment," by K. Kosar, T.T. Soong, K.L. Shen, J.A. HoLung and Y.K. Lin, 4/12/93, (PB93-198299, A07, MF-A02).

NCEER-93-0008 "Retrofit of Reinforced Concrete Frames Using Added Dampers," by A. Reinhorn, M. Constantinou and C. Li, to be published.

NCEER-93-0009 "Seismic Behavior and Design Guidelines for Steel Frame Structures with Added Viscoelastic Dampers," by K.C. Chang, M.L. Lai, T.T. Soong, D.S. Hao and Y.C. Yeh, 5/1/93, (PB94-141959, A07, MF-A02).

NCEER-93-0010 "Seismic Performance of Shear-Critical Reinforced Concrete Bridge Piers," by J.B. Mander, S.M. Waheed, M.T.A. Chaudhary and S.S. Chen, 5/12/93, (PB93-227494, A08, MF-A02).

NCEER-93-0011 "3D-BASIS-TABS: Computer Program for Nonlinear Dynamic Analysis of Three Dimensional Base Isolated Structures," by S. Nagarajaiah, C. Li, A.M. Reinhorn and M.C. Constantinou, 8/2/93, (PB94-141819, A09, MF-A02).

NCEER-93-0012 "Effects of Hydrocarbon Spills from an Oil Pipeline Break on Ground Water," by O.J. Helweg and H.H.M. Hwang, 8/3/93, (PB94-141942, A06, MF-A02).

NCEER-93-0013 "Simplified Procedures for Seismic Design of Nonstructural Components and Assessment of Current Code Provisions," by M.P. Singh, L.E. Suarez, E.E. Matheu and G.O. Maldonado, 8/4/93, (PB94-141827, A09, MF-A02).

NCEER-93-0014 "An Energy Approach to Seismic Analysis and Design of Secondary Systems," by G. Chen and T.T. Soong, 8/6/93, (PB94-142767, A11, MF-A03).

NCEER-93-0015 "Proceedings from School Sites: Becoming Prepared for Earthquakes - Commemorating the Third Anniversary of the Loma Prieta Earthquake," Edited by F.E. Winslow and K.E.K. Ross, 8/16/93, (PB94-154275, A16, MF-A02).

NCEER-93-0016 "Reconnaissance Report of Damage to Historic Monuments in Cairo, Egypt Following the October 12, 1992 Dahshur Earthquake," by D. Sykora, D. Look, G. Croci, E. Karaesmen and E. Karaesmen, 8/19/93, (PB94-142221, A08, MF-A02).

NCEER-93-0017 "The Island of Guam Earthquake of August 8, 1993," by S.W. Swan and S.K. Harris, 9/30/93, (PB94-141843, A04, MF-A01).

NCEER-93-0018 "Engineering Aspects of the October 12, 1992 Egyptian Earthquake," by A.W. Elgamal, M. Amer, K. Adalier and A. Abul-Fadl, 10/7/93, (PB94-141983, A05, MF-A01).

NCEER-93-0019 "Development of an Earthquake Motion Simulator and its Application in Dynamic Centrifuge Testing," by I. Krstelj, Supervised by J.H. Prevost, 10/23/93, (PB94-181773, A-10, MF-A03).

NCEER-93-0020 "NCEER-Taisei Corporation Research Program on Sliding Seismic Isolation Systems for Bridges: Experimental and Analytical Study of a Friction Pendulum System (FPS)," by M.C. Constantinou, P. Tsopelas, Y-S. Kim and S. Okamoto, 11/1/93, (PB94-142775, A08, MF-A02).

NCEER-93-0021 "Finite Element Modeling of Elastomeric Seismic Isolation Bearings," by L.J. Billings, Supervised by R. Shepherd, 11/8/93, to be published.

NCEER-93-0022 "Seismic Vulnerability of Equipment in Critical Facilities: Life-Safety and Operational Consequences," by K. Porter, G.S. Johnson, M.M. Zadeh, C. Scawthorn and S. Eder, 11/24/93, (PB94-181765, A16, MF-A03).

NCEER-93-0023 "Hokkaido Nansei-oki, Japan Earthquake of July 12, 1993, by P.I. Yanev and C.R. Scawthorn, 12/23/93, (PB94-181500, A07, MF-A01).

NCEER-94-0001 "An Evaluation of Seismic Serviceability of Water Supply Networks with Application to the San Francisco Auxiliary Water Supply System," by I. Markov, Supervised by M. Grigoriu and T. O'Rourke, 1/21/94, (PB94-204013, A07, MF-A02).

NCEER-94-0002 "NCEER-Taisei Corporation Research Program on Sliding Seismic Isolation Systems for Bridges: Experimental and Analytical Study of Systems Consisting of Sliding Bearings, Rubber Restoring Force Devices and Fluid Dampers," Volumes I and II, by P. Tsopelas, S. Okamoto, M.C. Constantinou, D. Ozaki and S. Fujii, 2/4/94, (PB94-181740, A09, MF-A02 and PB94-181757, A12, MF-A03).

NCEER-94-0003 "A Markov Model for Local and Global Damage Indices in Seismic Analysis," by S. Rahman and M. Grigoriu, 2/18/94, (PB94-206000, A12, MF-A03).

NCEER-94-0004 "Proceedings from the NCEER Workshop on Seismic Response of Masonry Infills," edited by D.P. Abrams, 3/1/94, (PB94-180783, A07, MF-A02).

NCEER-94-0005 "The Northridge, California Earthquake of January 17, 1994: General Reconnaissance Report," edited by J.D. Goltz, 3/11/94, (PB193943, A10, MF-A03).

NCEER-94-0006 "Seismic Energy Based Fatigue Damage Analysis of Bridge Columns: Part I - Evaluation of Seismic Capacity," by G.A. Chang and J.B. Mander, 3/14/94, (PB94-219185, A11, MF-A03).

NCEER-94-0007 "Seismic Isolation of Multi-Story Frame Structures Using Spherical Sliding Isolation Systems," by T.M. Al-Hussaini, V.A. Zayas and M.C. Constantinou, 3/17/94, (PB193745, A09, MF-A02).

NCEER-94-0008 "The Northridge, California Earthquake of January 17, 1994: Performance of Highway Bridges," edited by I.G. Buckle, 3/24/94, (PB94-193851, A06, MF-A02).

NCEER-94-0009 "Proceedings of the Third U.S.-Japan Workshop on Earthquake Protective Systems for Bridges," edited by I.G. Buckle and I. Friedland, 3/31/94, (PB94-195815, A99, MF-A06).

NCEER-94-0010 "3D-BASIS-ME: Computer Program for Nonlinear Dynamic Analysis of Seismically Isolated Single and Multiple Structures and Liquid Storage Tanks," by P.C. Tsopelas, M.C. Constantinou and A.M. Reinhorn, 4/12/94, (PB94-204922, A09, MF-A02).

NCEER-94-0011 "The Northridge, California Earthquake of January 17, 1994: Performance of Gas Transmission Pipelines," by T.D. O'Rourke and M.C. Palmer, 5/16/94, (PB94-204989, A05, MF-A01).

NCEER-94-0012 "Feasibility Study of Replacement Procedures and Earthquake Performance Related to Gas Transmission Pipelines," by T.D. O'Rourke and M.C. Palmer, 5/25/94, (PB94-206638, A09, MF-A02).

NCEER-94-0013 "Seismic Energy Based Fatigue Damage Analysis of Bridge Columns: Part II - Evaluation of Seismic Demand," by G.A. Chang and J.B. Mander, 6/1/94, (PB95-18106, A08, MF-A02).

NCEER-94-0014 "NCEER-Taisei Corporation Research Program on Sliding Seismic Isolation Systems for Bridges: Experimental and Analytical Study of a System Consisting of Sliding Bearings and Fluid Restoring Force/Damping Devices," by P. Tsopelas and M.C. Constantinou, 6/13/94, (PB94-219144, A10, MF-A03).

NCEER-94-0015 "Generation of Hazard-Consistent Fragility Curves for Seismic Loss Estimation Studies," by H. Hwang and J-R. Huo, 6/14/94, (PB95-181996, A09, MF-A02).

NCEER-94-0016 "Seismic Study of Building Frames with Added Energy-Absorbing Devices," by W.S. Pong, C.S. Tsai and G.C. Lee, 6/20/94, (PB94-219136, A10, A03).

NCEER-94-0017 "Sliding Mode Control for Seismic-Excited Linear and Nonlinear Civil Engineering Structures," by J. Yang, J. Wu, A. Agrawal and Z. Li, 6/21/94, (PB95-138483, A06, MF-A02).

NCEER-94-0018 "3D-BASIS-TABS Version 2.0: Computer Program for Nonlinear Dynamic Analysis of Three Dimensional Base Isolated Structures," by A.M. Reinhorn, S. Nagarajaiah, M.C. Constantinou, P. Tsopelas and R. Li, 6/22/94, (PB95-182176, A08, MF-A02).

NCEER-94-0019 "Proceedings of the International Workshop on Civil Infrastructure Systems: Application of Intelligent Systems and Advanced Materials on Bridge Systems," Edited by G.C. Lee and K.C. Chang, 7/18/94, (PB95-252474, A20, MF-A04).

NCEER-94-0020 "Study of Seismic Isolation Systems for Computer Floors," by V. Lambrou and M.C. Constantinou, 7/19/94, (PB95-138533, A10, MF-A03).

NCEER-94-0021 "Proceedings of the U.S.-Italian Workshop on Guidelines for Seismic Evaluation and Rehabilitation of Unreinforced Masonry Buildings," Edited by D.P. Abrams and G.M. Calvi, 7/20/94, (PB95-138749, A13, MF-A03).

NCEER-94-0022 "NCEER-Taisei Corporation Research Program on Sliding Seismic Isolation Systems for Bridges: Experimental and Analytical Study of a System Consisting of Lubricated PTFE Sliding Bearings and Mild Steel Dampers," by P. Tsopelas and M.C. Constantinou, 7/22/94, (PB95-182184, A08, MF-A02).

NCEER-94-0023 "Development of Reliability-Based Design Criteria for Buildings Under Seismic Load," by Y.K. Wen, H. Hwang and M. Shinozuka, 8/1/94, (PB95-211934, A08, MF-A02).

NCEER-94-0024 "Experimental Verification of Acceleration Feedback Control Strategies for an Active Tendon System," by S.J. Dyke, B.F. Spencer, Jr., P. Quast, M.K. Sain, D.C. Kaspari, Jr. and T.T. Soong, 8/29/94, (PB95-212320, A05, MF-A01).

NCEER-94-0025 "Seismic Retrofitting Manual for Highway Bridges," Edited by I.G. Buckle and I.F. Friedland, to be published.

NCEER-94-0026 "Proceedings from the Fifth U.S.-Japan Workshop on Earthquake Resistant Design of Lifeline Facilities and Countermeasures Against Soil Liquefaction," Edited by T.D. O'Rourke and M. Hamada, 11/7/94, (PB95-220802, A99, MF-E08).

NCEER-95-0001 "Experimental and Analytical Investigation of Seismic Retrofit of Structures with Supplemental Damping: Part 1 - Fluid Viscous Damping Devices," by A.M. Reinhorn, C. Li and M.C. Constantinou, 1/3/95, (PB95-266599, A09, MF-A02).

NCEER-95-0002 "Experimental and Analytical Study of Low-Cycle Fatigue Behavior of Semi-Rigid Top-And-Seat Angle Connections," by G. Pekcan, J.B. Mander and S.S. Chen, 1/5/95, (PB95-220042, A07, MF-A02).

NCEER-95-0003 "NCEER-ATC Joint Study on Fragility of Buildings," by T. Anagnos, C. Rojahn and A.S. Kiremidjian, 1/20/95, (PB95-220026, A06, MF-A02).

NCEER-95-0004 "Nonlinear Control Algorithms for Peak Response Reduction," by Z. Wu, T.T. Soong, V. Gattulli and R.C. Lin, 2/16/95, (PB95-220349, A05, MF-A01).

NCEER-95-0005 "Pipeline Replacement Feasibility Study: A Methodology for Minimizing Seismic and Corrosion Risks to Underground Natural Gas Pipelines," by R.T. Eguchi, H.A. Seligson and D.G. Honegger, 3/2/95, (PB95-252326, A06, MF-A02).

NCEER-95-0006 "Evaluation of Seismic Performance of an 11-Story Frame Building During the 1994 Northridge Earthquake," by F. Naeim, R. DiSulio, K. Benuska, A. Reinhorn and C. Li, to be published.

NCEER-95-0007 "Prioritization of Bridges for Seismic Retrofitting," by N. Basöz and A.S. Kiremidjian, 4/24/95, (PB95-252300, A08, MF-A02).

NCEER-95-0008 "Method for Developing Motion Damage Relationships for Reinforced Concrete Frames," by A. Singhal and A.S. Kiremidjian, 5/11/95, (PB95-266607, A06, MF-A02).

NCEER-95-0009 "Experimental and Analytical Investigation of Seismic Retrofit of Structures with Supplemental Damping: Part II - Friction Devices," by C. Li and A.M. Reinhorn, 7/6/95, (PB96-128087, A11, MF-A03).

NCEER-95-0010 "Experimental Performance and Analytical Study of a Non-Ductile Reinforced Concrete Frame Structure Retrofitted with Elastomeric Spring Dampers," by G. Pekcan, J.B. Mander and S.S. Chen, 7/14/95, (PB96-137161, A08, MF-A02).

NCEER-95-0011 "Development and Experimental Study of Semi-Active Fluid Damping Devices for Seismic Protection of Structures," by M.D. Symans and M.C. Constantinou, 8/3/95, (PB96-136940, A23, MF-A04).

NCEER-95-0012 "Real-Time Structural Parameter Modification (RSPM): Development of Innervated Structures," by Z. Liang, M. Tong and G.C. Lee, 4/11/95, (PB96-137153, A06, MF-A01).

NCEER-95-0013 "Experimental and Analytical Investigation of Seismic Retrofit of Structures with Supplemental Damping: Part III - Viscous Damping Walls," by A.M. Reinhorn and C. Li, 10/1/95, (PB96-176409, A11, MF-A03).

NCEER-95-0014 "Seismic Fragility Analysis of Equipment and Structures in a Memphis Electric Substation," by J-R. Huo and H.H.M. Hwang, (PB96-128087, A09, MF-A02), 8/10/95.

NCEER-95-0015 "The Hanshin-Awaji Earthquake of January 17, 1995: Performance of Lifelines," Edited by M. Shinozuka, 11/3/95, (PB96-176383, A15, MF-A03).

NCEER-95-0016 "Highway Culvert Performance During Earthquakes," by T.L. Youd and C.J. Beckman, 11/6/95, to be published.

NCEER-95-0017 "The Hanshin-Awaji Earthquake of January 17, 1995: Performance of Highway Bridges," Edited by I.G. Buckle, 12/1/95, to be published.

NCEER-95-0018 "Modeling of Masonry Infill Panels for Structural Analysis," by A.M. Reinhorn, A. Madan, R.E. Valles, Y. Reichmann and J.B. Mander, 12/8/95.

NCEER-95-0019 "Optimal Polynomial Control for Linear and Nonlinear Structures," by A.K. Agrawal and J.N. Yang, 12/11/95, (PB96-168737, A07, MF-A02).

NCEER-95-0020 "Retrofit of Non-Ductile Reinforced Concrete Frames Using Friction Dampers," by R.S. Rao, P. Gergely and R.N. White, 12/22/95.

NCEER-95-0021 "Parametric Results for Seismic Response of Pile-Supported Bridge Bents," by G. Mylonakis, A. Nikolaou and G. Gazetas, 12/22/95.

NCEER-95-0022 "Kinematic Bending Moments in Seismically Stressed Piles," by A. Nikolaou, G. Mylonakis and G. Gazetas, 12/23/95.

NCEER-96-0001 "Dynamic Response of Unreinforced Masonry Buildings with Flexible Diaphragms," by A.C. Costley and D.P. Abrams," 10/10/96.